Variabilité climatique récente de l'Antarctique : apports des enregistrements issus de carottes de névé

Sentia Goursaud

Communauté
UNIVERSITÉ Grenoble Alpes

THÈSE

Pour obtenir le grade de
DOCTEUR DE LA COMMUNAUTE UNIVERSITE GRENOBLE ALPES
Spécialité : Sciences de la Terre et Univers, Environnement
Arrêté ministériel : 25 mai 2016

Présentée par
Sentia GOURSAUD

Thèse dirigée par **Michel LEGRAND**
et codirigée par **Valérie MASSON-DELMOTTE**

préparée au sein de
l'Institut des Geosciences de l'Environnement
dans **l'École Doctorale Terre, Univers, Environnement**

Variabilité climatique récente de l'Antarctique : apports des enregistrements issus de carottes de névé

Thèse soutenue publiquement le **05/11/2018**,
devant le jury composé de :

M. Hubert GALLEE
Directeur de Recherche à l'IGE, Grenoble, Président
M. Roderik VAN DE WAL
Professeur à l'Université d'Utrecht, Rapporteur
M. Xavier CROSTA
Directeur de recherche à l'EPOC, Bordeaux, Rapporteur
M. Jean-Louis TISON
Professeur à l'Université de Bruxelles, Examinateur
M. Michel LEGRAND
Directeur de recherche, IGE, Grenoble, Directeur de thèse
Mme Valérie MASSON-DELMOTTE
Directrice de recherche, LSCE, Gif-sur-Yvette, Co-directrice de thèse

Remerciements.

A l'aboutissement de cet ouvrage, je me dois de rendre hommage aux personnes sans qui ce projet de thèse n'aurait non seulement pas pu se réaliser, mais aussi grâce à qui je garde le souvenir d'un si bel et agréable voyage.

Je tiens tout d'abord à te remercier, Valérie. Tu m'as encadré dans mon travail, en me donnant une direction scientifique, des outils, m'as initié aux techniques indispensables pour mener des recherches, et m'a inséré dans la communauté scientifique. Grâce à toi, je commence une carrière avec le sentiment d'avoir les principales clés en main. Mais tu as aussi toujours été là à chaque fois que des barrières émotionnelles entravaient à mon travail. Tu m'as montré que cette réalité personnelle faisait partie de l'intervalle moyenne ± 2 écart-types, et comment faire pour les sauter haut et réceptionner bien en avant.

Ma gratitude va aussi à vous Michel et Susanne, qui avez accompagné cette thèse, m'avez initié aux techniques expérimentales des analyses chimiques des carottes de glace. C'est aussi grâce à vous que j'ai pris goût au froid.

Merci à mes collègues, pour des moments chaleureux partagés, autour d'un café, d'un plateau ou d'un radiateur. J'en garde la mémoire de fous rires, de bienveillance, et d'attention. Cécile, Ambroise, Monique, Anaïs, et Aymeric … vous êtes encore aujourd'hui présents.

Mais mes plus grands collaborateurs sont mes amis et ma famille. Lulu, Ségo, Séb, Clem, Christelle, marraine, et beau-papa, je vous remercie bien que l'équivalent littéraire à ma reconnaissance ne connait pas d'égal. Maman chérie, plus qu'une collaboratrice, presque une partie de moi ou moi une partie de toi, ton soutien m'a été primordial. Votre Amour est salvateur, et réalisateur.

Enfin, Benjamin, mon amour, je te dédie ce travail, que tu accompagnes au quotidien.

Résumé.

Documenter la variabilité climatique récente est nécessaire à la compréhension des mécanismes en jeu, associés au rôle du bilan de masse de l'Antarctique pour l'élévation du niveau des mers globale. Les enregistrements issus des carottes peu profondes d'Antarctique sont des données précieuses, complémentaires aux observations instrumentales et satellitaires, pour couvrir en continu l'ensemble du continent. Mesurés le long de ces carottes de glace, les isotopes stables de l'eau sont traditionnellement utilisés pour quantifier les changements passés de la température locale.

Cette thèse doctorale a été initiée dans le cadre du programme de l'Agence Nationale de la Recherche ASUMA ("Improving the Accurancy of SUrface Mass balance of Antarctica"), ayant pour objectif de reconstruire et identifier les processus contrôlant la variabilité spatio-temporelle du bilan de masse de surface (BMS) de la Terre Adélie. J'ai utilisé des données d'isotopes stables de l'eau enregistrées dans des carottes de névé, des simulations atmosphériques produites par le modèle atmosphérique de circulation générale de haute résolution ECHAM5-wiso équipé des isotopes stables de l'eau, des réanalyses atmosphériques, des rétro-trajectoires, ainsi que des observations instrumentales satellitaires et de surface.

Dans une première partie, j'ai évalué les capacités du modèle ECHAM5-wiso à simuler les températures de l'Antarctique, le BMS, le $\delta^{18}O$ et l'excès en deutérium (ci-après, d-excess), comme prérequis à l'exploitation du modèle pour interpréter les compositions isotopiques. J'ai développé des diagnostics pour les relations $\delta^{18}O$-température et d-excess- $\delta^{18}O$ sur l'ensemble du continent de l'Antarctique, en montrant les différences issues des pentes des relations $\delta^{18}O$-température spatiales, inter-annuelles et saisonnières. Au sein du groupe de travail international de PAGES (Past Global Changes) Antarctica2k, j'ai utilisé des calibrations établies issues du modèle ECHAM5-wiso pour reconstruire la température de 7 régions d'Antarctique à partir d'une synthèse d'enregistrements de $\delta^{18}O$ issus de carottes de glace couvrant les 2 000 dernières années.

Dans une seconde partie, de nouveaux enregistrements issus de deux carottes de névé extraites en Terre Adélie, la S1C1 et la TA192A, ont été exploités, couvrant respectivement les périodes 1947-2007 et 1998-2014. Les BMS reconstruits décrivent une grande variabilité spatiale (74,11 ± 14,1 cm w.e. y^{-1} et 21,8 ± 6,9 cm w.e. y^{-1} pour la TA192A et la S1C1 respectivement), cohérente avec les données de balise disponibles. En utilisant une base de données mise à jour des isotopes stables de l'eau de l'Antarctique, j'ai montré que les valeurs moyennes isotopiques de Terre Adélie appartiennent à l'intervalle des valeurs côtières de l'Antarctique. Des analyses statistiques montrent une absence de relation entre nos enregistrements avec la température de surface locale à l'échelle inter-annuelle, mais des relations significatives avec des rétro-

trajectoires atmosphériques et des simulations isotopiques suggérant que les isotopes de l'eau de la Terre Adélie fournissent des indications de la variabilité de la dynamique atmosphérique et du transport d'humidité, aux échelles saisonnière et inter-annuelle.

Les analyses de cette thèse ont été limitées par la quantité d'enregistrements isotopiques disponibles pour la Terre Adélie, ainsi que par le manque de compréhension des effets de dépôt et de post-dépôt. Il est donc nécessaire d'exploiter les nouvelles carottes de névé extraites au cours du programme ASUMA, et d'effectuer en continu des mesures de la composition isotopique des précipitations, de la vapeur d'eau et de la neige de surface de Terre Adélie, en combinaison avec des outils de simulations atmosphériques, tels que des rétro-trajectoires associées à un diagnostic des sources d'humidité, et des modèles atmosphériques de circulation générale et régionaux équipés des isotopes stables de l'eau.

Mots clés : Variabilité climatique de l'Antarctique, carottes de névé, isotopes stables de l'eau, modèle atmosphérique de circulation général

Abstract.

Documenting recent Antarctic climate variability is needed in order to understand the mechanisms at play, associated with the role of Antarctic mass balance for global sea level rise. Proxy records from Antarctic shallow firn cores are precious data, which complement instrumental and remote sensing observations to continuously cover the whole continent. Within these ice cores, water stable isotopes are commonly used to quantify past changes in local temperature.

This PhD thesis was initiated within the French Agence Nationale de la Recherche "Improving the Accurancy of SUrface Mass balance of Antarctica" (ASUMA) project, which aims to reconstruct and to identify the processes controlling the spatio-temporal variability of the surface mass balance (SMB) in Adélie Land. I used water stable isotopes records from recently drilled shallow firn cores, as well as atmospheric simulations performed with the high resolution atmospheric general circulation model ECHAM5-wiso model, equipped with water stable isotopes, atmospheric reanalyses and back-trajectories, instrumental and remote sensing climate observations.

In a first part, I assessed the skills of the ECHAM5-wiso with respect to Antarctic temperature, SMB, $\delta^{18}O$ and deuterium excess (hereafter d-excess), as a prerequisite for the exploitation of the model to interpret isotope compositions. I developed Antarctic-wide diagnostics of the $\delta^{18}O$-temperature and d-excess- $\delta^{18}O$ relationships, showing differences in the spatial, seasonal and interannual $\delta^{18}O$-temperature slopes. Within the international working group of PAGES (Past Global Changes) Antarctica 2k, I used the calibrations inferred from ECHAM5-wiso to reconstruct temperatures over 7 Antarctic regions from a synthesis of ice core $\delta^{18}O$ records spanning the past 2,000 years.

In a second part, new water stable isotope records from two firn core drilled in Adélie Land, the S1C1 and the TA192A, were investigated, covering the periods 1947-2007 and 1998-2014 respectively. The reconstructed SMB display a high spatial variability (74.1 ± 14.1 cm w.e. y^{-1} and 21.8 ± 6.9 cm w.e. y^{-1} for the TA192A and S1C1 respectively), consistent with Adélie Land stake data. Using an updated database of Antarctic water stable isotope datasets, I showed that the mean isotopic values ($\delta^{18}O$ and d-excess) in Adélie Land are in line with the range of Antarctic coastal values. Statistical analyses show no relationship between our records and local surface air temperature, at the inter-annual scale, but significant relationships with atmospheric back-trajectories and isotopic simulations, suggesting that water stable isotopes in Adélie Land provide fingerprints of the variability of atmospheric dynamics and moisture transport, at the seasonal and inter-annual scales.

The analyses performed during this PhD thesis have been limited by the few available Adélie Land water stable isotope records, and by the lack of understanding of deposition and post-deposition processes. Further work is thus needed to exploit the new firn cores drilled within the ASUMA project, and to monitor continuously Adélie Land water stable isotopes in precipitation, surface water vapour and surface snow, in combination with tools of atmospheric simulations such as back-trajectory simulations provided with moisture sources diagnostics, as well as water stable isotopes-enabled atmospheric general and regional circulation models.

Keywords: Antarctic climate variability, firn cores, water stable isotopes, atmospheric general circulation models

Note au lecteur.

Dans la suite du manuscrit, le lecteur trouvera des encadrés ombrés insérés pour donner les prérequis nécessaires à une bonne compréhension de la thèse, et faisant l'objet de rappels. Les mots associés à un astérisque y sont définis.

Table des matières

CHAPITRE 1 : Introduction

1. Introduction

1.1 Pourquoi étudier le climat de l'Antarctique ?

1.1.1 Le changement climatique planétaire

Dans son dernier rapport, le Groupement Intergouvernemental d'experts (GIEC*) a conclu qu'un changement climatique était détecté* depuis les années 1950, notamment par une tendance de l'augmentation de la température moyenne à la surface de la Terre (cf. Fig. 1.1a) estimée à ~ 0,18 ± 0,01 °C par décennie sur la période 1951-2012. Le réchauffement climatique résulte d'une accumulation d'énergie dans le système climatique, et se manifeste également par une augmentation du contenu d'énergie des océans et une fonte de la cryosphère. La montée du niveau des mers est une conséquence planétaire de ce réchauffement, du fait de la dilatation thermique des océans, et de l'apport d'eau supplémentaire par la fonte des glaces continentales, glaciers et calottes polaires. Ces deux processus entraînent une hausse de l'élévation des mers observée à 2,0 ± 0,3 mm an^{-1} sur la période 1971-2000. Sur la période 1993-2010, le rythme de montée du niveau des mers s'est accéléré (Nerem et al., 2018). Cette élévation a été attribuée* à hauteur de 39,3 % à la dilatation thermique, et 52,1 % à la fonte des calottes polaires et glaciers (polaires et non polaires), dont 9,6 % à la fonte de la calotte Antarctique (cf Tableau 1.1). L'accélération récente de la montée du niveau des mers est cependant majoritairement attribuée à l'augmentation de la perte de masse de la calotte du Groenland, dont la contribution a été estimée à plus de 25 % en 2014 (Chen et al., 2017). Le réchauffement climatique s'accompagne également de modifications de la répartition des précipitations et de la fréquence et l'intensité d'évènements extrêmes, comme les vagues de chaleur et les pluies torrentielles, dans certaines régions (IPCC, 2013).

Tableau 1.1: Bilan des contributions à l'élévation du niveau de la mer observées sur la période 1993-2010 (Données extraites du chapitre 13 du cinquième rapport du GIEC; IPCC, 2013)

	Contribution	
	(mm y^{-1})	(%)
Océans (dilatation thermique)	1,1	39,3
Glaciers non polaires	0,76	27,1
Glaciers groenlandais	0,1	3,6
Calotte glaciaire groenlandaise	0,33	11,8
Calotte glaciaire antarctique	0,27	9,6
Stockage d'eaux continentales	0,38	13,6

Ce changement climatique est attribué sans équivoque à l'influence humaine (cf. Fig. 1.1b), et notamment au forçage radiatif à l'origine de l'augmentation des concentrations de gaz à effet de serre dans l'atmosphère. L'influence humaine est détectée dans le réchauffement de l'atmosphère et de l'océan, les changements du cycle de l'eau global, la réduction des zones enneigées et englacées, la montée du niveau des mers et certains évènements extrêmes. Néanmoins, toutes les variations climatiques régionales ne sont pas nécessairement pilotées par l'influence humaine, et peuvent également résulter de variations naturelles du climat. Ainsi, le 5ème rapport du GIEC (IPCC, 2014) souligne qu'il est probable que les forçages anthropiques* ont contribué de manière substantielle à l'augmentation de la température à la surface de chaque continent, à l'exception de l'Antarctique. Pour celle-ci, les incertitudes liées aux observations conduisent à un niveau de confiance faible dans la contribution de forçages anthropiques au réchauffement observé dans certaines stations. Ce constat motive la production de nouvelles sources d'information sur l'évolution récente du climat en Antarctique.

Le GIEC a été créé en 1988 et regroupe aujourd'hui 195 pays membres, dans l'objectif « d'évaluer, sans parti pris et de façon méthodique, claire et objective, les informations d'ordre scientifique, technique et socio-économique qui nous sont nécessaires pour mieux comprendre les risques liés au réchauffement climatique d'origine humaine, cerner plus précisément les conséquences possibles de ce changement et envisager d'éventuelles stratégies d'adaptation et d'atténuation. Il n'a pas pour mandat d'entreprendre des travaux de recherche ni de suivre l'évolution des variables climatologiques ou d'autres paramètres pertinents. Ses évaluations sont principalement fondées sur les publications scientifiques et techniques dont la valeur scientifique est largement reconnue ». Il recueille ainsi l'ensemble de l'information scientifique relative à **la détection**, **l'attribution**, des variations climatiques, ses conséquences, ainsi que les stratégies techniques et socio-économiques d'**adaptation** et d'**atténuation**.

Le climat (du grec « klima », inclinaison) est l'étude des paramètres météorologiques (e.g. température, pression, humidité) mesurables dans l'atmosphère. Ses variations spatiales et temporelles sont modulées par le bilan énergétique entre le flux incident solaire, le flux réfléchi par les nuages (effet parasol) et le sol (albédo), le flux sortant (effet de serre), ainsi que par la dynamique des composantes du système climatique (atmosphère, océan, géosphère, cryosphère et biosphère).

Un forçage est une contrainte engendrant une **perturbation** du bilan radiatif au sommet de l'atmosphère.

Naturel ou anthropique ? En climatologie, la variabilité climatique peut-être naturelle, c'est-à-dire spontanée (liée aux interactions entre océan, atmosphère, cryosphère, …) ou initiée par

une perturbation sans lien avec les activités humaines (e.g. éruption volcanique, activité solaire, activité tectonique, configuration astronomique). A contrario, si l'évolution du climat est attribuée par des méthodes objectives aux conséquences d'activités humaines, alors elle sera qualifiée d'anthropique (e.g. réchauffement anthropique lié au rejet de gaz à effet de serre).

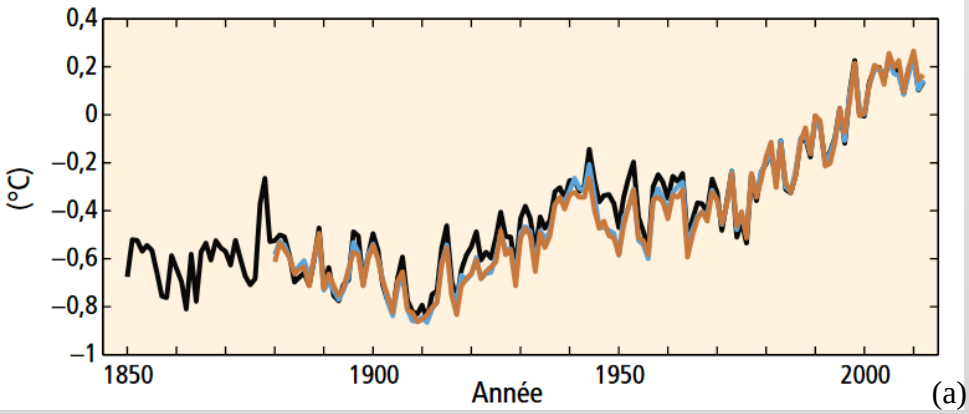

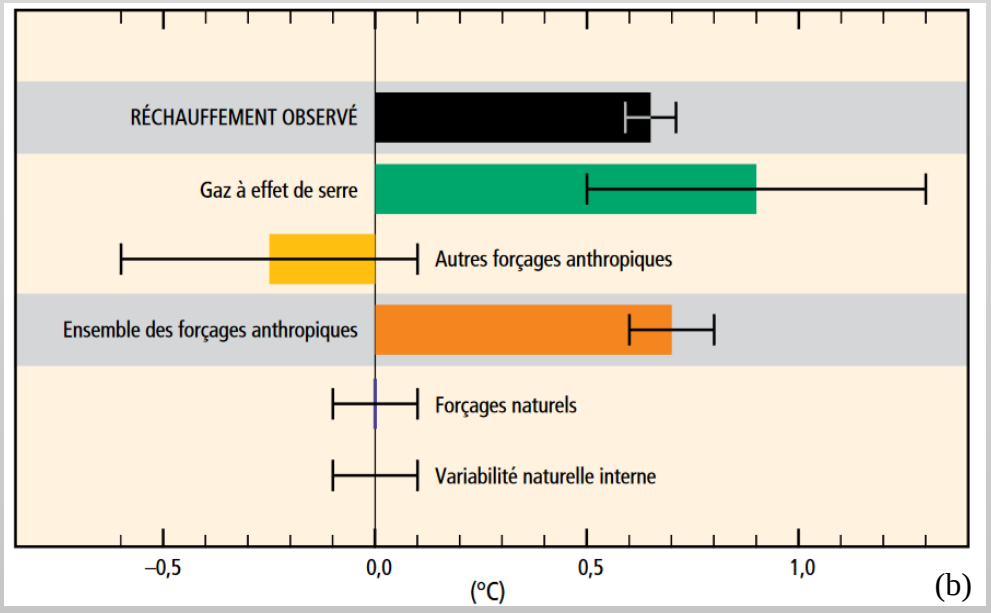

Figure 1.1: (a) Changement de température moyenne à la surface de la Terre, et (b) Plage probable (lignes noires horizontales) et médianes correspondantes (lignes noires verticales) pour les tendances du réchauffement sur la période 1951–2010 dû à des gaz à effet de serre, à d'autres forçages anthropiques (e.g. l'effet refroidissant net des aérosols), à l'ensemble des forçages anthropiques, aux forçages naturels et à la variabilité naturelle interne (i.e. spontanée, sans forçage). Figures extraites du cinquième rapport du GIEC (IPCC, 2014)

Géographie de l'Antarctique

L'Antarctique (du grec « ἀνταρκτικός ») désigne littéralement l'endroit diamétralement opposé à la grande ourse («Arkos »), qui est située au Pôle Nord. Cette position géographique actuelle singulière lui confère l'appellation de « continent des superlatifs » (Rémy, 2003). Cette région reçoit moins d'ensoleillement incident que les régions des latitudes plus basses. Ce grand continent de 14 000 000 km^2 (une superficie comparable à celle de la Russie) a aussi l'altitude moyenne la plus élevée (~ 2 200 m), et les températures les plus basses, avec des records de température inférieurs à -90 °C (Campbell et al., 2013)[1]. C'est également le continent le plus aride, avec une moyenne d'accumulation (i.e. le bilan net entre les apports de neige et la sublimation) de 143 ± 4 mm w.e. an^{-1} (Arthern et al., 2006). La somme de ces caractéristiques en fait un désert polaire. Néanmoins, malgré sa nature désertique, l'Antarctique est le lieu de stockage d'eau douce le plus important sur Terre (75% des ressources terrestres disponibles), à l'état de glace sur 98 % du continent. Communément appelée Inlandsis, cette épaisseur de glace résulte de l'accumulation de la neige au fil du temps, et de l'écoulement dynamique du plateau vers les côtes. Des modèles d'écoulement de la glace permettent de dater la glace (Parrenin et al., 2007). Actuellement, ces modèles glaciologique sont mis au service de la recherche de la glace la plus ancienne du continent Antarctique, dans le cadre du projet de forage « Oldest ice » (Fischer et al., 2013; Parrenin et al., 2017; Van Liefferinge et al., 2018).

La géographie et le climat de l'Antarctique sont étroitement liés. Leur variabilité spatiale se caractérise par des gradients de la côte vers le plateau : l'altitude augmente tandis que les températures atmosphériques et les taux de précipitations et de sublimation diminuent. La topographie et le gradient de température jouent un rôle important dans la formation des vents très intenses, appelés vents catabatiques. Du grec « cata », signifiant « vers le bas », ces vents se densifient le long de leur écoulement gravitaire du plateau vers la côte, du fait de l'inversion de température en Antarctique créant un gradient horizontal de densité (Ball, 1956; Pettré et al., 1986). L'orographie leur confère leur direction. Ces vents influencent le climat selon deux caractéristiques principales : (i) ils déplacent la glace de mer, créant des ouvertures dans la glace, les polynies (qui favorisent la formation de nouvelle glace de mer par congélation de l'eau de mer en surface) ; (ii) ils affectent le bilan de masse de surface en imposant une circulation atmosphérique méridionale contrôlant alors le transport d'humidité vers le continent (van Lipzig, 1999), ainsi qu'en générant un déplacement de la neige récemment déposée susceptible de sublimer (Bintanja, 1998); et (iii) ils participent à la formation des mésocyclones,

[1] A titre anecdotique, le record de froid planétaire enregistré à -93,2 °C, a été mesuré par le satellite NASA-UGSG Landsat en Antarctique de l'Est, entre Dôme F et Dôme A le 10/08/2010.

eux-même influencés par les vents d'ouest tout autour de l'Antarctique, associés au rail des dépressions (Gallée, 1995).

Enfin, le climat de l'Antarctique décrit une saisonnalité définie par la variation de températures plus élevées durant l'été austral, de décembre à février, et plus basses durant l'hiver austral, de mai à septembre (Comiso, 2000). Les hivers n'ont pas une période de froid particulièrement contrastée comparée à l'ensemble de la saison. On parle de phénomène de « coreless winter » (Van Loon, 1967). En hiver, les températures diminuant, les eaux de surface de la mer gèlent à ~ -1,8 °C (variable selon la salinité), créant ainsi de la glace de mer. Puis celle-ci s'épaissit progressivement pour atteindre jusqu'à 2 m. Sa formation peut-être ralentie par les forts vents catabatiques et les courants océaniques, perturbant la stabilité des flux propice à sa production. Une fois stabilisé, l'ensemble de la glace de mer et de la banquise peut atteindre jusqu'à 20 000 000 km^2. Cette glace de mer influence grandement le climat côtier, modulant l'apport d'air doux et humide venant de l'océan austral qui compense l'air sec et froid continental, et amplifiant les vents catabatiques côtiers très intenses (e.g. Parish and Waight III, 1987). Le rejet de saumures associé à la croissance de la glace de mer participe aussi à la formation des eaux profondes de la circulation océanique planétaire.

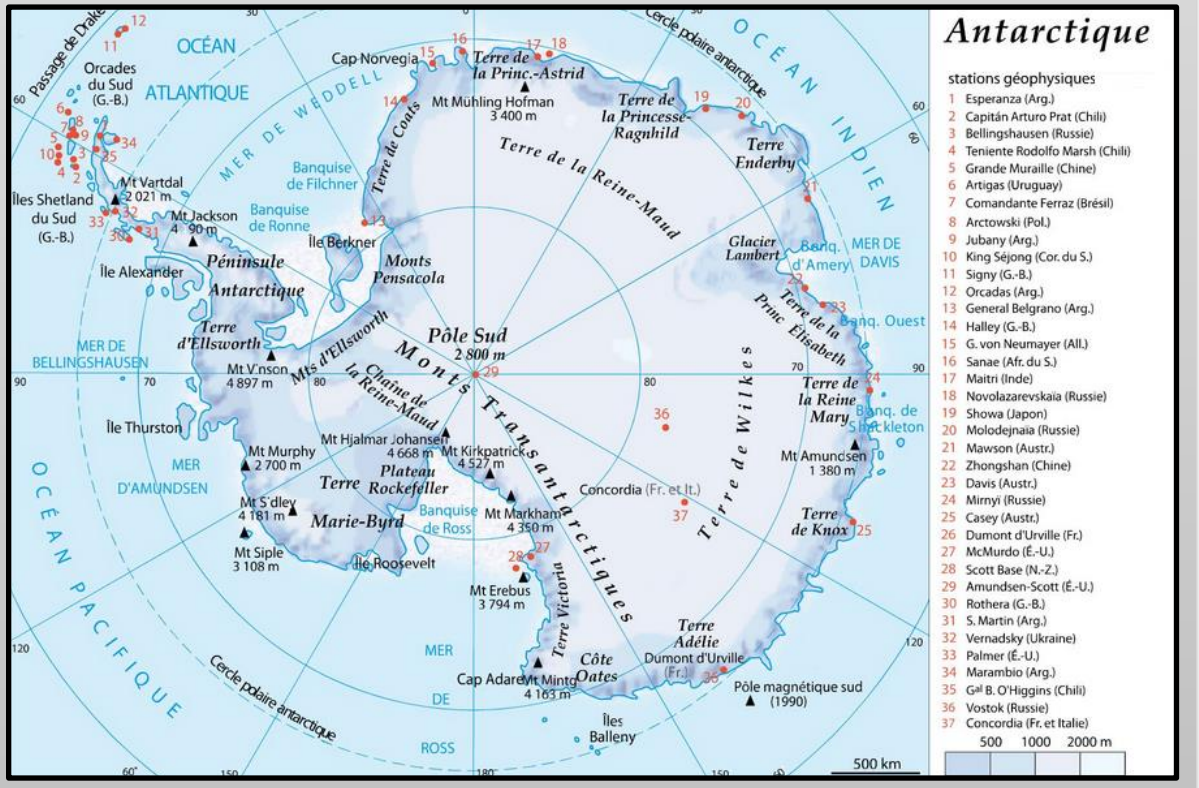

Figure 1.2: Carte de l'Antarctique. Extrait du Larousse, http://www.larousse.fr/encyclopedie/autre-region/Antarctique/105649, 06/2018.

1.1.2 L'Antarctique dans le système climatique

L'ensemble des composantes du climat (géosphère, atmosphère, hydrosphère, cryosphère, et biosphère) interagissent constamment. Ainsi, la calotte antarctique, ainsi que son atmosphère, influencent, et sont influencés par chacune des autres composantes du climat. Cependant, l'étude complète de ces interactions est complexe. Cette thèse propose de s'intéresser spécifiquement aux processus atmosphériques. Dans la suite, j'introduirai donc brièvement les conséquences pour le niveau des mers, puisqu'ils sont une des principales motivations actuelles de la compréhension du climat de l'Antarctique et de son évolution ; je me concentrerai sur les interactions atmosphériques entre l'Antarctique et les plus basses latitudes[2].

Pour le niveau des mers

La calotte de glace de l'Antarctique représente le plus grand volume d'eau douce terrestre. Son contact direct avec l'océan austral rend leur évolution interdépendante. Le bilan de masse* se calcule à partir du bilan de masse de surface* (ci-après, BMS, cf. Fig. 1.3), dont la composante principale est les précipitations (Bromwich, 1988). Les masses d'air précipitant en Antarctique se forment par évaporation au-dessus des océans et peuvent correspondre à une baisse du niveau des mers. A titre d'exemple, le 5ème rapport du GIEC rapporte un taux moyen d'accumulation* annuel équivalent à une baisse du niveau de la mer de 0,03 ± 0,01 mm an^{-1}, simulé par un ensemble de modèles intégrant des données d'observation, sur la période 1991-2010 (IPCC, 2014). A l'inverse, l'écoulement de la glace produit des icebergs qui se déchargent dans les océans. Le volume de la calotte est équivalent à une hauteur de ± 58,3 m de niveau de mer (Vaughan et al., 2013), ce qui souligne l'importance de l'évolution de la calotte Antarctique pour le niveau des mers planétaire.

Dans la circulation atmosphérique de grande échelle

A l'échelle synoptique (i.e. de grande échelle), la circulation atmosphérique structure des échanges entre basses et hautes latitudes. Son organisation est décrite par des modes de variabilité (SAM*, ENSO*, PSA1* et PSA2*) caractérisés par leur périodicité et leur influence sur la variabilité climatique régionale (Cassou and Guilyardi, 2007). Récemment, Welhouse et al. (2016) ont montré l'influence du signal ENSO sur les distributions spatiales de la température à 2 m d'altitude, et de la pression moyenne au niveau de la mer sur l'ensemble de l'Antarctique. De même, Marshall and Thompson (2016) ont montré l'influence des différents modes de variabilité sur la distribution de la température de surface en Antarctique, puis Marshall et al. (2017) ont mis en évidence leur influence sur la distribution des précipitations

[2] Il existe des interactions avec les autres composantes, notamment océaniques. Elles ne sont cependant pas traitées dans le cadre de ma thèse, et ne sont donc pas présentées dans cette introduction.

Le bilan de masse de surface (BMS) se définit par : BMS = P – D –E –S-R

Avec P les précipitations, D le dépôt, E l'érosion, S la sublimation et R le ruissellement.

Le bilan de masse (BM) se déduit du BMS et de l'écoulement dynamique.

L'accumulation représente la différence des précipitations par la sublimation.

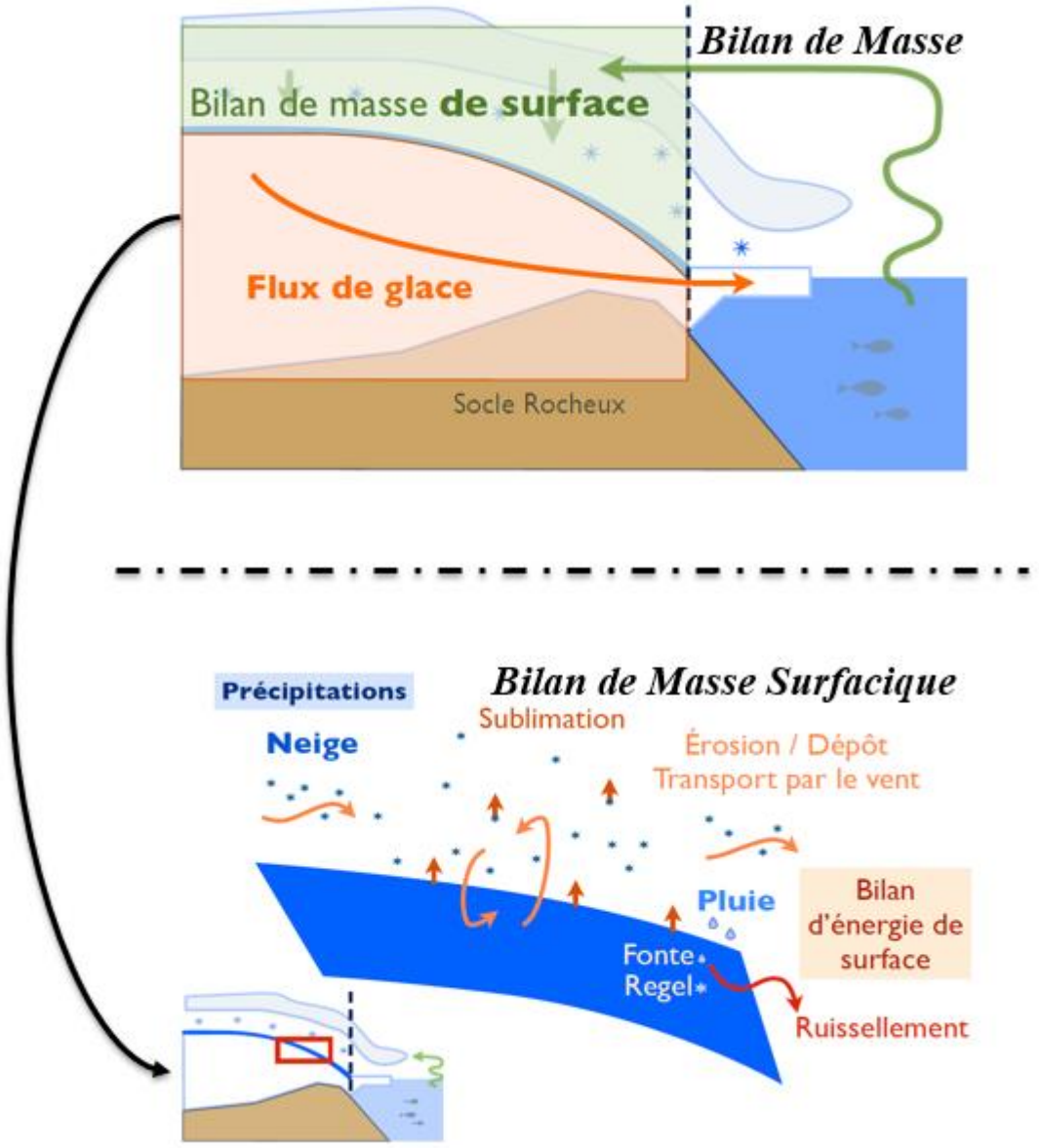

Figure 1.3: Illustration du bilan de masse, ainsi que du bilan de masse de surface. Le flux de glace correspond à l'écoulement dynamique. Schémas adaptés de Cécile Agosta (communication personnelle).

La dynamique atmosphérique (Cours d'Introduction à la physique de l'atmosphère, F. Hourdin, http://www.lmd.jussieu.fr/~hourdin/PEDAGO/)

En raison de la rotondité, le bilan radiatif du haut de l'atmosphère est cinq fois plus important au niveau de l'équateur comparé aux pôles, si bien que la Terre peut être modélisée comme une machine thermique avec l'équateur comme source chaude, et les pôles comme source froide. L'excès d'énergie dans les régions tropicales entraine un réchauffement en surface, une évaporation intensifiée au-dessus des océans, ainsi que des basses pressions atmosphériques à la surface. A l'inverse, les régions polaires expérimentent un déficit d'énergie, entrainant un refroidissement et de hautes pressions atmosphériques à la surface. La force de Coriolis dévie la trajectoire des masses d'air, dont le seul gradient thermique voudrait qu'elles se dirigent des pôles vers les tropiques (vents d'Est entre 30 °N et 30 °S, vents d'ouest entre 30 ° et 60 ° aux deux pôles), créant ainsi trois cellules méridionales (cellules de Hadley, Ferrel et polaires ; cf. Fig. 1.4). Au sein de chacune des cellules, des mouvements de subsidence et d'ascendance sont mises en place du fait des gradients de pression. Notamment, Au sein de la cellule polaire de l'hémisphère sud, le refroidissement en surface (et donc les hautes pressions en surface) à ~ 60 ° S crée une ascendance des masses d'air, puis le haut de la tropopause (à ~ 8 km aux pôles) contraint le flux à se déplacer horizontalement vers le sud, jusqu'à ce qu'un mouvement de subsidence soit imposé par instabilité négative à 90 °S, avec un air très sec (on dit que l'intérieur de l'Antarctique est un désert polaire).

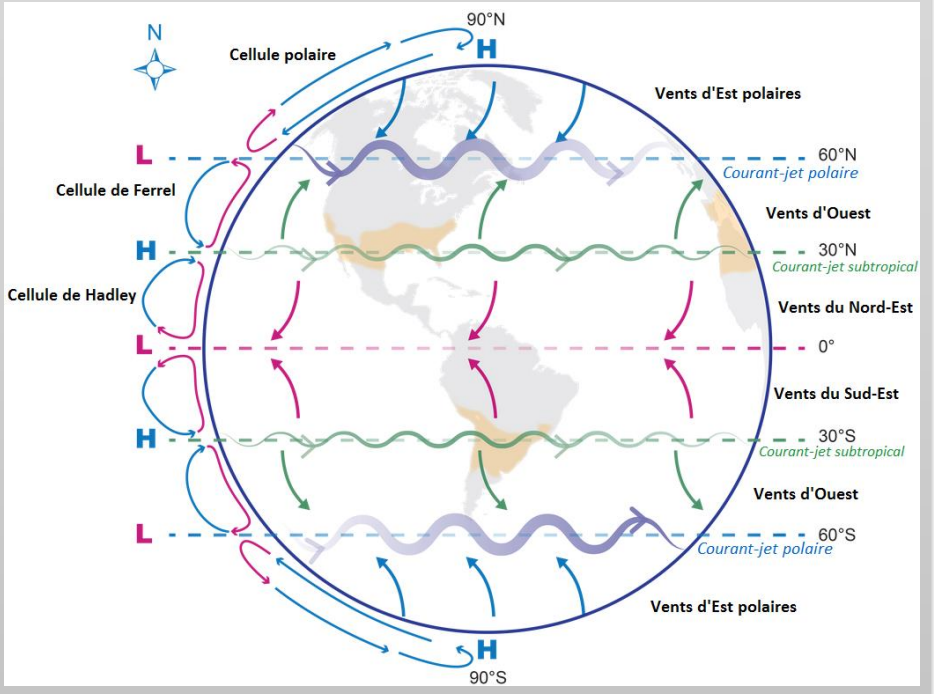

Figure 1.4: Cellules atmosphériques et vents associés, Adaptée de Wuebbles et al. (2017).

C'est la force de Coriolis qui divise la cellule convective initiale imposée par le gradient du bilan énergétique au sommet de la troposphère. Mais la circulation au sein de chacune des trois cellules reste dépendante de celle des deux autres. Ainsi, l'Antarctique situé au pôle Sud, est acteur et sujet de la circulation atmosphérique générale de grande échelle (i.e. sur une échelle horizontale de plus de 1 000 km), et cette circulation synoptique varie au cours du temps.

Les modes de variabilité atmosphériques

Le SAM (« Southern Annular Mode) est le principal mode de variabilité atmosphérique influençant l'hémisphère sud (Thompson and Wallace, 2000). L'indice du SAM se définit par la différence des pressions zonales moyennes au niveau de la mer à 40 °S et 65 °S (Marshall, 2003). Il peut également être calculé à partir de simulations ou analyses atmosphériques, comme la première fonction orthogonale empirique du géopotentiel à 500 hPa (Mo, 2000; Ding et al., 2012). Il indique principalement la position latitudinale du rail des dépressions : positif (négatif), il correspond à un rail situé plus au sud (nord). On observe, au cours des dernières décennies, une tendance positive. Toggweiler and Russell (2008) expliquent qu'une augmentation des températures tropicales (qu'il compare à titre comparatif à celles du dernier maximum glaciaire) augmente le contraste des températures tropicales/polaires, intensifiant ainsi les vents d'ouest (cf. Fig. 1.5a).

Les PSA1 et PSA2 (« Pacific South-American ») sont définis par les seconde et troisième fonctions orthogonales empiriques du géopotentiel à 500 hPa (Kidson, 1988; Mo and Higgins, 1998). Ils sont influencés par les anomalies de température de la mer tropicale, la force du jet-stream et les vents zonaux pacifiques extratropicaux.

L'ENSO (« El-Niño Southern Oscillation ») est le mode le plus important à l'échelle planétaire. Sa définition est basée sur les changements de la température de surface de la mer sur la zone tropicale de l'océan pacifique, et sa réponse couplée avec l'atmosphère (Wang and Fiedler, 2006). Ses variations se propagent via les ondes de Rossby jusqu'en Antarctique, et d'autant plus lorsque le SAM est dans sa phase négative (Abram et al., 2014).

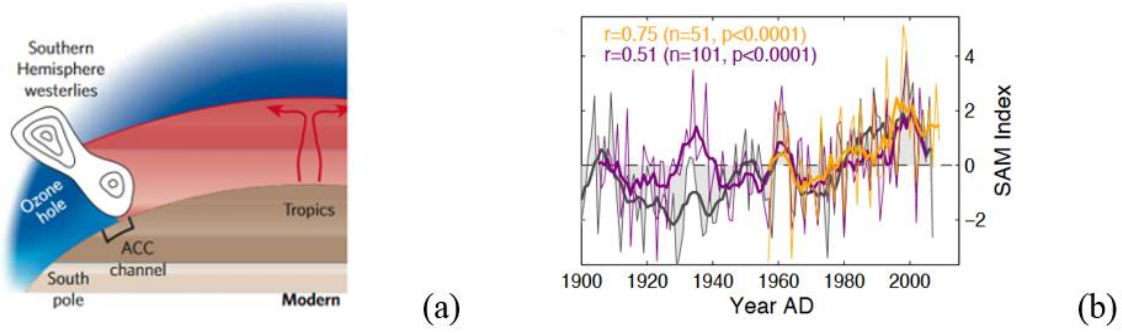

Figure 1.5: Evolution du SAM au cours des dernières décennies : (a) L'augmentation des températures de surface aux tropiques, accroit le contraste des températures entre les hautes et basses latitudes, intensifiant les vents d'ouest autour de l'Antarctique, et les déplaçant plus près des pôles. Adapté de Toggweiler and Russell (2008); (b) Reconstruction du SAM à partir des index définis par Marshall (2003; en orange, de 1957 à 2007), et Fogt et al. (2009; en violet, de 1905 à 2005) . Adapté de Abram et al. (2014).

en Antarctique. Cependant, les mécanismes physiques et forçages à l'origine de ces variabilités restent incompris. L'Antarctique est donc acteur du changement climatique global en participant à l'élévation du niveau des mers, mais aussi en participant à la redistribution énergétique au sein de la circulation atmosphérique de grande échelle. Les modes de variabilité basés sur les télé-connections entre les tropiques et les pôles, et notamment la tendance positive du SAM* d'été à l'échelle interannuelle (cf. Fig. 1.5b), suggèrent la possibilité que le changement climatique global des dernières décennies, dû aux rejets anthropiques de gaz à effet de serre, et observé dans les régions des basses et moyennes latitudes, affecte aussi le climat de l'Antarctique. Par ailleurs, la destruction de l'ozone stratosphérique semble également jouer un rôle clé dans l'évolution du SAM (e.g. Thompson et al., 2011).

1.1.3 Variations climatiques en Antarctique

Si le changement climatique récent est détectable à l'échelle globale, et que les modes de variabilité atmosphérique liés à l'hémisphère sud montrent des tendances aux cours des dernières décennies, comment le climat récent de l'Antarctique évolue-t-il? Et comment cette variabilité se situe-t-elle dans un contexte glaciaire-interglaciaire?

Au cours d'une transition glaciaire-interglaciaire, la température de surface de l'Antarctique, reconstruite à partir des isotopes stables des carottes de glace, a varié de l'ordre de 8 à 10 °C (Petit et al., 1999; Uemura et al., 2012). Cette variation diffère cependant selon que l'on considère l'Antarctique de l'Est (ci-après « EAIS », pour « East Antarctic Ice Sheet ») ou l'Antarctique de l'Ouest (ci-après « WAIS », pour « West Antarctic Ice Sheet »). Cuffey et al. (2016) ont montré que la différence de température de surface entre le dernier maximum glaciaire (il y a 20 à 23 000 ans) et le début de l'Holocène (de 12 000 à 10 000 ans) est estimée de 11,3 ± 1,8 °C pour la WAIS, alors qu'elle est estimée entre 7 et 9,3 °C pour l'EAIS.

Par rapport à ces variations glaciaires-interglaciaires, l'amplitude des variations climatiques récentes en Antarctique est modeste. Nicolas and Bromwich (2014) mentionnent une tendance inter-annnuelle de 0,11 ± 0,08 °C sur la période 1979-2009. Les quatre dernières décennies sont toutefois clairement marquées par des tendances régionales significatives (cf Fig. 1.6): (i) l'Antarctique de l'Ouest et la péninsule montrent une hausse significative des températures de surface (Steig et al., 2009), tandis que l'Antarctique de l'Est est caractérisée soit par une absence de tendance significative soit par une tendance non significative au refroidissement (Chapman and Walsh, 2007), (ii) l'extension de la glace de la mer de Amundsen-Bellinghausen diminue, alors que (iii) l'extension de la glace de la mer de Ross augmente (Hobbs et al., 2016). Une variabilité décennale d'été est observée pour la température de la surface de mer, le vent zonal, et l'extension de la glace de mer (Fan et al., 2014). Ces variations récentes sont explorées pour

identifier la part qui relève de la variabilité spontanée du climat austral, et la part qui peut être liée à l'influence humaine sur le climat, via la destruction de l'ozone stratosphérique, et la hausse des gaz à effet de serre. Le trou dans la couche d'ozone détecté en 1985 a causé un refroidissement de la stratosphère en hiver austral, induisant une intensification du vortex polaire stratosphérique à cette même période (Arblaster and Meehl, 2006; Thompson et al., 2011). En été et en automne, cette activité cyclonique de haute altitude se propage dans la couche limite de la troposphère, augmentant l'activité cyclonique au sud de 40 °S (Simmonds et al., 2003), et donc l'indice du SAM (Marshall, 2003). Une conséquence directe est une intensification des vents d'ouest (Marshall, 2002), et de la circulation antarctique circumpolaire. Les études de modélisation du climat montrent que l'augmentation des rejets de gaz à effet de serre devraient entraîner un réchauffement à la surface de la région antarctique, augmentant la température de surface de ces régions, et amplifiant les conséquences susmentionnées par le trou dans la couche d'ozone (Shindell and Schmidt, 2004). Le lien entre la perte d'ozone stratosphérique et l'augmentation des températures de surface de l'Antarctique de l'Ouest et de la péninsule apparaît comme clairement établi, tandis que les causes de la diminution de l'extension de la glace de la mer de Amundsen-Bellinghausen restent débattues (e.g. Bromwich et al., 2013; Sigmond and Fyfe, 2014).

La compréhension de la variabilté récente du climat de l'Antarctique est limitée par la somme des données disponibles, et par la fiabilité des modèles de climat utilisés pour comprendre les mécanismes à l'oeuvre. Afin d'obternir une meilleure couverture spatiale, il est fondamental (i) d'obtenir davantage de mesures in-situ : il n'existe que deux longues séries de mesure de température de surface sur le plateau Antarctique (Chapman and Walsh, 2007), et seulement 15 séries sur l'ensemble de l'Antarctique (Nicolas and Bromwich, 2014), (ii) de résoudre les incertitudes liées aux mesures satellitaires dues aux interférences avec les nuages, et à la résolution verticale proche de la surface (~20 m) (Xie and Arkin, 1997; Eisenman et al., 2014; Palm et al., 2017), et d'améliorer la résolution spatiale des informations issues de la télédétection.

Ma thèse s'inscrit dans ce contexte, et vise à évaluer la qualité de l'information climatique récente qui peut être extraite de carottes de névé (carottes courtes d'environ 20 m de profondeur), forées en Terre Adélie.

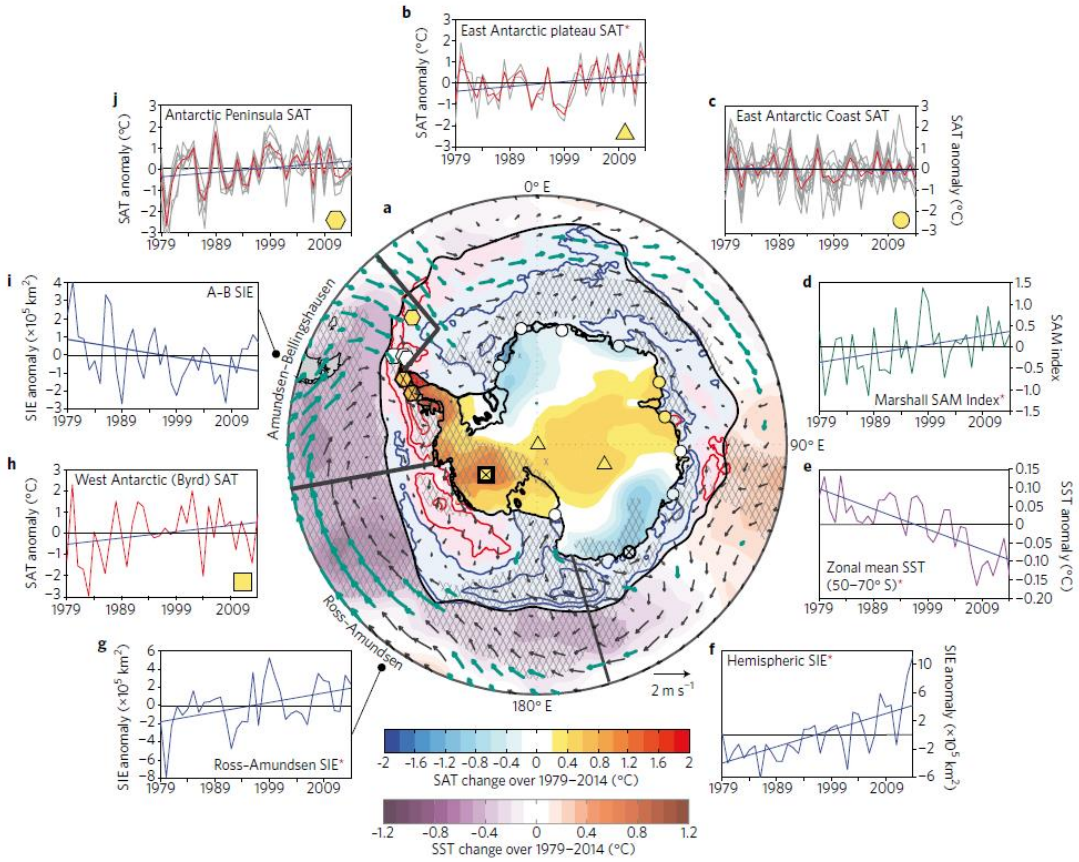

Figure 1.6: Tendances observées en Antarctique sur la période 1979-2014 pour la température de surface atmosphérique (balayage de couleurs bleu-rouge) et océanique (balayage de couleurs violet-rouge), de la concentration de la banquise (contour à 10 % de la concentration, en bleu pour des tendances négatives et en rouge pour des tendances positives) et champs de vents à 10 m (vecteurs). Les hachures représentent les tendances significatives à 95 % en appliquant un test de Student. Les graphiques (a-j) représentent les séries temporelles des températures de surface de la mer (« SST » en °C), atmosphérique (« SAT », en °C), de l'extension de la banquise (« SIE », en 105 km2) des différentes régions d'Antarctique, et de l'index du SAM. Les droites horizontales correspondent à la moyenne de la série tandis que les droites obliquent montrent les tendances. Figure extraite de Jones et al. (2016).

1.2 La Terre Adélie, une terre à explorer

1.2.1 Une terre exploitée par la France

Un peu plus d'un siècle après la découverte de la Terre Adélie (définie par le couloir longitudinal 142 °E -146 °E, cf. Fig. 1.2) par Jules Dumont d'Urville en 1840, des expéditions polaires françaises furent initiées par Paul Emile Victor, qui revendica la Terre Adélie comme région d'exploration française. Une première station fut créée en 1949 à Port-Martin, mais elle prit feu en 1952. En 1957, Année Géophysique Internationale (ci-après AGI), alors que le Conseil International des Unions Scientifiques lançait une série d'activités scientifiques visant à améliorer notre connaissance des géosciences, trente stations météorologiques furent crées en Antarctique, dont deux sont encore en fonctionnement en Terre Adélie : la station côtière de Dumont d'Urville (ci-après DDU) sur l'île des Pétrels, remplaçant dès lors celle de Port-Martin, et la station de Concordia sur le Plateau. Il est à noter que seules quatre stations sur le plateau Antarctique sont opérationelles : Pôle Sud, qui est une station américaine, Concordia, qui est une base franco-italienne, Dôme Fuji, qui est une base japonaise, et enfin Vostok qui est une

base russe. Depuis l'AGI, et jusqu'aujourd'hui, c'est sur cette région de la Terre Adélie que les recherches scientifiques françaises se concentrent, grâce à l'appui logistique apporté par l'Institut Polaire Paul Emile Victor.

1.2.2 Un climat très particulier

La Terre Adélie se distingue du reste de l'Antarctique principalement par quatre particularités : (1) l'existence de forts vents catabatiques, avec des records de vent mesurés à 90 $m.s^{-1}$, soit 324 $km.h^{-1}$ (Loewe, 1972) ; (2) une glace de mer d'hiver, constituée d'une banquise s'étendant jusqu'à 300 km en hiver (Massom and Stammerjohn, 2010), et de polynies au large de la côte (Adolphs and Wendler, 1995; Tamura et al., 2008) ; (3) sa proximité avec le rail des dépressions (Bromwich et al., 2011); (4) enfin, il s'agit de la seconde source de formation des eaux profondes antarctiques (Rintoul, 1998; Martin, 2016). La station météorologique de DDU située sur l'île des Pétrels, à 1 km de la côte continentale, a permis des mesures météorologiques tri-horaires, donnant ainsi accès à des informations sur les variations de la température de surface, de l'humidité, de l'intensité et de la direction des vents, en continu depuis janvier 1957 (à l'exception d'une brève période d'interruption s'étendant de mars 1959 à janvier 1961). Pettré and Périard (1996), puis König-Langlo et al. (1998) en ont fait une analyse climatologique sur les périodes 1957-1989 et 1991-1995, respectivement. Leurs résultats sont cohérents, et s'accordent aussi avec les moyennes que j'ai calculées sur l'ensemble des mesures disponibles (sur la période 1957-2014). Je rapporte donc mes résultats pour les caractéristiques

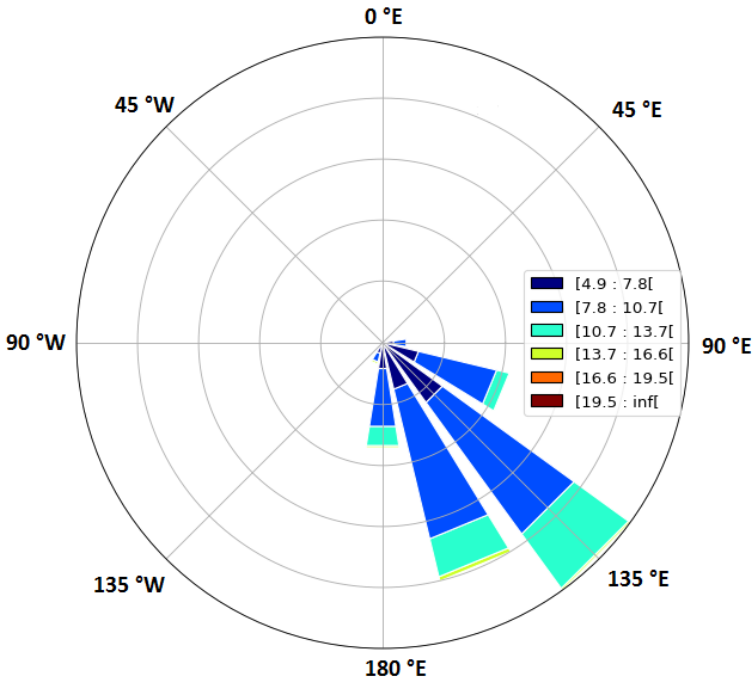

Figure 1.7: Rose des vents de surface mesurés à Dumont d'Urville toutes les trois heures de 1957 à 2017 à partir des données mensuelles archivées par Météo France. Les vitesses sont données en m s^{-1}.

climatologiques de DDU. La température de surface moyenne est de – 10,9 ± 6,0 °C, ce qui est cohérent avec la position côtière de cette station (Comiso, 2000). Comme König-Langlo et al. (1998), je trouve des vents moyens de 9,5 ± 2,1 $m.s^{-1}$, mais d'une large amplitude des valeurs tri-horaires définie par un intervalle allant de 4,9 à 19,5 $m.s^{-1}$, i.e. avec des périodes quasi sans vent, comme des périodes avec de forts vents catabatiques. König-Langlo et al. (1998) trouvent que les vents les plus fréquents viennent de 140 °E, moyenne cohérente 145,3 ± 22,4 °E avec celle que j'ai pu calculer sur la période 1957-2017. La direction des vents est relativement stable, variant de 90 à 220 °E, et qu'elle reste centrée autour de 135 °E (cf. Fig. 1.7). Enfin, l'humidité relative de 61,4 ± 7,6 % est relativement basse comparée à celle d'autres régions côtières : König-Langlo et al. (1998) rapportent des valeurs supérieures à 80 % pour les stations de Neumayer et Halley, explicable du fait que Dumont d'Urville est une île, conséquemment moins sujette aux vents catabatiques comparées aux stations de Neumayer et Halley (Barral, 2014; Vincent Favier, communication personnelle, 06/2018). Le climat côtier, relativement tempéré (comparé à celui du plateau) permet le développement d'un écosystème marin constitué de krills (Amakasu et al., 2011) et de manchots (Cherel et al., 2011). Deux espèces de manchots cohabitent, les manchots empereurs (*Aptenodytes forsteri*) et les manchots Adélie (*Pygoscelis adeliae*, cf. Fig. 1.8), avec des saisons de reproduction différentes (en hiver pour les manchots empereurs, en été pour les manchots Adélie; Cherel, 2008). Le taux de reproduction des manchots Adélie est d'autant plus important que le temps pour atteindre l'extension maximale est lente, que de la distance à l'océan libre le plus proche est courte (Par exemple, les années 1993, 1998 et 1999; Massom et al., 2009).

1.2.3 Les recherches scientifiques

(i) Etudes continentales

Les premières études scientifiques menées en Terre Adélie ont été initiées dans l'objectif de comprendre son climat si particulier (cf. Section 1.2.1), notamment son régime de vents (Ball, 1956, 1957), avec des événements de fortes intensités, qui avaient tant surpris Sir Douglas Mawson lors de son expédition en Terres Australes au cours des années 1912-1913 (Mawson, 1915). Ses observations avaient été confirmées par des mesures à 19,3 $m.s^{-1}$ à

Figure 1.8: Photo de manchots Adélie prise par Camille Bréant lors au cours de la campagne d'été 2016-2017 à au large de Dumont d'Urville.

Cap Denison, station côtière à ~ 90 km de DDU, l'amenant à décrire la Terre Adélie comme « Terre du Blizzard ». Au cours du siècle dernier et encore aujourd'hui, les régimes des vents font toujours l'objet de nombreux travaux de recherche (e.g. Wendler et al., 1997), notamment vis-à-vis des processus de transport de la neige de surface par le vent (Scarchilli et al., 2010; Gallée et al., 2013; Barral et al., 2014; Grazioli et al., 2017), rendant les mesures de précipitations difficiles (Grazioli et al., 2017).

Les recherches en sciences du climat menées en Terre Adélie se sont élargies à la compréhension de la variabilité spatio-temporelle du climat et du bilan de masse régionaux. Par exemple, l'installation de balises (piquets de polycarbonate plantés dans la neige), et l'utilisation de modèles de circulation générale du climat permettent l'étude de la variabilité spatiale du bilan de masse de surface (Favier et al., 2011; Agosta et al., 2012), ainsi que l'écoulement de la glace, grâce à l'extraction de carottes de glace et l'exploitation de la modélisation glaciologique (Lorius, 1967; Lorius et al., 1968; Raynaud et al., 1979; Young et al., 1984). Quelques carottes de glace ont été forées dans les années 1980 pour caractériser la variabilité climatique passée (jusqu'à une partie de la dernière période glaciaire), mais l'absence de datation précise en a limité l'exploitation en terme de variabilité climatique (Lorius et al., 1984; Yao et al., 1990).

Les mesures effectuées en continu depuis 1957 à la station météorologique de DDU ont permis de donner une climatologie des grandeurs météorologiques principales (température, vent, pression, humidité) représentative du climat local des dernières décennies (Kodama et al., 1989; Pettré and André, 1991; Pettré and Périard, 1996; König-Langlo et al., 1998). Par ailleurs, l'observatoire de DDU a été étendu au suivi de la composition atmosphérique, grâce à des mesures de composition chimique d'aérosols réalisées à l'échelle journalière en continu depuis 1991 (Jourdain, 2001; Jourdain and Legrand, 2002; Preunkert et al., 2008; Legrand et al., 2009; Legrand et al., 2016). La richesse de ces enregistrements a permis de caractériser les sources et les variabilités annuelles et saisonnières des sels de mer (e.g. du sodium, et du sulfate; Wagenbach et al., 1998), des aérosols biogéniques issus de l'oxyation du Dymethyl sulfoniopropionate émis par les phytoplanctons (du sulfate et de l'acide méthanesulfonique; Minikin et al., 1998), et d'espèces issues des sols ornithogéniques (Legrand et al., 1998). Ces résultats atmosphériques bien établis permettent d'utiliser les concentrations chimiques mesurées le long des carottes de glace afin d'en établir une datation en identifiant les pics annuels, observés pour chaque espèce, en été à Dumont d'Urville (cf. Chapitre 4, *Carottes côtières de la Terre Adélie*) [3].

[3] D'autres instruments ont été installés à DDU pour la mesure de concentrations d'espèces chimiques le long de profils verticaux de l'atmosphère, par exemple l'ozone.

(ii) Etudes océaniques et écologiques

Très tôt, l'extraction et l'analyse des diatomées dans les carottes sédimentaires ont été développées (Manguin, 1957) afin d'étudier l'évolution des composantes océaniques (e.g. la température océanique, la glace de mer) et les mécanismes associés[4]. La carotte MDO3-2601 a permis de reconstituer l'évolution de l'épaisseur des couches sédimentaires et des types d'assemblage des diatomés à l'échelle saisonnière au cours de l'Holocène. Une haute variabilité inter-annuelle indique une importante interaction entre la glace de mer, le ruissellement côtier continental et les courants océaniques au large de la Terre Adélie (Denis et al., 2006). L'information saisonnière de tels enregistrements permet aussi d'étudier les changements de saisonnalité de la glace de mer au cours de la période interglaciaire actuelle, avec une résolution typiquement de plusieurs centaines d'années (Crosta et al., 2008).

Les écosystèmes locaux font l'objet de suivis par des observations systématiques, notamment les populations de manchots (Wienecke et al., 2000; Cherel, 2008; Cherel et al., 2011), l'évolution de leur démographie en lien avec le climat local (Massom et al., 2009), et leur adaptation au changement climatique (Barbraud and Weimerskirch, 2006). Dans le cadre de l'étude de la variabilité climatique, le succès reproductif est une information intéressante puisqu'il dépend (1) de la saisonnalité et de l'extension de la glace de mer (Raymond et al., 2015) : les réseaux trophiques au sud de l'océan austral seraient plus approprié aux manchots, et une contraction de la glace de mer donne un accès direct à la mer pour les prédateurs; (2) de la température (Southwell et al., 2015) : une augmentation de la température peut augmenter le stress thermorégulateur des poussins, diminuant leur chance de survie, et entraine de la fonte de la glace, cause de noyade des nids. Ainsi, Southwell et al. (2015) ont observé une augmentation de la population des manchots Adélie (*Pygoscelis adeliae*, cf. Section 1.2.2) depuis les années 60, avec un doublement de la population depuis les années 1980, en accords avec une diminution de la banquise de glace de 0,3 à 0,5 % decade^{-1} et une augmentation de la durée d'extension de 20 à 30 jours decade^{-1}. A l'opposé, une diminution de la population des manchots empereurs (*Aptenodytes Forsteri*) avait été observée dans les années 70, initialement associée aux variations climatiques, et entre autres, un minimum de contraction de la banquise de glace. Or, il s'avère que cette diminution soit en réalité une conséquence d'un baguage massif des manchots les années précédentes, entraînant une gêne hydrodynamique des

[4] La compréhension et l'évolution de la formation des eaux profondes se formant face à la Terre Adélie font l'objet de nombreuses recherches et de suivis réguliers.

manchots au cours de leurs déplacements en mer (Cristofari et al., 2016). Les couveurs ayant échoués dans leur reproduction ont alors rejoint la colonie de Mertz (un peu plus à l'ouest).

L'ensemble des résultats de ces recherches contribuent à caractériser le climat de la Terre Adélie et sa variabilité, et forment un cadre très large dans lequel s'inscrit l'analyse des enregistrements de composition isotopique issus de carottes de glace effectuée pendant ma thèse.

1.3 L'analyse des carottes de glace

1.3.1 Les forages profonds

Théorie de Milankovitch : Cette théorie explique l'alternance de cycles glaciaires-interglaciaires, par des calculs de l'ensoleillement incident modulé par trois paramètres orbitaux (Berger, 1988)[5] : l'excentricité de l'orbite terrestre, qui fluctue avec des périodicités de l'ordre de 100 et 400 000 ans, l'inclinaison de l'axe de rotation de la Terre (ou obliquité), dont la périodicité approximative est de 41 000 ans, et la précession présentant une double périodicité à 19 000 et 23 000 ans.

Les recherches scientifiques en Antarctique initiées lors de l'AGI en 1957-1958 ont pris un essor avec le début de l'analyse des carottes de glace (Lorius et al., 1969). Ces archives ont le potentiel de témoigner des climats passés lointains. Les carottes recouvrant les plus longues périodes ont été forées à la station Vostok, reconstituant 420 000 ans (Petit et al., 1999), au Dôme F reconstituant 700 000 ans (Kawamura et al., 2017), et à Dôme C, dans le cadre du projet EPICA (« European Project for Ice Core in Antarctica », Jouzel et al., 2007), remontant 800 000 ans de l'histoire du climat Antarctique. Leur analyse ont permis de reconstituer la température de surface de l'Antarctique grâce au thermomètre isotopique (cf. Section 1.4.1), ainsi que les concentrations en gaz à effet de serre (dioxyde de carbone et méthane) contenus dans les clathrates de la glace (Lüthi et al., 2008). Ces enregistrements montrent qu'au cours des derniers 800 000 ans, la Terre a expérimenté des cycles glaciaires d'une durée moyenne de 100 000 ans, interrompus de courtes phases interglaciaires (10 000 – 30 000 ans), qui s'expliquent par la réponse du système climatique aux variations de répartition de l'ensoleillement, pilotées par les paramètres astronomiques de Milankovich* (Berger, 1988). Ce forçage astronomique étant calculé avec précision sur cette période, l'étude des variations glaciaires-interglaciaires permet de caractériser les rétroactions climatiques à l'œuvre (qui intègrent le couplage entre climat et cycle du carbone), et de caractériser la variabilité naturelle

[5] Astronome belge ayant apporté, avec l'astronome français Jacques Laskar, une contribution majeure à ces calculs.

du climat. Ces longues séries de données permettent de mettre en perspective les évolutions récentes et ainsi de caractériser la perturbation anthropique de la composition de l'atmosphère planétaire (Etheridge et al., 1998).

1.3.2 Carottes de névé

Des efforts importants pour obtenir des carottages de névé ont été mis en place dans les années 1990 en Antarctique (e.g. Isaksson and Karlén, 1994), motivés par le contexte du changement climatique, pour caractériser la variabilité spatio-temporelle du climat et du bilan de masse de surface de l'Antarctique au cours des dernières décennies (Abram et al., 2013; cf. Section 1.1.1), complétant ainsi les informations parcellaires issues des enregisterments instrumentaux (cf. Sections 1.2.1 et 1.2.3) et les informations de long terme issus de forages profonds. Ainsi, le programme internationnal ITASE[6] (International Trans-Antarctic Scientific Expedition, https://www2.umaine.edu/itase/content/Science/overview.html, 06/2018) a été mis en place avec pour objectif principal de caractériser la variabilité spatio-temporelle du climat de l'Antarctique (accumulation, température et circulation atmosphérique) sur les deux cent dernières années (Mayewski and Goodwin, 1997). Par rapport aux forages profonds, ces carottes courtes requièrent une logistique plus légère, de sorte que plusieurs carottes peuvent être extaites localement, permettant ainsi d'extraire un signal régional et d'étudier le rapport signal sur bruit (Schlosser et al., 2014; Altnau et al., 2015). Enfin, étudier le signal enregistré dans des carottes de névé est un moyen efficace d'explorer le potentiel des enregistrements climatiques de certains sites pour y poursuivre des forages profonds (Fernandoy et al., 2012; Caiazzo et al., 2016).

Dans les régions côtières où l'accumulation est la plus élevée (75 % de l'accumulation totale; Agosta, 2012), l'extraction d'un signal issu de carottes de glace peut être obtenue à l'échelle saisonnière (e.g. Isaksson and Karlén, 1994; Kreutz et al., 1999; Delmotte et al., 2000; Inoue et al., 2017), permettant ainsi l'exploitation des mécanismes responsables de la variabilité climatique saisonnière (e.g. Fernandoy et al., 2018).

1.3.3. Zoom sur les carottes de névé côtières de l'Antarctique de l'Est

La majorité des carottes de névé côtières forées en Antarctique de l'Est proviennent de la Terre de la Reine-Maud (cf. Fig. 1.2). C'est dans cette région que les premières extractions de carottes de névé ont été effectuées (Isaksson and Karlén, 1994), et se sont continuellement poursuivies

[6] Cette collaboration regroupait initialement 12 pays (Angleterre, Australie, Canada, Chine, Etats-Unis, France, Italie, Allemagne, Japon, Russie, Suède, et Suisse) puis s'est amplifiée, rejoints par l'Argentine, la Belgique, Brésil, le Chili, la Corée du Sud, la Hollande, l'Inde, la Norvège, et la Nouvelle-Zélande.

Les isotopes stables de l'eau : définition

Les atomes sont caractérisés par leur nombre de protons, et définis par le numéro atomique Z, et de neutrons contenus dans leur noyau. La somme du nombre de protons et de neutrons est indiqué par le nombre de masse A. A l'état naturel, un atome existe sous différentes formes se distinguant par leur nombre de neutrons et donc leur masse A, et appelés isotopes.

La molécule d'eau est thermodynamiquement stable sous la forme $^{1}H_2{}^{16}O$, composée des isotopes d'hydrogène et d'oxygène majoritaires ^{1}H et ^{18}O. Néanmoins, se trouve sur Terre aussi sous des formes isotopiques métastables plus lourdes, composée des isotopes de l'hydrogène et de l'oxygène, ^{2}H (ou D, appelé deutérium) , ^{18}O et ^{17}O (cf. Tableau 1.2) : $^{1}HD^{16}O$, $^{1}H_2{}^{18}O$, et $^{1}H_2{}^{17}O$.

Tableau 1.2: Caractéristiques des isotopes d'hydrogène et d'oxygène ; numéro atomique Z, masse atomique A, abondance (en %) et symbole. Adapté de Agency (2008).

Elément	Z	A	Abondance (%)	Symbole
Hydrogène	1	1	99,985	^{1}H
	1	2	0,0155	^{2}H, D
Oxygène	16	8	99,759	^{16}O
	17	9	0,037	^{17}O
	18	10	0,204	^{18}O

Pour reconstituer le climat, on compare principalement l'abondance de ^{2}H (ou D) par rapport à ^{1}H, et celle de ^{18}O par rapport à ^{16}O, en calculant leur ratio. Pour des raisons pratiques, on calcule ensuite leur déviation par rapport à une valeur standart, notée $\delta^{18}O$ et δD et définie par Craig and Gordon (1965) selon :

$$\delta\ (‰) = \left(\frac{R_{échantillon}}{R_{standard}} - 1\right) \times 1000 \text{ avec } R = \frac{[X_i]}{[X]} \quad (1)$$

$[X_i]$ étant la concentration de l'isotope lourd et [X] celle de l'isotope le plus abondant. Les valeurs des standards, commune à la communauté scientifique internationale et connues sous la dénomination V-SMOW (Vienna - Standart Mean Ocean Water), ont été définies par l'International Atomic Energy Agency (IAEA) (Gonfiantini, 1978) :

$R_{VSMOW}(D) = (155{,}75 \pm 0{,}05) \times 10^{-6}$ (Wit et al., 1980) (2)

$R_{VSMOW}(^{18}O) = (2005{,}20 \pm 0{,}45) \times 10^{-6}$ (Baertschi, 1976) (3)

Fractionnements isotopiques

Au cours de certains processus physiques ou chimiques, du fait de leur nombre de masse différent, les isotopes se répartissent dans des quantités différentes au cours de la réaction convertissant les réactifs en produits. C'est ce qu'on appelle le fractionnement isotopique. On distingue deux types de fractionnement : le fractionnement à l'équilibre, et le fractionnement cinétique.

(i) Le fractionnement à l'équilibre

Le fractionnement à l'équilibre (thermodynamique) dépend des grandeurs physiques déterminant l'état thermodynamique du système. Il a lieu notamment lors du changement de phase vapeur-liquide. Ce changement d'état dépend de la pression de vapeur saturante, fonction de la masse, et donc diffère d'un isotope à un autre.

Dans le contexte de l'histoire d'une masse d'air, il est modélisé par la distillation de Rayleigh (Dansgaard, 1953), régi par la loi :

$$R = R_0 \times f^{\alpha_{eq}-1} \quad (4)$$

Avec R_0 le rapport isotopique initial avant le changement de phase, f la quantité de vapeur résiduelle, α_{eq} le coefficient de fractionnement liquide/vapeur dépendant de la température (voir Majoube, 1971 pour leur définition; et Cappa et al., 2003 pour une mise à jour), et R le rapport isotopique final.

Les isotopes lourds condensent préférentiellement aux isotopes légers ($\alpha_{eq}>1$), et d'autant plus que la température est faible. Le paramètre f est quant à lui défni par la loi de Clausius Clapeyron, pour laquelle la quantité d'eau condensée augmente lorsque la température atmosphérique diminue. Ainsi, plus les températures diminuent, plus le fractionnement est important. On dit aussi que la masse d'air s'appauvrit en isotopes lourds sous l'effet de sa baisse de température, subissant ainsi une distillation isotopique.

(ii) Le fractionnement cinétique

Le fractionnement isotopique réfère aux réactions mettant en jeu les isotopes de l'eau dans un milieu saturé, i.e. que les isotopes de la phase liquide (solide) sont à l'équilibre avec la phase gaz. Au cours de l'histoire d'une masse d'air, le premier phénomène impliqué est l'effet cinétique isotopique, selon lequel un isotopologue plus lourd a des fréquences vibrationnelles moindres, et donc une diminution de l'énergie du point zéro. L'énergie d'activation à apporter pour initier la réaction est donc supérieure, et la vitesse de la réaction plus lente. Le second phénomène pris en compte dans la quantification du fractionnement isotopique est la diffusion des molécules en phase, la vitesse de diffusion augmentant avec la masse des isotopologues. Les deux phénomènes agissant dans le même sens au regard de la masse, il s'en suit qu'un tel

fractionnement résulte en l'appauvrissement en isopotes lourds et l'enrichissement en isotopes légers.

Au cours du cycle de l'eau, ce fractionnement cinétique a lieu lors de l'évaporation, de la condensation solide formant des cristaux de glace, et de la sublimation. Dans les deux cas, ce fractionnement se superpose à un fractionnement à l'équilibre. Dans le cas de l'évaporation, il dépend de la température de surface de l'océan, l'humidité relative à la surface et la vitesse du vent (cf. Craig and Gordon, 1965; Brutsaert, 1975 pour l'établissement d'équations empiriques). Les cristaux de glace se forment au sein des nuages, à ~ -15 °C dans un milieu en susaturation. La nucléation autour du noyau de condensation est trop rapide pour permettre l'équilibre entre les molécules d'eau en phase gaz et celles solides dans les cristaux de glace en formation, pour lesquelles la vitesse de diffusion est bien plus faible. Le fractionnement cinétique dépend donc non seulement d'une fonction de sursaturation correspondant au rapport des pressions de vapeur saturante dans le nuage par rapport à celle à la surface du cristal, ainsi que des rapports de coefficients de diffusion entre l'isotopologue lourd considéré ($HD^{18}O$ ou $H_2{}^{17}O$) par celui le plus stable ($H_2{}^{18}O$) (Merlivat, 1978; Jouzel and Merlivat, 1984).

L'histoire d'une masse d'air

Au cours de l'histoire d'une masse d'air, les molécules d'eau qu'elle contient sont sujets aux deux types de fractionnements. Une masse d'air se charge de la vapeur d'eau évaporée au-dessus des océans (cf. Fig. 1.9), induisant un fractionnement cinétique. Lors de ce processus, la masse d'air s'appauvrit une première fois en isotopes lourds (δD et $\delta^{18}O$ diminuent). Puis, au cours de sa trajectoire des moyennes vers les hautes latitudes, la masse d'eau condense. A chaque condensation liquide s'opére un fractionnement à l'équilibre, tandis qu'à des températures inférieures à -15 °C, des cristaux de glace sont formés par condensation solide au sein des nuages, alors accompagnés d'un fractionnement cinétique. Les cristaux de glace (précipitations solides) ou les précipitations liquides qui tombent à la surface entrainent un appauvrissement en isotopes lourds de la masse d'air résiduelle, alors que ces précipitations (solides ou liquides) s'enrichissent en isotopes lourds. Elles peuvent du fait des vents, sublimer au cours de leur chute, s'appauvrissant en isotopes lourds.

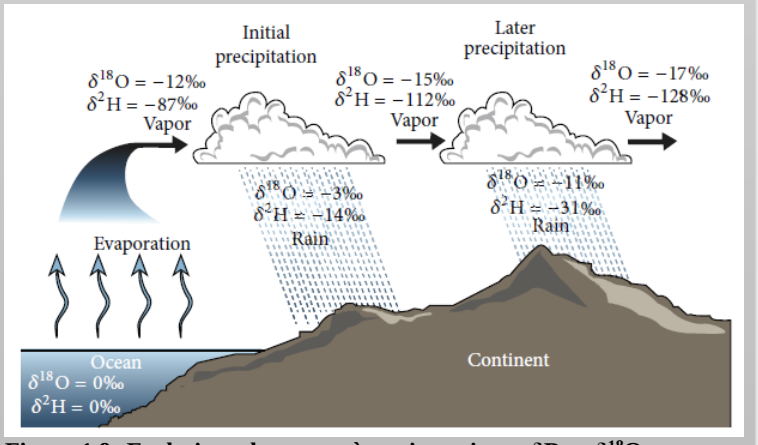

Figure 1.9: Evolutions des paramètres isotopiques δD et $\delta^{18}O$ au cours de l'histoire d'une masse d'air (Figure adaptée de Xi, 2014).

(Isaksson et al., 1996; Oerter et al., 2000; Graf et al., 2002; Karlöf et al., 2005; Schlosser et al., 2014). Récemment, Altnau et al. (2015) a rapporté l'analyse de 40 carottes de névé côtières, permettant l'extraction d'un signal climatique régional. Et c'est sans compter des forages plus récents (Vega et al., 2016). En moins grand nombre, quelques carottes de névé ont été forées sur la Terre des Wilkes, du Glacier de Lambert vers 90 °E (Cunde et al., 2001; Junying et al., 2002) jusqu'à sa frontière avec la Terre de Victoria (Caiazzo et al., 2016). Sur cette dernière région, ce ne sont que quelques carottes de névé qui ont été forées (Stenni et al., 1999; Stenni et al., 2000). Enfin, en Terre Adélie, seules des carottes d'environ 100 m ont été forées (Lorius, 1967; Lorius et al., 1968; Lorius et al., 1984; Yao et al., 1990), exploitées pour étudier l'écoulement dynamique de cette région côtière, et identifiées comme couvrant une partie de la dernière période glaciaire. Aucune carotte de névé récente forée en Terre Adélie n'a été analysée avant ma thèse.

1.4 Les isotopes stables de l'eau

Dans la partie précédente, j'ai souligné l'intérêt de l'utilisation des carottes de glace pour la reconstruction des climats passés de l'Antarctique. Au cours de ma thèse, je me suis particulièrement intéressée aux enregistrements des isotopes de l'eau. Pour faciliter la lecture de la suite du manuscrit, j'explique brièvement dans cette section la théorie des isotopes de l'eau, la limite de nos connaissances et de leur utilisation.

1.4.1 Le thermomètre isotopique remis en question

La relation isotope – température

La relation empirique qui lie la température de surface aux paramètres isotopiques du premier ordre (δD, $\delta^{18}O$) a été établie par Lorius and Merlivat (1975) à la suite de mesures effectuées sur de la neige fraîche le long d'un transect entre DDU et Dôme C en Terre Adélie. En effectuant une régression linéaire entre les températures de surface et les mesures de δD, ils ont obtenu une pente de 6,04 ‰ $°C^{-1}$. Appliquée sur des mesures effectuées sur l'ensemble de l'Antarctique, non seulement dans de la neige mais aussi dans des précipitations et des carottes de glace, Masson-Delmotte et al. (2008) ont obtenu une pente de 6,34 ± 0,09 ‰ $°C^{-1}$ (r^2=0,91, n=547) pour δD, et de 0,80 ± 0,01 ‰ $°C^{-1}$ pour $\delta^{18}O$ (r^2=0.92, n=745, cf. Fig. 1.10). Cette relation, utilisée pour les reconstructions de température à partir des analyses isotopiques effectuées le long des carottes de glace, est connue sous l'appellation de « thermomètre isotopique ».

Théoriquement, cette relation s'explique par la prédominance du fractionnement à l'équilibre lors de la dernière condensation de la masse d'air, en prenant en compte la particularité de la

relation linéaire qui lie la température de condensation (i.e. température d'inversation) à la température de surface en Antarctique (Phillpot and Zillman, 1970; Connolley, 1996). Les relations obtenues par Masson-Delmotte et al. (2008) reposent sur des mesures distribuées sur l'Antarctique, elles sont dites « spatiale ». Ce thermomètre isotopique est utilisé pour reconstruire les températures passées, mais repose sur un certain nombre d'hypothèses qui peuvent être matière à débats.

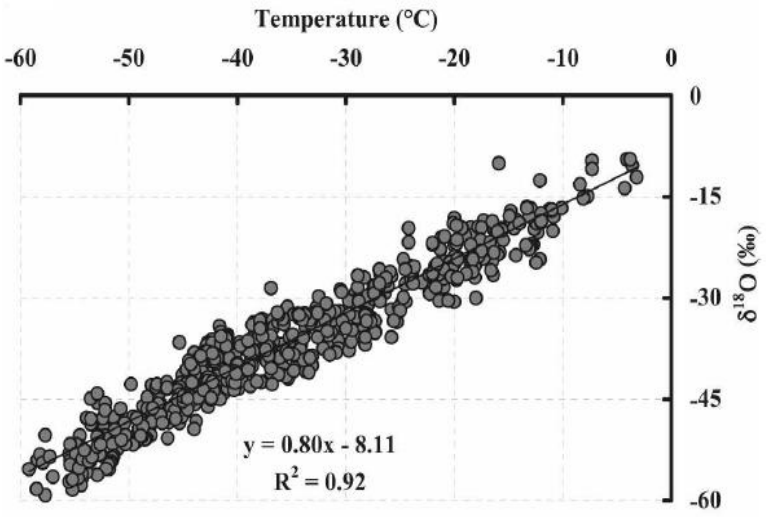

Figure 1.10: Relation linéaire entre les paramètres isotopiques du premier ordre (δD, $\delta^{18}O$) des eaux météoriques et la température de surface. Graphique extrait de Masson-Delmotte et al. (2008).

Limite du thermomètre isotopique

Utiliser le thermomètre isotopique, c'est faire l'hypothèse majeure que les variations de température de surface intervenant dans le fractionnement de la dernière condensation est la seule origine des variations de la composition isotopique des précipitations qui en sont issues, et donc que toutes les autres lois physiques régissant l'évolution des masses d'air au cours de leur existence sont invariables, et que le signal isotopique atmosphérique est préservé lors de son archivage dans la glace.

(i) La distribution dans le temps des précipitations

Le thermomètre isotopique repose tout d'abord sur l'hypothèse que les précipitations suivent une distribution statistique uniforme à l'échelle inter-annuelle. Or la circulation synoptique peut changer d'une année à l'autre (e.g. Masson-Delmotte et al., 2003), entraînant davantage d'intrusions marines d'air chaud et humide associées à de plus fortes précipitations certaines années, ou à l'inverse favorisant la prédominance de régimes de temps froids et secs, comme le montre Schlosser et al. (2016) pour les années 2009 et 2010 à Dôme C. Enfin, d'autres auteurs ont montré, en utilisant des modèles de circulation générale de l'atmosphère intégrant la

représentation des isotopes stables de l'eau (cf. Section 2.3), que différentes variations climatiques induisent un changement de l'intermittence des précipitations. Par exemple, Krinner and Werner (2003) ont montré qu'un tel changement au cours du dernier maximum glaciaire comparé à aujourd'hui, au Groenland, pourrait expliquer la différence entre la reconstruction de température obtenue pour cette période à partir des enregistrements isotopiques issus des carottes de glace, avec celle obtenue à partir des profils de température mesurés dans les trous de forage (Dahl-Jensen et al., 1998). Pour l'Antarctique, les simulations glaciaires suggèrent que le thermomètre isotopique spatial reste valide dans une gamme de conditions climatiques entre un état glaciaire et pré-industriel (Werner et al., in press). En revanche, pour des climats plus chauds, les simulations de Sime et al. (2008) en réponse à une augmentation future de la concentration atmosphérique en CO_2 ont montré que cela induit, en Antarctique, une pente isotope-température de moitié plus faible que le gradient spatial moderne. Enfin, Schmidt et al. (2007) ont effectué une simulation à partir d'un modèle couplé atmosphère-océan pour explorer la réponse climatique à la variabilité intrinsèque aux échelles inter-annuelles et décadales, mais aussi en utilisant des forçages orbitaux et concentrations en gaz à effet de serre différents afin de reproduire le climat du milieu de l'Holocène. Dans le premier cas, ils ont obtenu des pentes isotope-température plus de 60 % plus faibles que la pente spatiale. Dans le second cas, le modèle a montré des résultats contrastés entre les régions côtières (pentes négatives) et le centre de l'Antarctique, pour lequel les pentes sont proches de celles obtenues pour la variabilité intrinsèque.

(ii) Les variables climatiques à la source d'évaporation

A la formation d'une masse d'air (en considérant une unique source d'humidité), le fractionnement cinétique associé est invariant si la composition initiale, la température au-dessus des océans, l'humidité relative à leur surface, ainsi que les vents de surface le sont aussi. Or, on sait déjà que la température de surface de l'Océan austral a varié tant au cours de ces dernières décennies (cf. Fig. 1.6, Section 1.1.3) que pour des périodes plus lointaines (Dowsett et al., 1996). Certains auteurs ont donc appliqués une correction, afin d'enlever toute influence des variations de température de surface océanique (Stenni et al., 2001). Aussi, grâce à l'étude des carottes sédimentaires marines, il a été montré que sur de longs termes, la composition isotopique des océans a significativement varié au cours du temps (e.g. Lisiecki and Raymo, 2005). Ces estimations ont permis des corrections de la composition isotopique initiale à la source d'humidité pour une reconstruction à l'échelle glaciaire/interglaciaire sur le site de Vostok (Petit et al., 1999) et Dôme C (Jouzel et al., 2007).

(iii) Une unique et constante source d'évaporation

Les changements de la source d'évaporation des masses d'air précipitant à un même site sont un autre paramètre à prendre en compte pour l'interprétation du thermomètre isotopique. Peu étudiés il y a encore vingt ans, son étude a pris de l'essor avec le développement des outils de modélisation, notamment avec le traçage de la vapeur d'eau, de sa formation à sa condensation finale (Koster et al., 1992; Delaygue et al., 2000; Werner et al., 2001; Noone and Simmonds, 2002). Puis, depuis plus récemment, des outils de calculs de rétro-trajectoires ont permis d'identifier les régions sources des masses d'air (Draxler and Hess, 1998; Stein et al., 2015) et plus spécifiquement de repérer les régions sources pour le transport de vapeur d'eau (cf. Fig. 11; Sodemann and Stohl, 2009) arrivant en Antarctique. Ces calculs sont utilisés afin de mieux interpréter la composition isotopique mesurée dans des carottes de glace et des précipitations, permettant ainsi de les relier aux caractéristiques climatiques des régions d'évaporation océanique (e.g. Schlosser et al., 2008; Dittmann et al., 2016).

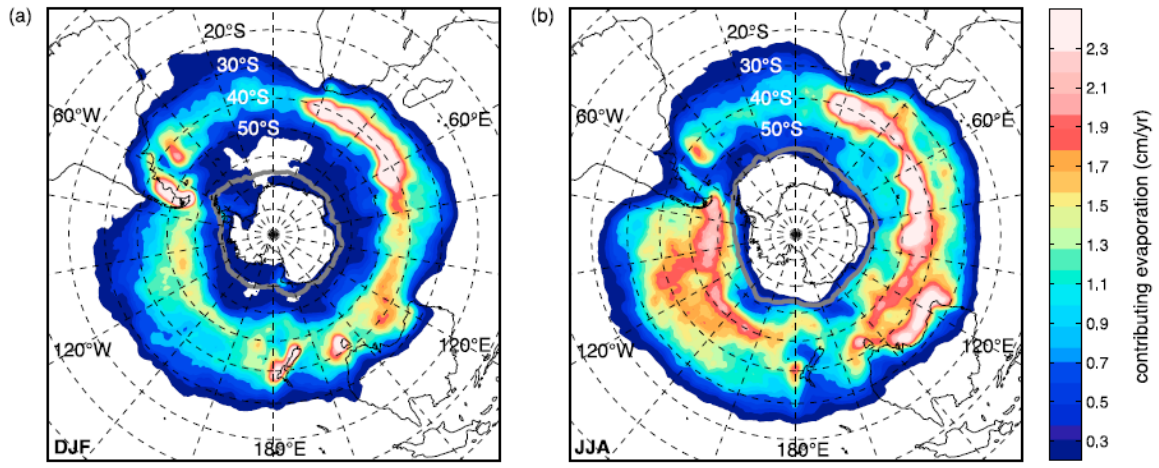

Figure 1.11: Sources d'humidité saisonnières moyennes pour l'Antarctique, diagnostiqué par le modèle lagrangien Flexpart sur la période allant d'octobre 1999 à avril 2005, pour (a) l'été (de décembre à février) et (b) l'hiver (de juin à août). La ligne grise indique la limite moyenne de l'extension saisonnière de la glace de mer. Extrait de Sodemann and Stohl (2009).

(iv) Altération du signal isotopique lors de sa déposition et son archivage dans la glace

Les mesures isotopiques effectuées le long des carottes de glace peuvent être affectées par des effets de dépôt de la neige, et de post-dépôt au sein du névé (cf. Annexe B). Lors de la déposition, de la sublimation initiant un fractionnement cinétique peut avoir lieu, puis les vents peuvent déplacer la neige récemment déposée (Bintanja, 1998). Enfin des échanges entre la vapeur et la neige de surface sont associés aux processus de métamorphisme de la neige (Casado et al., 2016; Ritter et al., 2016). Puis, des effets de post-dépôt peuvent avoir lieu au sein des premiers centimètres à décimètres en-dessous de la surface (Johnsen, 1977). Plusieurs modèles ont été construits pour décrire ces effets de post-dépôt, considérant la diffusion des isotopes de

l'eau dans les premiers mètres (Johnsen et al., 2000), mais aussi prenant en compte les échanges entre les bulles d'air emprisonnées dans le névé et la glace (Whillans and Grootes, 1985; Waddington et al., 2002; Neumann and Waddington, 2004; Jones et al., 2017). La théorie de Whillans and Grootes (1985) repose sur la diffusion du flux de vapeur entre les pores du névé, à l'origine d'un lissage du signal (amplitude du signal diminuée, e.g. Cuffey and Steig, 1998). Neumann and Waddington (2004) observent des échanges plus rapides en prenant en compte les effets de ventilation sur les processus de sublimation et de condensation entre les grains de neige et la vapeur contenue dans les pores du névé. Néanmoins, la validation de tels modèles, et notamment de leur paramétrisation, est limitée par le manque de données (mesures continues de compositions isotopiques dans les précipitations, la vapeur et la neige de surface sur plusieurs années). Une quantification réaliste et basée sur la compréhension des processus physiques des effets de position et de post-déposition reste à construire (Touzeau et al., 2017).

(v) Autres paramètres non discutés dans cette thèse

Tous les points discutés plus hauts affectent la relation isotope-température non seulement pour les périodes passées lointaines (à l'échelle des périodes glaciaire-interglaciaire) mais aussi pour les périodes passés récentes des dernières décennies. Certains paramètres cependant, sont exclusivement discutés pour les périodes passés lointaines, tel que la stabilité de la relation liant la température de condensation et température de surface (Jouzel and Merlivat, 1984), ou bien les changements de la topographie Antarctique (par exemple, Jouzel et al., 2007 a appliqué une correction de 0,9 °C tous les 100 m).

Définition du d-excess

Le deuterium excess (d-excess), paramètre isotopique du second ordre est défini par:

$$d = \delta D - 8 \times \delta^{18}O \quad (5)$$

Il correspond au résidu de la droite $\delta^{18}O$ vs δD des eaux météoriques (Dansgaard, 1964; Craig and Gordon, 1965), dont les compositions isotopiques ont été mesurées par Craig en 1961 pour des eaux échantillonnées sur l'ensemble de la planète. La pente de 8 ‰ $‰^{-1}$ obtenue en effectuant cette régression linéaire dérive des différences de fractionnement à l'équilibre, huit fois plus important pour le deuterium comparé

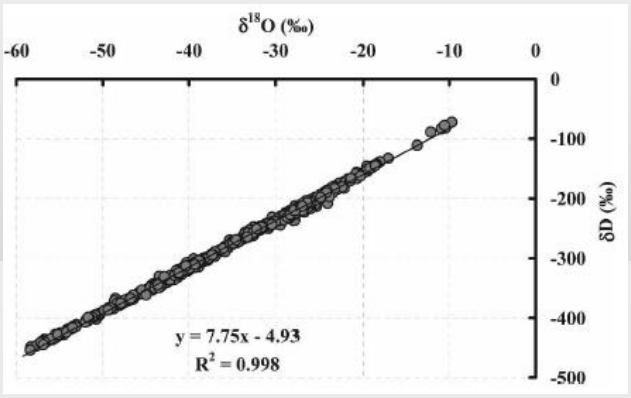

Figure 1.12: $\delta^{18}O$ vs δD des mesures isotopiques d'une base de donnée regroupant précipitations, neige fraîches, et carottes de de galce d'Antarctique (n=789). Extrait de Masson-Delmotte et al. (2008).

à l'oxygène. Elle dépend de la température, et varie donc selon les régions. Collectant des données isotopiques (issues de carottes de glace, neige fraîche et précipitations à 789 sites) pour l'ensemble de l'Antarctique, Masson-Delmotte et al. (2008) ont trouvé une pente de 7,75 ± 0,02 ‰ ‰$^{-1}$ (r^2=0,998 et n=789 , cf. Fig. 1.12). Le d-excess permet d'exclure l'influence du fractionnement à l'équilibre, et donc la dépendance de la composition isotopique à la température de surface, isolant les informations relatives au fractionnement cinétique, intervenant principalement lors de l'évaporation de la première vapeur au-dessus de l'océan.

Evolution au cours de l'histoire d'une masse d'air

La figure 1.13 illustre la variation théorique du d-excess au cours de l'histoire fictive d'une masse d'air, en représentant les valeurs de $\delta^{18}O$ versus δD au cours de son évolution. Avant que la masse d'air ne se forme, la composition isotopique dans l'océan décrit un point qui se situe sur la droite des eaux météoriques avec une pente de 8. La formation de la masse d'air par évaporation étant associée à un fractionnement cinétique fait dévier le point (2) le long d'une droite dont la pente est inférieure à 8 ‰ ‰$^{-1}$. La masse d'air s'appauvrit en isotopes lourds à chaque précipitation, déplaçant le point le long de cette même droite (3). Enfin, dans une gamme de température particulièrement basse (< ~ -15 °C), des cristaux de glace peuvent se former, initiant un nouveau fractionnement cinétique et déviant de nouveau le point sur une pente encore plus basse. Plus fort est le fractionnement cinétique, plus la pente sera faible. Finallement, la valeur du d-excess augmente tout au long de l'histoire de la masse d'air, et d'autant plus que le fractionnement cinétique est fort.

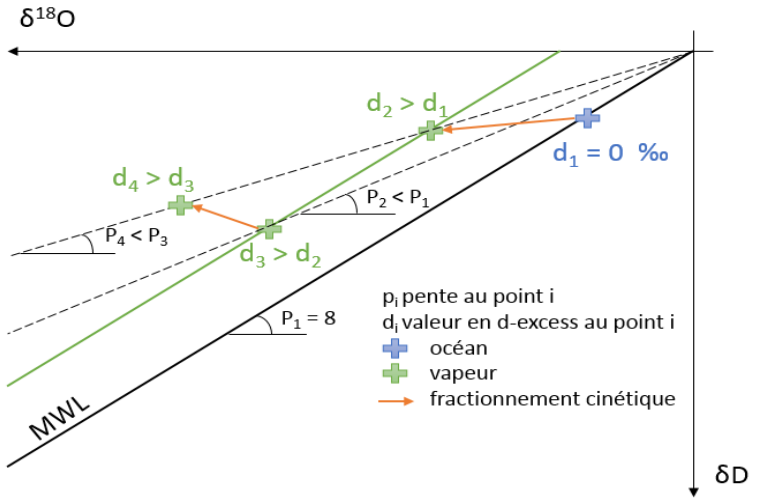

Figure 1.13: Variations qualitatives de la composition isotopique ($\delta^{18}O$, δD) au cours de l'histoire fictive d'une masse d'air, depuis l'océan (d_1), à son évaporation au-dessus de l'océan (d_2), à sa trajectoire durant laquelle une partie de sa masse se condense (d_3) ou se convertit en cristaux de glace (d_4).

1.4.2 Bref historique sur l'interprétation du d-excess

Le d-excess, paramètre isotopique de second ordre, a l'avantage comparé aux paramètres de premier ordre ($\delta^{18}O$, δD), d'être moins sensible au fractionnement à l'équilibre qu'au fractionnement cinétique. Ainsi, il permettrait non pas la reconstruction de la température de surface au lieu de prélèvement mais des paramètres à l'origine des masses d'air. Toutefois, une quantification des relations le liant avec ces paramètres reste délicate. Il fut initialement mesuré dans des carottes profondes forées sur le plateau de l'Antarctique afin de reconstituer les conditions d'évaporation (Craig and Gordon, 1965; Merlivat and Jouzel, 1979), et particulièrement la température surface de l'océan (Vimeux et al., 1999; Stenni et al., 2001; Vimeux et al., 2001) sur des échelles glaciaire-interglaciaire (faisant alors l'hypothèse que l'influence de la vitesse des vents et de l'humidité était négligeables à de telles échelles de temps). Des études plus récentes (Uemura et al., 2008; Benetti et al., 2014; Pfahl and Sodemann, 2014) ont montré que le d-excess mesuré dans la vapeur et les précipitations des périodes présentes varie linéairement avec l'humidité à la source (anti-corrélé), remettant alors en question les interprétations antérieures.

1.4.3 Relations indépendantes

(i) Humidité et température de surface de la mer à l'évaporation

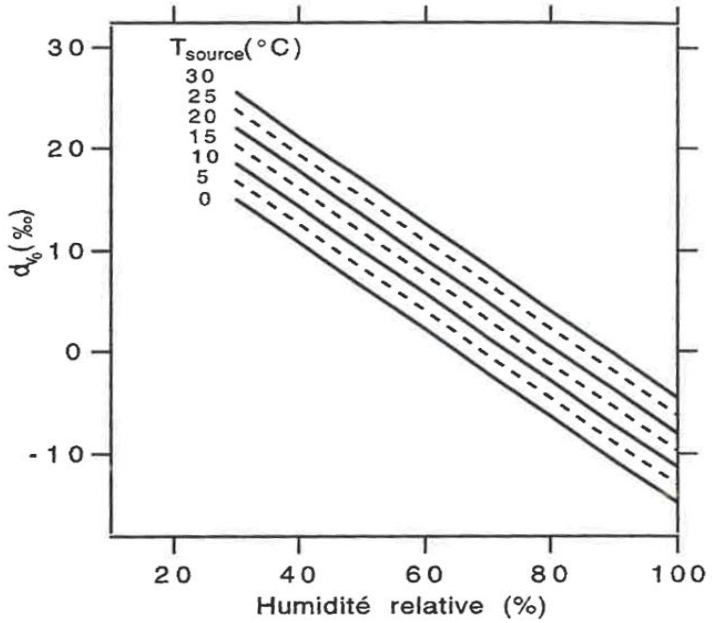

Figure 1.14: d-excess (en ‰) issu d'un calcul de fractionnement cinétique suivant la formule de Merlivat and Jouzel (1979), en fonction de l'humidité relative (en %), et pour différentes températures à la source (T_{source} en °C). Extrait de Vimeux (1999).

Le fractionnement cinétique ayant lieu lors de l'évaporation dépend des conditions d'évaporation: la température surface de l'océan, l'humidité relative à la surface de l'océan, et en moindre mesure, la vitesse des vents au-dessus de l'océan (cf. Secton 1.3.1). La

variation du d-excess en fonction de l'humidité relative et de la température de surface au-dessus de l'océan peut être calculée en utilisant l'équation empirique définie par Merlivat and Jouzel (1979). On montre alors que le d-excess augmente avec la température de surface au-dessus de l'océan, alors qu'il diminue avec l'augmentation de l'humidité relative (cf. Fig. 1.14).

(ii) Température du site

En ne considérant que le fractionnement à l'équilibre, le ratio entre δD et $\delta^{18}O$ est donné par:

$$\frac{\delta D}{\delta^{18}O} = \frac{\alpha_{eq,D}-1}{\alpha_{eq,^{18}O}-1} \times \frac{\delta D+1}{\delta^{18}O+1} \quad (6)$$

En faisant l'hypothèse que le terme $\frac{\delta D+1}{\delta^{18}O+1}$ est négligeable pour $\delta \ll 1$ et que le terme $\frac{\alpha_{eq,D}-1}{\alpha_{eq,^{18}O}-1}$ est constant. Cependant, en Antarctique, la plage des compositions isotopiques s'étend singulièrement : -491,5 ‰ < δD < 46,0 ‰ et -63,7 ‰ < $\delta^{18}O$ < -6,5 ‰ (Masson-Delmotte et al., 2008). Aussi, les fractionnements à l'équilibre varient avec la température, et le terme $\frac{\alpha_{eq,D}-1}{\alpha_{eq,^{18}O}-1}$ varie entre 9,6 et 11,6 pour une gamme de température allant de -40 °C à 0 °C. Il en résulte une dépendance du d-excess à la température de condensation, que l'on pourra qualifié d' « effet de site ». Cet effet est d'autant plus important à des températures inférieures à -40 °C, à partir de laquelle la température de condensation seule, fait augmenter le d-excess lorsque la température diminue. Ces températures sont atteintes en s'approchant de l'intérieur de l'Antarctique.

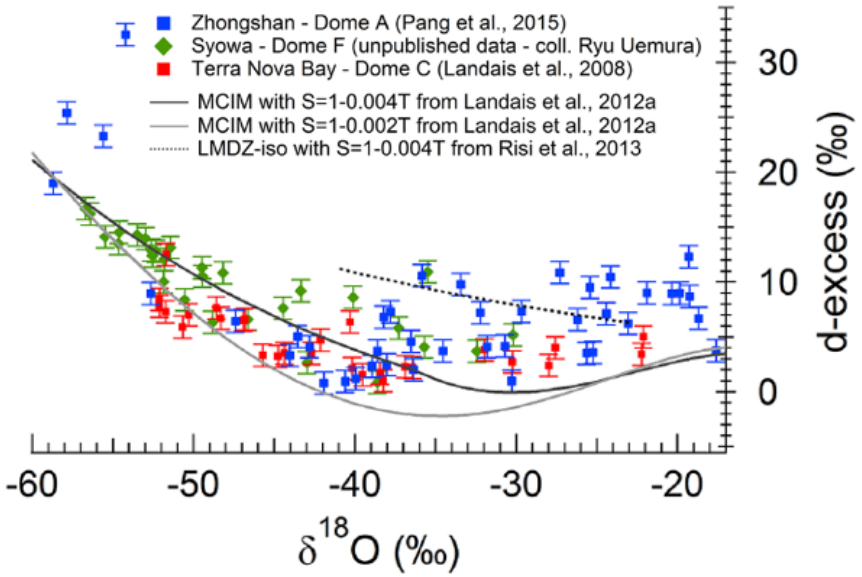

Figure 1.15: d-excess (en ‰) vs $\delta^{18}O$ (en ‰) mesurés le longs de transects (en bleu: Zhongshan–Dôme A; en vert: Syowa–Dôme F ; en rouge: Terra Nova Bay–Dôme C) et sorties de modèle (lignes noires et grises). Adapté de Touzeau, 2016.

1.4.4 Pistes d'amélioration

(i) Une définition alternative du d-excess

Une définition logarithmique polynomiale du second ordre a été introduite par Uemura et al. (2012) dans un contexte de variabilité glacial-interglacial :

$$d_{ln} = \ln(1+\delta D) - (-2{,}85 \times (\ln(1+\delta^{18}O))^2 + 8{,}47 \times \ln(1+\delta^{18}O)) \quad (7)$$

Elle a été réutilisée par Markle et al. (2017) pour des changements abrupts en période glaciaire. Uemura et al. (2012) appelle cependant à la prudence dans l'utilisation d'une telle définition, puisqu'elle exclut des caractéristiques de second ordre tel que les déphasages de déglaciation entre différents sites, contrairement à la définition classique du d-excess. Très récemment, Dütsch et al. (2017) ont montré que cette approche logarithmique présente l'avantage de s'abstraire de l'effet de site (cf. Section 1.4.3), particulièrement fort à l'échelle glaciaire-interglaciaire. Toutefois, l'inconvénient d'une telle définition est que le logarithme est sensible aux effets de mélange des masses d'air (Risi et al., 2013).

Finalement, Schoenemann and Steig (2016) ont identifié des valeurs très similaires entre le d-excess défini selon l'approche classique ou logarithmique. De plus, la définition commune classique du d-excess permet de comparer les résultats obtenus issus de différentes études. Dans ma thèse, j'ai testé que mes résultats ne différaient pas significativement d'une définition à une autre, et j'ai choisi d'utiliser la définition classique définie par Dansgaard (1964).

(ii) La variabilité saisonnière

Landais et al. (2012) ont montré la nécessité de coupler données isotopiques du premier et du second ordre à l'échelle saisonnière, afin de mieux en comprendre leur lien avec les paramètres climatiques locaux. Aussi, plusieurs études ont déjà mis en lumière le déphasage entre les cycles saisonniers du $\delta^{18}O$ et du d-excess en région côtière (Ciais et al., 1995; Delmotte et al., 2000; Markle et al., 2012; Vega et al., 2016), et sur le plateau (Ekaykin et al., 2004; Dittmann et al., 2016; Schlosser et al., 2016). Enfin, le développement récent des calculs de rétrotrajectoires (cf. Section 1.4.1) a permis de d'établir l'empreinte de la circulation synoptique, et des activités cycloniques sur la signature isotopique à l'échelle saisonnière (Schlosser et al., 2008; Markle et al., 2012; Dittmann et al., 2016; Schlosser et al., 2017). Cependant, des études systématiques pour chaque site avec des mesures à haute résolution seraient nécessaire pour décoder l'information locale extraite.

(iii) Les effets de déposition et de post-déposition

Les effets de déposition et de post-déposition affectent tant le signal isotopique du premier ordre que le signal isotopique du second ordre. Aussi les efforts déployés pour extraire un signal

isotopique régional qui se distingue du « bruit » (effets des processus de dépôt et post-dépôt) des carottes de glace sert tant les isotopes du premier que du second degré (cf. Section 1.4.1). Au-delà des exercices de modèles de diffusion, qui jusque là se sont principalement intéressés aux effets de déposition et de post-déposition sur le signal isotopique du premier ordre (δD, $\delta^{18}O$), des mesures conjointes de vapeur, précipitation et neige en $\delta^{18}O$ et d-excess permettraient d'étudier les potentiels échanges entre les différentes phases. Les premières mesures de vapeur ont été effectuées sur le plateau de l'Antarctique à Dôme C (Casado et al., 2016) et à la station Kohnen (Ritter et al., 2016), ainsi qu'à Dumont d'Urville (Bréant et al., submitted) pendant un mois, mais sans mesures synchrones dans les précipitations et la vapeur. De telles mesures seraient les bienvenues pour une amélioration de notre compréhension des mécanismes entre les différentes phases.

(iv) L'exploitation des modèles de climat

Enfin, des modèles de climat équipés des isotopes stables de l'eau permettent de mieux comprendre ces marqueurs du climat, en analysant et quantifiant leur réponse à différents forçages (e.g. Sime et al., 2008; Sime et al., 2009; Tindall et al., 2009; Holloway et al., 2016). Vice versa, les données isotopiques, qui ne sont pas utilisées pour la mise au point des modèles de climat et leurs paramétrisations physiques (Hourdin et al., 2017) fournissent un banc d'essai permettant d'évaluer le réalisme de ces modèles.

En résumé, les questions ouvertes concernant les recherches sur les climats passés récents par l'analyse des isotopes de l'eau sont : (1) d'étendre la banque d'enregistrements climatiques bien datés, à haute résolution, donnant accès aux variations intra-annuelles et inter annuelles en région côtière ; (2) d'exploiter les facteurs climatiques qui contrôlent le $\delta^{18}O$, et particulièrement en région côtière ; (3) d'identifier et quantifier la valeur ajoutée du d excess ; (4) d'évaluer les modèles atmosphériques intégrant les isotopes stables de l'eau.

1.5 Cette thèse

1.5.1 Contexte et objectifs

PAGES

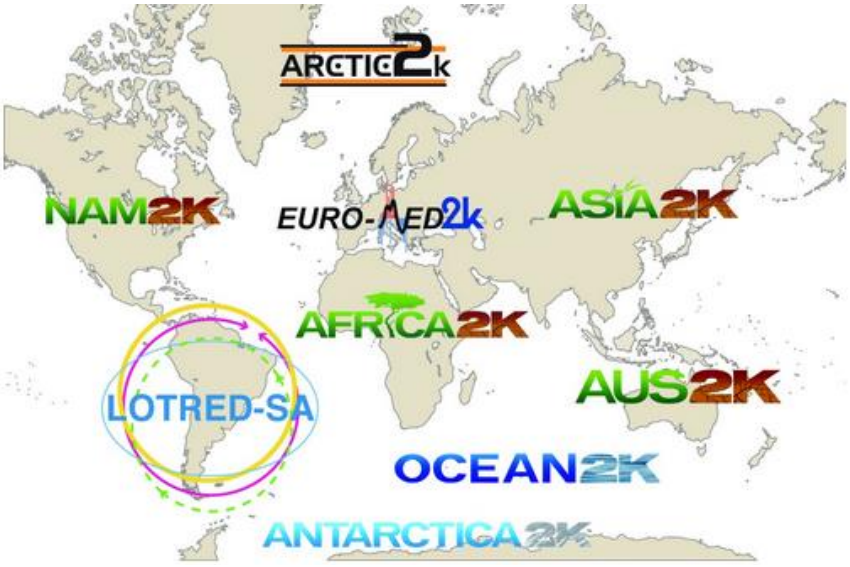

Figure 1.16: Les 9 groupes régionaux du réseau 2k. Extrait de http://www.pages-igbp.org/ini/wg/2k-network/former-2k-activities/regional-2k-groups, 06/2018.

PAGES (« PAst Global ChangES ») est le programme international majeur relatif à l'étude des climats et environnements passés, dans l'objectif d'améliorer les prévisions futures nécessaires aux stratégies mises en œuvre pour un développement durable. Il coordonne différents groupes de travail plus spécifiques (http://www.pages-igbp.org/ini/intro, 06/2018), et entre autres le réseau 2k, qui initié en 2008, a pour but d'étudier le climat des deux derniers millénaires, période appropriée pour replacer le forçage anthropogénique récent dans le contexte de la variabilité climatique naturelle. Une première phase a consisté à reconstruire la température des deux derniers millénaires sur 9 régions (cf. Fig. 1.16), dont l'Antarctique, au sein du groupe **« Ant2k »** (http://www.pages-igbp.org/ini/wg/2k-network/former-2k-activities/regional-2k-groups/antarctica2k/intro, 06/2018). J'ai participé à cette fructueuse collaboration au cours de ma thèse (cf. Section 3.2). A présent, la seconde phase tend à créer des groupes trans-régionaux ayant pour buts d'établir des bases de données planétaires, pour ensuite faire des comparaisons entre les données établies et les modèles de climat, et de caractériser les mécanismes de grande échelle de variabilité et de réponse du climat. Afin de poursuivre l'expérience de cette collaboration, j'ai récemment rejoint les groupes **« Iso2k »** (http://pastglobalchanges.org/ini/wg/2k-network/projects/iso2k/intro, 06/2018), ayant pour but de travailler à partir d'une base de donnée planétaire des isotopes stables de l'eau (issus donc non seulement des carottes de glace, mais aussi des spéléothèmes, des arbres, des lacs, des coraux, des carottes marines et des sclérosponges), et **CLIVASH2k** (http://pastglobalchanges.org/ini/wg/2k-network/projects/clivash/intro, 06/2018) dont le but est

d'étudier les mécanismes pilotant le climat de grande échelle, notamment en intégrant un couplage des enregistrements climatiques disponibles, des simulations de modèles de climat, en lien avec les modes de variabilité (e.g. le SAM, cf. Section 1.1.2).

Enfin, j'ai aussi intégré la communauté scientifque des carottes de glace IPICS (« International Partnership in Ice Core Sciences », http://pastglobalchanges.org/ini/end-aff/ipics/intro, 06/2018), soutenue par PAGES, qui se regroupe lors d'une conférence tous les quatre ans. J'ai participé à la plus récente conférence ouverte IPICS, qui a eu lieu en janvier 2016 à Hobart (Tasmanie, Australie).

Tous ces programmes de collaboration scientifique permettent d'établir les questions scientifiques prioritaires et d'y répondre collectivement. Comme souligné plus tôt (cf. Section 1.1), l'une de ces priorités porte sur l'étude de la variabilité spatio-temporelle du BMS de l'Antarctique, influençant le niveau des mers, dans le contexte du forçage antropogénique.

Etat de l'art des mesures de BMS en Antarctique

Les observations de SMB ont, jusqu'à récemment, reposé sur des relevés quantitatifs (König-Langlo et al., 1998), et des mesures annuelles en des points ponctuels (Agosta et al., 2012; Favier et al., 2013). Puis, le développement des radars à pénétration du sol (RPS) a permis d'analyser la composition ainsi que la structure interne des couches de neige / glace. L'identification des couches stratifiées et de leur profondeur réfléchies par le RPS donne accès à une estimation de l'accumulation annuelle (Eisen et al., 2008). Cette technique a déjà été grandement employée, que ce soit en Antarctique de l'Ouest (Spikes et al., 2004), sur la Terre de la Reine-Maud (Richardson et al., 1997), le long d'une traverse américano-norvégienne (Müller et al., 2010), à proximité de station Pôle Sud (Welch et al., 2009), entre Dome C et Vostok, en Terre Adélie (Verfaillie et al., 2012), et enfin le long du bassin Aurora. Beaucoup de zones restent néanmoins non couvertes. Des interpolations à partir de données ponctuelles ont été effectuées afin de reconstituer l'accumulation sur l'ensemble du continent (Arthern et al., 2006; Van de Berg et al., 2006; Vaughan et al., 2013), mais l'identification de biais dans les estimations spatiales de BMS, comparés à des simulations de modèles de climat montrent les limites des méthodes d'interpolation utilisées (Genthon et al., 2011). Les mesures de précipitation effectuées à distance par satellite ne permettent malheureusement pas de remédier à ces incertitudes, celles-ci étant limitées par l'incapacité du satellite à mesurer à des altitudes inférieures à 1.2 km (Maahn et al., 2014). Enfin, l'analyse des carottes de glace permet aussi de reconstruire l'accumulation annuelle sur le site d'extraction, dans la limite de l'incertitude de datation (Thomas et al., 2017). Obtenir une reconstruction spatio-temporelle précise et à résolution spatiale fine de l'accumulation sur l'ensemble de l'Antarctique est donc un défi

majeur. L'avancée des outils à notre disposition appelle au développement de mesures in-situ, permettant d'évaluer et améliorer les mesures satellitaires et d'obtenir des enregistrements en continu. Un premier effort mené par (Gorodetskaya et al., 2015) a déjà été initié en Terre de la Reine Maud en couplant des mesures in-situ à des mesures satellitaires, afin d'estimer précisément la précipitation. Les autres composantes du BMS, liées aux vents, compliquent les estimations précises d'accumulation, notamment en région côtière, où les forts vents catabatiques (cf. Section 1.2) créent des ondes gravitationnelles à l'origine des zones d'érosion et de re-déposition (Lenaerts et al., 2012; Gallée et al., 2013; Grazioli et al., 2017). Il est donc essentiel de multiplier le couplage des mesures localement afin d'améliorer la quantification et les mécanismes à l'origine de la variabilité spatio-temporelle du BMS**,** propos du projet ANR ASUMA en Terre Adélie.

Le projet ANR ASUMA

Cette thèse s'insère dans le projet de l'Agence Nationale de le Recherche ASUMA (« Improving the Accuracy of the SUrface MAss balance of Antarctica»), visant à caractériser et à comprendre les variations spatio-temporelles du BMS en Terre Adélie, et les processus en jeu. Ce projet a permis deux campagnes d'été (2014/2015 et 2015/2016) préliminaires à un raid lors de la campagne d'été 2016/2017, au cours desquels ont été effectuées des mesures sur le terrain (e.g. mesures radar), ainsi que le forage de carottes de glace. Les carottes rapatriées sont dédiées à des mesures isotopiques et chimiques, servant de support à ma thèse.

Initialement utilisés pour reconstruire les températures passées (e.g. Lorius et al., 1969; cf. Section 1.4.1), les isotopes de l'eau mesurés le long des carottes de glace peuvent aussi renseigner sur l'origine des masses d'air (Jouzel et al., 1982; cf. Section 1.4.2) via une signature des conditions d'évaporation préservée lors du transport atmosphérique (e.g. Bonne et al., 2015). Les mesures chimiques mesurées le long des carottes de glace peuvent aussi renseigner sur l'origine des masses d'air, puisque leur concentration dépend de la source qui les émet. Le sodium est un sel de mer, sa concentration dépend donc de sa proximité à l'océan ouvert, tandis que le sulfate non issu des embruns marins et le méthane sulfonique acide proviennent de l'oxydation des gaz sulfatés produits par les phytoplanctons agissant comme osmo-régulateur, et émis dans l'atmosphère lorsque la banquise se retire (Preunkert et al., 2007).

Les mesures isotopiques et chimiques pourraient donc être complémentaires afin de retracer l'origine des masses d'air. Aussi, mon travail de recherche doctorale a été initié dans l'objectif de répondre à la question suivante : **Quelle est la variabilité spatio-temporelle des signaux enregistrés dans les carottes de glace côtières forées en Terre Adélie ?**

Matériel et méthodes

J'ai combiné les enregistrements isotopiques issus des carottes de glace à des enregistrements de concentrations chimiques mesurées le long des mêmes carottes, aux observations météorologiques effectuées à la station côtière de Dumont d'Urville, à des données satellitaires d'extension de glace de mer, et des diagnostics du transport atmosphérique : réanalyses atmosphériques, rétro-trajectoires des masses d'air, et des simulations effectuées avec un modèle de circulation générale atmosphérique incluant les isotopes stables de l'eau.

Objectifs

Etant donné la problématique principale de ma thèse, l'état des connaissances et le matériel à ma disponibilité, j'ai abordé les questions suivantes :

(i) Les données isotopiques disponibles permettent-elle d'évaluer un modèle de circulation générale atmosphérique incluant les isotopes stables de l'eau; les productions d'un tel modèle sont-elles réalistes ?

(ii) Le thermomètre isotopique est-il applicable en région côtière, et tout particulièrement en Terre Adélie ?

(iii) Quelle information le d-excess enregistré dans les carottes de glace de la Terre Adélie apporte-t-il ?

(iv) Les enregistrements de chimie issus des carottes de glace peuvent-ils aider à l'interprétation du signal isotopique enregistré dans ces mêmes carottes ?

(v) Que peut-on déduire de l'analyse des isotopes stables de l'eau enregistrés dans les carottes de glace pour la quantification et la compréhension de la variabilité spatio-temporelle du BMS en Terre Adélie ?

1.5.2 Organisation du manuscript

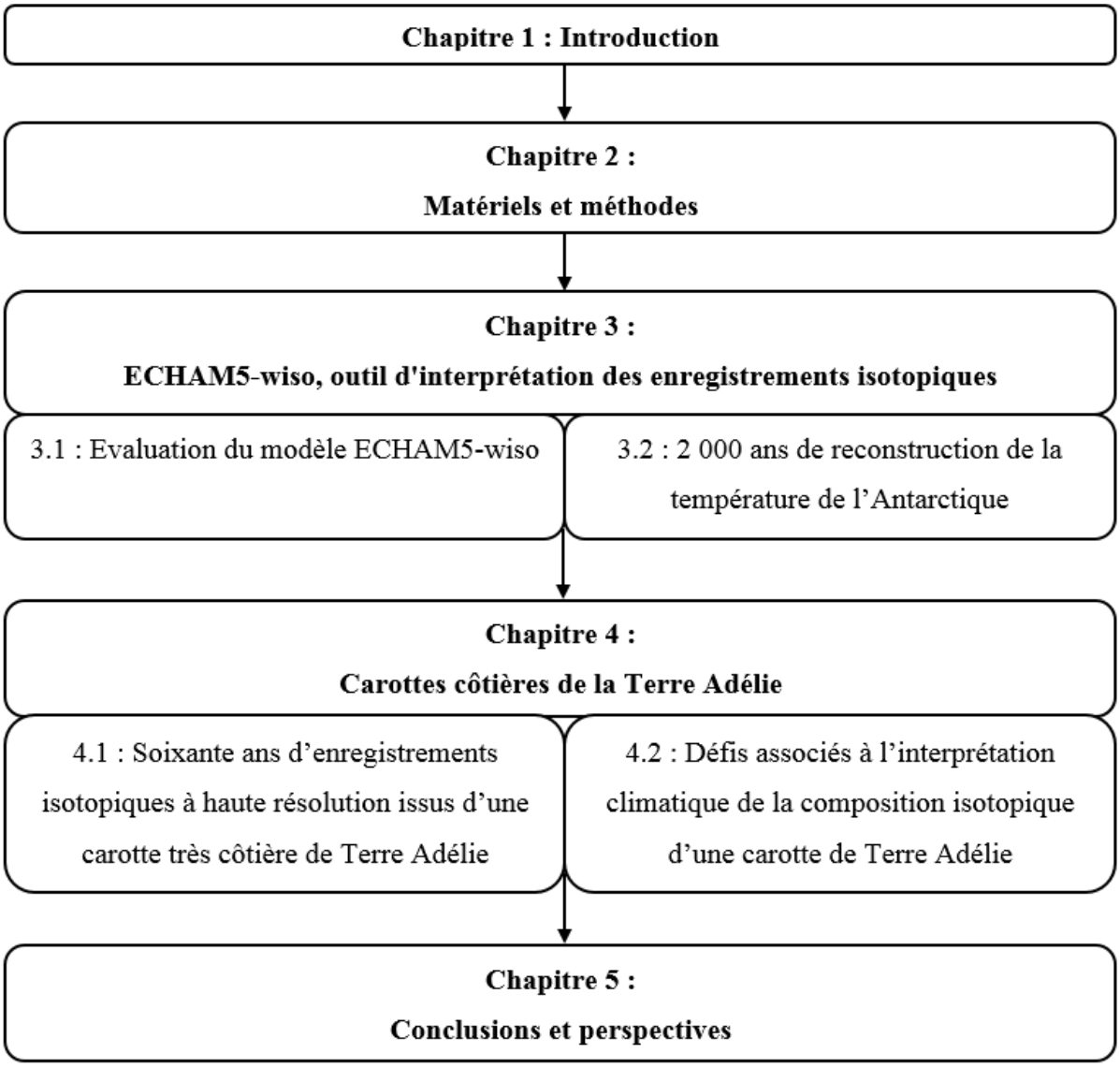

Figure 1.17: Structure du manuscrit

La figure 1.17 présente l'organisation de ce manuscrit, qui s'articule autour des quatre principaux articles préparés au cours de ma thèse (*Sections 3.1, 3 .2, 4.1, et 4.2*). La *Partie II* décrit l'ensemble des matériels et méthodes que j'ai employés. La *Partie III* a pour objectif de tester les performances du modèle atmosphérique de circulation générale ECHAM5-wiso que j'ai utilisé tout au long de ma thèse, afin d'en justifier son utilisation (*Section 3.1*. Puis une première application en est donnée pour une reconstruction de la température de l'Antarctique sur 2000 ans (*Section 3.2*). J'ai notamment proposé une méthode de calibration du thermomètre isotopique en utilisant la pente de la régression linéaire (au sens des moindres carrés) $\delta^{18}O$-température simulée par le modèle ECHAM5-wiso pour sept régions d'Antarctique. Cet exercice s'insère dans une collaboration internationale au sein du groupe de travail Antarctica2k. *La Partie IV* se concentre sur l'analyse des carottes de glace forées en Terre Adélie. La *Section 4.1* présente les résultats obtenus à partir de la carotte de névé S1C1, très

côtière, forée au cours de la campagne d'été 2006/2007 dans le cadre du projet TASTEIDEA/VANISH (Trans-Antarctic ScientificTraverse Expeditions – Ice Divide of East Antarctica). La *Section 4.2* résume les résultats obtenus à partir de la carotte de névé TA192A, plus continentale, et forée au cours de la campagne d'été 2014/2015 dans le cadre du projet ASUMA. Enfin, la *Partie V* apporte une conclusion générale et ouvre sur des perspectives.

CHAPITRE 2 : Matériels et méthodes

2. Matériels et méthodes

2.1 Carottes de névé

2.1.1 Terrain

Banque de carottes

J'ai démarré mon travail de thèse à partir de mesures précédemment effectuées mais non exploitées, le long de la carotte de névé S1C1 (66,71 °S ; 139,83 °E ; 279 m a.s.l), obtenue lors de la campagne d'été australe 2006/2007 dans le cadre d'un effort commun rassemblant les projets de l'Agence Nationale de la Recherche VANISH (« Vulnaribility of Antarctic Ice Sheet ») et de celui de l'institut Paul Emile Victor (IPEV) TASTE-IDEA (« Trans-Antarctic Scientific Traverses Expeditions – Ice Devide of East Antarctic »).

J'ai ensuite exploité des carottes de névé (~ 20 m de profondeur) issues du projet ANR ASUMA (cf. Section 1.4.1), dont l'objectif est d'étudier la variabilité spatio-temporelle du BMS sur la transition côte – plateau de la Terre Adélie, au moyen de l'acquisition de nouvelles données (météorologiques, radars et carottes) lors d'une série d'expéditions au cours de campagnes d'été et un raid.

En 2014/2015, six carottes très côtières ont été extraites, à une vingtaine de kilomètres de la station D10 (située à 10 km de la côte, cf. Encadré rouge, Fig. 2.1) et à une altitude d'environ 600 m a.s.l., sur deux sites distants: trois carottes (« TA162-15-X », X variant de 1 à 3 ; 66,75 ± 0.01 °S ; 139,59 ± 0,01 °E, altitude estimée à 579 m a.s.l) situées à 16,2 km de Cap Prud'Homme (station située à 5 km de DDU, au large du continent), et trois carottes situées à 19,2 km de Cap Prud'Homme (« TA192-15-X » X variant de 1 à 4 ; 66,78 ± 0,01 °S ; 139,56 ± 0,01 °E, altitude estimée à 602 m a.s.l). En 2015/2016, trois carottes ont été extraites sur un même site (« TA635-15-X », X variant de 1 à 3 ; 67,56 ± 0,02 °S ; 139,03 ± 0,04 °E,), à une altitude approximative de 1450 m, et à ~ 63,5 km de Cap Prud'Homme. La répétition des carottages sur chacun des trois sites vise à permettre la quantification du bruit créé lors du dépôt et de la densification de la neige, par rapport au signal atmosphérique local commun (cf. Section 1.4.4).

Enfin, le Raid a eu lieu du 03/12/2016 au 03/01/2017, sur 1380 km, et jusqu'à une distance de 1256 km de la côte, et sur une gamme d'altitudes variant de 1225 à 4589,5 m a.s.l. Ce ne sont pas moins de vingt-cinq carottes de glace (> 30 m de profondeur) et de névé qui ont été extraites, sur un parcours débutant à la station D10, se prolongeant vers l'intérieur du continent, et terminant sa boucle à proximité de D47 (située à 110 km de la côte). Six arrêts de quelques jours (« STOPS ») furent définis en amont de la campagne, pour permettre le forage de carottes de glace d'environ 50 m de profondeur et de plusieurs carottes de névé.

Le laps de temps accordé à mon doctorat ne m'a permis que d'initier l'étude de ces carottes. Je me suis donc concentrée sur des carottes côtières, en-dessous de 1500 m a.s.l., et à moins de 110 km de la côte, obtenues avant le raid (cf. lignes en gras, Tableau 2.1).

Méthode de carottage

L'ensemble des carottes a été extrait à l'aide du système électro-magnétique FELICS (« Fast Electrochemical lightweight Ice Coring System »), dont la méthode est décrite par Ginot et al. (2002) et Verfaillie et al. (2012). Le carottier effectue plusieurs passes variables de 25 à 100 cm en fonction de la longueur du carottier et de la quantité de copeaux, jusqu'à la profondeur désirée. Les segments de carottes issues de ces passes sont ensuite découpés à des longueurs inférieures à 50 cm, afin de pouvoir être stockées dans des caisses isothermes. Lors du Raid ASUMA uniquement, chaque fragment a été pesé et mesuré sur site, ce qui a permis de reconstituer les profils de densité sur le terrain. Les segments de carottes sont ensuite scellés dans des films de polyéthylène, soudés thermiquement, agrafés et placés dans des caisses propres isothermes. Ces caisses sont ensuite stockées à une température de ~- 20 °C à DDU ou Cap Prud'Homme jusqu'au jour de leur départ. Leur acheminement vers la France s'effectue intégralement par voie maritime dans des containers à ~ - 20 °C. Tout d'abord envoyées à Hobart de l'Astrolabe (bateau dédié aux voyages Antarctique – Tasmanie), elles sont ensuite transportées par bateau jusqu'en France. La durée du voyage importe peu pour les mesures que j'ai à effectuer, tant que la chaîne du froid est bien respectée. Enfin, les caisses sont entreposées dans une installation réfrigérée à ~ -25 °C, localisée au Fontanyl, non loin de l'IGE.

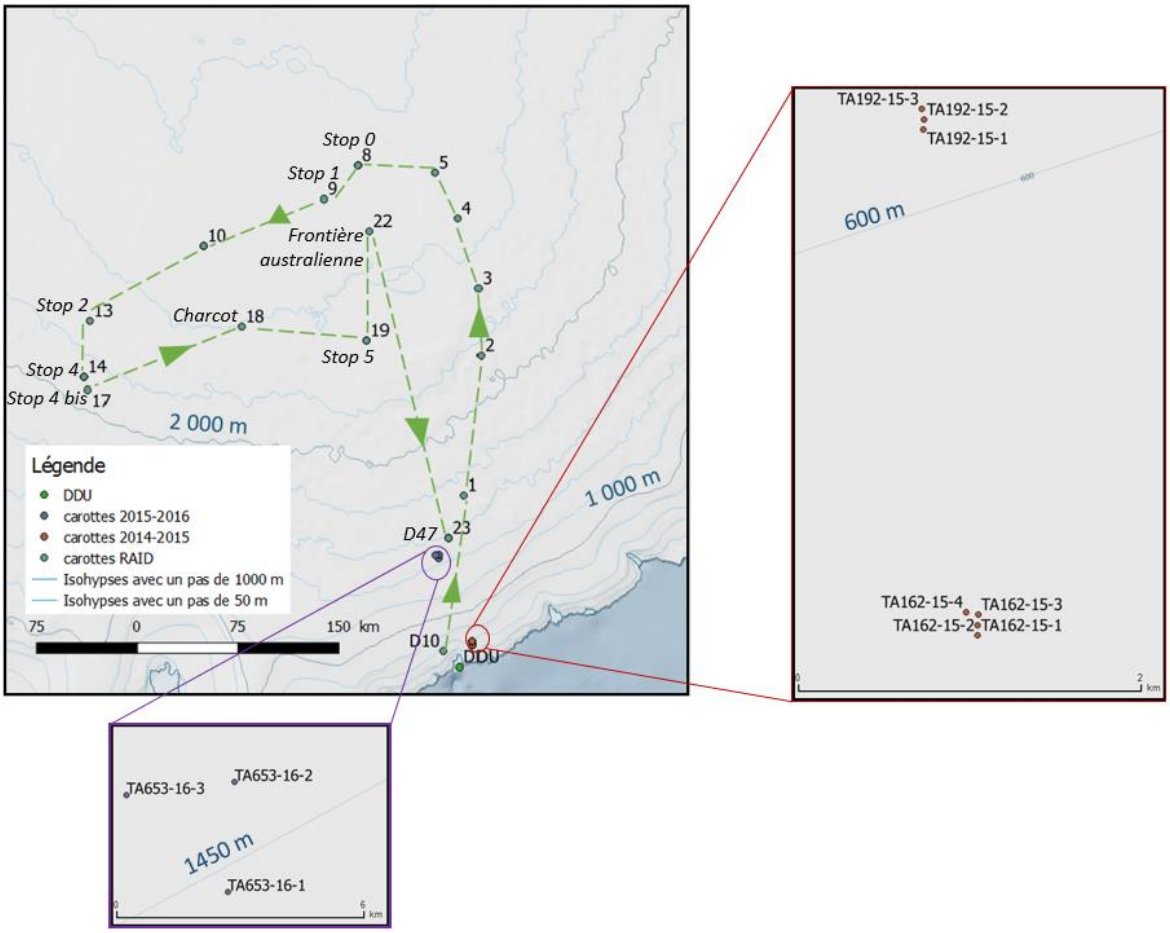

Figure 2.1: Carte représentant le raid ASUMA (ligne pointillée verte), depuis la station D10 jusqu'à la station D47 (sens donné par les flèches vertes). Les numéros (associés à des points verts) correspondent aux points de forage. Les « stops » 0 à 5 ainsi que les stations de Dumont d'Urville (« DDU »), Charcot et la « frontière australienne »[7] sont aussi indiqués. Le zoom autour de D10 correspondant à l'encadré rouge montre les 6 carottes TA192-15-X et TA162-15 (avec X de 1 à 3 ou 4, points rouges) extraites en janvier 2015. Le zoom autour de D47 correspondant à l'encadré violet montre les 3 carottes TA653-X (avec X de 1 à 3) extraites en décembre 2016. La carotte S1C1 n'est pas représentée sur cette figure, car à cette échelle, elle est superposée avec la station de DDU. Les isohypses (lignes bleues) sont extraites du modèle d'élévation digital « Digital elevation model Radarsat Antarctic Mapping Project Digital Elevation Model Version 2 » (Liu et al., 2001).

[7] La « frontière australienne » ne constitue pas une frontière, mais est le nom du site répertorié dans la base de données de l'Institut Polaire Emile Victor (IPEV). Il correspond certainement à une délimitation de la Terre Adélie par rapport au raid IAGP 1, dirigé en 1970 par R. Guillard, et C. Lorius responsable scientifique.

Tableau 2.1: Carottes obtenues au cours du projet ASUMA. Pour chacune des carottes, sont précisés la campagne, le nom de la carotte, sa position géographique et sa date de carottage (latitude en °S et longitude en °E), sa profondeur (en cm) et la distance la séparant de D10 (« dist. De D10 » en km). Les lignes en gras indiquent les carottes que j'ai échantillonnées au cours de ma thèse.

Campagne	Nom	Lat, (°S)	Lon, (°E)	Date de forage	Prof, (cm)	Dist, de D10 (km)
	TA162-15-1	66,7537	139,5950	18/01/2015	1225	22,24
	TA162-15-2	**66,7541**	**139,5942**	**18/01/2015**	**2177**	22,25
	TA162-15-3	66,7545	139,5932	18/01/2015	2171	22,27
2014-2015	TA162-15-4	66,7550	139,5942	26/01/2015	2133,5	22,2
	TA192-15-1	66,7753	139,5577	26/01/2015	1986,5	22,69
	TA192-15-2	66,7757	139,5568	29/01/2015	2157	22,71
	TA192-15-3	**66,7762**	**139,5561**	**29/01/2015**	**2162**	22,72
	TA653-16-1	67,3400	139,0714	09/12/2016	2148,5	68,74
2015-2016	**TA653-16-2**	**67,3569**	**139,0283**	**10/12/2016**	**2127,5**	71,36
	TA653-16-3	67,3700	139,0786	10/12/2016	2071,5	72,5
	ASUMA 2016-1	67,5451	138,0139	03/12/2016	1161,5	135
	ASUMA 2016-2	68,1501	136,1167	05/12/2016	1988,5	230
	ASUMA 2016-3	68,4813	135,3046	06/12/2016	2079	280
	ASUMA 2016-4	68,9130	134,6508	07/12/2016	2019	330
	ASUMA 2016-5	69,2352	134,3476	08/12/2016	2032,5	365
	ASUMA 2016-6	69,6359	135,2796	09/12/2016	2037	423
	ASUMA 2016-7	69,6359	135,2796	10-11/12/2016	4460,5	423
	ASUMA 2016-8	69,6359	135,2796	12/12/2016	2043,5	423
	ASUMA 2016-9	69,6355	136,2106	14/12/2016	2041	460
	ASUMA 2016-10	69,9539	138,5514	16-17/12/2016	4589,5	557
	ASUMA 2016-11	69,9539	138,5514	16/12/2016	2015	557
	ASUMA 2016-12	69,9539	138,5514	16/12/2016	2021	557
2016-2017	ASUMA 2016-13	70,0597	141,1976	19/12/2016	1864	660
	ASUMA 2016-14	69,7875	141,9746	20/12/2016	2013	703
	ASUMA 2016-15	69,7875	141,9746	22/12/2016	1953	703
	ASUMA 2016-16	69,7875	141,9746	21-22/12/2016	3241	703
	ASUMA 2016-17	69,7050	142,0696	23/12/2016	1959,5	713
	ASUMA 2016-18	69,3762	139,0162	25/12/2016	1998,5	843
	ASUMA 2016-19	68,7473	137,4428	26/12/2016	1998,5	937
	ASUMA 2016-20	68,7473	137,4428	27/12/2016	2003	937
	ASUMA 2016-21	68,7473	137,4428	27/12/2016	3273	937
	ASUMA 2016-22	69,2673	136,0040	29/12/2016	2008	1019
	ASUMA 2016-23	67,3989	138,7094	02/01/2017	2098	1256
	ASUMA 2016-24	67,3989	138,7094	02/01/2017	4047	1256
	ASUMA 2016-25	67,3989	138,7094	03/01/2017	1758,5	1256

Différences attendues entre les sites

Des mesures d'accumulation antérieures au projet ASUMA permettent d'estimer la variabilité du taux d'accumulation annuel le long d'une ligne s'étendant de Cap Prud'Homme (1 km de la côte) jusqu'à une distance de 156 km de la côte, grâce à mesures d'accumulation annuelles par le biais de balises (piquets de polycarbonate plantés dans la neige):

- couvrant la période 1971-1992 (21 ans), le long d'une ligne s'étendant de 1 à 16 km de la côte (21 balises) ; ces données ont été archivées par l'IPEV.
- couvrant la période 2004-2008 (5 ans), le long d'une ligne s'étendant de 1 à 156 km de la côte (91 balises), et initiées par le service national d'observation GLACIOCLIM-SAMBA (GC-SB dans la suite du manuscrit, cf. Section 2.2.1 pour plus de détails)

Agosta et al. (2012) ont publié ces données et les ont comparées. La figure 2.2 montre une représentation de la variabilité spatiale des données.

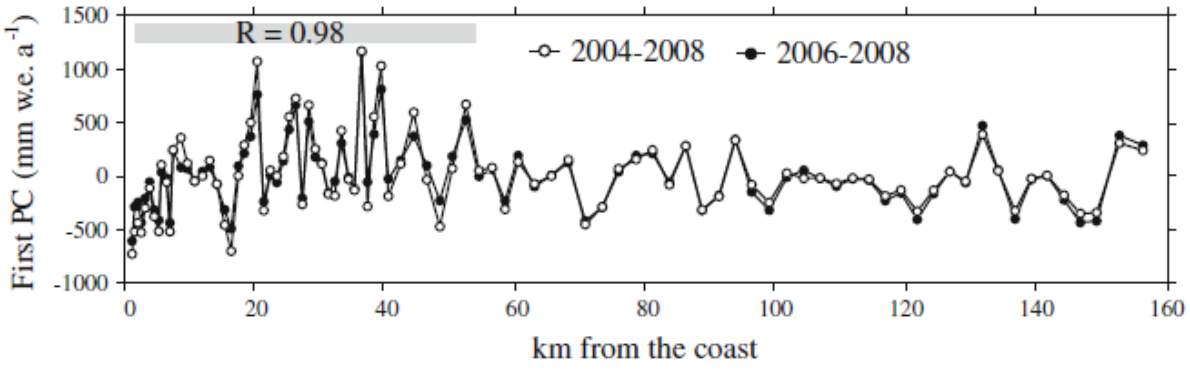

Figure 2.2: Première composante d'une analyse en composantes principales (fonctions orthogonales empiriques) des mesures GC-SB sur les périodes 2004-2008 (points blancs) et 2006-2008 (points noirs). La corrélation donnée en haut à gauche du graphique est issue de la régression linéaire entre ces deux composantes sur les 50 premières balises, i.e. jusqu'à 52 km de la côte. Extrait de Agosta et al. (2012).

Puis, au cours du raid, des mesures in-situ permettent d'appréhender les différences entre sites, et donc d'axer la sélection des carottes à analyser. En premier lieu, la température dans le trou de forage à 20 m a été mesurée à chaque campement (cf. Tableau 2.2). Cette information renseigne sur les gradients spatiaux de température moyenne annuelle, et donc l'appauvrissement relatif de la composition isotopique attendu dans les carottes extraites sur les différents sites, en faisant l'hypothèse que les gradients de température de névé sont représentatifs des

Tableau 2.2: Température à 20 m de profondeur (en °C) pour chaque arrêt.

site	$T_{20\,m}$ (°C)
STOP0	-41,14
STOP0	-41,2
STOP1	-40,92
STOP2	-40,37
STOP3	-38,92
STOP4	-36,76
STOP4_bis	-36,32
Charcot	-37,92
STOP5	-37,22
Frontière Australienne	-39,61
D47	-25,86

gradients de température de condensation, et que celle-ci est le contrôle principal sur la composition isotopique.

Enfin, des mesures de rugosité de surface ont été couplées à des mesures de vents (permettant la quantification de la rugosité aérodynamique), afin de caractériser les endroits les plus affectés par des processus de déposition/redéposition de la neige par les vents. Ces processus sont une source d'incertitude pour le signal isotopique enregistré dans les carottes (cf. Section 1.2), créant un bruit altérant le signal. On s'attend notamment à une partie lisse (et donc peu affectée par de tels processus) dans la région délimitée par les « STOP5 », « STOP0 » et « STOP1 ». Dans le cadre de ma thèse, je n'ai pas pu exploiter des carottes extraites au-delà de D47. Néanmoins, cette information est à retenir pour les études ultérieures.

2 .1.2 Analyses en laboratoire

Découpe

Je n'ai pas effectué la découpe de la carotte de névé S1C1 issue du programme couplé VANISH/TASTE-IDEA. J'ai cependant participé à la découpe des carottes « TA192-15-3» et « TA162-15-2 » (appelées dans la suite du manuscrit « TA192A » et « TA162A »), considérablement aidée de Susanne Preunkert (chargée de recherche, IGE) et de Bruno Jourdain (physicien adjoint, IGE).

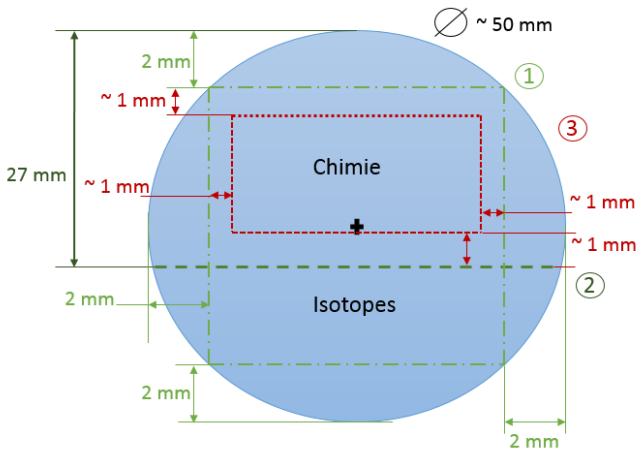

Figure 2.3: Plan de coupe d'une carotte de glace et indications des distances de découpe en différenciant les 3 étapes : 1) l'épurage à la scie (en vert clair), 2) la séparation longitudinale à la scie de la carotte pour la partie dédiée à la chimie et celle aux isotopes (vert foncé), 3) le rabotage pour la partie dédiée à la chimie.

J'ai ensuite mené la découpe de la carotte « TA653-15-2 » en totale autonomie. L'estimation du BMS annuel moyen fournie grâce au service national d'observation GC-SB permet de prévoir une résolution temporelle en fonction de la résolution de découpe. La compaction relativement faible du névé le rendant friable (densité variant de 0.4 à la surface du névé, à 0.6 g cm^{-3} à ~20 m de profondeur), nous avons choisi une résolution de découpe de 4 à 5 cm, permettant ainsi de recueillir un minimum de 15,5 mL par échantillon pour les analyses isotopiques (cf. Tableau 2.3).

La découpe s'effectue dans une chambre froide de l'IGE à ~ - 15 °C, dans un espace ventilé et décontaminé. Sur ses premiers mètres, la carotte, s'effritant facilement, n'est pas parfaitement cylindrique. Pour les carottes de névé courtes que j'ai découpées (~ 20 m), leur diamètre est en

Tableau 2.3: Volume d'eau minimum et maximum des échantillons d'isotopes et de chimie calculés à partir des surfaces exposées sur la Fig. 2.2, de la résolution des échantillons (4 cm pour les carottes TA192-15-3 et TA653-16-2, et 5 cm pour la carotte TA162-15-2), ainsi que des densités minimales et maximales observées le long des carottes de névés (0.4 et 0.6 g cm^{-3})

Résolution (cm)	4		5	
Densité (g cm^{-3})	0,4	0,6	0,4	0,6
Isotopes	15,5	23,2	19,3	29,0
Chimie	16,2	24,3	20,2	30,4

moyenne de 5 cm (± 1 cm). Chaque fragment est pesé, mesuré (pour construire le profil de densité), puis découpé. Une première découpe permet d'épurer le fragment, en sciant des surfaces planes à 2 mm de chaque extrémité (cf. pointillés verts clairs, Fig. 2.2), puis une seconde de la départager en deux tronçons (cf. pointillés verts foncés, Fig. 2.2) : le tronçon de plus petit volume est dédié aux isotopes stables de l'eau tandis que l'autre est dédié à la chimie. Avant d'échantillonner les tronçons, celui dédié à la chimie est raboté de toutes parts sur une épaisseur ~ 1 mm, le prémunissant contre toute impureté (cf. pointillés rouges, Fig. 2.2). Finalement, les tronçons résultant sont échantillonnés au couteau à la longueur désirée. Les échantillons ainsi obtenus sont recueillis dans des sachets de polyéthylène thermo-soudés pour les isotopes, et dans des flacons propres pour la chimie. Les échantillons dédiés aux mesures chimiques sont stockées dans la même chambre froide en attendant leur analyse, tandis que les échantillons dédiés aux mesures isotopiques sont transvasés dans des flacons avant d'être transportés au Laboratoire des Sciences du Climat et de l'Environnement (LSCE, Gif-sur-Yvette) dans une caisse isotherme.

Mesures isotopiques

Bénédicte Minster (Technicienne CEA au LSCE) a procédé aux mesures isotopiques selon deux méthodes complémentaires décrites plus en détail ci-dessous : (1) le $\delta^{18}O$ a tout d'abord été analysé par spectrométrie de masse sur les échantillons issus des carottes de glace, en phase gaz ; (2) le $\delta^{18}O$ et le δD ont été analysés conjointement dans un spectromètre à cavité raisonnante avec injection d'une source laser en continu.

Spectrométrie de masse

Cette méthode se décompose en deux phases explicitées ci-dessous :

(1) Passage en phase gaz

Après que les échantillons aient été laissés à température ambiante pour passer à l'état liquide, l'oxygène est passé en phase gaz par équilibration avec du CO_2 selon l'équation :

$$C^{16}O_2 + 2H_2^{18}O \leftrightarrow C^{18}O_2 + 2H_2^{16}O \quad (8)$$

(2) Spectrométrie de masse

Le gaz (au LSCE il s'agit du CO_2) est introduit dans le spectromètre de masse, ionisé puis accéléré par un champ électrique. Un champ magnétique dévie la trajectoire des atomes composant le gaz dépendamment de leur masse. Cette déviation se traduit mathématiquement par la relation qui lie le rayon de courbure r d'un atome ionisé quand il est soumis à champs magnétique B et accéléré par un potentiel v, au rapport de sa masse par sa charge $\frac{m}{q}$, énoncée par la loi de Lorentz :

$$r^2 = \frac{m}{q} \times \frac{2v}{B^2} \quad (9)$$

Les ions terminent leur course sur une cage de Faraday qui convertit les charges électriques détectées en courant électrique. Tandis que la position sur la cage détermine l'identité de l'ion détecté, le signal électrique permet d'obtenir sa concentration.

Au sein du LSCE, l'installation est composée de deux unités :

(i) Les deux bacs d'équilibration accueillant 31 flacons placés dans un bain thermostaté, et dans lesquels sont introduits 3 mL d'échantillons. Une pompe permet de faire le vide à une pression de 5.10^{-1} bar, avant que du CO_2 soit introduit, initiant la réaction d'équilibration, qui dure de 8 à 12 heures. Un piège à froid à -90 °C élimine l'humidité rémanente.

(ii) Le spectromètre de masse de la marque Finnigan MAT252 mesure les isotopologues du CO_2 les plus abondants $^{12}C^{16}O^{16}O$ ($\frac{m}{q} = 44$), $^{13}C^{16}O^{16}O$ ($\frac{m}{q} = 45$) et $^{12}C^{16}O^{18}O$ ($\frac{m}{q} = 46$) au moyen de trois collecteurs. Pour prévenir de la dérive de l'appareil au cours du temps, trois standards calibrés aux valeurs standards internationales SMOW (cf. Section 1.4.1) sont mesurés successivement avec les échantillons.

Les intensités étant proportionnelles aux concentrations, $\delta^{18}O$ est déductible en calculant :

$$\delta^{18}O = \left(\frac{\left(\frac{i_{46}}{i_{44}}\right)_{échantillon}}{\left(\frac{i_{46}}{i_{44}}\right)_{standard}} - 1 \right) \times 10^3 \quad (10)$$

Avec i_X l'intensité mesurée pour l'isotopologue de rapport $\frac{m}{q} = X$. Le standard utilisé pour ce calcul est celui se rapprochant le plus de la gamme de valeurs des échantillons analysés. Finalement, 31 échantillons de glace peuvent être mesurés par jour. La précision résultante pour la mesure de $\delta^{18}O$ est de 0.05 ‰, soit la précision la plus haute disponible pour des mesures de routine sur de petits volumes d'échantillons[8].

[8] Historiquement, le LSCE effectuait les mesures des isotopes stables de l'hydrogène sur un autre type de spectromètre de masse, permettant d'atteindre une précision de 0,5 ‰. Depuis les années 2010, ces analyses ne se font plus que par spectrométrie laser.

En plus de la précision obtenue, cette méthode a les avantages principaux de ne pas présenter d'effets mémoire, i.e. que les analyses sont indépendantes de celles qui ont précédées. En revanche, elle ne mesure que les isotopes stables de l'oxygène, et ne permet donc pas d'obtenir le paramètre de second ordre d-excess nécessitant des mesures conjointes en oxygène et hydrogène.

Spectrométrie laser à cavité raisonnante avec laser continu

Cette méthode plus couramment connu par son acronyme anglais CW-CRDS (« Continuous Wave - Cavity Ring Down Spectroscopy ») repose sur la capacité d'une espèce à absorber de la lumière (absorbance).

Une source laser est introduite en continu dans une cavité optique de 25 cm. Son intensité est amplifiée par résonnance au fur et à mesure que ses rayons se réfléchissent sur trois miroirs. Une fois que son intensité a atteint un certain seuil (détecté grâce à un détecteur photosensible), le laser est abruptement arrêté. L'intensité décroît alors selon la loi exponentielle:

$$I(t) = I_0 \times e^{-\frac{t}{\tau}} \quad (11)$$

Avec τ le temps d'amortissement dépendant non seulement des caractéristiques de la cavité optique, mais aussi de l'absorbance du milieu, c'est-à-dire du gaz inséré. L'absorbance du gaz est proportionnel à sa concentration (loi de Beer-Lambert). Ainsi, le profil de décroissance de l'intensité permet d'obtenir sa concentration[9].

Au LSCE, $\delta^{18}O$ et δD sont mesurés à l'aide d'un spectromètre laser à cavité résonnante PICARRO (modèle L240-i, 09/2013), et les trois mêmes standards qu'utilisés pour la spectrométrie de masse. Une routine permet l'analyse d'une séquence de 30 échantillons à l'état liquide (par mise à température ambiante). Un échantillonneur automatique introduit successivement un volume de ~2 µL dans un vaporiseur dilué à l'azote sec à 110 °C et ~ 2000 ppm. Le vide est fait dans la cavité, le gaz est injecté, puis la mesure est effectuée pour une durée de 9 minutes. Pour augmenter la précision, chaque échantillon est mesuré sept fois. La valeur enregistrée correspond à la moyenne des trois dernières mesures. Le standard utilisé est mesuré tous les sept échantillons, et l'ensemble des trois standards, en amont et en aval de la série d'échantillons, afin de corriger la dérive de l'instrument et de prévenir de l'effet mémoire. Une description technique plus détaillée est donnée par Law (2000). Finalement, la séquence dure deux jours, et permet l'analyse de 21 échantillons de carotte de glace avec des précisions

[9] Pour les férus de mathématiques désirant approfondir les lois mathématiques sur lesquelles repose le système, je réfère au livre de Onofri, F.: Métrologie laser pour la mécanique des fluides: granulométrie et techniques spectroscopiques, Boutier A (Ed), Hermès-Lavoisier, Paris, 2012 (ISBN 978-2-7462-3822-0), p.2006).

de 0,2 ‰ et de 0,7 ‰ pour $\delta^{18}O$ et δD, respectivement. Il en découle une précision du d-excess (calcul d'erreur quadratique) de 1,7 ‰ (en utilisant uniquement les mesures PICARRO), mais une précision de 0,8 ‰ est atteinte en combinant les mesures plus précises de $\delta^{18}O$ du MAT252 et les mesures de δD du PICARRO.

Cette méthode présente l'avantage de mesurer conjointement $\delta^{18}O$ et δD. Aussi, la source laser ainsi que le trajet d'absorption relativement long, pouvant atteindre 20 km, en fait une méthode extrêmement sensible. En revanche, le temps nécessaire à la mesure peut être long (de quelques secondes à quelques minutes), et l'incertitude est relativement élevée comparée à la première méthode (justifiant ainsi sa mise en œuvre).

2.1.3 Mesures de concentrations chimiques par chromatographie ionique

La chromatographie ionique (en phase liquide) repose sur l'habilité d'une espèce ionique à passer d'une phase mobile (éluent) à une phase stationnaire (résine). Cet échange ionique se déroule dans des colonnes de séparation cationique et anionique, selon la charge de l'ion. Le temps de rétention sur la résine permet l'identification de l'ion, tandis que la conductivité mesurée dans l'éluant au moyen d'une cellule de conductivité, permet d'obtenir sa concentration.

Les analyses chimiques ont été effectuées en quasi-totalité par Susanne Preunkert, parfois aidée de Bruno Jourdain à l'IGE, selon une routine bien établie depuis de nombreuses années (cf. Jourdain, 2001 pour les détails de la méthode). Un échantillonneur automatique permet d'effectuer 70 mesures en continu, d'une durée de 12.8 min chacune. Le temps est optimisé en cela que l'injection s'effectue au cours des 6 minutes de la mesure précédente. La mesure de six étalons anioniques et six étalons cationiques[10] en amont de celle des échantillons permet ad fine une calibration corrigeant la dérive de l'instrument. Puis les échantillons sont mesurés, ainsi qu'un blanc tous les neuf échantillons. Pour chaque mesure, neuf espèces ont été mesurées : les anions de fluor (F^-), acétate, formiate ($CHOO^-$), acide méthane sulfonique (CH_4O_3S), chlore (Cl^-), sulfate (SO_4^{2-}) et oxalate (CH_3COO^-) ; et les cations de potassium (K), magnésium (Mg) et calcium (Ca) ; à l'aide d'une colonne de séparation AS11 pour les anions, et CS12 pour les cations. Finalement, une routine avec un échantillonneur complet s'effectue

[10] Les espèces et concentrations utilisées pour la réalisation des étalons sont inchangées depuis la thèse de Bruno Jourdain Jourdain, B.: Etude du maillon atmosphérique du cycle biogéochimique du soufre aux hautes latitudes sud (station Dumont d'Urville), Th. : Océan, Atmosphère, Université Joseph-Fourier - Grenoble, I, 2001.

sur ~15 h, et permet l'analyse de 52 échantillons de glace si les étalons sont inclus, et 63 échantillons dans le cas contraire.

2.2 Observations climatiques régionales

Figure 2.4: Représentation artistique de l'ensemble des systèmes d'observation regroupant des stations et plateformes terrestres, marines et spatiales. Extrait du "World Meteorological Organization" (https://public.wmo.int/en/files/02jpg-8)

2.2.1 Observations en station

Mesures in-situ internationales

L'installation de stations météorologiques a été initiée suite à l'AGI (cf. Section 1.2.1). Cependant jusqu'en 1986, on ne décompte que vingt-cinq stations au sud de la latitude 60°S, dont deux seulement sont situés à l'intérieur du continent (Fogg and Fogg, 1992). Pour pallier à cette disparité, des stations météorologiques automatiques (« Antarctic Weather Station », AWS dans la suite du manuscrit) ont été déployées et largement installées sur l'ensemble du continent, puisqu'on en compte une centaine aujourd'hui. Contrairement aux stations météorologiques dans lesquelles des opérateurs effectuent manuellement les mesures, les AWS sont pourvus de panneaux solaires permettant l'alimentation de capteurs mesurant automatiquement la température, la pression atmosphérique, l'humidité, la direction et la vitesse du vent. Depuis le développement du système satellitaire Argos en 1978, les données sont envoyées par satellites toutes les 200 s (Lazzara et al., 2012). Que les stations soient manuelles ou automatiques, les changements d'instruments au cours du temps posent des difficultés d'homogénéité pour l'analyse de tendances sur plusieurs décennies (Turner et al., 2004). Les observations manuelles restent néanmoins les plus fiables. En Terre Adélie, on dénombre deux stations météorologiques à DDU et Dôme C (cf Section 1.1.1). En 1980, trois AWS ont été installées entre DDU et Dôme C, notamment dans l'optique d'étudier les vents catabatiques (Gallée and Pettré, 1998). Elles ont été complétées par l'installation de deux AWS au cours du raid ASUMA (à STOP0 et STOP4, cf. Fig. 2.1).

Grâce au Comité Scientifique pour la Recherche en Antarctique (« Scientific Committee on Antarctic Research », SCAR), la majorité de ces données est en accès libre. Ce comité a été créé à la fin de l'AGI afin de faciliter la coordination internationale des recherches menées en Antarctique (incluant l'Océan Austral). Regroupant 43 pays, il est le conseiller scientifique des décideurs du Traité de l'Antarctique et autres organisations suscitant des questions d'ordre scientifique et de conservation de l'Antarctique et de l'Océan Austral. Un de ces objectifs est de produire des publications, des cartes et des bases de données regroupant l'ensemble des données internationales. La première base de données de températures de surface étaient constituée grâce à la collecte de données pour seulement ~ 20 stations (Jones, 1995). Puis en 2003, une nouvelle base de donnée « Reference Antarctic Data for Environmental Research » (READER) a été initiée. Continuellement mise à jour, elle regroupe actuellement des données moyennes mensuelles sur un pas de 6h (00h, 06h, 12h, et 18h) pour 47 stations manuelles et 73 AWS (Turner et al., 2004). Les données de température, pression moyenne au niveau de la mer, pression à la station et vitesse des vents ainsi regroupées sont disponibles sur une plateforme dédiée (https://legacy.bas.ac.uk/met/READER/). Cette base de données fait l'objet d'un contrôle de qualité : la direction des vents a été exclue car sa mesure est influencée par l'orographie locale et n'est donc pas représentative de la circulation de grande échelle ; les données de surface des stations météorologiques sont sélectionnées si elles sont opérationnelles au moins depuis les 25 dernières années de manière discontinue, ou continue depuis 10 ans ; les données mesurées par AWS doivent être en fonctionnement depuis 10 ans de manière discontinue, ou continue depuis 5 ans. Enfin, les observations suspectes (e.g. valeurs aberrantes) sont aussi exclues. Au cours de ma thèse, j'ai extrait les données de température de surface, en privilégiant celles mesurées manuellement.

Mesures in-situ françaises

MétéoFrance

MétéoFrance est le service météorologique et climatique national français. Il a pour missions principales d'assurer une collecte des données météorologiques sur le réseau d'observation français, de traiter ces données, notamment en effectuant des bilans climatiques, et de prévoir la météorologie au moyen d'un modèle de climat. Puisque la Terre Adélie appartient aux Terres Antarctiques et Australes Françaises (TAAF), la station météorologique de DDU participe à la collecte de ces données. Depuis 1956, des hivernants effectuent des mesures en continu sur l'ensemble de l'année. Les données sont recueillies, puis rendues disponibles sur la plateforme en ligne de MétéoFrance (https://donneespubliques.meteofrance.fr/). Elles sont, au besoin,

partagées librement avec la communauté de la recherche scientifique. Au cours de ma thèse, j'ai extrait la température de surface, l'humidité, ainsi que la vitesse et la direction des vents. La température et l'humidité sont actuellement mesurées à l'aide d'une sonde Vaisala HMP 110 abritée à 1,5 m du sol. La vitesse et la direction du vent sont mesurées depuis une tour de 10 m.

GLACIOCLIM-SAMBA (GC-SB)

Le programme Glacioclim « Les GLAciers, un Observatoire du CLIMat » est un Service National d'Observation (« SNO ») labellisé par l'Institut National des Sciences de l'Univers (« INSU ») en 2003, afin de répondre au besoin de la communauté scientifique à documenter le suivi de glaciers et sites froids, dont la Terre Adélie en Antarctique. Cette composante Antarctique du programme s'intitule GLACIOCLIM SAMBA (« SurfAce Mass Balance of Antarctica »). Elle est coordonnée par l'IGE et soutenue par l'Institut Paul Emile Victor (IPEV). Elle a été initiée en janvier 2004, avec l'installation d'un réseau de balises dont l'incertitude moyenne associée est de ± 10 %. Ce réseau se déploie de la région côtière (Cap Prud'Homme) vers Dome C, sur une distance de 156 km (Agosta et al., 2012; Favier et al., 2013). Ces données sont en libre accès sur le site dédié au programme GLACIOCLIM (pp.ige-grenoble.fr/pageperso/favier/glacioclim-samba.php). Avec l'aide de Vincent Favier, j'ai pu exploiter ces données afin d'estimer l'accumulation moyenne globale de Antarctique, ainsi qu'à proximité des sites de forages des carottes que j'ai exploitées.

2.2.2 Mesures satellitaires

Afin d'étudier l'influence du signal local et régional de la glace de mer sur les signaux isotopiques, j'ai extrait les données satellitaires de glace de mer issues du programme satellitaire Nimbus-7 basé sur des mesures microondes passives par les techniques « Scanning Multichannel Microwave Radiometer » (SMMR) et « Defense Meteorological Satellite Program Special Sensor Microwave/Imagers - Special Sensor Microwave Image/Sounder » (DMSP SSM/I-SSMIS), rendues librement disponibles sur la plateforme du centre d'information et d'archives satellitaires américain pour la cryosphère (« National Snow and Ice Data Center », NSIDC, http://nsidc.org/data/nsidc-0051).

Le programme NIMBUS initia les observations satellitaires de la glace de mer en 1973 par des techniques de télédection micro-ondes passives (Parkinson et al., 1987). A la différence des techniques actives, les mesures peuvent être effectuées de jour comme de nuit, et sans être interrompues par la couverture (Gignac, 2012). A sa septième version, le programme employa une technique de balayage SMMR fonctionnelle de 1978 à 1987(Gloersen, 1981), succédé par

la technique SSMI. Avant d'être rendu disponibles, les données sont traitées par le centre de vol spatial Goddard (NASA Goddard Space Flight Center, GSFC). Elles ont déjà été utilisées dans de nombreuses études portant sur l'évolution du climat Antarctique (e.g. Abram et al., 2011; Shu et al., 2012; Thomas et al., 2013).

Au cours de ma thèse, j'ai extrait les données satellitaires de glace de mer au voisinage de l'Antarctique sur la période 1979-présent, afin de les comparer aux signaux que j'ai analysés dans les carottes de glace.

2.3 Simulations

2.3.1 La modélisation du climat

Implémentation générale

Un modèle de circulation générale atmosphérique (« General Circulation Model », GCM dans la suite du manuscrit) simule l'évolution temporelle des paramètres physiques météorologiques de l'atmosphère. Ces paramètres sont des variables d'état pour le modèle, et sont représentés en trois dimensions. Ils sont discritisés dans le temps (t) et dans l'espace (x,y,z), à l'aide d'un maillage tridimensionnelle : un maillage bidimensionnelle en surface (dont la maille peut s'étendre de quelques dizaines à quelques centaines de kilomètres), et des niveaux verticaux.

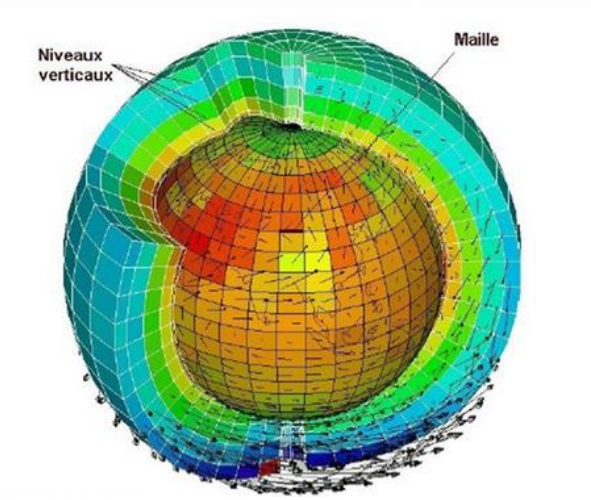

Figure 2.5: Maillage tridimensionnelle des modèles de circulation générale atmosphérique. Figure extraite de l'IPSL.

Le modèle intègre dans le temps et l'espace les équations primitives de la circulation atmosphérique, qui modélisent la dynamique atmosphérique:

- ➔ les équations de Navier et Stokes, qui décrivent l'écoulement atmosphérique
- ➔ la conservation de la masse (première loi thermodynamique), du moment cinétique et de l'énergie totale (second principe de Newton)
- ➔ La loi des gaz parfaits
- ➔ L'hypothèse hydrostatique selon laquelle les forces de gravité et de pressions verticales se compensent

A ces paramétrisations dynamiques, s'ajoutent des paramétrisations physiques intégrées au sein des colonnes verticales qui redistribuent le moment, l'énergie (chaleur sensible et latente) et l'eau (vapeur, condensats, précipitations) (e.g. Randall et al., 1996; Jakob, 2003).

Analyses rétrospectives, dites réanalyses

« Réanalyse » est l'abbréviation d' « analyse rétrospective ». Les réanalyses atmosphériques sont construites en utilisant un modèle de prévision météorologique, auquel est couplée une méthode d'assimilation d'observations, permettant une représentation de l'état tri-dimensionnel de l'atmosphère au plus près des observations. Parmi les données d'observations, on dénombre les mesures de surface (stations météorologiques, bouées et rapports de navire), les mesures issues des radiosondes, des aéronefs, et des satellites (cf. Fig. 2.5). L'assimilation s'effectue à intervalles réguliers, assurant une intégration en continu. Cette méthode rectifie la marche du modèle, en minimisant une fonction de coût donnant les valeurs les plus proches de l'état de l'atmosphère issu des observations, tout en respectant le continuum physique liant les variations atmosphériques par les équations du climat (cf Fig. 2.6). Ainsi, non seulement les variables du modèle correspondant à des données d'observations synchrones à l'heure synoptique de l'assimilation peuvent être rectifiées, mais aussi les données d'observations asynchrones, arrivant trop tôt ou trop tard pour y être intégrées. Les réanalyses permettent de tirer parti des observations (surtout de pression et de température), mais restent parfois délicates à exploiter à l'échelle du changement climatique (hétérogénéités des données assimilées au cours du temps, limites des modèles de prévisions atmosphériques) (e.g. Nicolas and Bromwich, 2011).

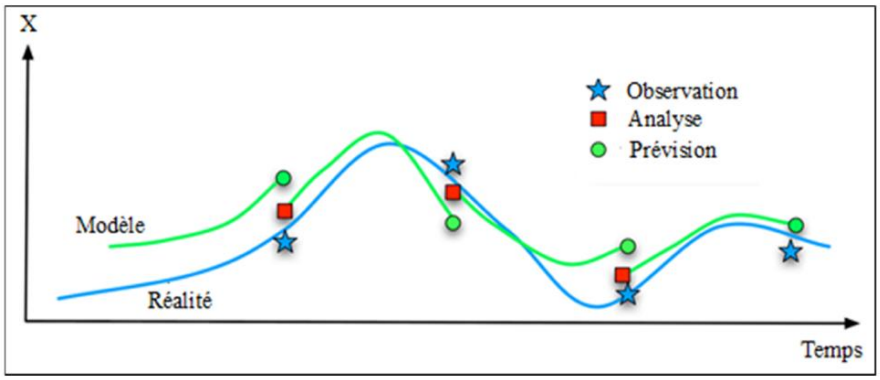

Figure 2.6: Description schématique de la méthode exploitée par les réanalyses. Figure extraite de Essou (2016).

Implémentation des isotopes stables de l'eau

Plusieurs modèles de circulation générale de l'atmosphère ont été équipés d'une représentation des isotopes stables de l'eau, et parfois également de diagnostics permettant d'identifier la région océanique source d'évaporation (par un marquage de l'eau au moment de l'évaporation) (e.g. Koster et al., 1992; Delaygue et al., 2000; Werner et al., 2001; Noone and Simmonds, 2002). Pour les isotopes stables de l'eau, cela implique de multiplier la modélisation du cycle de l'eau pour chaque isotope stable de l'eau (^{1}H, D, ^{16}O, ^{17}O et ^{18}O), et de conserver la masse pour chacun de ceux-ci lors du schéma d'advection. A chaque changement de phase sont

représentés les fractionnements, qu'ils soient à l'équilibre ou cinétique : lors de l'évaporation, la condensation atmosphérique (y compris la formation de cristaux) et la réévaporation des gouttes d'eau (Jouzel and Merlivat, 1984).

Les premières implémentations des isotopes de l'eau ont eu lieu dans les années 1980 (Joussaume et al., 1984), et ont connu un essor depuis ces vingt dernières années (e.g. Hoffmann et al., 1998). Les sources d'incertitudes sont liées à la résolution des modèles atmosphériques par rapport aux processus sous-jacents et à leur représentation du cycle de l'eau (ex. paramétrisations pour l'évaporation), mais aussi aux valeurs des coefficients de fractionnement en-dehors de la gamme de leur détermination expérimentale. Certaines paramétrisations, comme la fonction de sur-saturation liée à la formation des cristaux de glace (Risi et al., 2010; Werner et al., 2011), sont optimisées pour améliorer la simulation de la composition isotopique des précipitations (données extraites de la base de données GNIP, "Global Network of Isotopes in Precipitation", Rozanski et al., 1993). Des travaux récents ont mis en évidence l'intérêt de la confrontation entre simulations et observations de composition isotopique de la vapeur d'eau, que ce soit par rapport aux processus convectifs tropicaux (Yoshimura et al., 2011) ou bien par rapport à la vapeur d'eau en surface dans le secteur Atlantique Nord-Arctique (Steen-Larsen et al., 2017).

Récemment, des méthodes ont été développées pour guider les simulations effectuées à l'aide de modèles de circulation générale de l'atmosphère équipés des isotopes stables de l'eau, par les réanalyses atmosphériques. Cette approche permet des comparaisons entre observations et simulations à l'échelle des évènements météorologiques individuels, l'effet de la circulation atmosphérique de grande échelle étant représenté de manière la plus réaliste possible.

Intérêts de la simulation des isotopes de l'eau

La modélisation des isotopes stables de l'eau a été développée initialement pour mieux comprendre les processus de grande échelle contrôlant la composition isotopique des précipitations, en allant au-delà des approches très théoriques comme celles d'une distillation de Rayleigh. Plusieurs applications de ces méthodes ont été développées, comme l'utilisation des mesures isotopiques pour évaluer les modèles atmosphériques, indépendemment des données avec lesquels ils ont pu être mis au point ; et pour comprendre les facteurs qui contrôlent les changements de composition isotopique des précipitations (gradients spatiaux ; variations synoptiques, saisonnières, inter-annuelles, et pour différentes périodes paléoclimatiques). Ces modèles ont ainsi permis d'évaluer l'incertitude associée à l'utilisation du thermomètre isotopique pour quantifier les variations climatiques passées à partir des

enregistrements isotopiques issus de carottes de glaces polaires (Noone and Simmonds, 2002; Werner and Heimann, 2002; Werner et al., in press).

2.3.2 Réanalyses ERA-interim

Présentation

ERA, acronyme de « European ReAnalysis » est le nom des réanalyses globales atmosphériques du Centre Européen de Prévision Météorologique (« ECMWF », European Center of Meterological Weather Forecast). La version ERA-interim succède à la seconde génération de réanalyses ERA40 qui débuta en 1998 et dont les productions couvrent la période 1957-2002 (Uppala et al., 2005). Elle sert d'intermédiaire à une nouvelle génération amenée à remplacer la version d'ERA40.

Les réanalyses ERA-interim utilisent le modèle de prévision du centre européen IFS Cy31r2 (« Integrated Forecast Model »), couplé à une méthode d'assimilation variationnelle en quatre dimensions (4DVAR) sur un pas de temps de 12 h, et avec une correction de biais des données de radiations satellitaire. Les productions couvrent la période 1979 à nos jours, et ont une résolution spectrale T255 (~80 km) sur 60 niveaux verticaux (jusqu'à une altitude à 0.1 hPa, soit ~64 km). Une description détaillé est donnée par Dee et al. (2011).

Evaluation d'ERA-interim pour l'Antarctique

Différents paramètres climatiques issus des réanalyses ERA-interim ont été évalués pour le continent Antarctique, par comparaisons avec les jeux de données disponibles. J'en fais ici une description non exhaustive, afin de justifier son utilisation pour l'Antarctique.

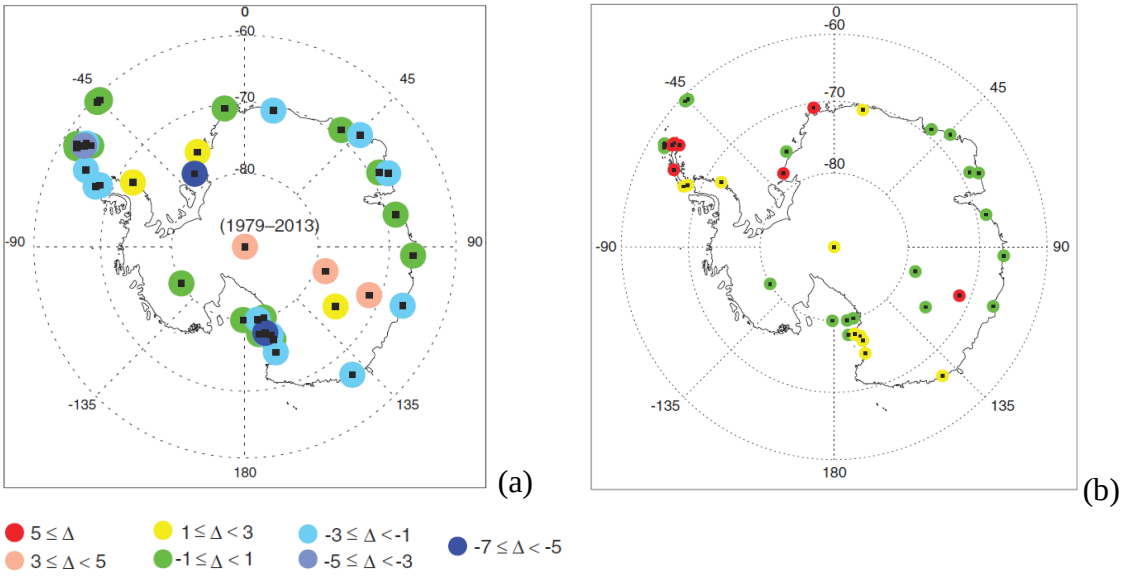

Figure 2.7: Diagnostic de la différence entre température de l'air en surface simulée par ERA-interim et observée. (a) Différences (en °C) entre les simulations ERA-interim et les mesures effectuées en stations pour quatre périodes (1979-2013, 1979-1990, 1991-2001 et 2002-2013). (b) Corrélation entre les anomalies des séries temporelles mesurées en station et simulées par ERA-interim sur la période 1979- 2013. Les cercles rouges indiquent des corrélations inférieures à 0.80,

en jaune entre 0.80 et 0.89, et en vert, supérieures ou égal à 0.90. Les rectangles noirs sont centrés sur la position de la station. Figures adaptées de Jones and Lister (2015).

Température

La température de l'air en surface issue de ERA-interim a été récemment comparée avec les données météorologiques des stations manuelles et automatiques par Jones and Lister (2015). Ces auteurs ont observé un biais chaud sur le plateau Antarctique s'élevant jusqu'à 5 °C. Néanmoins, la variabilité est bien reproduite, le coefficient de corrélation sur les valeurs mensuelles étant supérieur ou égal à 0,89 pour 33 des 40 stations.

Accumulation

Bromwich et al. (2011) ont comparé la différence entre précipitations et évaporation (P-E) produite par différentes réanalyses, avec une base de données de BMS interpolée par méthode de krigeage, permettant ainsi de couvrir l'ensemble de l'Antarctique (Arthern et al., 2006). Ils ont montré que les réanalyses ERA-interim étaient les plus réalistes, puisque contrairement aux autres étudiées, elles ne montrent pas de tendances ni de discontinuités suspicieuses. Cependant, elles restent associées à une incertitude liée à la faible densité des mesures d'observation couvrant l'Antarctique, à leur propre incertitude, et aux changements des matériels utilisés pour les effectuer. Nicolas and Bromwich (2011) ont complété cette étude en montrant le réalisme de la variabilité inter-annuelle des productions P-E issues de ERA-interim. Plus récemment, Wang et al. (2016) ont montré qu'ERA-interim reproduisait le mieux la variabilité interannuelle des précipitations en Antarctique par rapport aux réanalyses disponibles. Palerme et al. (2017) ont confirmé ce résultat en comparant les précipitations issues des mesures satellitaires Cloudstat avec celles de plusieurs réanalyses, dont ERA-interim. Ils ont montré des variabilités interannuelles et saisonnières similaires entre les réanalyses mais des taux de précipitation meilleurs pour ERA-interim.

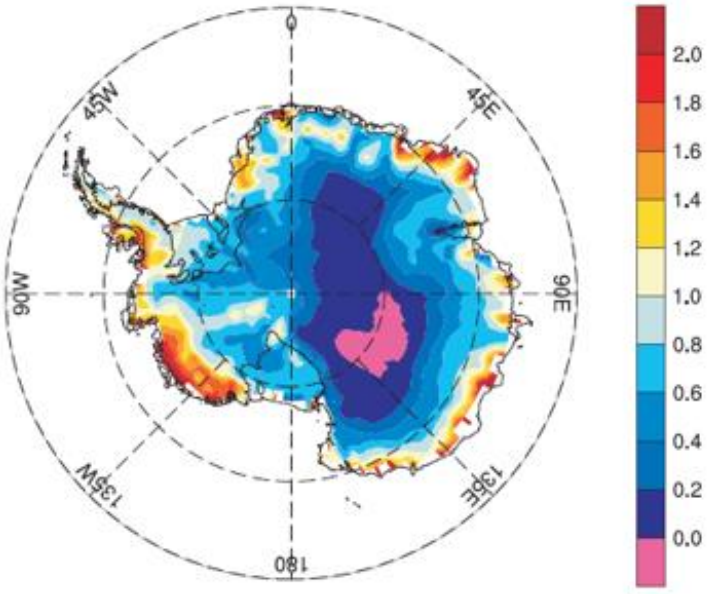

Figure 2.8: Ratio des simulations (P-E) moyennées sur la période 1989-2009 par la base de données d'accumulation de Arthern et al. (2006). Figure adaptée de Bromwich et al. (2011)

Vents

Rodrigo et al. (2013) ont évalué la distribution des vents sur le continent Antarctique. Ils ont montré que la distribution de Weibull (notamment le facteur k) était généralement sous-estimée à cause d'une topographie lissée par une résolution horizontale pas assez fine. Les biais les plus importants ont été observés en région côtière, dans les zones d'escarpement, et notamment les zones de confluence des vents catabatiques au sein de sillons les intensifiant grandement.

Couverture nuageuse

Naud et al. (2014) ont évalué la couverture nuageuse, en comparant les productions ERA-interim avec les observations satellitaires de la NASA, MODIS («Moderate Resolution Imaging Spectroradiometer ») et MISR (« Multi-angle Imaging SpectroRadiometer »). Ils ont trouvé que le taux de nuage moyen correspond aux observations à ± 5 %, mais qu'il y a un biais négatif de la couverture nuage à basse altitude au niveau des cyclones extratropicaux, notamment derrière les fronts froids. Ces résultats impliquent une répercussion sur les précipitations simulées pour l'Antarctique côtière.

Pression atmosphérique au niveau de la mer

Enfin, en comparant les productions ERA-interim aux données météorologiques et radiosondages répertoriées dans la base READER, Bracegirdle and Marshall (2012) ont montré qu'ERA-interim simule la pression moyenne au niveau des mers et le géopotentiel à 500 hPa les plus réalistes comparées aux autres réanalyses atmosphériques globales exploitées pour le continent antarctique.

En conclusion, malgré des biais variant spatialement (côte vs plateau), les réanalyses ERA-interim sont les plus réalistes et reproduisent correctement la variabilité climatique inter-annuelle de la température, de l'accumulation, et des pressions.

Exploitation d'ERA-interim pour l'Antarctique

Les réanalyses ERA-interim ayant les meilleures performances pour le climat de la région antarctique, ces réanalyses ont été utilisées pour différentes reconstructions.

L'ensemble des stations météorologiques et des AWS est associé à une couverture spatiale éparse du continent. A contrario, bien que les réanalyses soient spatialement discrétisées, elles présentent l'avantage de couvrir l'ensemble de l'Antarctique. Elles ont donc été utilisées afin d'effectuer des reconstructions, notamment celle de la pression moyenne au niveau des mers de

l'Antarctique (Fogt et al., 2017; Fogt et al., 2018), ou d'évaluer le réalisme des productions de modèle, comme celles de l'accumulation simulée par le modèle de circulation général atmosphérique RACMO2.4 (Thomas et al., 2017). Elles ont permis l'étude de la variabilité climatique des dernières décennies en Antarctique. Par exemple, Bromwich et al. (2011) ont montré qu'il n'y avait aucune tendance significative du BMS en Antarctique de l'Est. Par ailleurs, Bromwich et al. (2013) ont montré un réchauffement significatif en Antarctique de l'ouest sur la période 1958-2010.

Les réanalyses permettent aussi l'exploitation des paramètres climatiques associés à la circulation de grande échelle, comme les champs de pression, de vent et de géopotentiels (Jones et al., 2016; Marshall et al., 2017), ainsi que leur influence sur le climat régional. De nombreuses études se concentrent sur l'influence de la circulation synoptique sur la glace de mer (Pope et al., 2017; Paolo et al., 2018), par les vents (Holland and Kwok, 2012), la pression moyenne au niveau des mers (Turner et al., 2017; Schlosser et al., 2018). Steig et al. (2012) ont étudié le lien entre la formation des eaux profondes circumpolaires et les vents. Enfin, Hosking et al. (2017) ont utilisé les champs de pression et de vapeur d'eau pour étudier le lien entre les cyclones et l'apport d'humidité.

Les réanalyses sont aussi utilisées comme outil d'analyse des enregistrements issus de carottes de glace extraites en Antarctique. Elles permettent d'étudier l'influence de la circulation synoptique sur le signal isotopique enregistré dans les carottes de glace (Schwanck et al., 2017), en le comparant avec les champs simulés, mais aussi l'influence de la circulation régionale, en comparant les mêmes enregistrements avec les paramètres climatiques simulés pour le point de grille le plus proche du site de forage (Fudge et al., 2016; Bertler et al., 2018). Enfin, la température de surface de la mer et l'humidité simulées par les réanalyses peuvent servir de conditions initiales d'un modèle de distillation de Rayleigh (Dittmann et al., 2016) afin d'explorer quantitativement les relations entre régions sources et signaux isotopiques.

Pour terminer, ERA-interim est utilisé pour fixer les conditions initiales de modèles de circulation générale du climat atmosphérique (e.g. RACMO2.1, Lenaerts et al., 2012), ou les paramètres d'advection de modèles de rétro-trajectoires (Sinclair et al., 2010; Drumond et al., 2016).

2.3.3 Réanalyses NCEP-2

Bien que j'aie montré précédemment que les réanalyses ERA-interim sont les plus performantes en Antarctique (cf Section 2.3.2), j'ai utilisé les réanalyses NCEP-2 pour effectuer des simulations de rétro-trajectoires de masses d'air par le modèle HYSPLIT (cf Section 2.3.5). Adapter le format des réanalyses ERA ou le logiciel HYSPLIT pour pouvoir les analyser

représentait un investissement de temps incompatible avec mon calendrier de thèse (Nancy Bertler, personnal communication, 2018).

Performances des réanalyses NCEP-2 pour l'Hémisphère Sud

Des comparaisons avec les premières observations régionales de la Troposphère (« First Regional Observating Sutdy of the Troposphre », FROST) ont montré tant que les réanalyses ERA-interim que les réanalyses NCEP-2 reproduisent les caractéristiques principales de la circulation synoptique de l'Hémisphère Sud (Bromwich and Smith, 1993; Turner et al., 1996; Turner et al., 1999). Les réanalyses NCEP-2 présentent néanmoins des tendances suspicieuses non seulement dans les simulations de température à 2 m (Wang et al., 2016), mais aussi des simulations de BMS (Bromwich et al., 2011), de pression moyenne à la surface de la mer et du géopotentiel à 500 hPa (Hines et al., 2000; Marshall and Harangozo, 2000). Ces discordances s'expliquent principalement par les différentes méthodes utilisées pour assimiler les données satellitaires : tandis qu'ERA-interim assimile les données brutes de rayonnement satellitaires, NCEP-2 utilise des estimations de données satellitaires à partir de relations statistiques basés sur les profils verticaux de température et d'humidité. La variabilité interannuelle est cependant bien reproduite tant pour la température (Lejiang et al., 2010; Wang et al., 2016), le BMS (Bromwich et al., 2011) et la pression moyenne à la surface de la mer (Lejiang et al., 2010). Aussi, malgré ces biais, les réanalyses NCEP-2 restent les plus utilisées avec ERA-interim pour l'étude de la variabilité climatique interannuelle de la circulation de grande échelle de l'Hémisphère Sud (e.g. Blázquez and Solman, 2017) , mais aussi pour l'évaluation de modèles (e.g. Xin et al., 2014).

2.3.4 Le modèle de circulation atmosphérique générale ECHAM5-wiso

Intérêt des AGCM pour les isotopes stables de l'eau

L'utilisation d'un GCM permet d'étudier l'influence de la circulation générale sur le signal isotopique enregistré dans les carottes de glace. Les GCM sont décomposés en modules atmosphériques, de surface continentale, et d'océan, qui peuvent être couplés ou pris séparément. Les GCM atmosphériques (« Atmospheric General Circulation Model », AGCM dans la suite du manuscrit) ont pour conditions limites les variables climatiques des couches océaniques et les caractéristiques des surfaces continentales et de la cryosphère. En particulier, la température de surface de la mer et la concentration de glace de mer doivent être prescrites. Les simulations climatiques demandent également de prendre en compte les forçages externes (e.g. paramètres astronomiques, évolution de la composition atmosphérique ou de la surface continentale). Ces modèles peuvent être également guidés par des réanalyses d'observations

météorologiques, i.e. que l'état de l'atmosphère en trois dimension (vents, parfois également température et humidité) sont les plus proches possibles, jour après jour, des valeurs des réanalyses. Ce guidage (« nudging ») par les réanalyses permet de reproduire un climat plus proche des observations (Telford et al., 2008). Le cycle de l'eau qui reste libre, mais qui dépend des paramètres physiques climatiques contraints par les réanalyses, est alors plus réaliste (Noone and Simmonds, 2002; Yoshimura et al., 2008; Risi et al., 2012), même si il demeure que sa qualité dépend des paramétrisations physiques du modèle atmosphérique.

Etat de l'art des AGCM équipés d'isotopes stables de l'eau

Dans cette partie, je présente un portrait non exhaustif des différents AGCM équipés des isotopes de l'eau afin de justifier le choix du modèle ECHAM5-wiso. Le tableau 2.5 présente une carte d'identité de ces modèles. Les modèles diffèrent principalement par la résolution des simulations, par l'approche numérique, et par leurs paramétrisations physiques. Les isotopes de l'eau simulés dans les précipitations ont été évalués dans sept des dix modèles en les confrontant aux données du réseau global des isotopes de l'eau des précipitations (« Global Network of Isotopes in Precipitation », GNIP, Rozanski et al., 1993). Cependant, ce réseau ne dénombre que quatre enregistrements isotopiques en Antarctique, dont trois en Péninsule Antarctique. Les modèles HadAM3 (Sime et al., 2008), LMDZiso (Risi et al., 2010) et ECHAM5-wiso ont quant à eux été évalués en comparant les simulations avec la base de données constituée par Masson-Delmotte et al. (2008) regroupant des enregistrements isotopiques issus de précipitations, neige fraîche, et de glace, de 1279 sites (dont 938 pourvus de mesures en δD et 1125 de mesures en $\delta^{18}O$).

Le diagnostic de l'évaluation dépend de la physique du modèle, de l'implémentation des isotopes, de sa résolution et de son forçage. Malgré leur différence, les modèles présentent des biais communs : un biais chaud sur le plateau de l'Antarctique, accompagné d'une surestimation du $\delta^{18}O$ (Lee et al., 2007). Cependant, si certains modèles montrent un biais isotopique non négligeable, la reproduction des gradients spatiaux est considérée comme suffisante pour permettre d'utiliser ces modèles afin de tester des mécanismes de grande échelle via des tests de sensibilité. Ainsi, Lewis et al. (2013) a testé l'influence des conditions aux limites représentatives de l'ENSO, du Dernier Maximum Glaciaire et de l'Holocène moyen (il y a 6 000 ans), en couplant le modèle GISS ModelE à un diagnostic de distribution de source de vapeur. En revanche, l'utilisation d'un modèle dans l'objectif de comprendre et quantifier précisément les processus expliquant la variabilité des mesures isotopiques nécessite que le modèle soit le plus réaliste possible, ne reproduisant pas seulement la circulation synoptique mais aussi résolvant des processus de petite échelle.

L'initiative internationale « Stable Water Intercomparison Group » (http://atoc.colorado.edu/~dcn/SWING/index.php) initiée en 2003 a pour but d'effectuer une inter-comparaison entre les modèles de circulation générale équipée des isotopes stables de l'eau et les données isotopiques disponibles (Werner et al., 2004). Ce groupe ne rassemble que 6 modèles de circulation générale, dont les versions ne sont pas nécessairement les plus récentes utilisées dans les exercices standardisées d'inter-comparaisons des projections climatiques (en cause, le temps requis pour l'implémentation des isotopes stables de l'eau). De plus, alors que des comparaisons des productions isotopiques du premier ordre ($\delta^{18}O$), et à l'échelle globale ont été entreprises (Noone, 2006; Noone, 2007), aucune étude n'a comparé systématiquement les simulations isotopiques issues des dernières versions de modèles isotopiques pour l'Antarctique, cohérentes avec les simulations climatiques CMIP5 ou CMIP6.

ECHAM5-wiso

Les isotopologues de l'eau ($H_2{}^{16}O$, $HD^{16}O$, $H_2{}^{18}O$) ont été implémentés dans l'AGCM ECHAM5 (Roeckner et al., 2003) par Werner et al. (2011), de la même manière que dans les versions précédentes ECHAM3 (Hoffmann et al., 1998) et ECHAM4 (Werner et al., 2001), en appliquant les fractionnements à l'équilibre et cinétiques décrits dans la Section 1.2.1. Les conditions aux limites (température de surface de la mer et glace de mer) sont forcées par les réanalyses du centre européen de prévision météorologique ERA40 (Uppala et al., 2005) et ERA-interim (cf. Section 2.3.2, Dee et al., 2011).

Tableau 2.4 : Moyenne et erreur quadratique moyenne (EQM) de la température de surface (« Tsurf. » en °C), $\delta^{18}O$ (en ‰), et δD (en ‰) simulés par ECHAM5-wiso sur l'ensemble de l'Antarctique sur la période 1979-1999

	Moyenne	EQM
Tsurf. (°C)	-37,8	6,3
$\delta^{18}O$ (‰)	-39,3	4,6
δD (‰)	-307,9	36,1

Le choix du modèle ECHAM5-wiso pour ma thèse tient de son évaluation préalable, soulignant les performances du modèle pour l'Antarctique. Tout d'abord, dix-neuf des modèles couplés utilisés dans le quatrième rapport du Groupe d'experts Intergouvernemental sur l'Evolution du Climat (GIEC) ont été évalués puis classés (Connolley and Bracegirdle, 2007), basé sur des simulations de pression moyenne au niveau de la mer, altitude, température à 500 hPa, température de surface de la mer et BMS couvrant la période 1979-2000 sur l'ensemble du continent Antarctique. Les résultats montrent qu'en considérant l'ensemble des paramètres, ECHAM5 est le plus performant. Puis, Werner et al. (2011) a évalué spatialement les isotopes de l'eau simulés dans les précipitations à l'échelle globale, et en zoomant sur l'Antarctique en confrontant les simulations à la base de données de Masson-Delmotte et al. (2008). L'erreur quadratique moyenne de la température de l'air en surface, $\delta^{18}O$ et δD ne représentent que 10 à 15 % de la

moyenne. Le modèle représente les tendances spatiales et est globalement en accord avec les données de Masson-Delmotte et al. (2008; cf. Fig. 2.9).

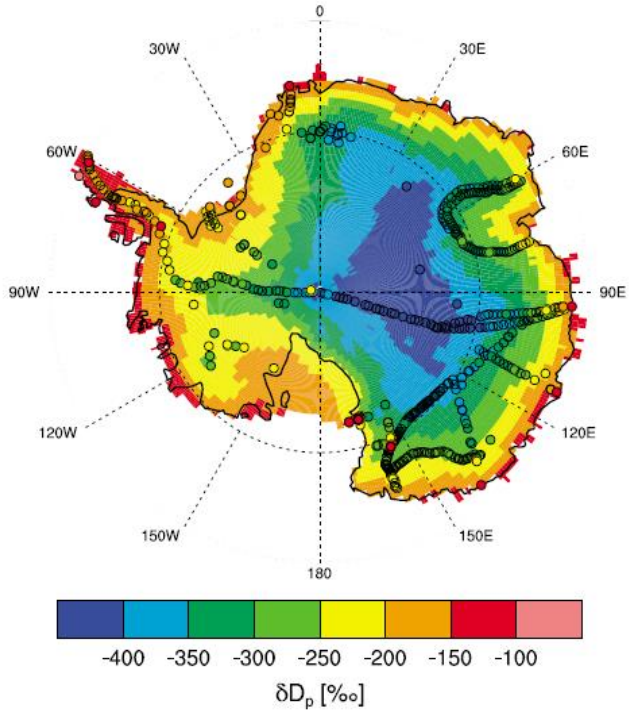

Figure 2.9: δD (en ‰) simulé dans les précipitations par ECHAM5-wiso (arrière-plan) et enregistré dans les données de Masson-Delmotte et al. (2008) (cercles). Figure extraite de Werner et al. (2011).

Quatre études ont déjà utilisées les simulations d'ECHAM5-wiso pour interpréter des enregistrements isotopiques mesurées en Antarctique. Je ne reporterai ici que les résultats qui ont à trait à l'évaluation du modèle. Ritter et al. (2016) ont comparé des simulations de température à 2 m au-dessus du sol, d'humidité et de compositions isotopiques de la vapeur correspondant à la grille la plus proche de la station Kohnen, aux mesures effectuées entre Décembre 2013 et Janvier 2014. Les moyennes sont reproduites par le modèle, cependant l'amplitude du cycle diurne de la température est sous-estimée, dû à un déficit dans le bilan énergétique de surface, ainsi que de la dynamique de la couche limite, notamment une mauvaise reproduction de la couverture nuageuse et des évènements de précipitations neigeuses. Xiao et al. (2013) ont comparé des simulations de la composition isotopique des précipitations à des mesures effectuées le long d'un transect partant de la région côtière à 1415 m a.s.l. jusqu'à Dome A, à 4093 m a.s.l., ainsi couvrant une large variabilité topographique. Ils notèrent une surestimation du $\delta^{18}O$ par le modèle, mais uns bonne reproduction du δD. En conséquence, le d-excess est sous-estimé à ~ 11 ‰ par rapport aux données isotopique. La tendance à l'augmentation du d-excess depuis la côte vers le plateau central antarctique est cependant bien simulée. Enfin, Dittmann et al. (2016) ont comparé la variabilité inter-annuelle du signal isotopique enregistré dans les précipitations à Dome F (3810 m a.s.l.) de février 2003 à janvier 2004 avec les simulations correspondantes.

Tableau 2.5: Description non exhaustive des AGCM équipés des isotopes de l'eau

Laboratoire de développement	Modèle	Référence	Evaluation	Résolution horizontale	Niveaux verticaux	Forçage
National Center for Atmospheric Research (NCAR)	NCAR Community Atmosphere Model 2 (CAM 2)	Lee et al. (2007)	Globale	2,8 °N x 2,8 °E	26	Température de surface de la mer et couverture de la glace de mer issues de simulations du modèle couplé océan-atmosphère CCSM (Kiehl and Gent, 2004; Collins et al., 2006; Hack et al., 2006)
	NCAR Community Atmosphere Model 3 (CAM 3)	Sturm et al. (2010)	Globale	2,8 °N x 2,8 °E	19	
	NCAR Community Atmosphere Model 5 (CAM5)	Nusbaumer (2016)	Globale	1,9 °N x 2,5 °E	30	Etat de l'océan et données de surface du sol de la composante extrait du modèle couplé CESM (Kay et al., 2015)
European Center	ECHAM5-wiso	Werner et al. (2011)	Globale avec un zoom sur l'Antarctique	De 3,8 °N x 3,8 °E à T159 0,75 °N x 0,75 °E	31	ERA-interim (Dee et al., 2011)

Goddard Institute for space studies (GISS)	GISS modelE	Schmidt et al, 2005; Schmidt et al, 2007	Globale	4°N x 5 °E 2 °N x 2,5 °E	20	Différents forçages selon les études (Lewis et al., 2013)
Hadley Center	Hadley Center Atmospheric Model 3 (HadAM3)	Sime et al. (2008)		3,75 °N × 2,5 °E	19	Température de surface de la mer et couverture de la glace de mer issues du modèle couplé HadCM3 (Gordon et al., 2000)
National Centers for Environmental Prediction (NCEP)	NCEP Isotopic Atmospheric Global Spectral *Model (*IsoGSM)	Yoshimura et al. (2008)		1,85 °N x 1,85 °E	28	NCEP Reanalysis 2 (Saha et al., 2014)
Laboratoire de Météorologie Dynamique (LMD)	Laboratoire de Météorologie Dynamique Zoom 4 (LMDZ4)	Risi et al. (2010)	Globale	3,75 °N × 2,5 °E	19	ERA-interim (Dee et al., 2011)
University of Tokyo	Model for Interdisciplinary Research on 3.2 Climate (MIROC3.2)	Kurita et al. (2011)		1,1 °N × 1,1 °E	40	Climatologie des températures de surface de mer mensuelles
Melbourne University	Melbourne University General Circulation Model (MUGCM)	Noone and Simmonds (2002)	Globale	3,25 °N × 5,625 °E	9	Climatologie des températures de surface de mer mensuelles

Ils reportent un coefficient de corrélation de 0,85 pour $\delta^{18}O$ mais de 0,21 pour d-excess. Globalement, l'ensemble de ces évaluations confortent dans l'utilisation du modèle ECHAM5-wiso pour l'interprétation des signaux isotopiques mesurés.

Au cours de ma thèse, Martin Werner (chercheur à l'Institut Alferd Wegner, Bremerhaven, Allemagne) m'a fourni des simulations effectuées par le modèle ECHAM5-wiso à une résolution T106 (i.e. ~ 110 km x 110 km) et sur 31 niveaux verticaux, sur la période 1960-2013, guidé par les réanalyses ERA-40 et ERA-interim (décrire exactement la méthode de nudging). J'ai principalement utilisé la température de surface, la température à 2 m d'altitude, la précipitation, l'évaporation, et δD et $\delta^{18}O$ simulées dans les précipitations.

2.3.5 Rétro-trajectoires

Afin d'étudier l'influence de la circulation synoptique sur les signaux isotopiques, j'ai simulé des rétro-trajectoires de masses d'air. J'ai utilisé le modèle HYbrid Single-Particle Langrangian Integrated Trajectory (HYSPLIT) développé par le « National Oceanic and Atmospheric Administration's (NOAA) Air Research Laboratory » (Draxler and Hess, 1998) (NOAA), librement disponible en ligne (https://ready.arl.noaa.gov/HYSPLIT.php), et qui a déjà été utilisé par la communauté des isotopistes en région polaire (Schlosser et al., 2008; Fernandoy et al., 2012; Markle et al., 2012; Sinclair et al., 2014; Dittmann et al., 2016; Rahaman et al., 2016). Il a aussi déjà été utilisé pour le cas particulier de masses d'air arrivant à DDU (Preunkert et al., 2008; Legrand et al., 2009).

Présentation du modèle HYSPLIT

HYSPLIT est un modèle de transport et de dispersion atmosphérique basé sur un couplage des approches lagrangiennes et eulériennes (Stein et al., 2015), sur une grille tridimensionnelle discrétisée. L'advection est paramétrée par les vents, nécessitant l'intégration d'observations atmosphériques. Par soucis de disponibilités, j'ai choisi d'utiliser les rénanalyses NCEP-2 (« National Center of Environmental Prediction – Department of Energy», NCEP-2, Kanamitsu et al., 2002), et non ERA-interim. Les réanalyses NCEP utilisent une méthode d'assimilation variationnelle en trois dimensions (3DVAR). Le maillage tridimensionnel est défini à une résolution de 1,89 °N x 1,89 °E et 28 niveaux verticaux.NCEP-2 est une version améliorée des réanalyses initiales NCEP1 (Kalnay et al., 1996), qui couvre la période de 1979 à nos jours.

Calculs de rétro-trajectoires HYSPLIT pour l'étude de la circulation synoptique sur le signal isotopique enregistré dans des carottes de glace d'Antarctique

Une des premières études utilisant le modèle de rétro-trajectoires HYSPLIT pour l'interprétation des compostions isotopiques de l'eau en Antarctique a consisté à identifier les origines des masses d'air grâce à HYSPLIT afin de paramétrer les conditions initiales d'évaporation des masses d'air (humidité et température de surface de la mer) dans le modèle isotopique MCIM (Mixed Cloud Isotopic Model, Ciais and Jouzel, 1994), en extrayant les productions d'humidité et de température de surface de la mer simulées par l'AGCM ECHAM4 et correspondant aux origines des masses d'air (Helsen et al., 2006; Helsen et al., 2007). Leurs résultats ont montré que la distribution spatiale de la relation linéaire δ^{18}O-température issue des simulations isotopiques ainsi générées est très variable, confirmant qu'une commune formule de la reconstruction de la température pour l'ensemble de l'Antarctique ne peut s'appliquer. Ils ont ainsi souligné la possibilité que le signal isotopique soit affecté par des fluctuations saisonnières des trajectoires du transport d'humidité.

Le d-excess (cf. Section 1.2.2) permet d'identifier ces changements puisqu'il dépend principalement des conditions aux sources d'évaporation. Un certain nombre d'études a de fait, exploité des rétro-trajectoires pour identifier leur origine et les classer en différentes catégories (e.g. continentales, océaniques) afin de les comparer aux variations du d-excess enregistré à un site spécifique. Markle et al. (2012) ont montré que la variabilité de la direction des rétro-trajectoires venant de l'océan était corrélée à la variabilité du d-excess enregistré dans une carotte du secteur de Ross à l'échelle saisonnière et inter-annuelle. De façon similaire, Fernandoy et al. (2012) ont calculé les rétro-trajectoires des évènements de précipitation entre 2008 et 2010 en Péninsule. Ils ont montré que les précipitations prenaient leur source au sud de l'océan Pacifique (entre 50 °S et 60 °S), mais aussi bien plus localement, au sud de 60 °S, en mer de Bellingshausen. Enfin, ils ont montré que la valeur moyenne du d-excess enregistré dans les carottes de glace extraites à la pointe de la Péninsule dépend de l'origine des rétro-trajectoires. De manière similaire, Schlosser et al. (2008) ont montré que la valeur moyenne du d-excess enregistré dans de la neige fraîche à la station de Neumayer en Terre de la Reine Maud sur la période 1981-1999 est associée à l'origine des rétro-trajectoires.

D'autres études ont testé la relation qui lie le d-excess aux conditions d'évaporation. Dittmann et al. (2016) ont interrogé la corrélation entre le d-excess mesuré dans les précipitations de Dome F de février 2003 à janvier 2004, et le d-excess calculé par le modèle isotopique MCIM (Mixed Cloud Isotopic Model, Ciais and Jouzel, 1994), dont les conditions d'évaporation correspondent à celles données par les calculs de rétro-trajectoires HYSPLIT. Ils n'ont cependant trouvé aucune relation significative entre les observations et ces calculs. Fernandoy

et al. (2018) ont effectué un exercice similaire, en utilisant cette fois-ci des mesures isotopiques issues de carottes de glace de Péninsule : ils ont calculé un d-excess théorique à partir de l'humidité et de la température de surface de la mer (Uemura et al., 2008), et ont trouvé une corrélation significative entre les valeurs expérimentales et théoriques.

Enfin, des études très récentes ont considéré le d-excess mesurées le long des carottes de glace, couplées à des mesures chimiques et de rétro-trajectoires afin de reconstruire l'histoire de la glace de mer (Rahaman et al., 2016; Mezgec et al., 2017).

A ce stade, les études basées sur des analyses de corrélations statistiques suggèrent, dans certaines régions (Péninsule antarctique) que la variabilité du d-excess enregistré dans les carottes de glace peut être liée à la variabilité des trajectoires des masses d'air et/ou aux conditions à la surface océanique, mais il n'y a pas encore de compréhension physique quantitative de ces relations.

Au cours de ma thèse, j'ai utilisé des calculs de rétro-trajectoires (HYSPLIT-NCEP), pour explorer les relations entre circulation atmosphérique et signal isotopique enregistré dans les carottes de glace de Terre Adélie, à différentes échelles de temps (cycle saisonnier, évènements remarquables, variabilité inter-annuelle).

Evaluations de rétro-trajectoires de masses d'air arrivant à DDU calculées à partir du modèle HYSPLIT et utilisant les réanalyses NCEP-2

Quelques études sont disponibles vis-à-vis des performances de calculs de rétro-trajectoires de masses d'air arrivant à DDU. Legrand et al. (2009) ont montré que les valeurs d'ozone mesurées à DDU au cours de l'année 2009 sont cohérentes avec la simulation de rétro-trajectoires continentales, suggèrant donc que HYSPLIT capture correctement la distinction entre masses d'air d'origine antarctique ou maritime. Plus récemment, Pépy (2011) a comparé des rétro-trajectoires simulées par le modèle Flexpart (Stohl et al., 2005) utilisant les données ERA, avec celles simulées par HYSPLIT utilisant les données NCEP. Plus précisément, il a comparé les pourcentages de masses d'air arrivant à DDU transportées sur les 24, 48 et 72 dernières heures, issues de simulations HYSPLIT moyennées sur trois altitudes (0, 250 et 500 m au-dessus du sol), et du modèle Flexpart (dont le nombre de rétro-trajectoire est intégré sur une grille de résolution 1 °N x 0,5 °E x 500 m), du 25/12/2010 au 10/01/2011. Bien que les données météorologiques utilisées pour paramétrer les modèles (les réanalyses NCEP pour HYSPLIT, et ERA-interim pour Flexpart) ne sont pas les mêmes, il reporte des variabilités comparables malgré une surestimation de l'advection marine par HYSPLIT par rapport à Flexpart à l'échelle journalière, néanmoins lissée sur trois jours. Cette étude suggère une convergence entre les

réanalyses NCEP et ERA pour la variabilité des trajectoires, même s'il faudrait une comparaison systématique (qui n'a pas été effectuée dans le cadre de cette thèse).

Paramétrisation

L'ensemble des rétro-trajectoires que j'ai simulées a été paramétrées de sorte que le transport s'effectue sur une altitude maximale de 10 000 m au-dessus de la mer (couche troposphérique), et sur 5 jours, avec un pas de temps d'une heure par jour.

Les coordonnées et la date d'arrivée des rétro-trajectoires ont été fixées pour correspondre aux points de carottage et aux périodes couvertes par les carottes de glace que j'ai analysées (cf. Sections 3 et 4). Enfin, l'altitude d'arrivée des masses d'air a été fixée après analyse des radiosondages d'humidité spécifique à Dumont d'Urville (cf. Fig. 2.10, Durre et al., 2006) montrant que la majorité de l'humidité se trouve dans les premiers 2 kilomètres d'altitude. Une comparaison des rétro-trajectoires à 250, 500 et 1500 m d'altitude (cf. Fig. 2.11) a pu montrer que l'origine des masses d'air est peu variable selon l'altitude choisie, que la trajectoire soit tangente au continent (cf. Fig 2.11a et 2.11b), océanique (cf. Fig. 2.11c) ou continentale (cf. Fig. 2.11d). J'ai donc choisi de m'aligner avec des études antérieures en fixant une altitude d'arrivée de 1500 m (e.g. Markle et al., 2012).

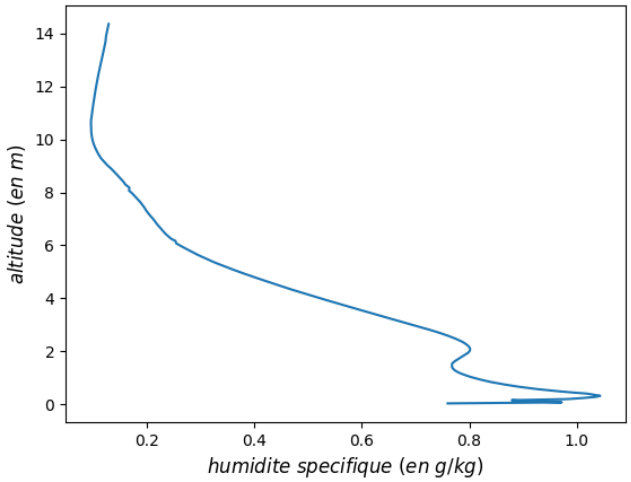

Figure 2.10: Profil vertical de l'humidité spécifique (en g/kg) mesurée par radiosondage à Dumont d'Urville moyenné sur la période 1970-2017 (données extraites de Durre et al., 2006).

Limites

Le couplage du schéma d'interpolation, de la résolution spatiale issus du modèle HYSPLIT, ainsi que les performances des réanalyses NCEP-2 à reproduire les champs de vents, participent à une incertitude de 1 000 km de la position des masses d'air au bout de 5 jours (Stohl et al., 1995; Helsen, 2006). Cette incertitude peut-être davantage estimée si on prend en compte les systèmes convectifs (fronts de précipitations, tempêtes) non reproduits par le modèle HYSPLIT (incertitude associée non quantifiable). Aussi on notera que cette méthode ne permet pas d'extraire l'information relative à l'humidité transportée.

Les résultats issus de ces calculs sont donc à prendre avec un regard critique. Cependant cette procédure a été le meilleur moyen d'estimer l'origine du transport d'humidité dans le temps imparti de ma thèse.

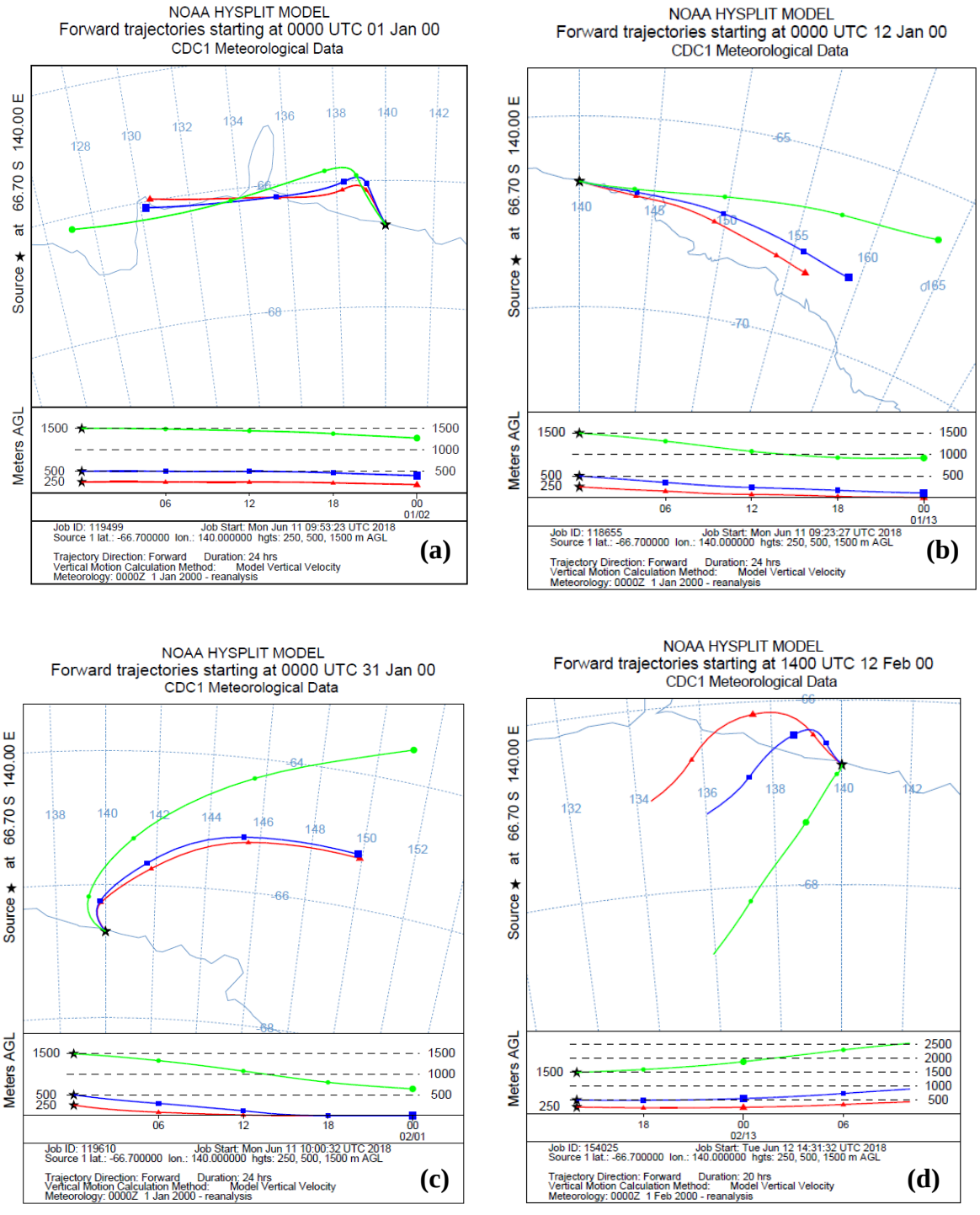

Figure 2.11 : Rétro-trajectoires représentatives des différentes catégories de trajectoires identifiées pour Dumont d'Urville, simulées par le modèle HYSPLIT sur les 24 dernières heures de masses d'air arrivant à Dumont d'Urville (66.7 °S, 140 °E) à des altitudes de 250 m (courbes rouges), 500 m (courbes bleues) et 1500 m (courbes vertes) les (a) 01er janvier 2000, (b) 12 janvier 2000, (c) 31 janvier 2000 et (d) 12 Février 2000.

2.4 Tests sur les séries temporelles

Afin de décrire et comparer tous les outils à ma disponibilité, i.e. enregistrements issus des carottes de glace, séries temporelles d'observations météorologiques, et simulations, j'ai principalement effectué des calculs statistiques de base en utilisant les modules de python (McKinney, 2011; Walt et al., 2011; Jones et al., 2014) disponibles:

Pour chaque série temporelle:

- Des descriptions statistiques : moyenne, écart-type, et extrema pour chaque série temporelle.
- J'ai considéré des valeurs comme étant « anormales » ou « remarquables » lorsqu'elles se situaient hors de l'intervalle borné par la moyenne plus ou moins deux écart-types.

Pour le calcul de tendances et de corrélations entre deux séries temporelles :

- Calcul de régressions linéaires, au sens des moindres carrés, en utilisant la fonction python scipy.stats.linregress. J'ai fait l'hypothèse que les relations étaient significatives pour une p-value inférieure ou égale à 0.05, où p est basé sur l'hypothèse nulle que la pente est égale à 0.

2.5 Conclusion

Au cours de ma thèse, j'ai exploité les informations enregistrées dans les carottes de glace forées en Antarctique, et plus particulièrement en Terre Adélie, en les comparant statistiquement à des séries temporelles issues d'observations climatiques régionales (température, accumulation, vents, pression et humidité) et de simulations représentant la circulation synoptique (réanalyses ERA-interim, AGCM ECHAM5-wiso et rétro-trajectoires calculées par le modèle HYSPLIT).

CHAPITRE 3 : ECHAM5-wiso, outil d'interprétation des enregistrements isotopique

3. ECHAM5-wiso, outil d'interprétation des enregistrements isotopiques

3.1 Introduction

Les simulations produites par les modèles de circulation atmosphérique générale sont couramment utilisées dans le but d'améliorer la compréhension de l'information climatique préservée dans les signaux isotopiques enregistrés dans les carottes de glace (Section 1.4.4). Les deux questions principales abordées par la communauté des isotopistes des carottes de glace, et dans lesquelles s'inscrivent ma thèse, sont : (1) le thermomètre isotopique est-il invariable dans le temps et dans l'espace ? et (2) quelle information peut-on extraire du deutérium excess ? (cf. Section 1.5.1).

Dans le cadre de ma thèse, j'ai utilisé le modèle ECHAM5-wiso (Section 2.3.4). Ce modèle a été une première fois évalué par Werner et al. (2011). Plusieurs simulations produites à différentes résolutions (dont celle que j'ai utilisée au cours de ma thèse) ont été comparées, à la base de données surfaciques de compositions isotopiques issues de précipitations, neige fraîche, et glace, constituée par Masson-Delmotte et al. (2008). Cependant, seule la variabilité spatiale a été évaluée, et uniquement pour le paramètre du premier ordre $\delta^{18}O$. L'utilisation du modèle dans le but d'apporter des réponses robustes aux deux questions énoncées précédemment, nécessite donc une évaluation de la variabilité temporelle des isotopes stables de l'eau, tant pour les paramètres isotopiques du premier ordre ($\delta^{18}O$), que du second ordre (deutérium excess).

J'ai donc choisi d'évaluer plus systématiquement les performances du modèle ECHAM5-wiso pour l'Antarctique, en le confrontant à une base de données d'enregistrements isotopiques que j'ai mise à jour. Le résultat de cette analyse est un article publié dans Climate of the Past, et constitue la Section 3.2. Dans cet article, j'ai proposé une démarche pour guider l'interprétation des signaux extraits des carottes de glace antarctiques pour différents paramètres et différentes régions, en prenant en compte la confiance qui peut être accordée aux résultats du modèle (Section 3.2.4). J'ai ensuite, au sein du groupe Antarctica2k, utilisé les résultats de ce modèle pour proposer une méthode de calibration permettant, à partir d'une synthèse de données de carottes de glace en Antarctique couvrant les derniers 2000 ans, de reconstruire les variations récentes de température dans différentes régions de l'Antarctique, en y associant une quantification de l'incertitude associée. Ces résultats font l'objet d'un article auquel j'ai contribué, également publié dans Climate of the Past, et qui constitue la Section 3.3.

Ce chapitre se termine par des conclusions (Section 3.4).

3.2 Evaluation du modèle ECHAM5-wiso

Cette étude a été publiée dans le journal *Climate of the Past* (Goursaud et al., 2018). La version ci-retranscrite a simplement été formatée pour être intégrée au manuscrit de thèse. Je réfère le lecteur à plusieurs reprises à un matériel supplémentaire. Celui-ci est disponible en ligne (https://www.clim-past.net/14/923/2018/, dernier accès : 07/2018).

Abstract. Polar ice core water isotope records are commonly used to infer past changes in Antarctic temperature, motivating an improved understanding and quantification of the temporal relationship between $\delta^{18}O$ and temperature. This can be achieved using simulations performed by atmospheric general circulation models equipped with water stable isotopes. Here, we evaluate the skills of the high-resolution water-isotope-enabled atmospheric general circulation model ECHAM5-wiso (the European Centre Hamburg Model), nudged to European Centre for Medium-Range Weather Forecasts (ECMWF) reanalysis using simulations covering the period 1960-2013 over the Antarctic continent.

We compare model outputs with field data, first with a focus on regional climate variables and, second on water stable isotopes, using our updated dataset of water stable isotope measurements from precipitation, snow, and firn/ice core samples. ECHAM5-wiso simulates a large increase in temperature from 1978 to 1979, possibly caused by a discontinuity in the European Reanalyses (ERA) linked to the assimilation of remote sensing data starting in 1979.

Although some model-data mismatches are observed, the (precipitation minus evaporation) outputs are found to be realistic products for surface mass balance. A warm model bias over central East Antarctica and a cold model bias over coastal regions explain first-order $\delta^{18}O$ model biases by too-strong isotopic depletion on coastal areas and underestimated depletion inland. At the second order, despite these biases, ECHAM5-wiso correctly captures the observed spatial patterns of deuterium excess. The results of model-data comparisons for the inter-annual $\delta^{18}O$ standard deviation differ when using precipitation or ice core data. Further studies should explore the importance of deposition and post-deposition processes affecting ice core signals and not resolved in the model.

These results build trust in the use of ECHAM5-wiso outputs to investigate the spatial, seasonal and inter-annual $\delta^{18}O$-temperature relationships. We thus make the first Antarctica-wide synthesis of prior results. First, we show that local spatial or seasonal slopes are not a correct surrogate for inter-annual temporal slopes, leading to the conclusion that the same isotope-temperature slope cannot be applied for the climatic interpretation of Antarctic ice core for all timescales. Finally, we explore the phasing between the seasonal cycles of deuterium excess and $\delta^{18}O$, as a source of information on changes in moisture sources affecting the $\delta^{18}O$-

temperature relationship. The few available records and ECHAM5-wiso show different phase relationships in coastal, intermediate and central regions.

This work evaluates the use of the ECHAM5-wiso model as a tool for the investigation of water stable isotopes in Antarctic precipitation, and calls for extended studies to improve our understanding of such proxies.

Résumé. Les enregistrements d'isotopes de l'eau issus des carottes de glace polaires sont couramment utilisés pour reconstruire les changements passés de la température de l'Antarctique, motivant une meilleure compréhension, ainsi qu'une quantification de la relation temporelle entre le $\delta^{18}O$ et la température. Ces exploitations peuvent être réalisées par l'utilisation de simulations effectuées par des modèles atmosphériques de circulation générale équipés des isotopes stables de l'eau. Ici, nous évaluons les capacités du modèle atmosphérique de circulation générale de haute résolution ECHAM5-wiso (the European Centre Hamburg Model), équipé des isotopes stables de l'eau, forcé au réanalyses du centre européen de prévisions météorologiques (European Centre for Medium-Range Weather Forecasts, ECMWF), pour la période 1960-2013 et sur l'ensemble du continent antarctique.

Nous avons comparé les sorties de modèle avec les données de terrain, tout d'abord en nous concentrant sur les variables du climat régional, puis sur les isotopes stables de l'eau, en utilisant notre base de données mise à jour des isotopes stables de l'eau issues des précipitation, de la neige, et des échantillons de carotte de glace. ECHAM5-wiso simule une importante augmentation de la température de 1978-1979, potentiellement due à une discontinuité dans les réanalyses européennes (ERA) liée à l'assimilation des satellites à partir de 1979.

Bien que nous observions des biais entre le modèle et les données, les sorties de (précipitation – évaporation) sont réalistes comparées au bilan de masse de surface. Un biais chaud simulé au centre de l'Antarctique de l'Est et un biais froid sur les régions côtières expliquent des biais du paramètre de premier ordre $\delta^{18}O$, par un appauvrissement isotopique trop fort en région côtière et sous-estimé à l'intérieur du continent. Au second ordre, malgré ces biais, ECHAM5-wiso capture correctement le gradient spatial observé du deutérium excess. Les résultats de la comparaison modèle-données pour l'écart type inter-annuel du $\delta^{18}O$ sont différents selon que l'on utilise des données de précipitation ou de carottes de glace. Des études plus approfondies devraient enquêter l'importance des processus de dépôt et de post-dépôt affectant les signaux enregistrés dans les carottes de glace et non résolus dans le modèle.

Ces résultats renforcent la confiance que nous accordons au modèle ECHAM5-wiso pour exploiter les relations $\delta^{18}O$-température aux échelles spatiale, saisonnière et inter-annuelle. Nous avons donc effectué la première synthèse pour l'ensemble de l'Antarctique.

Tout d'abord, nous avons montré que les pentes locales saisonnières et spatiales ne peuvent pas remplacer les pentes inter-anuelles, nous amenant à la conclusion qu'une même pente isotope-température ne peut pas être appliqué pour l'interprétation des carottes de glace d'Antarctique quelle que soit l'échelle de temps. Finalement, nous explorons le déphasage entre les cycles saisonniers du deutérium excess et du $\delta^{18}O$, comme marqueur des changements des sources d'humidité affectant la relation $\delta^{18}O$-température. Le peu d'enregistrements disponible, ainsi que les simulations d'ECHAM5-wiso montrent différentes phase en régions côtières, intermédiaires, et dans les régions centrales.

Ce travail évalue l'utilisation du modèle ECHAM5-wiso comme outil d'exploitation des isotopes stables de l'eau dans les précipitations d'Antarctique, et appelle à d'autres études pour améliorer notre compréhension de tels marqueurs.

3.2.1 Introduction

The Antarctic climate has been monitored from sparse weather stations, providing instrumental records starting at best in 1957 (Nicolas and Bromwich, 2014). Water stable isotopes in Antarctic ice cores are key to expanding the documentation of spatio-temporal changes in polar climate and the hydrologic cycle (Jouzel et al., 1997) for the recent past (PAGES 2k Consortium, 2013; Stenni et al., 2017) as well as for glacial-interglacial variations (Jouzel et al., 2007; Schoenemann et al., 2014). Water stable isotopes measured along ice cores were initially used to infer Antarctic past temperatures using the spatial isotope-temperature slope (Lorius et al., 1969). The focus on inter-annual variations is motivated by the goal to quantifying temperature changes at the Earth's surface, including Antarctica, during the last millennia, to place current changes in the perspective of recent natural climate variability (Jones et al., 2016), to understand the drivers of this variability, and to test the ability of climate models to correctly represent it. This timescale is relevant for the response of the Antarctic climate to e.g. volcanic forcing, and for the Antarctic climate fingerprint of large-scale modes of variability such as ENSO and the Southern Annular Mode (Smith and Stearns, 1993; Turner, 2004; Stammerjohn et al., 2008; Schroeter et al., 2017). The various climate signals potentially recorded in precipitation isotopic composition are, however, difficult to disentangle.

First, the original signal from precipitation may be altered due to deposition and post-deposition (e.g. Sokratov and Golubev, 2009; Jones et al., 2017; Münch et al., 2017; Laepple et al., 2018). Wind erosion and sublimation during or after precipitation have long been known to affect ice core records (Eisen et al., 2008; Grazioli et al., 2017). Other processes such as melt and diffusion processes can also alter the preservation of isotopic signals in firn and ice and cause smoothing of the initial snowfall signals (Johnsen, 1977; Whillans and Grootes, 1985; Johnsen

et al., 2000; Jones et al., 2017). So far, the mechanisms of such post-deposition processes on the alteration of the initial precipitation signals are not fully understood and quantified (Touzeau et al., 2017). Second, the Antarctic snowfall isotopic composition may be affected by the origin of moisture and the associated evaporation conditions, changes in the relationship between condensation and surface temperature, by changes in the intermittency of precipitation (e.g. Sime et al., 2009; Hoshina et al., 2014; Touzeau et al., 2016). Although the surface snow isotopic composition signal has classically been interpreted as a precipitation-weighted deposition signal (Krinner and Werner, 2003), recent studies evidenced isotopic exchanges between the Antarctic snow surface and the atmosphere associated with snow metamorphism occurring at the diurnal and sub-annual scales (Steen-Larsen et al., 2014; Casado et al., 2016; Ritter et al., 2016; Touzeau et al., 2016).

Second, the climatic interpretation of water stable isotopes in Antarctic ice cores is still challenging. Quantitative approaches have relied on empirical relationships the use of theoretical and atmospheric models including water stable isotopes. Pioneer studies evidenced a close linear relationship between the spatial distribution of water stable isotopes and local temperature (e.g. Lorius and Merlivat, 1975), and explained this feature as the result of the distillation along air mass trajectories. Thereupon, local temperature (i.e. at a specific site) was reconstructed using $\delta^{18}O$ measurements and based on the slope of the aforementioned spatial empirical relationship, as a surrogate for relationships at annual to multi-annual scales. However, recent data syntheses have shown that other effects had to be taken into account (e.g. Masson-Delmotte et al., 2008): It was found that Antarctic snowfall isotopic composition is also linked to the initial vapour isotopic composition (Stenni et al., 2016), atmospheric transport pathways (Schlosser et al., 2008; Dittmann et al., 2016), Antarctic sea ice extent (Bromwich and Weaver, 1983; Noone and Simmonds, 2004; Holloway et al., 2016) and local condensation temperature, itself related to surface temperature through complex boundary layer processes (Krinner et al., 2007). Evaporation conditions, transport and boundary layer processes may vary through time, from seasonal (Fernandoy et al., 2018) to annual or multi-annual scale, thereby potentially distorting the quantitative relationship between snow isotopic composition and local surface air temperature estimated empirically for present-day conditions (Jouzel et al., 1997).

Model studies have been key to quantitatively exploring the spatio-temporal aspects of the relationships between precipitation isotopic composition and temperature (Jouzel et al., 2000). Mixed-cloud isotopic models have been used to propose a coherent interpretation of $\delta^{18}O$ and δD data in terms of changes in site and source temperatures (Uemura et al., 2012), or to simulate isotopic variations along individual atmospheric trajectories (Dittmann et al., 2016). However, such theoretical distillation models rely on the closure assumption at the ocean surface to

calculate the initial evaporation isotopic composition, and do not account for atmospheric dynamics and mixing of air masses (Jouzel and Koster, 1996; Delmotte et al., 2000). Atmospheric general circulation models equipped with water stable isotopes offer a physically coherent, three-dimensional framework to investigate the weather and climate drivers of Antarctic precipitation isotopic composition (Jouzel et al., 2000). They play a key role in assessing how different boundary conditions (e.g. changes in orbital forcing, changes in atmospheric greenhouse gas concentration) affect the simulated relationships between precipitation isotopic composition and climate variables. Most of these simulations support the idea that the present-day isotope-temperature spatial relationship is a good approximation for the relationships between glacial conditions and today (Delaygue et al., 2000; Werner et al., in press), with one exception (Lee et al., 2008). One study used climate projections in response to increased atmospheric CO_2 concentration to explore isotope-temperature relationships in a world warmer than today and suggested a changing temporal, isotope-temperature relationship, due to changing covariance between temperature and precipitation (Sime et al., 2009). Several observational and modelling studies have also evidenced different isotope-temperature relationships between the spatial relationship and those calculated at the seasonal (Morgan and van Ommen, 1997), or inter-annual scale (Schmidt et al., 2007).

Our study is motivated by the need for a synthesis over all of Antarctica, using a proper interpretation of processes that affect water stable isotopes on the appropriate spatial and temporal scales. It aims to address the following questions: (i) what is the performance of a state-of-the-art atmospheric general circulation model with respect to existing Antarctic observations of spatio-temporal variations in temperature, surface mass balance, precipitation and snow isotopic composition for present day? (ii) What can we learn from such a model for the regional relationships between isotopic composition from the precipitation and temperature at the inter-annual scale for the recent past, and considering all of Antarctica?

For this purpose, we focus on the high-resolution atmospheric general circulation model equipped with water stable isotopes ECHAM5-wiso (the European Centre Hamburg model) which demonstrated remarkable skills for Antarctica (Werner et al., 2011). We explore a simulation performed for the period 1960-2013, in which the atmospheric model is nudged to the European Reanalyses (ERA) ERA-40 and ERA-interim reanalyses (Uppala et al., 2005), ensuring that the day-to-day simulated variations are coherent with the observed day-to-day variations in synoptic weather and atmospheric circulation (see Butzin et al., 2014 for more explanation). This framework is crucial to performing comparisons between simulations and observations for temporal variations. Second, we compile a database of precipitation, snow, and firn-ice isotopic composition, using data from precipitation sampling and ice core records and

considering $\delta^{18}O$ and deuterium excess (hereafter, d). These methods are described in Section 3.2.2. We then compare the model outputs with the available datasets (Section 3.2.3). After evaluating the near-surface temperature and the surface mass balance (hereafter SMB, Section 3.2.3.1), we focus on the water stable isotopes (Section 3.2.3.2). We emphasise spatial patterns, the magnitude of inter-annual variability (Sections 3.2.3.2.1 and 3.2.3.4), the pattern and the amplitude of seasonal variations (Section 3.2.3.2.2 and 3.2.3.4). We explore the simulated and estimated isotope-temperature relationships (Section 3.2.3.3) and the relationships between d and $\delta^{18}O$ (Section 3.2.3.4). Highlighting the strengths and limitations of the model (Section 3.2.3.5), we use the simulation framework to explore the $\delta^{18}O$-temperature relationship (Section 3.2.4.1) and the phase lag between seasonal variations in d and $\delta^{18}O$ (Section 3.2.4.2). Finally, we focus on the implications of our results for the climatic interpretation of water stable isotope records for seven Antarctic regions (central plateau, coastal Indian, Weddell Sea coast, West Antarctic Ice Sheet, Victoria Land, and Droning Maud Land). The Antarctica2k group (Stenni et al., 2017) indeed identified these seven Antarctic regions, which are geographically and climatically consistent, to produce regional temperature reconstructions using ice core records. The results of our study thus contribute to the reconstruction of past Antarctic climate spanning the last 2000 years (the Antarctica2k initiative) of the Past Global Changes (PAGES) PAGES2K project (PAGES 2k Consortium, 2013), by providing quantitative calibrations of the regional temperature reconstructions using ice core water stable isotope records.

3.2.2 Material and methods

3.2.2.1 Observations and reanalysis products

3.2.2.1.1 Temperature and surface mass balance instrumental records

Station temperature records have been extracted from the READER database (https://legacy.bas.ac.uk/met/READER, last access: 08/2017; Turner et al., 2004). We have selected surface station data following two conditions: to cover the seven Antarctic regions aforementioned (see Section 3.2.1 and Fig. 3.2.1) with at least one station for each, and to cover the period 1960-2013. As a result, we have selected Neumayer, Mawson, Vostok, Casey, Dumont d'Urville (hereafter DDU), McMurdo, Palmer and Esperanza station surface data. Due to the short duration of surface station records for the 90-180° W sector, we have added data from the automatic weather station (hereafter, AWS) of Dome C, but we have used it with caution as these records are associated with a warm bias in thermistor measurements due to solar radiation when the wind speed is low (Genthon et al., 2011). Finally, we extracted the reconstruction of temperature for Byrd station by Bromwich et al. (2013), based on AWS data and infilled with observational reanalysis data. No record meets our criteria for the Weddell

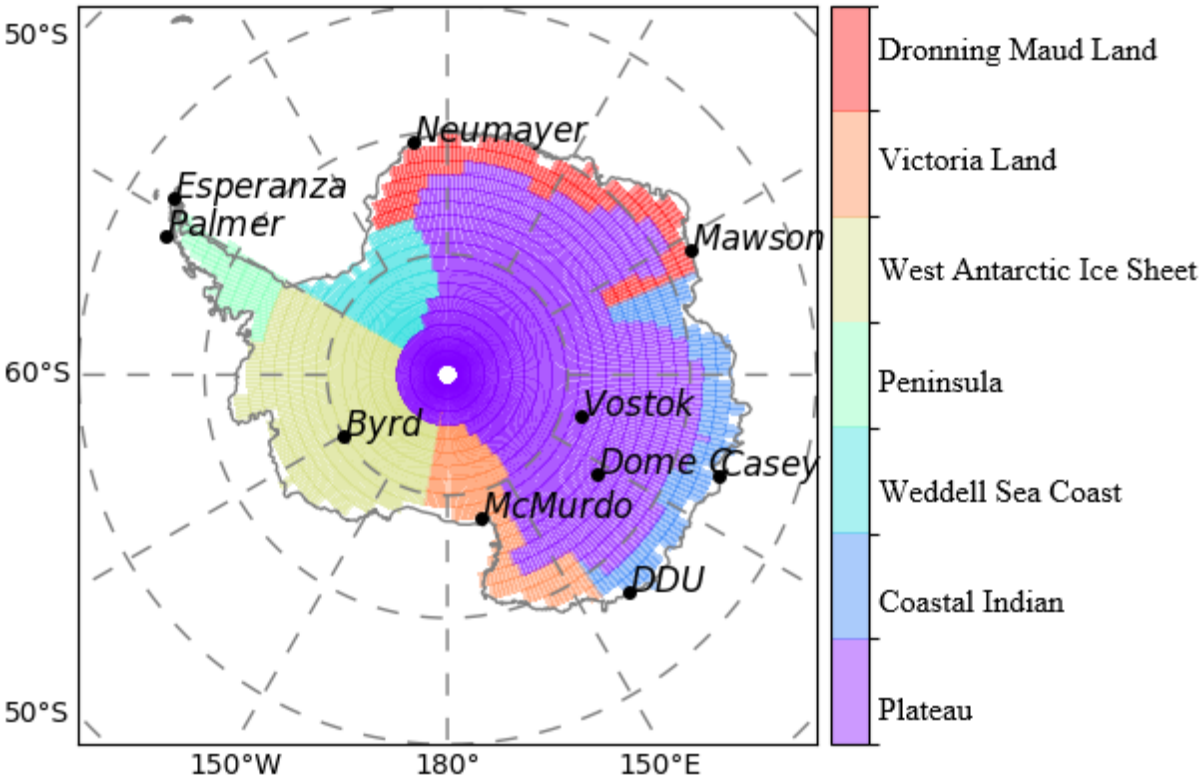

Figure 3.2.1: Spatial distribution of Antarctica in seven regions: East Antarctic Plateau, coastal Indian, Weddell sea, West Antarctic Ice Sheet, Victoria Land and Droning Maud Land regions. The location of the selected READER surface stations: Neumayer, Mawson, Vostok, Dome C, Casey, Dumont d'Urville (noted as "DDU"), McMurdo, Byrd, Palmer and Esperanza.

Sea coast region (Fig. 3.2.1). SMB data have been extracted from the quality-controlled GLACIOCLIM-SAMBA (GC) database (Favier et al., 2013). We have selected data spanning the twentieth century, corresponding to 3242 punctual values, which have then been clustered within the corresponding ECHAM5-wiso grid cells for the calculation of gridded annual average values. As described by Favier et al. (2013), the spatial coverage of SMB field data is particularly poor

in the Antarctic Peninsula, in West Antarctica and along the margins of ice sheet. As a result, SMB is not correctly sampled at elevations between 200 and 1000 m a.s.l., where accumulation rates are the highest. In central Antarctica, areas characterised by wind glaze and megadunes are also insufficiently documented.

3.2.2.1.2 ERA reanalyses

The ECHAM5-wiso model run for this study is nudged to ERA-40 (Uppala et al., 2005) and ERA-interim (Dee et al., 2011) global atmospheric reanalyses produced by the European Centre for Medium-Range Weather Forecasts (ECMWF). ERA-40 covers the period 1957-2002 at a daily resolution, with a spatial resolution of 125 km x 125 km. ERA-Interim covers the period 1979 to present at a 6-hourly resolution, with a spatial resolution of 0.75° x 0.75°.

For comparison with instrumental records and ECHAM5-wiso outputs, we have extracted 2-meter temperature outputs (hereafter 2m-T) over the periods 1960-1978 and 1979-2013 for

ERA-40 and ERA-Interim, respectively, at grid cells closest to the stations where meteorological measurements have been selected (see previous section). We have then calculated annual averages.

3.2.2.1.3 A database of Antarctic water stable isotopic composition from precipitation, surface snow and firn-ice core records

This database consists of water stable isotope measurements performed on different types of samples (precipitation, surface snow or shallow ice cores), and at different time resolutions (sub-annual, annual or multi-annual average values, see S1 in Supplementary Material). Sample data consist of $\delta^{18}O$ and/or δD, providing d, if both $\delta^{18}O$ and δD have been measured. Altogether, we have gathered data from:

1. A total of 101 high-resolution ice core records, including 79 annually resolved records and 18 records with sub-annual resolution (including 5 records with both $\delta^{18}O$ and δD data). These data have been extracted from the Antarctica2k data synthesis (Stenni et al., 2017) with a filter for records spanning the interval 1979-2013, thus restricting the original 122 ice cores to a resulting 101 ice core data. Primary data sources, geographical coordinates and covered periods are reported in Table S1, in Supplementary Material.
2. Average surface snow isotopic composition data compiled by Masson-Delmotte et al. (2008; available on http://www.lsce.ipsl.fr/Phocea/Pisp/index.php?nom=valerie.masson, last access: 08/2017) expanded with datasets from Fernandoy et al. (2012); in this case, the averaging period is based on different time periods, with potential non-continuous records (see Supplementary Material, Table S1).
3. Precipitation records extracted from the International Atomic Energy Agency / Global Network of Isotopes in Precipitation (IAEA / GNIP) network (IAEA/WMO, 2016) with monthly records available for four Antarctic Stations, complemented by daily records for four Antarctic stations from individual studies. Precipitation records from Vostok are available but are excluded from our analysis, due to an insufficient number of measurements (29). See orange part of Table S1 in Supplementary Material.

Each of the 1205 locations have given an individual index number. Data have been processed to calculate time-averaged values (available at 1089 locations for $\delta^{18}O$ values, 879 locations for δD and 770 locations for d). The ice core records with sub-annual resolution were averaged at annual resolution over the period 1979-2013, resulting in 88 ice core records for $\delta^{18}O$ and only 5 for d. Most precipitation records are not continuous and do not cover a full year, preventing the calculation of annual mean values. We have also used sub-annual records from 22 highly

resolved ice cores (including 18 records giving access to $\delta^{18}O$ and 5 records giving access to d) and precipitation sampling from eight stations to characterise the seasonal amplitude. For ice core records, we have only calculated the yearly amplitude from available measurements, as chronologies cannot be established at monthly scales. Note that this database is publicy available on the PANGAEA data archive (https://www.pangaea.de/?t=Cryosphere, last access: 06/2018).

3.2.2.2 ECHAM5-wiso model and simulation

The atmospheric general circulation model (AGCM) ECHAM5-wiso (Roeckner et al., 2003; Werner et al., 2011) captures the global pattern of precipitation and vapour isotopic composition, including the spatial distribution of annual mean precipitation isotopic composition over Antarctica (Masson-Delmotte et al., 2008). Several studies using ECHAM5-wiso have been dedicated to model-data comparisons for temporal variations in other regions (e.g. Siberia, Greenland) (Butzin et al., 2014; Steen-Larsen et al., 2016).

The ECHAM5-wiso outputs analysed in this study consist of daily values simulated over the period 1960-2013. ECHAM5-wiso was nudged to atmospheric reanalyses from ERA-40 (Uppala et al., 2005) and ERA-interim (Dee et al., 2011), which are shown to have good skills for Antarctic precipitation (Wang et al., 2016), surface pressure fields, and vertical profiles of winds and temperatures. The ocean surface boundary conditions (sea ice included) are also prescribed based on ERA-40 and ERA-interim data. Isotope values of ocean surface isotopic composition are based on a compilation of observational data (Schmidt et al., 2007). The simulation was performed at a T106 resolution (which corresponds to a mean horizontal grid resolution of approx. 1.1 ° x 1.1 °) with 31 vertical model levels.

3.2.2.3 Methods for model-data comparisons

In the model, we have extracted specific daily variables for comparison with available data and then averaged them. We have extracted daily 2m temperature outputs (hereafter 2m-T) for comparison with surface air instrumental records, daily (precipitation minus evaporation) outputs (hereafter P-E) for comparison with SMB data, and daily precipitation isotopic composition outputs for comparison with measurements of isotopic composition data in the precipitation. For ice core data, we averaged daily precipitation isotopic composition weighted by the daily amount of precipitation.

For each specific site, we selected the model grid cell including the coordinates of the site. When comparing model outputs with the database of surface data (time-averaged SMB and isotopic composition), available data have been averaged within each model grid cell.

Time selection was dependent on the variables. The 2m-T outputs have been compared with temperature records for the period 1960-2013 based on annual averages and selecting the same years as in the data (see Section 3.1.1). The comparison with other datasets (SMB, snow, and water stable isotopes from firn-ice cores) is restricted to the period 1979-2013 due to concerns about the skills of the reanalyses used for the nudging prior to 1979 in Antarctica (see next section). Daily (P-E) outputs were all extracted over the whole period 1979-2013 and averaged (see Section 3.1.2). For comparison with the surface isotopic database (Section 3.2.1), daily precipitation isotopic composition was averaged by weighting by the daily amount of precipitation over the whole period 1979-2013. For the inter-annual variability (same Section) or annual values (e.g. for d outputs, see Section 4), daily precipitation isotopic composition was averaged by weighting by the daily amount of precipitation for each year of the period 1979-2013. For sub-annual isotopic composition, we used precipitation isotopic compositions (amplitude and mean seasonal cycle) and highly resolved ice cores (amplitude only). Precipitation isotopic composition data consist of a very small number of measurements, sometimes taken before 1979 (e.g. observations from DDU consist of 19 measurements during 1973), and thus model precipitation isotopic composition outputs were extracted at the very exact sampling date. Then, monthly averages were performed and mean seasonal cycles were calculated. The resulting mean seasonal cycles of precipitation isotopic composition were obtained the same way in both precipitation data and the model. For comparison with the mean seasonal amplitude of the highly resolved ice cores, the mean seasonal amplitude was calculated from the mean seasonal cycle based on the monthly averages (weighted by the precipitation amount) over the period covered by the ice core record. .

Finally, for the spatial linear relationships, the calculations reported for each grid cell are based on the relationship calculated by including the 24 grid cells (± 2 latitude steps, ± 2 longitude points) surrounding the considered grid cell.

Our comparisons are mainly based on linear regressions. Note that through the paper, we consider a linear relationship to be significant for a p-value<0.05.

3.2.3 Model skills

In this section, we assess ECHAM5-wiso skills, with the perspective of using the model outputs for the interpretation of water stable isotope data. In polar regions, isotopic distillation is driven by fractionation occurring during condensation, which is itself controlled by condensation temperature (Dansgaard, 1964). We thus first compare ECHAM5-wiso outputs with regional climate records, as this comparison may explain potential isotopic biases. This includes a

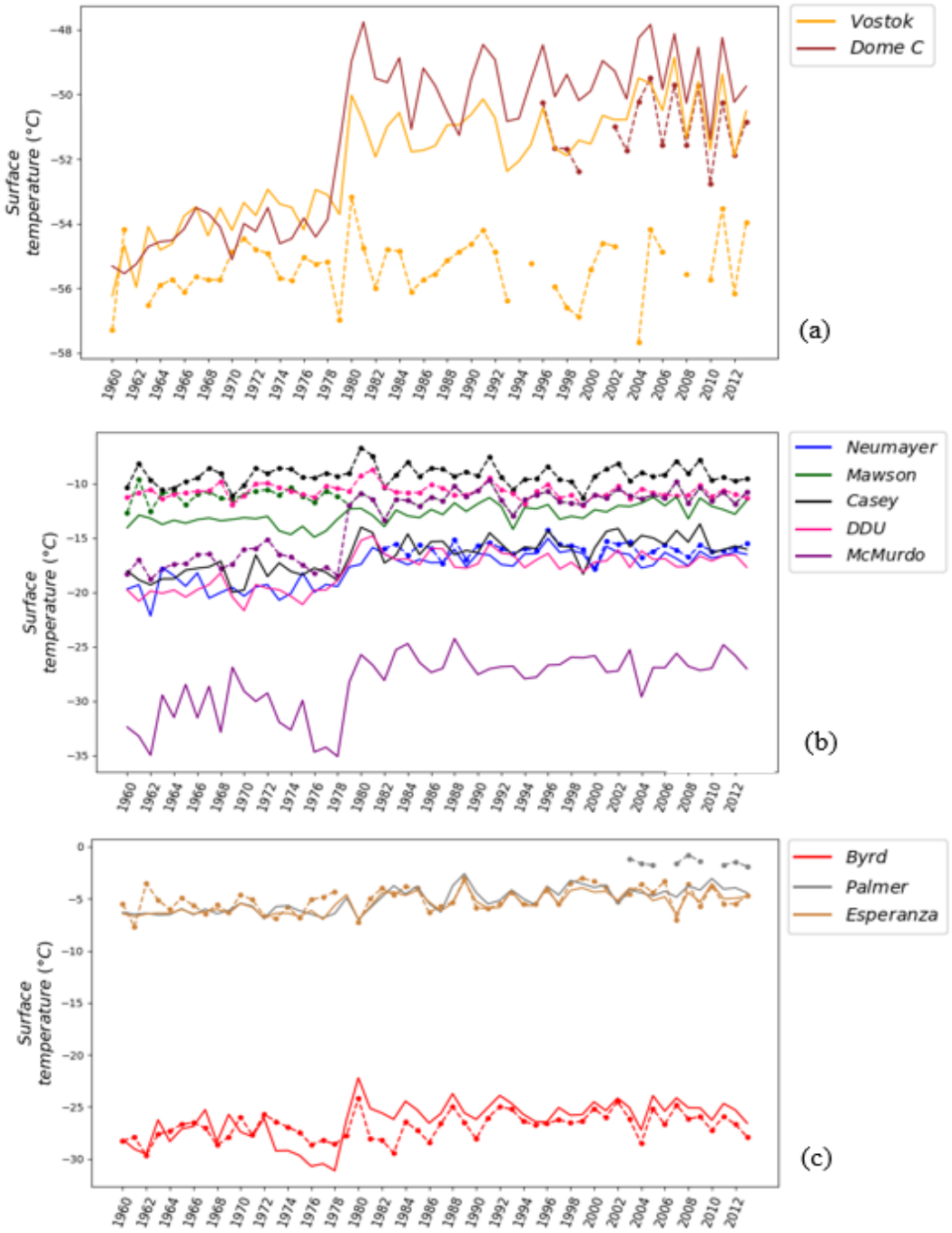

Figure 3.2.2: Surface air temperature (in °C) from station instrumental records (points and dashed lines) and simulated by the ECHAM5-wiso model (solid lines) over the period 1960-2013 for (a) the Plateau, (b) coastal East Antarctic Ice Sheet and (c) the West Antarctic Ice Sheet. Note that the plots were organised by regions to make it more readable: inland (a), coastal (b) and West Antarctic Ice Sheet plus peninsula (c).

comparison with reanalyses in order to explore the role of nudging in model-data mismatches. We then compare ECHAM5-wiso outputs with our isotopic database.

3.2.3.1 Temperature and surface mass balance

3.2.3.1.1 Comparison with instrumental temperatures records and ERA output

We compare time series of instrumental temperature records (filled circles and dashed lines, Fig. 3.2.2) with model outputs (solid lines, Fig. 3.2.2) from 1960 to 2013. This comparison first

Table 3.2.1: Differences between observed (READER) and simulated (ECHAM5-wiso) annual surface air temperature: observed average (noted as "observed μ", in °C), average difference (noted as "μ differences", in °C), standard deviation from observations (noted as "observed σ", in °C) and standard deviation from the model (noted as "simulated σ", in °C) for the period 1979-2013.

	Neumayer	Mawson	Vostok	Casey	Dome C	DDU	McMurdo	Byrd	Palmer	Esperanza
Observed										
μ (°C)	-16.0	-11.2	-55.4	-9.2	-51.1	-10.7	-13.4	-26.9	-1.5	-5.1
μ differrences (°C)	-0.8	-1.6	3.2	-7.3	1.7	-7.2	-14.9	1.4	-2.8	-0.3
Observed σ (°C)	0.67	0.74	0.99	0.92	0.97	0.66	0.74	1.2	0.33	1.1
Simulated σ (°C)	0.79	0.71	1.00	1.10	1.20	0.80	1.70	1.4	0.96	0.84

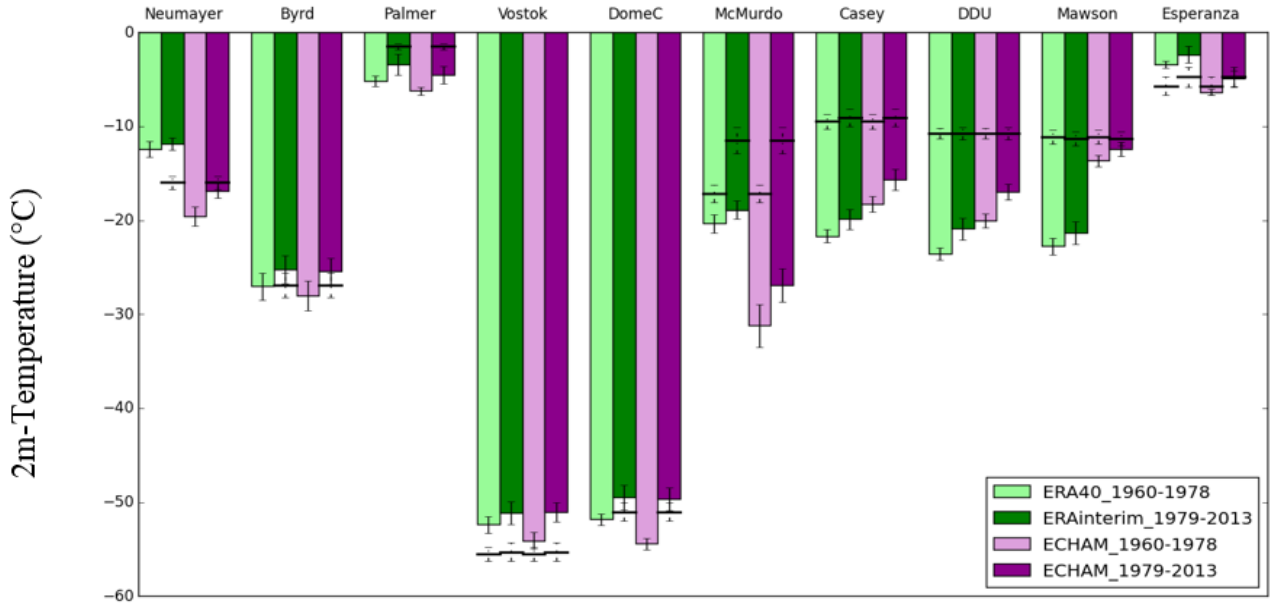

Figure 3.2.3: 2m temperature outputs (in °C) from ERA-40 (light green), ERA-interim (dark green) and ECHAM5-wiso outputs over the periods 1960-1979 (light purple) and 1979-2013 (dark purple) at the locations of Neumayer, Byrd, Palmer, Vostok, Dome C, McMurdo, Casey, Dumont d'Urville (written as DDU), Mawson and Esperanza stations. Horizontal black lines correspond to the mean data. Vertical black lines correspond to inter-annual standard deviations: dotted lines are associated with data, while solid lines are associated with model outputs (ERA or ECHAM).

highlights local offsets between observed and simulated mean values at each site, without a systematic overall warm or cold bias. Table 3.2.1 reports the statistical analysis of annual differences between observations and simulations (observed mean, mean difference between the data and the model outputs, observed versus simulated standard deviation). ECHAM5-wiso has a cold bias for 7 out of 10 stations. While this bias is less than 2°C for Dronning Maud Land (Mawson and Neumayer) and over the peninsula (Palmer and Esperanza), it reaches 7°C for the coastal Indian region (Casey and Dumont d'Urville) and is very strong over the Victoria Land region (McMurdo), reaching 15°C. This cold bias may be due to the model resolution and the location of coastal stations in the ice-free region, where the small-scale topographic features are not accounted for at the model resolution. In contrast, ECHAM5-wiso has a warm bias for all the stations located inland (Vostok, Dome C and Byrd). Werner et al (2011) also reported this warm bias for the central Antarctic Plateau, and suggested that it could be linked to problems in correctly simulating the polar atmospheric boundary layer. Our comparison also shows that the simulated inter-annual temperature variability is larger than observed for seven out of nine sites, and particularly overestimated for locations such as DDU, McMurdo and Palmer, where the cold bias is large.

Figure 3.2.2 depicts a sharp simulated increase in temperature from 1978 to 1979 for all stations, except for the peninsula region (Esperanza and Palmer). Such a feature is not displayed in instrumental records, with one exception, at McMurdo (Fig. 3.2.2). As a result, the model-data correlation coefficient for McMurdo is higher over 1960-2013 than over 1979-2013 (Table 3.2.2), possibly because it is dominated by the sharp increase just prior to 1979. For all other stations, the correlation coefficient is significantly higher in 1979-2013 than in 1960-2013. In order to assess whether ECHAM5-wiso reproduces the temperature bias displayed by ERA-40 (Bromwich et al., 2007), we compare outputs from ERA-40 and ERA-interim (green bars, Fig. 3.2.3) with ECHAM5-wiso outputs (purple bars, Fig. 3.2.3) nudged by these reanalyses (i.e. over 1960-1978 and 1979-2013, respectively) and with the station temperature data (horizontal black lines, Fig. 3.2.3).

All datasets reveal a cold bias simulated by both the reanalyses and ECHAM5-wiso at all stations but Byrd and Vostok over the two periods (only over 1960-1978 for Neumayer and Esperanza), but this bias is larger over the period 1960-1978 compared to the period 1979-2013. This finding supports our earlier suggestion for Dumont d'Urville (Goursaud et al., 2017) that the 1978-1979 shift simulated by ECHAM5- wiso arises from the nudging to ERA-40 reanalyses. We note that mean values and the amplitude of inter-annual variations are different for ECHAM5-wiso and ERA (not shown), as expected from different model physics despite

the nudging technique. This finding has led us to restrict, as far as possible, the subsequent analysis of the ECHAM5-wiso outputs to the period 1979-2013.

For this period, marked by small temperature variations, we note that the correlation coefficient between data and model outputs (Table 3.2.2) is very small for McMurdo (r=0.2) and rather small for Vostok (r=0.6), questioning the ability of our simulation to resolve the drivers of inter-annual temperature variability at these locations. We observe that the model reproduces the amplitude of inter-annual variations, with a tendency to underestimate the variations as shown by model-data slopes from 0.6 to 1°C per °C. As a result, ECHAM5-wiso underestimates the magnitude of inter-annual temperature variability for these central regions of the West and East Antarctic Ice Sheet. It will therefore be important to test whether similar caveats arise for water isotopes.

Table 3.2.2: Linear relationship between surface temperatures (in °C) from station instrumental records and ECHAM5-wiso outputs (in °C) over the periods 1960-2013 and 1979-2013: the slope (in °C °C-1), the correlation coefficient (noted as "r") and the p-value. Data are not reported for 1960-2013 for stations for which records only cover the second period (1979-2013). Numbers in brackets correspond to standard errors.

	Period 1960-2013			Period 1979-2013		
	slope (in °C °C^{-1})	r	p-value	slope (in °C °C^{-1})	r	p-value
Neumayer				0.8 (<0.1)	0.8	<0.001
Mawson	0.5 (0.2)	0.4	0.002	0.8 (<0.1)	0.9	<0.001
Casey	1.1 (0.2)	0.6	<0.001	0.9 (0.1)	0.9	<0.001
Dome C				1.0 (<0.1)	0.9	<0.001
DDU	1.0 (0.4)	0.4	0.004	1.1 (0.1)	0.9	<0.001
McMurdo	0.8 (<0.1)	0.8	<0.001	0.3 (0.2)	0.2	0.2
Byrd	1.1 (0.2)	0.7	<0.001	0.8 (0.1)	0.8	<0.001
Palmer				0.7 (0.3)	0.7	0.05
Esperanza	0.7 (<0.1)	0.7	<0.001	0.7 (<0.1)	0.9	<0.001

3.2.3.1.2 Comparison with GLACIOCLIM database accumulation

For each grid cell in which at least one stake record is available, we have calculated the ratio of the P-E values (which we use as a surrogate for accumulation) simulated by ECHAM5-wiso to the averaged SMB estimate for that grid region based on stake measurements (Fig. 3.2.4a). Due to the limited number of grid cells containing SMB data points from 1979 to 2013 (100 cells), located almost only on the East Antarctic Ice Sheet, we have decided to use the dataset covering the entire twentieth century (521 cells) spread over the continent. The spatial distribution of

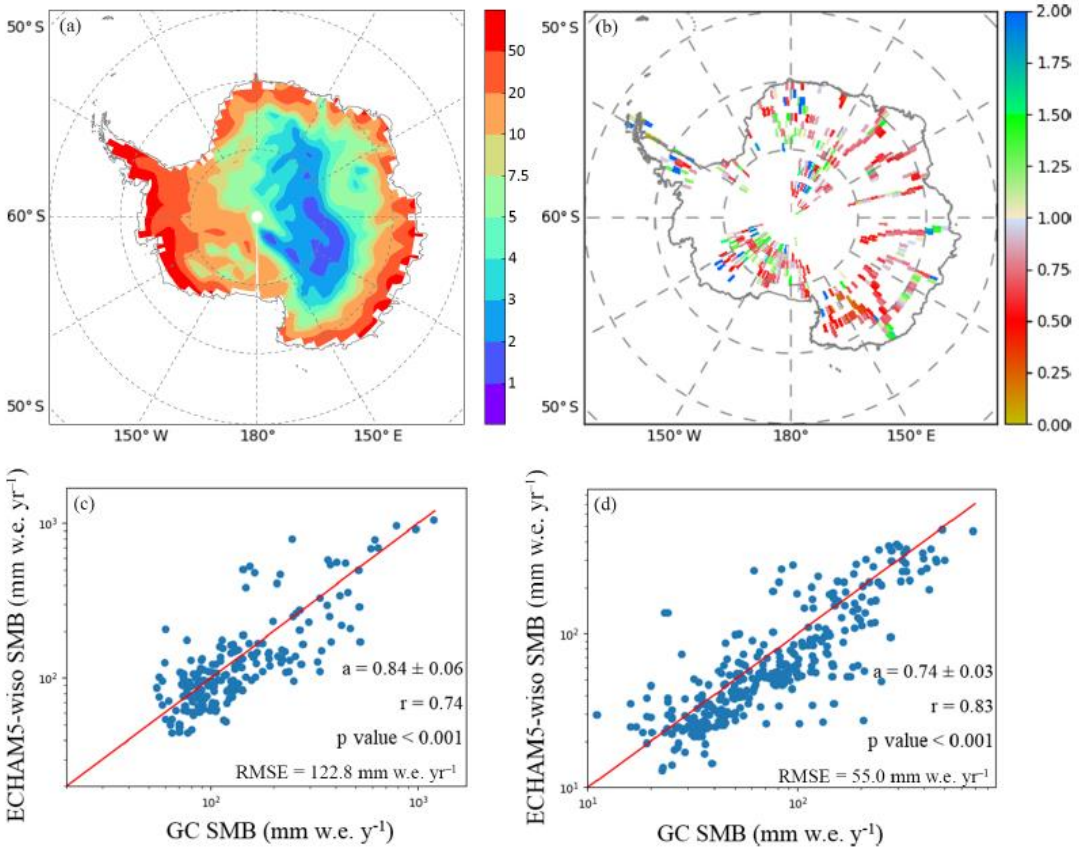

Figure 3.2.4: Comparison of the GLACIOCLIM (hereafter and noted in the plots "GC") SMB database averaged within the ECHAM5-wiso grid cells and the SMB (i.e. precipitation – evaporation) simulated by the model, with the spatial distribution of the accumulation (a) as simulated by the model (in cm w.e. y^{-1}), (b) the ratio of the ECHAM5-wiso annual accumulation (precipitation minus evaporation) to the GC averaged SMB (no unit), and GC-averaged SMB values against SMB values simulated by the model (blue dots) associated with the corresponding linear relationships (red solid line); displayed at the logarithm scale for elevation ranges of 0-2200 m a.s.l. (with the upper limit excluded) (c) and 2200-4000 m a.s.l. (d).

SMB is well captured by ECHAM5-wiso, with decreasing SMB values from the coast to the interior plateau (Fig. 3.2.4a). However, the model quantitatively shows some discrepancies when compared with the GC database. The area-weighted (by the model grid cells) mean GC SMB is 141.3 mm w.e. y^{-1}, while the simulated area-weighted mean P-E over the same model grid is 126.6 mm w.e. y^{-1}. This underestimation covers 69.7% of the compared areas. The 30.3% remaining areas associated with an overestimation of the model are located in sparse regions like in the north of the plateau, and over coastal areas (Fig. 3.2.4b). Note that the low P-E rates over the plateau (75 mm w.e. y^{-1}, see Fig. 3.2.4a) counterbalance the local overestimation at the coast, supporting the ability of ECHAM5-wiso to resolve the integrated surface mass balance for the Antarctic ice sheet. Figures 3.2.4c and 3.2.4d confirm the global underestimation by the model, with slopes of simulated P-E against GC SMB lower than 1. This aspect is emphasized for elevations higher than 2200 m a.s.l. (r= 0.74 and rmse=122.8 mm w.e. y^{-1} for elevation lower than 2200 m a.s.l., and r =0.83 and rmse=55 mm w.e. y^{-1} for elevations higher than 2200 m a.s.l., with "r" the correlation coefficient, and "RMSE" the root mean square error). The correlation coefficient (considering all elevations) is 0.79, reflecting the non-homogenous bias

over the whole continent. This can be due first to a failure in the representativity of SMB spatial variability when averaging GC data within ECHAM5-wiso grid cells due to a too-small number of point measurements. Second, the model grid resolution may be too coarse to reproduce coastal topography and thus associated amounts of precipitation. Finally, several key processes such as blowing snow erosion and deposition are not taken into account in the model. For instance, the lowest value from the GC database is -164 mm w.e. y^{-1}, measured at the Bahia del Diablo glacier, a small glacier covering important elevation ranges in a narrow spatial scale between the front and the summit. It was the only one within the corresponding model grid cell, so the resulting GC value within this grid cell could not be representative of the model scale, and the simulated P-E value is not representative of this small glacier-wide value.

When considering the whole Antarctic grounded ice sheet, the area-weighted P-E simulated by the model amounts to 164.4 mm w.e. y^{-1}. This value falls within the highest values of the 11 simulations displayed by Monaghan et al. (2006), varying from 84 to 188 mm w.e. y^{-1}. However, the high range of values between the different simulations illustrates the uncertainties related to the SMB model, mainly due to model resolution which is crucial to reproducing the impact of topography on precipitations and to non-resolved physical processes (e.g. drifting snow transport, including the erosion, deposition, and sublimation of drifting snow particles, and clouds microphysics; Favier et al., 2017). Moreover, this simulated value is very close to the best estimations of Antarctic grounded ice sheet SMB, which range between 143.4 mm w.e. y^{-1} (Arthern et al., 2006) and 160.8 mm w.e. y^{-1} (Lenaerts et al., 2012). This simulated value is also very close to the one obtained by Agosta et al. (2013) for the LMDZ4 model over the period 1981-2000 (160 mm w.e. y^{-1}), but slightly lower than with the SMHiL model forced by LMDZ4 (189 mm w.e. y^{-1}).

To conclude, although the ECHAM5-wiso simulation presented in this study has a relatively coarse resolution (110 km x 110 km compared to 15 km x 15 km for the SMHiL model forced by LMDZ4), and does not resolve processes contributing in the SMB (e.g. drifting snow processes), the P-E outputs are realistic products when compared with SMB data.

3.2.3.2 Comparison with water stable isotope data

Limited by the availability of the data, we could only study model skills with respect to spatio-temporal patterns, including seasonal and inter-annual variations, and the simulated relationships between $\delta^{18}O$ and temperature. We have also extended the model-data comparison to the second-order parameter, d.

3.2.3.2.1 $\delta^{18}O$ time-averaged values and inter-annual variability

The model-data difference of the time-averaged values is positive for 88% of all grid cells, suggesting a systematic underestimation of isotopic depletion by ECHAM5-wiso (Fig. 3.2.5a). The few areas for which ECHAM5-wiso overestimates the isotopic depletion are restricted to coastal regions. This pattern is coherent with the temperature anomalies: ECHAM5-wiso produces too-low isotopic values where ECHAM5-wiso has a cold bias, likely causing too-strong distillation towards coastal areas and too-high isotopic values inland, where the warm bias limits the distillation strength. The statistical distribution of model-data $\delta^{18}O$ differences (not shown) shows a wide range but an interquartile range (50% of all values) of 1.4 to 3.9 ‰, which is therefore within 1.3 ‰ of the median. We conclude that, beyond the systematic offset linked to climatic biases, ECHAM5-wiso correctly captures the spatial gradient (continental effect) of annually avera ged $\delta^{18}O$ data. These results also suggest that the spatial distribution of annual mean $\delta^{18}O$ values from shallow ice cores is driven by transport and condensation processes well resolved by ECHAM5-wiso, probably with secondary effects of non-resolved processes such as snow drift, wind erosion, and snow metamorphism. The largest deviations are encountered in coastal regions, where the model resolution is too low to correctly resolve topography, advection and boundary layer processes (e.g. small-scale storms, katabatic winds). Katabatic winds also have the potential to enhance ventilation-driven post-deposition processes (Waddington et al., 2002; Neumann and Waddington, 2004).

$\delta^{18}O$ inter-annual standard deviation is underestimated by the model for 92% of the 179 grid cells in which this comparison can be performed (Fig. 3.2.5b).The interquartile range of the ratio between the simulated and observed standard deviation varies from 0.4 to 0.6 (not shown), with an underestimation by a factor of 2 for about 50% of the grid cells. No such underestimation of inter-annual standard deviation was identified for the simulated temperature.

We now focus on our model-data comparison of precipitation data. Both precipitation isotopic composition and temperature measurements are available for only eight locations and for short time periods (Table 3.2.3). These data evidence the altitude and continental effect with increased isotopic depletion from Vernadsky (averaged $\delta^{18}O$ of -9.9 ‰) to Dome F (averaged $\delta^{18}O$ of -61.3 ‰). For five out of the eight records, the isotopic depletion is stronger in ECHAM5-wiso than observed (Dome C included). The observations depict an enhanced inter-daily $\delta^{18}O$ standard deviation for inland sites, from 3.1 ‰ at Vernadsky to 10.8‰ at Dome F. The simulated $\delta^{18}O$ inter-daily standard deviation is 1.1 to 3.8 times larger than observed, ranging from 5.1 to 19.2 ‰. For the exact same time period corresponding to the short precipitation isotopic records, ECHAM5-wiso simulates colder than observed temperatures at

Table 3.2.3: Comparison between measurements from precipitation samples and ECHAM5-wiso simulated precipitation isotopic composition for grid cells closest to sampling locations over the same period as the data (at daily or monthly scale, when the name of the station is associated with an asterisk). We report the mean value ± the standard deviation for $\delta^{18}O$ (in ‰) and for temperature (°C).

		Data		Model	
	Number of points	Temperature (°C)	$\delta^{18}O$ (‰)	Temperature (°C)	$\delta^{18}O$ (‰)
Rothera*	194	-12.9 ± 3.4	-4.0 ± 4.1	-12.3 ± 6.4	-6.7 ± 5.3
Vernadsky*	372	-9.9 ± 3.1	-3.1 ± 3.6	-13.5 ± 6.0	-9.0 ± 7.2
Halley*	552	-22.0 ± 5.5	-18.7 ± 1.7	-25.7 ± 7.1	-20.1 ± 7.6
Marsh*	19	-12.1 ± 4.1	-3.4 ± 3.0	-10.4 ± 5.1	-4.2 ± 3.6
Dome F	351	-61.3 ± 10.8	-54.7 ± 12.6	-58.3 ± 12.2	-53.4 ± 12.1
Dome C	501	-58.0 ± 8.6	-55.2 ± 13.8	-59.6 ± 17.4	-52.9 ± 10.9
DDU	19	-18.0 ± 3.8		-23.4 ± 5.1	-21.3 ± 7.8
Neumayer	336	-20.8 ± 6.6	-13.4 ± 8.0	-21.3 ± 7.9	-15.8 ± 7.9

all stations but Dome F and Dome C, i.e. over the plateau. This finding is consistent with results from ice core records reported previously and consistent with the isotopic systematic biases. From this limited precipitation dataset, there is no systematic relationship between model biases for temperature (mean value or standard deviation) or for $\delta^{18}O$ in contrast with the outcomes of the model-data comparison using the whole dataset, including surface snow. At Dome C, ECHAM5-wiso underestimates the standard deviation of temperature, but strongly overestimates the standard deviation of $\delta^{18}O$.

As a conclusion, while $\delta^{18}O$ time-averaged model-data biases are consistent with temperature biases using the whole dataset, no systematic relationships emerge between model biases for temperature and $\delta^{18}O$ measured in precipitation.

3.2.2.2.2 $\delta^{18}O$ seasonal amplitude

High-resolution $\delta^{18}O$ data allow us to explore seasonal variations. This includes 18 ice core records with sub-annual resolution, four IAEA / GNIP monthly precipitation datasets, and four daily precipitation monitoring records.

In order to quantify post-deposition effects in ice cores, we calculated the ratio of the first three seasonal amplitudes by using the mean seasonal amplitude in sub-annual ice cores (See Table S2 in Supplementary Material). We find a mean ratio of 1.40 ± 0.47. We explored whether this ratio was related to annual accumulation rates (See S3 in Supplementary Material), without any straightforward conclusion. We also observe that five ice cores depict a ratio lower than 1, including one with a mean yearly accumulation of 15 cm w.e. y^{-1}, a feature which may arise

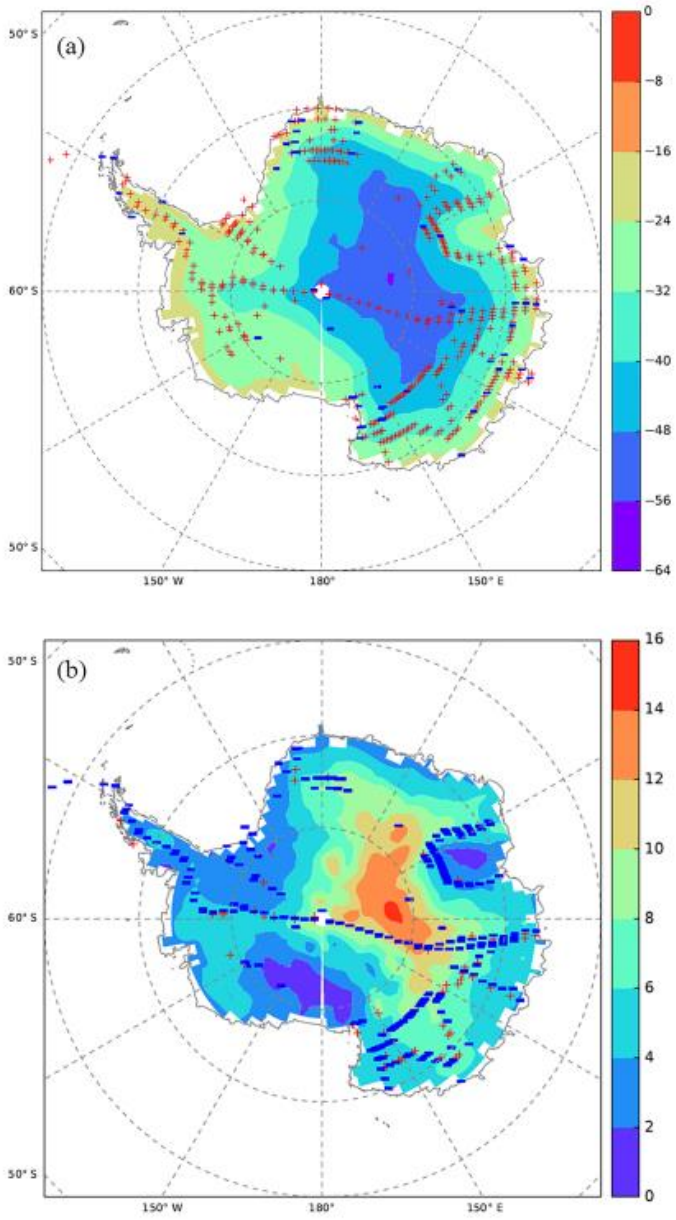

Figure 3.2.5: Maps displaying model-data comparisons for $\delta^{18}O$ time-averaged values (a) and inter-annual standard deviations (b). Backgrounds correspond to ECHAM5-wiso simulations over the period 1979-2013, while signs correspond to the model-data comparison. For the time-averaged values, the comparison consists in calculating the model-data differences. Red "+" symbols indicate a positive model-data difference while blue "-" symbols correspond to a negative model-data difference. For the inter-annual standard deviations, the comparison consists of calculating the ratio of the simulated value to the corresponding grid cell data. Red "+" symbols indicate a ratio higher than 1, while blue "-" symbols correspond to a model/data ratio lower than 1.

from inter-annual variability in the precipitation seasonal amplitude or in post-deposition processes. This empirical analysis shows that a loss of seasonal amplitude due to post-deposition processes is likely in most cases, with

an average loss of the seasonal amplitude of approximately 70% compared to the amplitude recorded in the upper part of the firn cores (first 3 years).

We have calculated the mean of the $\delta^{18}O$ annual amplitude (i.e. maximum – minimum values within each year) in ice core records (triangles in Fig. 3.2.7a) and the mean seasonal amplitude of precipitation time series (circles in Fig. 3.2.7a) for comparison with ECHAM5-wiso outputs (Fig. 3.2.7, Table 3.2.4). Unfortunately, a too-small number of measurements (19 daily

measurements) were monitored at DDU, preventing the representation of the full seasonal cycle. The data depict the largest seasonal amplitude in the central Antarctic Plateau, reaching up to 25.9 ‰ at Dome F. ECHAM5-wiso underestimates the seasonal amplitude (by 14 to 69%) when compared to precipitation data, but overestimates the seasonal amplitude when compared to ice core data (from 11 to 71%). The overestimation when comparing with ice core data is consistent with the attenuation of signal by post-deposition effects (as previously mentioned) rather than a model bias.

The simulated mean seasonal $\delta^{18}O$ amplitude increases gradually from coastal regions to central Antarctica (more than 15 ‰ and up to 25 ‰ for some previously reported for annual mean values, systematic offsets are also identified for seasonal variations, with a systematic overestimation of monthly isotopic levels inland (e.g. for Dome C and Dome F), and a

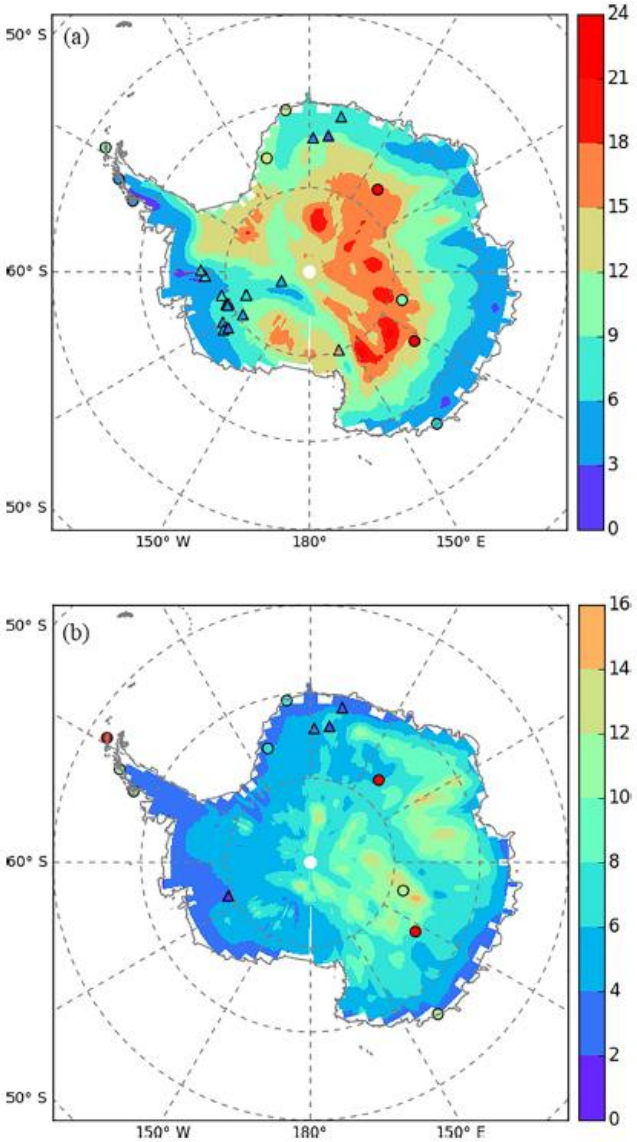

Figure 3.2.7: Average seasonal amplitude of precipitation $\delta^{18}O$ (a) and d (b) (in ‰) simulated by ECHAM5-wiso (colour shading) over the period 1979-2013 and calculated from precipitation data (circles) and ice core records (triangles) over their respective available periods.

systematic underestimation on the coast (e.g. for Vernadsky and Halley). The model-data mismatch is largest during local winter months.

Minima are observed and simulated in winter (May-September) at most locations, except for Rothera and Vernadsky where the data show a minimum in July but the model produces a minimum in late autumn (April). Maximum values are observed and simulated in local summer (December-January); a secondary maximum is also sometimes observed and simulated in late winter (August-September). Data from Marsh station show maxima in January, April and August, whereas the model only produces a single summer maximum value.

Table 3.2.4: $\delta^{18}O$ mean seasonal amplitude (in ‰) calculated for precipitation and sub-annual ice core data, as well as simulated by ECHAM5-wiso for the same time period as the data. The time resolution used in the model corresponds to the time resolution of the precipitation data, and to the annual scale for the ice core data (i.e. yearly averages based on daily precipitation isotopic composition weighted by the amount of daily precipitation). The data type is identified as 1 for precipitation samples and 2 for ice core data.

Station	Type	$\delta^{18}O$ observed amplitude (‰)	ECHAM5-wiso averaged over the observed period (‰)
Rothera	1	4.1	1.9
Vernadsky	1	4.1	2.3
Halley	1	13.2	6.7
Marsh	1	10.4	7.3
Dome F	1	25.9	15.3
Dome C	1	20.1	13.5
DDU	1	6.1	3.7
Neumayer	1	12.8	7.9
USITASE-1999-1	2	7.2	13.2
USITASE-2000-1	2	4.8	10.6
USITASE-2000-2	2	7.7	10.4
USITASE-2000-4	2	4.0	12.0
USITASE 2000-5	2	5.2	13.7
USITASE-2000-6	2	2.8	14.2
USITASE-2001-1	2	7.3	9.4
USITASE-2001-2	2	7.3	12.0
USITASE-2001-4	2	6.2	8.9
USITASE-2001-5	2	6.8	9.0
USITASE-2002-1	2	4.2	12.2
USITASE-2002-2	2	6.3	10.7
USITASE-2002-4	2	5.3	13.8
NUS 08-7	2	3.4	16.6
NUS 07-1	2	2.1	14.8
WDC06A	2	4.0	10.8
IND25	2	5.3	12.6
GIP	2	15.1	16.8

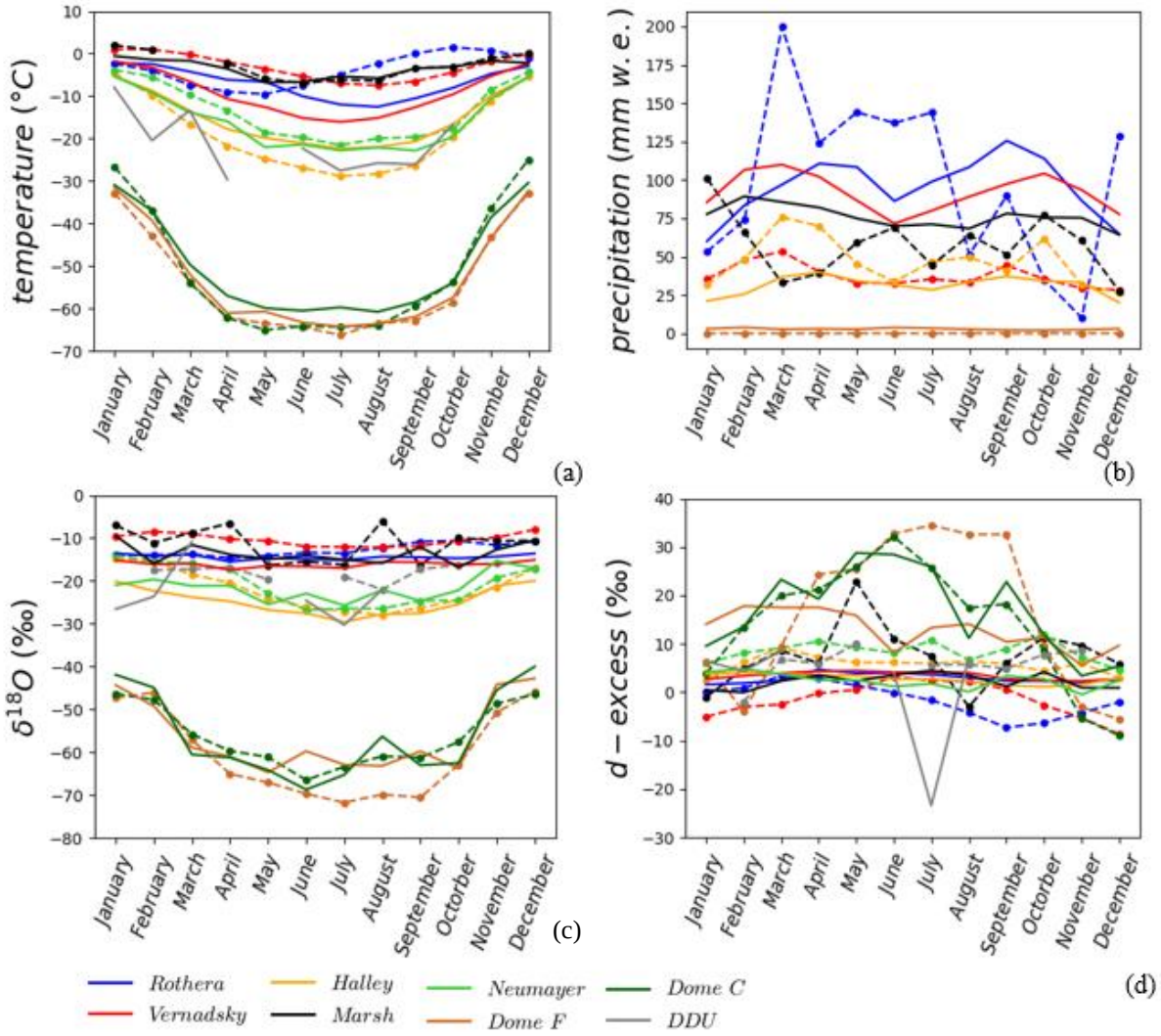

Figure 3.2.8: Average seasonal cycles from precipitation data over the available period (dashed lines with points) and simulated by the ECHAM5-wiso model over the period 1979-2013 (solid lines) of the temperature (in °C) (a), the precipitation (in mm w.e. y^{-1}), the precipitation $\delta^{18}O$ (in ‰) (c) and the deuterium excess (in ‰) (d). Data are shown for different durations depending on sampling, while model results are shown for the period 1979-2013. The number of points used for the observations is given in Table 3.2.3.

In summary, we report no systematic bias of the seasonal temperature amplitude (Fig. 3.2.8a). The seasonal pattern for the temperature is similar compared to $\delta^{18}O$, with minima in winter and the largest model-data mismatch in winter. Secondary minima or maxima cannot be discussed with confidence, as they have low amplitudes. We also highlight that model-data offsets are larger in winter. Note that precipitation and d seasonal cycles are described in Section 3.2.3.4.

3.2.3.3 $\delta^{18}O$ – T relationships

Table 3.2.5 reports the temporal $\delta^{18}O$ – T relationships established from precipitation and temperature observations, and those simulated by ECHAM5-wiso. This calculation is based on daily or monthly values (depending on the sampling resolution) and includes seasonal variations. The data display significant linear relationships for all sites but Marsh (p-

value=0.07), with an increased strength of the correlation coefficient from the coast (e.g. r= 0.38 at Rothera) to the East Antarctic Plateau (e.g. r= 0.88 at Dome F).

The lowest slopes are identified in the peninsula region, with a mean slope of 0.32 ‰ °C^{-1} for Rothera and Vernadsky, while the highest slopes occur over the East Antarctic Plateau, with a mean slope of 0.68 ‰ °C^{-1} for Dome C and Dome F. These temporal slopes appear mostly lower than the spatial slopes and those expected a Rayleigh distillation with a single moisture source (typically 0.8 ‰ °C^{-1}).

In the ECHAM5-wiso model, as for the data, the simulated isotope-temperature relationship is statistically significant for all sites but Marsh (p-value=0.06). However, correlation coefficients are very small for Rothera and Vernadsky which are thus excluded from further analyses. In the simulation, correlation coefficients are the highest for Halley, Dome C and Dome F (up to 0.55), and the lowest for Neumayer (as low as 0.29). The slope is the lowest at Neumayer, with a value of 0.29 ‰ °C^{-1}, increases at Halley with a value of 0.48 ‰ °C^{-1}, and is the highest over the plateau with values of 0.70 ‰ °C^{-1} at Dome C and up to 0.94 ‰ °C^{-1} at Dome F.

To summarise, ECHAM5-wiso tends to underestimate the strength of the isotope-temperature relationship, but correctly simulates a larger strength of the correlation in the central Antarctic Plateau compared to coastal regions. There are significant differences in the isotope-temperature slopes for both coastal and central plateau locations. While there is some agreement (e.g. for Dome F and Halley), the model also produces non-realistic slopes, with a much larger slope than observed at Dome C, for instance.

Table 3.2.5: Slope (in ‰ °C^{-1}), correlation coefficient and p-value of the $\delta^{18}O$ -temperature linear relationship from precipitation measurements over the available period and at daily or monthly (when the name of the station is associated with an asterisk) scale depending of the time resolution of the data, and from the ECHAM5-wiso model over the observed period at the time resolution of the data. Numbers in brackets correspond to the standard errors.

	Number of points	Data			ECHAM5-wiso over the observed period		
		Slope (‰ °C^{-1})	r	p-value	Slope (‰ °C^{-1})	r	p-value
Rothera*	194	0.31 (0.06)	0.38	<0.001	0.01 (0.03)	0.23	<0.001
Vernadsky*	372	0.32 (0.04)	0.39	<0.001	0.09 (0.02)	0.25	<0.001
Halley*	552	0.47 (0.02)	0.76	<0.001	0.48 (0.02)	0.68	<0.001
Marsh*	19	0.61 (0.31)	0.44	0.07	0.47 (0.23)	0.43	0.06
Dome F	351	0.76 (0.02)	0.88	<0.001	0.70	0.62	<0.001
Dome C	501	0.59 (0.02)	0.64	<0.001	0.94 (0.07)	0.55	<0.001
Neumayer	336	0.57 (0.03)	0.69	<0.001	0.29 (0.06)	0.29	<0.001

3.2.3.4 The δD-δ^{18}O relationship and d patterns

The δ^{18}O- δD linear relationship is expected to be affected by different kinetic fractionation processes, for instance associated with changes in evaporation conditions. We first compare the δ^{18}O- δD linear relationship in the available precipitation and ice core data, and simulated by ECHAM5-wiso (Table 3.2.6). Significant correlation is observed for all observational datasets but Marsh, as expected from meteoric samples, assuming correct preservation of samples and accurate isotopic measurements. We stress that the smallest correlation coefficient is identified at Vernadsky (r=0.96), suggesting potential artefacts for this record. In the observations, the δD-δ^{18}O slope varies across regions. While slopes higher than for the global meteoric waterline (i.e. >8 ‰ ‰$^{-1}$) are identified at DDU and in Dronning Maud Land, lower slopes are identified in the Antarctic peninsula (6.6 to 7.0 ‰ ‰$^{-1}$) and in the central East Antarctic Plateau (6.5 and 6.4 ‰ ‰$^{-1}$ at Dome C and Dome F respectively). In the model, outputs also display significant linear relationships. They show higher values of the slope than observed in the Antarctic Peninsula, at DDU, and at Dome F, and lower than observed for the other regions, including Dome C. These results appear coherent with associated coastal versus inland temperature and isotopic distillation biases.

Figure 3.2.6 compares the spatial patterns of the d time-averaged model-data difference (characterized at 293 grid cells in our database, see Fig. 3.2.6a), the situation is contrasted with 50% of positive and negative differences. We can identify systematic trends, with an underestimation of the mean d levels in ECHAM5-wiso for the central East Antarctic Plateau and the Peninsula, and an overestimation above Victoria Land (Fig. 3.2.6a). Due to the temperature dependency of equilibrium fractionation coefficients leading to a gradual deviation from the meteoric waterline (calculated at the global scale, at which a coefficient of 8 results from the average equilibrium fractionation coefficients), d increases when temperature decreases (Masson-Delmotte et al., 2008; Touzeau et al., 2016).For central Antarctica, the d bias is thus consistent with the warm bias and the lack of isotopic depletion. The upper and lower quartiles of the model-data differences range within ±1.5 ± 0.1 ‰, suggesting that the model outputs remain close to those observed.

The d pattern is similar to that of δ^{18}O: ECHAM5-wiso underestimates the d standard deviation for 90 % of grid cells, with an interquartile range comparable to the one for the ratio of standard deviations for δ^{18}O (Fig. 3.2.6b). Table 3.2.7 displays the comparison of the statistics between d in the observations and in ECHAM5-wiso. In the observations, the time-averaged d is particularly low in the peninsula (-3.6 to 8.6 ‰), intermediate in coastal regions of Dronning

Table 3.2.6: Slope (in ‰ ‰$^{-1}$), correlation coefficient and p-value of the $\delta^{18}O$-δD linear relationship from precipitation measurements (top of the table) and ice core data (bottom of the table) over the available period at daily or monthly scale (identified with an asterisk), and from the ECHAM5-wiso model over the observed period at the time resolution of the data for the precipitation and at the annual scale for the ice core data. Numbers in brackets correspond to the standard errors.

	Number of points	Observations slope (‰ ‰$^{-1}$)	r	p-value	ECHAM5-wiso slope (‰ ‰$^{-1}$)	r	p-value
Rothera*	194	7.0 (<0.1)	9.81×10^{-1}	<0.001	7.9 (<0.1)	9.97×10^{-1}	<0.001
Vernadsky*	372	6.6 (<0.1)	9.62×10^{-1}	<0.001	7.8 (0)	9.96×10^{-1}	0
Halley*	552	7.8 (0)	9.91×10^{-1}	0	7.8 (<0.1)	9.95×10^{-1}	<0.001
Marsh*	19	7.1 (<0.1)	9.80×10^{-1}	<0.001	8.0 (<0.1)	9.94×10^{-1}	<0.001
Dome F	351	6.4 (<0.1)	9.92×10^{-1}	<0.001	7.3 (<0.1)	9.91×10^{-1}	<0.001
Dome C	501	6.5 (0)	9.89×10^{-1}	0	6.3 (<0.1)	9.73×10^{-1}	<0.001
DDU	19	8.5 (<0.1)	9.92×10^{-1}	<0.001	9.0 (<0.1)	9.86×10^{-1}	<0.001
Neumayer	336	7.9 (<0.1)	9.90×10^{-1}	<0.001	7.8 (<0.1)	9.98×10^{-1}	<0.001
NUS 08-7	256	8.6 (<0.1)	9.96×10^{-1}	<0.001	8.0 (<0.1)	9.95×10^{-1}	<0.001
NUS 07-1	118	8.3 (<0.1)	9.94×10^{-1}	<0.001	7.6 (<0.1)	9.94×10^{-1}	<0.001
WDC06A	540	8.2 (0)	9.95×10^{-1}	0.00	8.1 (<0.1)	9.98×10^{-1}	<0.001
IND25	349	8.2 (<0.1)	9.82×10^{-1}	<0.001	7.8 (<0.1)	9.94×10^{-1}	<0.001
GIP	495	7.8 (0)	9.90×10^{-1}	0	8.3 (<0.1)	9.98×10^{-1}	<0.001

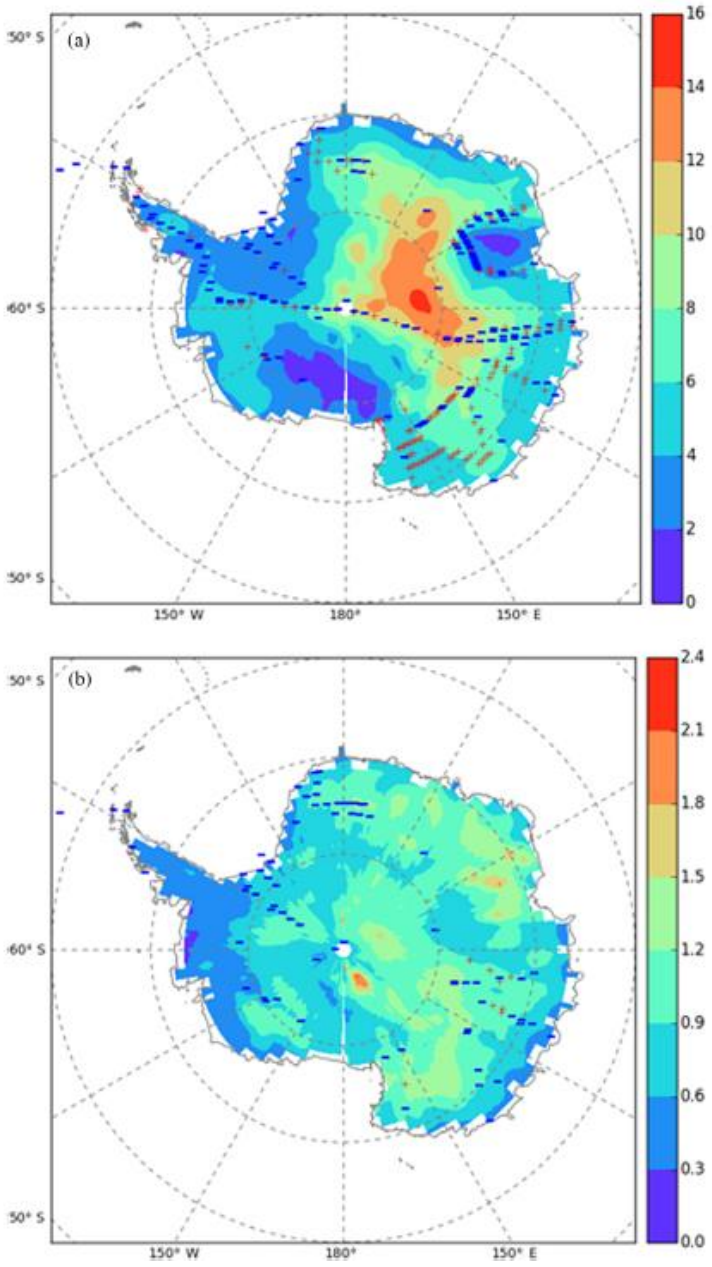

Figure 3.2.6: Maps displaying model-data comparisons for d time-averaged (in ‰, a) values and inter-annual standard deviations (in ‰, b). Backgrounds correspond to ECHAM5-wiso simulations over the period 1979-2013, while signs correspond to the model-data comparison. For the time-averaged values, the comparison consists of calculating the model-data differences. Red "+" symbols indicate a positive model-data difference while blue "-" symbols correspond to a negative model-data difference. For the inter-annual standard deviation, the comparison consists of calculating the ratio of the simulated value to the corresponding grid point data. Red "+" symbols indicate a ratio higher than 1 while blue "-" symbols correspond to a model / data ratio lower than 1.

Maud Land, Victoria Land and Adélie Land (4.4 to 8.6 ‰), and very high in the central Antarctic Plateau (up to 17.5 ‰ for Dome C). Lower coastal values and higher inland values are captured by ECHAM5-wiso, albeit with large offsets for each site, reaching several per mille. These findings are consistent with the map showing the time-averaged precipitation d simulated by ECHAM5-wiso over the period 1979-2013 (Fig. 3.2.6a), with very low coastal values (close to zero) and increasing values towards the interior of Antarctica, reaching values

Table 3.2.7: Mean value ± standard deviation (in ‰) of sub-annual d in observational time series at daily or monthly scale (identified with an asterisk) for the precipitation and for the ice core data, and simulated d by ECHAM5-wiso for the same time period as the observations for precipitation and at the annual scale for the ice core. Mean values which are overestimated by ECHAM5-wiso are written in italic.

	Data (‰)	ECHAM5-wiso over the observed period (‰)
Rothera*	-1.1 ± 5.7	*2.9* ± 1.5
Vernadsky*	-1.5 ± 7.0	*3.5* ± 1.5
Halley*	5.77 ± 6.1	*2.8* ± 1.9
Marsh*	8.6 ± 7.0	2.4 ±1.7
Dome F	17.4 ± 19.5	15.3 ± 14.2
Dome C	17.5 ± 15.2	14.2 ± 24.3
DDU	5.9 ± 4.5	2.8 ± 9.5
Neumayer	8.7 ± 5.6	2.4 ± 4.7
NUS 08-7	5.0 ± 2.7	*6.6* ± 1.0
NUS 07-1	5.8 ± 2.3	*7.0* ± 1.1
WDC06A	3.6 ± 1.5	*4.5* ± 0.5
IND25	4.4 ± 19.2	4.1 ± 0.9
GIP	6.0 ± 4.4	2.1 ± 0.9

higher than 16 ‰ on the plateau. ECHAM5-wiso mainly underestimates the d intra-annual standard deviation for 10 sites out of 15 (Table 3.2.7 and Fig. 3.2.6b).

Figure 3.2.8d depicts the mean d seasonal patterns of the precipitation data and corresponding model outputs. The data show different patterns from one location to another. While d measured at Neumayer, Halley and Rothera displays a maximum in autumn (March-April), it appears in late autumn (May) at Marsh and in winter (June-August) at Vernadsky. Maxima for central stations are observed later, in May-July for Dome C and July-September for Dome F. In short, most coastal areas are associated with a maximum d in autumn while central areas are associated with a later maximum d, i.e. in winter or late winter, thus in anti-phase with $\delta^{18}O$ and temperature. The seasonal amplitude increases from the coast to the plateau. In the model, for central areas, a first d maximum is simulated earlier than observed (February-March for Dome F, and May-June for Dome C), followed by a second maximum in late winter (August for Dome F and September for Dome C). For coastal areas, the amplitude of the simulated d signal is too small to unequivocally estimate the timing of the maximum. Note the very low value simulated at DDU in July, which appears to be an outlier when comparing this value with the average modelled d value for all days in August 1973 (+5.9 ‰). No link emerges between

the modelled seasonal patterns in d and in temperature (Fig. 3.2.8a), accumulation (Fig. 3.2.8b), or $\delta^{18}O$ (Fig. 3.2.8c).

Finally, Table 3.2.8 reports the d mean seasonal amplitude values for the precipitation data and ice core records, as well as for the model outputs covering the observation. They clearly show an increase in d seasonal amplitude from the coast to the plateau (see also Fig. 3.2.7b), with values varying from 6.7 ‰ at Halley to 41 ‰ at Dome C. ECHAM5-wiso systematically underestimates the d mean seasonal amplitude when compared with precipitation data, while it systematically overestimates it when compared with ice core data (from 9.4 to 15.5 ‰), with the exception of the GIP ice core. Again, we cannot rule out a loss of amplitude in ice core data compared to the initial precipitation signal, due to the temporal resolution and post-deposition effects.

3.2.3.5 Strength and limitations of the ECHAM5-wiso model outputs

The isotopic model-data time-averaged biases appear coherent with temperature. A warm bias over central East Antarctica and a cold bias over coastal regions lead to a too-low and too-strong isotopic depletion, respectively. Temperature and distillation biases also explain the underestimation of d above the central East Antarctic Plateau.

However, some characteristics are not explained by model skills for temperature. At sub-annual timescales, ECHAM5-wiso always overestimates the standard deviation of $\delta^{18}O$ in precipitation (Table 3.2.3), but results for d are mixed (Table 3.2.7). ECHAM5-wiso always underestimates seasonal amplitude of $\delta^{18}O$ and d in precipitation but always overestimates the seasonal amplitude of $\delta^{18}O$ and d in firn-ice cores (Table 3.2.4 and 3.2.8). Differences between the model and firn-core data are at least partially due to diffusion processes, but no clear reason can be given for the other isotopic biases.

We do not find any clear link between other model biases for d and those for temperature or $\delta^{18}O$.

Sampling Antarctic snowfall remains challenging (Fujita and Abe, 2006; Landais et al., 2012; Schlosser et al., 2016; Stenni et al., 2016). Sampling is likely to fail to capture small events, and may also collect surface snow transported by winds or hoar. Snow samples may undergo sublimation before collection. The fact that ECHAM5-wiso appears to overestimate the variability of precipitation isotopic composition may be related to an improper characterisation of the full day-to-day variability of real-world precipitation from daily precipitation sampling. Alternatively, this feature may also arise from a lack of representation of small-scale processes (boundary layer processes, wind characteristics, snow-atmosphere interplays) in ECHAM5-wiso. These processes may contribute to a local source of Antarctic moisture (through local

Table 3.2.8: d mean seasonal amplitude (in ‰) calculated for precipitation at daily or monthly scale (identified with an asterisk) and sub-annual ice core data, as well as simulated by ECHAM5-wiso for the same time period as each record. The data type is identified as 1 for precipitation samples and 2 for ice core records. Amplitude values that are overestimated by ECHAM5-wiso are written in italic.

Station	Type	Observed amplitude (‰)	ECHAM5-wiso outputs for the observed period (‰)
Rothera*	1	10.7	3.1
Vernadsky*	1	11.8	2.1
Halley*	1	6.7	3.8
Marsh*	1	25.8	4.5
Neumayer	1	7.3	5.3
Dome F	1	40.1	12.2
Dome C	1	41.0	25.4
NUS 08-7	2	3.5	*14.0*
NUS 07-1	2	1.9	*15.8*
WDC06A	2	1.0	*16.5*
IND25	2	2.3	*11.7*
GIP	2	17.8	6.9

recycling), reducing the influence of large-scale moisture transport (resolved by ECHAM5-wiso nudged to reanalyses) on the isotopic composition of precipitation and its day-to-day variability.

Caveats also limit the interpretation of the comparison of ECHAM5-wiso precipitation outputs with surface snow or shallow ice core data. Such records are potentially affected by post-deposition processes, such as wind scoring, erosion, snow metamorphism between precipitation events and diffusion.

Our apparently contradictory findings for model-data comparisons with respect to inter-annual variations (from ice cores) and inter-daily variations (from precipitation data) call for more systematic comparisons between $\delta^{18}O$ records of precipitation and ice cores at the same locations, over several years.

3.2.4 Use of ECHAM5-wiso outputs for the interpretation of ice core records

In this section, we use the model outputs to help in the interpretation of ice core data: we quantify the inter-annual isotope-temperature relationships (Section 3.2.4.1) and characterise the spatial distribution of seasonal $\delta^{18}O$-d phase lag (Section 3.2.4.2). Based on the confidence we can have in the model for each of the seven aforementioned regions (See Section 1 and Fig. 3.2.1), we formulate recommendations for the future use of ECHAM5-wiso outputs (Section (Section 3.2.4.3).

3.2.4.1 Spatial and temporal isotope-temperature relationships

First, we use ECHAM5-wiso to investigate spatial $\delta^{18}O$-temperature relationships (Fig. 3.2.9a and 3.2.9b) and then inter-annual (Fig. 3.2.9c and Fig. 3.2.9d) and seasonal relationships (Fig. 3.2.9e and Fig. 3.2.9f). For spatial relationships, the strength of the linear correlation coefficient is higher than 0.8. The spatial slope shows regional differences. It is generally smaller near the coasts (less than 0.8 ‰ $°C^{-1}$), with the exception of Dronning Maud Land , and increases at elevations higher than 2500 m a.s.l., with values above 1.2 ‰ $°C^{-1}$ in large areas. Furthermore, ECHAM5-wiso simulates spatial heterogeneity of the gradient in the central East Antarctic Plateau, around Dome C, Dome A and Dome F. Such variability may arise from the simulated intermittency of precipitation and from differences in condensation versus surface temperature. At the inter-annual scale (Fig. 3.2.9c and 3.2.9d), results are not significant for large areas encompassing the Dronning Maud Land region, the Antarctic Peninsula, the Transantarctic Mountain region, the Ronne and Filchner ice shelf regions, part of Victoria Land and along the Wilkes Land coast. For the whole continent, the correlation coefficient varies between 0.5 and 0.6 (with few values reaching 0.6 at the upper limit and 0.3 at the lower limit). Where correlations are significant, the inter-annual $\delta^{18}O$-temperature slope increases from the coasts (0.3‰ $°C^{-1}$ to 0.6‰ $°C^{-1}$) to the inland regions, where it can exceed 1‰ $°C^{-1}$ for some high-elevation locations. The low correlation may be due to the small range of mean annual temperature over the period 1979-2013 and is not necessarily indicative of a weak sensitivity to temperature change.

Finally, at the seasonal scale, results are significant almost over the whole continent (with the exception of two little areas in peninsula and East Antarctica) and the correlation coefficients are equal to 1 everywhere but along the coastal regions in the Indian Ocean sector, where the correlation coefficient can decrease down to 0.75. Slopes are lower than for spatial and inter-annual relationships, with values from 0.0 to 0.3 ‰ $°C^{-1}$ along the coast (higher over Dronning Maud Land and the Ross Ice Shelf region), around 0.5 ‰ $°C^{-1}$ inland for altitudes lower than 2500 m a.s.l. (with the exception of lower values above the Transantarctic Mountains), and up to 0.8 ‰ $°C^{-1}$ over the East Antarctic Plateau.

To conclude the coherent framework provided by the ECHAM5-wiso simulation covering the period 1979-2013 shows that annual $\delta^{18}O$ and surface temperatures are only weakly linearly related in several areas. This suggests that the inter-annual variability of $\delta^{18}O$ is controlled by other processes, for instance those associated with synoptic variability and changes in moisture source characteristics (Sturm et al., 2010; Steiger et al., 2017). Moreover, our results rule out

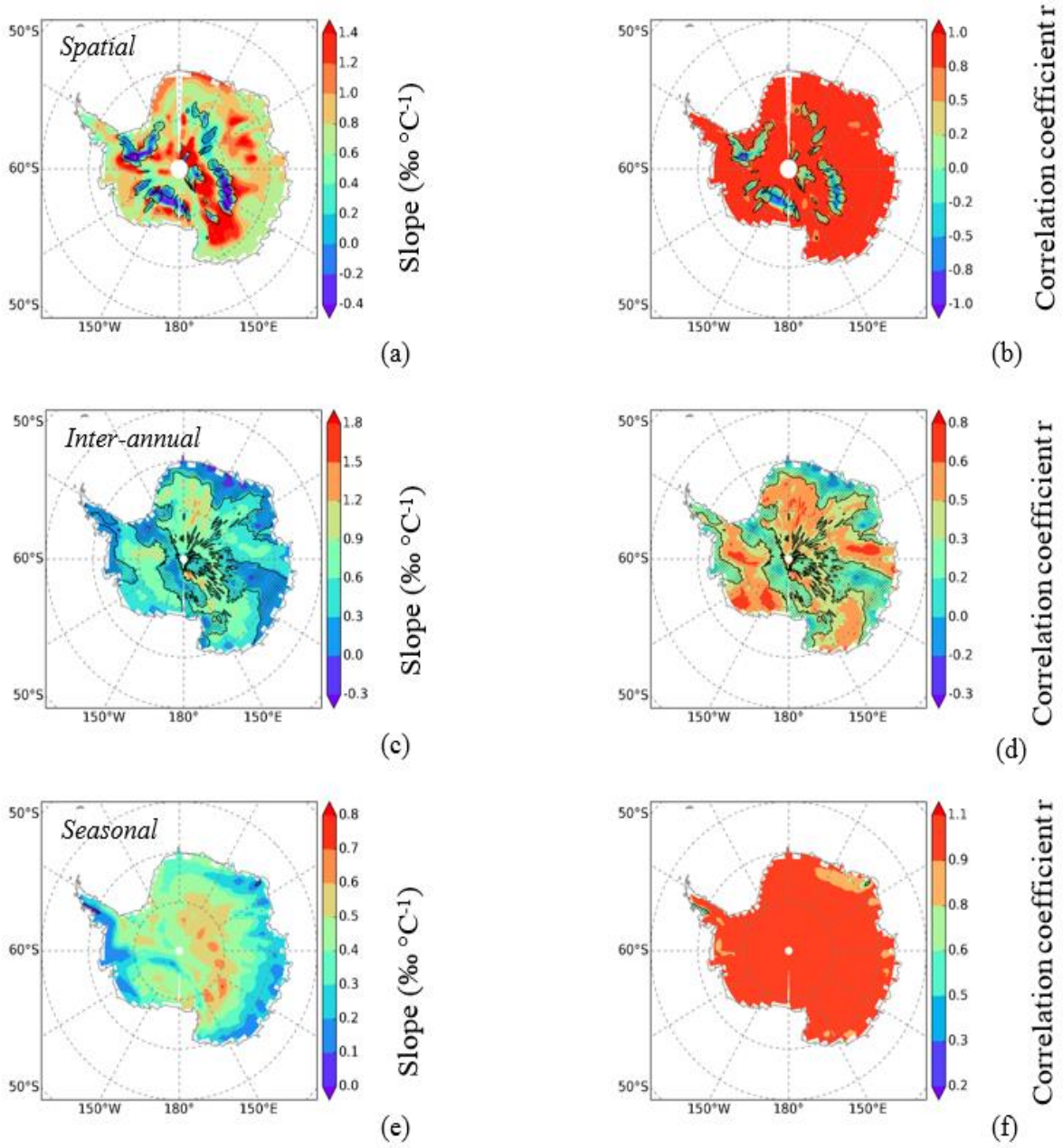

Figure 3.2.9: Linear analysis of annual ECHAM5-wiso outputs from 1979-2013 for the temporal δ18O-temperature relationship (using the 2-meter temperature and the precipitation-weighted δ18O). Maps show the slope of the linear regression (‰ °C-1) at the right side (a, c and e) and the correlation coefficient at the left side (b, d, and f). The upper plots use outputs at the spatial scale (a and b), the middle plots at the inter-annual scale (c and d) and the lower plots at the seasonal scale (e and f). Areas where the results of the linear analysis are not significant are hatched (p-value>0.05).

the application of a single isotope-temperature slope for all Antarctic ice core records on the inter-annual timescale, and the seasonal isotope-temperature slope is not a surrogate for scaling inter-annual $\delta^{18}O$ to temperature.

We have also used the simulation to explore linear relationships between d and surface air temperature, without any significant results (not shown).

3.2.4.2 $\delta^{18}O$ –d phase lag

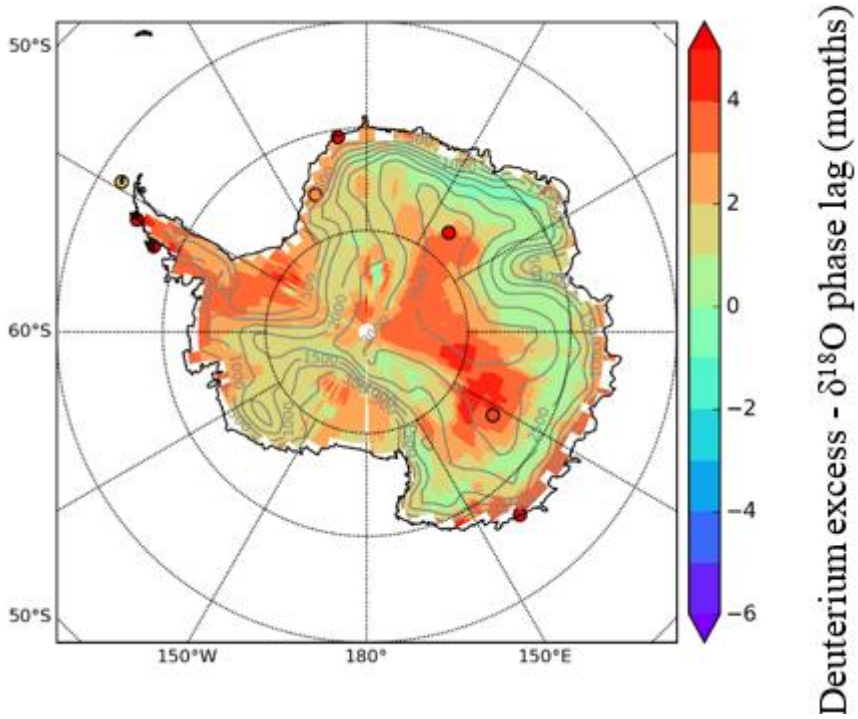

Figure 3.2.10: Best correlated phase lag between the mean seasonal cycle of deuterium excess and that of $\delta^{18}O$ simulated by ECHAM5-wiso over the period 1979-2013 (colour shading) and calculated from precipitation data (circles). The sign provides information on the sign of the correlation between $\delta^{18}O$ and d (e.g. positive numbers correspond to a correlation, while negative numbers correspond to an anti-correlation). The absolute value corresponds to the lag (in months) between $\delta^{18}O$ and deuterium excess corresponding to the highest correlation of monthly averaged values. This figure also displays the Antarctic topography, with isohypses (in m a.s.l.).

Deuterium excess (d) has originally been interpreted as a proxy for relative humidity at the moisture source (Jouzel et al., 2013; Pfahl and Sodemann, 2014; Kurita et al., 2016). However, recent studies of Antarctic precipitation data combined with back-trajectory analyses did not support this interpretation (e.g. Dittmann et al., 2016; Schlosser et al., 2017), calling for further work to understand the drivers of seasonal d variations. The phase lag between d and $\delta^{18}O$ was initially explored to identify changes in evaporation conditions (Ciais et al., 1995). In ECHAM5-wiso, this phase lag is calculated as the lag that gives the highest correlation coefficient between d and $\delta^{18}O$ (Fig. 3.2.10), using the mean seasonal cycle from monthly averaged values. If there were no seasonal change in moisture origin and climatic conditions during the initial evaporation process, one would expect d to be in anti-phase with $\delta^{18}O$, due to the impact of condensation temperature on equilibrium fractionation. For regions with small seasonal amplitude in condensation temperature, a constant initial isotopic composition at the moisture source would imply a stable d year-round. In such regions, the simulated phase lag likely therefore reflects seasonal changes in the d of the initial moisture source. The comparison with precipitation data (Section 3.2.2.2.2) showed that ECHAM5-wiso had low seasonal amplitude in coastal regions (Fig. 3.2.8d), making the discussion of seasonal maxima difficult.

These comparisons are also limited by the duration of the precipitation records. Here, we use the full simulation (1979-2013) to investigate the phase lag between the mean seasonal cycle of d and $\delta^{18}O$. Clear spatial patterns are identified for the distribution of this phase lag (see Fig. 3.2.10). At intermediate elevations (between 1000 and 3000 m a.s.l.), d seasonal variations occur in phase (within 2 months) with the seasonal cycle of $\delta^{18}O$ (and surface air temperature). By contrast, a phase lag of several months is identified over coastal areas and over the central East Antarctic Plateau. Along the Wilkes Land coast and the Dronning Maud Land region, the time lag is between 2 and 4 months, below 1000 m a.s.l. and 500 m a.s.l. respectively. Over the West Antarctic Ice Sheet, the phase lag is higher than 2 months below 500 m a.s.l. and can even reach 6 months (indicating an anti-phase between d and $\delta^{18}O$). Over the central East Antarctic Plateau (above 3000 m elevation), the phase lag reaches several months again, especially near Dome C. Obtaining longer precipitation records and comparing the phase lag identified in precipitation and surface snow records would be helpful to understand whether post-deposition processes, which are not included in ECHAM5-wiso, affect this phase lag. The different characteristics of seasonal d changes suggest different seasonal changes in moisture origin at coastal, intermediate and central plateau regions, supporting the identification of specific coastal versus inland regions to assess the isotope-temperature relationships. Note that the few available datasets are in line with the simulation.

3.2.4.3 Recommendations for the different regions of Antarctica

In this section, we summarise our findings, based on the model-data comparisons and the analysis of model outputs for the seven Antarctic regions selected by the Antarctica2k program, as shown in Fig. 3.2.1 (Stenni et al., 2017). The regions depend on geographical and climatic characteristics. Results from Section 3.2.3 were averaged over each region and are given in Table 3.2.9.

We first discuss the systematic model biases. The maximum time-averaged model-data differences (3.8 ‰ and 2.6 ‰ for $\delta^{18}O$ and d respectively) are identified in the Weddell Sea area. Minimum time-averaged model-data differences occur in different regions for $\delta^{18}O$ and d (Victoria Land and Dronning Maud Land respectively).

For inter-annual standard deviation, the model-data mismatch is smallest for Victoria Land (ratio of 1.1 and 1.0 for $\delta^{18}O$ and d respectively). Results for $\delta^{18}O$ show that the simulated inter-annual variability can be considered close to reality (model-data ratio higher than 0.7) only for Victoria Land and the plateau, acceptable (model-data ratio higher than 0.5) for the Weddell Sea area and the West Antarctic Ice Sheet, but significantly different from observations in the other three regions. The model-data mismatch is larger for d inter-annual variability, with

Table 3.2.9: Evaluation of ECHAM5-wiso model for 7 Antarctic regions: East Antarctic Plateau, Coastal Indian, Weddel Sea, Peninsula, West Antarctic Ice Sheet, Victoria Land and Dronning Maud Land (7). We regionally averaged the time-averaged $\delta^{18}O$ mean (model – data) differences (in ‰), the inter-annual $\delta^{18}O$ standard deviation (model/data) ratio, the time-averaged d mean (model – data) differences (in ‰), the inter-annual d (model-data) standard deviation ratio using only precipitation data. Italic cells correspond to parameters for which we support the validity of the use of ECHAM5-wiso for the considered region, underlined cells to parameters we suggest some cautions, and bold cells to parameters we suggest not to use ECHAM5-wiso outputs for the considered region. Numbers in brackets correspond to the number of data points.

Region	Plateau	Coastal Indian	Weddell Sea	Peninsula	West Antarctic Ice Sheet	Victoria Land	Dronning Maud Land
$\delta^{18}O$ mean difference (in ‰)	*2.5 (551)*	*1.8 (68)*	*3.8 (38)*	*2.6 (30)*	*3.7 (48)*	*0.6 (246)*	*1.1 (70)*
$\delta^{18}O$ standard deviation ratio	*0.9 (62)*	**0.3 (3)**	0.6 (12)	**0.1 (1)**	0.5 (7)	*1.1 (2)*	**0.3 (13)**
d mean difference (in ‰)	*0.4 (402)*	*1.3 (20)*	*-2.6 (12)*	*-1.1 (25)*	*-0.6 (31)*	*2.3 (232)*	*0.2 (18)*
d standard deviation ratio	*0.7 (62)*	**0.3 (3)**	**0.4 (12)**	**0.1 (1)**	**0.3 (7)**	*1.0 (2)*	**0.2 (13)**

Table 3.2.10: Exploration of the ECHAM5-wiso model outputs (1979-2013) for 7 Antarctic regions: East Plateau, coastal Indian, Weddell Sea, peninsula, West Antarctic Ice Sheet, Victoria Land and Dronning Maud Land (7). For each of the variables precipitation (in mm w.e. y^{-1}), temperature (in °C), $\delta^{18}O$ (in ‰) and d (in ‰), we regionally averaged the annual mean values (lines 1 to 4), the inter-annual standard deviation (lines 5 to 8), and the mean seasonal amplitude (lines 9 to 12). Finally, we calculated the statistics of the inter-annual $\delta^{18}O$ -temperature linear relationship: the slope (noted as "a", in ‰ $°C^{-1}$), the correlation coefficient (noted as "r") and the p-value for each region.

	Regions	Plateau	Coastal Indian	Weddell Sea	Peninsula	West Antarctic Ice Sheet	Victoria Land	Dronning Maud Land
Time-averaged values	Precipitation (in cm w.e. y^{-1})	6.7	40.7	9.0	68.8	25.9	14.1	24.3
	Temperature (in °C)	-39.8	-20.1	-29.3	-14.2	-24.2	-27.7	-19.7
	$\delta^{18}O$ (in ‰)	-42.3	-24.3	-30.6	-18.9	-26.6	-28.8	-25.2
	d (in ‰)	6.9	4.7	3.6	3.1	3.3	3.3	3.8
Inter-annual standard deviation	Precipitation (in cm w.e. y^{-1})	0.6	4.2	1.6	9.0	2.5	2.4	3.3
	Temperature (in °C)	0.5	0.7	0.8	0.9	0.7	0.7	0.5
	$\delta^{18}O$ (in ‰)	0.6	0.4	0.8	0.4	0.7	0.9	0.4
	d (in ‰)	0.4	0.4	0.4	0.2	0.4	0.5	0.5
Mean seasonal amplitude	Precipitation (in cm w.e. y^{-1})	5.2	28.4	7.2	45.0	19.2	12.2	19.3
	Temperature (in °C)	23.9	16.5	24.2	17.8	21.7	24.4	18.1
	$\delta^{18}O$ (in ‰)	10.9	4.4	12.2	4.1	8.8	10.7	7.3
	d (in ‰)	7.3	4.3	4.7	2.5	4.1	5.1	4.2
Inter-annual $\delta^{18}O$ - temperature relationship	a (in ‰ $°C^{-1}$)	0.7	0.2	0.3	0.1	0.6	0.6	0.4
	r	0.6	0.4	0.3	0.3	0.6	0.5	0.4
	p-value	5.9×10^{-5}	8.5×10^{-3}	4.5×10^{-2}	6.5×10^{-2}	1.9×10^{-4}	2.7×10^{-3}	2.2×10^{-2}

acceptable inter-annual variability only for Victoria Land and the plateau. However, these results are clearly limited by the low number of observational records for some regions.

Table 3.2.10 provides a brief overview of ECHAM5-wiso outputs for our seven regions of interest in terms of mean climate and isotopic variables, their standard deviation, seasonal amplitude, and the calculated regional $\delta^{18}O$ – T relationship. The main findings are again the highest slope simulated for the central Antarctic Plateau, followed by the Dronning Maud Land and West Antarctic Ice Sheet regions, and weak correlations in some regions (Weddell Sea, Antarctic Peninsula) where water stable isotope outputs are not good predictors of inter-annual temperature change within ECHAM5-wiso, together with low correlations and slopes for the other coastal regions (Indian Ocean sector, Victoria Land).

3.2.5. Conclusions and perspectives

This study presents a systematic evaluation of a present-day Antarctic climate simulation using the ECHAM5-wiso atmospheric circulation model equipped with water stable isotopes. For this simulation, covering the period 1960-2013, the model has been nudged to ERA atmospheric reanalyses. In particular, we tested its ability to correctly capture time-averaged values, inter-annual variations, and seasonal cycles in surface mass balance, temperature, and precipitation isotopic composition in Antarctica. As far as possible, we discarded model results prior to 1979, as model-data differences prior to 1979 may arise from uncertainties in the reanalyses, prior to the period for which satellite data were assimilated.

Despite some divergences, simulated P-E values are found to be a good surrogate for SMB. Most artefacts in modelled $\delta^{18}O$ are coherent with those for temperature, with systematic biases in different regions. Some of these artefacts may be linked to the nudging method and the reanalyses. Model-data comparisons are limited by data availability and by the fact that deposition and post-deposition processes are not considered in the simulation. This is particularly true for precipitation amounts, for which there is a lack of direct measurements, and isotopic analysis for many regions at a multi-annual timescale. A systematic comparison between water isotope measurements from precipitation and surface snow or ice core samples is needed for further in-depth studies of this topic. We note a lower quantitative performance from ECHAM5-wiso for d (time-averaged values and inter-annual standard deviations) than for $\delta^{18}O$, beyond its remarkable ability to resolve the spatial distribution of time-averaged d values. Our findings confirm several other studies conducted in other regions highlighting the fact that atmospheric models including ECHAM5-wiso tend to underestimate the variability of d in surface vapour (e.g. Steen-Larsen et al, 2016). Expanding earlier site-specific studies, we show that the strength and slope of the $\delta^{18}O$-temperature linear relationship is dependent on the

timescale in Antarctica over the last 4 decades. This finding has implications for past temperature reconstructions using ice core records. Finally, interesting results emerge for regional differences in the phase lag between the mean seasonal cycle in $\delta^{18}O$ and d, calling for further studies to better characterise this feature in precipitation and ice core records and better understand its implications of these lags for the representation of seasonal changes in moisture source effects.

Our study deserves to be expanded to other atmospheric models equipped with water stable isotopes and other nudged simulations using different reanalyses datasets to assess the robustness of our findings. Furthermore, obtaining more high-resolution ice core records is crucial to better assessing model skills for inter-annual variations. More measurements of precipitation, surface snow and vapour monitoring for water isotopes would also help to better characterise deposition and post-deposition processes, their implication for model-data evaluation studies, and for an improved climatic interpretation of ice core records.

Data availability

All data used in this chapter are publicy available. Table S1, from the Supplementary material, resumes the type, location, covered period and data citation of each record. The isotopic time-averaged values and standard deviations from precipitations, snow and firn-ice cores, and seasonal precipitation data (accumulation, temperature and isotopic composition), were archived on the PANGAEA data library at https://doi.pangaea.de/10.1594/PANGAEA.891279. Ice core data extracted from the Antarctica2k working group are available on the NOAA World Data Center for paleoclimatology (https://www.ncdc.noaa.gov/paleo-search/study/22589).

Acknowledgements

This study was supported by the ASUMA project supported by the ANR (Agence Nationale de la Recherche, project no. ANR-14-CE01-0001), which funded the PhD grant of Sentia Goursaud and the publication costs of this paper.

3.3 2 000 ans de reconstruction de la température de l'Antarctique

Ce travail résulte d'une collaboration internationale menée dans le cadre du groupe Antartica2k de PAGES (cf. Section 1.5.1), et coordonnée par Barbara Stenni (enseignant-chercheur à l'université Ca'Foscari, Venise, Italie). Fortement impliquée, j'ai effectué la calibration issue des simulations produites par ECHAM5-wiso (Section 3.3.3.4.1), et j'ai co-écrit l'article consécutif, publié dans le journal *Climate of the Past* (Stenni et al., 2017). Il s'accompagne d'un second article (Thomas et al., 2017), dans lequel est proposé une reconstruction de l'accumulation de l'Antarctique sur le dernier millénaire à partir des enregistrements de carotte de glace. La version ci-retranscrite a été adaptée au manuscrit de thèse. Le matériel supplémentaire, auquel nous nous référons dans l'article, est disponible en ligne (https://www.clim-past.net/13/1609/2017/, dernier accès : 07/2018).

Abstract. Climate trends in the Antarctic region remain poorly characterised, owing to the brevity and scarcity of direct climate observations and the large magnitude of interannual to decadal-scale climate variability. Here, within the framework of the PAGES Antarctica 2k working group, we build an enlarged database of ice core water stable isotope records from Antarctica, consisting of 112 records. We produce both unweighted and weighted isotopic ($\delta^{18}O$) composites and temperature reconstructions since 0 CE, binned at 5 and 10-year resolution, for 7 climatically-distinct regions covering the Antarctic continent. Following earlier work of the Antarctica 2k working group, we also produce composites and reconstructions for the broader regions of East Antarctica, West Antarctica, and the whole continent. We use three methods for our temperature reconstructions: i) a temperature scaling based on the $\delta^{18}O$-temperature relationship output from an ECHAM5-wiso model simulation nudged to ERA-interim atmospheric reanalyses from 1979 to 2013, and adjusted for the West Antarctic Ice Sheet region to borehole temperature data; ii) a temperature scaling of the isotopic normalized anomalies to the variance of the regional reanalysis temperature and iii) a composite-plus-scaling approach used in a previous continental scale reconstruction of Antarctic temperature since 1 CE but applied to the new Antarctic ice core database. Our new reconstructions confirm a significant cooling trend from 0 to 1900 CE across all Antarctic regions where records extend back into the 1st millennium, with the exception of the Wilkes Land coast and Weddell Sea coast regions. Within this long-term cooling trend from 0-1900 CE we find that the warmest period occurs between 300 and 1000 CE, and the coldest interval from 1200 to 1900 CE. Since 1900 CE, significant warming trends are identified for the West Antarctic Ice Sheet, the Dronning Maud Land coast and the Antarctic Peninsula regions, and these trends are robust across the distribution of records that contribute to the unweighted

isotopic composites and also significant in the weighted temperature reconstructions. Only for the Antarctic Peninsula is this most recent century-scale trend unusual in the context of natural variability over the last 2000-years. However, projected warming of the Antarctic continent during the 21st Century may soon see significant and unusual warming develop across other parts of the Antarctic continent. The extended Antarctica 2k ice core isotope database developed by this working group opens up many avenues for developing a deeper understanding of the response of Antarctic climate to natural and anthropogenic climate forcings. The first long-term quantification of regional climate in Antarctica presented herein is a basis for data-model comparison and assessments of past, present and future driving factors of Antarctic climate.

Résumé. Les tendances climatiques d'Antarctique restent à ce jour peu caractérisées, étant donné les rares et courts enregistrements issus d'observations instrumentales, et les larges variabilités aux échelles inter-annuelles à décennales. Dans le cadre du groupe de travail PAGES Antarctica 2k, nous avons étendu une base de données d'isotopes stables de l'eau enregistrés dans des carottes de glace d'Antarctique, pour atteindre un nombre de 112 enregistrements. Nous avons produit des composites ($\delta^{18}O$) avec et sans pondération, ainsi que des reconstructions de la température à partir de 0 EC, à des résolutions de 5 ans 10 ans, et pour 7 régions distinctes par leur climat couvrant le continent Antarctique. Suivant la précédente étude menée par le groupe de travail Antarctica 2k, nous avons aussi produit des composites et des reconstructions pour les plus larges régions de l'Antarctique de l'Est, l'Antarctique de l'Ouest, et l'ensemble du continent. Nous avons utilisé trois méthodes de reconstructions de la température : i) une calibration de la température par la relation linéaire qui lit $\delta^{18}O$ et la température dans le modèle ECHAM5-wiso forcé par les réanalyses ERA-interim de 1979 à 2013, et ajusté à l'aide de données de température dans les trous de forage pour la région de l'Antarctique de l'Ouest, ii) une calibration de la température des anomalies des isotopes normalisés par la variance de la température régionale issue des réanalyses, et iii) une approche de calibration « composite-plus-scaling » utilisée dans la précédente reconstruction de la température de l'Antarctique à l'échelle continentale depuis 1 EC, mais cette fois-ci avec notre nouvelle base de données de carottes de glace d'Antarctique. Nos nouvelles reconstructions confirment une tendance de refroidissement significative de 0 à 1900 EC pour l'ensemble des régions de l'Antarctique pour lesquelles les enregistrements remontent à un million d'années, à l'exception des régions côtières de la Terre des Wilkes et de la mer de Weddell. Au cours de ce long refroidissement de 0 à 1900 EC, des tendances de réchauffement significatives ont eu lieues de 300 à 1000 ED, et le plus froid intervalle de 1200 à 1900 EC. Depuis 1900 EC, des tendances de réchauffements significatives pour la région de l'Antarctique de l'Ouest, la région

côtière de la Terre de la Reine Maud, et la péninsule antarctique, et ces tendances sont robustes parmi la distribution des enregistrements qui contribuent aux composites isotopiques non pondérés, mais aussi pour les reconstructions de température pondérées. Seule la région de la péninsule antarctique présente une tendance inhabituelle à l'échelle du dernier siècle dans le contexte de la variabilité naturelle sur les 2000 dernières années. Cependant, les projections de réchauffement du continent de l'Antarctique au cours du 21ème siècle pourraient bientôt faire émerger des tendances inhabituelles significatives dans d'autres régions d'Antarctique. La base de données isotopiques issues de carottes de glace couvrant les deux derniers millénaires étendue, développée par ce groupe de travail ouvre davantage de champs d'investigations pour développer une compréhension approfondie de la réponse du climat de l'Antarctique aux forçages climatiques naturel et anthropogénique. La première quantification de long terme du climat de l'Antarctique à l'échelle régionale, présentée ici, fournit une base pour des comparaisons modèle-données, ainsi que pour une évaluation des facteurs passés, présents et futurs contrôlant le climat de l'Antarctique.

3.3.1 Introduction

Antarctica is the region of the world where instrumental climate records are shortest and sparsest. Estimates of temperature change with reasonable coverage across the full Antarctic continent are only available since 1958 CE (Nicolas and Bromwich, 2014), and the large magnitude of year-to-year climate variability that characterises Antarctica makes the interpretation of trends in this data sparse region problematic (Jones et al., 2016). As a result, the knowledge of past Antarctic temperature and climate variability is predominantly dependent on proxy records from natural archives. While coastal proxy records are being developed from terrestrial and marine archives, information on Antarctic climate above the ice sheet exclusively relies on the climatic interpretation of ice core records.

Within the variety of measurements performed in boreholes and ice cores, only water stable isotopes can provide subdecadal resolution records of past temperature changes (Küttel et al., 2012). In high accumulation areas of coastal zones and West Antarctica, annual layer counting is feasible during the last centuries to millennia (Plummer et al., 2012; Abram et al., 2013; Thomas et al., 2013; Sigl et al., 2015; Winstrup et al., 2017), and annual water stable isotope signals can be delivered. However, in the dry regions of the central Antarctic plateau, where the longest ice core records are available, chronologies are less accurate and rely on the identification of volcanic deposits that can be used to tie ice cores from different sites to a common Antarctic ice core age scale (Sigl et al., 2014; Sigl et al., 2015).

The chemical and physical signals measured in an individual ice core reflect a local climatic signal archived through the deposition and reworking of snow layers. The intermittency of Antarctic precipitation (Sime et al., 2009; Masson-Delmotte et al., 2011), variability in precipitation source regions (Sodemann and Stohl, 2009), and post-depositional effects of snow layers including wind drift and scouring, sublimation, and snow metamorphism (Frezzotti et al., 2007; Ekaykin et al., 2014; Hoshina et al., 2014; Steen-Larsen et al., 2014; Casado et al., 2016; Touzeau et al., 2016) can distort the climate signal preserved within ice cores and produces non-climatic noise. As a result, obtaining a robust climate signal can only be achieved through the combination of multiple ice core records from a given site and/or region, and through the site-specific calibration of the relationships between water stable isotopes and temperature.

Water can be characterised by the stable isotope ratios of oxygen ($\delta^{18}O$: the deviation of the ratio of $^{18}O/^{16}O$ in a sample, relative to that of the standard, Vienna Standard Mean Ocean Water) and of hydrogen (δD: the deviation of the ratio of $^{2}H/^{1}H$). Both of these parameters within ice cores provide information on past temperatures. There is solid theoretical understanding of distillation processes relating moisture transport towards the polar regions with air mass cooling and the progressive loss of heavy water molecules along the condensation pathway (Jouzel and Merlivat, 1984). This theoretical understanding is further supported by numerical modelling performed using atmospheric general circulation models equipped with water stable isotopes (Jouzel, 2014). The effects of these processes are observed in the spatial relationships between the isotopic composition of Antarctic precipitation/surface snow and surface air temperature across the continent. However, relationships between water stable isotopes in snow and surface temperature may vary through time as a result of changes between condensation and surface temperature (in relationship to changes in boundary layer stability), changes in moisture origin and initial evaporation conditions, changes in atmospheric transport pathways and changes in precipitation seasonality or intermittency (Masson-Delmotte et al., 2008). Investigations based on the sampling of Antarctic precipitation have demonstrated that seasonal and inter-annual isotope versus temperature slopes are generally smaller than spatially-derived relationships (van Ommen and Morgan, 1997; Ekaykin et al., 2004; Schlosser et al., 2004; Schneider et al., 2005; Fernandoy et al., 2010; Stenni et al., 2016). Moreover, emerging studies combining the monitoring of surface water vapour isotopic composition with the isotopic composition retained in surface snow and precipitation have revealed that snow-air isotopic exchanges during snow metamorphism affect surface snow isotopic composition (Casado et al., 2016; Ritter et al., 2016; Touzeau et al., 2016). It is not yet possible to assess the importance of such post-deposition processes for the interpretation of ice core water stable

isotope records, but they may enhance the relationship between snow isotopic composition and surface temperature more than expected from the intermittency of snowfall (Touzeau et al., 2016). Changes in ice sheet height due to ice dynamics may also affect the surface climate trends inferred from water stable isotope records; however, this influence should be of second order over the last 2000-year interval that is the focus of this study (Fegyveresi et al., 2011).

As a result, the two key challenges to reconstruct past changes in Antarctic temperature from ice core isotope records are (1) to develop methodologies to combine different individual or stacked ice core records in order to deliver regional-scale climate signals, and (2) to quantify the temperature changes represented by water stable isotope variations.

Goosse et al. (2012) first calculated a composite of Antarctic temperature simply by averaging seven standardized temperature records inferred from water stable isotopes using a spatial isotope-temperature relationship for the last millennium. The first coordinated effort to reconstruct Antarctic temperature during the last 2000 years (PAGES 2k Consortium, 2013) screened published ice core records for annual layer counting or alignment of volcanic sulphate records and overlap with instrumental temperature data (Steig et al., 2009), leading to the selection of 11 records. The reconstruction procedure used a composite-plus-scaling approach similar to the methodology of Schneider et al. (2006), and produced reconstructions of the continent-wide temperature history as well as specific West Antarctica and East Antarctica reconstructions. The skill of the reconstructions was limited by the number of available records through time (for instance, only one predictor in each region prior to 166CE). This analysis identified significant ($p<0.01$) cooling trends from 166 to 1900 CE, 2.5 times larger in West Antarctica than in East Antarctica. A robust cooling trend over this time period has also been identified from terrestrial and marine reconstructions from other regions (PAGES 2k Consortium, 2013; McGregor et al., 2015).

The comparison of these first Antarctic 2k time series with those from other regions obtained within the PAGES 2k working groups identified three specificities: (i) Antarctic reconstructed centennial variations did not correlate with those from other regions; (ii) the Antarctic region was the only one where a protracted cold period was not starting around 1580 CE; (iii) the Antarctic region was the only one where the 20th century was not the warmest century of the last 2000 years. A recent effort to characterize Antarctic and sub-Antarctic climate variability during the last 200 years also concluded that most of the trends observed since satellite climate monitoring began in 1979 CE cannot yet be distinguished from natural (unforced) climate variability (Jones et al., 2016), and observed instrumental climate trends are of the opposite sign to those produced by most forced climate model simulations over the same post-1979 CE interval. The only exception to this conclusion was for changes in the Southern Annular Mode

(SAM), the leading mode of atmospheric circulation variability in the high latitudes of the SH, which has showed a significant and unusual positive trend since 1979 CE.

While changes in the SAM have been related to the human influence on stratospheric ozone and greenhouse gases (Thompson et al., 2011), major gaps remain in identifying the drivers of multi-centennial Antarctic climate variability. For instance, the influence of solar and volcanic forcing on Antarctic climate variability remains unclear. This is due to both the lack of observations and to the lack of confidence in climate model skill for the Antarctic region (Flato et al., 2013). Goosse et al. (2012) have used simulations from an intermediate complexity model to attribute the Antarctic annual mean cooling trend from 850 to 1850 CE to volcanic forcing. Recent comparisons of climate model simulations with the PAGES2k regional reconstructions have highlighted greater model-data disagreement in the Southern Hemisphere (SH) than in the Northern Hemisphere (Bothe et al., 2015; Abram et al., 2016); such disagreement could be due either to model deficiencies or to large uncertainties in the reconstructions which were built on relatively small number of records. Changes in ocean heat content and ocean heat transport have likely contributed to the different temperature evolution at high southern latitudes compared to other regions of the Earth (Goosse, 2017), and model based studies have suggested that circulation in the Southern Ocean may act to delay by centuries the development of sustained warming trends in high southern latitudes (Armour et al., 2016). Antarctic temperature reconstructions spanning the last 2000 years may help to better constrain the processes and timescales by which natural and anthropogenic forcing act to affect climate changes in the Antarctic region.

This motivates our efforts to produce updated Antarctic temperature reconstructions. The previous continent-scale reconstruction (PAGES 2k Consortium, 2013), where only a limited number of records have been used, may mask important regional-scale features of Antarctica's climate evolution. Here we use an expanded paleoclimate database of Antarctic ice core isotope records and new reconstruction methodologies to reconstruct the climate of the past 2000 years, at decadal scale and on a regional basis. Seven distinct climatic regions have been selected: the Antarctic Peninsula, the West Antarctic Ice Sheet, the East Antarctic Plateau, and four coastal domains of East Antarctica. This regional selection, which is supported by regional atmospheric RACMO2.3p2 model results (Van Wessem et al., 2014; Thomas et al., 2017), is applied to both Antarctic ice core-derived isotopic (temperature-proxy) and snow accumulation rate reconstructions (see companion paper in the same issue by Thomas et al.). Section 3.3.2 describes the ice core and the temperature data sets used in this study, as well as the modelling framework used to support the analysis. The climate region definition, the pre-processing of the data and the different reconstruction methods are presented in Section 3.3.3. Section 3.3.4

discusses our new regional isotopic and temperature reconstructions for Antarctica, including the application of the previous methodology to the new database. Finally, section 3.3.5 presents the summary of our results and their implications.

3.3.2 Datasets

3.3.2.1 Ice core records

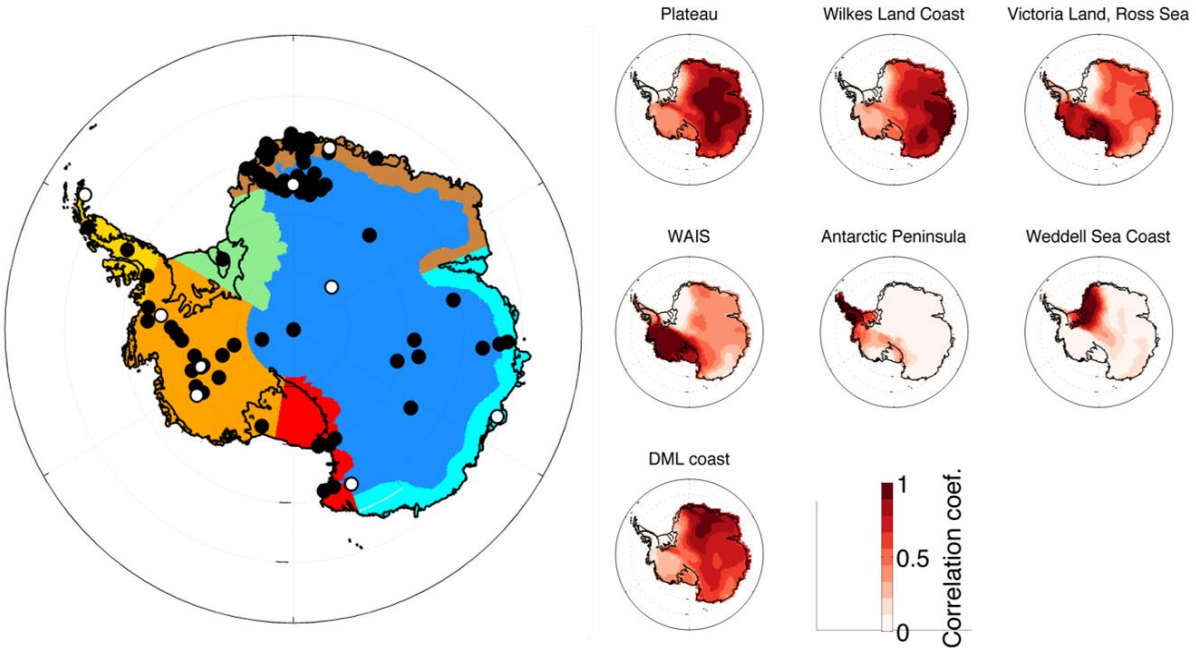

Figure 3.3.1: Left panel: schematic map of the seven Antarctic regions selected for the regional reconstructions. In blue the East Antarctic Plateau, in light blue the Wilkes Land Coast, in green the Weddell Sea Coast, in yellow the Antarctic Peninsula, in orange the West Antarctic Ice Sheet, in red the Victoria Land Coast – Ross Sea and in brown the Dronning Maud Land Coast. The dots show the site locations. The white dots represent the sites that have been used in the previous continental scale reconstruction (PAGES 2k Consortium, 2013). Right panel: Correlation maps between the regional mean temperature and each grid point using the Nicolas and Bromwich (2014) data set.

Here we present and use a new expanded database which has been compiled in the framework of the PAGES Antarctica 2k working group. The initial selection criteria are those requested by the PAGES 2k network (http://www.pages-igbp.org/ini/wg/2k-network/data) for the building of the community-sourced database of temperature-sensitive proxy records (PAGES 2k Consortium, 2013). Briefly, i) the records must be publically available and published, ii) a relation between the climate proxies and variables should be stated, iii) the record duration should be between 300 and 2000 years, iv) the chronology, certified by the data owner, should contain at least one chronological control point near the end (most recent) part of the record and another near the oldest part of the record, v) the resolution should be at least one analysis every 50 years.

In building the Antarctica2k database we also allow shorter records to be included, although request a stratigraphic control using volcanic markers (Sigl et al., 2014) and whenever possible,

a dating by annual layer counted chronology. This last requirement is only possible in the high-accumulation regions of West Antarctica, the Antarctic Peninsula and coastal areas of East Antarctica. The inclusion of shorter records is designed to improve data coverage for assessments of climatic trends in Antarctica during the past century. The 11 records included in the previous continental-scale reconstruction (PAGES 2k Consortium, 2013) relied on a highly precise chronological framework consisting of a common chronology, which used 42 volcanic events to synchronize the records. Here, we use both high and low-resolution records. Most of the records have a data resolution ranging from 0.025 to 5 years (only three records have a resolution of >10 years). Previous studies (Frezzotti et al., 2007; Ekaykin et al., 2014) have shown that post-depositional and wind scouring effects, acting more effectively when the accumulation rate is very low, limit our ability to obtain temperature reconstructions at annual resolution in most of the interior of Antarctica. Because of this, in our regional reconstructions we use 5-year averaged data for reconstructing the last 200 years, and 10-year averages for reconstructing the last 2000 years. Using 5, or 10-year averages also decreases our dependence on an annually precise chronological constraint between the ice core records, allowing us to more confidently use the expanded database. The data have been also screened for glaciological problems, with those records that are very likely to be affected by ice flow dynamics excluded. This enlarged database consists of 112 isotopic records. A list of the records used are reported in Table S1 (Supplementary Material) and their spatial distribution is shown in Figure 3.3.1. Figure B.1 shows the location of the ice core sites along with a visualization of the record lengths. Most of the records of this new database cover the last 200 years and this is particularly true for the more coastal areas. Within the database, 36 records cover just the last 50 years or less, while 50 records cover the whole length of the past 200 years. There are 15 records that cover the last 1000 years, while only 9 records reach as far back as 0 CE.

3.3.2.2 Temperature product

The instrumental record is very short in Antarctica, and most ice core sites do not have weather station measurements associated with the cores. In addition, the retrieval of the first meter of firn can be difficult, due to poor cohesion of the snow. As a result, for many sites, there is no overlap between instrumental and proxy data, which complicates the proxy calibration exercise. To enlarge the calibration dataset, we use the climate field reconstruction from Nicolas and Bromwich (2014) (hereafter NB2014; http://polarmet.osu.edu/datasets/Antarctic_recon/). This surface temperature dataset provides homogeneous data at 60 km resolution, extends from 1957 to 2013, and includes the revised Byrd temperature record (Bromwich et al., 2013) that improves the skill of the temperature product over West Antarctica. It covers a longer timespan

than reliable atmospheric reanalysis products for Antarctica (which begin only 1979 CE), and has a higher spatial resolution than available isotope enabled GCM outputs. This dataset is used to estimate the spatial representativeness of individual core sites (Section 3.3.3.3.2), to scale the normalized isotopic anomaly data to temperature (Section 3.3.3.4.2), and to calculate the surface temperature reconstructions with the Composite-Plus-Scale (CPS) method (Section 3.3.3.4.4).

3.3.2.3 Modelling framework

In order to use model information on isotope-temperature relationships in Antarctic precipitation, we use a reference simulation performed using the Atmospheric General Circulation Model ECHAM5-wiso. The initial ECHAM5 model (Roeckner et al., 2003) has been equipped with water stable isotopes (Werner et al., 2011), following earlier work on ECHAM3 (Hoffmann et al., 1998) and ECHAM4 (Werner et al., 2001), and accounting for fractionation processes during phase changes. This model is used here because recent studies, based on model-data comparisons using observations of precipitation and surface vapour isotopic composition at a global scale and in the Arctic (e.g. Werner et al, 2011; Steen-Larsen et al., 2017), have shown strong model skill of ECHAM5-wiso when it is run in high resolution as in this study (T106, with a mean horizontal grid resolution of approximately 1.1° x 1.1°). A study of the 2012 atmospheric river event in Greenland has demonstrated the skill of ECHAM5-wiso to reproduce these events, with a good representation of the water isotope signature (Bonne et al., 2014). In Antarctica, model performance was assessed against a compilation of surface data (Masson-Delmotte et al., 2008) and recent measurements of vapour and precipitation (Ritter et al., 2016; Dittmann et al., 2016).

Here, we use a 1958-2014 CE simulation where ECHAM5-wiso was nudged to atmospheric reanalyses from ERA40 (Uppala et al., 2005) and ERA interim (Dee et al., 2011), and run using the same ocean surface boundary conditions (SST and sea-ice) as in ERA40 and ERA interim. Ocean surface water isotopic values were set to constant values using a compilation of observational data (Schmidt et al., 2007). Inter-comparisons of reanalysis products showed good skills of ERA-interim for Antarctic precipitation (Wang et al., 2016), surface temperature, as well as vertical profiles of winds and temperatures. However, comparisons with in-situ observations reveal an underestimate of precipitation and slight cold bias in the surface temperatures in some regions (Thomas and Bracegirdle, 2015).

The ECHAM5-wiso simulations produce a large increase in the temperature and the $\delta^{18}O$ outputs prior to 1979, which is not observed in instrumental or ice core data (Goursaud et al., 2018). This arises from a discontinuity in the ERA-40 reanalyses due to the lack of observations

available for assimilation and boundary conditions prior to the satellite era (e.g. Antarctic sea ice) (Nicholas and Bromwich, 2014). We therefore use the ECHAM5-wiso simulations only for 1979-2013 CE.

For the analysis of the isotope-temperature relationships at each individual ice core site, we extracted the grid point data closest to each site. For the analysis of isotope-relationships at regional scale, we calculated the area-weighted average of model outputs at grid points within the region. The $\delta^{18}O$-temperature relationship was calculated using the annual or seasonal average 2-meter temperature and annual precipitation-weighted $\delta^{18}O$, to mimic deposition processes. The simulation does not account for post-deposition processes (i.e., diffusion, which is not important on the 5 and 10-year timescales considered here; e.g. Küttel et al., 2012).

3.3.3 Methodology

3.3.3.1 Defining climatic regions

Earlier work of the PAGES Antarctica 2k working group produced a continent-scale temperature reconstruction for the whole of Antarctica, as well as reconstructions for East and West Antarctica based on a separation approximated by the Transantarctic mountain chain (PAGES 2k Consortium 2013). These broad-scale groupings mask important regional climatic trends noted in individual studies. In particular, the absence of recent significant warming in the Antarctica 2k continent-scale temperature reconstruction is known to not be representative of all Antarctic locations (e.g. Steig et al., 2009; Mulvaney et al., 2012; Abram et al., 2013; Steig et al., 2013).

In this study, we choose seven climatic reconstruction regions (see Fig. 3.3.1). These regions are defined based on our knowledge of regional climate and snow deposition processes in the Antarctic region, as well as the availability of ice core isotope records. In particular, we separated coastal regions (below 2000 m altitude) from the East Antarctic Plateau: coastal sites receive moisture from the high-latitude Southern Ocean, and are affected by the nearby sea ice cover (Masson-Delmotte et al., 2008). In contrast, high altitude sites receive moisture that has travelled at higher altitude, originating from further afield, and from clear sky precipitation (Ekaykin et al., 2004). The regional selections were further validated and refined by spatial correlation of temperature using the NB2014 data product. The seven climatic regions are defined as follows (see Table B.1):

1. EAST ANTARCTIC PLATEAU: All East Antarctic contiguous regions at an elevation higher than 2000 m, including everything south of 85 °S. We exclude high peaks of the Transantarctic Mountains if they belong to the Victoria Land - Ross Sea coast (e.g. Taylor Dome or Hercules Névé).

2.WILKES LAND COAST: A region that sits at an altitude <2000m, and extends from Lambert Glacier (67 °E) east to the start of Victoria Land and the Transantarctic Mountains (160 °E).
3. WEDDELL SEA COAST: Extending eastward from longitude 60 °W to 30 °W, and south of 75 °S, and lying at an altitude < 2000 m. Eastward of the 30°W longitude, the 75 °S latitude defines the boundary with the Dronning Maud Land coast region, with the northeastern corner of the Weddell Sea coast region occurring where the 75 °S latitude meets the 2000 m elevation contour. This region includes the Filchner Ice Shelf and most of the Ronne Ice Shelf.
4. ANTARCTIC PENINSULA: This region encompasses the mountainous Antarctic Peninsula. Between 74°S and 70°S the longitudinal boundaries lie between 60-80 °W, while north of 70 °S the longitudinal boundaries increase to 50-80 °W so as to capture the northern end of the peninsula.
5. WEST ANTARCTIC ICE SHEET: A region bounded by longitudes 60 °W to 170 °W, and north of 85 °S. In the Peninsula region (60-80 °W) a northern bound of 74 °S is also applied.
6. VICTORIA LAND COAST - ROSS SEA: This region is north of 85 °S, and at an altitude <2000 m, with the exception of some localised peaks within the Trans-Antarctic mountain range. It extends from 160 °E to 190 °E (i.e. 170 °W) and incorporates most of the Ross Ice Shelf.
7. DRONNING MAUD LAND COAST: Extending eastward from 30 °W to 67 °E (Lambert glacier). The southern-most boundary lies at 75°S (where this region borders with the Weddell Sea region), or at the 2000-meter elevation contour elsewhere.
In addition to these seven climatic regions, we also produce reconstructions for a continent-wide Antarctic region. Broad-scale East Antarctic (incorporating the climatic regions of the East Antarctic Plateau, as well as the Weddell Sea, Dronning Maud Land, Wilkes Land and Victoria Land coasts) and West Antarctic (incorporating the climatic regions of the West Antarctic Ice Sheet and Antarctic Peninsula) reconstructions are also presented. These additional reconstructions facilitate comparisons of our new results, using additional methods and an expanded database, with earlier findings of the Antarctica 2k working group and subsequent research using the 2013 continent-scale reconstruction for Antarctic temperature.

3.3.3.2 Data pre-processing

All ice core records in the Antarctica 2k database were assigned to one of the climatic regions described in section 3.3.3.1 (as well as to East *vs.* West Antarctica, and to the Antarctic-wide classifications). The majority (94 out of 112) of ice core water isotope records in the database are based on oxygen isotope ratios ($\delta^{18}O$). In cases where only deuterium isotope (δD) data is available, the ice core time series were converted to $\delta^{18}O$-equivalent by dividing by 8, a value

that represents the slope of the global mean meteoric relationship of oxygen and deuterium isotopes in precipitation, and is close to the ratio of 7.75 observed in surface Antarctic snow (Masson-Delmotte et al., 2008).

The ice core $\delta^{18}O$ (and $\delta^{18}O$-equivalent) records were compiled on a common annual average age scale. For records with sub-annual resolution this involved averaging all data from within a calendar year to generate an annual average dataset. Pseudo-annual records were generated for the ice core $\delta^{18}O$ records with lower than annual resolution. These pseudo annuals assume that each low-resolution isotopic value represents an average of the full-time interval that the sample covers. As such, a nearest-neighbour interpolation method was used to generate stepped (piecewise constant) pseudo-annual records that continue the measured isotopic value across all of the calendar years that it represents.

Records were next binned to 5y and 10y average resolution and converted to $\delta^{18}O$ anomalies. This reduction in resolution is designed to reduce the influence of small age uncertainties between the records, as well as the non-climatic noise induced by post-deposition (e.g. wind erosion, diffusion) processes (Frezzotti et al. 2007; Ekaykin et al., 2014). The 5y resolution records were converted to anomalies relative to their mean over the 1960-1990 CE interval, and records that don't include a minimum of 6 bins (30y) coverage since 1800 CE are excluded based on length. Overall, 79 records in the new Antarctica 2k water isotope database meet the minimum requirement of having at least 30y data coverage since 1800 CE. In some cases, records meet this minimum length requirement but do not include data for the full 1960-1990 CE reference interval. We adjust the mean value of each of these records by matching the mean $\delta^{18}O$ of their most recent 6 bins (30y) of data to the mean of all anomaly records from the same climatic region and over the same 6-bin interval. We also produce normalised records by adjusting the variance of the records using the same reference period and method as for the anomaly records.

The 10y resolution anomaly and normalised records were generated using the same method but using a reference period of 1900-1990 CE and a minimum data coverage of 9 bins (90y) since 0 CE. Similarly, records that don't include the full 1900-1990 CE reference period have the mean of their most recent 9-bin (90y) interval adjusted to match the mean of all other anomaly records from the same region and over the same 9-bin interval. Overall, 67 records in the new Antarctica 2k water isotope database meet the minimum requirement of having at least 90y data coverage since 0 CE.

Some regions of Antarctica include dense networks of ice core data, such as coastal and plateau sites in Dronning Maud Land (Fig. S1 in Supplementary Material). To reduce possible bias

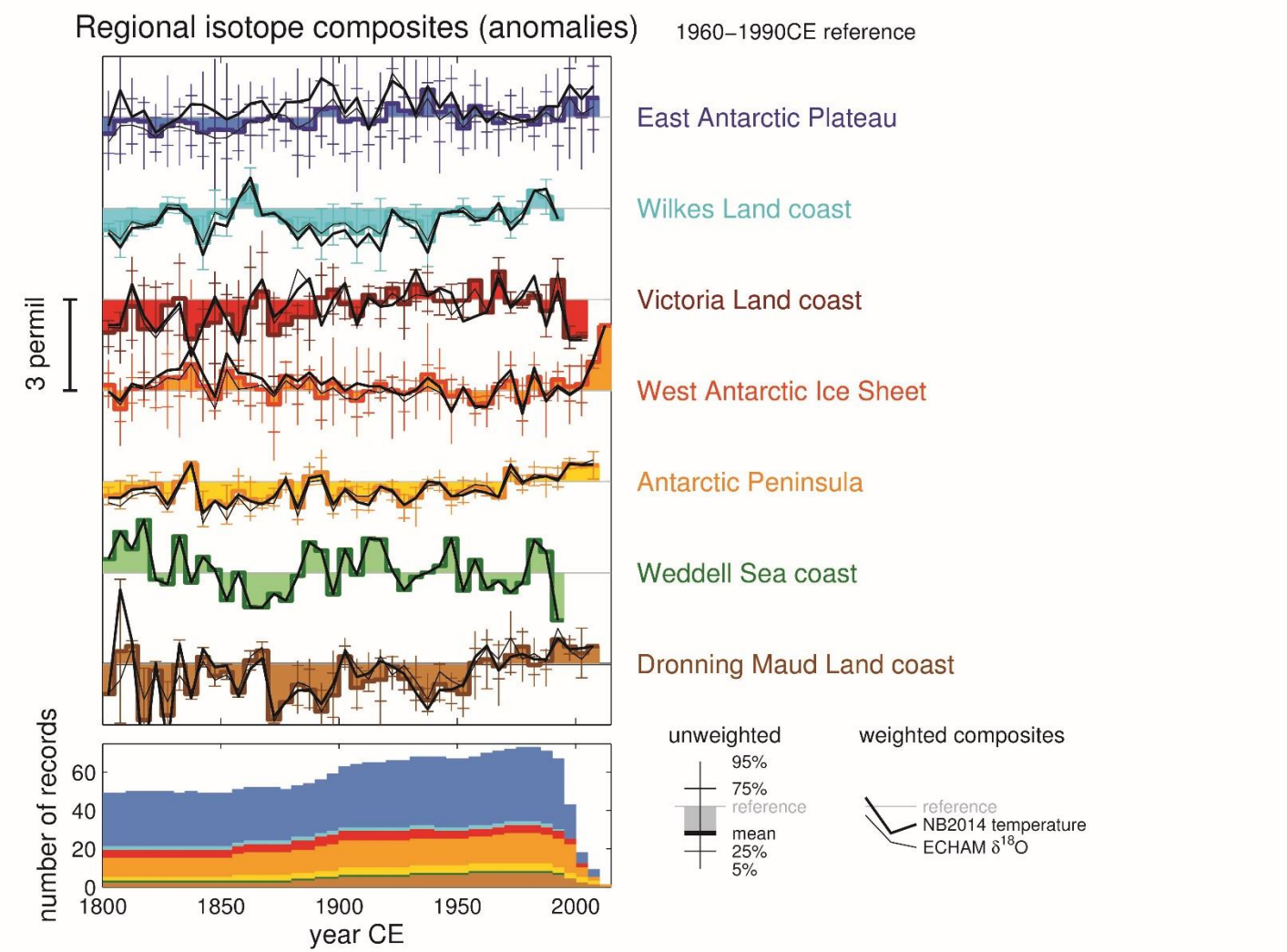

Figure 3.3.2: Regional δ18O composite reconstructions over the last 200 years using 5y-binned anomaly data. Both unweighted composites and weighted composites (using both NB2014 temperature and ECHAM δ18O weighting methods) are shown. For each 5y-bin of the unweighted data, the mean δ18O anomaly across all records in the climatic region is calculated, as well as the distribution of δ18O anomalies within each bin. All anomalies are expressed relative to the 1960-1990CE interval. The number of records that contribute to the reconstructions for each region are displayed in the lower panel.

towards these data-rich regions an additional data reduction method was used, based on a 2° latitude by 10° longitude grid. Where multiple ice core records from the same climatic-region fall within the same grid cell, their isotopic anomalies (or normalised data) are averaged to produce a single composite time series for the grid. This replicates the simple unweighted compositing method described in section 3.3.3.3.1, but at the grid-scale to reduce the representation of data-rich areas prior to the regional compositing. Supplementary figures S2 and S3 show the distribution of records by region that meet the 6-bin (30y) and 9-bin (90y) minimum requirements for the 5y and 10y composites, respectively, after the gridded data reduction step.

3.3.3.3 Compositing Methods

We use a suite of reconstruction methods of varying complexity in order to assess robust trends and variability in Antarctic ice core $\delta^{18}O$ records and temperature.

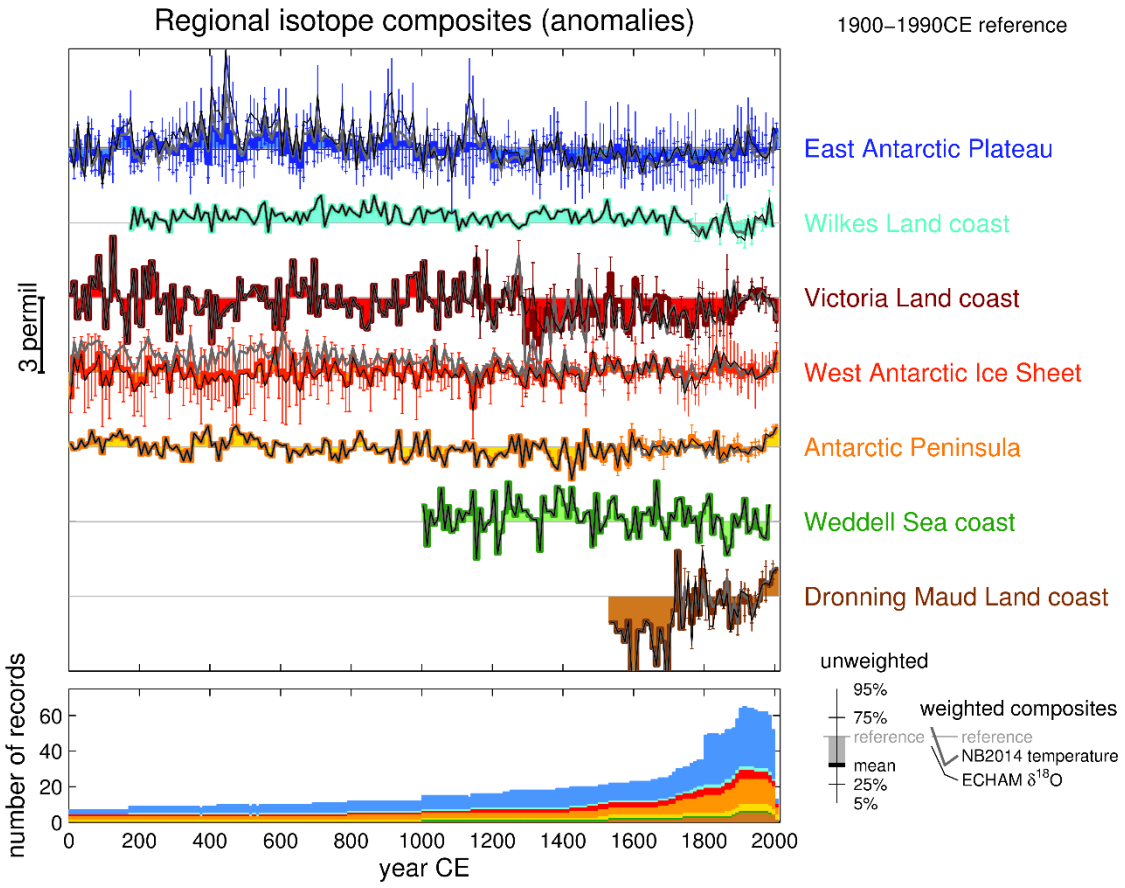

Figure 3.3.3: Regional $\delta^{18}O$ composite reconstructions over the last 2000 years using 10y-binned anomaly data. Both unweighted composites and weighted composites (using both NB2014 temperature and ECHAM $\delta^{18}O$ weighting methods) are shown. For each 10y-bin of the unweighted data, the mean $\delta^{18}O$ anomaly across all records in the climatic region is calculated, as well as the distribution of $\delta^{18}O$ anomalies within each bin. All anomalies are expressed relative to the 1900-1990CE interval. The number of records that contribute to the reconstructions for each region are displayed in the lower panel.

3.3.3.3.1 Unweighted Composites

Our first reconstruction method involves calculating simple composites of $\delta^{18}O$ anomalies. For each 5 or 10y bin we calculate the mean $\delta^{18}O$ anomaly across all records in the climatic region, as well as the distribution of $\delta^{18}O$ anomalies within each bin (see Fig. 3.3.2 and 3.3.3). This basic reconstruction method is analogous to that used for the Ocean 2k low-resolution reconstruction (McGregor et al. 2015). The benefit of this simple method is that it requires no weighting or calibration assumptions, which is advantageous for data sparse regions such as Antarctica (and the global oceans). The disadvantage is that it applies equal weighting to all records within a climatic region, which may introduce biases related to record length, location and climatic skill.

3.3.3.3.2 Weighted composites based on site-level temperature regressions

In order to avoid biases from uneven data sampling, we performed, for each region, a multiple regression between each site temperature and the relevant regional average temperature (see Fig. 3.3.2 and 3.3.3). Most of the ice core records do not cover the full instrumental period, so it is problematic to use the $\delta^{18}O$ anomalies directly to determine the regression vectors required for a weighted temperature reconstruction. Instead, we use the climate field reconstruction of NB2014 to estimate the weights: the annual mean temperature time series at the grid cell corresponding to each ice core site is extracted from the NB2014 product, and the regional average is also calculated for each reconstruction region. Regression-based weightings are calculated based on the relationship between site temperature and regional average temperature, and the regression is performed for each combination of ice core records through time. The weights are then applied to the ice core $\delta^{18}O$ anomalies to produce regional averaged standardized anomalies.

We further reproduced this regression method using both the $\delta^{18}O$ and temperature field outputs from the ECHAM5-wiso experiments. The regression of site-$\delta^{18}O$ against regional average-$\delta^{18}O$, or site-temperature onto regional-temperature gave nearly identical weighting factors, supporting the use of the temperature field to calculate regressions. The effects of the different weighting methods on each regional isotopic composite, as well as the initial 10y isotopic anomaly records, are reported in the Supplementary Material (Fig. from S4 to S10). The small differences between ECHAM and NB2014-based regressions were due to the lower resolution of ECHAM-5wiso, which does not include islands and topographic features such as Roosevelt Island and Law Dome. For this reason, we preferentially use the NB2014 dataset for the temperature regression reconstruction method.

3.3.3.4 Temperature Reconstructions

The relationship between $\delta^{18}O$ and local surface temperature is complicated by the influence of a large range of processes (origin of moisture sources, intermittency in precipitation, snow drift, snow-air exchanges, snow metamorphism, and diffusion in ice cores). It is not possible to consider each process independently, because in many cases, there are simply no observations to constrain them well enough. However, the atmospheric circulation often leads to several processes to be correlated (reduced sea ice, increased precipitation and warmer temperature, for instance). We follow here the classical approach, which is to perform a linear regression of ice core $\delta^{18}O$ with local surface temperature, on the regional average products. This method has the advantage of looking at all the climatic processes influencing $\delta^{18}O$ in "bulk", and the use of regional average allows us to limit the influence of small-scale processes. The lack of an overlap period between our site $\delta^{18}O$ records and direct temperature observations makes the proxy calibration difficult. The CPS method (Section 3.3.3.4.4), which replicates the 2013 PAGES 2k reconstruction method, is limited to sites where this calibration is possible. To overcome this limitation and include the largest number of records, we also use models to scale the regional isotope composites. A first method uses ECHAM5-wiso to determine the regional $\delta^{18}O$-temperature relationship in a mechanistic way (Section 3.3.3.4.1). A second method uses a more statistical approach, and simply scales the normalized record to the instrumental period temperature variance (Section 3.3.3.4.2). Both approaches are equally valid and share the same hypothesis: that the instrumental period (1979-2013) is representative of the longer-term climate variability. Finally, for the West Antarctic Ice Sheet region, an independent longer-term temperature record is available from borehole temperature measurements (Orsi et al., 2012). We use this independent temperature record to scale the long term 1000-1600 temperature trend for the West Antarctic Ice Sheet region, to provide our best estimate of temperature change in line with current knowledge (Section 3.3.3.4.3).

In the figure captions, we refer to the different methods as "ECHAM", "NB2014" and "borehole", respectively.

3.3.3.4.1 Scaling using model-based regional $\delta^{18}O$-Temperature relationships

We use the coherent physical framework of the 1979-2013 CE simulation performed at T106 resolution with ECHAM5-wiso to infer constrains on regional $\delta^{18}O$-temperature slopes through linear regression analysis between regional averages of simulated annual mean temperature and precipitation-weighted $\delta^{18}O$ (Table 3.3.1). These regional $\delta^{18}O$-temperature regressions were applied to the regional ice core composites ($\delta^{18}O_{region}$ anomalies) to scale them from $\delta^{18}O$ to temperature units (see Fig. 3.3.4 and 3.3.5), and produce temperature anomalies (T_{region}). The

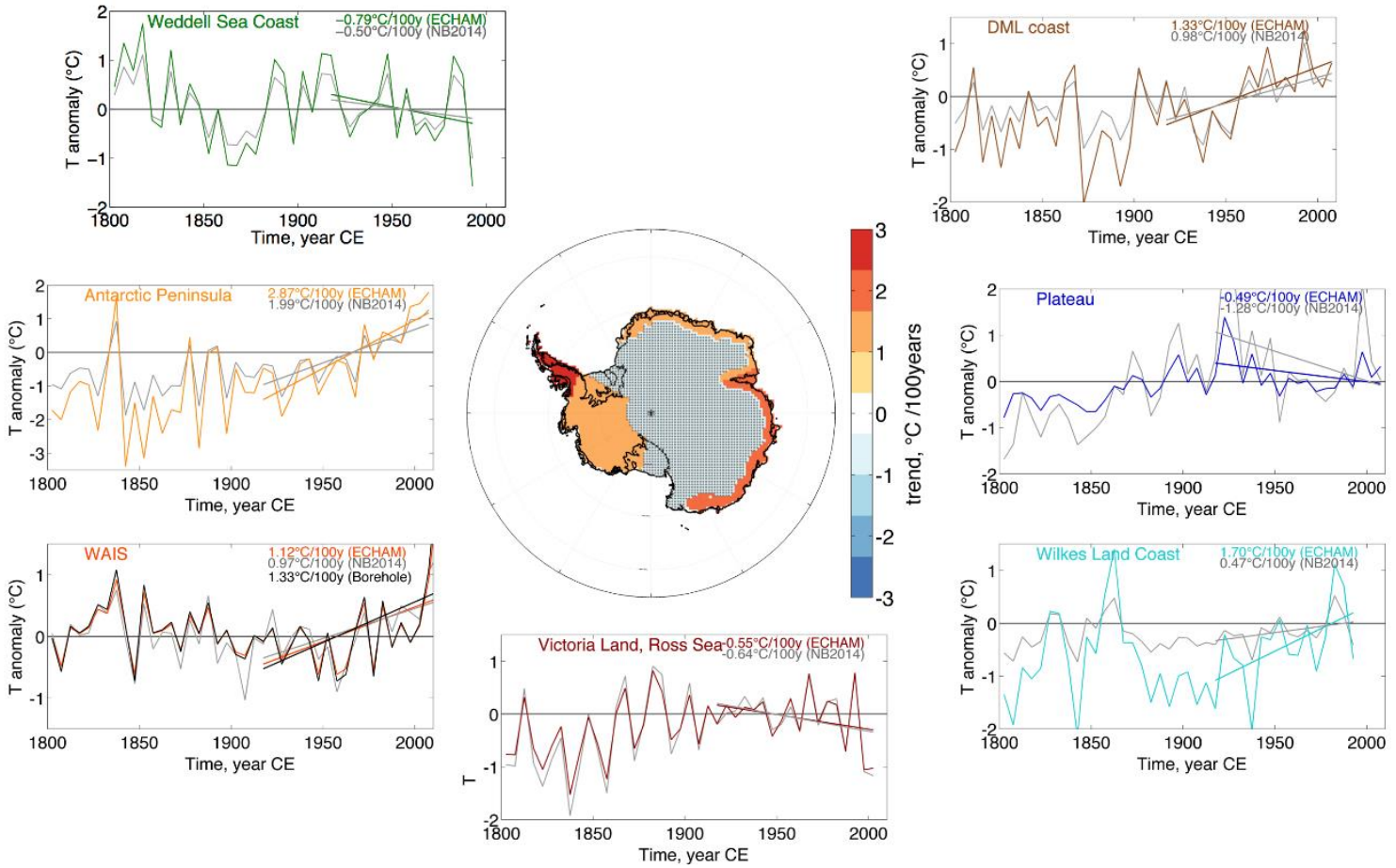

Figure 3.3.4: Regional temperature (T anomalies in °C, referenced to the 1960-1990 CE interval) reconstructions using 5y-binned data for the past 200y. Weighing method based on the correlation between site T and regional T from NB2014. Temperature scaling method: i) based on the correlation between annual mean regional $\delta^{18}O$ and regional T from ECHAM5-wiso forced by ERA-Interim (coloured lines), ii) scaled on NB2014 target over 1960-1990 CE (grey lines), iii) West Antarctic Ice Sheet region adjusted to match the temperature trend between 1000 and 1600 CE based on borehole temperature measurements (black line, Orsi et al., 2012). Linear trends are calculated over the last 100 years of the reconstructions (colours match associated reconstruction methods). The map at the centre reports regional trends over the last 100y trend using 5y data based on the ECHAM method adjusted for the West Antarctic Ice Sheet region to borehole data. Hatched areas are not significant (p>0.05).

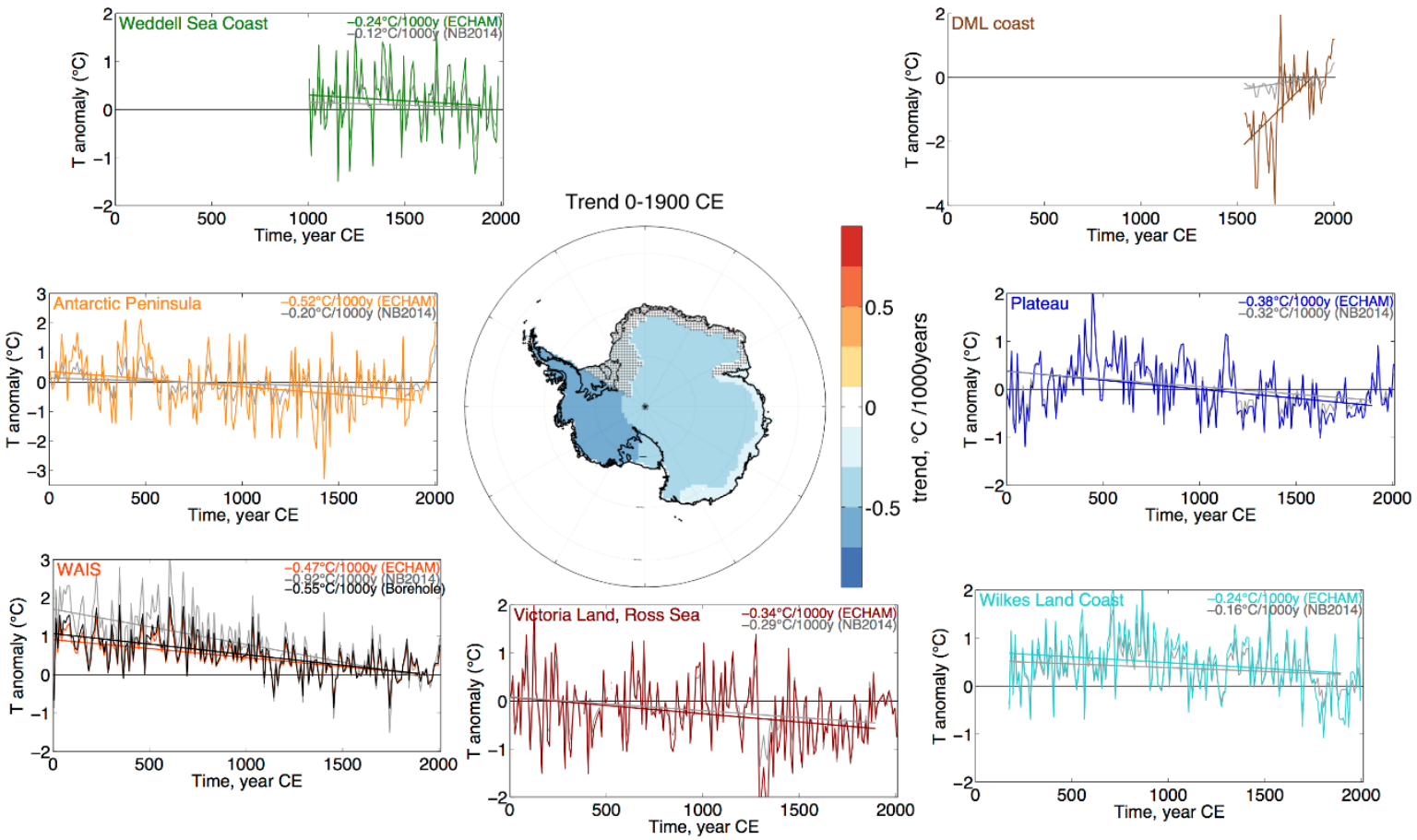

Figure 3.3.5: Regional temperature (T anomalies in °C, referenced to the 1900-1990 CE period) reconstructions using 10y data for the past 2000y. Weighing method based on the correlation between site T and regional T from NB2014 forced by ERA-Interim. Temperature scaling method: i) based on the correlation between annual mean regional $\delta^{18}O$ and regional T from ECHAM5-wiso forced by ERA-Interim (coloured lines), ii) scaled on NB2014 target over 1960-2010CE (grey lines), iii) West Antarctic Ice Sheet region adjusted to match the temperature trend between 1000 and 1600 CE based on borehole temperature measurements (black line, Orsi et al., 2012). Linear trends are calculated over the period 0-1900 CE using 10y binned data. The map at the centre reports the trend values calculated between 0 and 1900 CE using 10y data based on the ECHAM method adjusted for the West Antarctic Ice Sheet region to borehole data (the hatched area is not significant).

correlation coefficient α_{region} is calculated using the York et al. (2004) method, taking into account uncertainties both in T_{region} and in $\delta^{18}O_{region}$, with each prior uncertainty equals to 20% of the variance.

$$T_{region} = \alpha_{region}\delta^{18}O_{region} = \alpha_{region} \sum_{sites\ i} w_i\, \delta^{18}O_i$$

In this equation, w_i represents the weights assigned to each site i, and $\delta^{18}O_i$ the site $\delta^{18}O$ anomalies in 5 or 10 year averaged records. The limited length of the observational period (1979-2013 CE), does not allow us to precisely estimate the slope α on 10-year averages, and we preferred to use 1-year anomalies, where the slopes are significant (Table 3.3.1), and apply these slopes on the 10-year binned composites. It implies that the interannual $\delta^{18}O$-temperature relationship comes from mechanisms that are also applicable to decadal scale variability. It is impossible to further test this hypothesis without longer independent temperature records. The use of the ECHAM-wiso isotope enabled climate model is the most up-to-date tool we have to quantify the $\delta^{18}O$-temperature on broad spatial-temporal scales, and is our best tool to infer the $\delta^{18}O$-temperature relationship in the absence of data. Its main limitation is the model resolution: it is missing some coastal topographical features, notably James Ross Island, Roosevelt Island, and Law Dome, and cannot faithfully represent regions where these sites are important.

All regional $\delta^{18}O$ temperature relationships produced by the ECHAM-wiso output are statistically significant (at 95 % confidence) with the exception of the Antarctic Peninsula. Weak correlations are also found for the Weddell Sea coast (r = 0.34). Stronger correlation coefficients are obtained inland, for the larger-scale East and West Antarctic sectors, and maximum values (r=0.62) are identified for the East Antarctic Plateau.

Similarly, the simulated regional $\delta^{18}O$-temperature slopes are highest for Victoria Land (1.21 ‰ °C^{-1}) and lowest for the Peninsula (0.40 ‰ °C^{-1}). This low slope for the Antarctic Peninsula does not agree with the temporal $\delta^{18}O$-temperature relationship that has been reported for the highly-resolved James Ross Island ice core (0.86 ‰ °C^{-1}; Abram et al., 2011) , while it is similar to one reported for the Gomez ice core (0.5 ‰ °C^{-1}; Thomas et al., 2009) and precipitation samples collected at the O'Higgins Station (0.41 ‰ °C^{-1}, Fernandoy et al., 2012). ECHAM finds that the only site on the peninsula with a significant correlation between $\delta^{18}O$ and temperature is Bruce Plateau (66 °S, 64 °W) (slope=0.63±0.58 ‰ °C^{-1}, r=0.13, p=0.03), and the overall low $\delta^{18}O$-temperature slope is largely attributable to model resolution. We expect that the ECHAM scaling will produce a temperature reconstruction with a high-amplitude bias in the Antarctic Peninsula.

High slopes similar to the Victoria Land are identified in the inland East Antarctic plateau, Weddell Sea Coast and West Antarctic Ice Sheet regions (1.05, 0.99 and 0.96 ‰ °C^{-1}, respectively), together with intermediate values in coastal Dronning Maud Land with a 0.93 ‰ °C^{-1} mean slope. At the whole Antarctic ice sheet scale, the overall temporal slope is dominated by inland regions and simulated at 0.98 ‰ °C^{-1}. This analysis is more thoroughly examined in a study comparing an isotopic dataset from surface snow, snowfalls and ice cores (Goursaud et al., 2018).

Table 3.3.1: Linear regression analysis (slope with ±1σ uncertainty, correlation coefficient r, and p-value) of the simulated δ^{18}O-temperature relationships extracted from the ECHAM5-wiso model for each climatic region, as well as the broad East Antarctic, West Antarctic and whole Antarctic regions.

Geographic region	Slope (°C/‰)	Slope (‰/°C)	r	p-value
1. East Antarctic Plateau	0.95 ± 0.05	1.05 ± 0.06	0.62	0.0001
2. Wilkes Land Coast	1.91 ± 0.11	0.52 ± 0.03	0.44	0.0084
3. Weddell Sea Coast	1.01 ± 0.06	0.99 ± 0.06	0.34	0.0449
4. Antarctic Peninsula	2.50 ± 0.15	0.40 ± 0.02	0.31	0.0658
5. West Antarctic Ice Sheet	1.04 ± 0.06	0.96 ± 0.05	0.59	0.0002
6. Victoria Land Coast	0.83 ± 0.05	1.21 ± 0.07	0.49	0.0027
7. Dronning Maud Land Coast	1.08 ± 0.06	0.93 ± 0.05	0.39	0.0217
West Antarctica	1.03 ± 0.06	0.97 ± 0.05	0.62	0.0001
East Antarctica	1.00 ± 0.05	1.00 ± 0.05	0.58	0.0002
All Antarctica	1.02 ± 0.06	0.98 ± 0.05	0.56	0.0004

3.3.3.4.2. Scaling based on NB2014 variance

In addition, we used an independent method of scaling the normalized δ^{18}O anomalies to the standard deviation ($\sigma(T)$) of the regional temperature from NB2014, over the 1960-1990 CE interval for the 5-year binned averages, and the period 1960-2010 CE for the 10-year binned averages. This scaling is similar to the one used for the CPS method (see next section).

$$T_{region} = \sigma(T)_{region} \delta^{18}O_{region}(normalized)$$

This scaling method implies that the δ^{18}O-temperature relationship can be inferred from the ratio of temperature to δ^{18}O standard deviation, which would be true if the relationship between the two was purely linear. If some of the δ^{18}O variance is due to something else than temperature, this scaling will under-estimate temperature variations. This method also assumes that the last 30 to 50 years provide a good estimate of the 5 or 10-year temperature variance. In the absence of longer temperature reconstructions, this is the best estimate of $\sigma(T)_{region}$ that we can provide.

3.3.3.4.3. Scaling based on borehole temperature for the WAIS region.

In the West Antarctic Ice Sheet region, the approaches described above give different results (Fig. 3.3.4 and 3.3.5), with the first method (temperature scaling from the $\delta^{18}O$-T relationship in ECHAM-wiso) giving a smaller amplitude. At WAIS–Divide, there is an independent temperature record, which can be used to scale the long-term temperature evolution. We used the borehole temperature reconstruction at WAIS Divide (Orsi et al, 2012) to adjust the amplitude of temperature variations, matching the cooling trend over the period 1000-1600 CE (-1.1 °C.1000y^{-1}), with a correction factor relating the WAIS-Divide site to the West Antarctic region ($c=\sigma_{WAIS}/\sigma_{WDC}$ = 0.65), with σ_{WAIS} the standard deviation of the annual NB2014 WAIS regional mean dataset, and σ_{WDC} the standard deviation of the annual NB2014 time series at the WAIS-Divide site, which gives a 1000-1600 cooling trend of -0.76 °C.

This scaling is actually in line with the other two scalings: 1000-1600 slope of -0.65 °C for ECHAM and -1.01 °C for NB2014 scaling. The temperature calibration presented here is the best estimate we can provide with current knowledge, but we expect it to be revised in the future, with more precise $\delta^{18}O$ modeling, and more independent quantitative temperature reconstructions.

3.3.3.4.4 Replication of the 2013 Antarctica2k reconstruction method

To facilitate comparison with the preceding Antarctica2k temperature reconstruction published by the PAGES 2k Consortium (2013), we apply their reconstruction method to the updated ice-core isotope data collection. The method is a simple Composite-Plus-Scale (CPS) approach (Jones et al., 2009), updated from Schneider et al. (2006) and implemented similarly to Neukom et al. (2014). We apply this method to all sub-regions defined above, the broad East and West Antarctic divisions and to the Antarctic-wide database, replicating the Antarctic reconstructions presented in the PAGES 2k Consortium (2013) study.

First, the annual-average records are allocated to the climatic regions as defined above. The following steps are then repeated for each region separately. Second, only the records with no missing values in the 1961-1991 CE calibration period are selected. These records are then scaled to mean zero and unit standard deviation over their common interval of data availability. Next, the normalised records are correlated against the NB2014 regional mean temperatures over 1961-1991 CE. Between 0 % and 33 % of the ice core records within each region have negative correlations (physically implausible) with the target and are removed from the proxy matrix. A composite of the remaining records is then calculated by creating a weighted average, where the weighting of each ice core record is based on its temperature correlation from the previous step. The composite is then scaled to the mean and standard deviation of the NB2014

regional temperatures over the 1961-1991 CE period. The compositing and scaling steps are done in a nested approach, i.e. repeated for all periods with different proxy data availability.
In the reconstruction of the PAGES 2k Consortium (2013), three records were infilled with neighbouring sites to have no missing data in the calibration window: WDC06A was infilled with data from WDC05A, Siple Station and Plateau Remote were infilled by least median of squares multiple linear regression using nearby records (PAGES 2k Consortium, 2013). To allow comparison, we also used the infilled data for these records. Thus, the only difference to the reconstruction of PAGES 2k Consortium (2013) is that we use an extended proxy database with more records and an updated temperature target (NB2014 instead of Steig et al. 2009).
While this CPS approach allows a quantitative calibration to the NB2014 temperature data, it has some limitations compared to the above methods. First, in this implementation it allows only the inclusion of data covering the calibration period, thereby removing more than half of the available records (62 out of 112). Second, the calibration period is extremely short and therefore individual years (for example with outliers) can significantly bias the reconstruction and reasonable validation of the reconstruction is hardly possible. The main difference from the other compositing methods described above is the weight of each record and the interval, over which the data are standardized.

3.3.4 Results and Discussion

We use the varying reconstruction methods to identify robust trends in the Antarctic ice core database. We present results based on isotopic trends, as well as temperature reconstructions, and examine these for the seven climatic regions and for the larger-scale Antarctic regions (Section 3.3.4.1); compare our results to the previous Antarctic temperature reconstruction (Section 3.3.4.2), and investigate the link between temperature and volcanic activity (Section 3.3.4.3).

3.3.4.1 Regional-scale $\delta^{18}O$ and temperature reconstructions

Five year-binned $\delta^{18}O$ composite records since 1800 CE years are reported for each of the seven climatic regions Figure S2 (unweighted isotope anomalies, Supplementary Material) and Figure 3.3.2 (weighted and unweighted data). The unweighted composites are shown with respect to the distributions of data within each bin, and expressed relative to the 1960-1990 CE interval. Figure 3.3.2 also shows the reconstructions that are obtained by weighting the records within each region based on the NB2014 temperature field and by the ECHAM5-wiso $\delta^{18}O$ field. Figure 3.3.3 (and Figure S3 in Supplementary Material) shows equivalent data, but for 10y averages since 0 CE relative to the 1900-1990 CE interval.

The highest density of ice core records is present in the last century, but these are not evenly distributed over Antarctica (Fig. S1 in Supplementary Material) with most of the records in the plateau and coastal areas of Dronning Maud Land and across the West Antarctic Ice Sheet. On the other hand, only 1 and 3 records are present in the Weddell Sea and Wilkes Land coastal areas, respectively.

In order to separate the uncertainties due to the stacking procedure from uncertainties in the temperature scaling, we first discuss the main features of the un-weighted regional $\delta^{18}O$ anomalies (Section 3.3.4.1.1), and then proceed to discuss the weighted regional $\delta^{18}O$ anomalies, and finally the temperature reconstructions. The weighted and unweighted composites produce similar results for the seven climatic regions (see figures in Supplementary Information from B.4 to B.10), suggesting that our reconstructions are robust, and don't depend on the exact methodology used (see Fig. 3.3.2 and 3.3.3). There are two exceptions to this: the Antarctic Plateau (Fig. B.4), where the many sites in Dronning Maud Land perhaps still bias the simple average towards this area even with the gridded data-reduction process, and the West Antarctic ice Sheet (Fig. B.8) where the two long records from WAIS-Divide and Roosevelt Island (RICE) have diverging trends for much of the last 2000 years. The weighted reconstruction gives a higher weight to WAIS-Divide, which maintains a long-term negative isotopic trend over the last 2ka in this region (see section 3.3.4.1.2). We further checked that WAIS-Divide is indeed more representative of temperatures averaged across the West Antarctic Ice Sheet region than RICE looking at temperature correlation maps which use the NB2014 temperature field (Fig. B.8). The temperature reconstructions obtained with the different methods are further shown in Fig. B.15. We assess trends for the seven climatic regions (and in the larger-scale Antarctic groupings) for the reconstructions prior to 1900 CE (up to 1,900 years length) (Section 3.3.4.1.2), and since 1900 CE (up to 110 years length) (Section 4.1.3), and estimate the significance of the most recent 100-year trend relative to natural variability (Section 3.3.4.1.4).

3.3.4.1.1 Trend significance in unweighted composites

We first use a Monte Carlo approach to assess the significance of trends in the unweighted composites. This test is designed to test the significance of trends in relation to the distribution of data within each bin of the isotopic composites. For each bin where 2 or more ice cores contribute data we scale random Gaussian data about the median value and $\pm 2\sigma$ distribution of isotopic data within that bin. We then sample from this scaled Gaussian data to produce 10,000 simulations of each regional composite. We then assess the proportion of ensemble members which produce trends of the same sign as the mean composite, and the proportion of ensemble members where the trend is of the same sign as the mean composite and also significant at

greater than 95 % confidence. These trend analyses are based on 10-year binned isotopic anomalies for trends prior to 1900 CE, and 5-year binned data for trends over the last 100 years of the composites (although equivalent results are found if 10-year binned data are used to assess trends in the last 100 years).

Results of unweighted composite trend analysis are summarised in Table 3.3.2. This analysis shows that for the unweighted composites the long-term cooling trend from 0-1900 CE is only significant for the East Antarctic plateau. Visual examination of the unweighted composites (Fig. 3.3.3) suggest that many of the other climate regions appear to also have a negative unweighted isotopic trend over part of the last 2000 years (e.g. Wilkes Land and West Antarctic Ice Sheet regions), but these trends are not significant in the unweighted composites when calculated across the full interval from 0-1900 CE. The Victoria Land coast trend prior to 1900 CE is not significant in the mean or median unweighted composites, but over the interval where two or more ice cores contribute to the composites the Monte Carlo assessments indicate that negative isotopic trends are produced in all 10,000 ensemble members and are significant ($p<0.05$) more often than can be explained by chance alone.

The significant trend that is produced in the unweighted composite for the East Antarctic Plateau climate region is also evident in the broader East Antarctic compilation and for the Antarctic continent-scale composite. The continent-scale cooling trend produced in unweighted composites using the expanded Antarctica 2k database is in agreement with the PAGES 2k Consortium (2013) results where a long-term cooling trend over the Antarctic continent was identified. It is also consistent with robust pre-industrial cooling trends that have been identified in other continental reconstructions (PAGES 2k Consortium, 2013) and in the global oceans (McGregor et al., 2015).

Isotopic trends in the last 100 years of the unweighted composites show significant positive trends across a number of regions. In particular, significant isotopic trends, indicative of climate warming, are evident in the unweighted composites for the Antarctic Peninsula, and the Wilkes Land and Dronning Maud Land coasts. The West Antarctic Ice Sheet region does not display a significant ($p<0.05$) positive trend in the mean or median of the unweighted composites, but the Monte Carlo analysis across the distribution of isotopic data within each 10-year bin suggests that positive trends are produced in 99.5 % of the 10,000 simulations and are significant ($p<0.05$) more often than can be explained by chance alone (20.5 % of simulations). Similarly, the Victoria Land-Ross Sea region shows a negative but insignificant trend in the mean and median composites, but in the Monte Carlo simulations this negative (cooling) trend is produced in 99.9% of ensemble members and is significant in 13.6 % of ensemble members. The apparent inverse isotopic trends during the last century between the Victoria Land-Ross

Sea region and the West Antarctic Ice Sheet and Antarctic Peninsula regions may be indicative of dynamical processes in the Amundsen Sea sector, which on interannual time scales are known to cause opposing climate anomalies between these regions.

The PAGES 2k Consortium (2013) study concluded that Antarctica was the only continent-scale region to not see of the long-term cooling trend of the past 2000 years reverse to recent significant warming. However, at the regional scale examined in this study recent significant warming is suggested by many of the unweighted isotopic composites, particularly for coastal regions of Antarctica and the West Antarctic ice sheet. It should be stressed that these results are based only upon the simple unweighted compositing of the regional isotopic data, and the significance of trends is further assessed in the following section after weighting of the individual ice core records based on how representative they are of isotopic and temperature variability within each climatic region.

3.3.4.1.2 Long term trends in weighted reconstructions

To extend this trend analysis further we next assess the pre-1900 CE (see Fig. 3.3.5) trends in the temperature reconstructions produced by scaling the ice core data based on our different approaches (see section 3.3.3.3.3). We estimate the uncertainty of the slope based on the $\pm 2\sigma$ uncertainty in the regression parameters. The robustness of the slope estimation to individual data points was further checked by taking out 10 % of data points randomly and calculating the slope again, but the uncertainty estimates this yields is much smaller than the uncertainty based on regression parameters. The slopes obtained by each of the temperature scaling methods are presented in Table 3.3.3. The uncertainty in the amplitude of the 0-1900 CE trend is dominated by the uncertainty in the temperature scaling of the composite. To make the discussion clear, we first focus on the trend in terms of normalised $\delta^{18}O$ anomalies, with respect to the 1900-1990 CE periods, which circumvents the temperature scaling issues.

The period 0-1900 CE exhibits significant negative trends in most regions, from -0.4 to -1.3 ‰ y^{-1}. The trend is largest in West Antarctic Ice Sheet (-1.3 ± 0.2 ‰ y^{-1}), Victoria Land (-0.9 ± 0.4 ‰ y^{-1}), and the Antarctic Plateau (-0.8 ± 0.3 ‰ y^{-1}) regions. It is smaller but still significant for the Wilkes Land coast (-0.6 ± 0.5 ‰ y^{-1}, p=0.007) and Antarctic Peninsula (-0.5±0.2 ‰ y^{-1}). It is insignificant on the Weddell Sea coast (p=0.4), and the dataset is not long enough to estimate millennial-scale trends on the DML coast. These observations indicate a broad scale cooling trend over the continent that is comparable in amplitude to the variance over the past 100 years. As previously mentioned, the 0-1900 CE negative trend is largest in the normalized datasets for the West Antarctic Ice Sheet region, but this feature masks sub-regional scale differences, with the RICE record indicating increasing rather than decreasing anomalies. This result is puzzling because both WAIS Divide (to the west) and Victoria Land cores (e.g. VLG,

Table 3.3.2: Summary of trend statistics for isotopic anomalies using unweighted composites. Trends are expressed as isotopic anomalies, in per mil $\delta^{18}O$ per decade units. Trends and their significance (p; based on the Student's t-statistic) are calculated using a linear additive model, and reported for the mean and median composites. Monte Carlo testing is applied to 10,000 ensemble members based on the unweighted composite distributions, which are assessed to determine the percentage of trends with the same sign as the mean trend, and the percentage with the same sign and a significance of $p < 0.05$. Bold values indicate mean and median trends with a significance of $p < 0.05$, and Monte Carlo simulations where significant, same-signed trends exceed 5% of the ensemble.

	Pre-1900 CE trends			Last 100y trends		
Region	Mean trend ‰ $10y^{-1}$ (p)	Median trend ‰ $10y^{-1}$ (p)	Monte Carlo % (% p<0.05)	Mean trend ‰ $10y^{-1}$ (p)	Median trend ‰ $10y^{-1}$ (p)	Monte Carlo % (% p<0.05)
1. East Antarctic Plateau	**-0.003 (0.000)**	**-0.002 (0.000)**	**100 (99.2)**	0.011 (0.675)	0.040 (0.096)	**96.2 (14.1)**
2. Wilkes Land coast	0.017 (0.444)	0.017 (0.444)	80.6 (2.3)	**0.098 (0.001)**	**0.098 (0.001)**	**100 (90.5)**
3. Weddell Sea coast	-0.002 (0.376)	-0.002 (0.376)	-	-0.060 (0.318)	-0.060 (0.318)	-
4. Antarctic Peninsula	0.006 (0.188)	0.004 (0.361)	84.3 (2.9)	**0.112 (0.000)**	**0.111 (0.000)**	**100 (98.2)**
5.West Antarctic ice sheet	0.000 (0.435)	0.000 (0.428)	85.4 (1.4)	0.033 (0.226)	0.042 (0.091)	**97.0 (14.4)**
6. Victoria Land Coast	-0.006 (0.118)	-0.006 (0.101)	**100 (12.76)**	-0.054 (0.220)	-0.074 (0.102)	**99.9 (13.6)**
7. Dronning Maud Land Coast	-0.032 (0.366)	-0.027 (0.448)	95.3 (0.1)	**0.147 (0.000)**	**0.158 (0.001)**	**100 (99.8)**
West Antarctica	0.000 (0.437)	-0.001 (0.118)	**95.57 (11.2)**	**0.054 (0.021)**	**0.082 (0.001)**	**100 (79.8)**
East Antarctica	**-0.003 (0.000)**	**-0.002 (0.000)**	**100 (100)**	**0.037 (0.035)**	**0.064 (0.003)**	**99.8 (55.1)**
All Antarctica	**-0.002 (0.000)**	**-0.002 (0.000)**	**100 (99.5)**	**0.044 (0.005)**	**0.073 (0.000)**	**99.9 (76.2)**

to the east of RICE) show a clear cooling trend prior to 1900 CE, and together this points to a more complex picture of the evolution of the atmospheric circulation around the Ross Sea than can be captured with the current network of cores. The RICE $\delta^{18}O$ record, situated on Roosevelt Island on the Ross Ice Shelf, is more influenced by air masses from the eastern Ross Sea sector than the rest of the West Antarctic Ice Sheet region which is influences predominantly by air masses from the Amundsen Sea (Neff and Bertler, 2015; Emanuelsson et al., 2018). Moreover, borehole temperature and $\delta^{15}N$ thermal fractionation records at RICE highlight some notable differences to the isotope temperature reconstruction, which suggest that sea ice extent exerts an important control, perhaps masking aspects of the longer-term temperature trends in the region (Bertler et al., 2018). Over the period from 0-1900 CE the ECHAM temperature scaling suggests that the mean cooling trends are -0.38ºC $1000y^{-1}$ for the east Antarctic Plateau, -0.47ºC $1000y^{-1}$ for the West Antarctic ice sheet, -0.52°C $1000y^{-1}$ for the Antarctic Peninsula, and -0.34°C $1000y^{-1}$ for Victoria Land. Coastal East Antarctic regions do not show significant trends (Weddell Sea, Dronning Maud Land coast and Wilkes Land coast). The NB2014 temperature scaling produces lower trends overall (Table 3.3.3), except for the West Antarctic Ice Sheet where the trend doubles (-0.92 ºC $1000y^{-1}$). The trend in the West Antarctic Ice Sheet region can be assessed independently by comparing the WAIS composite to the borehole temperature record of Orsi et al. (2012) at WAIS-Divide for the period 1000-1600 CE. The borehole-derived trend at WAIS divide is -0.55°C $1000y^{-1}$ for the 0-1900CE period, in between the -0.92 °C $1000y^{-1}$ value found with the NB2014 method and the -0.47 °C $1000y^{-1}$ found with the ECHAM scaling. The CPS method finds a slope of -0.59°C $1000y^{-1}$ for the period 0-1900 CE, very close to the borehole method.

Over all of Antarctica, we find a cooling trend of -0.26 to -0.4 °C $1000y^{-1}$ between 0-1900 CE across the various scaling approaches (Table 3.3.3). This trend is comparable in magnitude to the -0.22±0.06 °C $1000y^{-1}$ found for the Arctic region (Kaufman et al., 2009). This trend was attributed to a decrease in JJA solar insolation due to precession of the equinoxes.

3.3.4.1.3 Trends of the last 100 years in weighted reconstructions

Studies based on individual ice cores have identified significant positive trends in the last century (Mulvaney et al., 2012; Steig et al., 2013). Similar to the findings for unweighted composites, significant warming trends in the last 100 years (Table 3.3.4) of the weighted anomalies are evident for the Antarctic Peninsula (+2.65σ $100y^{-1}$ with respect to the 1960-1990 CE normalisation period), Dronning Maud Land coast (+2.51σ $100y^{-1}$) and the West Antarctic Ice Sheet (+1.17σ $100y^{-1}$) regions. The trends in other regions are not significant (Table 3.3.4). In temperature units, the NB2014 method gives a scaling within 30 % of ECHAM, while CPS is generally 50 % lower (Table 3.3.4). Since 1900 CE, the reconstructions indicate that the

Table 3.3.3: Trend analysis of the period 0-1900 CE (or shorter depending on maximum record length), for the various temperature scaling approaches detailed in Section 3.3.3.4.

			ECHAM		NB2014		Borehole	
Geographic region	Start date	End date	Slope (°C/1000y)	p-value	Slope (°C/1000y)	p-value	Slope (°C/1000y)	p-value
1. East Antarctic Plateau	0	1900	**-0.38 ± 0.14**	**<0.0001**	**-0.32 ± 0.12**	**<0.0001**	NaN	NaN
2. Wilkes Land Coast	170	1900	**-0.24 ± 0.17**	**0.0072**	**-0.16 ± 0.13**	**0.0161**	NaN	NaN
3. Weddell Sea Coast	1000	1900	-0.24 ± 0.54	0.3763	-0.12 ± 0.27	0.3763	NaN	NaN
4. Antarctic Peninsula	0	1900	**-0.52 ± 0.23**	**<0.0001**	**-0.20 ± 0.09**	**<0.0001**	NaN	NaN
5. West Antarctic Ice Sheet	0	1900	**-0.47 ± 0.10**	**<0.0001**	**-0.92 ± 0.16**	**<0.0001**	**-0.55 ± 0.11**	**<0.0001**
6. Victoria Land Coast	0	1900	**-0.34 ± 0.18**	**0.0003**	**-0.29 ± 0.12**	**<0.0001**	NaN	NaN
7. Dronning Maud Land Coast	1530	1900	**5.96 ± 3.27**	**0.0007**	**0.97 ± 0.62**	**0.0032**	NaN	NaN
West Antarctica	0	1900	**-0.24 ± 0.07**	**<0.0001**	**-0.44 ± 0.10**	**<0.0001**	**-0.55 ± 0.10**	**<0.0001**
East Antarctica	0	1900	**-0.30 ± 0.10**	**<0.0001**	**-0.32 ± 0.10**	**<0.0001**	NaN	NaN
All Antarctica	0	1900	**-0.36 ± 0.08**	**<0.0001**	**-0.40 ± 0.08**	**<0.0001**	**-0.26 ± 0.06**	**<0.0001**

	Normalized		CPS			
Geographic region	Slope (σ/1000y)	p-value	Slope (°C/1000y)	p-value	Start date	End date
1. East Antarctic Plateau	**-0.76 ± 0.28**	**0**	**-0.15 ± 0.06**	**0**	10	1900
2. Wilkes Land Coast	**-0.59 ± 0.48**	**0.0161**	**-0.10 ± 0.07**	**0.008**	180	1900
3. Weddell Sea Coast	-0.41 ± 0.92	0.3763	-0.09 ± 0.27	0.4935	1000	1900
4. Antarctic Peninsula	**-0.50 ± 0.23**	**0**	**-0.09 ± 0.09**	**0.0479**	0	1900
5. West Antarctic Ice Sheet	**-1.32 ± 0.23**	**0**	**-0.59 ± 0.08**	**0**	0	1900
6. Victoria Land Coast	**-0.89 ± 0.39**	**0**	-0.54 ± 0.58	0.0661	1140	1900
7. Dronning Maud Land Coast	**4.98 ± 3.20**	**0.0032**	**NaN**	**NaN**	1890	1900
West Antarctica	**-0.76 ± 0.16**	**0**	**-0.55 ± 0.07**	**0**	0	1900
East Antarctica	**-0.59 ± 0.19**	**0**	**-0.18 ± 0.06**	**0**	10	1900
All Antarctica	**-0.76 ± 0.15**	**0**	**-0.38 ± 0.05**	**0**	0	1900

Antarctic Peninsula has been warming by 1.14-2.87 °C $100y^{-1}$, West Antarctic Ice Sheet by 0.46-1.32 °C $100y^{-1}$, and the Dronning Maud Land coast by 0.59 to 1.33 °C $100y^{-1}$. The borehole temperature adjustment needed to match the long-term trend leads to an over-estimation of the 100-year trend in the WAIS region. Indeed, the same borehole temperature record finds a warming trend of 0.70 °C $100y^{-1}$ for the past 100 years, and 1.22 °C $50y^{-1}$ for the past 50 years. This example shows that a simple linear scaling cannot be valid for all timescales, and that another approach will be needed to improve quantitative temperature reconstructions for Antarctica.

Despite these uncertainties on absolute scaling, our analyses underline that the sustained warming of the Antarctic Peninsula over the last century stands out as being a robust feature across all methods. Moreover, while the West Antarctic Ice Sheet and the Peninsula regions have now seen reversal of the long-term cooling trend of the past 2000 years, this is not the case for the rest of the continent, where temperatures changes over the last century have not been significant (Fig. 3.3.4, Table 3.3.4).

3.3.4.1.4 Significance of most recent 100y trends relative to natural variability

Finally, we assess how significant the trends in the most recent 100-years of the regional temperature reconstructions are relative to the range of all other 100-year trends in the reconstructions since 0 CE (Figure 6). The most recent 100y trend and its (±1σ) uncertainty range are compared to the distribution of all other 100y trends for that region. This assessment method uses overlapping trend analysis intervals that are not fully independent, but captures the full range of possible trends in all 100y intervals of the regional reconstructions. In this

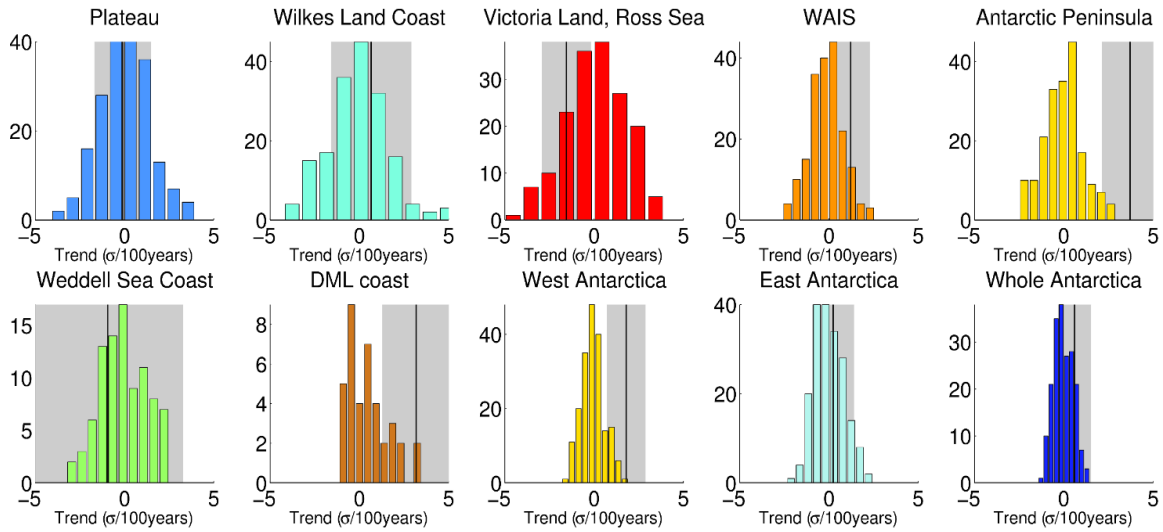

Figure 3.3.6: Histograms showing the distributions of all 100y trends on normalised, weighted composites over the last 2000 years. Distributions are shown for each climatic region, as well as for East, West and Whole Antarctica composites, and are calculated on 10-year binned composites. The solid vertical lines represent the most recent 100y trend in each reconstruction, and grey shading corresponds to the 5-95% uncertainty range of the last 100y trends. Only for the Antarctic Peninsula does the most recent 100-year trend stand out as unusual compared to the natural range of century-scale trends over the last 2000 years.

Table 3.3.4: Regression of the last 100-year slope based on the 5-year averages

			ECHAM		NB2014		Borehole	
Geographic region	Start date	End date	Slope (°C/100y)	p-value	Slope (°C/100y)	p-value	Slope (°C/100y)	p-value
1. East Antarctic Plateau	1915	2010	-0.49 ± 0.73	0.174	-1.28 ± 1.71	0.133	NaN	NaN
2. Wilkes Land Coast	1915	1995	**1.70 ± -0.55**	**0.034**	0.47 ± 0.60	0.115	NaN	NaN
3. Weddell Sea Coast	1915	1995	-0.79 ± 1.75	0.351	-0.50 ± 1.12	0.351	NaN	NaN
4. Antarctic Peninsula	1915	2010	**2.87 ± 1.12**	**<0.001**	**1.99 ± 0.75**	**<0.001**	NaN	NaN
5. West Antarctic Ice Sheet	1915	2015	**1.12 ± 0.92**	**0.020**	**0.97 ± 0.75**	**0.014**	**1.32 ± 1.08**	**0.020**
6. Victoria Land Coast	1915	2005	-0.55 ± 0.97	0.247	-0.64 ± 1.00	0.195	NaN	NaN
7. Dronning Maud Land Coast	1915	2010	**1.33 ± 0.90**	**0.006**	**0.98 ± 0.73**	**0.012**	NaN	NaN
West Antarctica	1915	2015	**1.25 ± 0.86**	**0.007**	**1.12 ± 0.62**	**0.001**	0.97 ± 0.78	0.019
East Antarctica	1915	2010	0.09 ± 0.58	0.743	0.06 ± 1.23	0.924	NaN	NaN
All Antarctica	1915	2015	0.79 ± 0.82	0.060	**0.99 ± 0.94**	**0.040**	0.21 ± 0.38	0.262

	Normalized		CPS			
Geographic region	Slope (σ/100y)	p-value	Slope (°C/100y)	p-value	Start date	End date
1. East Antarctic Plateau	-0.85 ± 1.14	0.133	**0.77 ± 0.46**	**0.004**	1900	2000
2. Wilkes Land Coast	1.08 ± 1.37	0.115	0.05 ± 0.49	0.820	1900	1980
3. Weddell Sea Coast	-1.10 ± 2.45	0.351	-0.25 ± 0.93	0.544	1900	1980
4. Antarctic Peninsula	**2.65 ± 0.99**	**<0.001**	**1.14 ± 0.60**	**0.002**	1900	2000
5. West Antarctic Ice Sheet	**1.17 ± 0.90**	**0.014**	0.46 ± 0.63	0.132	1900	2000
6. Victoria Land Coast	-0.79 ± 1.23	0.195	0.22 ± 0.52	0.364	1900	1990
7. Dronning Maud Land Coast	**2.51 ± 1.88**	**0.012**	0.59 ± 0.61	0.057	1900	1990
West Antarctica	**1.50 ± 0.83**	**0.001**	0.60 ± 0.61	0.052	1900	2000
East Antarctica	0.04 ± -0.85	0.924	**0.43 ± 0.33**	**0.017**	1900	2000
All Antarctica	**0.72 ± 0.68**	**0.040**	**0.43 ± 0.32**	**0.013**	1900	2000

analysis, the significant recent positive trends for the Dronning Maud Land coast and West Peninsula over the last century stands out as being robust to the binning of multiple isotopic anomaly records for the region, significant after weighting and scaling of the regional isotopic records to represent regional temperature, and unusual compared with the range of natural Antarctic ice sheet do not emerge as unusual in the context of similar length trends of the last two millennia, consistent with the findings of Steig et al. (2013) based on the WAIS Divide ice core. However, the most recent 100-year warming of the Antarctic Peninsula is unusual century-scale temperature variability of this region over the last two thousand years. The companion Antarctica 2k paper (Thomas et al., 2017) that examines snow accumulation across Antarctica over the last 1000 years also concludes that the most robust recent changes in snowfall are evident for the Antarctic Peninsula. Temperature and precipitation increases over the Antarctic Peninsula in recent decades have previously been linked to the Southern Annular Mode (Abram et al., 2014) and the effects of the coupling between SAM and ENSO on the strength and position of the Amundsen Sea Low pressure and sea ice conditions offshore of West Antarctic and the Antarctic Peninsula. The variability of these driving forcings over the past 2000 years could also explain part of the opposite regional climate variability that appears to be present at decadal-centennial scales between our reconstructions for the Antarctic Peninsula and the Victoria Land-Ross Sea regions.

Prior to this recent warming, which has been most significant for the Antarctic Peninsula region of Antarctica, long-term cooling is evident for many regions of Antarctica. In particular, it is the long-term cooling of the East Antarctic Plateau which emerges as significant in the weighted reconstructions and also robust across the distribution of contributing records in the unweighted composites. This is also in agreement with what was recently found by Hakim et al. (2016) using a data assimilation approach to identify a very strong SH cooling trend through the last 2000 years, up to about 1850 CE.

3.3.4.2 Continent-scale temperature reconstructions

Figure 3.3.7 shows the results obtained by applying the Composite-Plus-Scale (CPS) method published in 2013 (PAGES2k Consortium, 2013) to the expanded Antarctica2k database to reconstruct temperature across the whole Antarctic continent. A good agreement is observed between the new reconstruction and the previously published one (see Fig. 3.3.7), both at annual and decadal scale (r=0.89 and 0.91, respectively). There is a slightly stronger negative temperature trend in the new Antarctic continent-scale reconstruction, which is related mainly to a slightly cooler temperature estimate for the 1600-1900 CE interval using the expanded database. Figures in supplementary material similarly repeat this CPS comparison for the West

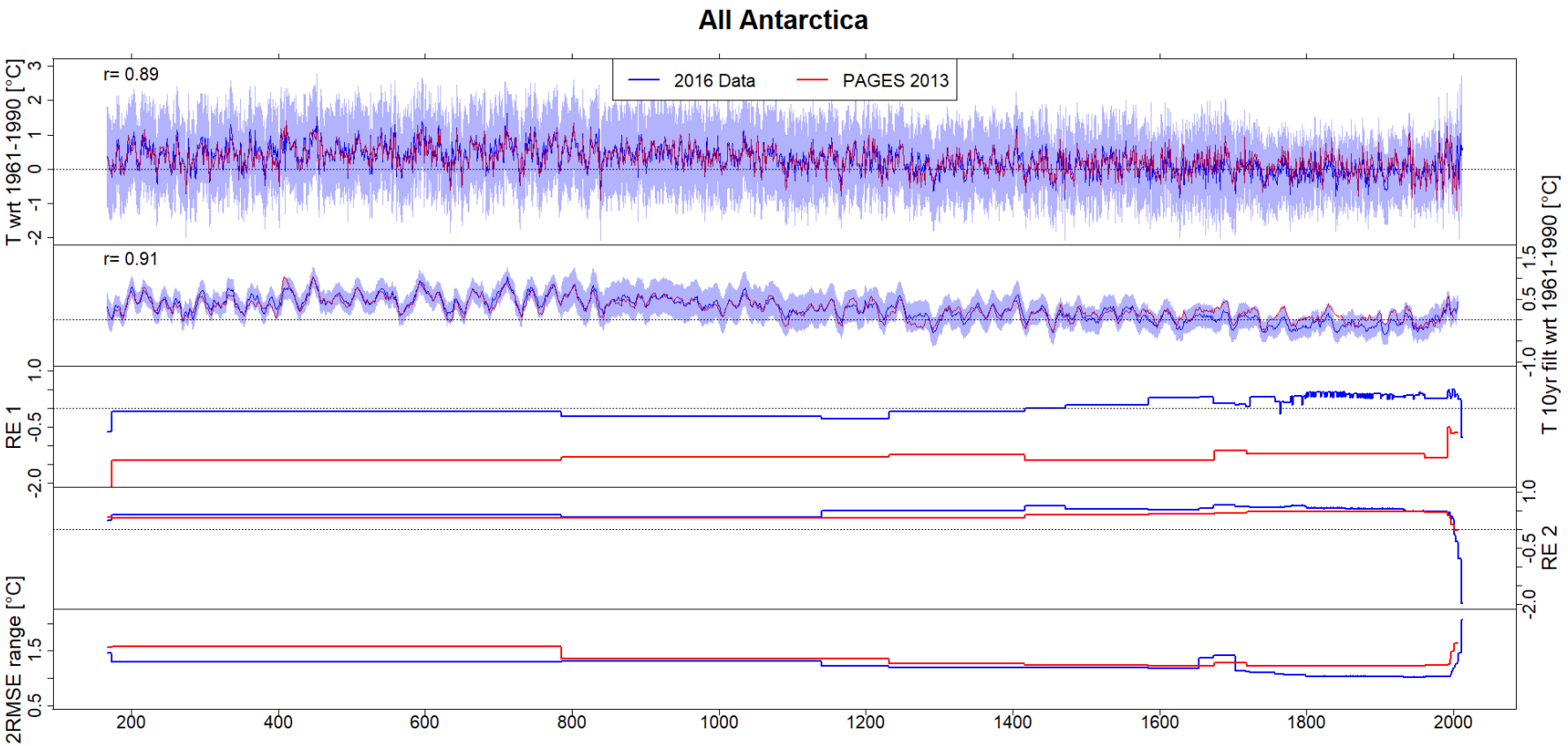

Figure 3.3.7: Comparison of CPS reconstructions of Antarctic mean temperatures over 167-2010 CE. Red: results from PAGES 2k Consortium (2013). Blue: Updated results using the new ice core isotope data collection described herein and the NB2014 temperature target. Blue shading: 2RMSE uncertainties of the updated reconstruction. Top panel: Unfiltered interannual reconstructions. Second panel: 10-year running mean of reconstructions. Third (fourth) panel Reduction of Error skill from a split-calibration-verification exercise using 1961-1976 for calibration (verification) and 1977-1991 for verification (calibration). Bottom panel: 2RMSE reconstruction uncertainty ra

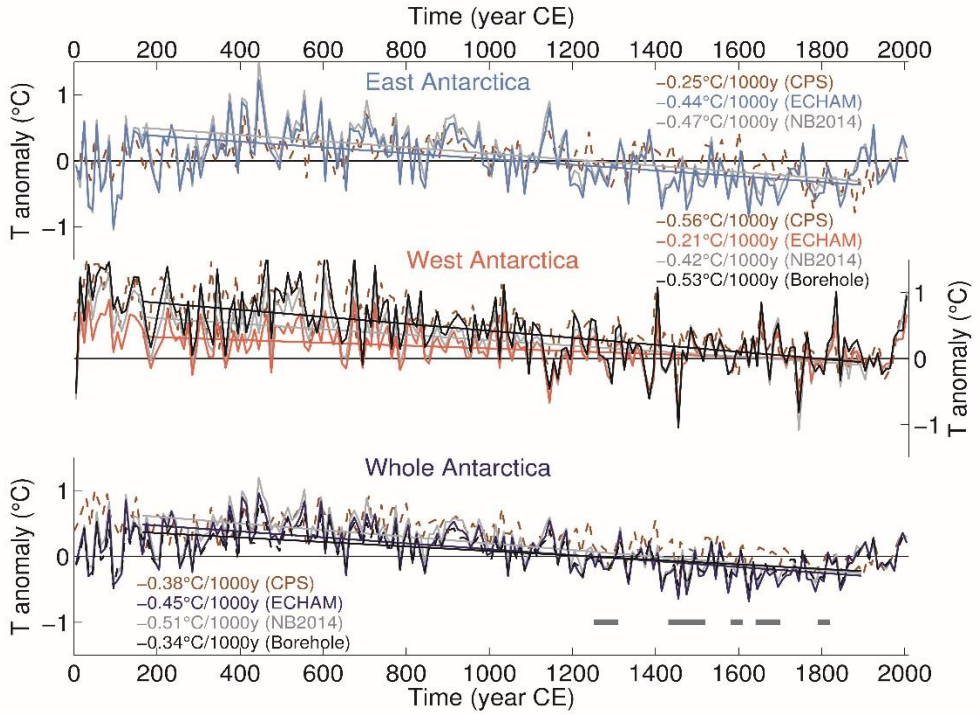

Figure 3.3.8: Composite temperature reconstructions (T anomalies in °C) for East, West and Whole Antarctica using 10y averages and the different temperature scaling approaches: dotted coloured lines for the CPS method (2013 method applied to the new database); grey lines for the method which uses the NB2014 variance for scaling (different weighting method compared to CPS); coloured lines for the method based on the correlation between annual mean regional $\delta^{18}O$ and regional T from ECHAM5-wiso forced by ERA-Interim; black lines for the method adjusted to match the temperature trend between 1000 and 1600 CE based on borehole temperature measurements at WAIS divide (Orsi et al., 2012). Linear trends are calculated between 165 and 1900 CE. The grey horizontal segments correspond to volcanic-solar downturns intervals as defined in PAGES2k Consortium (2013) and corresponding to the following periods: 1251-1310 CE, 1431-1520 CE, 1581-1610 CE, 1641-1700 CE and 1791-1820 CE.

Antarctica and East Antarctica regions and find similar agreement between the 2013 results and those using the expanded ice core database (Fig. B.11, B.12, and B.13 respectively).

Figure 3.3.8 shows the continental scale (All Antarctica), East Antarctica and the West Antarctic temperature reconstructions that have been obtained from the different temperature scaling approaches in comparison with the CPS method. The period between 1200 and 1900 CE appears as the coldest interval in the East Antarctic reconstruction, and this is also reflected in the reconstruction at the whole continental scale. The warmest interval is identified between 300 and 1000 CE, especially for West Antarctica. The comparison between the CPS method and our new reconstruction methods shows a better agreement in East Antarctica than in West Antarctica when considering the ECHAM temperature scaling (Fig. 3.3.8). However, a better agreement between the CPS method and the temperature reconstruction obtained with the borehole scaling method is observed for West Antarctica. Note that ECHAM and NB2014 use two independent datasets for scaling the $\delta^{18}O$ signal to temperature, and that the difference between them is a measure of the uncertainty in the temperature reconstruction.

Over the period from 165-1900 CE (the reconstruction interval of the 2013 PAGES 2k reconstruction for Antarctica), a cooling trend is common to all three broad-scale reconstruction

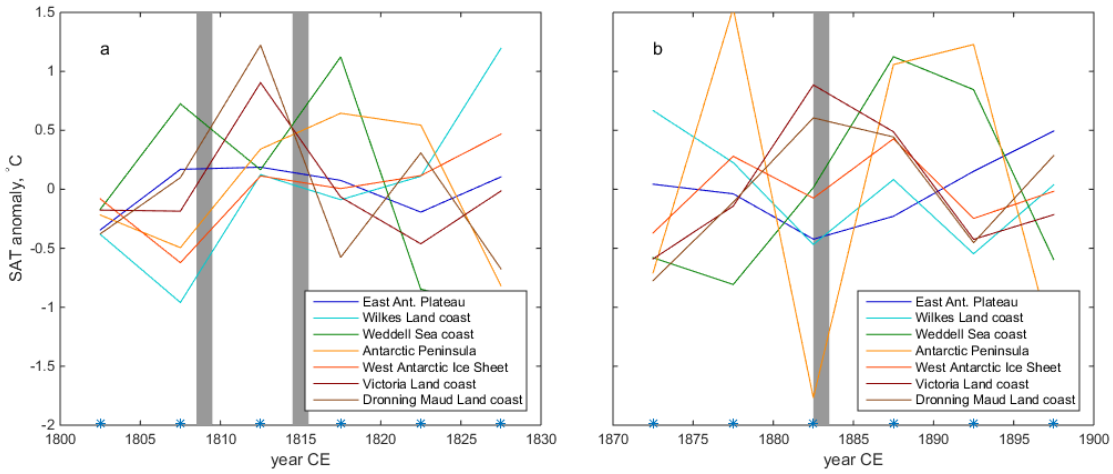

Figure 3.3.9: Reconstructed regional surface atmospheric temperature anomalies during the periods of 1802.5-1827.5CE (a), and 1872.5-1897.5CE (b) overlapping with the three major tropical volcanic eruptions of 1808/09 and Tambora 1815, and Krakatoa (1883). The reconstruction segments for each region were centred on the means of the corresponding intervals. Stars mark the bin centres of the reconstructions, and the years of the eruptions are highlighted in grey.

regions and across all reconstruction methods (see Table B.2). Cooling trends range between -0.21 and -0.45 °C $1000y^{-1}$for the ECHAM method, and between -0.34 and -0.53 °C $1000y^{-1}$ for the borehole method. These values are in the range of those previously reported by the 2013 reconstruction (PAGES2k Consortium, 2013) where cooling trends of -0.18 and -0.46 °C $1000y^{-1}$ were calculated, for the same interval, for East and West Antarctica, respectively. By comparison, cooling trends of -0.25 and -0.56 °C $1000y^{-1}$ are calculated from the 10y binned data obtained with the same CPS methods but applied to this new database.

East Antarctica is one of the last places on the globe where the long-term cooling trend of the last millennium has not been inverted (PAGES 2k Consortium, 2013; Abram et al., 2016). This feature of delayed onset of industrial warming is clear in our reconstruction, but is not captured by climate models (Bothe et al., 2015). Climate models are known to overestimate inter-hemispheric synchronicity (Neukom et al., 2014). The model-data mismatch may come from an over-estimation of the response to external forcing in climate models, an under-estimation of the role of internal ocean-atmosphere dynamics in models, or incorrect inference from proxy data. This quantitative reconstruction will provide an important constraint on the forced vs unforced nature of trends observed for the last century.

3.3.4.3 Response to volcanic forcing

The radiative forcing caused by major volcanic eruptions is known to drive hemispheric-scale cooling at subdecadal to decadal timescale (e.g. Sigl et al., 2015; Stoffel et al., 2015). Previous model-based assessments have suggested that the long-term cooling trend over Antarctica during the 850-1850 CE interval may be attributed to volcanic forcing of the climate(Goosse et al., 2012). Volcanic forcing may also affect atmospheric and oceanic dynamics, including

modes of variability, causing substantial seasonal and regional variations in the climate footprint of volcanic forcing (e.g. Otterå et al., 2010; Ortega et al., 2015; Schleussner et al., 2015; Swingedouw et al., 2015). For example, the long-term cooling trend of the global oceans during the last two millennia has been attributed to the effects of short-term cooling from episodic eruptions being cycled into subsurface layers of the oceans (McGregor et al., 2015).

We use the composite reconstructions of Antarctic temperature anomalies to explore whether a signatures/imprints of past major eruptions can be identified. Since different normalizations applied during the reconstruction procedure are not expected to affect a qualitative interpretation of the results, we present the analysis based on the reconstruction that fits 5-year annual $\delta^{18}O$ to regional temperature anomaly from ECHAM-wiso forced by ERA-Interim.

A robust identification of the climate impacts of volcanism from Antarctic ice cores faces a number of challenges. In addition to chronological uncertainties due to low accumulation and post-depositional alterations, processes other than local temperature may affect water stable isotopes in Antarctic precipitation, therefore making the detection of a temperature response to volcanic forcing more challenging. Finally, stacking the individual core records acts as a low-pass filter, suppressing the variability in the shorter, interannual timescales, thereby eliminating potentially short-lived cooling signals triggered by volcanic forcing.

Despite these limitations, it should be possible to record a volcanic cooling signal from well-dated cores from high accumulation areas and/or around the time periods with clear markers of volcanic origin, widely used as precise age control points for constructing ice core chronologies. For example, the chemical fingerprints of two consecutive tropical eruptions of 1808/09 (VEI 6-7) and Tambora 1815 (VEI 7) are detected in many Antarctic ice cores as a pronounced double peak in a number of measured ice parameters such as electrical conductivity or non-sea salt-SO_4^{2-} profiles (Sigl et al., 2015).

Due to the aforementioned difficulties in the identification of a potential Antarctic temperature response to volcanic forcing, we restrict our analysis to the eruptions associated with the estimated strongest volcanic forcing, which are more likely to leave a clear footprint in ice core records. The highest resolution reconstruction (5 year averages) is available for a period which experienced only three eruptions with a Volcanic Explosivity Index (VEI) of 6-7, namely the tropical eruptions of 1808/09, 1815 Tambora and 1883 Krakatoa. The signatures of the first two eruptions are commonly used as reference horizons when constructing the core chronologies. Due to a low number of replicates, we cannot use a Superposed Epoch Analysis, commonly applied for detecting the signature of the climate response to volcanic forcing (e.g. Fischer et al., 2007; Stoffel et al., 2015). Figure 3.3.9 simply displays the regional surface atmospheric temperature anomalies for the two periods centred at 1815 CE and 1883 CE.

Following the Tambora eruption, cooling is recorded in 5 out of our 7 regional reconstructions, namely in the Dronning Maud Land coast, Wilkes Land coast, Victoria Land coast, East Antarctic Plateau and possibly West Antarctic Ice Sheet regions. Following the 1808/09 eruption, cooling appears in 3 out of our 7 regional reconstructions (West Antarctic Ice Sheet, Wilkes Land coast regions and to a lesser extent the Antarctic Peninsula). Following the Krakatoa eruption, regional cooling emerges for 4 out of 7 regions (East Antarctic Plateau, Antarctic Peninsula, Wilkes Land coast and West Antarctic Ice Sheet regions). Potential response time lags should be interpreted with caution due to effects of the data binning procedure as well as age scale uncertainties.

Within the limitations associated with our reconstructions and with the small number of large eruptions in the studied time period, we can only report a lack of consistent pan-Antarctic cooling, and a variable regional response. Such features have also been identified for the largest volcanic eruptions in the Northern Hemisphere (e.g. Guillet et al., 2017). Local negative anomalies following major eruptions may arise from non-temperature drivers of water stable isotope records and be an artefact of inconsistencies in chronologies; they may also reflect an actual regional cooling. Further studies will require to focus on ice core records with a solid chronological control, and sufficient regional records to assess the common climatic signal from the deposition noise. Second order isotopic parameters such as deuterium excess which preserve a signal associated with moisture source characteristics may also provide insights on the response of the Southern Ocean surface state to volcanic forcing.

This analysis represents only a preliminary attempt to assess the possible short-term climatic response of Antarctic climate to volcanic forcing, and we suggest that this is a good avenue for further detailed study using the expanded Antarctica 2k isotope database assembled here.

3.3.5 Conclusions and Implications

We have presented a new enlarged database of high and low resolution ice core water stable isotope records from Antarctica, which has been compiled in the framework of the PAGES Antarctica2k working group. To further develop our scientific understanding based on continental scale reconstructions of Antarctic temperature, we define seven climatic regions based on our knowledge of the regional Antarctic climate and further supported by spatial correlation of temperature using the NB2014 reanalysis data. In our reconstructions of both regional and continental scale climate, we use 5y and 10y averaged data in order to limit our dependence on annually precise dating which faces real problems, especially in interior Antarctica, due to the very low snow accumulation there. Similar conclusions are reached using different approaches (ECHAM, NB2014 and borehole methods) giving support to our

temperature reconstructions. Furthermore, a replication of the CPS approach used in a previous continental scale reconstruction but adapted to the new database also produces consistent results. The range of the values obtained by these four methods provide information on the uncertainties related to the temperature reconstructions at regional and continental scale.

Our new continental scale reconstructions, based on the extended database, corroborate previously published findings for Antarctica from the PAGES2k Consortium (2013): (1) temperatures over the Antarctic continent show an overall cooling trend during the period from 0 to 1900 CE, which appears strongest in West Antarctica, and (2) no continent-scale warming of Antarctic temperature is evident in the last century.

The robust and significant long-term cooling trend of Antarctic-wide temperatures from 0-1900 CE is also reflected in the broader East Antarctic and West Antarctic regions. In East Antarctica, the coldest interval occurs from 1200 and 1900 CE. During the same time period five intervals of volcanic-solar downturns have been previously linked to cooling in temperature reconstructions for other continental regions (PAGES2k Consortium, 2013). These intervals of negative radiative forcings are in agreement with our lower temperature estimates during this time (Fig. 3.3.8).

The absence of significant continent-scale warming of Antarctica over the last 100 years is in clear contrast with the significant industrial era warming trends that are evident in reconstructions for all other continents (except Africa) and the tropical oceans (Abram et al., 2016). As noted in other studies (e.g. Abram et al., 2016; Jones et al., 2016) the absence of continent-scale warming over Antarctica is not in agreement with climate model simulations, which consistently produce a 20^{th} century warming trend over Antarctica in response to greenhouse gas forcing. The high interannual climate variability with respect to the magnitude of climate trends over Antarctica, and the small number of ice core records that have contributed to previous continent-scale reconstructions of Antarctic temperature, have been suggested as possible sources for the lack of detection of continent-scale warming trends in palaeoclimate records from Antarctica. However, we replicate this finding of a continent-scale absence of 20^{th} Century warming using our greatly expanded ice core database and with composites and reconstructions based on a range of methods. This suggests that the absence of continent scale warming over Antarctica during the last century is a robust result and alternate reasons for data-model divergences need to be investigated.

Despite the lack significant warming over the last 100 years at the continent scale, there are three regions which show positive and significant isotopic and temperature trends: the Antarctic Peninsula, the West Antarctic Ice Sheet and the coastal Dronning Maud Land. However, currently only for the Antarctic Peninsula is the last 100 y trend unusual in the context

of natural century-scale trends over the last 2000 years, although if sustained and significant warming of Dronning Maud Land coast and the West Antarctic ice sheet continues during the coming decades (as would be expected based on climate model simulations), then these areas may soon also see the recent warming emerge as unusual in the context of natural variability. A companion paper (Thomas et al., 2017), which examines the snow accumulation rate variability over Antarctica during the last millennium, reaches the same conclusion showing that in the Antarctic Peninsula region the late 20th century snowfall increase is unusual in the context of the past 300 years. The regional to local scale patterns of climate changes, and the processes that these illustrate, are another target for future research that could be explored using the new Antarctica2k database. Future work will also consider the comparison of the results obtained in this study with those by Thomas et al. (2017) assessing the snow accumulation rate variability in the same regions, with the aim of exploring a long-standing question about the relationship between temperature and precipitation in Antarctica.

Our new regional and continental scale reconstructions of Antarctic temperatures highlight again the urgent need to increase the spatial coverage of this sparse data continent with new temperature records, particularly focusing in the coastal areas. These regions are typically seen to be data-poor areas in our extended database. However, the coastal areas are also the places where high-resolution ice cores can be retrieved, where strong climatic differences can occur over relatively short distances, where there is some evidence for non-significant but emerging development of warming trends, where even small amounts of warming can rapidly move the local climate beyond the threshold and where surface melting of snow occurs potentially leading to widespread impacts of any future Antarctic warming.

Data availability

The target dataset of NB2014 is archived at: http://polarmet.osu.edu/datasets/Antarctic_recon/. The table B.1 (Supplementary Information) contains the data citations, as well as the primary bibliographic reference, for each record used in this study. We used the URL links for existing published data from public repositories.

The regional and continental scale isotopic composites, including the statistical information for the 5y and 10y unweighted composites, and temperature reconstructions generated during the current study and the table B.1 are available in the NOAA World Data Center for Paleoclimatology (WDC Paleo) at the following link: https://www.ncdc.noaa.gov/paleo/study/22589.

Supplementary Information

Supplementary figures (from Fig. S1 to S15) and tables (from table S1 to S4) are available as Supplementary Information.

Author contribution

BS led Phase 2 of the Antarctica 2k project, and MAJC was data manager. The data analysis presented in this paper was carried out by NJA, AO, SG, RN and DD. BS, NJA and AO led the writing of the manuscript, with contributions by MAJC, SG, RN, VM-D, HG, DD and EJS. All authors contributed to discussions on the analysis design and manuscript.

Acknowledgements

This manuscript is the Antarctic contribution to the international effort to characterise global climate variability during the last 2000 years, coordinated within the Past Global Changes PAGES 2k network working group (http://www.pages-igbp.org/ini/wg/2k-network/intro) and the planning group International Partnership for Ice Core Science, IPICS (http://www.pages-igbp.org/ini/end-aff/ipics/intro). We thank all of the scientists who made their ice core data available for this study.

This is a contribution to the PAGES 2k Network [through the Antarctica2k working group]. Past Global Changes (PAGES) is supported by the US and Swiss National Science Foundations. NJA acknowledges funding from the Australian Research Council through Discovery Project DP140102059. BS acknowledges funding from PNRA (Italian Antarctic Research Programme) IPICS-2kyr-It project. RN is funded by the Swiss NSF (Ambizione grant PZ00P2_154802).

3.4 Résumé et Conclusions

Le premier volet de ma thèse a été consacré à l'évaluation des isotopes stables des précipitations simulés dans ECHAM5-wiso sur l'ensemble du continent Antarctique, et sur la période 1958-2013.Cette évaluation est un travail préliminaire à l'utilisation des simulations dans le cadre de ma thèse, pour l'exploitation des signaux isotopiques enregistrés dans les carottes de glace, et notamment celles extraites en Terre Adélie.

Une première comparaison des températures simulées par le modèle avec des mesures effectuées dans des stations météorologiques, ainsi qu'avec les réanalyses ERA-interim, montrent que les simulations sont peu fiables avant 1979. Ce biais est attribué au fait que, avant 1979, les données satellitaires (en particulier les observations d'extension de glace de mer) n'étaient pas disponibles et donc pas intégrées dans les réanalyses, utilisées pour guider cette simulation effectuée avec le modèle ECHAM5-wiso. Ce premier résultat majeur m'a amené à n'utiliser les simulations qu'à partir de 1979.

La confrontation des simulations avec une base de données d'enregistrements isotopiques issues des précipitations, de la neige et de la glace à ce jour disponibles, a montré que le modèle produisait un biais froid sur le Plateau, ainsi qu'un biais chaud sur les côtes de l'Antarctique, cohérents avec les simulations du $\delta^{18}O$ des précipitations, trop appauvries sur le plateau et trop enrichies sur la côte. Le biais moyen reste cependant acceptable (biais moyen de 6.6 % par rapport aux données[11]), et le gradient spatial simulé est bien réaliste, avec un appauvrissement de la côte vers le Plateau. Une comparaison des cycles saisonniers de $\delta^{18}O$ simulés par le modèle avec les compositions isotopiques des précipitations indique que ces biais systématiques sont les plus importants en hiver. De même, bien qu'un peu plus important, le biais moyen du deutérium excess simulé par rapport aux données reste convenable (biais moyen de 10 %[12]), et le gradient spatial simulé est cohérent avec les données décrivant une augmentation de la côte vers le Plateau. En revanche, l'évaluation de la variabilité, qu'elle soit inter-annuelle ou saisonnière (pour $\delta^{18}O$ et d-excess), reste discutable, le signe du ratio modèle/donnée étant opposé selon que l'on compare les simulations avec des données isotopiques issues des carottes de glace ou des précipitations. Cette observation pose la question de la confiance qu'il est possible d'accorder aux données pour une telle évaluation. En effet, des processus de déposition et de post-déposition ont pu affecter les signaux isotopiques enregistrés dans les carottes de

[11] Ce biais correspond au ratio de la différence modèle-donnée moyenne de 2.4 ± 3.1 ‰, par la valeur moyenne de -36.3 ± 9.7 ‰ dans les données.

[12] Ce biais correspond au ratio de la différence modèle-donnée de 0.4 ± 6.8 ‰, par la valeur moyenne de 4.0 ± 16.5 ‰ dans les données.

glace (cf. Section 1.4.1) ; ils ne sont pas pris en compte dans les comparaisons entre composition isotopique simulée et mesurée dans la neige de surface ou les carottes de névé. Quelques travaux sont en cours pour améliorer la compréhension de ces processus et quantifier leur influence, par exemple via l'intégration des isotopes stables de l'eau dans les modèles de densification de la neige, ou bien par la représentation des processus liés aux vents de surface (e.g. redéposition par le vents) dans ces modèles de circulation atmosphérique régionale. Néanmoins, ces processus ne sont pas résolus par les modèles de climat, et leurs effets ne peuvent pas être simplement corrigés dans les enregistrements isotopiques.

Cette identification des biais systématiques du modèle ECHAM5-wiso m'a permis d'évaluer la confiance accordée au modèle ECHAM5-wiso pour différentes variables et différents secteurs de l'Antarctique, puis de réaliser des diagnostiques afin de guider l'interprétation des isotopes de l'eau en Antarctique. J'ai confirmé, en montrant pour la première fois de manière systématique sur l'ensemble du continent de l'Antarctique, que le thermomètre isotopique variait selon les échelles de temps considérées. J'ai montré que la relation linéaire dite spatiale, issue des mesures isotopiques surfaciques de la neige, ne permet pas de reconstruire la température à partir des enregistrements isotopiques mesurés le long des carottes de glace et résolues à l'échelle annuelle. Enfin, j'ai décrit la variabilité spatiale du retard de phase entre les cycles saisonniers du $\delta^{18}O$ et du d-excess, et j'ai identifié le potentiel de ce diagnostic pour la caractérisation et la compréhension des changements saisonniers des sources d'humidité. J'ai terminé cette étude par un diagnostic régional des valeurs moyennes isotopiques et de la relation linéaire $\delta^{18}O$-température, préliminaire à ma collaboration au sein de groupe Antarctica2k.

Cette collaboration internationale avait pour but de reconstruire la température de l'Antarctique, à l'échelle continentale, et pour sept régions d'Antarctique (le Plateau de l'Antarctique de l'Est, la côte de la Terre des Wilkes, la côte de la mer de Weddel, Péninsule Antarctique, l'Antarctique de l'Ouest, la côte de Victoria Land et de la mer de Ross, et la côte de la Reine Maud), sur les deux derniers millénaires, à partir de l'ensemble des enregistrements isotopiques disponibles ($\delta^{18}O$, δD) mesurés le long des carottes de glace. Les enregistrements ont été normalisés, puis moyennés sur 5 ans ou 10 ans selon la longueur des séries afin de minimiser les variations issues des échelles de temps inférieures et des processus locaux non liés à la température. Pour s'extraire des biais liés à la variabilité de la densité des sites d'extraction sur le continent, les enregistrements ont été moyennés sur des grilles de 2° de latitude par 10° de longitude. Les composites isotopiques ont ensuite été corrigés des évènements chauds particuliers, en les pondérant par la corrélation entre les températures issues des reconstructions de Nicolas and Bromwich (2014) du site de chaque enregistrement, avec celle de la région associée. Enfin, en plus de la méthode de moyenne sans pondération, différentes calibrations ont été appliquées

afin de reconstituer les températures régionales à partir de: (1) la pente $\delta^{18}O$-température simulée par le modèle ECHAM5-wiso à partir des simulations sur la période 1979-2013 à l'échelle inter-annuelle, (2) l'écart type de la température du site extrait des reconstructions de Nicolas and Bromwich (2014) sur la période 1960-1990 à l'échelle inter-annuelle, et (3) de la reconstruction de la température à partir des trous de forage pour le WAIS uniquement. Les tendances observées des reconstructions issues des différentes méthodes sont similaires, ce qui montre leur robustesse. Cet exercice confirme les capacités du modèle ECHAM5-wiso pour l'interprétation des isotopes stables de l'eau mesurés en Antarctique, et l'utilisation de ces simulations pour guider des reconstructions à des échelles de temps plus longues (multi-décennales à multi-centennales). Les résultats des reconstructions confirment une tendance négative de la température de l'Antarctique à l'échelle décennale sur la période 0-1900 CE, et une tendance positive sur le dernier siècle en Antarctique de l'Ouest, majoritairement en Péninsule.

Dans ce chapitre, j'ai donc mis en évidence les capacités du modèle ECHAM5-wiso à produire des simulations réalistes de la composition isotopique des précipitations à l'échelle inter-annuelle, et proposé une méthodologie pour en tirer pari afin de guider l'interprétation de données isotopiques. L'évaluation de la capacité du modèle à représenter correctement la variabilité intra et inter-annuelle est cependant limitée par les jeux de données. Le premier facteur limitant tient à l'incertitude liée aux enregistrements isotopiques issus des carottes de glace, tant pour la représentativité d'un seul enregistrement (signal/bruit) que pour les effets de dépôt et post-dépôt non intégrés dans la comparaison modèle-données. Le second facteur limitant est lié au faible nombre de points de données de compositions isotopiques des précipitations mesurées à ce jour en Antarctique.

Ces limitations mettent en lumière (1) la nécessité de mieux quantifier l'influence des processus de déposition et post-déposition sur les enregistrements isotopiques des carottes de glace, par les outils de modélisation mathématique, et par l'analyse de mesures synchrones dans la vapeur, les précipitations et la neige, (2) d'augmenter significativement la banque de données isotopiques issues des précipitations, et (3) d'améliorer les capacités des modèles à resoudre les processus locaux de déposition (e.g. redéposition et métamorphisme de la neige), et de post-déposition, affectant le signal isotopique enregistré dans les carottes de glace.

Enfin, notre approche a été restreinte à l'utilisation d'un seul modèle atmosphérique équipé de la représentation des isotopes stables de l'eau. Il serait pertinent d'évaluer la robustesse des résultats d'ECHAM5-wiso par une comparaison systématique entre simulations guidées par réanalyses et simulations libres (uniquement forcées par les conditions aux limites), et une

comparaison systématique du même type de simulation avec différents modèles atmosphériques.

CHAPITRE 4 : Carottes côtières de la Terre Adélie

4. Carottes côtières de la Terre Adélie

4.1 Introduction

Cette partie présente deux publications portant sur l'analyse de deux carottes de névé forées en Terre Adélie: la carotte S1C1 (cf. Section 4.2) qui a été extraite au cours d'un programme de forage précédent, mais dont les analyses isotopiques et chimiques n'avaient pas été exploitées ; et la carotte TA192A (cf. Section 4.3) extraite au cours de la campagne australe 2014/2015 menée par l'équipe scientifique impliquée dans le projet ASUMA (cf. Section 2.1.1). Pour chaque carotte, j'ai étayé l'interprétation climatique des enregistrements issus des carottes en les confrontant à des observations climatiques régionales (cf. Section 2.2), ainsi qu'à des simulations atmosphériques, en particulier issues du modèle atmosphérique de circulation générale ECHAM5-wiso, dont j'ai évalué les capacités dans la partie précédente.
L'analyse de ces carottes de glace avait été planifiée pour répondre aux questions du projet ANR ASUMA sur le bilan de masse de la Terre Adélie :

(1) Quelle est estimation du BMS régional peut-on faire à partir des carottes de glace extraites en Terre Adélie ?
(2) Comment le BMS moyen et la variabilité interannuelle sont-ils comparables d'un site d'extraction à un autre ?
(3) Comment le BMS reconstruit à partir des carottes de glace extraites en Terre Adélie évolue-t-il au regard des autres paramètres climatiques couvrant la même période ? Peut-on en tirer des explications mécanistiques à l'origine de la variabilité spatio-temporelle du BMS ?

Une partie importante de mon travail a porté sur la datation des carottes de glace. J'ai effectué celle-ci en utilisant toutes les informations disponibles, avec la volonté d'estimer le plus précisément et objectivement possible l'incertitude associée au comptage de couches annuelles via les enregistrements d'éléments chimiques. Par ailleurs, j'ai aussi utilisé les enregistrements d'éléments chimiques et des isotopes stables de l'eau dans l'optique de caractériser également la variabilité du climat et du transport atmosphérique. Les paramètres du premier ordre ($\delta^{18}O$, δD) sont classiquement utilisés comme marqueurs de la température de surface du site d'extraction, tandis que les variations du d-excess ont été utilisées pour tracer des variations des conditions d'évaporation à la source des masses d'air, par exemple en relation avec la température ou l'humidité de surface océanique. Ces interprétations reposent sur la compréhension des processus affectant la distillation isotopique, également sur des hypothèses simplificatrices par rapport aux conditions de cette distillation et du transport atmosphérique

(cf. Section 1.4). J'ai d'ailleurs montré dans la partie précédente que le « thermomètre isotopique » n'est pas applicable pour les variations récentes dans certaines régions de l'Antarctique (cf. Section 3.2.4.3 et 3.3.3.4.1). Dans ces deux publications, je me suis donc attachée à apporter des éléments de réponse précis et objectifs aux questions suivantes :

(1) Le « thermomètre isotopique » est –il applicable pour les variations climatiques récentes en Terre Adélie ?

(2) Quelle information peut-on extraire de l'analyse du d-excess issu des carottes extraites en Terre Adélie ?

(3) Peut-on combiner les informations extraites des enregistrements isotopiques et chimiques (par exemple les sels de mer) pour caractériser les masses d'air parvenant en Terre Adélie ?

4.2 S1C1

Cette étude a été publiée dans un numéro spécial du journal *The Cryosphere* (Goursaud et al., 2017) dédié aux résultats présentés lors de la conférence IPICS (« International Partnership in Ice Core Sciences ») 2016 à Hobart (Tasmanie). La version ci-retranscrite a été formatée pour être intégrée au manuscrit de thèse. Le matériel supplémentaire correspondant est disponible en ligne (https://www.the-cryosphere.net/11/343/2017/, dernier accès : 07/2018).

Abstract. A 22.4 m-long shallow firn core was extracted during the 2006/2007 field season from coastal Adélie Land. Annual layer counting based on sub-annual analyses of $\delta^{18}O$ and major chemical components was combined with 5 reference years associated with nuclear tests and non-retreat of summer sea ice to build the initial ice core chronology (1946-2006), stressing uncertain counting for 8 years. We focus here on the resulting $\delta^{18}O$ and accumulation records. With an average value of 21.8 ± 6.9 cm w.e. y^{-1}, local accumulation shows multi-decadal variations peaking in the 1980s, but no long-term trend. Similar results are obtained for $\delta^{18}O$, also characterized by a remarkably low and variable amplitude of the seasonal cycle. The ice core records are compared with regional records: temperature, stake area accumulation measurements, and variations in sea ice extent, and outputs from two models nudged to ERA atmospheric reanalyses: the high resolution atmospheric general circulation model (AGCM) including stable water isotopes ECHAM5-wiso and the regional atmospheric model MAR. A significant linear correlation is identified between decadal variations in $\delta^{18}O$ and regional temperature. No significant relationship appears with regional sea-ice extent. A weak and significant correlation appears with Dumont d'Urville wind speed, increasing after 1979. The model-data comparison highlights the inadequacy of ECHAM5-wiso simulations prior to 1979, possibly due to the lack of data assimilation to constrain atmospheric reanalyses. Systematic biases are identified in the ECHAM5-wiso simulation, such as an over-estimation of the mean accumulation rate and its inter-annual variability, a strong cold bias, and an under-estimation of the mean $\delta^{18}O$ value and its inter-annual variability. As a result, relationships between simulated $\delta^{18}O$ and temperature are weaker than observed. Such systematic precipitation and temperature biases are not displayed by MAR, suggesting that the model resolution plays a key role along the Antarctic ice sheet coastal topography. Inter-annual variations in ECHAM5-wiso temperature and precipitation accurately capture signals from meteorological data and stake observations, and are used to refine the initial ice core chronology within 2 years. After this adjustment, remarkable positive (negative) $\delta^{18}O$ anomalies are identified in the ice core record and the ECHAM5-wiso simulation, respectively in 1986 and 2002 (1998-99). Despite uncertainties associated with post-deposition processes and signal-to-noise issues in one single

coastal ice core record, we conclude that the S1C1 core can correctly capture major annual anomalies in $\delta^{18}O$ as well as multi-decadal variations. These findings highlight the importance of improving the network of coastal high resolution ice core records, and stress the skills and limitations of atmospheric models for accumulation and $\delta^{18}O$ in coastal Antarctic areas, particularly important for the overall East Antarctic ice sheet mass balance.

Résumé. Une carotte de névé de 22,4 m de long a été extraite pendant la campagne d'été 2006/2007 dans la région côtière de la Terre Adélie. Un comptage des couches annuelles basé sur des analyses sub-annuelles de $\delta^{18}O$ et de composants chimiques majeurs a été combiné à 5 années de référence associées à des tests nucléaires et pour lesquelles la contraction de la banquise d'été est particulièrement faible, afin de construire une première chronologie de la carotte de glace (1946-2006), soulignant une incertitude dans le comptage de 8 ans. Nous nous concentrons ici sur les résultats des enregistrements de $\delta^{18}O$ et d'accumulation. Avec une valeur moyenne de 21,8 ± 6,9 cm w.e. y^{-1}, l'accumulation locale décrit des variations multi-décennales atteignant des valeurs maximales dans les années 1980, mais sans tendance à long terme. Des résultats similaires sont obtenus pour le $\delta^{18}O$, aussi caractérisé par une amplitude du cycle saisonnier particulièrement faible et variable. Les enregistrements de la carotte de glace sont comparés avec des enregistrements régionaux : température, des mesures d'accumulation issues de balises, et des variations de l'extension de la glace de mer ; et avec des simulations produites par deux modèles forcés par les réanalyses atmosphériques ERA : le modèle atmosphérique de circulation générale de haute résolution ECHAM5-wiso équipé des isotopes stables de l'eau, et le modèle atmosphérique régional MAR. Une corrélation significative est détectée entre les variations décennales en $\delta^{18}O$ et la température régionale. Aucune relation significative n'apparait avec l'extension régionale de la glace de mer. Une faible relation significative apparaît cependant avec la vitesse du vent mesurée à Dumont d'Urville, augmentant après 1979. La comparaison entre le modèle et les données met en lumière l'inadéquation des simulations produites par ECHAM5-wiso avant 1979, potentiellement due à un défaut du schéma d'assimilation à contraindre les réanalyses atmosphériques. Des biais systématiques sont identifiés dans les simulations d'ECHAM5-wiso, telle qu'une surestimation du taux moyen d'accumulation et de sa variabilité inter-annuelle, un biais froid important, et une sous-estimation de la valeur moyenne du $\delta^{18}O$ et de sa variabilité inter-annuelle. Par conséquent, les relations entre le $\delta^{18}O$ et la température simulés sont plus faibles que dans les observations. De tels biais systématiques dans les précipitations et la température ne sont pas représentés par MAR, suggérant que la résolution du modèle joue un rôle clé pour la topographie côtière de la calotte de l'Antarctique. Les variations inter-annuellles de la température et des précipitations

simulées par ECHAM5-wiso capturent correctement les signaux issus des données météorologiques et des balises, et sont utilisés pour affiner la chronologie initiale de la carotte de glace de 2 ans. Après l'ajustement, des anomalies particulières positives (négatives) de $\delta^{18}O$ sont identifiés dans l'enregistrement de la carotte et dans les simulations produites par ECHAM5-wiso en 1986 et 2002 respectivement (1998-99). Malgré des incertitudes associées aux processus de post-dépôt et aux problèmes de signal sur bruit dans l'enregistrement d'une seule carotte de glace, nous concluons que la carotte S1C1 peut capturer correctement les anomalies annuelles majeures en $\delta^{18}O$, ainsi que les variations multi-décennales. Ces résultats montrent l'importance d'améliorer le réseau de carottes de glace côtières de haute résolution, et souligne les capacités et limites des modèles atmosphériques pour l'accumulation et le $\delta^{18}O$ des régions côtières de l'Antarctique, particulièrement important pour le bilan de masse de l'Antarctique de l'Est.

4.2.1 Introduction

Deep ice cores from coastal Antarctic areas are crucial to retrieve highly resolved, multi-millennial records, a priority of the International Partnership for Ice Core Science within the Past Global Changes 2k project (PAGES 2k Consortium, 2013). Obtaining highly resolved records spanning the last decades is therefore a pre-requisite to identify the potential of a given site. Moreover, climate variability of the last decades in Antarctica remains poorly documented and understood (e.g. Jones et al., 2016). This is particularly the case in coastal Antarctic areas, which play a key role for the overall Antarctic mass balance (Agosta et al., 2013; Palerme et al., 2016), with relevance for global sea level (Church et al., 2013). Finally, field data are needed to assess the validity of climate models for multi-decadal variability and change in coastal Antarctic temperature and mass balance (Krinner et al., 2007).

Here, we focus on coastal Adélie Land (Fig. 4.2.1), an area where regional climate is marked by the interplay of katabatic winds accelerating downslope from Antarctic interior to the coast (Périard and Pettré, 1993), large seasonal variations in sea-ice extent (Simmonds and Jacka, 1995; König-Langlo et al., 1998) and its proximity to the circumpolar storm track (Jones and Simmonds, 1993). These features lead to dominant southerly (160 plus or minus 20°) intense katabatic winds (Wendler et al., 1997). During summer open sea conditions, a reverse pattern of wind direction can occur, associated with sea breezes. At Dumont d'Urville station (hereafter DDU), Périard and Pettré (1993) reported an average wind speed of 10 m s^{-1}, as well as events when wind speeds exceed 20 m s^{-1} during several days (with an observed local maximum wind speed at 90 m s^{-1}). The region is therefore marked by sastrugi formed by snow erosion and redeposition, The resulting high spatial variability in accumulation challenges the climatic

interpretation of a single ice core record, especially for accumulation rates lower than 20 cm w.e. y^{-1} (Frezzotti et al., 2007). The knowledge of Adélie Land climate variability therefore requires a spatial network of field data.

Multi-decadal climate variability in this region is documented since 1958 from DDU meteorological measurements, and since 1979 from sea ice remote sensing. Only a few shallow ice cores were drilled near DDU (Masson-Delmotte et al, 2008), and none was dated (Jean Jouzel, personal communication, 2016), preventing any comparison of ice core records with meteorological measurements.

In the framework of the International TASTE-IDEA / VANISH programs (Trans-Antarctic Scientific Traverse Expeditions - Ice Divide of East Antarctica), a 22.4 m-long shallow firn core (named S1C1) was extracted in January 2007 from the Adélie Land sector (67.71 °S, 139.83 °E, 279 m a.s.l.) (Fig. 4.2.1). The core was collected close to a stake network which provides records of accumulation spatio-temporal variability from 1971 to 2015 (Favier et al., 2013).

Following the classical approach for other coastal Antarctica areas, the chronology of the S1C1 core is established through the annual layer counting of seasonal cycles in chemical species, water isotopes records and absolute horizons (e.g. Graf et al., 1991; Mulvaney et al., 2002). This task was feasible thanks to multi-year aerosol monitoring at sub-seasonal scale at DDU providing detailed information on the seasonal cycle of aerosols. However, no such monitoring is available for precipitation isotopic composition at this site. Indeed, very few multi-year direct records of snowfall isotopic composition are available from Antarctica (Fujita and Abe, 2006; Schlosser et al., 2008; Landais et al., 2012; Schlosser et al., 2016; Stenni et al., 2016), and emerging records of water vapour isotopic composition only span one month (Casado et al., 2016; Ritter et al., 2016).We therefore investigated seasonal variations in precipitation isotopic composition from a simulation performed with the isotopically enabled ECHAM5-wiso AGCM (Roeckner et al., 2003; Werner et al., 2011) nudged to ERA40 (Uppala et al., 2005) and ERA-interim atmospheric reanalyses (Dee et al., 2011). This high-resolution model was chosen for its good skills with respect to the present-day spatial distribution of water stable isotopes and mass balance in Antarctica (Masson-Delmotte et al., 2008; Werner et al., 2011). The 50 year long simulation is used to identify uncertainties associated with annual layer counting based on the seasonal cycle in precipitation $\delta^{18}O$. Vice-versa, the ice core record and the stake area network will allow assessing the skills of this simulation in coastal Adélie Land. This model-data was further expanded through investigation of recent mass balance and temperature variations from the regional atmospheric model MAR (Gallée and Schayes, 1994).

Section 4.2.2 describes the material and methods underlying this study, including our new measurements, the methodology for the annual layer counting, as well as the regional instrumental (near surface air temperature, wind speed and stake area measurements) and remote sensing (sea-ice extent) datasets, the simulations performed with these two atmospheric models. Section 4.2.3 reports our results. In section 4.2.4, we discuss our new ice core records, and compare $\delta^{18}O$ and accumulation records with local to regional climate information as well as atmospheric model outputs. We summarize our main findings and suggest future research directions in our conclusions (Section 4.2.5).

4.2.2 Material and method

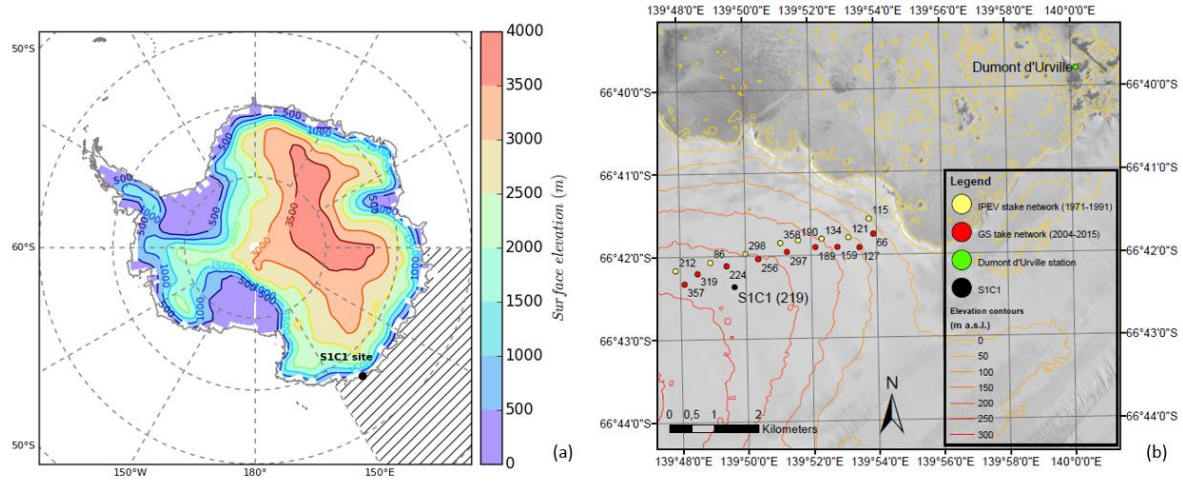

Figure 4.2.2: Maps showing the areas of interest with (a) a map of Antarctica representing the local topography (contours), the location of the S1C1 drilling site and the area used to extract regional sea-ice extent from the Nimbus-7 SMMR and DMSP SSM/I-SSMIS Passive Microwave Data (hatched area), and (b) an orientation map showing stake networks around S1C1 drilling site. Data from 1971 to 1991 were measurement by IPEV, whereas data from 2004 to 2015 were measured in the framework of GLACIOCLIM-SAMBA (GS) observatory. Elevation lines are from the digital elevation model of Korona et al. (2009), which was computed from SPOT5 images obtained during the fourth International Polar Year (2007–2009). The SPOT5 image is also included as a background map. Labels are mean accumulation values at each stake computed over the period with measurements.

Here, we briefly describe the ice core sampling, the chemical and isotopic analyses, the density measurements and the dating methodology. We then introduce the regional climate datasets used for statistical analyses, as well as the atmospheric simulations used for model-data comparisons.

4.2.2.1 Field work and ice core sampling

The field campaign was conducted from the 16th to the 26th of January 2007 in Adélie Land by a French joint LGGE (Laboratoire de Glaciologie et Géophysique de l'Environnement) and IPEV (Institut Français Polaire Paul-Emile Victor) expedition. Several shallow firn cores were drilled along a transect between the Italian-French Cap Prud'Homme station, at sea level, and D47 point, located around 1600 m a.s.l. and approximately 100 km from the coast. This round-trip traverse was part of the ANR-VANISH (*Vulnerability of the Antarctic Ice-Sheet*) and IPEV-

TASTE-IDEA (*Trans-Antarctic Scientific Traverses Expeditions – Ice Divide of East Antarctica*) scientific programs. The scientific aim of the programs was to obtain new firn core records and ground-penetrating radar measurements to improve the knowledge of coastal East Antarctic accumulation.

The present paper is focused on one ice core drilled at the S1C1 site (66.71 °S, 139.83 °E, 279 m a.s.l.), the closest sampling site to the coast and the French Dumont-D'Urville station (Fig. 4.2.1). At this site, the measured temperature of the firn was -13.1±0.5 °C at 10 m-depth. Data obtained during 3 days at 25 cm depth show a mean value of -5.0 °C. At DDU and Dome C, July 2007 temperatures were close to the climatological average conditions from the period 1995-2015. As a result, our measurements from summer 2007 are assumed to be representative of average summer conditions. Such negative near surface air summer temperature ensures preservation of snow signals (e.g. water stable isotopes, chemical species).

A portable solar powered electromechanical drilling system was used to extract the 22.4 m long and 58 mm diameter firn core (Ginot et al., 2002; Verfaillie et al., 2012; Lemeur, submitted). The recovered core pieces were sealed in polyethylene bags in the field, stored in clean isothermal boxes and transported in frozen state to the cold-room facilities of the LGGE in Grenoble, France. Sample preparation for chemical measurements was performed under clean-room laboratory conditions. After stratigraphic observations and measurements of bulk density, the firn core was divided in two half cores. One half was dedicated to radioactivity measurements and the other half was analysed in ion chromatography and mass spectrometry (Section 4.2.2.2). Sub-annual resolution sampling and gross beta radioactivity and gamma spectrometry for bomb test markers allowed to build the S1C1 firn core chronology (Section 4.2.2.3).

4.2.2.2 Measurements

Discrete density values were calculated based on snow sample volume and mass measurements with a 50 cm resolution, from the surface to 22.4 meters depth. The resulting values range from 400 to 700 kg m^{-3} (Table S2 in Supplementary Material). Accounting for measurement difficulties due to weak cohesion of snow in the first few meters, and considering measurement errors, the associated uncertainties are ±20-25 kg m^{-3} (± 4%) from the surface to 7 meters depth, and ±15 kg m^{-3} (± 2%) from 7 to 22.4 meters. Hereafter, density values are used to convert snow depths into water equivalent depths.

Firn core sections were processed for artificial radioactivity measurements by low-level (i) beta counting and (ii) gamma spectrometry, with a continuous sampling every 50 cm from the surface to 22.4 m-depth. Using a method developed by Delmas and Pourchet (1977) and

improved by Magand (2009), snow samples (100-200 g) were melted, weighed, acidified and filtered on ion exchange paper, on which radionuclides of interest (^{90}Sr, ^{137}Cs, ^{241}Am – daughter of ^{241}Pu) were trapped. All steps were realized in the LGGE clean room laboratory to prevent any contamination. After drying (in an oven at 60 °C), these filters were first analysed by a beta gas-proportional counting system (gross beta measurement) to determine the presence of beta emitters peaks corresponding to nuclear weapons global fallout of the 1950s and the 1960s. In a second step, very low level gamma spectrometry (coaxial germanium detector) measurements were performed on the filters to determine activities of ^{137}Cs and ^{241}Am. Both 1955±1 AD and 1965±1 AD peaks were clearly identified in the S1C1 core, respectively at 19.5-20.0 m and 16.5-17.0 m-depth (red vertical lines, Fig. 4.2.2).

Along the S1C1 core, each 5 cm sample was analysed for ionic concentrations and the oxygen isotopic ratio. The firn pieces dedicated to the ion analysis were decontaminated under a clean air bench located in a cold room (−15 °C) using a pre-cleaned electric plane tool on which the ice is slid (Preunkert and Legrand, 2013). A total of 427 subsamples were obtained along the 22.4 m S1C core, with a 5 cm sample resolution. Concentrations of cations (Na^+ and NH_4^+), and anions (Cl^-, NO_3^-, SO_4^{2-}, and methanesulfonate, hereafter MSA), were analysed by ion chromatography (IC) equipped with a CS12 and an AS11 separator column, respectively. Finally, the oxygen isotopic ratio analysis was processed using the CO_2/H_2O equilibration method on a Finnigan MAT252, using two different internal water standards calibrated to SMOW/SLAP international scales. The accuracy of each measurement is ±0.05 ‰ (1σ) (Table S1 in Supplementary Material).

4.2.2.3 Methodology for layer counting

As shown by Jourdain and Legrand (2002), all ions exhibit a summer maximum at DDU, as also found for different Antarctic coastal stations for nitrate (Wagenbach et al., 1998), ammonium (Legrand et al., 1998), MSA and sulfate (Minikin et al., 1998). The sodium seasonal pattern at DDU (maximum in summer) is reversed compared to those observed at other coastal Antarctic sites (e.g. Halley and Neumayer), a feature already discussed by Wagenbach et al. (1998).

The outstanding summer maximum of sea-salt concentrations only detected at DDU is related to its location on a small island, immediately surrounded by open-ocean from December to February. With the aim to use the seasonality of sulfate and MSA produced by oxidation of dimethyl sulfur emitted in summer by marine phytoplankton, we have calculated the non-sea-salt sulfate concentrations in the S1C1 core. Wagenbach et al. (1998) showed that at the coastal Antarctic sites, sea-salt aerosol exhibits a strong depletion of atmospheric sulfate in winter due

to precipitation of mirabilite ($Na_2SO_4.10H_2O$) on the sea-ice surface (Wagenbach et al., 1998). In order to quantify non-sea-salt (nss) SO_4^{2-} contribution, different sulfate to sodium ratio should be defined for summer (0.25, i.e. the reference seawater value) and winter (0.13 derived by Jourdain and Legrand (2002) for DDU):

$$[nssSO_4^{2-}]_{summer} = [SO_4^{2-}] - 0.25\,[Na^+] \quad (1)$$

$$[nssSO_4^{2-}]_{winter} = [SO_4^{2-}] - 0.13\,[Na^+] \quad (2)$$

Note that the volcanic horizons related to the eruptions of Mt Agung (1963) and Pinatubo (1991) are not detected in the $nssSO_4^{2-}$ profile. Legrand and Wagenbach (1999) explained this feature by the fact that, in coastal Antarctica, the volcanic perturbation remained weak with respect to the year-to-year variability of marine biogenic sulphate. While the relationship between concentrations in snow and in simultaneously sampled air remains poor for all compounds (Wolff et al., 1998), there is a general seasonal coincidence of the maxima. Annual layer counting is therefore based on our assessment of the concurrence of synchronous maximum values for Na^+, MSA, SO_4^{2-}, NH_4^+, NO_3^- and $\delta^{18}O$ to objectively identify summer horizons. The combination of information on annual layer counting as well as absolute age markers used to build the S1C1 age scale is described in Section 4.2.3.1 (Results).

4.2.2.4 Regional climate records

We extracted DDU monthly near surface air temperature data spanning the period 1958-2006 from the READER dataset (https://legacy.bas.ac.uk/met/READER/; Turner et al., 2004). We also calculated annual mean values of wind speed spanning the period 1950-2006 (with gaps in years 1953-1955) at DDU (P. Pettré, pers. comm.). Finally, we extracted the average sea ice concentration from the Nimbus-7 SMMR and DMSP SSM/I-SSMIS Passive Microwave Data (http://nsidc.org/data/nsidc-0051) and focused on the region situated between 90 °E and 150 °E (Center, 1996). We used these datasets to perform linear regression analysis with the S1C1 $\delta^{18}O$ and accumulation records.

4.2.2.5 Atmospheric simulations

In this paper, we refer to two simulations, one by the AGCM ECHAM5-wiso and one by the regional atmospheric model MAR.

ECHAM5 (Roeckner et al., 2003) has been equipped with stable-water isotopes (Werner et al., 2011). This model, named ECHAM5-wiso, leads to realistic simulations when evaluated against observations of isotopic composition in precipitation and water vapour on a global scale. More specifically, the simulated distribution of annual mean precipitation isotopic composition over Antarctica is in good agreement with the spatial isotopic dataset compiled from snow and ice core data (Masson-Delmotte et al., 2008).

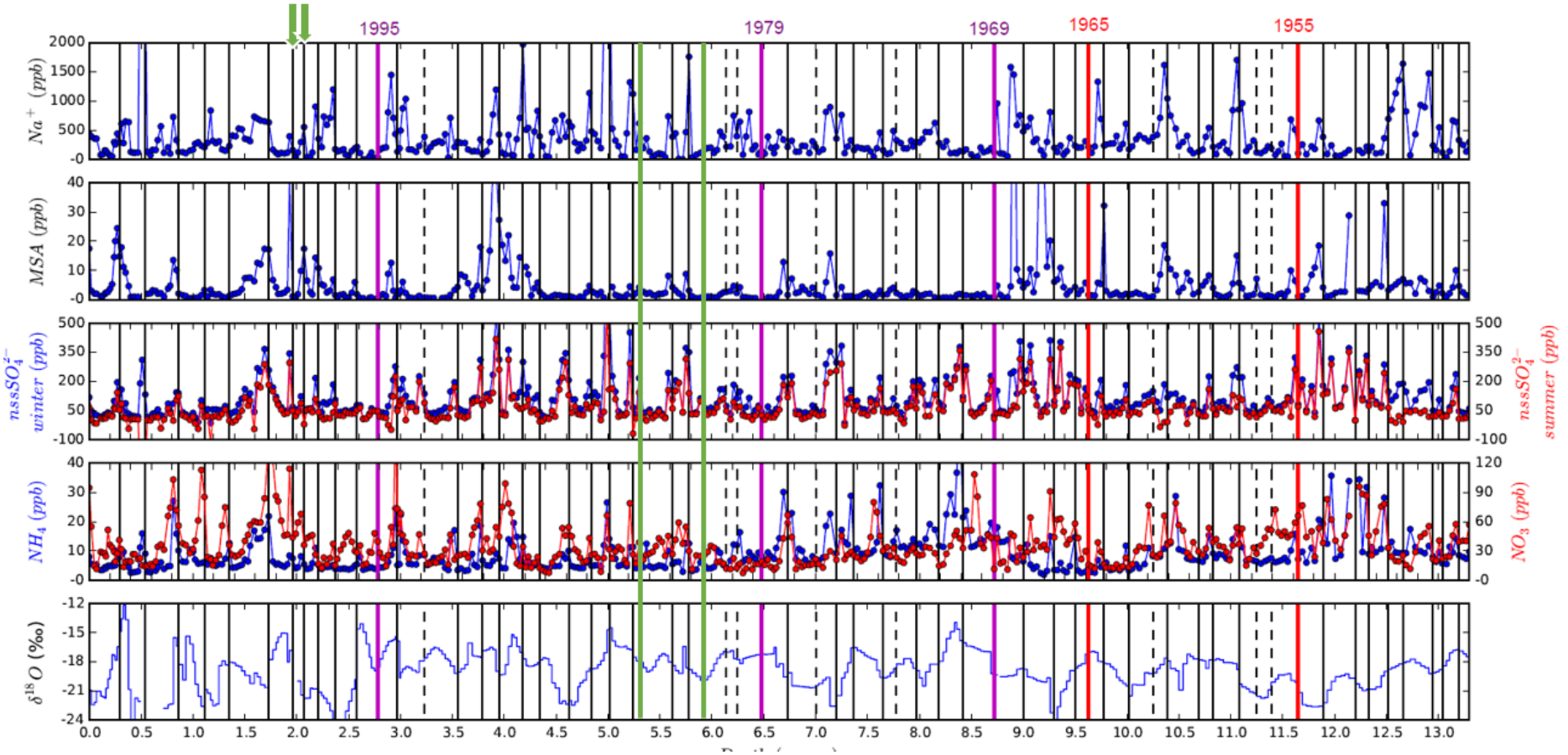

Figure 4.2.3: Dating of the S1C1 core based on sodium Na^+, methanesulfonic acid (MSA), non-sea-salt sulfate ($nssSO_4^{2-}$), ammonium NH_4^+, nitrate (NO_3), and $\delta^{18}O$. The black lines correspond to the December-January period of each year (solid lines are the layers for which all sources of information are consistent, while dashed lines are the layers for which we have contrasted results from one or more sources of information), the purple lines to the non-full sea-ice retreat horizons and the red lines to the nuclear test horizons. $\delta^{18}O$ data are shown as horizontal steps because one measurement corresponds to a value averaged over a 5 cm sample. Green lines stress the years which were added for the second dating, while the green stress those which were deleted (see text for details).

In addition to the most common water stable isotope $H_2{}^{16}O$, $H_2{}^{18}O$ and HDO were implemented into the hydrological cycle of ECHAM5-wiso, in an analogous manner than in the previous model releases of ECHAM3 (Hoffmann et al., 1998) and ECHAM4 (Werner et al., 2001). Each water phase (vapour, cloud liquid and cloud ice) being transported independently in ECHAM5-wiso contains its isotopic counterpart, implemented in the model code. Equilibrium and kinetic fractionation processes are taken into account during any phase change of a water mass.

The ECHAM5-wiso model simulation analysed in this study covers the period 1960-2006. ECHAM5-wiso was nudged to atmospheric reanalyses from ERA40 (Uppala et al., 2005) and ERA interim (Dee et al., 2011), which was shown to have good skills for Antarctic precipitation (Wang et al., 2016), surface pressure fields as well as vertical profiles of winds and temperature. The ocean surface boundary conditions (sea-ice included) are prescribed based on ERA40 and ERA interim data. Isotopic values of ocean surface waters are based on a compilation of observational data (Schmidt et al., 2007). The simulation was performed at a T106 resolution (which corresponds to a mean horizontal grid resolution of approx. 1.1 ° x 1.1 °). We used the model results at the grid point closest to our site of interest.

The MAR (Modèle Atmosphérique Régional) model is a limited area coupled atmosphere – blowing snow – snow pack model. Atmospheric dynamics are based on the hydrostatic approximation of the primitive equations (Gallée and Schayes, 1994). The vertical coordinate is the normalized pressure. The parameterisation of turbulence in the surface boundary layer (SBL) takes into account the stabilization effect by the blowing snow flux, as in Gallée et al. (2001). Turbulence above the SBL is parametrized using the local E - ε model of (Bintanja, 2000). Prognostic equations are used to describe five water species (Gallée, 1995): specific humidity, cloud droplets and ice crystals, rain drops and snow particles. A sixth equation is added describing the number of ice crystals. Cloud microphysical parameterisations are based on the studies of Kessler (1969), Lin et al. (1983), Meyers et al. (1992) and Levkov et al. (1992). The radiative transfer through the atmosphere is parameterised as in Morcrette (2002).Surface processes in MAR are modelled using the Soil – Ice – Snow – Vegetation – Atmosphere – Transfer (SISVAT) scheme (Gallée et al., 2001). In particular, the snow surface albedo depends on the snow properties (dendricity, sphericity and size of the snow grains). Finally the blowing snow model is described in Gallée et al. (2013). MAR is set up over Antarctica with a horizontal resolution of 40 km over 200 x 200 grid points. Lateral forcing and sea surface conditions (SST and sea – ice fraction) are taken from ERA-Interim (Dee et al., 2011). There are 33 levels in the vertical with a high vertical resolution in the low troposphere. The first level is situated at 3 m a.g.l. The simulation was performed from January 1st, 1990, to December 31st, 2010.

Hereafter, we use the ECHAM5-wiso simulation to explore the suitability of local precipitation $\delta^{18}O$ to identify seasonal cycles, as no regional precipitation monitoring data are available. We then compare the ECHAM5-wiso ($\delta^{18}O$, temperature and accumulation) and MAR (temperature and accumulation) outputs with our ice core records.

4.2.3 Results

4.2.3.1 Age scale

4.2.3.1.1 Information from ECHAM5-wiso on annual $\delta^{18}O$ cycles

In order to assess whether annual layer counting was possible using a $\delta^{18}O$ seasonal cycle, we investigate seasonal patterns in ECHAM5-wiso outputs and the timing of the maximum precipitation $\delta^{18}O$ value for each year. The mean simulated precipitation $\delta^{18}O$ seasonal cycle over the period 1979-2006 (28 years) shows a maximum in December-January, a minimum in May, and an overall amplitude of 4.5 ‰. The timing of the simulated monthly precipitation $\delta^{18}O$ maximum fluctuates from year to year. Out of the 29 years, it was simulated at 80 % during local spring-summer: 7 times in December (i.e. 24 %), 8 times in November (i.e. 28 %) and 8 times in January (i.e. 28 % of the time). However, several occurrences were simulated in autumn: 3 times in March (i.e. 10 %), once in February (i.e. 3 %), and in winter: 2 times in August (i.e. 7 %) (Table S3 in Supplementary Material). From this analysis, assuming that the ECHAM5wiso model is a perfect representation of reality, peak $\delta^{18}O$ has a 80% likelihood to occur in December ± 1 month. If a chronology was purely based on $\delta^{18}O$, the occurrence of maxima during other seasons may therefore lead to age scale errors of up to 6 months.

Table 4.2.1: Occurrence of species not showing a summer peak for a identified summer (data missing in summer, peaks not identified at all, or 2 or 3 peaks appearing for the same year)

	Data missing in summer	Peaks not identified	2 or 3 peaks
Na^+	0	4	9
MSA	4	10	2
$nssSO_4^{2-}{}_{summer}$	0	4	5
$nssSO_4^{2-}{}_{winter}$	0	0	6
NH_4^+	0	7	5
NO_3^-	0	1	7
$\delta^{18}O$	2	25	0

4.2.3.1.2. Absolute age horizons

Following major nuclear tests in the atmosphere, radioactive debris wasinjected in the stratosphere in 1953-54 and 1963-64 and reported to be deposited in Antarctica in 1955 and

1965 (± 1 year) (Picciotto and Wilgain, 1963). These two dates are indicated by red vertical lines in Fig. 4.2.2.

Aerosol monitoring data from DDU (1991-2015) show an unequivocal fingerprint of rare summers during which the sea-ice retreat was not complete offshore the site through the absence of sodium maximum. Such events were observed in January 1995 (Jourdain and Legrand, 2002), and more recently in January 2012 and 2013 (Legrand et al., 2016). Prior to the start of DDU atmospheric monitoring in 1991 and to the availability of satellite sea-ice data in January 1979, two other years were characterized by a non-complete sea-ice retreat in summer offshore DDU, namely January 1969 and January 1979 (Patrice Godon, personal communication). The identification of years 1995, 1969 and 1979 in S1C1 records is indicated by purple vertical lines in Fig. 4.2.2. Note that the chemical fingerprint of summer 1969 is equivocal, as it is defined by the absence of a sodium maximum, but coincides with a sulfate maximum, contrary to what is expected.

4.2.3.1.3 Combining layer counting with absolute age horizons

We assessed the concurrence of synchronous maximum values for Na^+, MSA, SO_4^{2-}, NH_4^+, NO_3^- and $\delta^{18}O$ to objectively identify summer horizons, indicated by the vertical continuous black lines in Fig. 4.2.2. Only 4 layers showed simultaneous peaks in all species (in 1959, 1966, 1984 and 2001). In the other cases, the determination was equivocal: either data were missing for the depth interval corresponding potentially to summer or peaks were not identified in some of the or, conversely 2 or 3 peaks appeared. Table 4.2.1 reports the number of occurrence of such cases for each species. We note that maxima in NO_3^- and $\delta^{18}O$ were often delayed with respect to maxima in other species. These two parameters can potentially be affected by diffusion in the firn, due to snow-vapor interactions (Johnsen, 1977; Mulvaney et al., 1998). Mulvaney et al. (1998) also reported that MSA could migrate in the firn. Potential seasonal signals had a very low amplitude (e.g. 1969 to 1975), and sometimes no signal could be discerned. Altogether, $nssSO_4^{2-}{}_{,winter}$ seems to be the most reliable species to identify seasonal cycles in the S1C1 core, as a seasonal pattern appears for every layer.

The remaining difficulty is associated with multiple peaks within one year. This appears for instance in year 1993 (represented in dashed vertical line in Fig. 4.2.2). Double peaks may be associated with year 1993 only, or with two successive years. Such situations were encountered 8 times (dashed vertical lines in Fig. 4.2.2). As a result, we made subjective choices for the identification of annual or sub-annual peaks in order to optimize the coherency with absolute age markers.

We found 60 summer peaks (solid lines, Fig. 4.2.2), whereas the initial layers excluded from the final chronology are represented with dashed lines. As a result, the S1C1 ice core spans the period 1946-2006, as displayed in a depth (expressed in meter water equivalent)-age scale.

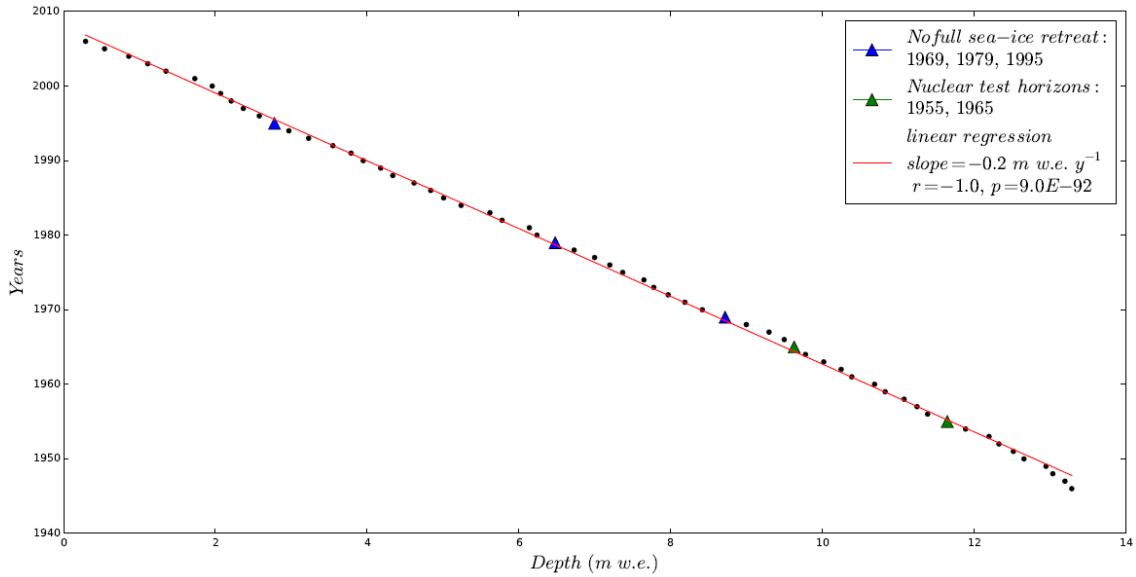

Figure 4.2.4: Depth-age relationship based on the dating of the S1C1 core.

4.2.3.2 Record of accumulation variability and comparison with stake measurements

Annual accumulation variations were extracted from the S1C1 core by combining density measurements with annual mean layer counting (Fig. 4.2.4). The resulting annual accumulation varies between 9.4 and 38.0 cm w.e. y^{-1}, with a mean value of 21.8 cm w.e. y^{-1}, and a standard deviation of 6.9 cm w.e. y^{-1}. This value is 15% lower than the annual accumulation of 25.6 cm w.e. y^{-1} (standard deviation of 15.1 cm w.e. y^{-1}) measured between 2004 and 2015 on one stake located closest to the drilling site (Agosta et al., 2012) (Fig. 4.2.1b), or 27% lower than the mean value measured nearly at the same location between 1971 and 1991 (mean value of 29.9 cm w.e. y^{-1} and standard deviation of 26.6 cm w.e. y^{-1}). We identified remarkable years as those for which accumulation deviates from the mean value by more than two standard deviations. Remarkable high accumulation rates were encountered in 1981, 1983 and in 2001 (at respectively 35.9, 37.3 and 38.0 cm w.e. y^{-1}). No remarkable low accumulation rates were found. For stake accumulation measurements performed at the stake closest to S1C1, the highest values were measured in 1979 and 1981 (75.8 and 73.8 cm w.e. y^{-1}). These remarkable years can be found neither in the stake average record nor in the stake data the closest to the S1C1 site. Moreover, small and non-significant linear correlation coefficients are found with the stake average record, and with the stake data the closest to the S1C1 site. Spectral analyses performed using the Multi-Taper method (Paillard et al., 1996) reveal significant periodicities of 6 and 8 years (harmonic F-test $\geq$ 0.94). We also note a periodicity of 12 years, but which is not detected as significant (harmonic F-test=0.8). Decadal variability is characteristic of the

high latitudes of the Southern Hemisphere (Yuan and Yonekura, 2011). This motivates filtering using a 13-point binomial filter with bounce end-effects (Fig. 4.2.5), i.e. repeating the first (last) value six times in order to calculate the six first (last) running means. From this analysis, we observe a slight accumulation increase from the 1950s until the 1980s, with secondary maxima in 1970s and 1990s (Fig. 4.2.5). A decrease appears from the 1980s to the 2000s, back to the initial mean level. Finally, the S1C1 core displays an unprecedented accumulation increase from the 1990s to the 2000s.This latter feature is surprising, as recent stake measurements from this area show no increase in mean values in 2004-2015 compared with earlier surveys (1971-1991). We therefore remain cautious about the recent accumulation increase inferred from one single ice core record, unless this finding can be supported by other lines of evidence. Finally, note that only a 5 year periodicity emerges from spectral analysis of DDU temperature (harmonic F-test=0.99).

4.2.3.3 Record of $\delta^{18}O$

With our age scale, each year is documented with 2 to 14 $\delta^{18}O$ 5 cm measurements, with a mean number of 7 values per year. Hereafter, the $\delta^{18}O$ record is resampled at this average temporal resolution using the Fourier method (Fig. 4.2.4). Annual mean $\delta^{18}O$ values are then calculated from January to December, for comparison with accumulation and other observational or simulation datasets (Fig. 4.2.5).

4.2.3.3.1 Other sources of information for $\delta^{18}O$ regional variability

Very few multi-year direct records of snowfall isotopic composition are available from Antarctica (Fujita and Abe, 2006; Landais et al., 2012; Schlosser et al., 2016), and none in our region of interest. Near S1C1, the single direct observation arises from a collection of 19 samples of precipitation at DDU, spanning the period from February to November of 1977 (*J. Jouzel, pers. comm.*). These data depict a mean $\delta^{18}O$ value of -18.0 ‰, a standard deviation of 3.9 ‰, with the lowest value in August (~ -27.7 ‰) and the highest values in March (-10.0 ‰) and November (-11.5 ‰). Despite its brevity, this dataset shows less depleted values, a different seasonal pattern (i.e. maxima do not appear at the same months), and lower variability than at Dome C, where recent measurements are available for the period 2008-2010 (Stenni et al., 2016). At Dome C, precipitation isotopic composition values range from -80.6 to -35.5 ‰, with a mean $\delta^{18}O$ value of -58.0 ‰, a standard deviation of 8.6 ‰ and a ~37 ‰ mean seasonal amplitude, with maximum values in December-January, as for near surface air temperature. This comparison is of course limited by the short dataset available for DDU and the fact that these measurements were not performed for the same time period. The distribution of $\delta^{18}O$ data at DDU appears consistent with the range of values observed in a multi-decadal (1982-1996)

record of surface snow isotopic composition obtained from the coastal station of Neumayer, with a mean $\delta^{18}O$ value of -20.6 ‰, and a seasonal amplitude varying from 14.6 to 29.0 ‰ (Schlosser et al., 2008). Finally, the Dumont d'Urville precipitation mean $\delta^{18}O$ value is also quite close to that of shallow ice cores from Law Dome (66.73 °S, 112.83 °E, 1395 m a.s.l.) (Delmotte et al, 2000; Masson-Delmotte et al, 2003), which display a mean value of ~ -21 ‰, and an average seasonal $\delta^{18}O$ amplitude of ~ 6 ‰, together with a larger inter-annual variability rather in local winter than in local summer.

4.2.3.3.2 Record of δ18O variability and links with accumulation and regional climate records

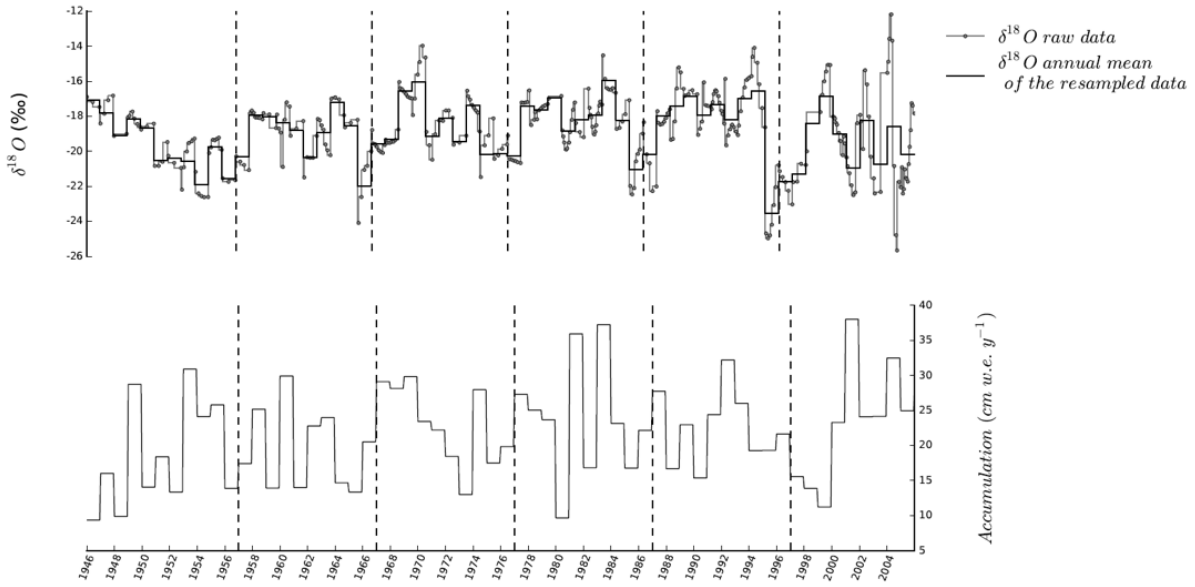

Figure 4.2.5: Time series of $\delta^{18}O$ (in ‰) and accumulation (in cm w.e. y^{-1}) extracted from the S1C1 core. Dark green points correspond to the raw data, while pale green points correspond to the resampled data (with 7 steps). Finally, the red and black lines correspond to the annual mean of the resampled data and the accumulation data resulting from the annual layer counting respectively.

The sub-annual record from raw measurements and resampling at an average of 7 points per year displays large year-to-year variations in the amplitude of the seasonal cycle, varying from 0.2 ‰ (in 1980) to 13.5 ‰ (in 2005), with a mean value of 2.5 ‰. The S1C1 record clearly displays a smaller intra-annual range than observed in DDU precipitation (17.7 ‰ for one single year), and an average intra-annual range about twice smaller than shallow ice core records from Law Dome (typically 5 ‰). Note that the annual accumulation rate at Law Dome (64 cm. w.e. y^{-1}) is ~3 times higher than in the S1C1 core (21.9 cm. w.e. y^{-1}). However, the confidence in this finding is limited by the resolution of our record as well as by potential post-deposition processes affecting the preservation of the sub-seasonal to seasonal precipitation isotopic composition signal (Johnsen, 1977; Touzeau et al., 2016).

We again identified remarkable years as those deviating from the mean value by more than two standard deviations. Only one remarkable low $\delta^{18}O$ values was encountered in 1996, while no remarkable high $\delta^{18}O$ values was encountered. The year 1984 is marked by the most enriched

Table 4.2.2: Statistical analyses : minimum (Min), maximum (Max), mean (μ) and standard deviation (σ) of the precipitation (extracted from ECHAM5-wiso) or the accumulation (from the S1C1 ice core) in cm w.e. y^{-1}, the $\delta^{18}O$ (extracted from ECHAM5-wiso or from the S1C1 ice core) in ‰ and the 2-meter temperature (2m-T, extracted from ECHAM5-wiso or from the READER database) in °C over the different available periods (1946-2007 for the S1C1 ice core and 1956-2007 for the READER database), and over the period 1979-2007.

		Precipitation (ECHAM) or Accumulation (S1C1) (cm w.e. y^{-1})				2m-T (°C)				$\delta^{18}O$ (‰)			
		Min	Max	μ	σ	Min	Max	μ	σ	Min	Max	μ	σ
S1C1	1946-2006	9.4	38.0	21.8	7.0					-23.6	-15.9	-18.9	1.7
	1979-2006	9.7	38.0	23.1	7.5					-23.6	-15.9	-18.7	1.8
READER	1956-2006					-12.2	-8.6	-10.7	1				
	1979-2006					-11.9	-8.6	-10.6	0.7				
ECHAM	1979-2006	52.1	96.6	68.7	12.0	-18.1	-14.8	-16.9	0.8	-22.4	-19.6	-20.8	0.6

Table 4.2.3: Linear relationship between the S1C1 $\delta^{18}O$ and regional climate records showing the coefficient correlation and the p-value. Note that all data from the S1C1 core are annual averages from the 1st dating.

Period	Resolution	Record	r	p
1946-2006	annual	accumulation	4.4×10^{-3}	0.97
1956-2006	annual	READER surface temperature	-0.13	0.35
1956-2006	decadal	READER surface temperature	0.72	2.6×10^{-9}
1979-2006	annual	READER surface temperature	-0.15	0.44
1979-2006	annual	sea ice concentration in Adélie Land	0.04	0.82
1950-2006	annual	wind speed	-0.27	0.0666
1979-2001	annual	wind speed	-0.47	0.029

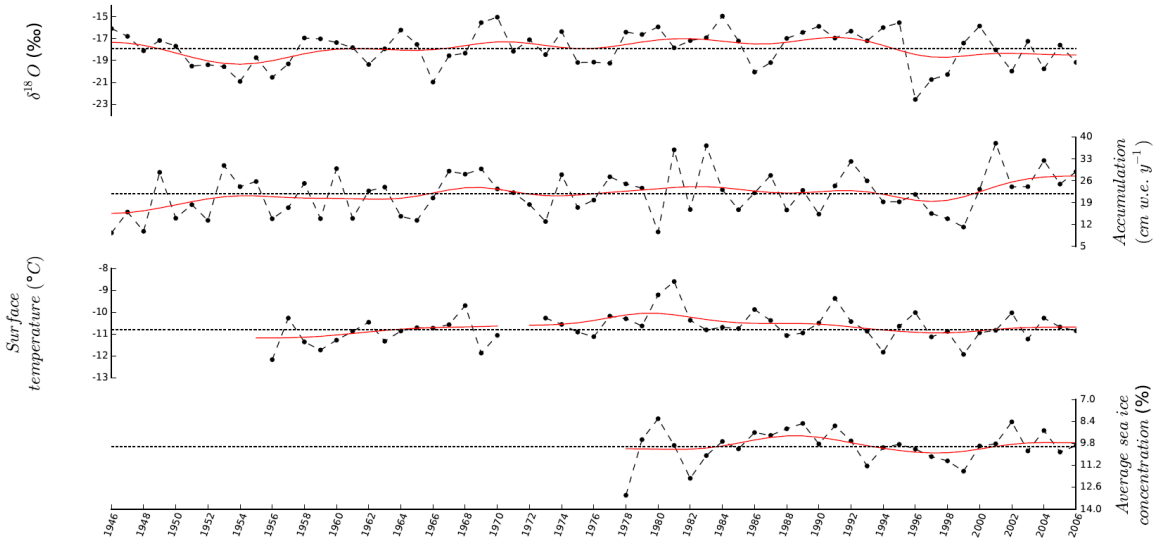

Figure 4.2.6: Comparison of the (resampled) δ18O (‰) and the annual accumulation (cm w.e. y-1) from the S1C1 core, with the near surface temperature (in °C) extracted from the READER data base for Dumont d'Urville Station (https://legacy.bas.ac.uk/met/READER/) and the Average sea ice concentration extracted between 90°E and 150°E from the Nimbus-7 SMMR and DMSP SSM/I-SSMIS Passive Microwave Data (http://nsidc.org/data/nsidc-0051). Note that the y-axis of the lowest panel is reversed, to ensure visual coherency between lower sea-ice extent and higher temperatures. Black points linked by a dotted line correspond to the annual time series while the red lines correspond to the 13-point binomial filters with bounce end-effects.

annual mean $\delta^{18}O$ values of the whole series. No long-term trend is observed. Spectral analyses performed using the Multi-Taper method evidence highly significant periodicities of 6 and 14 years (harmonic F-test > 0.99), close to those identified for accumulation. . This former result lead us to use a 13-point binomial filter with bounce end-effects, allowing us to explore the S1C1 $\delta^{18}O$ record at the decadal scale and to compare it with accumulation at the same scale (Figure 4.2.5). The resulting calculations depict a sharp decrease in the 1950s, with the strongest decadal minimum peaking in 1955. It is followed by a gradual increase, reaching the highest $\delta^{18}O$ decadal-mean values in ~1982 and ~1992, with secondary maxima in ~1962 and ~1972. A sharp decrease occurs in the 1990s, when mean levels from the 1950s are reached again. There is an anti-phase of the $\delta^{18}O$ and accumulation smoothed signals in the 1950s and the 2000s, while they appear in phase from the 1970s to 1990s, with multi-decadal variations.

We now explore linear relationships between the S1C1 records and regional climate records (Table 3). No significant linear correlation is identified between annual mean S1C1 $\delta^{18}O$ and accumulation records from 1946 to 2006. We also note that there is no coincidence between remarkable years for $\delta^{18}O$ and for accumulation. There is no significant correlation between annual mean S1C1 $\delta^{18}O$ and DDU near surface air temperature over the available period at the annual scale. At the decadal scale, we observe a significant positive correlation, with a slope of 1.49 ‰ per °C. Linear relationships between $\delta^{18}O$ and near surface air temperature were found in other Antarctic stations. At Law Dome, the DE08 ice Australian $\delta^{18}O$ record displays a weak

negative correlation with Casey near surface air temperature with a slope of -0.31 ‰ per °C (r=-0.45 and p=9.0 x $10^{-}3$ for the period 1959-1991) (Masson-Delmotte et al., 2003). At Dome C, over 3 years, daily precipitation $\delta^{18}O$ displays a significant positive correlation with daily AWS near surface air temperature, with a slope of 0.49 ‰ per °C (r=0.79 and p=3.2 x 10^{-109}). No significant relations are detected between annual mean S1C1 $\delta^{18}O$ and annual mean sea ice concentration in the Adélie land sector (Table 4.2.3).

4.2.3.4 Model-data comparison

4.2.3.4.1 Comparison between the ECHAM5-wiso and the S1C1 data

This comparison is limited by the fact that we only have one firn core record, and no estimation of the deposition noise. In the future, the latter may be estimated from signal-to-noise analyses of multiple ice core records from the same area (Masson-Delmotte et al., 2015). Moreover, recent monitoring of surface snow and surface vapour isotopic composition in polar regions have suggested isotopic exchanges between surface snow an water vapour in-between snowfall events (Steen-Larsen et al., 2014; Ritter et al., 2016). Such processes are not accounted for in the atmospheric models, and we can therefore only compare simulated precipitation-weighted $\delta^{18}O$ with our firn measurements. Similarly, we compare the ECHAM5-wiso model simulated precipitation with the ice core accumulation data, which may also reflect the impact of wind erosion.

The ECHAM5-wiso simulation produces a large increase in $\delta^{18}O$ and precipitation after 1979 (not shown). As such increase is not observed in the S1C1 record, we suggest that it may arise from a discontinuity in the ERA reanalyses data used as boundary conditions. Indeed, the lack of sea ice observations prior to the satellite era in the ERA-40 dataset leads to the unrealistic set of climatological sea ice coverage values around Antarctica prior to 1979. This deficit does not exist in the ERA interim dataset, starting from year 1979. Therefore, in the following, the model-data comparison is restricted to the period 1979-2006 (Fig. 4.2.6).

The ECHAM5-wiso simulation underestimates the average seasonal amplitude of $\delta^{18}O$ at the S1C1 grid point by a factor of 2.0, and its inter-annual standard deviation by a factor of 1.4. No strong similarity appears for year-to-year values. Weak but significant decreasing long-term trends appear in both the S1C1 record and in the model outputs (r=-0.36 and p=0.058 and r=-0.43 and p=0.022 respectively).

By contrast, the model precipitation amount (68.4 ±11.7 cm w.e. y^{-1}) is much higher than observed (23.1 ±7.3 cm w.e. y^{-1}) at S1C1 site on the same period. This difference cannot be explained by the impact of sublimation (in average, -4.8 cm w.e. y^{-1} in the simulation). Note that the model may not fully account for the impact of wind erosion, due to missing

parameterizations for wind scouring and misrepresentation of small-scale katabatic winds. However, snow accumulation is highly variable in this region, due to the orographic effect on precipitation and to wind scouring. Along the first 50 km of the stake network (Agosta et al., 2012), the mean accumulation rate is estimated at 34.6 cm w.e. y^{-1} between 2004 and 2014. This result confirms that ECHAM5-wiso overestimates the regional accumulation rate. When considering deviations from average values (Fig. 4.2.6), no similarity emerges between inter-annual variations in the S1C1 record and in the simulation. The simulation captures the observed positive anomalies in 1993. No significant long-term trend is identified from 1979 to 2006.

The model-data mismatch may arise from the topographic effect of the Antarctic ice sheet margin on the distribution of precipitation, and the associated isotopic distillation. The model grid size used here (approx. 1.1 ° x 1.1 °, i.e. 110 x 110 km^2) might also be too coarse for a direct comparison of the simulation results to the S1C1 drill site. Further investigations are needed, and this requires also a regional network of shallow firn core records on the Antarctic ice sheet margin, in order to characterize spatio-temporal variations and signal-to-noise ratios.

In the simulation, we have also explored the δ^{18}O-precipitation and the δ^{18}O-temperature relationship at the annual scale. A significant linear relationship appears for temperature, with

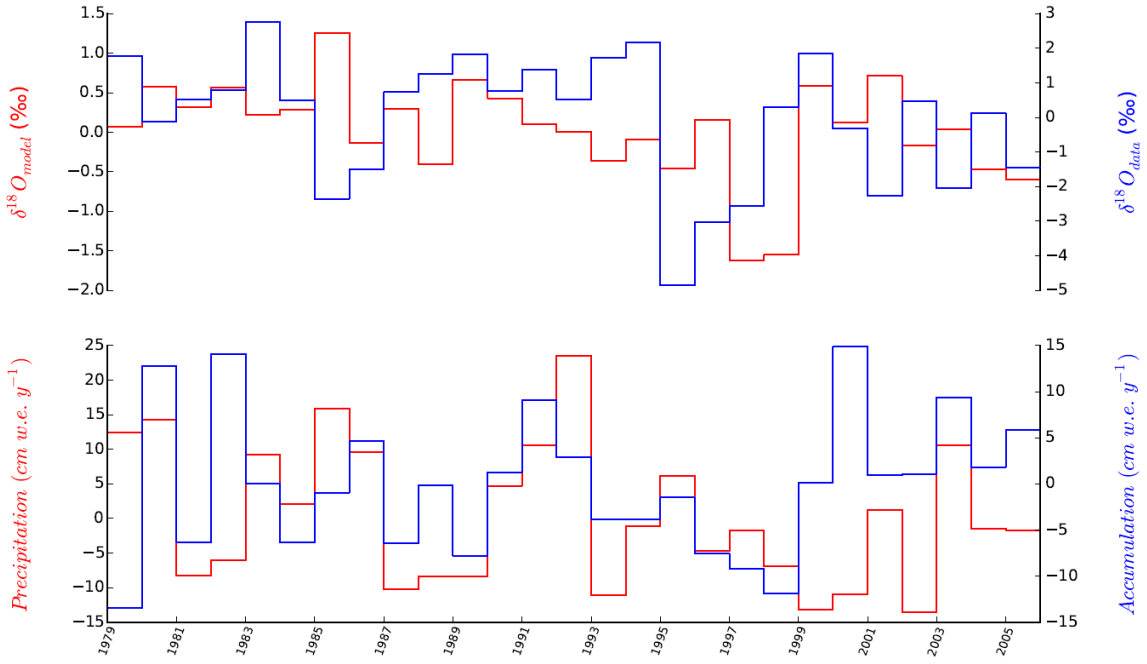

Figure 4.2.7: Model-data comparison of the anomalies (annual value minus the 1979-2006 average value) of δ^{18}O (‰) and accumulation (cm w.e. y-1). The blue points and dashed lines correspond to the data from the S1C1 core while the red stair steps correspond to the simulations.

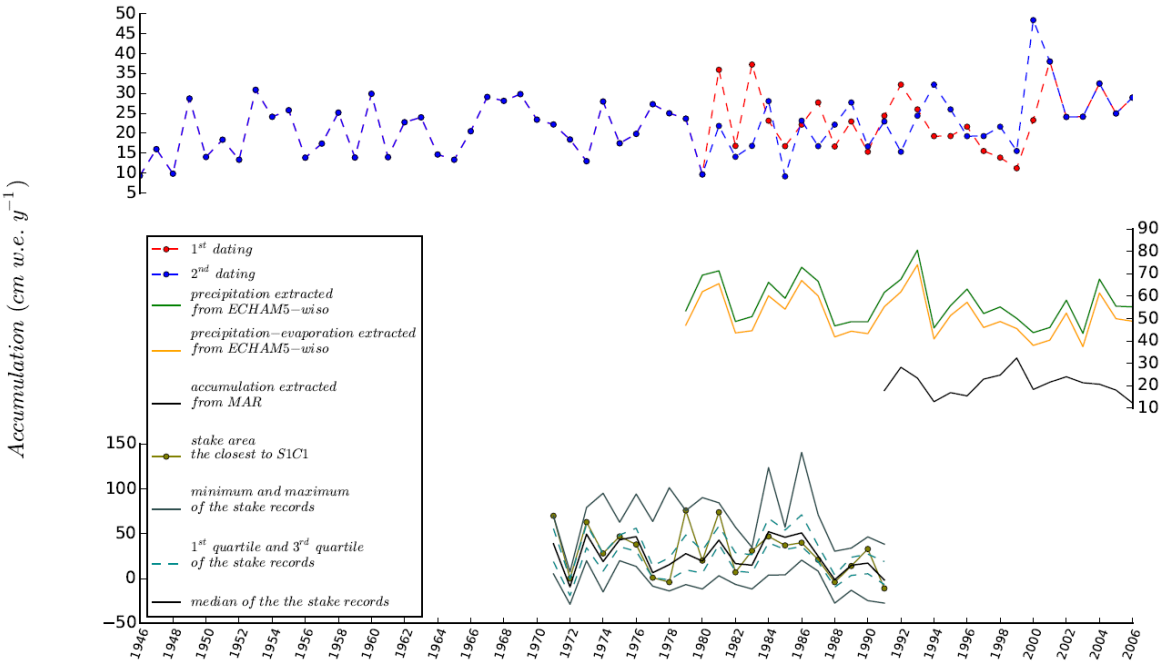

Figure 4.2.7: Comparison of accumulation data. Top panel: S1C1 reconstruction obtained from the first (red) and second (blue) dating. Note that the accumulation resulting from first dating and second dating overlap over 1946-1980 and 2001-2006 so only one colour line appears. Middle panel: precipitation (green) and precipitation minus evaporation (orange) simulated by ECHAM5-wiso (1979-2006), and accumulation simulated by MAR (1991-2006) (black). Lower panel: distribution of accumulation measurements from stake records, illustrated by minima and maxima (grey lines), first and third quartiles (dashed green lines), median value of stake measurements (black line) and measurements from one single stake, closest to the S1C1 site (solid green line). Two dashed vertical lines correspond to years 1984 and 1990.

a slope of 0.29 ‰ °C^{-1} (r=0.39, p= 0.038). By contrast, no significant linear relationship is simulated for precipitation (r=0.19, p=0.34).

In summary, the ECHAM5-wiso model outputs appear to have a wet and δ^{18}O-depleted bias at the S1C1 drill site, overestimate the inter-annual accumulation variability, underestimate the δ^{18}O variability and its relationship with surface air temperature, and fail to capture the observed δ^{18}O-accumulation relationship.

Our model-data comparison is of course limited by comparing two different datasets. For the modelling results, we have analysed a pure atmospheric signal (precipitation). The signal recorded in the S1C1 core is produced by precipitation, but also potentially altered by post-deposition processes (such as sublimation, wind scouring and snow metamorphism). Also, the fact of having just one ice core record (also associated with age scale uncertainties) precludes an assessment of the signal-to-noise ratio. Indeed, with similar mean accumulation values, it was shown that 4-5 shallow ice cores may be needed to extract the common climatic signal in North-West Greenland (Masson-Delmotte et al, 2015).

4.2.3.4.2 Comparison between the ECHAM5-wiso model and the MAR model

We now investigate the results of the regional model MAR for accumulation. MAR produces a more realistic range of accumulation, with simulated values varying from 12.3 cm w.e. y^{-1} (in 2006) to 32.4 cm w.e. y^{-1} (in 1999). At this 40 km horizontal scale (against 110 km in the

ECHAM5-wiso model), the slope of the East Antarctic ice sheet is better represented, a critical aspect for orographic precipitation. However, the inter-annual variability simulated by MAR is very different from that inferred from the S1C1 core compared to ECHAM5-wiso. This result may arise from the nudging technique: while the ECHAM5-wiso model is strongly nudged to reanalyses, the MAR model is only forced by large-scale circulation at the lateral boundaries and layers above 20 km, allowing the model to build its own atmospheric circulation. We conclude that systematic caveats of the ECHAM5-wiso model for coastal Antarctic precipitation amounts may arise from its resolution.

4.2.4 Discussion

Here, we propose an alternative ice-core chronology, given the annual layer counting uncertainties. For that purpose, we have screened peak-to-peak relationships between S1C1 record, stake accumulation measurements, and ECHAM5-wiso outputs. We first tried to optimize the match between S1C1 accumulation and stake data. However, the inter-annual standard deviation of S1C1 accumulation is approximately three times lower than calculated from either individual stake records, or from the average stake record. As a result, we could not identify unequivocally remarkable low or high accumulation years as a robust signal. For instance, all stake area data show very low (close to zero) accumulation in years 1972 and 1988, but no such signal can be identified in the S1C1 record. We therefore used the ECHAM5-wiso $\delta^{18}O$ to test an alternative chronology (Section 4.2.4.1). We identified a high similarity between ECHAM5-wiso inter-annual precipitation variability and average stake data (Section 4.2.4.2). We then discussed processes that can produce non climatic noise (Section 4.2.4.3). After assessing $\delta^{18}O$-temperature relationships (Section 4.2.4.4), we finally explored the spatial relevance of climatic records from the S1C1 location (Section 4.2.4.5).

4.2.4.1 An alternative age scale can improve the model-data comparison for $\delta^{18}O$

The comparison of the most remarkable annual anomalies in the S1C1 and simulated $\delta^{18}O$ series from ECHAM5-wiso reveals a one year shift: the minimum value is identified in 1996 for S1C1 but simulated in 1998, while the 1984 maximum value in the S1C1 core may coincide with the simulated maximum value in 1986. Given the uncertainties of age chronology of at least one year and potentially several years (Section 4.2.3.1), we reconsidered the annual layer counting to assess whether the S1C1 chronology can be reconciled with the ECHAM5-wiso $\delta^{18}O$ outputs. Indeed, the identification of the summers 1999-2000 and 2000-2001 in our initial chronology (years 2000 and 2001 in Fig. 4.2.2) are based on equivocal evidence due to multiple peaks in NO_3^- and the lack of a peak in $\delta^{18}O$. Vice-versa, we could have missed one year between the

initial layers associated with the summers 1981-1982 and 1982-1983, where peaks are identified in Na^+, $nssSO_4^{2-}{}_{winter}$, $nssSO_4^{2-}{}_{summer}$, NO^{3-} and $NH4^+$. We therefore built an alternative depth-age scale (Table S4 in Supplementary Material) following these two findings (Fig. 4.2.7 and Fig. 4.2.8), and discussed the implications for the S1C1 records. Consequently, we have produced new annual mean accumulation and $\delta^{18}O$ time series, from 1979 to 2006, following the same approach (Section 4.2.2.3).

With this alternative chronology, the resulting mean accumulation does not change, and the inter-annual standard deviation is slightly increased (21.8 ± 7.4 cm w.e. y^{-1}). It has no impact on $\delta^{18}O$ or accumulation multi-decadal variations or trends. The resulting accumulation dataset remains non-significantly correlated with the stake average record and with the closest stake data. In the alternative chronology, there is still no significant $\delta^{18}O$-temperature relationship between the S1C1 record and the DDU near surface air temperature time series, and no relationship between S1C1 accumulation dataset and the ECHAM5-wiso precipitation output at the annual scale. However, it improves (by construction!) the strength of the correlation between the S1C1 $\delta^{18}O$ and the ECHAM5-wiso $\delta^{18}O$, from r=0.17 with p=0.39 for the initial chronology to r=0.57 with p=1.6 x 10^{-3} for the alternative chronology.

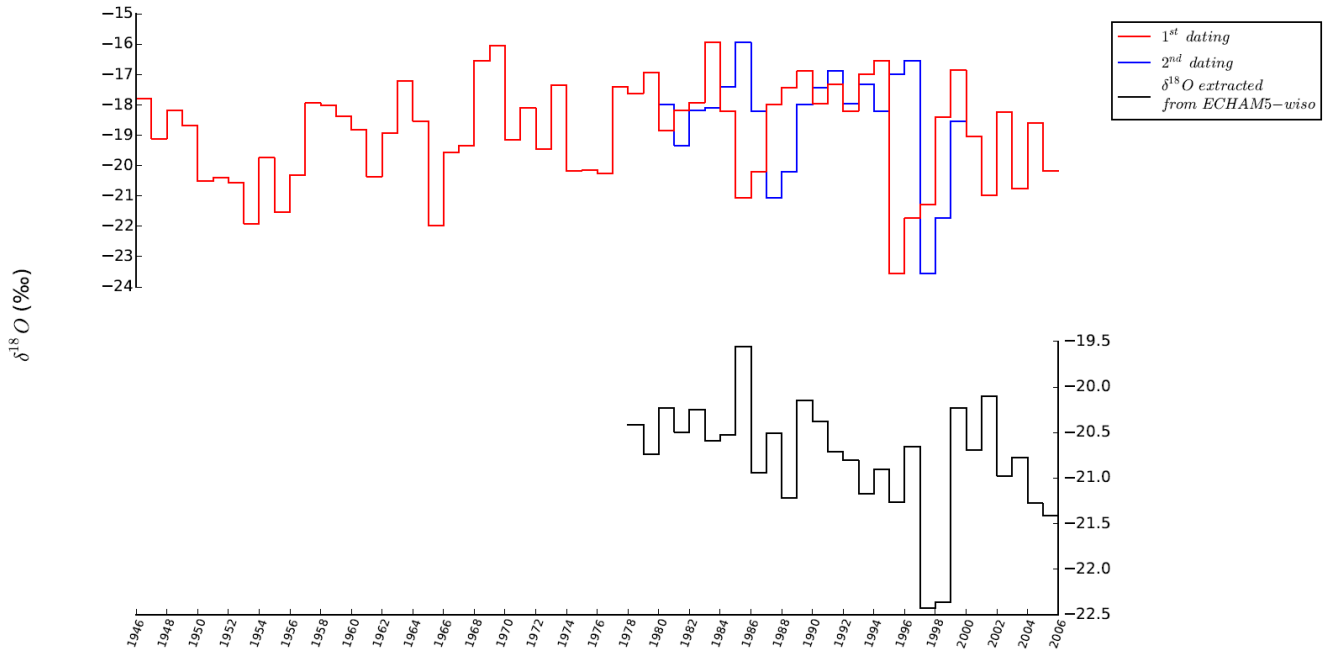

Figure 4.2.8: Comparison of dO18 data. Top panel: annual mean dO18 data from the S1C1 core on the first (red) and second (blue) dating, over 1946-2006. Note that the S1C1 dO18 resulting from first dating and second dating overlap in 1946-1980 and 2001-2006, when only one colour line is displayed. Bottom: annual mean (precipitation-weighted) precipitation dO18 simulated by the ECHAM5wiso-model. Small vertical black lines and arrows illustrate the shift between the two S1C1 age scales for the years with the highest and lowest dO18 values of our record. Long vertical lines illustrate the match between the ECHAM5-wiso and S1C1 peaks used to build the second chronology.

4.2.4.2 Comparison between stake data and ECHAM5-wiso simulation

No significant linear correlation is found neither between the S1C1 accumulation record (whatever chronology is used) and the stake accumulation measurements, nor between the S1C1 accumulation record and the ECHAM5-wiso simulated precipitation. We therefore compared the stake measurements and the ECHAM5-wiso output, with the goal to investigate if there is a common climatic signal (for the period 1979-1991).

We observe a high and significant correlation between the ECHAM5-wiso simulated precipitation and the average stake record at the inter-annual scale ($r=0.62$ and $p=0.030$). This finding shows that the nudged ECHAM5-wiso simulation is able to capture almost 40% of the inter-annual average accumulation variance, and that there is a clear synoptic climatic deposition (and not only local deposition) in the stake accumulation record. We also note that there is a high dispersion in the inter-annual variability of accumulation across the individual stake records, as evidenced by the quartile distribution (Fig. 4.2.7). Each stake record is significantly correlated with the average stake record (r varies from 0.57 to 0.90, reaching 0.78 for the stake closest to S1C1, $p=3.2 \times 10^{-5}$). However, significant differences are encountered. For instance, the sharp peak in accumulation displayed by the stake closest to S1C1 in 1979 is an outlier and is not recorded in the average stake signal. Similarly, the correlation coefficient between the ECHAM5-wiso simulated precipitation and individual stake records varies from 0.3 to 0.7, stressing potential non-climatic noise in local accumulation data.

We conclude that the common climatic signal in average stake accumulation time series is related to regional-scale circulation, and is captured by the ECHAM5-wiso simulation. The lack of correlation between the S1C1 accumulation record and both stake records and ECHAM5-wiso precipitation outputs may therefore reflect local non-climatic noise.

4.2.4.3 Processes causing non-climatic noise

The significant correlation between the ECHAM5-wiso precipitation and the stake average accumulation record stresses the fact that the inter-annual variability of the average accumulation is dominated by large-scale atmospheric circulation controls on precipitation. Given the spatio-temporal variability of accumulation reported previously, we could not use accumulation information to refine the initial S1C1 chronology, and conclude that the S1C1 accumulation record is probably heavily affected by non-climatic noise. The significant correlation between the ECHAM5-wiso precipitation and the stake average accumulation record stresses the fact that the inter-annual variability of the average accumulation is dominated by large-scale atmospheric circulation controls on precipitation. However, snow accumulation is spatially variable at the study site (Agosta et al., 2012). Indeed, the mean

accumulation given by the stake located at D10 is 25.6 cm w.e y^{-1} and the standard deviation of mean accumulation values from the 14 stakes located within the first 10 km is 12.0 cm w.e y^{-1}. A high variability reaching tens of milimeter over few meters was also reported by Genthon et al. (2007) and Favier et al. (2011) over an ablation site located 4 km from D10.

This high variability can be associated to wind erosion, wind redistribution, sublimation, occurrence of gravity waves in the katabatic flow, and other processes during or after the precipitation event (Eisen et al., 2008). This leads to very high variability even at very small spatial scales, down to deca-meter scale (Libois et al., 2014), as reflected by the presence of sastrugi (Amory et al., 2015). Local features associated either with the distribution of precipitation or with wind-driven post-deposition erosion or deposition appear dominant for a given stake record, and for the S1C1 record as well.

Liquid precipitation or melting and subsequent refreezing appear of secondary importance in this region. Indeed, 2.5-m snow cores were collected every 0.5 km from the 156-km stake network of the Glacioclim observatory. These shallow cores were used for density measurements and screened for stratigraphic analysis. Small ice layers exceeding 2 mm were identified at the same depth. Near D10, one event of liquid precipitation event followed by refreezing was observed between December 31th, 2014 and January 1st, 2014. This single event led to ice layers reaching up to 6 cm of thickness. According from meteorological monitoring performed at the Météo France DDU station, this is the single such occurrence of a heavy liquid precipitation event since 1957. From stratigraphic analyses of pits and shallow ice cores at D10, spanning the last 10 years (prior to 2014), only one ice layer thicker than 3 mm was identified: a 3 cm thick ice layer was observed at 60 cm depth in the surface core collected in 2008-2009. There is therefore evidence for rare occurrence of liquid precipitation, and very limited melting and refreezing of surface snow at D10, with limited percolation effects, when compared to annual accumulation amounts.

Differences in accumulation estimates from the stake data and from S1C1 may also arise from variations in surface snow density. Indeed, stake height measurements were converted into water equivalent using a spatial estimate of mean density distribution (Agosta et al., 2012). Lastly, this analysis also highlights the limited information which can be extracted from one single ice core. In the future, obtaining several ice cores from this sector will help to quantify the common climatic signal and better characterize the non-climatic noise. It will also to confirm our hypothesis that there is a significant climatic signal from this single core, as suggested by the comparison of the average stake area record with the ECHAM5-wiso output.

4.2.4.4 $\delta^{18}O$-temperature relationship

We now report the various estimates of the $\delta^{18}O$-temperature relationship based on our S1C1 record, instrumental temperature data, and ECHAM5-wiso outputs (Table 4.2.4).

Correlations and slopes in the $\delta^{18}O$-temperature relationship from the data (both chronologies) over the whole available period (1956-2006), are not significant at the annual scale contrary to the decadal scale. It suggests that the $\delta^{18}O$-temperature is not stationary through time. This may arise from non-climatic noise at the inter-annual scale. Moreover, the decadal slopes are stronger than expected from a Rayleigh distillation, possibly resulting from either a decoupling between surface and condensation temperature, or from changes in moisture sources through time.

We note that over the period 1979-2006, although the $\delta^{18}O$-temperature relationship from the fist chronology is not significant, the relationship from the second one is significant but weak, with a slope close to the Rayleigh distillation.

The ECHAM5-wiso simulation shows that the seasonal cycle of $\delta^{18}O$ is not in phase with the seasonal cycle of temperature. Moreover, the inter-annual variability of $\delta^{18}O$ simulated in the S1C1 area is maximum in local spring (November), in contrast with the maximum inter-annual variability of DDU temperature, occurring in winter. This finding are also different from Dome C precipitation data (Stenni et al., 2016), showing a larger inter-annual variability of both temperature and $\delta^{18}O$ during local winter (possibly due to variability in frequency of maritime air mass intrusions). These model results suggest that processes other than local temperature play a key role in local $\delta^{18}O$ seasonal cycle and inter-annual variability, as suggested by Schlosser et al. (2016).

In the ECHAM5-wiso model, the $\delta^{18}O$ – temperature relationship is significant (but weak) at the annual scale, and therefore stronger than observed from the S1C1 record. At the decadal scale, as in the data, the correlation is higher. However, the slope is lower (0.63) than in the data, being closer to the Rayleigh distillation. To understand this mismatch between data and simulations, we investigated alternative approaches for the $\delta^{18}O$-temperature relationship obtained using annual data through the combination of temperature extracted from the READER database and simulated $\delta^{18}O$, and the temperature extracted from the ECHAM5-wiso model and S1C1 $\delta^{18}O$ record (Table 4.2.4).

We found a high and significant correlation between inter-annual variations in temperature from the READER database and ECHAM5-wiso simulated near surface air temperature ($r=0.91$ and $p=2.2 \times 10^{-12}$) but no significant correlation between inter-annual variations in $\delta^{18}O$ from the S1C1 core (from the first dating) and simulated by ECHAM5-wiso. The variance of the ECHAM5-wiso model result is about twice as small as in the S1C1 core (inter-annual standard

Table 4.2.4. Linear relationships between temperature and $\delta^{18}O$ showing the slope, the coefficient correlation and the p-value. The indices associated with "S1C1" indicate the chronology (1, initial; 2, revised).

Period	Resolution	Source of the temperature	Source of the $\delta^{18}O$	Slope	r	p
1956-2006	annual	READER database	$S1C1_1$	-0.33	-0.13	0.35
		READER database	$S1C1_2$	0.36	0.15	0.30
	decadal	READER database	$S1C1_1$	1.49	0.72	2.6×10^{-9}
		READER database	S1C1,2	1.32	0.60	3.2×10^{-6}
1979-2006	annual	READER database	$S1C1_1$	-0.33	-0.15	0.44
		READER database	$S1C1_2$	0.77	0.31	0.11
	decadal	READER database	$S1C1_1$	1.82	0.72	1.30×10^{-5}
		READER database	$S1C1_2$	1.38	0.51	5.7×10^{-3}
	annual	ECHAM	ECHAM	0.29	0.39	0.038
	decadal	ECHAM	ECHAM	0.63	0.80	4.0×10^{-7}
	annual	READER database	ECHAM	0.42	0.48	0.010
	decadal	READER database	ECHAM	0.98	0.89	3.6×10^{-10}
	annual	ECHAM	$S1C1_1$	-0.37	-0.17	0.40
	annual	ECHAM	$S1C1_2$	0.58	0.27	0.16

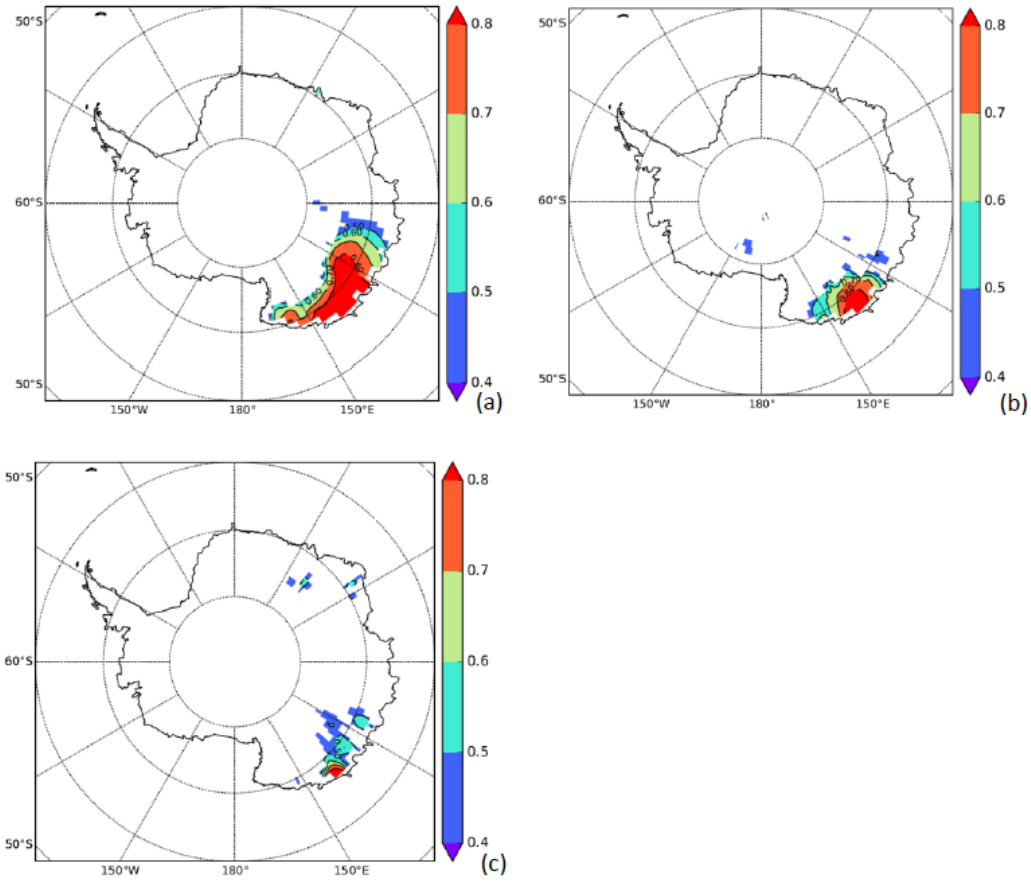

Figure 4.2.9: Correlation between simulated annual mean 2m-temperature (a), annual precipitation amount (b), precipitation annual mean $\delta^{18}O$ (c) at the S1C1 site with the same variable at each grid point of the ECHAM5-wiso model for r>0.4 and p<0.03. Only significant values are represented (p<0.05).

deviation 0.6 ‰ for the ECHAM5-wiso model and 1.8 ‰ in the S1C1 core respectively for the period 1979-2006) (Table 4.2.2). Also, note that the strength of the correlation coefficient and the magnitude of the slope are higher for ECHAM $\delta^{18}O$ versus READER temperature than within ECHAM outputs for both annual and decadal time scales. This could be explained by a near surface temperature closer to the condensation temperature in the case of READER compared to ECHAM.

So far, we cannot conclude on the cause for such a difference in variance: the ice core record may be affected by post-deposition features that generate noise (Section 4.2.4.3), or the atmospheric model may not adequately resolve moisture transport pathways driving variability in the precipitation signal. Systematic comparisons between ECHAM5-wiso and results from direct precipitation sampling or from surface water vapour isotopic composition monitoring are needed to understand whether this mismatch arises from the atmospheric model or from signal-to-noise issues in one individual ice core record. So far, no such measurements are available in Adélie Land. This finding calls for a cautious use of simulated $\delta^{18}O$-temperature relationships in coastal areas, before a full assessment of the model skills can be achieved.

4.2.4.5 Spatial extent of the representativeness of S1C1 site

We finally take advantage of the ECHAM5-wiso simulation in order to investigate the spatial relevance of the S1C1 site. For that purpose, we have calculated the correlation coefficients of the annual surface air temperature, precipitation amount and $\delta^{18}O$ between the model output at the S1C1 site and the model outputs for each other Antarctic grid point (cf. Fig. 4.2.9). Regarding temperature, S1C1 temperature appears closely related ($r \geq 0.8$) with regional temperature in an approximative ~1000 km from ~120 °E to 150 °E. S1C1 is strongly correlated

4.2.5 Conclusions and perspectives

Documenting inter-annual climatic variations in coastal Antarctica is important to characterize natural climate variability, and provide a long-term context for recent changes beyond the instrumental period. The study of the S1C1 core addresses this challenge.

The initial chronology of the S1C1 ice core was established combining multi-parameter annual layer counting using major ions and $\delta^{18}O$, as well as references horizons (nuclear test horizons and fingerprints of summers with no sea-ice retreat). The latter approach would not have been feasible without the knowledge provided by long-term aerosol monitoring at DDU. The S1C1 records encompass the period 1946-2006 with equivocal identification of 8 annual years.

The mean accumulation rate estimated from the S1C1 record is coherent with information from stake area measurements in Adélie Land. No long-term trend is detected in the stake data

(Agosta et al., 2012) and in the S1C1 accumulation record. This robust finding challenges a recent regional modeling study showing a decrease of accumulation in coastal Adélie Land from 1979 to 2010 (Lenaerts et al., 2012). We are not confident in the signal of higher accumulation rates in the 2000s, because no such signal is detected in the comparison of recent and historical stake measurements. The average stake area record is significantly correlated with results from the ECHAM5-wiso model, but not with the S1C1 record. This finding may arise from post-deposition noise associated with e.g. wind scouring. The lack of similarity between the S1C1 ice core records and the stake measurements may also arise from the fact that the location of stake measurements may have moved through time (Agosta et al., 2012), and from the correction of height measurements using an average density value along the profile rather than simultaneous measurements of density which were not available.

The S1C1 $\delta^{18}O$ record shows a remarkable small amplitude of the seasonal cycle, when compared to other isotopic datasets from coastal East Antarctica. But note that the accumulation rate is site-dependent. We have stressed that remarkable years in $\delta^{18}O$ and accumulation records do not coincide. Both records display a multi-decadal variability. The S1C1 $\delta^{18}O$ record is significantly correlated with DDU near surface air temperature only at the decadal scale, with a particularly large slope. We showed that the ECHAM5-wiso model strongly underestimates the inter-annual variability in $\delta^{18}O$. This features calls for a systematic assessment of the skills of the isotopically enabled atmospheric general circulation models against the whole variety of data regarding the temporal variability. In order to better understand the drivers of isotopic variability in coastal Adélie Land, obtaining continuous vapour and precipitation isotopic composition measurements at DDU will offer the possibility of a direct comparison with atmospheric transport pathways, and with aerosol chemical data.

Implementing water stable isotopes in the regional MAR model is underway. Resolving regional aspects of the atmospheric circulation, especially related to katabatic winds and boundary layer dynamics, may indeed be important to resolve changes in moisture origin at the inter-annual scale. Contrary to the regional MAR model, the ECHAM5-wiso model captures inter-annual variations in Adélie Land accumulation rate (as inferred from the average stake measurements) and remarkable $\delta^{18}O$ anomalies (as identified in the S1C1 record). Therefore, these variations are driven by large-scale atmospheric circulation. We have highlighted the fact that model outputs cannot be used in a climate sense prior to 1979, probably due to the lack of sea ice data used in the assimilation systems.

In this manuscript, we have also used the ECHAM5-wiso model outputs to challenge our initial ice core chronology. None of our key conclusions is affected by the alternative chronology implying a two-year shift. Finally, we have used the ECHAM5-wiso model to explore the

spatial relevance of precipitation and precipitation $\delta^{18}O$ outputs at the S1C1 site, and stressed the differences between a large-scale representativeness of temperature (typically, 1000 km), and a smaller-scale representativeness of $\delta^{18}O$ (typically, 100 km around the S1C1 site). In the future, obtaining a network of shallow ice core records in coastal East Antarctica will be critical to assess signal-to-noise aspects and test the validity of these findings. Obtaining longer records will also allow to better characterize the multi-decadal variability and assess past changes in Antarctic temperature (PAGES 2k Consortium, 2013; Jones et al., 2016). Moreover, characterizing spatio-temporal variations in deuterium excess will provide a complementary line of information, for the identification of seasonal variations, and for assessing past changes in moisture origin.

Further investigations are finally needed to explore the relationships between large-scale modes of variability such as the Southern Annular Mode (SAM), the Pacific – South American patterns (PSA), ENSO and climate variability in the Adélie Land sector. Indeed, composite analyses performed from 1979 to 2013 show significant imprints of SAM and PSA2 (associated with the tropical heating anomalies in the Pacific) on DDU temperature (Marshall and Thompson, 2016), and of La Niña on coastal East Antarctic climate (Welhouse et al., 2016). No significant relationships emerge with our S1C1 records.

Our records, available back to 1946 (therefore 10 years earlier than the instrumental temperature series from DDU) depict decadal variations with a $\delta^{18}O$ minimum in the mid-1950s, within the range of subsequent variability. Altogether, these results imply no major climatic reorganization in this sector of East Antarctica prior to the 1970s. It contradicts suggestions for dramatic sea ice contraction in the mid-1950s, based on whaling ship records (William, 1997; Cotte and Guinet, 2007). Given discussions with respect to drivers of penguin demography (Raymond et al., 2015; Southwell et al., 2015), reconciling all sources of information for Adélie Land climate variability prior to the 1970s remains to be achieved.

4.3 TA192A

Cette dernière étude est en cours de relecture dans le journal *The Cryosphere (Goursaud et al., 2018)*. Le matériel supplémentaire correspondant est disponible en ligne (https://www.the-cryosphere-discuss.net/tc-2018-121/, dernier accès : 01/2019).

Abstract. A new 21.3 m firn core was drilled in 2015 at a coastal Antarctic high accumulation site in Adélie Land (66.78 °S; 139.56 °E, 602 m a.s.l.), named Terre Adélie 192A (TA192A). The mean isotopic values (-19.3 ± 3.1 ‰ for $\delta^{18}O$ and 5.4 ± 2.2 ‰ for deuterium excess) are consistent with other coastal Antarctic values. No significant isotope-temperature relationship can be evidenced at any timescale. This rules out a simple interpretation of in terms of local temperature. An observed asymmetry in the $\delta^{18}O$ seasonal cycle may be explained by the precipitation of air masses coming from the eastern and western sectors in autumn and winter times, recorded in the d-excess signal showing outstanding values in austral spring versus autumn. Significant positive trends are observed in the annual d-excess record and local sea ice extent (135 °E–145 °E) over the period 1998-2014.

However, processes studies focusing on resulting isotopic compositions and particularly the deuterium excess- $\delta^{18}O$ relationship, evidenced as a potential fingerprint of moisture origins, as well as the collection of more isotopic measurements in Adélie Land are needed for an accurate interpretation of our signals.

Résumé. Une nouvelle carotte de 21,3 cm a été forée en 2013 sur un site côtier d'Antarctique de haute accumulation en Terre Adélie (66,78 °S; 139,56 °E, 602 m a.s.l.).

Les valeurs moyennes isotopiques (-19,3 ± 3,1 ‰ pour le $\delta^{18}O$ et 5,4 ± 2,2 ‰ pour le d-excess) sont cohérentes avec les autres valeurs côtières pour l'Antarctique. Il n'existe aucune relation significative entre la température et les isotopes, à aucune échelle de temps, écartant une simple interprétation en termes de température locale. Une asymétrie observée du cycle saisonnier du $\delta^{18}O$ pourrait trouver son explication dans la précipitation des masses d'air venant des secteurs de l'Est et de l'Ouest en automne et en hiver, enregistré dans le signal du d-excess montrant des valeurs remarquables durant le printemps austral comparé à l'automne. Des tendances inter-annuelles significatives positives sont observées pour l'enregistrement du d-excess et l'extension de la glace de mer locale (135 °E-145 °E) sur la période 1998-2014.

Cependant, des études mécanistiques se concentrant sur les compositions isotopiques résultantes, et particulièrement la relation d-excess-$\delta^{18}O$, témoignant de l'origine de l'humidité, ainsi que des collectes de nouvelles mesures isotopiques en Terre Adélie, sont nécessaires pour une interprétation plus fidèle de nos signaux.

4.3.1 Introduction

Motivation for new coastal Antarctic firn cores

Polar ice cores are exceptional archives of past climate variations. In Antarctica, many deep ice cores have been drilled and analyzed since the 1950s. For instance, Stenni et al. (2017) compiled water stable isotope data from 112 ice cores spanning at least part of the last 2000 years. Most deep ice cores were drilled in the central Antarctic plateau where low accumulation rates and ice thinning give access to long climate records. In today's context of rapid global climate change, it is of paramount importance to also document recent past climate variability around Antarctica. Many Antarctic regions still remain undocumented due to the lack of accumulation and water stable isotope records from shallow ice cores or pits (Jones et al., 2016;Masson-Delmotte et al., 2008). An accurate knowledge of changes in coastal Antarctic surface mass balance (SMB), an evaluation of the ability of climate models to resolve the key processes affecting its variability, and thus an improved confidence in projections of future changes in coastal Antarctic surface mass balance is important to reduce uncertainties on the ice sheet mass balance and its contribution to sea level change (Church et al., 2013).

Meteorological observations have been conducted since 1957 in manned and automatic stations (Nicolas and Bromwich, 2014), and considerable efforts have been deployed to compile and update the corresponding dataset (Turner et al., 2004). This network is marked by gaps in spatio-temporal coverage (Goursaud et al., 2017a) as well as systematic biases of instruments such as thermistors (Genthon et al., 2011). Satellite remote sensing data have been available since 1979 and provide large-scale information for changes in Antarctic sea-ice and temperature (Comiso et al., 2017), but do not provide sufficient accuracy and homogeneity to resolve trends at local scales (Bouchard et al., 2010). Coastal shallow (20 – 50 m long) firn cores are thus essential to provide continuous climate information spanning the last decades at sub-annual resolution, at local but also regional scales. They complement stake area observations of spatio-temporal variability in surface mass balance (Favier et al., 2013), which also help assessing the representativeness of a single record.

Since the 1990s, efforts have been made to retrieve shallow ice cores in coastal Antarctic areas.Most of these efforts have been focused on the Atlantic sector, in Dronning Maud Land (Altnau et al., 2015;Graf et al., 2002;e.g. Isaksson and Karlén, 1994) and the Weddell Sea Sector (Mulvaney et al., 2002). Fewer annually resolved water stable isotope records have been obtained from ice cores in other regions, such as the Peninsula (Fernandoy et al., 2018), the Ross sea sector (Bertler et al., 2011), Law Dome (Masson-Delmotte et al., 2003;Delmotte et al., 2000;Morgan et al., 1997), Adélie Land (Yao et al., 1990;Ciais et al., 1995;Goursaud et al., 2017b), and Princess Elizabeth region (Ekaykin et al., 2017). However, the recent 2k

temperature and SMB reconstructions for Antarctic (Stenni et al., 2017;Thomas et al., 2017) highlighted the need for more coastal records. In this line, new drilling efforts have recently been initiated in the context of the ASUMA project (improving the Accuracy of SUrface Mass balance of Antarctica) from the French Agence Nationale de la Recherche, which aims to assess spatio-temporal variability and change in SMB over the transition zone from coastal Adélie Land to the central East Antarctic Plateau (towards Dome C).

Climatic interpretation of water stable isotope records

Water stable isotope ($\delta^{18}O$, δD) records from central Antarctic ice cores have classically been used to infer past temperature changes (e.g. Jouzel et al., 1987). The isotope-temperature relationship was nevertheless shown not to be stationary and to vary in space (Jouzel et al., 1997), calling for site-specific calibrations relevant for various timescales (Stenni et al., 2017). In coastal regions, several studies showed no temporal isotope-temperature relationship at all between water stable isotope records in firn cores covering the last decades and near-surface air temperature measured at the closest station. This is for instance the case in Dronning Maud Land, near the Neumayer station (three firn cores, for which the longest covered period is 1958-2012, Vega et al., 2016), in the Ross Sea sector (one snow pit covering the period 1964-2000, Bertler et al., 2011), and in Adélie Land, close to DDU (one firn core covering the period 1946-2006, Goursaud et al., 2017b). While several three-dimensional atmospheric modelling studies have suggested a dominant role of large-scale atmospheric circulation on the variability of coastal Antarctic snow $\delta^{18}O$ (e.g. Noone, 2008;Noone and Simmonds, 2002), understanding the drivers of coastal Antarctic $\delta^{18}O$ variability remains challenging (e.g. Fernandoy et al., 2018;Bertler et al., 2018;Schlosser et al., 2004;Dittmann et al., 2016). While distillation processes are expected theoretically to relate condensation temperature with precipitation isotopic composition, a number of deposition processes can distort this relationship: changes in moisture sources (Stenni et al., 2016), intermittency or seasonality of precipitation (Sime et al., 2008), boundary layer processes affecting the links between condensation and surface air temperature (Krinner et al., 2008), as well as several post-deposition processes, such as the effects of winds (Eisen et al., 2008), snow-air exchanges (Casado et al., 2016;Ritter et al., 2016), and diffusion processes in snow and ice (e.g. Johnsen, 1977). Nevertheless, all these processes remain poorly quantified. As a result, comparisons between firn core records with precipitation records or simulations have to be performed carefully.

Changes in the atmospheric water cycle can also be investigated using a second order parameter, deuterium excess (d-excess). The definition given by Dansgaard (1964) as d-excess = $\delta D - 8 \times \delta^{18}O$ aims to remove the effect of equilibrium fractionation processes to identify

differences in kinetic fractionation between the isotopes of hydrogen and oxygen. In Antarctica, spatial variations of d-excess have been documented through data syntheses, showing an increase from the coast to the plateau (Masson-Delmotte et al., 2008;Touzeau et al., 2016), but temporal variations of d-excess (seasonal cycle, inter-annual variations) remain poorly documented and understood.

Theoretical isotopic modeling studies show that d-excess depends on evaporation conditions, mainly through the impacts of relative humidity (RH), and sea surface temperature (SST) on kinetic fractionation at the moisture source (Merlivat and Jouzel, 1979;Petit et al., 1991;Ciais et al., 1995), and the preservation of the initial vapor signal during transportation towards polar regions (e.g. Jouzel et al., 2013;Bonne et al., 2015). The effect of wind speed on kinetic fractionation is secondary and thus has been neglected in climatic interpretations of d-excess. Some studies usually privileged one variable (RH or SST). For instance, glacial – interglacial d-excess have classically been interpreted to reflect past changes in moisture source SST, neglecting RH effects or assuming co-variations of RH and SST (Vimeux et al., 2001;Vimeux et al., 1999;Stenni et al., 2001). Recent measurements of d-excess in water vapor from ships have evidenced a close relationship between d-excess and oceanic surface conditions, especially RH, at sub-monthly scales (Pfahl and Sodemann, 2014;Uemura et al., 2008;Kurita et al., 2016). Other recent studies have suggested that evaporation at sea ice margins may be associated with a high d-excess value due to low RH effects, a process which may not be well captured in atmospheric general circulation models (e.g. Kurita, GRL, 2011; Steen-Larsen et al, 2017). Several authors have thus identified the potential to identify changes in moisture sources using d-excess (Delmotte et al., 2000;Sodemann and Stohl, 2009;Ciais et al., 1995). The comparison between multi-year isotopic precipitation datasets with the identification of air mass origins using back-trajectories showed however a complex picture, with no trivial relationship between the latitudinal air mass origin and d-excess (Dittmann et al., 2016;Schlosser et al., 2008). A few studies have also explored sub-annual d-excess variations, and suggested that seasonal d-excess signals cannot be explained without accounting for seasonal changes in moisture transport (e.g. Delmotte et al., 2000). These features have been explored through the identification of back-trajectory clusters and their relationship with $\delta^{18}O$–d-excess relationships, including phase lags (Markle et al., 2012;Caiazzo et al., 2016;Schlosser et al., 2017).

Most of these d-excess studies have been performed using firn records and not precipitation samples. We stress that the impact of post-deposition processes on d-excess remain poorly documented and understood. While relationships between moisture origin and d-excess should in principle be conducted on vapour measurements to circumvent the uncertainties associated

with deposition and post-deposition processes, the available vapour water stable isotope records from Antarctica only cover one or two summer months (Ritter et al., 2016;Casado et al., 2016) and do not yet allow to explore the relationships between moisture transport and seasonal or inter-annual isotopic variations. Also, state-of-the-art atmospheric general circulation models equipped with water stable isotopes such as ECHAM5-wiso can capture d-excess spatial patterns in Antarctic snow, but they fail to correctly reproduce its seasonal variations (Goursaud et al., 2017a). Finally, the understanding of the climatic signals preserved in d-excess is limited by the available observations. This motivates the importance of retrieval of more highly resolved d-excess records from coastal Antarctic firn cores.

This study

In this study, we focus on the first highly resolved firn core drilled in coastal Adélie Land, at the TA192A site (66.78 ° S, 139.56 ° E; 602 m a.s.l., hereafter named "TA"). Only two ice cores and one snow pit were previously studied for water stable isotopes in this region, without any d-excess record: the S1C1 ice core (14 km from the TA, 279 m a.s.l., Goursaud et al., 2017b), the D47 highly resolved pit (78 km from the TA, 1550 m a.s.l., Ciais et al., 1995) and the Caroline ice core (Yao et al., 1990). The climate of coastal Adélie Land is greatly influenced by katabatic winds (resulting in a very high spatial variability of accumulation), and by the presence of sea ice (Périard and Pettré, 1993;König-Langlo et al., 1998), including the episodic formation of winter polynya (Adolphs and Wendler, 1995), which lead to nearby open water during winter time. The regional climate is well documented since March 1957 at the meteorological station of Dumont d'Urville, where multi-year atmospheric aerosol monitoring has also been performed (e.g. Jourdain and Legrand, 2001). The spatio-temporal variability of regional SMB has also been monitored at annual time scale since 2004 through stake height and snow density measurement over a 156-km stake-line (91 stakes) (Agosta et al., 2012; Favier et al., 2013). The TA firn core was analysed at sub-annual resolution for water isotopes ($\delta^{18}O$ and δD) and chemistry (Na, SO_4^{2-}, and MSA). These records were used to establish the age scale for the firn core. Using these records, we explore: (i) the links between the TA isotopic signals, local climate and atmospheric transport, (ii) the possibility to extract a sub-annual signal from such a highly-resolved core, and (iii) how to interpret the d-excess signal of coastal Antarctic ice cores.

In this manuscript, we first present our material and methods (Sect. 2), then describe our results (Sect. 3) and compare them with other Antarctic records and the outputs of the ECHAM5-wiso model in our discussion (Sect. 4), before summarizing our key findings and formulating suggestions for future studies (Sect. 5).

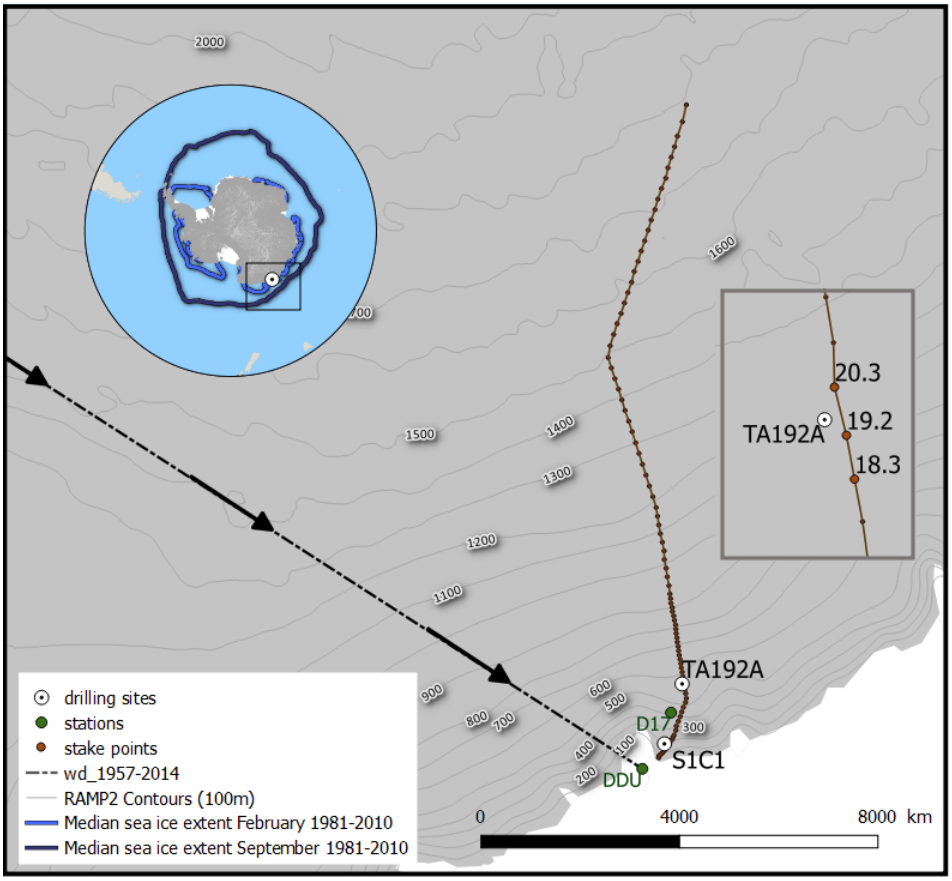

Figure 4.3.1: Map showing the location of the drilling sites of the S1C1 and TA192A firn cores (black points), the Dumont d'Urville and D17 stations (green points), and the stake points (in brown. included the three closest stake points from the TA192A. namely the "18.3", the "19.2" and the "20.3, and the "156 km" stake line), the mean wind direction over the periods 1957-2014 (in black). Isohypses (grey lines) shown on the main figure are simulations from Digital elevation model, large scale resolution. Radarsat Antarctic Mapping Project Digital Elevation Model Version 2 (Liu et al., 2001). The map of Antarctica on the top left displays the mean February and September sea ice extent over the period 1981-2010 extracted from the Nimbus-7 Scanning Multichannel Microwave Radiometer (SMMR) and Defense Meteorological Satellite Program Special Sensor Microwave/Imagers - Special Sensor Microwave Image/Sounder (DMSP SSM/I-SSMIS) passive microwave data (http://nsidc.org/data/nsidc-0051) (Cavalieri et al., 1996) (light blue. and dark blue lines respectively), and the zoomed area (grey rectangle), while the grey rectangle in the middle right zooms the area around the TA192A drilling site in order to show the three closest stake locations.

4.3.2 Material and method

4.3.2.1 Field work and laboratory analyses

We present here the results of one firn core drilled at the TA site (66.78 ° S; 139.56 ° S, 602 m a.s.l.), located at 25 km from Dumont d'Urville station (hereafter, DDU) and at 14 km from the S1C1 ice core (Goursaud et al., 2017; see Fig. 4.3.1). The 21.3 m long firn core was drilled on the 29th of January in 2015, when the daily surface air temperature and wind speed were -8.5°C and 3.9 m/s respectively, at the D17 station (9 km from the drilling site).

The FELICS (Fast Electrochemical lightweight Ice Coring System) drill system was used (Ginot et al., 2002; Verfaillie et al., 2012). Firn core pieces were then sealed in polyethylene bags, stapled and stored in clean isothermal boxes. At the end of the field campaign, the boxes were transported in a frozen state to the cold-room facilities of the Institute of Environmental

Geoscience (IGE, Grenoble, France). Every core piece was weighted and its length measured in order to produce a density profile. The cores were sampled at 4 cm resolution, leading to a total of 533 samples for oxygen isotopic ratio and ionic concentrations following the method described in Goursaud et al. (2017). Samples devoted to ionic concentration measurements were stored in the cold room until concentrations of sodium (hereafter Na^+), sulfate (hereafter SO_4^{2-}), and methane sulfonate (hereafter MSA) were analyzed by ion chromatography equipped with a CS12 and an AS11 separator column, respectively. Samples devoted to oxygen isotopic ratio were sent to LSCE (Gif-sur-Yvette, France) and analyzed following two methods. First, $\delta^{18}O$ was measured by the CO_2/H_2O equilibration method on a Finnigan MAT252, using two standards calibrated to SMOW/SLAP international scales, with an accuracy of 0.05 ‰. Second, $\delta^{18}O$ and δD were also measured using a laser cavity ring-down spectroscopy (CRDS) PICARRO analyzer, using the same standards, leading to an accuracy of 0.2 ‰ and 0.7 ‰ for $\delta^{18}O$ and δD respectively. The resulting accuracy of d-excess, calculating using a quadratic approach, is 1.7 ‰.

4.3.2.2 Datasets

Instrumental data

To assess potential climate signals archived in our firn core records, we extracted meteorological data to explore regional climate signals, and outputs of atmospheric models to explore synoptic scale climate signals. The regional climate is well documented since 1957 thanks to the continuous meteorological monitoring at DDU station (https://donneespubliques.meteofrance.fr/?fond=produit&id_produit=90&id_rubrique=32), with one gap between March 1959 and January 1960. We extracted near-surface temperature, humidity, surface pressure, wind speed and wind direction data computed monthly and annual averages over the periods 1957–2014 and 1998–2014.

The monthly average sea ice concentration was extracted from the Nimbus-7 Scanning Multichannel Microwave Radiometer (SMMR) and Defense Meteorological Satellite Program Special Sensor Microwave/Imagers - Special Sensor Microwave Image/Sounder (DMSP SSM/I-SSMIS) passive microwave data (http://nsidc.org/data/nsidc-0051), over the 50 – 90 °S latitudinal range at a 25 km x 25 km grid resolution (Cavalieri et al., 1996). D'Urville summer sea ice extent was estimated by extracting the number of grid points covering the area (50 – 90 °S, 135 – 145 °E) where the sea ice concentration is higher than 15 %, from December to January (included) for each year from 1998 to 2014.

SMB measurements from stake point data were obtained from the Glacioclim observatory (https://glacioclim.osug.fr/). We extracted data from the three stakes closest to the TA drilling

site, namely “18.3” (66.77 °S, 139.57 °E; 1.04 km from the TA drill site), “19.2” (66.77 °S, 139.56 °E; 83 m from the drilling TA site), and “20.3” (66.78 °S, 139.55 °E; 1.00 km from the drilling TA site), all spanning the period 2004–2014.

Database of surface snow isotopic composition

In order to compare the d-excess record from the TA firn core with available Antarctic values, we have updated the database of Masson-Delmotte et al. (2008), by adding 26 new data points from precipitation and firn core measurements provided with d-excess (Table 1). This includes data from five ice cores from the database constituted by the Antarctica2k group (Stenni et al., 2017). Altogether, the updated database includes 777 locations. This includes 64 coastal sites at an elevation lower than 1000 m a.s.l., (with 19 new datasets). These data were extracted from our updated isotope database (Goursaud et al., 2018) archived on the PANGAEA data library (https://doi.org/10.1594/PANGAEA.891279).

Atmospheric reanalyses and back-trajectories

Unfortunately, because of the katabatic winds around DDU, no instrumental method allows reliable measurements of precipitation (Grazioli et al., 2017a). We use outputs from ERA-interim reanalyses (Dee et al., 2011b), which were shown to be relevant for Antarctic surface mass balance (Bromwich et al., 2011), to provide information on DDU intra-annual precipitation variability. We extracted these outputs from the grid point (0.75 ° x 0.75 °, ~ 80 km x 80 km, point centered at 66.75 °S and 139.5 °E) closest to the TA drilling site over the period 1998–2014, at a 12-hours resolution, and calculated daily, monthly and annual average values. We also extracted 2-meter temperature (2mT), 10-meter u and v wind components (u10 and v10), and the geopotential height at 500 hPa (z500) over the whole southern hemisphere (50 – 90 °S), in order to investigate potential linear relationships between our records and the large-scale climate variability.

In order to identify the origin of air masses, back-trajectories were computed using the HySPLIT (Hybrid Single-Particle Lagrangian Integrated Trajectory) model. It is an atmospheric transport and dispersion model developed by the National Oceanic and Atmospheric Administration’s (NOAA) Air Research Laboratory (Draxler and Hess, 1998), based on a mixing between Lagrangian and Eulerian approaches (Stein et al., 2015). We set the arrival point at the coordinates of the TA drilling site, at an initial height of 1500 m a.s.l., and used the NCEP/NCAR Global Reanalysis ARL archived data for forcing the meteorological conditions, as the ERA-interim reanalyses are not available in the required extension. Earlier studies (e.g. Markle et al., 2012;Sinclair et al., 2010) highlighted good performances of NCEP

outputs when compared with Antarctic station data after 1979. For instance, previous studies showed that the mean sea level pressure simulated at DDU and averaged on a 5 year running window, was well captured in NCEP reanalyses after 1986 (correlation coefficient > 0.8, bias < 4 hPa and RMSE < 5 hPa) (Bromwich and Fogt, 2004;Bromwich et al., 2007). Also, Simmons et al. (2004) showed quasi-equal twelve months running mean of 2-meter temperatures for the Southern Hemisphere between the European Re-Analyses ERA-40, the NCEP/NCAR and the Climatic Research Unit CRUTEM2v products. We thus run daily five days back-trajectories from January 1998 to December 2014. Each back-trajectory was analyzed for the geographical position of the last simulated point (the estimated start of the trajectory, 5 days prior arrival at DDU), and classified into one of the following four regions, represented on Figure 4.3.2 and defined by their longitude (lon) and latitude (lat) as follows : (i) the eastern sector: (0 – 66 °S, 0 – 180 °E), (ii) the Plateau: (66 – 90 °S, 0 – 180 °E), (iii) the Ross sea sector: (0 – 75 °S, 180 – 240 °E), and finally (iv) the western sector: (0 – 75 °S, 180 – 240 °E), and (50 – 90 °S, 240 – 360 °E).

Atmospheric general circulation and water stable isotope modeling: ECHAM5-wiso

The potential relationships between large-scale climate variability and regional precipitation isotopic composition was also investigated through outputs of a nudged simulation performed with the atmospheric general circulation model ECHAM5-wiso (Roeckner et al., 2003), equipped with stable-water isotopes (Werner et al., 2011). We chose this model due to demonstrated skills to reproduce spatial and temporal patterns of water stable isotopes in Antarctica (Masson-Delmotte et al., 2008;Steen-Larsen et al., 2017;Werner et al., 2011;Goursaud et al., 2017a), and in Greenland (Steen-Larsen et al, 2017).

In this study, we use the same simulation as Goursaud et al. (2017a), in which the large-scale circulation (winds) and air temperature were nudged to outputs of the ERA interim reanalyses (Dee et al., 2011a). The skills of the model were assessed over Antarctica for the period 1979–2014. The model was run in a T106 resolution (i.e. ~ 110 km x 110 km horizontal grid size). In the following, we used the subscripts “ECH”, “TA”, and “S1C1” to differ ECHAM5-wiso outputs from the TA and S1C1 firn cores records respectively (e.g. $\delta^{18}O_{TA}$ and $\delta^{18}O_{ECH}$). Note also that linear relationships are considered significant when the p-value < 0.05.

Modes of variability

We tested either the main modes of variability were imprinted in our recorded, especially:

- the Southern Annual Mode (SAM) using the index defined by Marshall (2003), and archived on the National Center for Atmospheric Research website (Marshall, Gareth & National Center

Table 4.3.1: Site, latitude (in °), longitude (in °E) and reference of new d-excess data added to Masson-Delmotte et al. (2008). Data in orange correspond to precipitation, blue data correspond to ice cores extracted from the Antarctica2k database (Stenni et al., 2017), purple data are new data compared to our prior database (Goursaud et al., 2017). Finally, data associated with "*" were not provided with a dating while data in italic have a sub-annual resolution. Note that DE08-2 and D15 ice cores were not dated.

Site	Latitude	Longitude	Reference
Frei (south shetland islands)*	-62.20	301.04	(Fernandoy et al., 2012)
O'Higgins (north peninsula)*	-63.32	302.10	(Fernandoy et al., 2012)
Halley	*-75.58*	*333.50*	*(Rozanski et al., 1993)*
Base tte. Marsh	*-62.12*	*301.44*	*(Rozanski et al., 1993)*
Rothera Point	*-67.57*	*291.87*	*(Rozanski et al., 1993)*
Vernadsky	*-65.08*	*296.02*	*(Rozanski et al., 1993)*
Vostok	*-78.5*	*106.9*	*(Landais et al., 2012)*
DDU	*-66.7*	*140.00*	*Pers. Comm., Jean Jouzel*
Neumayer	*-70.7*	*351.60*	*(Schlosser et al., 2008)*
Dome F	*-77.3*	*39.7*	*(Fujita and Abe, 2006)*
Dome C	*-75.1*	*123.4*	*(Schlosser et al., 2017)*
EDC Dome C	-75.10	123.39	(Stenni et al., 2001)
NUS 08-7	*-74.12*	*1.60*	*(Steig et al., 2013)*
NVFL-1	-77.11	95.07	(Ekaykin et al., 2017)
WDC06A	*-79.46*	*247.91*	*(Steig et al., 2013)*
IND 25B5 Coastal DML	*-71.34*	*11.59*	*(Rahaman et al., 2016)*
OH-4*	-63.36	302.20	(Fernandoy et al., 2012)
OH-5*	-63.38	302.38	(Fernandoy et al., 2012)
OH-6*	-63.45	302.24	(Fernandoy et al., 2012)
OH-9*	-63.45	302.24	(Fernandoy et al., 2012)
OH-10*	-63.45	302.24	(Fernandoy et al., 2012)
KC	*-70.52*	*2.95*	*(Vega et al., 2016)*
KM	*-70.13*	*1.12*	*(Vega et al., 2016)*
BI	*-70.40*	*3.03*	*(Vega et al., 2016)*
GIP	*-80.10*	*159.30*	*(Markle et al., 2012)*
DE08-2	-66.72	112.81	(Delmotte et al., 2000)
DSSA	*-66.77*	*112.81*	*(Delmotte et al., 2000)*
*D15**	*-66.86*	*139.78*	*Pers. Comm., Jean Jouzel*
TA192A	*-66.78*	*139.56*	*This study*

for Atmospheric Research Staff (Eds). Last modified 19 Mar 2018. "The Climate Data Guide: Marshall Southern Annular Mode (SAM) Index (Station-based)." Retrieved from https://climatedataguide.ucar.edu/climate-data/marshall-southern-annular-mode-sam-index-station-based.)

- the El Niño Southern Oscillation (ENSO) using el Ni*ño 3.4 index defined* by the Climate Prediction Center of NOAA's National Centers for Environmental Prediction, and archived on their website (Trenberth, Kevin & National Center for Atmospheric Research Staff Eds). Last modified 06 Sep 2018. "The Climate Data Guide: Nino SST Indices (Nino 1+2, 3, 3.4, 4; ONI and TNI)." Retrieved from https://climatedataguide.ucar.edu/climate-data/nino-sst-indices-nino-12-3-34-4-oni-and-tni.)

- the Interdecadal Pacific Oscillation (IPO), using the IPO Tripole Index (TPI) defined by Henley et al. (2015) based on filtered HadISST and ERSSTv3b sea surface temperature data and archived on the internet (Accessed on 09 20 2018 at "https://www.esrl.noaa.gov/psd/data/timeseries/IPOTPI".).

- the Amundsen Sea Low pressure center (ASL) archived one the National Center for Atmospheric Research website (Hosking, Scott & National Center for Atmospheric Research Staff Eds). Last modified 19 Mar 2018. "The Climate Data Guide: Amundsen Sea Low indices." Retrieved from https://climatedataguide.ucar.edu/climate-data/amundsen-sea-low-indices.)

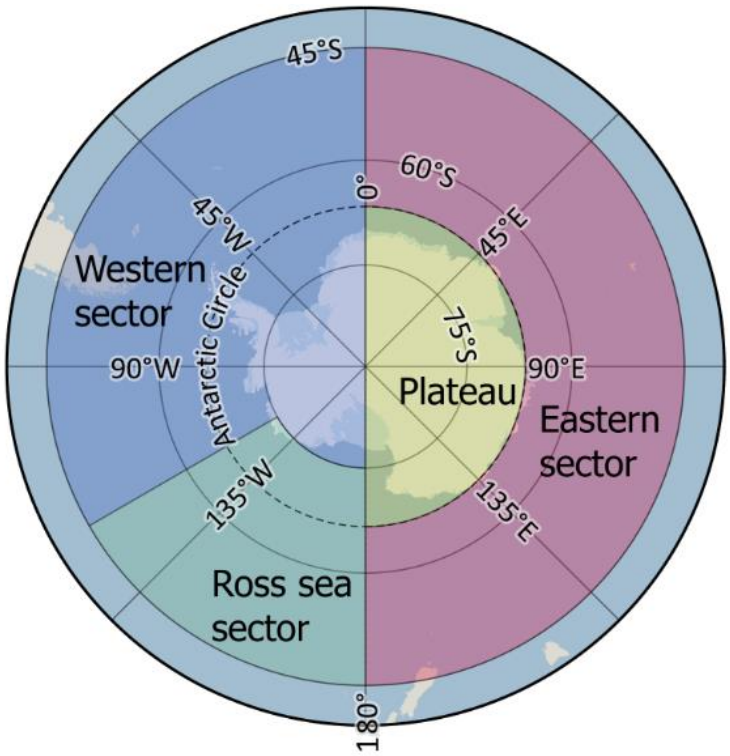

Figure 4.3.2: Representation of the sectors used to classify the last point of the simulated back-trajectories by HYSPLIT over the period 1998-2014, defined as follows: (i) the eastern sector: (0 – 66 °S, 0 – 180 °E), (ii) the Plateau: (66 – 90 °S, 0 – 180 °E), (iii) the Ross sea sector: (0 – 75 °S, 180 – 240 °E), and finally (iv) the western sector: (0 – 75 °S, 180 – 240 °E), and (50 – 90 °S, 240 – 360 °E).

4.3.3 Results

4.3.3.1 Firn core chronology

Ice core dating

The firn core was dated using an annual layer counting method (Fig. 4.3.3). As in Goursaud et al. (2017b), we used concentrations in MSA and non-sea-salt (nss) SO_4^{2-} ($nssSO_4$).

We have explored the validity of an approach using a definition of $nssSO_4$ based on a sulfate to sodium mass ratio of 0.25 inferred from summer observations only. The multi-year study of size-segregated aerosol composition conducted at the coast of TA (the DDU station) has demonstrated that sea-salt aerosol is depleted in sulfate with respect to sodium in winter, with a sulfate to sodium mass ratio of 0.13 from May to October instead of 0.25 (i.e. the sea-water composition) in summer (Jourdain and Legrand, 2002). Even at the high plateau station of Concordia, Legrand et al. (2017a) showed that sea-salt aerosol is depleted in sulfate in winter (sulfate to sodium ratio of 0.13 from May to October). We resampled the sulfate time series recorded in the TA with 12 points per year and inferred seasonal average values from averages over the corresponding subsets of points, as previously done for isotopic records (Section 3.2). We then calculated $nssSO_4$ (noted as $nssSO_4^*$) using a sulfate to sodium ratio of 0.25 for points associated to months from November to February and 0.13 for points associated from months from March to September. Note that when ignoring the change in sulfate to sodium ratio in winter, (i.e. applying a sulfate to sodium ratio of 0.25 for all the points of the year), the mean $nssSO_4$ value is lower by 18.2 %, decreasing from 36.5 ± 12.3 ppb to 43.1 ± 11.8 ppb for $nssSO_4^*$ (Figure S1 in the Supplementary Material). We thus applied a calculation of $nssSO_4$ for all points of our firn core, only using the sulfate to sodium ratio obtained from summer observations, as $[nssSO_4^{2-}] = [SO_4^{2-}] - 0.25\,[Na^+]$.

For depths lower than 10 m w.e., summer (December-January) peaks were identified (i) from $nssSO_4$ values higher than 100 ppb, synchronous with MSA peaks (with no threshold), and (ii) for $nssSO_4$ values higher than 200 ppb (with or without a simultaneous MSA peak). Double $nssSO_4$ peaks were counted as one summer (e.g. 2012, 2003, and 2001). For depths higher than 10 m w.e., summer peaks were identified for $nssSO_4$ values higher than 27 ppb. The outcome of layer counting allowed us to estimate annual layer thickness, which, combined with the density profile, allowed us to estimate annual SMB in the firn core. This estimated SMB was then compared with stake area data. The three stake data closest to the TA firn core ("18.3", "19.2" and "20.3", not shown) depict the same inter-annual variability (pairwise coefficient correlations, $r>0.93$ and p-values, $p<0.05$), giving confidence in the use of these measurements to characterize the inter-annual variability of local SMB. The comparison with the stake data shows that our initial layer counted chronology results in a mismatch in the measured versus

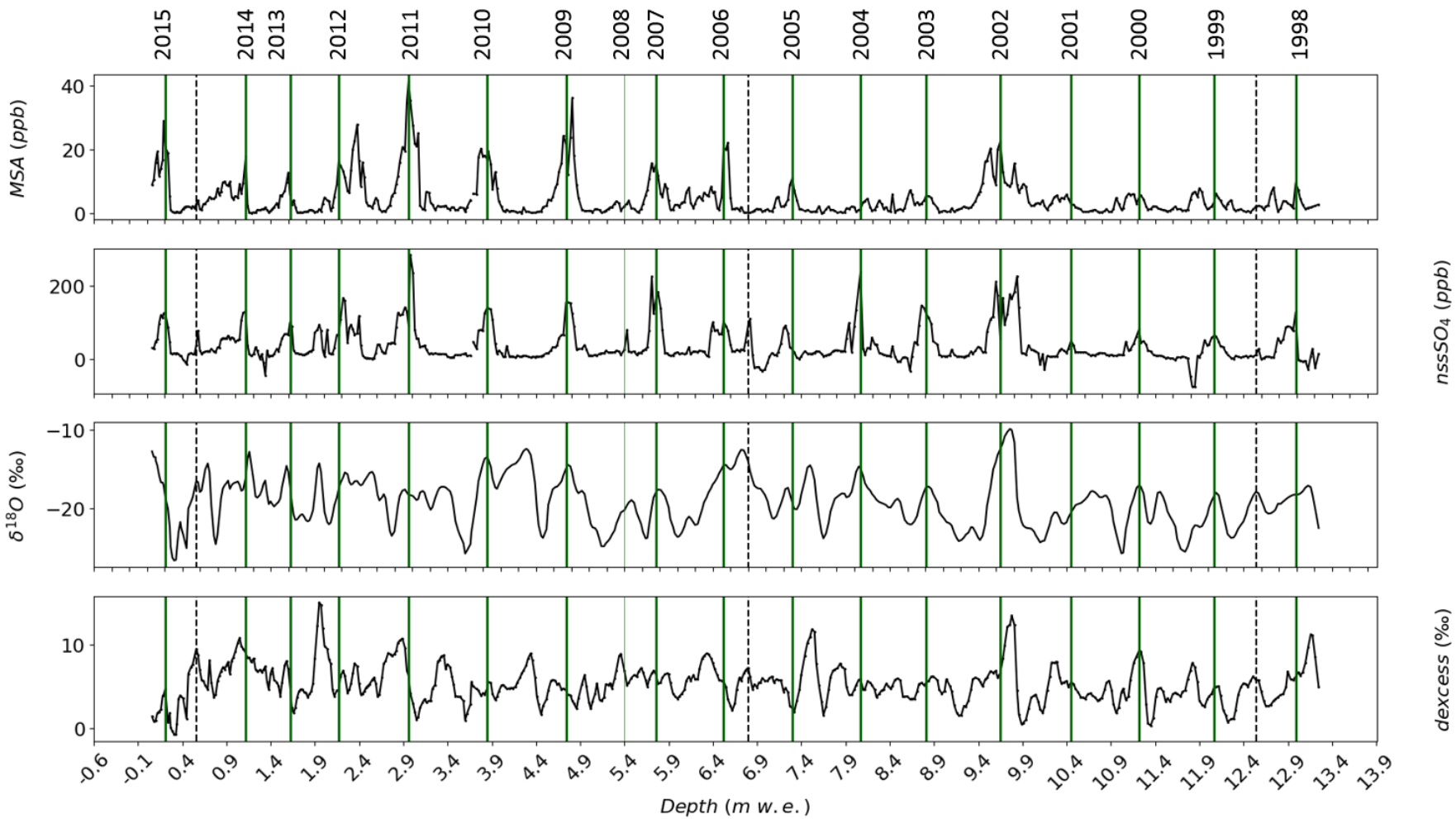

Figure 4.3.3: Identification of annual layers in the TA192A ice core based on the dual identification of nssSO42- and MSA summer peaks, and comparison of estimated accumulation with annual accumulation measured at the closest stakes (not shown). The thick vertical green lines correspond to summer peaks identified from chemical signals, while the thin vertical green line shows the additional identification of summer 2008 added to the counted summers from the comparison between the estimated accumulation and the accumulation record from the closest stake data (see Fig. 4.3.3). Vertical dashed lines highlight equivocal summer peaks with a sometimes small signal in only one of the chemical records. Water stable isotope records were not used to build the time scale. Note that double peaks in both δ18O and d-excess occur repeatedly within one counted year.

estimated SMB for year 2008 (Fig. 4.3.4a). This mismatch can be resolved by identifying one more summer peak in the chemical records (thin green line, Fig. 4.3.3). The revised firn core SMB record from this revised chronology shows correlation coefficients between the stake data and the TA firn core varying from 0.64 for the "20.3" to 0.83 for the "19.2" ($p<0.05$), with coherent inter-annual variability (Fig. 4.3.4b).

Peaks in $\delta^{18}O_{TA}$ or d-excess$_{TA}$ were not used in our layer counting, so that our age scale is independent of a climatic interpretation of water stable isotopes (e.g. assumption of synchronicity between temperature seasonal cycles and water stable isotope records). We note an uncertainty in layer counting of 3 years when comparing the outcome of layer counting using chemical records with $\delta^{18}O_{TA}$ peaks, which have nonetheless been excluded from our dating, as they do not improve the correlations, neither between the reconstructed SMB and the stake data, nor between our records and the ECHAM5-wiso simulations (Tables S1 to S3 in the Supplementary Material).

As a result, we consider that the "best guess" chronology results from the annual layer counting based on nssSO_4 and MSA refined with the comparison with stake data, giving a total of 18 summer peaks (green vertical lines, Fig. 4.3.3). In the following, we thus use the dated firn core records covering the complete period 1998–2014. We note that our chronology is more robust for the period 2004–2014, for which stake area SMB data are available.

Potential post-deposition effects

In order to test whether the available d-excess$_{TA}$ records are not affected by post-deposition effects, one may apply calculations of diffusion (e.g. Jones et al., 2017;Johnsen et al., 2000;van der Wel et al., 2015). However, many records are not available as depth profiles, and annual accumulation rate data are missing, precluding a systematic approach. We thus applied a simple approach to quantify how the seasonal $\delta^{18}O_{TA}$ and d-excess$_{TA}$ amplitudes vary through time in firn records, as an indicator of potential post-diffusion effects. For this purpose, we calculate the ratio between the mean amplitude of the most recent three complete seasonal cycles (2011–2014 for TA) and the average seasonal amplitude for the whole record (1998–2014 for TA). If seasonal cycles are stable through time, and if there is no significant smoothing due to post-deposition effects, we should obtain a ratio of 1. However, it is expected to be above 1 in the case of large post-deposition smoothing. We obtain a ratio of 0.5 for $\delta^{18}O_{TA}$ data, possibly reflecting the inter-annual variability of the $\delta^{18}O$ seasonal amplitude. We repeated the same exercise with all the 8 other sub-annual $\delta^{18}O$ records from our database (Table S4 in the Supplementary Material.). Discarding an outlier (NUS 08-7), all ratios are between 1.0 and 2.9. Ratios based on d-excess amplitudes are similar to those found for $\delta^{18}O$ (Table S5 in the

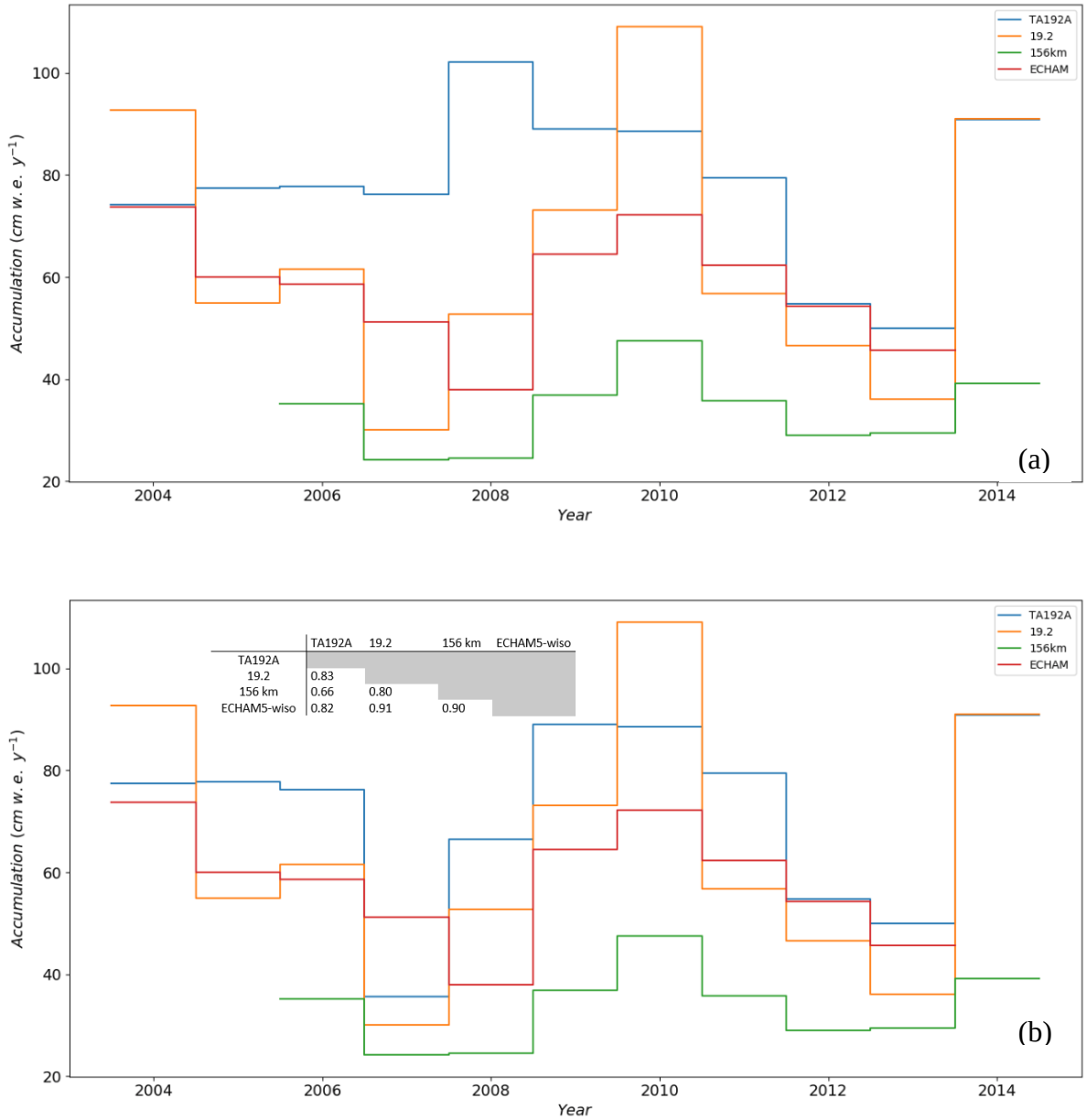

Figure 4.3.4: Annual accumulation (cm w.e. y^{-1}) estimated from the layer counting in the TA192A firn core (blue line), measured at the closest stake point "19.2" (orange line), from the 156 km network stake data (green line) and extracted from the ECHAM5-wiso model (red line), before (a) and after (b) adding the identification of summer 2008 in a time interval of low accumulation rates and skipped in the initial layer counting approach due to the lack of a signal in the MSA record (thin green line in Fig. 4.3.2). Correlations between time series (TA192A series inferred from the second dating) are inserted in the lower plot, all linear relationships being significant ($p<0.05$).

Supplementary Material). For the TA firn core, we again obtain a ratio of 1.1 for d-excess$_{TA}$. We also note high ratios for d-excess data in the NUS 08-7. Except for the ratios calculated in the WDC06A, which notably differs for d-excess (1.1) compared to $\delta^{18}O$ (2.9), other ratios for d-excess data vary between 1.0 and 1.4, with 20 % maximum difference compared to the corresponding ratio for $\delta^{18}O$ data.

For the TA, we also estimated the diffusion length (Küttel et al., 2012), and found mean diffusion lengths of 1.4 ± 0.3 months for $\delta^{18}O_{TA}$ (with a maximum of 1.9 months in 2007), and 1.6 ± 0.5 months for d-excess$_{TA}$ (with a maximum of 2.4 months in 2007).

These results suggest that potential post-deposition effects in the TA can be neglected. Notwithstanding, a potential loss of seasonal amplitude in the other average time series compared to the most recent seasonal cycles cannot be discarded, and has to be considered in the comparison of seasonal amplitudes, from one core to the other, in the comparison with the seasonal amplitude of precipitation $\delta^{18}O$ time series, and with ECHAM5-wiso outputs.
which notably differs for d-excess (1.1) compared to $\delta^{18}O$ (2.9), other ratios for d-excess data vary between 1.0 and 1.4, with 20 % maximum difference compared to the corresponding ratio for $\delta^{18}O$ data. These results suggest that (i) potential post-deposition effects in the TA can be neglected. Notwithstanding, a potential loss of seasonal amplitude in the other average time series compared to the most recent seasonal cycles cannot be discarded, and has to be considered in the comparison of seasonal amplitudes, from one core to the other, in the comparison with the seasonal amplitude of precipitation $\delta^{18}O$ time series, and with ECHAM5-wiso outputs.

4.3.3.2 Mean values

Mean climate from instrumental data

Before reporting the mean values from TA records, we describe the available meteorological data. A time-averaged statistical description of the available meteorological data measured at DDU, the station closest to the drilling site, is given in Table 2 for the whole available measurement period prior to 2015 (1957–2014), and over the period covered by our TA records, 1998-2014. For all the considered parameters (near-surface temperature, wind direction, wind speed, humidity, and surface pressure), the time-averaged values differ by less than 8% (the maximum deviation being for the wind direction) over the period 1998-2014 compared to the whole available period. Standard deviations calculated over these two time periods also differ by less than one respective standard deviation unit, except for wind direction which shows much less variability over the recent period. We conclude that the local climate of the period 1998–2014 is representative of the multi-decadal climate state since 1957. In ERA-interim, the average precipitation is 46.0 ± 26.9 cm w.e. y^{-1} over the period 1998–2014.
Finally, we compare the statistical description of the sea ice concentration for the four aforementioned regions (Section 2.2) over the available period 1979–2014, with the period covered by the TA firn core 1998-2014 (Table 3). We note that the mean difference between the two periods is maximum for the local sea ice concentration (135 – 145 °E), with 8.9 % difference, whereas it is remains below 1.5 % for the other sectors. The extrema (minimum and maximum values) varies of 0.5 % on average (all regions included) from one sector to another, with a maximum difference of 2.9 %. As a result, the mean sea ice concentrations of the period

1998–2014 are also representative for the last decades over large sectors from Amundsen to Indian Ocean.

Mean values recorded in the TA firn core

Time-averaged values calculated from TA records are reported in Table 4. The average SMB_{TA} is 75.2 ± 15.0 cm w.e. y^{-1}. Stake data points from Glacioclim show that this site of high accumulation is located in an area of large spatial variability. This features is confirmed by the values given by (i) the stake data closest to the TA site ("19.2", 100 m for the TA site and associated to a 76.6 ± 25.8 cm w.e. y^{-1} mean accumulation rate) compared to further stake data ("18.2", 1.04 km from the TA site and associated to a 47.7 ± 15.7 cm w.e. y^{-1} mean accumulation rate), (ii) our mean SMB reconstruction from the S1C1 ice core almost four times lower than for the TA (21.8 ± 6.9 cm w.e. y^{-1} (Goursaud et al., 2017b)) (iii) and meso-scale fingerprints such as the SMB estimated for coastal Adélie Land by Pettré et al. (1986), based on measurements at stakes located from 500 m to 5 km from the coast (Table 2).
The average $\delta^{18}O_{TA}$ value is -19.3 ± 3.1 ‰, close to the average $\delta^{18}O_{S1C1}$ of -18.9 ± 1.7 ‰, and the average $d\text{-}excess_{TA}$ is 5.4 ± 2.2 ‰. Compared to the 64 points located at an elevation lower than 1000 m a.s.l. from our database, the $\delta^{18}O_{TA}$ and $d\text{-}excess_{TA}$ average values are slightly higher than the average low-elevation records (-22.7 ± 8.8 ‰ and 4.8 ± 2.3 ‰ for $\delta^{18}O$ and d-excess respectively, Fig. 4.3.5). Finally, the average TA concentrations in Na^+, MSA and $nssSO_4$ are of 126.0 ± 276.5 ppb, 4.5 ± 5.6 ppb and 36.5 ± 44.2 ppb respectively. Note that the Na^+ average concentration value is affected by strong peaks in 2003 and 2004 with annual values of 369.4 and 388.5 ppb. Excluding these two peaks, the average Na^+ concentration is reduced to 93.2 ppb (with a standard deviation of 38.6 ppb). These concentrations will be discussed later in Section 4.4.

To summarize our findings, the TA records encompass a period (1998–2014) representative of multi-decadal mean climatic conditions. The isotopic mean values appear lower than the average of other Antarctic low elevation records (as shown in Fig. 4.3.4). The local SMB is remarkably high for East Antarctica, consistent with stake measurements performed close to the TA site.The TA average $\delta^{18}O$ value is -19.3 ± 3.1 ‰, close to the average S1C1 $\delta^{18}O$ of -18.9 ± 1.7 ‰, and the average TA d-excess is 5.4 ± 2.2 ‰. Compared to the 64 points located

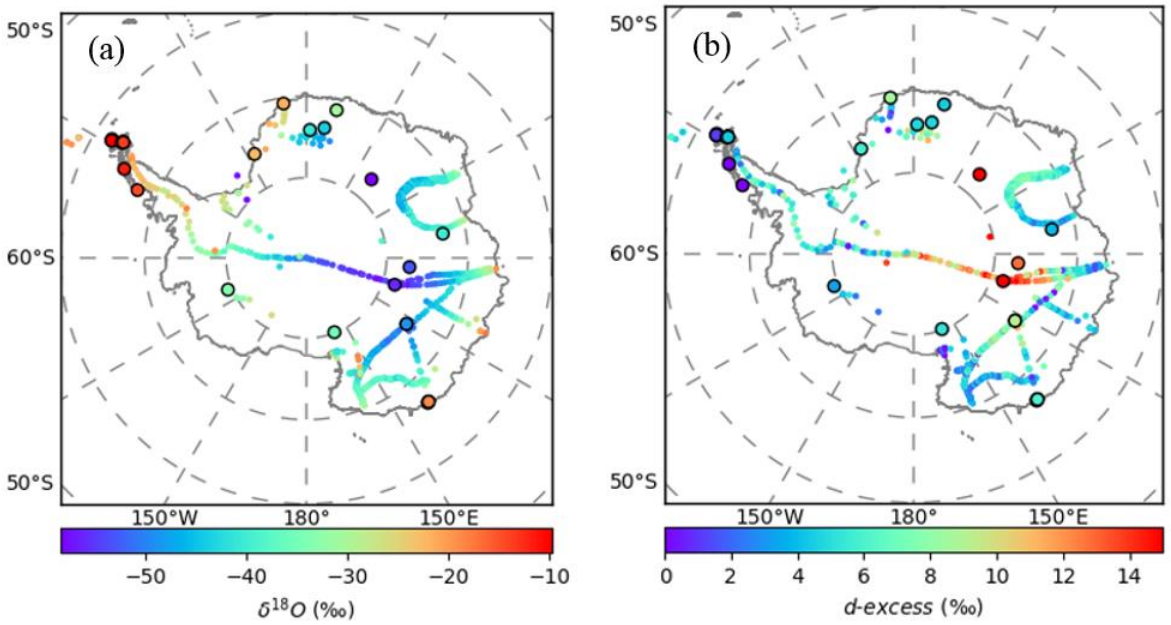

Figure 4.3.5: Spatial distribution of $\delta^{18}O$ (a. in ‰) and d-excess (b. in ‰) in surface Antarctic snow based on our updated database combining data from precipitation, surface snow, pits and shallow ice cores. Bigger points with a black edge correspond to new data compared to Masson-Delmotte et al. (2008).

at an elevation lower than 1000 m a.s.l. from our database, the TA $\delta^{18}O$ and d-excess average values are slightly higher than the average low-elevation records (-22.7 ± 8.8 ‰ and 4.8 ± 2.3 ‰ for $\delta^{18}O$ and d-excess respectively, see Fig. 4.3.5). Finally, the average TA concentrations in Na^+, MSA and $nssSO_4$ are of 126.0 ± 276.5 ppb, 4.5 ± 5.6 ppb and 36.5 ± 44.2 ppb respectively. Note that the Na^+ average concentration value is affected by strong peaks in 2003 and 2004 with annual values of 369.4 and 388.5 ppb. Excluding these two peaks, the average Na^+ concentration is reduced to 93.2 ppb (with a standard deviation of 38.6 ppb). These concentrations will be discussed later in Section 4.3.4.4.

To summarize our findings, the TA records encompass a period (1998-2014) representative of multi-decadal mean climatic conditions. The isotopic mean values appear lower than the average of other Antarctic low elevation records (as shown in Fig. 4.3.4). The local SMB is remarkably high for East Antarctica, consistent with stake measurements performed close to the TA site.

4.3.3.3 Inter-annual variations

In the following, we refer to seasons as follows: summer (December to February), autumn (March to May), winter from (June to September) and spring (October and November). This cutting was defined based on the mean seasonal cycle of temperature, showing the highest values from December to February, and a plateau of low values from May to September (Fig. 4.3.8a). In the TA records, resampled with 12 points per year, we identified seasonal average values

Table 4.3.2: Number of points ("n"), time averages ("μ"), standard deviation ("σ"), minimum ("min") and maximum ("max") values of all the monthly meteorological observations at Dumont d'Urville from Météo France over the period 1957-2014 (with a gap between March 1959 and January 1960, included) and over the period 1998-2014 for near-surface temperature ("Ts", in °C), wind speed ("ws", in m/s), wind direction ("wd", in °E), and relative humidity ("RH", in %), and of annual precipitation and accumulation (precipitation minus evaporation/sublimation) from ERA-interim reanalyses ("Prec. ERA' and "Accu. ERA" respectively, both in mm w.e. y^{-1}).

	1957-2014				1998-2014					
	Ts (°C)	ws (m/s)	wd (°E)	RH (%)	Ts (°C)	ws (m/s)	wd (°E)	RH (%)	Prec. ERA (cm w.e. y^{-1})	Accu ERA (cm w.e. y^{-1})
n	730	719	383	717	202	201	201	199		
μ	-10.9	9.6	145.3	61.4	-11.1	9.1	133.8	60	53.7	40.5
σ	6	2.1	22.4	7.6	6.0	1.8	15.8	8.3	7.6	8.3
min	-23.5	4.9	90	34	-22.1	4.8	1.5	34.0	39.3	24.7
max	1	19.5	220	86	0.9	14.1	172.4	85.5	70.3	56.1

Table 4.3.3: Number of points ("n"), time averages ("μ"), standard deviation ("σ"), minimum ("min") and maximum ("max") values of monthly meteorological sea ice concentration over the periods 1979-2014 and 1998-2014 extracted from the Nimbus-7 Scanning Multichannel Microwave Radiometer (SMMR) and Defense Meteorological Satellite Program Special Sensor Microwave/Imagers - Special Sensor Microwave Image/Sounder (DMSP SSM/I-SSMIS) passive microwave data (http://nsidc.org/data/nsidc-0051; Cavalieri et al., 1996), and for the four regions defined as "Indian": 0 °E<lon < 160 °E and lat > -66 °, "Plateau": 0 °E < lon < 180 °E and lat<-66°, "Ross-Sea Secor": 160 °E <lon< 190° E and lat > -75 °, and "WAIS + Pacific": 190 °E <lon (see Section 4.3.2.2).

	1979-2014				1998-2014			
	Indian	local	Amundsen	Regional	Indian	local	Amundsen	Regional
n	432	432	432	432	204	204	204	204
μ	41.1	47.0	56.6	42.9	41.6	51.2	57.4	43.4
σ	6.8	7.7	11.5	8.7	6.6	8.0	11.6	8.8
min	31.0	38.2	36.3	28.7	31.1	38.4	36.6	28.9
max	55.4	66.0	74.2	58.8	53.8	65.2	73.9	57.7

Table 4.3.4: Time averages ("μ") and standard deviation ("σ") of the reconstructed accumulation (in cm w.e.) and of the signals recorded in the TA192A ice core obtained from the resampling of the isotopic and chemical variables) for $\delta^{18}O$ (in ‰), d-excess (in ‰), Na, MSA, and $nssSO_4$ (in ppb), over the 17 annual values.

	Accumulation (cm w.e.)	$\delta^{18}O$ (‰)	d-excess (‰)	Na^+ (ppb)	MSA (ppb)	$nssSO_4$ (ppb)
μ	75.2	-19.3	5.4	126.0	4.5	36.5
σ	15.0	3.1	2.2	276.5	5.6	44.2

by calculating averages over the corresponding subsets of points (e.g. for autumn, we select from the 3rd to the 5th points out of the 12 resampled points within the year). We are fully aware that this is a simplistic approach, assuming a regular distribution of precipitation year round, and that our chronology is more accurate for summer than for other seasons, due to the layer counting method. We nevertheless checked that the distribution of precipitation simulated by ERA-interim within each year is rather homogeneous (Table S6 in the Supplementary Material).

Trends in time-series

We report here the analysis of potential trends from 1998 to 2014, and the identification of remarkable years. Figure 4.3.6 and 4.3.7 display the time series of meteorological variables, d'Urville summer sea-ice extent and TA records over 1998–2014. In Figures 4.3.6 and 4.3.7, we chose not to display standard deviations for readability, but they are reported in the Supplementary Material (Fig. S2 and S3).

Significant increasing trends are detected in the annual values of $d\text{-excess}_{TA}$ (0.11 ‰ y^{-1}, r=0.61 and $p<0.05$) as well as of d'Urville summer sea ice extent (r=0.77, $p<0.05$)

Pairwise linear regressions between variables

We performed pairwise linear regressions for all records (meteorological and firn core records), using on one side, annual averages and on the other side, monthly or seasonal values. As previously observed by Comiso et al. (2017), we report a significant anti-correlation between annual regional sea ice concentration (i.e. 100 – 205 °E, but not with other sectors) and DDU near-surface air temperature (r=-0.56 and $p<0.05$). This relationship is strongest in autumn (r = -0.75 and $p<0.05$), where it holds for sea-ice in all sectors, and disappears in spring or summer. Confirming earlier studies (Minikin et al., 1998), we observe a close correlation between annual concentrations of MSA and $nssSO_4$ (r=0.76, $p<0.05$). Statistically significant linear relationships appear between the isotopic signals ($\delta^{18}O_{TA}$ and $d\text{-excess}_{TA}$) and $nssSO_4$ in spring (r=0.65 and r=0.55 for $\delta^{18}O_{TA}$ and $d\text{-excess}_{TA}$ respectively, $p<0.05$), and only between $d\text{-excess}_{TA}$ and $nssSO_4$ in autumn (r=0.65 and $p<0.05$). We

Table 4.3.5: d-excess versus $\delta^{18}O$ linear relationship of data from our database provided with d-excess over the whole time series (left side of the table) and over annual averages ('inter-annual scale', right side of the table): slope (in ‰‰$^{-1}$), correlation coefficient ('r'), p-value ("p-val") and standard error of the slope ('stderr' in ‰‰$^{-1}$). Cells in bold show significant relationship (p<0.05) and the cell in italic is to be taken with caution (see "DDU" line, p<0.10). Inter-annual relationships could not be computed for not dated data (D15 and OH ice cores) as well as for too short time monitored precipitation data, and thus appear as empty cells.

	Whole time series					Inter-annual scale				
	Number of points	Slope (‰‰$^{-1}$)	r	p-val	stderr	Number of points	Slope (‰‰$^{-1}$)	r	p-val	stderr
EDC Dome C	**140**	**-0.41**	**-0.31**	**0.00**	**0.11**	**623**	**-0.41**	**-0.31**	**0.00**	**0.11**
NUS 08-7	**2413**	**-0.36**	**-0.28**	**0.00**	**0.08**	**626**	**-0.36**	**-0.28**	**0.00**	**0.08**
NUS 07-1	299	0.17	0.25	0.15	0.12	299	0.17	0.25	0.15	0.12
NVFL-1	**233**	**0.47**	**0.40**	**0.00**	**0.02**	**233**	**0.47**	**0.40**	**0.00**	**0.02**
WDC06A	**41120**	**0.25**	**0.25**	**0.00**	**0.00**	**2056**	**0.05**	**0.06**	**0.01**	**0.02**
IND 25B5	1297	0.17	0.08	0.45	0.22	140	0.17	0.08	0.45	0.22
BI	404	0.01	0.02	0.70	0.03	**17**	**-0.57**	**-0.57**	**0.01**	**0.20**
KC	**343**	**0.22**	**0.23**	**0.00**	**0.05**	48	0.05	0.06	0.70	0.12
KM	425	0.04	0.06	0.24	0.04	**18**	**-0.86**	**-0.57**	**0.01**	**0.29**
DSSA	161	-0.03	-0.04	0.58	0.05	**6**	**-0.41**	**-0.74**	**0.04**	**0.15**
DE08-2	58	-0.11	-0.08	0.57	0.19	58	-0.11	-0.08	0.57	0.19
D15-1	126	-0.03	-0.03	0.72	0.07					
D15-2	191	-0.06	-0.10	0.19	0.04					
OH4	318	-0.11	-0.11	0.13	0.07					
OH5	213	-0.05	-0.04	0.45	0.07					
OH6	124	0.01	0.01	0.86	0.08					
OH9	232	-0.05	-0.04	0.57	0.08					
OH10	190	-0.10	-0.04	0.58	0.17					
DDU	*19*	*0.48*	*0.41*	*0.08*	*0.26*					
Dome C	**501**	**-1.48**	**-0.84**	**0.00**	**0.04**	**4**	**-2.75**	**-0.98**	**0.02**	**0.42**
Dome F	**351**	**-1.60**	**-0.89**	**0.00**	**0.05**					
Halley	**532**	**-0.20**	**-0.18**	**0.00**	**0.05**	49	-0.23	-0.12	0.41	0.28
Marsh	**19**	**-0.86**	**-0.51**	**0.03**	**0.35**					
Neumayer	336	-0.06	-0.07	0.21	0.05	19	0.28	0.31	0.20	0.21
Rothera	**194**	**-1.00**	**-0.58**	**0.00**	**0.10**	**18**	**-1.21**	**-0.86**	**0.00**	**0.18**
Vernadsky	**372**	**-1.33**	**-0.57**	**0.00**	**0.08**	**35**	**-1.89**	**-0.69**	**0.00**	**0.29**
Vostok	**27**	**-0.73**	**-0.63**	**0.00**	**0.18**					

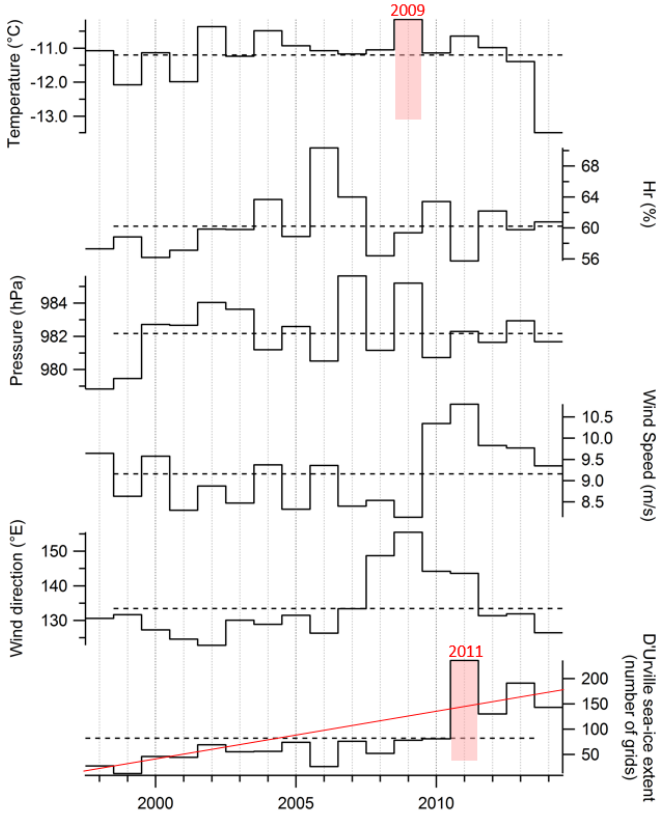

Figure 4.3.6: Meteorological time series over the period 1998-2014 averaged at the inter-annual scale. Near-surface temperature (°C), relative humidity (%), sea level pressure (hPa). wind speed (m s-1) and direction (°E) were provided by Meteo France. The local sea ice concentration (%) is extracted in the 135 – 145°E sector (with a latitudinal range of 50 – 90 °S) from the Nimbus-7 Scanning Multichannel Microwave Radiometer (SMMR) and Defense Meteorological Satellite Program Special Sensor Microwave/Imagers - Special Sensor Microwave Image/Sounder (DMSP SSM/I-SSMIS) passive microwave data (Cavalieri et al., 1996). Horizontal dashed lines correspond to the climatological averages over 1998-2014 for each parameter. Remarkable years. i.e. associated with values deviating by at least 2 standard deviations from the climatological mean value are highlighted with a red shading (positive anomalies) or blue shading (negative anomalies). The same figure with standard deviations is available in the Supplementary Material (Fig. S2).

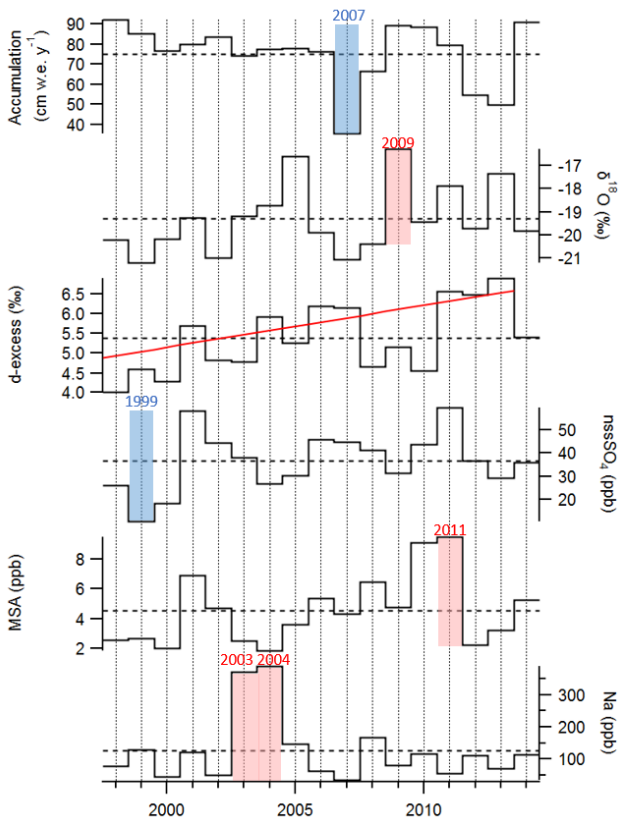

Figure 4.3.7: Dated TA192A ice core annually averaged records over the period 1998–2014: accumulation cm w. e. y-1), concentrations of Na+ (ppb), nssSO4 (ppb), MSA (ppb), δ18O (‰) and d-excess (‰). Horizontal dashed lines correspond to 1998–2014 average values. Remarkable years (i.e. associated with values deviating by at least 2 standard deviations from the climatological mean value) are highlighted with a red shading (positive anomalies) or blue shading (negative anomalies). The same figure with standard deviations is available in the Supplementary Material (Fig. S3).

find no annual regional sea-ice concentration (i.e. 100 – 205 °E, but not with other sectors) and DDU near-surface air temperature ($r=-0.56$ and $p<0.05$). This relationship is strongest in autumn ($r =$

-0.75 and $p<0.05$), where it holds for sea ice in all sectors, and disappears in spring or summer. Confirming earlier studies (Minikin et al., 1998), we observe a close correlation between annual concentrations of MSA and $nssSO_4$ ($r=0.76$, $p<0.05$). Statistically significant linear relationships appear between the isotopic signals ($\delta^{18}O$ and d-excess) and $nssSO_4$ in spring ($r=0.65$ and $r=0.55$ respectively, $p<0.05$), and only between d-excess and $nssSO_4$ in autumn ($r=0.65$ and $p<0.05$). We find no relationship between $\delta^{18}O_{TA}$ and the DDU near-surface temperature. Our record depicts a significant anti-correlation between annual values of SMB_{TA} and d-$excess_{TA}$ ($r=-0.59$ and $p<0.05$), as well as a significant correlation between d-$excess_{TA}$ and d'Urville summer sea ice extent ($r=0.65$ and $p<0.05$). Finally, a systematic positive significant correlation is identified between d-$excess_{TA}$ and $\delta^{18}O_{TA}$, except in summer. It is the strongest in austral spring, with a correlation coefficient of 0.75 (with a slope of 0.61 ‰ ‰$^{-1}$). In order to understand the specificities of the TA record, we explored the temporal correlation between $\delta^{18}O$ and d-excess from all available Antarctic records (Table 5, cells in bold for significant relationships), using all data points (in order to be able to exploit non-dated depth profiles) as well as inter-annual variations, when available. When focusing on significant results, we note that most precipitation datasets depict an anti-correlation between d-excess and $\delta^{18}O$ (3 out of 9 precipitation records). Although we are cautious with the short DDU precipitation time series (with only 19 points, and p-values = 0.08, cell in italics in Table 5), it shows a positive relationship, similar to the one identified in the TA record. We conclude that the positive correlation observed in the TA records is specific to the coastal Adélie Land region, what is unusual in an Antarctic context.

Remarkable years

Using only annual SMB, water stable isotope and chemistry TA records, we finally searched for remarkable years, defined here as deviating from the 1998–2014 mean value by at least 2 standard deviations. We highlight three remarkable years (red-shaded for high values and blue-shaded for low values, Fig. 4.3.6 and 4.3.7):

→ Year 2007: very low SMB_{TA}.

→ Year 2009: remarkably high $\delta^{18}O_{TA}$.

→ Year 2011: high MSA, d'Urville summer sea ice extent, and wind speed values.

We had previously noted that years 2003 and 2004 are associated with very high Na^+ values and add that year 1999 experienced low $nssSO_4$ values.

In summary, we identify increasing trends in d-excess$_{TA}$ and sea-ice concentration, no significant correlation between $\delta^{18}O_{TA}$ and DDU near-surface temperature, and an anti-correlation between d-excess$_{TA}$ and SMB$_{TA}$. We also note 2 remarkable years in SMB$_{TA}$ ("dry" 2007) and $\delta^{18}O_{TA}$ ("high" 2009). Finally, no systematic relationships are identified between chemistry and water stable isotope signals (e.g. parallel trends, inter-annual correlation, and remarkable years).

4.3.3.4 Intra-annual scale

Mean cycles

The high resolution of the TA record allows us to describe the mean seasonal cycles (Fig. 4.3.8), as well as to explore the inter-annual variability of the seasonal cycle.

Among the meteorological variables, only near-surface temperature, relative humidity and sea level pressure show a clear seasonal cycle. Temperature (Fig. 4.3.8a) is minimum in July and maximum in January, while relative humidity and pressure (Fig. 4.3.8b and 4.3.8c respectively) are minimum in spring (in November and October respectively), and a maximum in winter (in August and June respectively), as reported in earlier studies (Pettré and Périard, 1996). The average seasonal cycles of wind speed and wind direction are flat but marked by large inter-annual variations (Fig. 4.3.8d and 4.3.8e). Finally, the local sea ice concentration shows a rapid advance from March to June, a plateauing from June to October and a rapid retreat from October to November, with a minimum in February (Fig. 4.3.8c), as previously reported by Massom et al. (2013).

In the TA firn core, Na, nssSO_4, and MSA show symmetric cycles with minima in winter and maxima in summer (by construction of our time scale) (Fig. 4.3.8 g-i), consistent with previous studies of aerosols and ice core signals (e.g. Preunkert et al., 2008). The $\delta^{18}O_{TA}$ seasonal cycle is surprisingly asymmetric (Fig. 4.3.8j), with a maximum in December and a minimum in April, thus not in phase with the seasonal cycles of local sea-ice concentration (Fig. 4.3.8f) nor DDU temperature (Fig. 4.3.8a). The mean d-excess$_{TA}$ seasonal cycle (Fig. 4.3.8k) is marked by a maximum in February, two months after the $\delta^{18}O_{TA}$ maximum, and a minimum in October, six months after the $\delta^{18}O_{TA}$ minimum. We then calculated the mean of the isotopic seasonal amplitudes, preferentially to the amplitude of the mean seasonal cycle, due to the different timing of peaks from one year to another. The mean $\delta^{18}O_{TA}$ seasonal amplitude is 8.6 ± 2.1 ‰, more than three times higher than found in the S1C1 ice core, and close to the DSSA mean $\delta^{18}O$ seasonal cycle of 8.0 ± 2.8 ‰. The mean d-excess$_{TA}$ seasonal amplitude is 6.5 ± 2.8 ‰, close

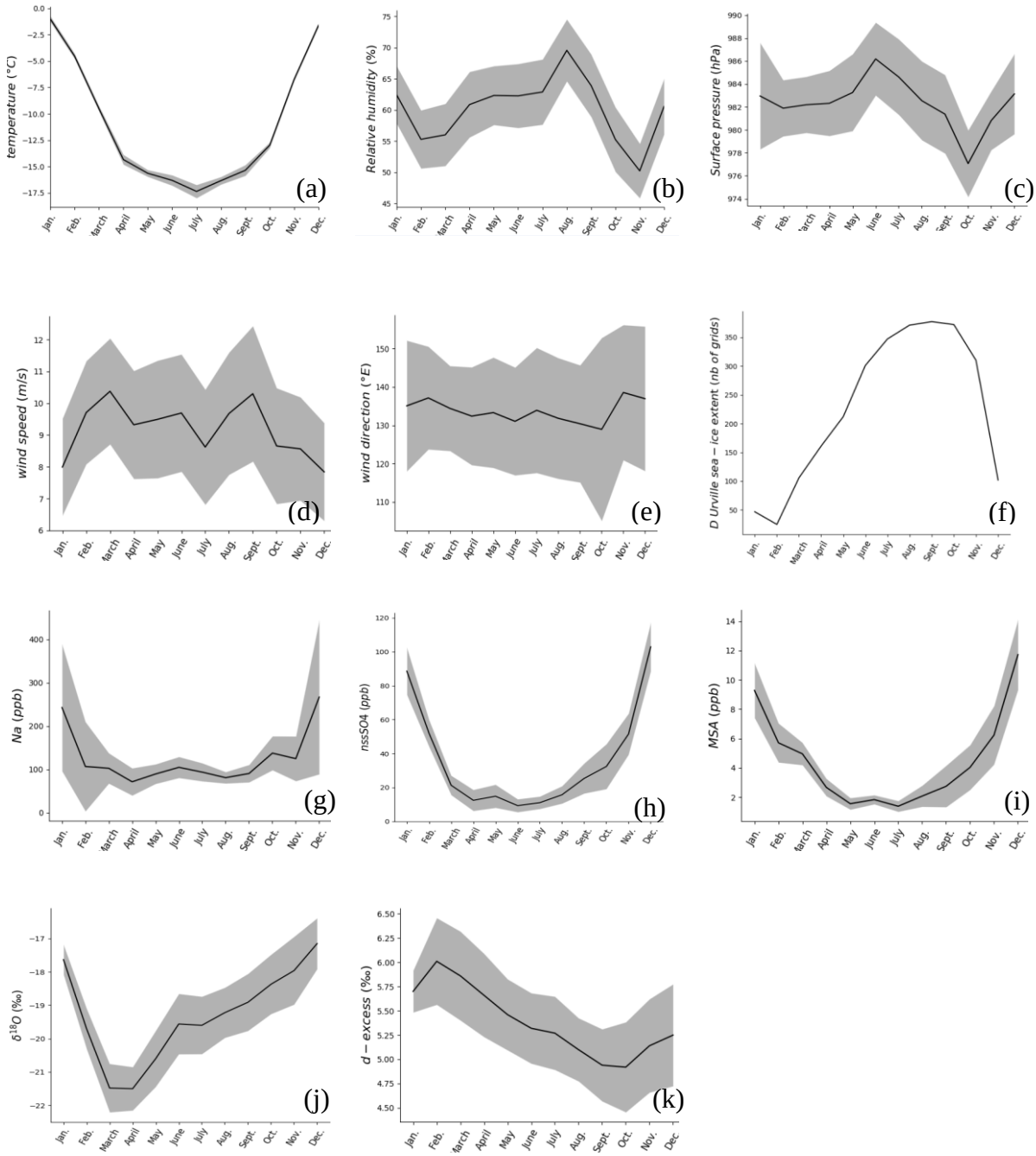

Figure 4.3.8: Mean seasonal cycles over the period 1998-2014. Meteorological observations are averaged from daily data, for near-surface temperature (a, °C), relative humidity (b, i%), surface pressure (c, hPa), wind speed (d, m/s), wind direction (e, °E), and local sea ice concentration. i.e. averaged over a 135 – 145 °E ridge (f, %). Seasonal cycles from ice core records are averaged from the resampled time series for Na (g, ppb), nssSO4 (h, ppb), MSA (i, ppb), δ18O (j, ‰) and d-excess (k, ‰). The inter-annual standard deviation is highlighted with the grey shading.

to the DSSA value of 5.3 ± 1.0 ‰. Compared with other precipitation and firn/ice core isotopic data from other regions of Antarctica (Table S7 in the Supplementary Material), the average seasonal amplitude obtained from TA $\delta^{18}O$ is closest to the one obtained at KM, BI sites in Dronning Maud Land, and Vernadsky or Rothera in Peninsula, but is much larger than identified from NUS 08-7 or WDC06A, and significantly smaller than at Halley (by a factor of almost 2), Neumayer (a factor of 2.3), Dome C or Dome F (a factor of ~4). In addition to DSSA, the average seasonal amplitude obtained from TA d-excess is also comparable to the one obtained in the KM, BI, and the IND25B5 firn cores in Dronning Maud Land, but is systematically higher (by a factor higher than 3) than in precipitation datasets. This calls for systematic comparisons of d-excess seasonal amplitudes in precipitation and snow data.

Due to their common symmetric aspect, significant positive linear relationships emerge from the mean seasonal cycles of (i) temperature, $nssSO_4$ and MSA ($r>0.93$ and $p<0.05$), (ii) $nssSO_4$ and MSA ($r=0.97$ and $p<0.05$), (iii) $nssSO_4$ and Na^+ ($r=0.93$ and $p<0.05$) and finally (iv) $\delta^{18}O$ with $nssSO_4$ ($r=0.75$ and $p<0.05$). Due to the asymmetry of water stable isotope seasonal cycles, no linear relationship is detected between the seasonal cycles of DDU near-surface temperature, $\delta^{18}O_{TA}$, and d-excess$_{TA}$. Finally, the seasonal cycle of d-excess$_{TA}$ is clearly anti-correlated with all sea-ice concentration indices (local, Indian, Amundsen and regional), with correlation coefficients varying between -0.83 and -0.80.

Inter-annual variability of peaks

Over the whole period covered by the TA firn core (1998–2014), the seasonal cycle of $\delta^{18}O_{TA}$ shows a large inter-annual variability (Table 6). $\delta^{18}O_{TA}$ maximum values occur primarily in summer (41 % of the time) and winter (41 %), and more rarely in spring (12 %) and in autumn (6%). The same feature is observable for d-excess$_{TA}$, which most of the time has its maximum in summer (38 %) and winter (43 %), and more scarcely in spring (6%) and in autumn (13%).

In summary, the TA water stable isotope seasonal cycles displays an asymmetry, with higher isotopic values in austral spring than in austral autumn. The d-excess$_{TA}$ seasonal cycle is anti-correlated withthe reconstructed SMB. Finally, the TA isotopic seasonal cycles show a high inter-annual variability from one seasonal cycle to another one, with no recurrent pattern between those of $\delta^{18}O_{TA}$ and d-excess$_{TA}$.

Table 4.3.6: Fraction of annual maxima (in %) of $\delta^{18}O$ and d-excess identified during each season: austral summer ("DJF", i.e. from December to February), austral autumn ("MAM", i.e. from March to May), austral winter ("JJAS", i.e. from June to September) and austral spring ("ON", i.e. from October to November) in the data over the period 1998-2014, and in the ECHAM5-wiso simulation ("model") over the period 1998-2013. The analysis is based on resampled data (ice core) and monthly values (model).

Variable	Source	Period	DJF	MAM	JJAS	ON
$\delta^{18}O$	data	1998-2014	41	6	41	12
	model	1998-2013	63	0	12	25
d-excess	data	1998-2014	41	12	41	6
	model	1998-2013	0	69	31	0

4.3.3.5 Influence of synoptic weather on TA records: insights from ECHAM5-wiso simulation and back-trajectories

In order to explore the influence of the synoptic scale weather on TA records, we explore outputs of ECHAM5-wiso and back-trajectory calculations, driven by atmospheric reanalyses. None of the associated atmospheric simulations does resolve local processes such as katabatic winds or sea breeze. We used the ECHAM5-wiso model outputs to explore the following questions: (i) ECHAM5-wiso outputs show similarities with the corresponding observed variables for their inter-annual variability, trends and remarkable years? (ii) What are the simulated seasonal cycles for $\delta^{18}O$ and d-excess? (iii) What are the simulated relationships between local near-surface air temperature and $\delta^{18}O$, and $\delta^{18}O$ and d-excess at the seasonal and inter-annual scales? (iv) Are there significant relationships between our isotopic records and the large-scale climatic variability?

ECHAM5-wiso similarities with the corresponding observed variables

For inter-annual variations, the annual means of DDU near-surface temperature and the simulated 2-meter temperature ($2m\text{-}T_{ECH}$) are significantly correlated (slope of 0.50 ± 0.14, r=0.67 and $p<0.05$). This relationship is valid for all seasons. It is the strongest in winter (slope of 1.1 ± 0.1 °C $°C^{-1}$, r=0.93 and $p<0.05$), and the weakest in summer (slope of 0.98 ± 0.3 °C $°C^{-1}$, r=0.69 and $p<0.05$). There are no significant correlation between water stable isotope records from the TA and simulated by the ECHAM5-wiso, neither for $\delta^{18}O$, nor for d-excess. Finally, we found no significant trend in any model output over 1998–2014.

In terms of remarkable years, ECHAM5-wiso shows a low $\delta^{18}O_{ECH}$ mean value in 1998 and a high $d\text{-}excess_{ECH}$ mean value in 2007 (Fig. S4 in the Supplementary Material). Only year 2007 is remarkable in both the data (low reconstructed SMB) and the model. We thus explored more deeply the model. The highest d-excess value was simulated the 7th of May (Table S8 in the Supplementary Material). When comparing from the 6th to the 8th of May in 2007, with daily

averages over the period 1979-2014, the model simulates similar near-surface temperature, but particularly low precipitation, and wind components (zonal and meridional). Despite the small precipitation amount, the daily isotopic anomaly is sufficiently large to drive the annual anomaly (Fig. S5 in the Supplementary Material). D-excess values higher than 30 ‰ (threshold chosen as it corresponds to the maximum d-excess mean + standard deviation simulated by ECHAM5-wiso over Antarctica at the monthly scale, see Fig. S6 in the Supplementary Material) occur only 4 other timer over 1998–2014. We nevertheless remain cautious with these values which could be due to a numerical artefact.

Neither $t2m_{ECH} - \delta^{18}O_{ECH}$, nor SMB_{ECH} – $d\text{-}excess_{ECH}$, nor $\delta^{18}O_{ECH}$ – $d\text{-}excess_{ECH}$ relationships are identified in ECHAM5-wiso seasonal or annual outputs. Likewise, no significant relationship could be identified between $d\text{-}excess_{TA}$ and SMB simulated by ERA using both annual and seasonal values.

Simulated seasonal cycles for $\delta^{18}O$ and d-excess

We now explore the seasonal variations in $\delta^{18}O_{ECH}$ and $d\text{-}excess_{ECH}$ over the period of simulation (1998-2014, Table 6). The peaks in t $\delta^{18}O_{ECH}$ predominantly occur in spring and summer (25 % and 63 % respectively), while it only happens 12 % of the time in winter and never in autumn. The $d\text{-}excess_{ECH}$ peaks most often in autumn (69 %) and secondarily in winter (31 %), but never during the other seasons. As a result, the model simulates more regular isotopic seasonal cycles with $\delta^{18}O$ maxima during spring to summer seasons, and d-excess maxima during autumn to winter seasons, than identified in the TA record.

Relationships with the large-scale climatic variability

The ERA-interim outputs allow us to investigate whether the large-scale climatic variability influence the isotopic composition of Adélie Land precipitation recorded in the TA firn core. We looked at the simulated linear relationships between the TA isotopic records ($\delta^{18}O_{TA}$ and $d\text{-}excess_{TA}$) with the ERA-interim outputs (2mT, u10, v10 and z500, Section 2.2). We here report only significant relationships with absolute correlation coefficients higher than 0.6. For $\delta^{18}O_{TA,}$ we found a correlation with 2m-T over the Antarctic plateau (Fig.4.3.12a), as well as a correlation with v10 (Fig. 4.3.12b) along the westerly wind belt, at ~ (55 °S, 100 °E) and ~ (55 °S, 130 °E) in the Indian Ocean, and at ~ (55 °S, 10-50 °E) in the Atlantic Ocean, and a very little area on coastal Dronning Maud Land at ~ (60 °S, 30-40 °E). For $d\text{-}excess_{TA}$, we found a correlation with 2m-T (Fig. 4.3.12c) toward the Lambert Glacier at ~ (70-80 °S, 30-40 °E), and an anticorrelation in the south of the Peninsula at ~ (55-65 °S, 250-300 °E). Finally, we noted

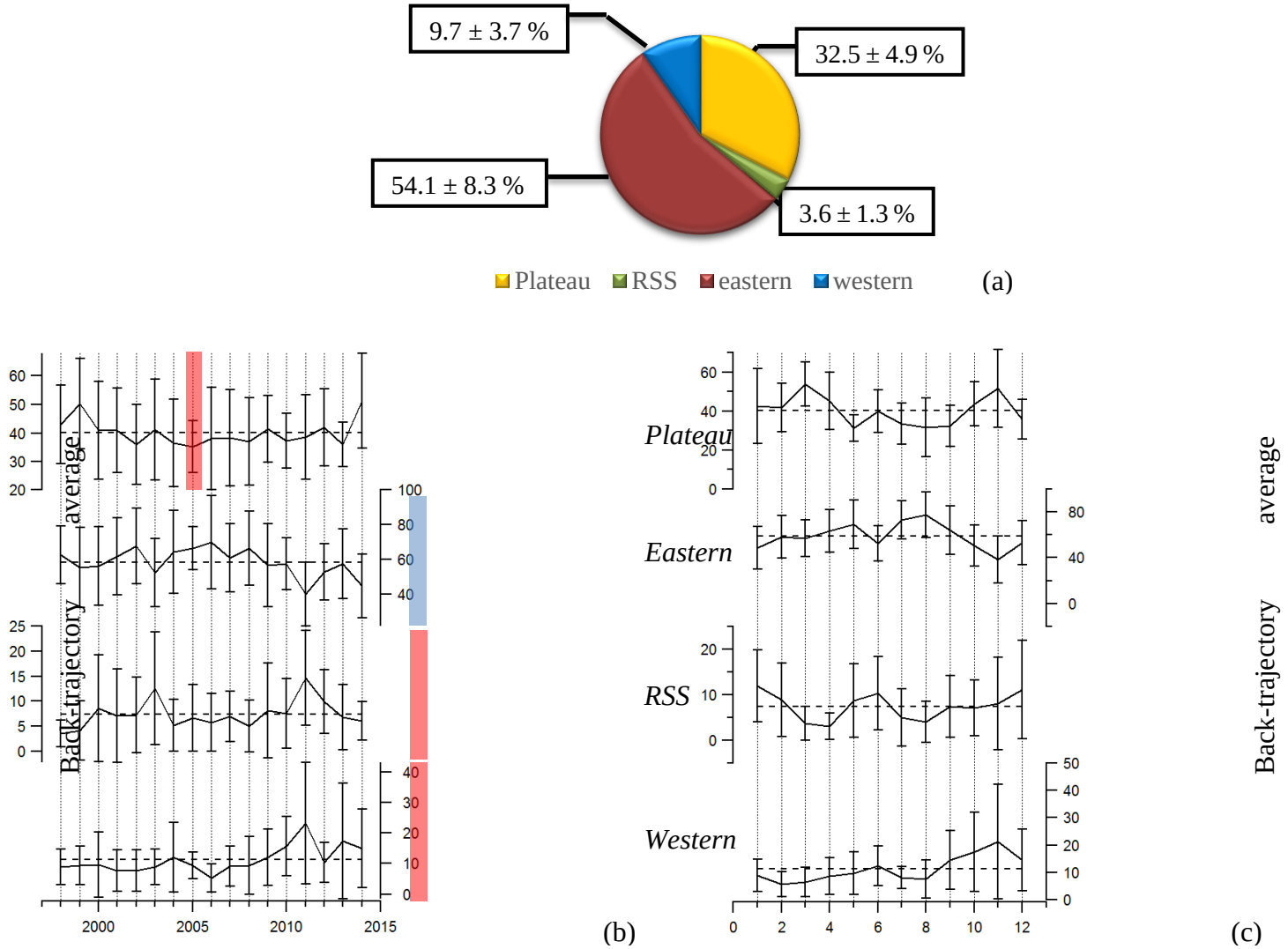

Figures 4.3.9: Results of daily back-trajectories calculations over the period 1998-2014 with (i) percentage (%) of the sum of back-trajectories passing over each defined region: (i) the eastern sector: (0 – 66 °S, 0 – 180 °E), (ii) the Plateau: (66 – 90 °S, 0 – 180 °E), (iii) the Ross sea sector: (0 – 75 °S, 180 – 240 °E), and finally (iv) the western sector: (0 – 75 °S, 180 – 240 °E), and (50 – 90 °S, 240 – 360 °E)(see Section 4.3.2.3); and (ii) averages at the annual scale (a and c) and at the mean seasonal scale (c and d). On the bottom panels. Horizontal dashed lines correspond to the mean value and vertical solid lines to standard deviations. Remarkable years. i.e. associated with values deviating by at least 2 standard deviations from the climatological mean value are highlighted with a red shading (positive anomalies) or blue shading (negative anomalies).

a correlation between d-excess$_{TA}$ and u10 (Fig. 4.3.12d) at a very narrow area of Dronning Maud Land at ~ (80 °S, 10-20 °E), and an anticorrelation on the westerly wind belt in the Atlantic Ocean at ~ (55 °S, 40-50 °E). No correlation is found with z500, neither with $\delta^{18}O_{TA}$ nor d-excess$_{TA.}$

Note that no significant relationship is obtained between the TA records and any mode of variability.

Origin of air masses

Finally, we used the HYSPLIT back-trajectory model to count the proportion (in percentage) of air mass back-trajectories, based on daily calculations over the period 1998-2014, and averaged at the annual and seasonal scale, from four different regions (Section 4.3.2.3): the plateau, the eastern Atlantic Ocean and th Indian Ocean (eastern sector), the Ross Sea sector (RSS), and the West Antarctic Ice Sheet with the Pacific Ocean and the western Atlantic Ocean (western sector), as displayed on Fig. 4.3.2. On average, the highest annual proportion of air masses comes from the eastern sector (54.1 ± 8.3 %) and the East Antarctic plateau (32.5 ± 4.9), while a small proportion of air masses come from the western sector (9.7 ± 3.7 %), and from the RSS (3.6 ± 1.3 %). A k-mean clustering over the last points of the whole back-trajectories indicate two main origins, in the Indian Ocean (62.4 °S, 131.7 °E) and in the coastal West Antarctic Ice Sheet (73.4 °S, 227.5 °E).

Inter-annual variations in back trajectories (Fig. 4.3.9b) reveal a positive trend for the fraction of air masses coming from western sector (slope of 0.41 ± 0.16 % y^{-1}, r=0.55 and p<0.05), and remarkable years: 1999, which was identified as a remarkable high $\delta^{18}O$ value and low nssSO_4 in our TA records, is here associated with a minimum of back-trajectories from the Plateau, and year 2011 which was associated with particular high MSA in our TA record, shows a particular low proportion of air masses coming from the estern sector while particular high proportion of air masses coming from the Ross and western sectors.

The seasonal cycles of back-trajectories per region is shown on Figure 4.3.9c. The percentage of back-trajectories coming from the Plateau display peaks in autumn and spring (March and November), those from the Ross Sea sector in winter and summer (January and June), those from the eastern sector in autumn and winter (May and August), and finally those from the western sector in spring (November). We note a significant linear correlation between the seasonal cycles of the percentage of $\delta^{18}O$ and back-trajectories coming from the Ross sea sector (r=0.68 and p<0.05), and from the western sector (r=0.59 and p<0.05), and between the seasonal cycles of d-excess and the percentage of back-trajectories coming from the western sector (r=-0.67 and p<0.05).

Finally, we associated each daily back-trajectory to daily precipitation $\delta^{18}O$ and d-excess values simulated by ECHAM5-wiso in the precipitation, and classified the time series for each variable by back-trajectories sectors. We then computed the corresponding seasonal cycles (Fig. 4.3.10). The mean $\delta^{18}O_{ECH}$ value is slightly higher for air masses coming from the eastern sector (-20.6 ‰ compared to -21.9± 0.2 for the other sectors). The asymmetry in $\delta^{18}O_{ECH}$ is particularly well marked for air masses coming from the Ross sea and western sectors, with peaks in August and September respectively (resulting in a winter amplitude more than twice higher compared to the eastern and Plateau sectors), and correspond to higher precipitation amounts during these months during the winter season. The d-excess mean seasonal cycles substantially differ by their amplitude: for air masses coming from the western sector, it is 11.8 ‰, with outstanding values in March and October (minima) and in May (higher than the mean plus two standard deviations), whereas it varies between 3.2 ‰ and 3.6 ‰ for the other sectors.

The back-trajectory of the 7th of May in 2007 (shown to be remarkable of simulated d-excess by ECHAM5-wiso) was identified as coming from the western sector, but those associated with the 4 other remarkable simulated d-excess (i.e. > 30 ‰) indicate air masses coming the three other regions, and sometimes varying with the hour of the day (S6 in the Supplementary Material).

In summary, we found a mismatch between ECHAM5-wiso outputs and the TA data for d-excess variations. There are no similarities for trends, for seasonal cycles, or for inter-annual isotopic variations. Similarly than in the TA firn core, ECHAM5-wiso simulates no $\delta^{18}O_{ECH}$ – $t2m_{ECH}$ correlation, but no $d\text{-}excess_{ECH}$ – $\delta^{18}O_{ECH}$. Both TA records and ECHAM5-wiso depict an unusual feature in 2007, with dry conditions and high d-excess values. The comparison between TA records and air mass back trajectories suggests that the asymmetry in the $\delta^{18}O$ seasonal cycle is due to the precipitation of air masses coming from the the western sector, and that an increased occurrence of (rare) air masses coming from the the western sectoris associated with high d-excess values.

4.3.4 Discussion

4.3.4.1 SMB

The estimated SMB of East Antarctica does not show a clear trend since 1900 (Favier et al., 2017). Recent studies (Altnau et al., 2015;Ekaykin et al., 2017;Vega et al., 2016) report negative SMB trends in coastal areas contrary to positive trends for the plateau. Especially, Thomas et al. (2017) report an unprecedented negative trend observed in Victoria Land for the last 50 years (1961-2010). For our study period (17 years for the TA record, and the ECHAM5-wiso simulation), we observe no significant trend.

In Adélie Land, a quality controlled SMB dataset has been developed (Favier et al., 2013), but the drivers of SMB spatio-temporal variability remain unexplored (Favier et al., 2017). This is related to the challenges in monitoring 1) precipitation in windy areas 2) sublimation of precipitating snowflakes (Grazioli et al., 2017) in the katabatic flow, 3) and the amounts of surface erosion or deposition according to surface wind convergence or divergence, of drifting snow fluxes, and of sublimation of the drifting snow particles (Gallée et al., 2013; Amory et al., 2016; Amory et al., 2017). The low correlation (over 1998-2006) between TA192A annual accumulation and from the first shallow ice core ("S1C1" (Goursaud et al., 2017b)), collected 14 km from TA192A site, demonstrates this complexity, even though this mismatch may be explained by age scale uncertainties. The S1C1 reconstructed accumulation was also weakly correlated with stake data and model outputs, reflecting the random snow accumulation

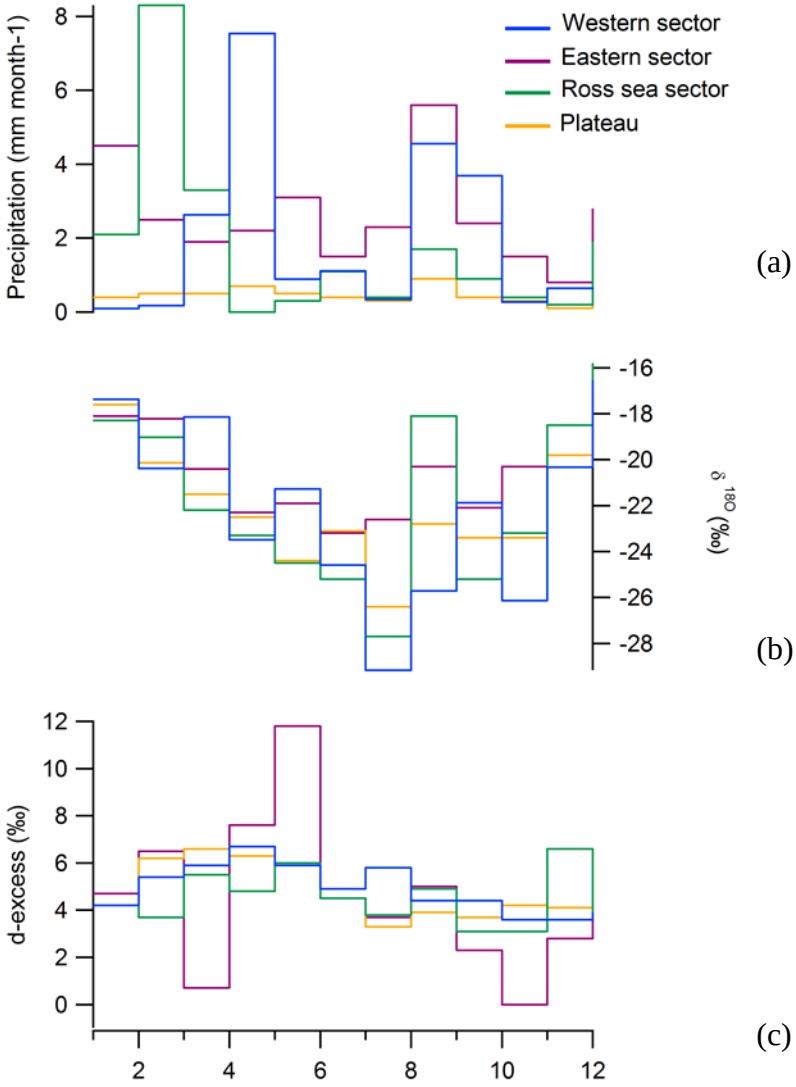

Figure 4.3.10: Seasonal cycles of precipitation (in mm month^{-1}. a), $\delta^{18}O$ (in ‰, b) and d-excess (in ‰, c) simulated by ECHAM5-wiso by back-trajectories regions "Indian" (corresponding to 0° E<longitude<160° E and latitude>-66 °), "Ross" (corresponding to -160° E<longitude<120° E and latitude>-75 °), "Plateau" (corresponding to 0° E<longitude<180° E and latitude<-66 °) and "WAIS + Pacific" (corresponding to -150° E<longitude<0 °E) (see Section 4.2.2.3).

amounts due to the presence or absence of sastrugi, and the potential occurrence of annual erosion at S1C1 site (Fig. S7 in the Supplementary Material). Here, the TA accumulation record is highly correlated not only with the closest stake data, but also with the ECHAM5-wiso model output over the period 2004–2014, showing the robustness of our reconstruction for this period. The fact that the TA record, the ECHAM5-wiso output for the corresponding grid point, and the "156 km" stake area data are pairwise correlated ($0.79 \leq r \leq 0.90$ and $p<0.05$), indicates that the TA firn core captures a 100 km- scale regional signal. The differences between the local and regional SMB signal are (Fig. 4.3.3b): (i) a higher local SMB average compared to the regional SMB, and (ii) the shift of minimum peak of 2007 in the local signal (i.e. the TA firn core and the "19.2" stake data) to 2008 in the regional signal (see the 2007–2008 plateau in the "156 km" network and the 2008 minimum value simulated by the ECHAM5-wiso model in Fig. 4.3.3b).

The anticorrelation between the d-excess$_{TA}$ and SMB$_{TA}$ shows the possibility to use water isotope firn core records from Adélie Land to complete the document of the SMB spatio-temporal variability. Dry air masses from the western sector may be associated with particular high d-excess values. The remaining uncertainty in the dating and the extraction of a pure signal limited our investigation.

As a conclusion, the absence of similarity between the TA and the S1C1 accumulation reflects the uncertainty in the S1C1 dating resulting from the large spatial variability and from more frequent erosion processes occurring at the S1C1 site. More ice core records within a 100 km area will allow reducing uncertainties in the interpretation of ice core signals, in particular on the link with the atmospheric variability.

4.3.4.2 The $\delta^{18}O$ – temperature relationship in coastal Antarctic regions

Several studies have shown that the annual $\delta^{18}O$ – temperature relationship is weak in coastal regions. As an example, over Dronning Maud Land, Isaksson and Karlén (1994) found a weaker correlation between $\delta^{18}O$ records and Halley temperature for coastal ice cores, i.e. for sites below 1000 m a.s.l., with a correlation coefficient of 0.56 compared to a correlation coefficient of 0.91 for site above 1000 a.s.l. More recently, Abram et al. (2013) reported a coefficient correlation of 0.52 for the relationship between $\delta^{18}O$ recorded in the James Ross Island ice core (at a high of 1524 m a.s.l., with a mean reconstructed SMB of 63 cm w.e. y^{-1}), and the near-surface temperature measured at Esperanza station ($n=56$ and $p<0.05$,). In coastal West Antarctica, Thomas et al. (2013) also reported a significant but weak correlation between the the $\delta^{18}O$ recorded in an ice core drilled on the Bryan coast and the near-surface temperature simulated by ERA-interim, over the period 1979-2009. Closer to Adélie Land, in Victoria Land,

Bertler et al. (2011) found a correlation coefficient of 0.35 between the $\delta^{18}O$ recorded in the Victoria Lower Glacier ice core (at a high of 626 m a.s.l.) and the summer near-surface temperature measured in Scott Base station (n=30 and p<0.0005). In this study, we find no relationship between the DDU near-surface temperature and the $\delta^{18}O_{TA}$, based on annual averages. Similarly, no relationship had been identified in the S1C1 core (Goursaud et al., 2017b), and was here not simulated by the ECHAM5-wiso model.

Our study shows that changes in air mass trajectories (dynamics) may dominate over thermodynamical controls (condensation temperature) on coastal Adélie Land $\delta^{18}O$ signal, as shown by the asymmetry of the $\delta^{18}O$ seasonal cycle recorded in the TA firn core (Section 4.3.3.4 and Fig. 4.3.8). The coupling of calculations of air masses back-trajectory and ECHAM5-wiso outputs suggests that $\delta^{18}O$ outstanding high values occurring during winter time would be brought by air masses coming from the western sector (Section 4.3.3.5 and Fig. 4.3.10).

The $\delta^{18}O$ measured in the ice of coastal Adélie Land may thus not allow to reconstruct surface temperatures of this region. However, correlations between $\delta^{18}O_{TA}$ and the 2m-temperature by ERA-interim over each grid point of Antarctica (Fig. 4.3.12a) show significant relationships over the plateau, confirmed by a significant correlation between annual $\delta^{18}O_{TA}$ and the near-surface temperature measured at Dome C over the period 1998-2014 (slope of 0.70 ± 0.29 ‰ $°C^{-1}$, r=0.53, p<0.05). These results support previous studies suggesting warm intrusions offshore Dumont d'Urville towards Dome C (Naithani et al., 2002).

Finally, the significant linear relationships with the u10 wind component above the westerly wind belt and at some coastal Antarctic area (Fig 4.3.12b) stress the influence of other processes than thermodynamic drive the isotopic composition of Adélie Land precipitations.

4.3.4.3 Water stable isotope, a fingerprint of changes in air mass origins

The mean d-excess$_{TA}$ is 5.4 ± 1.0 ‰, close to the 4.7 ± 0.4 ‰ value simulated by the ECHAM5-wiso model for the "coastal Indian" region defined in Goursaud et al. (2017a, different definition than in this study), and the 5.2 ± 0.6 ‰ value for the grid point corresponding to the TA drilling site. Inter-annual variations of d-excess$_{TA}$ (Fig. 4.3.7) are anti-correlated with TA reconstructed SMB, a feature not depicted by ECHAM5-wiso.

Main trajectories imprinted in the TA isotopic records

We suggest that air masses associated with small/large precipitation amounts are associated with different trajectories and moisture sources: main air mass origins from the Indian Ocean. These maritime air masses, isotopically enriched may transport water vapor , to the plateau, as shown by the significant relationship between $\delta^{18}O_{TA}$ and the near-surface temperature of the

plateau, especially in winter.Rare dry air masses may also come from the western sector, with a signal preserved in d-excess. Last point is led by the following hints:

(i) the positive trends both for the TA d-excess and the percentage of air masses coming from the western sector

(ii) an anti-correlation between the seasonal cycles of the TA d-excess and percentages of air masses coming from the western sector

(iii) the high simulated d-excess amplitude simulated by ECHAM5-wiso for air masses coming from the western sector, reflecting outstanding values occurring in autumn and winter times

(iv) The particular case of the 7th of May in 2007 with very high d-excess values simulated by ECHAM5-wiso, corresponding to an air mass trajectory from the western sector

As discussed earlier, the last item should be considered with caution as the four other remarkable d-excess values (i.e. higher than 30 ‰) simulated by the ECHAM5-wiso are associated to air masses coming from other regions (S6 in the Supplementary Material), and also to the fact that such high values could be due to potential numerical artefacts.

Linear relationships between d-excess$_{TA}$ and ERA-interim outputs strengthen the link between the climate variability of western Antarctic and associated southern oceans, as we note an anticorrelation between d-excess$_{TA}$ and the 2m-T in the south of the Peninsula, the Ellsworth region and the Bellingshausen sea ($r>0.6$); and an anticorrelation between d-excess$_{TA}$ and the u10 wind component over the coastal Ross sector, consistent with air mass trajectories coming from western Antarctica towards Adélie Land via the Ross sea sector. These dry air masses might origin from the Amundsen Bellingshausen sea (Emanuelsson et al., 2018;Winstrup et al., 2017), but cannot be directly linked to the Amundsen sea cyclonic, as we obtain no significant relationship with the ASL center pressure indices.

Potential interaction with sea ice

Noone and Simmonds (2004) have shown, thanks to climate modelling, that water stable isotopes were conditioned by changes in sea ice extent (a contraction in sea ice increases the local latent heat and temperature due to open water), but confirmed that a thorough understanding of main mechanisms controlling the d-excess was still needed. Also, earlier studies have suggested the use of d-excess ice core recordsto reconstruct past sea ice extent (e.g. Sinclair et al., 2014). Although we find a significant correlation between the d-excess$_{TA}$ and the d'Urville summer sea ice extent (section 4.3.3.3), a correlation map between the annual d-excess$_{TA}$ and the summer sea ice concentration (S8 in the Supplementary Material) show

significant correlations with further sea ice areas (e.g. an anticorrelation in the Amundsen sea and correlations in the Belligshausen, Scotia and Lazarev seas). We also noted a coincidence between the sign of the correlation of the relationship between the d-excess$_{TA}$ and the sea ice concentration, and the sea ice extent trend over the period 1998-2014 (S9 in the Supplementary Material), especially positive correlations (negative) associated to positive sea ice concentration trends. These findings call for mechanistic studies to understand the different processes behind d-excess associated to each air mass origins.

As we suggested a particular d-excess signature in the TA firn core, associated with air masses coming from the western sector, we tested the possibility for the d-excess$_{TA}$ to imprint changes in the Ross polynya. We thus estimated it, by counting the annual sea ice concentration over the polygon (60 – 70 °S; 150 – 210 °E), lower than 15 %. But we find no significant correlation between this estimated Ross polynya and the d-excess$_{TA}$ over the period 1998-2014.

The $\delta^{18}O$ – δD relationship

Earlier studies showed empirically that the relationship between d-excess and $\delta^{18}O$, and mainly the phase lag between signals within the seasonal cycle may indicate variations of the origin of the moisture source. This phage lag was shown to be of ~ 3–4 months over coastal regions such as Law Dome (Masson-Delmotte et al., 2003), Dronning Maud Land (Vega et al., 2016) and in the Ross Sea sector (Sinclair et al., 2014). By contrast, most studies identified an anti-phase over the East Antarctic plateau (e.g. Landais et al., 2012;Ciais et al., 1995), and at D47, situated close to the TA drilling site (Ciais et al., 1995).

We thus focus on the outcome of the running linear regression between d-excess$_{TA}$ and $\delta^{18}O_{TA}$ over 10 points all along the core (Fig. 4.3.11). We focus on the periods (53.3%) when a significant linear relationship is identified (i.e. $p<0.05$). The time-averaged correlation coefficient is 0.71 ± 0.45, which is consistent with the results obtained from the annual averages (varying from 0.51 in autumn to 0.75 in spring, Section 4.3.3.3). The time-averaged slope is 0.83 ± 0.83 ‰ ‰$^{-1}$. These positive values prevail for 91.5 % of the significant linear regressions. However, we observe remarkable deviations from this overall relationship. Particularly, linear regressions within year 2007 show slopes lower than the time-averaged minus two standard deviations (with a minimum value of -1.46 ‰ ‰$^{-1}$), and others within year 2011 show surprisingly very high slopes up to 6.9 ‰ ‰$^{-1}$. The years 2007 and 2011 were also previously noticed: the mean d-excess$_{ECH}$ simulated by ECHAM5-wiso for the year 2007 was shown to be driven by the high value occurring the 7th of May, associated to air masses coming from the western sector; and year 2011 is associated with a minimum of annual back-trajectories percentage from the eastern sector and maxima of back-trajectories from the Ross and the

western sector. As a result, the $\delta^{18}O$-d-excess relationship may be a fingerprint of changes in air mass origins, and particularly of the occurrence of precipitation of air masses coming from the western sector.

We undertook the same exercise with outputs of the ECHAM5-wiso model (Fig. S10 in the Supplementary Material), where only 19.2 % of the simulated linear regressions are significant (i.e. $p<0.05$). All significant relationships have negative correlation coefficients and slopes of time-averaged values -0.72 ± 0.25 ‰ ‰$^{-1}$ and -0.39 ± 0.23 ‰ ‰$^{-1}$ respectively (this is consistent with the annual means, Section 4.3.3.4). Moreover, these significant relationships do not occur during the remarkable years 2007 and 2011 identified in the TA firn core.

As a result, we propose that remarkable anomalies in d-excess / $\delta^{18}O$ running linear relationships provide an isotopic fingerprint associated with changes in dominant air mass trajectories. But a more comprehensive mechanistic study would be necessary to quantify the fractionation processes associated with different moisture source and transport characteristics.

4.3.4.3 Limits associated with model-data isotopic comparisons

We note a mismatch between ECHAM5-wiso outputs and the data (Section 4.3.3.5 and Fig. S4 in the Supplementary Material). This could be related to (i) to post-deposition processes associated with wind scoring or snow metamorphism not resolved in ECHAM5-wiso, (ii) the key role of very local atmospheric circulation effects related to katabatic wind processes, not

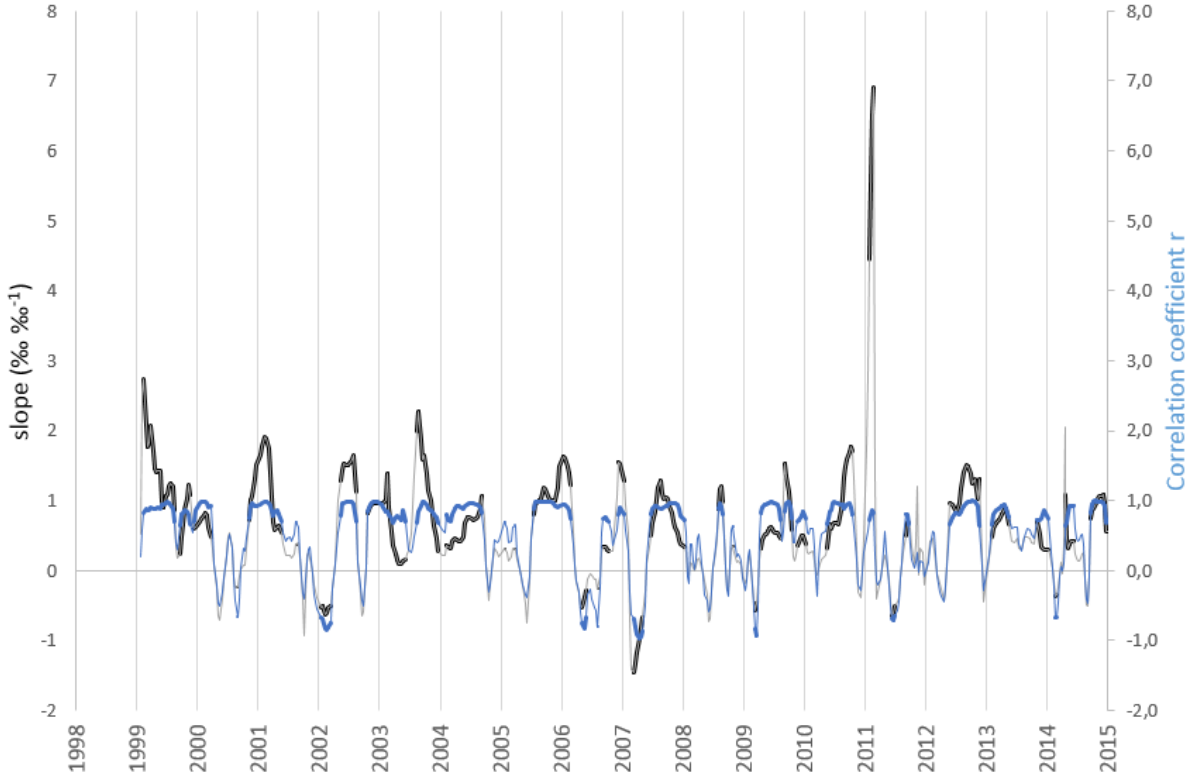

Figure 4.3.11: 10-point running slope ((‰ ‰$^{-1}$) and running correlation coefficient calculated between d-excess versus $\delta^{18}O$ calculated from the raw data of TA192A. Only significant results are reported ($p<0.05$). The date associated with the results correspond to the first point of the regression calculation (applied on 10 points).

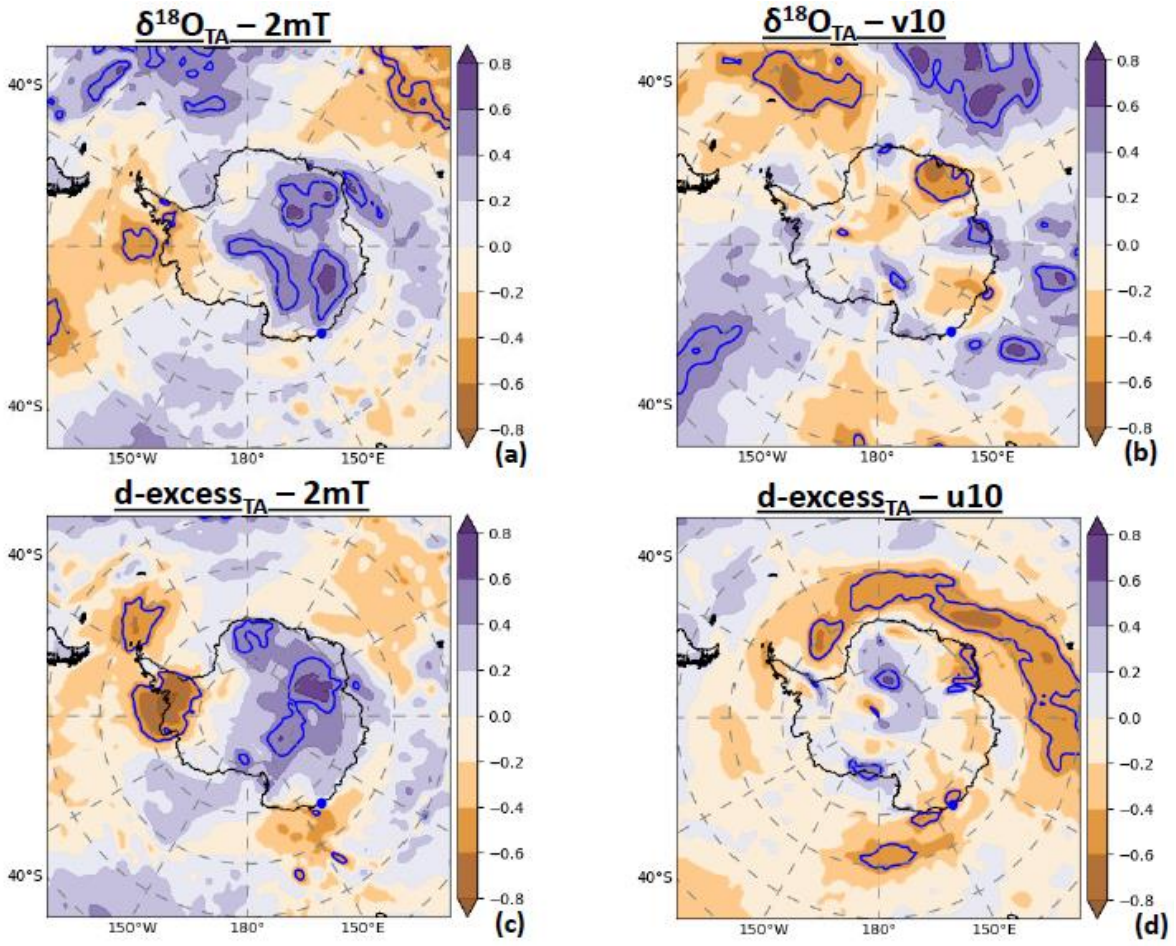

Figure 4.3.12: Coefficient correlation between the TA isotopic records and ERA-interim reanalyses, (a) between δ18OTA and the 2-meter temperature, (b) between δ18OTA and the 10-meter v wind component, (c) between d-excessTA and the 2-meter temperature, and finally (d) between d-excessTA and the 10-meter u wind component. The blue point locates the TA192A drilling site, and the blue lines contour the significant correlations.

resolved in large-scale atmospheric reanalyses and simulations, (iii) or the difficulties of ECHAM5-wiso to resolve the processes associated with the ocean boundary vapour d-excess, a mismatch already identified in the Arctic (Steen-Larsen et al., 2017).

The first issue is related with the robustness of records from a single coastal firn core. Several studies have evidenced signal to noise limits (e.g. Mulvaney et al., 2002;Graf et al., 2002). Given the high SMB estimated from TA, diffusion effects can be ignored (Frezzotti et al., 2007), and the estimated inter-annual variations in TA SMB are closely correlated not only with stake data closest to the drilling site, but also with the 156 km network stake data and to precipitation from the corresponding grid point of ECHAM5-wiso within a 100 x 100 km area. This finding supports an interpretation of the TA record to be representative of a regional SBM signal (100 km scale). However, we cannot draw any conclusion of the signal to noise aspects of the water stable isotope records, given the lack of coherency between the inter-annual variability in the TA and S1C1 $\delta^{18}O$ records for the few years of overlap (Unfortunately, there

are no striking features during the records common period, which makes it challenging to match the isotope records), and the lack of any other d-excess record within hundreds of kilometers.

The second source of uncertainty lies in the mismatch between inter-annual variations from coastal Adélie Land meteorological observations and the TA records, with ECHAM5-wiso outputs. For instance, we only see high correlation for the surface air temperature inter-annual variations for winter, and weak correlation for wind speed in spring and summer. These findings suggest limitations in the skills of either atmospheric reanalyses or the ECHAM5-wiso model to correctly capture the processes responsible for local climate variability. We had previously reported the capability of ECHAM5-wiso to correctly simulate observed large-scale features of water stable isotopes and SMB across Antarctica, for spatio-temporal patterns identified from datasets spanning the last decades such as mean values, amplitudes and phases of mean seasonal cycles, amplitude of inter-annual variance, strength of isotope-temperature relationships, d-excess versus $\delta^{18}O$ relationships) (Goursaud et al., 2017a). We thus highlight here specific challenges related to the Antarctic coastline, where local processes associated with katabatic winds, open water (e.g. polynya), and local boundary layer processes (e.g. snow drift) may affect isotopic records without being resolved at the resolution of reanalyses and ECHAM5-wiso simulation.

Our study therefore depicts limited understanding of the drivers of seasonal and inter-annual variability in coastal Adélie Land hydrological cycle, and thus calls for more isotopic measurements (from ice cores, snow precipitation, and water vapour) in Adélie Land to reduce uncertainties.

4.3.4.4 Chemistry

We now compare the chemical concentrations recorded in the TA firn core compared to the costal S1C1 firn core (Goursaud et al., 2017a). On the common covered period (1998-2006), we observe that mean chemical concentrations are slightly lower in the TA than the S1C1 firn core from 30 % for Na^+, to 50 % for MSA (see Table S11 in Supplementary Material). This decrease with the increasing distance from the coast (or elevation above sea level) is consistent with atmospheric studies showing a decrease of levels from the coast to the plateau for sea-salt (Legrand et al., 2017) and sulfur aerosols (Legrand et al., 2017). No significant linear regression emerges from any chemical species, highlighting a high spatial variability and/or the uncertainty in the dating of the S1C1 firn core.

Finally, we initially processed chemical measurements in our firn core, to support the isotopic records not only for dating, but also to identify air mass origins, making the hypothesis of three possible cases: (i) Air masses formed near the sea ice margin may be associated with relatively

high d-excess and $\delta^{18}O$ values, due to respectively a high kinetic fractionation due to evaporation under low humidity levels, and limited distillation effects. Such a configuration should be associated to low sea-salt concentrations due to reduced sea-salt emissions when summer sea-ice is present at the site as shown by atmospheric studies (Legrand et al., 2016). (i) By contrast, air masses formed over the Ocean in the absence of sea-ice may be associated with high $\delta^{18}O$ values, low d-excess and high sea-salt concentrations. (iii) Finally, air masses from central Antarctica may be associated with depleted $\delta^{18}O$ values and high d-excess, while air masses from ocean regions may lead to intermediate $\delta^{18}O$ and d-excess values, due to distillation effects, and evaporation under relatively humid conditions, but with low sea-salt concentrations.

The period from December 2003 to February 2004, associated with Na^+ values higher than the mean plus five standard deviations, probably caused marine advections, is not distinguishable in the isotopic records. And none of the three aforementioned cases was systematically observed.

To make it short, taking into account the definition of summer observations only does not alter our results. The sea-salt and sulfur concentrations measured along the TA records are slightly lower compared to the S1C1 firn core, consistently with the coast-to-plateau depletion previously observed in atmospheric measurement. Unfortunately, we could not use the sea-salt measurements to support our hypotheses regarding the air mass origins associated with isotopic compositions.

4.3.5 Conclusions and perspectives

In this study, we report the analysis of the first highly resolved firn core drilled in Adélie Land covering the very recent period 1998–2014, with a sub-annual resolution. The chronology was based on chemical tracers (Na, $nssSO_4$ and MSA) and adjusted by one year based on stake area information. Three $\delta^{18}O$ peaks found no counterparts in the chemical records. The high estimated SMB rate of 74.1 ± 14.1 cm w.e. y^{-1} limits the effects of diffusion and ensures that records with sub-annual resolution are preserved (e.g. Johnsen, 1977). The good consistency of the estimated annual SMB variations with observations on stakes reflects that high accumulation amounts are needed to ensure that small-scale SMB random variability caused by presence of sastrugi, dunes and barchans is negligible when compared to the mean accumulation value. This condition allows avoiding the erosion of seasonal or annual layers, which would lead to removal of the annual cycle of the recorded signal. For this reason, getting long term observations on distributed stake networks around a drilling site, or ground penetrating radar

data is crucial to accurately select a drilling site, by retrieving the location of mesoscale accumulation maxima, and by rejecting zones with potential erosion.

Using an updated database of Antarctic surface snow isotopes, we showed that not only $\delta^{18}O_{TA}$ but also d-excess$_{TA}$ mean values are in line with the range of coastal values in other locations. Neither in the TA – DDU dataset, nor in the ECHAM5-wiso output do we see any significant relationship between inter-annual variations in $\delta^{18}O$ and local surface air temperature. The anti-correlation between annual reconstructed SMB$_{TA}$ and d-excess$_{TA}$ leads us to suggest that changes in large-scale atmospheric transport could lead to an explanation for this feature. Particularly back-trajectory simulations from HYSPLIT and atmospheric outputs from ECHAM5-wiso at the seasonal cycle show the occurrence of air masses coming from the western sector during autumn and winter times, corresponding to high simulated d-excess values. Also, the identification of remarkable years both in back-trajectory percentages and in the relationships between d-excess and $\delta^{18}O$ also lead us to evidence a potential in the d-excess –$\delta^{18}O$ to identify remarkable features in moisture transport.

We cannot explain at this stage the observed positive trends in the d-excess$_{TA}$. We suggest that an improved understanding of the drivers of moisture transport towards coastal Adélie Land can benefit from the interpretation of water stable isotope tracers, especially d-excess, through mechanistic studies and the exploration of global atmospheric models. Ways forward include a better documentation of the spatio-temporal variability in SMB and water stable isotopes using a matrix of coastal firn core records spanning longer periods over the last decades (17 points being small to assess linear relationships, and record climate shifts, e.g. the IPO shift occurring in 1998 (Turner et al., 2016)); a better documentation of the relationships between precipitation and ice core records through the monitoring of the isotopic composition of surface vapour, and precipitation snow and firn (Casado et al., 2016;Ritter et al., 2016); and the implementation of water stable isotopes in regional models resolving the key missing processes linked for instance with katabatic winds, boundary layer processes, wind drift (Gallée et al., 2013).

Data availability

The TA192A isotope and chemical firn core records were archived on the PANGAEA data library at **https://doi.pangaea.de/10.1594/PANGAEA.896623**.

Acknowledgements

This study has been supported by the ASUMA project supported by the ANR (Agence Nationale de la Recherche, Project n°: ANR-14-CE01-0001), which funded the PhD grant of Sentia Goursaud and the publication costs of this manuscript.

4.4 Résumé et conclusions

Pour la première fois, deux carottes de névé côtières de Terre Adélie, caractérisées par des mesures isotopiques et chimiques relativement fines (à résolution sub-annuelle), ont été datées : la carotte S1C1 (66,71 °S; 139,83 °E; 279 m a.s.l.), extraite en 2007 dans le cadre du programme TASTE-IDEA, et la carotte TA (66,78 ° S; 139,56 ° S ; 602 m a.s.l) extraite en 2015 dans le cadre du programme ASUMA, 14 km plus loin vers l'intérieur du continent (cf. Fig. 4.3.2). De plus, le haut BMS du site d'extraction de la TA (74,1 ± 14,1 cm w.e. y^{-1} contre 21,8 ± 6,9 cm w.e. y^{-1} pour la S1C1), rare pour l'Antarctique de l'Est, permet d'exploiter les variations saisonnières, bien caractérisées. La datation de ces deux carottes repose sur un comptage des couches annuelles des enregistrements présentant un extrema saisonnier en été. Je souligne que malgré le soin apporté à l'identification objective des pics estivaux des espèces chimiques, un réajustement de la datation a dû être effectué en comparant le BMS annuel reconstruit résultant avec les mesures de balise Glacioclim et le signal isotopique enregistré avec celui simulé par ECHAM5-wiso sur la même période. Une comparaison statistique des signaux isotopiques issus des carottes avec des observations du climat régional (mesures météorologiques à la station de Dumont d'Urville, BMS mesuré extrait de l'observatoire Glacioclim, et données de mer de glace satellitaire) permet d'extraire les informations du climat régional enregistré dans les carottes, tandis qu'une comparaison avec les simulations extraites des réanalyses ERA-interim et du modèle ECHAM5-wiso m'a permis d'évaluer les informations du climat synoptique préservées dans les carottes.

Les deux carottes couvrent des périodes différentes : la S1C1 couvre la période 1946-2006 avec une incertitude maximale de 8 ans, et la TA la période 1998-2014 avec une incertitude maximale de 3 ans. Le recoupement entre ces deux carottes est donc réduit à quelques années. Les BMS annuels reconstruits montrent une grande variabilité spatiale, la TA ayant un BMS annuel moyen 3.4 fois plus important que celui de la S1C1 (75.2 ± 15 cm w.e. y^{-1} contre 21.8 ± 6.9 cm w.e. y^{-1} pour la TA et la S1C1 respectivement), et ne présentent ni corrélation significative, ni années remarquables communes. En outre, le BMS annuel issu de la TA est significativement corrélé (i) avec celui mesuré par la plus proche balise, et (ii) avec l'accumulation (précipitations – évaporations) simulée par ECHAM5-wiso sur le point de grille le plus proche. Il semblerait que ce résultat s'explique par l'emplacement du site d'extraction de la S1C1, situé sur une zone d'érosion par les vents, ce qui augmente le bruit de post-dépôt et limite le signal climatique préservé. Enfin, bien que de récentes études relatives à des constructions de BMS à partir de carottes de glace (Altnau et al., 2015; Vega et al., 2016; Ekaykin et al., 2017) reportent une tendance négative du BMS annuel côtier contrairement à une tendance positive du BMS sur le plateau central, aucune tendance n'est détectée dans les

séries temporelles de Terre Adélie (carottes, mesures de balise, ERA-interim). Nos résultats vont aussi à l'encontre de résultats de modélisation simulant une tendance à la diminution du BMS pour l'Antarctique de l'Est (Lenaerts et al., 2012).

Par rapport à la base de données que j'ai mise à jour des compositions isotopiques des précipitations, neiges et carottes de glace en Antarctique, les valeurs isotopiques moyennes enregistrées dans la S1C1 et la TA correspondent bien aux valeurs côtières couramment observées, et les différences entre les deux sites reflètent le léger appauvrissement attendu en rentrant vers l'intérieur du continent (valeurs moyennes du $\delta^{18}O$ de -18.9 ± 1.7 ‰ et -19.3 ± 3.1 ‰ pour la S1C1 et la TA respectivement). Aucune corrélation n'est observée entre la température de surface mesurée à DDU et le $\delta^{18}O$ enregistré dans les carottes à l'échelle interannuelle. En revanche, une corrélation significative existe à l'échelle décennale avec le $\delta^{18}O$ issu de la S1C1 ; ce résultat est à considérer avec prudence compte-tenu du petit nombre de points permettant cette analyse décennale sur un enregistrement de 60 ans. Nous en déduisons que d'autres paramètres que la température locale conditionnent l'évolution de la composition isotopique des masses d'air précipitant en région côtière de la Terre Adélie. Le d-excess enregistré dans la TA, ainsi que des simulations de rétro-trajectoires de masses d'air, permettent d'explorer l'influence de la dynamique atmosphérique. Un faisceau d'éléments suggèrent que la circulation atmosphérique pourrait jouer un rôle déterminant dans la variabilité isotopique en Terre Adélie : le déphasage des cycles saisonniers de la température de surface mesurée à DDU et du $\delta^{18}O$ issu de la TA, l'anti-corrélation entre le BMS annuel reconstruit à partir de la TA et le d-excess enregistré, l'anti-corrélation des cycles saisonniers du d-excess et de la fréquence des rétro-trajectoires provenant de l'Antarctique de l'ouest et du Pacifique, avec une augmentation du d-excess en automne/hiver synchrone avec un maximum de rétro-trajectoires ventant de l'Antarctique de l'ouest et du Pacifique.

J'ai également noté des tendances positive à la fois du d-excess enregistré dans la TA et de la banquise locale sur la période 1998-2014, mais n'avons pas pu fournir une explication pour ces tendances récentes. Alors que nous pensions que la combinaison de mesures d'élements chimiques et isotopiques pourrait permettre de caractériser des changements de masses d'air associées au transport atmosphérique, mes analyses montrent qu'il n'y a aucune corrélation significative entre tout élément chimique mesuré dans la TA et le d-excess. Ceci pourrait s'expliquer par la différence de transport entre les conditions d'atmosphère sèche permettant le dépôt des aérosols, et le transport d'air humide donnant lieu à des précipitations et l'enregistrement isotopique ainsi produit dans les carottes de glace. L'interprétation climatique du d-excess est rendue complexe par le faible accord entre observations et simulations, même avec le modèle ECHAM5-wiso (cf. partie précédente).

Je note à l'issue de ce travail sur des carottes de glace récentes en Terre Adélie, que deux problématiques majeures devraient être approfondies :

- Mieux comprendre les processus de dépôt et post-dépôt affectant le signal isotopique enregistré dans les carottes de glace de la Terre Adélie. Sur le terrain, des strasturgis, dunes et barchans témoignent de l'érosion par les vents. Les mesures de radar permettent également de caractériser les variations spatiales et temporelles de cet effet d'érosion. Aussi, il est désormais essentiel d'examiner ces mesures avant d'envisager une extraction ou l'analyse d'une carotte pour rechercher les sites de forage permettant de réduire le bruit associé. Enfin, des observations systématiques de compositions isotopiques de la vapeur, des précipitations et de la neige fraîche permettraient d'estimer quantitativement les effets de post-dépôt pour en tenir compte dans l'interprétation des carottes de névé ou les comparaisons entre données issues de carottes de névé et simulations atmosphériques.
- Améliorer la compréhension des processus contrôlant le transport d'humidité vers la Terre Adélie. Pour cela, il serait intéressant d'analyser les rétro-trajectoires de masse d'air humides simulées par le modèle lagrangien Flexpart, et d'utiliser les zones d'évaporation identifiées le long des trajectoire pour quantifier l'impact de ces changements de conditions d'évaporation et de transport sur le signal isotopique des précipitations, par exemple en utilisant le modèle isotopique simple MCIM. Cela pourrait également être abordé à l'aide d'un modèle atmosphérique régional comme MAR qui devrait prochainement être équipé des isotopes de l'eau. Grâce à une résolution plus fine que celle du modèle ECHAM5-wiso, et à des paramétrisations spécifiques pour représenter de nombreuses spécificités du climat de l'Antarctique et des interactions neige-atmosphère, résolvant notamment explicitement l'érosion par les vents (bien qu'à plus grande échelle que dans la réalité), ce modèle permettrait de mieux comprendre les liens entre circulation atmosphérique synoptique, phénomènes locaux (e.g. couche limite), affectant aussi bien les conditions d'évaporation à proximité de DDU que les conditions de condensation, et composition isotopique des précipitations et de la neige de surface. Les données issues de carottes de glace en Terre Adélie sont particulièrement importantes pour l'évaluation d'une telle modélisation isotopique à vocation régionale. Ce bouquet d'outils de modélisation pourrait être utilisé pour interpréter les premières données isotopiques mesurées dans la vapeur d'eau atmosphérique de Dumont d'Urville (cf. Annexe A).

Enfin, il serait intéressant en perspectives, d'analyser et exploiter d'autres carottes extraites dans la région de la Terre Adélie au cours du programme ASUAM, afin d'obtenir une variabilité

spatio-temporelle plus fine, notamment en interrogeant les gradients spatiaux par rapport à la distance à la côte, à l'altitude, mais aussi afin d'améliorer le rapport signal sur bruit (e.g. Schlosser et al., 2014).

CHAPITRE 5 : Conclusions et perspectives

5. Conclusions et perspectives

Dans un contexte du changement climatique pour lequel l'élévation du niveau des mers aura des répercussions importantes sur les régions littorales, leurs écosystèmes et habitants, il est indispensable de mieux connaître et comprendre les processus contribuant à cette montée du niveau des mers, pour évaluer notre capacité à les prendre en compte dans les simulations d'évolution future, et ainsi guider les stratégies de gestion des risques.

L'une des principales sources d'incertitude vis-à-vis de l'évolution future du niveau des mers tient à notre capacité à connaître et comprendre les variations du bilan de masse de la calotte antarctique, tant pour les aspects d'écoulement dynamique que pour le bilan de masse de surface. Caractériser la variabilité spatio-temporelle de ce bilan de masse de surface est important pour pouvoir évaluer la pertinence des outils de modélisation essentiels pour les projections d'évolution future.

Les technologies d'observation instrumentale du bilan de masse de surface sont en progrès constant, mais la connaissance de la variabilité spatio-temporelle du bilan de masse de surface reste limitée. Dans ce contexte, les « rétro-observations » offertes par les informations issues des carottes de glace sont une source précieuse d'informations, malgré les limitations intrinsèques de ces archives climatiques. De plus, les enregistrements issus de l'analyse des aérosols atmosphériques et de la composition isotopique de l'eau de ces carottes de glace permettent d'apporter des informations complémentaires pour caractériser la variabilité climatique régionale en Antarctique, en relation avec les trajectoires des masses d'air, et pour évaluer la capacité des modèles de circulation atmosphérique à représenter correctement le transport d'air et d'humidité vers l'Antarctique. Les travaux que j'ai effectués au cours de ma thèse s'inscrivent dans ce contexte. Cette section est structurée en deux grandes parties, l'une portant sur la reconstitution de la variabilité de la température en Antarctique à partir des informations isotopiques issues des carottes de glace, et l'autre portant spécifiquement sur la variabilité climatique en Terre Adélie.

5.1 Situer la variabilité climatique récente dans un contexte plus large

Etudier le climat des deux derniers millénaires permet de replacer la variabilité climatique des dernières décennies potentiellement affectée par l'influence des activités humaines dans le contexte de la variabilité climatique naturelle. De même, mieux comprendre la variabilité climatique en Terre Adélie demande de confronter la variabilité climatique régionale à la variabilité climatique à l'échelle du continent Antarctique. Pour permettre la quantification des changements passés de température en Antarctique, j'ai combiné les informations issues

d'enregistrements isotopiques aux résultats issus de la modélisation de la circulation atmosphérique incluant les isotopes stables de l'eau.

Démarche. J'ai dans une première partie montré les capacités du modèle de circulation générale atmosphérique équipé des isotopes ECHAM5-wiso à produire des simulations isotopiques réalistes, en le confrontant à une base de données que j'ai mise à jour à partir de données isotopiques issues de précipitations, neige fraîche et carottes de glace. J'ai donc identifié les points forts mais aussi les biais systématiques de ce modèle pour le bilan de masse de surface, pour la température de l'air en surface et pour les isotopes stables de l'eau. J'ai ensuite effectué des diagnostics permettant de guider l'interprétation des isotopes de l'eau pour différentes régions antarctiques. Cette méthode a ensuite été appliquée à une base de donnée d'enregistrements isotopiques des derniers 2000 ans pour produire des reconstitutions de température quantifiées et associées à une estimation de l'incertitude, pour ces différentes régions ainsi que pour l'ensemble du continent antarctique.

Valeur ajoutée.

(1) J'ai constitué une base de données isotopiques rassemblant toutes les données disponibles à l'heure de sa constitution pour l'Antarctique, issues de précipitations, neige fraîche et carottes de glace à partir non seulement du $\delta^{18}O$, mais aussi du d-excess, et balayant les échelles de temps saisonnières, annuelles, et en donnant des moyennes temporelles de chaque enregistrement. Cette base de données est en libre accès sur la base d'archives PANGAEA.

(2) J'ai établi une méthode rigoureuse d'évaluation des isotopes de l'eau simulés par un modèle atmosphérique de circulation générale du climat, appliquée au modèle ECHAM5-wiso mais avec des diagnostics généralisables à d'autres simulations.

(3) J'ai établi la première analyse systématique pour caractériser la régression linéaire entre le $\delta^{18}O$ et la température de surface (gradients spatiaux, relations temporelles à l'échelle saisonnière et inter-annuelle), ainsi que le retard de phase entre le $\delta^{18}O$ et le d-excess, sur l'ensemble de l'Antarctique.

(4) J'ai proposé une méthode de calibration pour reconstruire la température de l'Antarctique à partir des enregistrements en $\delta^{18}O$, en utilisant la pente issue de la régression linéaire entre le $\delta^{18}O$ et la température de surface simulée dans le modèle ECHAM5-wiso.

Résultats clés. J'ai validé l'utilisation du modèle ECHAM5-wiso pour l'interprétation des isotopes stables de l'eau mesurés en Antarctique, en soulignant les limites d'utilisation de la simulation guidée par les réanalyses atmosphériques, en fonction des régions et des paramètres considérés. J'ai confirmé le fait que la relation linéaire entre le $\delta^{18}O$ et la température de surface de l'échelle saisonnière dépend de la région et de l'échelle de temps considérées. J'ai montré que le « thermomètre isotopique » ne peut pas être appliqué pour la Péninsule antarctique, et que la corrélation entre le $\delta^{18}O$ et la température de surface est faible dans les régions côtières. L'étude à laquelle j'ai participé au sein du groupe Antarctica2k a permis de reconstituer la température de l'Antarctique des deux derniers millénaires. Nous avons notamment montré la robustesse de la méthode de calibration de la relation $\delta^{18}O$-température en utilisant la pente de la relation simulée par le modèle ECHAM5-wiso, la représentativité de la variabilité climatique du $\delta^{18}O$ et de la température simulés par le modèle (couvrant la période 1979-2013) pour la reconstituion des températures sur 2000 ans à l'échelle régionale, et les différences dans les relations linéaires $\delta^{18}O$-température entre les différentes régions d'Antarctique.

Perspectives.

(1) Il faudrait désormais appliquer la méthode d'évaluation des isotopes stables de l'eau simulés à l'ensemble des modèles équipés des isotopes stables de l'eau et d'en faire une inter-comparaison. Ces diagnostics pourraient également permettre d'évaluer d'éventuelles améliorations de différentes versions d'un même modèle en fonction de la résolution spatiale, de différentes paramétrisations physiques, ou de la manière de représenter les isotopes stables de l'eau (e.g. coefficients de fractionnements, sur-saturation, etc).

(2) Mon étude a été limitée par les données disponibles, et notamment les données de composition isotopique de précipitations et de vapeur. Celles-ci permettent en effet de limiter les artefacts liés aux processus de dépôt et de post-dépôt qui peuvent affecter le signal issu de carottes de névé et biaiser les comparaisons modèles-données. Mon travail souligne la nécessité de renforcer le dispositif d'observations continues en Antarctique en tirant parti des bases scientifiques pour les équiper de systèmes de prélèvement de précipitations (relativement léger) et d'instruments de mesure en continu de la composition isotopique de la vapeur d'eau de surface (ce qui est plus ambitieux).

(3) La reconstruction de la température sur les deux derniers millénaires n'était qu'une première étape dans la reconstruction et la compréhension des processus en œuvre dans la variabilité climatique des derniers millénaires. Les nouveaux groupes de travaux transverses ISO2k et Clivash2k permettront désormais de comprendre les télé-

connections entre les moyennes latitudes et les hautes latitudes sur les mêmes échelles de temps. Pour le moment, ces projets sont à leur tout début et les premières problématiques à aborder ne sont pas encore clairement énoncées. Elles seront définies lors du workshop « Climate Variability in Antarctica and the Southern Hemisphere in the past 2000 years » qui aura lieu les 4 et 5 Septembre à Cambridge, et au cours duquel je présenterai les résultats récents, problématiques et perspectives sur lesquels l'équipe du LSCE se concentre.

5.2 Caractériser et comprendre la variabilité climatique récente en Terre Adélie

La constitution d'une banque de carottes par le projet ASUMA de 2014 à 2017 a permis de fournir de nouvelles archives pour caractériser la variabilité climatique spatio-temporelle récente de la Terre Adélie, dans un secteur marqué par de fortes différentes de distance à la côte, altitude, régimes de vent.... Au cours de ma thèse, je n'ai pu exploiter que deux carottes côtières, la S1C1 et la TA192A.

Démarche. J'ai regroupé l'ensemble des observations et simulations disponibles du climat de la Terre Adélie. J'ai daté les carottes de glace par comptage de couche annuel, puis j'ai réajusté en comparaison les reconstructions de bilan de masse de surface (BMS) avec des données issues de mesures de balises, et, lorsqu'un signal commun pouvait être identifié, entre les moyennes annuelles du $\delta^{18}O$ enregistré de la carotte et les simulations de $\delta^{18}O$ produites par le modèle ECHAM5-wiso. J'ai effectué une description statistique de l'ensemble des enregistrements des carottes. J'ai comparé les données isotopiques aux données côtières issues de la base de données que j'avais consistué antérierement, puis j'ai effectué des régressions linéaires avec l'ensemble des séries temporelles issues des observations et des simulations.

Valeur ajoutée.

(1) J'ai proposé une approche étendue de la méthode de datation traditionnelle par comptage des couches annuelles, en l'ajustant par comparaison de la variabilité interannuelle du BMS reconstitué et du $\delta^{18}O$ issus de la première datation, avec des mesures de BMS et des simulations de $\delta^{18}O$ par un modèle atmosphérique de circulation générale. Cette démarche a permis d'évaluer objectivement l'incertitude associée au comptage de couches, et de comprendre les sources d'incertitude (e.g. forme des signaux saisonniers dans les enregistrements chimiques).

(2) Mon travail a permis de fournir les premières données isotopiques datées issues de carottes de glace forées en Terre Adélie pour les dernières décennies.

Résultats clés. J'ai confirmé la grande variabilité spatiale du BMS en Terre Adélie, déjà caractérisée à l'aide de mesures de balises et de données radar. Certains sites sont fortement impactés par l'érosion par les vents. Aussi, une estimation préalable du BMS grâce aux mesures des balises est essentielle pour sélectionner les sites à forer. Aucune relation significative n'a été trouvée entre les isotopes stables de l'eau et la température de surface à l'échelle interannuelle. Comme dans d'autres régions côtières, la variabilité du signal isotopique n'est pas contrôlée par la variabilité de la température de surface locale, mais probablement par le transport atmosphérique. Plusieurs indices montrent en effet que les isotopes de l'eau sont principalement modulés par la dynamique atmosphérique plutôt que par la thermodynamique : (i) les cycles saisonniers de la température de surface et du $\delta^{18}O$ ne sont pas en phase ; et (ii) les cycles saisonniers du d-excess et de la fréquence de rétro-trajectoires provenant de différents secteurs de l'Océan austral sont significativement corrélés. J'ai également montré que le d-excess enregistré dans la TA, et la banquise de la côte de l'océan indien décrivent une tendance négative sur la période 1998-2014, sans pouvoir apporter d'explication à cette caractéristique, en particulier parce que cette tendance du d-excess n'est pas simulée par ECHAM5-wiso. Enfin, je n'ai pu identifier aucune relation significative entre les enregistrements isotopiques ($\delta^{18}O$, d-excess) et ceux des éléments chimiques (Na^+, SO_4^{2-}, MSA). Cela exclut la possibilité de combiner ces différents enregistrements pour mieux caractériser les changements de transport atmosphérique dans cette région.

Perspectives.

(1) Renforcer le signal climatique extrait des carottes de glace. A certains sites de forage des campagnes de terrain ASUMA, plusieurs carottes ont été forées, ce qui permetta, lorsque toutes les analyses et datations auront été effectuées, d'extraire, au moyen d'outils statistiques, le signal climatique potentiel du bruit lié aux processus de déposition et post-déposition (cf. Section 1.4). Par exemple, pour chacun des sites TA192-15, et TA162-15, trois carottes ont été forées (cf. Section 2.1.1). Leur analyse et leur exploitation permettra donc de rendre les signaux obtenus plus robustes.

(2) Quantifier les processus à l'interface neige de surface/atmosphère. Obtenir des mesures isotopiques conjointes de vapeur, précipitation et neige fraîche et en continu permettra de mieux quantifier les processus de déposition par le vent, mais aussi les possibles fractionnements entre les différentes phases atmosphériques. De telles mesurées seront effectuées dans le cadre de la thèse de Christophe Leroy-Dos Santos (LSCE, Gif-sur-Yvette), cet été austral à Dumont d'Urville.

(3) Affiner les comparaisons entre simulations atmosphériques et données isotopiques locales. L'implémentation des isotopes de l'eau dans le modèle régional atmosphérique MAR a très récemment initiée par Cécile Agosta (post-doctorante au LSCE, Gif-sur-Yvette). Ce modèle prend en compte des processus spécifiques à la couche limite atmosphériques en Antarctique, ainsi que la re-déposition de la neige par les vents (Amory et al., 2015). La comparaison entre simulation globale (e.g. ECHAM5-wiso) et régionale (MAR-iso) permettra de comprendre l'importance relative des processus atmosphériques régionaux dans la variabilité spatiale et temporelle du signal isotopique en Terre Adélie.

5.3 Mieux comprendre le transport d'humidité vers l'Antarctique

Le travail de ma thèse a montré les limites de l'interprétation du d-excess pour diagnostiquer le transport d'humidité. Davantage d'outils sont nécessaires pour affiner la compréhension de ce marqueur.

Une première approche porte sur la combinaison entre observations (issues de mesures de vapeur, de précipitations ou de carottes de névé) et diagnostics de transport atmosphérique. Le modèle de rétro-trajectoires Flexpart a l'avantage, comparé aux modèle Hysplit, d'apporter un diagnostic du transport d'humidité. L'utiliser de manière systématique en le couplant à la modélisation isotopique est une piste à explorer pour l'exploitation des signaux observé en d-excess. La confrontation entre ces diagnostics de transport d'humidité issus de réanalyses et le transport d'humidité simulé par ECHAM5-wiso pourrait aussi permettre de comprendre pourquoi il reste si difficile de simuler de manière réaliste le d-excess en Antarctique.

Une seconde piste porte sur l'exploitation d'autres outils de dynamique atmosphérique que les modèles atmosphériques de circulation générale, comme des diagnostiques de l'activité cyclonique à partir des réanalyses ERA-interim (http://eraiclim.ethz.ch/) ou des algorithmes(e.g. recherches menées par Ambroise Dufour, post-doctorant à l'IGE, Grenoble; Dufour, 2016). En outre, la thèse de Jonathan Wille (IGE, Grenoble) permettra de mieux caractériser les évènements de « rivières atmosphériques ». Le travail de Jean-Louis Bonne avait montré lors d'un événement remarquable de « rivière atmosphérique » au Groenland que la signature du d-excess était conservée lors du transport atmosphérique depuis la région source d'humidité. Evaluer l'importance de ces tempêtes extra-tropicales pour le bilan de masse des régions côtières comme la Terre Adélie et pour le signal isotopique déposé dans les carottes de glace ouvrirait de nouvelles perspectives.

Enfin, le groupe de travail Iso2K (cf Section 1.5.1) a constitué une base de données globale des isotopes de l'eau issus des différentes archives existantes. Cette base de donnée pourrait

permettre d'explorer les relations entre la variabilité climatique en Antarctique et aux moyennes latitudes, avec un même traceur (isotopes stables de l'eau), et de renforcer l'évaluation des modèles climatiques équipés des isotopes stables de l'eau. Ces thématiques font l'objet d'une proposition de sujet de thèse au LSCE.

5.4 Mieux caractériser la variabilité du climat en Terre Adélie et en comprendre les mécanismes

Analyser et exploiter les autres carottes forées au cours du programme ASUMA (cf. Section 2.1.1), est bien sûr fondamental pour progresser dans la quantification de la variabilité spatio-temporelle du BMS et des isotopes de l'eau de la Terre Adélie, ainsi que la compréhension des mécanismes à leur origine. Des mesures isotopiques et chimiques ont déjà été effectuées le long des carottes TA162-15-2 et TA653-16-2. Je souhaite poursuivre l'exploitation de ces données dans les mois à venir (datation, reconstitution du SMB, analyse des enregistrements) pour pouvoir effectuer une première reconstruction régionale via une analyse composite des quatre carottes coupées et analysées au cours de ma thèse (e.g. Schlosser et al., 2014; Ekaykin et al., 2017).

A terme, la combinaison des informations issues des carottes de névé et de glace de la Terre Adélie, avec des informations climatiques extraites de carottes marines à très haut taux de sédimentation (cf. Section 1.2.3., e.g. Denis et al., 2006; Crosta et al., 2008), et les informations issues de l'évolution des écosystèmes de ce secteur (cf. Section 1.2.3; e.g. Massom et al., 2009; Mezgec et al., 2017), est nécessaire pour permettre de caractériser la variabilité du climat de la Terre Adélie au cours des dernières décennies et des derniers siècles.

Comprendre les mécanismes de grande échelle agissant sur la variabilité du climat de ce secteur (e.g. le lien avec les grands modes de variabilité du climat), évaluer la réponse du climat de ce secteur à des perturbations naturelles (e.g. éruptions volcaniques majeures, activité solaire), et aux perturbations anthropiques (e.g. destruction de l'ozone stratosphérique, influence humaine sur le climat planétaire) sont autant de questions qui restent ouvertes. Pour y répondre, il est indispensable de disposer de davantage d'observations (y compris les informations issues des archives naturelles du climat), mais aussi d'améliorer la fiabilité des outils de modélisation du climat pour cette région, et leur capacité à représenter correctement le spectre de variabilité naturelle, et les processus clé (e.g. glace de mer antarctique, transport d'humidité, couche limite polaire, vents catabatiques, interactions atmosphère-cryosphère-océan). Ces développements sont également essentiels pour pouvoir évaluer les risques futurs pour cette région associés au changement climatique.

Bibliographie

Abram, N. J., Mulvaney, R., and Arrowsmith, C.: Environmental signals in a highly resolved ice core from James Ross Island, Antarctica, Journal of Geophysical Research: Atmospheres, 2011, 116; D20, p. 1-15.

Abram, N. J., Mulvaney, R., Wolff, E. W., Triest, J., Kipfstuhl, S., Trusel, L. D., Vimeux, F., Fleet, L., and Arrowsmith, C.: Acceleration of snow melt in an Antarctic Peninsula ice core during the twentieth century, Nature Geoscience, 2013, 6; 5, p. 404-411.

Abram, N. J., Mulvaney, R., Vimeux, F., Phipps, S. J., Turner, J., and England, M. H.: Evolution of the Southern Annular Mode during the past millennium, Nature Climate Change, 2014, 4; 7, p. 564-569.

Abram, N. J., McGregor, H. V., Tierney, J. E., Evans, M. N., McKay, N. P., Kaufman, D. S., Thirumalai, K., Martrat, B., Goosse, H., and Phipps, S. J.: Early onset of industrial-era warming across the oceans and continents, Nature, 2016, 536; 7617, p. 411-418.

Adolphs, U., and Wendler, G.: A pilot study on the interactions between katabatic winds and polynyas at the Adélie Coast, eastern Antarctica, Antarctic Science, 1995, 7; 3, p. 307-314.

Agency, I. A. E.: Isotopes de l'environnement dans le cycle hydrologique, Agence internationale de l'energie atomique, 2008.

Agosta, C.: Evolution du bilan de masse de surface Antarctique par régionalisation physique et contribution aux variations du niveau des mers, Th. : Terre Univers Environnement, Université Grenoble Alpes, 2012, 175 pp.

Agosta, C., Favier, V., Genthon, C., Gallée, H., Krinner, G., Lenaerts, J. T., and van den Broeke, M. R.: A 40-year accumulation dataset for Adelie Land, Antarctica and its application for model validation, Climate dynamics, 2012, 38; 1-2, p. 75-86.

Agosta, C., Favier, V., Krinner, G., Gallée, H., Fettweis, X., and Genthon, C.: High-resolution modelling of the Antarctic surface mass balance, application for the twentieth, twenty first and twenty second centuries, Climate dynamics, 2013, 41; 11-12, p. 3247-3260.

Altnau, S., Schlosser, E., Isaksson, E., and Divine, D.: Climatic signals from 76 shallow firn cores in Dronning Maud Land, East Antarctica, The Cryosphere, 2015, 9; 3, p. 925-944.

Amakasu, K., Ono, A., Hirano, D., Moteki, M., and Ishimaru, T.: Distribution and density of Antarctic krill (Euphausia superba) and ice krill (E. crystallorophias) off Adélie Land in austral summer 2008 estimated by acoustical methods, Polar Science, 2011, 5; 2, p. 187-194.

Amory, C., Trouvilliez, A., Gallée, H., Favier, V., Naaim-Bouvet, F., Genthon, C., Agosta, C., Piard, L., and Bellot, H.: Comparison between observed and simulated aeolian snow mass fluxes in Adélie Land, East Antarctica, The Cryosphere Discussions, 2015, 9, p. 1373-1383.

Amory, C., Naaim-Bouvet, F., Gallée, H., and Vignon, E.: Brief communication: Two well-marked cases of aerodynamic adjustment of sastrugi, The Cryosphere, 2016, 10; 2, p. 743-750.

Amory, C., Gallée, H., Naaim-Bouvet, F., Favier, V., Vignon, E., Picard, G., Trouvilliez, A., Piard, L., Genthon, C., and Bellot, H.: Seasonal variations in drag coefficient over a sastrugi-covered snowfield in coastal East Antarctica, Boundary-Layer Meteorology, 2017, 164; 1, p. 107-133.

Arblaster, J. M., and Meehl, G. A.: Contributions of external forcings to southern annular mode trends, Journal of climate, 2006, 19; 12, p. 2896-2905.

Armour, K. C., Marshall, J., Scott, J. R., Donohoe, A., and Newsom, E. R.: Southern Ocean warming delayed by circumpolar upwelling and equatorward transport, Nature Geoscience, 2016, 9; 7, p. 549-554.

Arthern, R. J., Winebrenner, D. P., and Vaughan, D. G.: Antarctic snow accumulation mapped using polarization of 4.3-cm wavelength microwave emission, Journal of Geophysical Research: Atmospheres, 2006, 111; D6, p. 1-10.

Baertschi, P.: Absolute18O content of standard mean ocean water, Earth and Planetary Science Letters, 1976, 31; 3, p. 341-344.

Ball, F.: The theory of strong katabatic winds, Australian Journal of Physics, 1956, 9; 3, p. 373-386.

Ball, F.: The katabatic winds of adélie land and king george v land, Tellus, 1957, 9; 2, p. 201-208.

Barbraud, C., and Weimerskirch, H.: Antarctic birds breed later in response to climate change, Proceedings of the National Academy of Sciences, 2006, 103; 16, p. 6248-6251.

Barral, H.: Couches limites atmosphériques en Antarctique: observation et simulation numérique, Th., Université Grenoble Alpes, 2014, 211 pp.

Barral, H., Genthon, C., Trouvilliez, A., Brun, C., and Amory, C.: Blowing snow in coastal Adélie Land, Antarctica: three atmospheric-moisture issues, The Cryosphere, 2014, 8; 5, p. 1905-1919.

Benetti, M., Reverdin, G., Pierre, C., Merlivat, L., Risi, C., Steen-Larsen, H. C., and Vimeux, F.: Deuterium excess in marine water vapor: Dependency on relative humidity and surface wind speed during evaporation, Journal of Geophysical Research: Atmospheres, 2014, 119; 2, p. 584-593.

Berger, A.: Milankovitch theory and climate, Reviews of geophysics, 1988, 26; 4, p. 624-657.

Bertler, N., Mayewski, P., and Carter, L.: Cold conditions in Antarctica during the Little Ice Age—Implications for abrupt climate change mechanisms, Earth and Planetary Science Letters, 2011, 308; 1, p. 41-51.

Bertler, N. A., Conway, H., Dahl-Jensen, D., Emanuelsson, D. B., Winstrup, M., Vallelonga, P. T., Lee, J. E., Brook, E. J., Severinghaus, J. P., and Fudge, T. J.: The Ross Sea Dipole–temperature, snow accumulation and sea ice variability in the Ross Sea region, Antarctica, over the past 2700 years, Climate of the Past, 2018, 14; 2, p. 193-214.

Bintanja, R.: The contribution of snowdrift sublimation to the surface mass balance of Antarctica, Annals of Glaciology, 1998, 27, p. 251-259.

Bintanja, R.: Snowdrift suspension and atmospheric turbulence. Part I: Theoretical background and model description, Boundary-layer meteorology, 2000, 95; 3, p. 343-368.

Blázquez, J., and Solman, S. A.: Interannual variability of the frontal activity in the Southern Hemisphere: relationship with atmospheric circulation and precipitation over southern South America, Climate Dynamics, 2017, 48; 7-8, p. 2569-2579.

Bonne, J.-L., Masson-Delmotte, V., Cattani, O., Delmotte, M., Risi, C., Sodemann, H., and Steen-Larsen, H.: The isotopic composition of water vapour and precipitation in Ivittuut, southern Greenland, Atmospheric Chemistry and Physics, 2014, 14; 9, p. 4419-4439.

Bonne, J. L., Steen-Larsen, H. C., Risi, C., Werner, M., Sodemann, H., Lacour, J. L., Fettweis, X., Cesana, G., Delmotte, M., and Cattani, O.: The summer 2012 Greenland heat wave: In situ and remote sensing observations of water vapor isotopic composition during an atmospheric river event, Journal of Geophysical Research: Atmospheres, 2015, 120; 7, p. 2970-2989.

Bothe, O., Evans, M., Donado, L. F., Bustamante, E. G., Gergis, J., Gonzalez-Rouco, J., Goosse, H., Hegerl, G., Hind, A., and Jungclaus, J. H.: Continental-scale temperature variability in PMIP3 simulations and PAGES 2k regional temperature reconstructions over the past millennium, Climate of the Past, 2015, 11, p. 1673-1699.

Bouchard, A., Rabier, F., Guidard, V., and Karbou, F.: Enhancements of satellite data assimilation over Antarctica, Monthly Weather Review, 2010, 138; 6, p. 2149-2173.

Bracegirdle, T. J., and Marshall, G. J.: The reliability of Antarctic tropospheric pressure and temperature in the latest global reanalyses, Journal of Climate, 2012, 25; 20, p. 7138-7146.

Bréant, C., Leroy Dos Santos, C., Casado, M., Fourré, E., Goursaud, S., Masson-Delmotte, V., Favier, V., Agosta, C., Cattani, O., Prié, F., Golly, B., Orsi, A., and Martinerie, P.: Coastal water vapor isotopic composition driven by katabatic wind variability in summer at Dumont d'Urville, coastal East Antarctica, Earth and Planetary Science Letters, submitted.

Bromwich, D. H., and Weaver, C. J.: Latitudinal displacement from main moisture source controls δ18O of snow in coastal Antarctica, Nature, 1983, 301; 5896, p. 145-147.

Bromwich, D. H.: Snowfall in high southern latitudes, Reviews of Geophysics, 1988, 26; 1, p. 149-168.

Bromwich, D. H., and Smith, S. R.: US FROST: Data and Science Plan Report from the US FROST Workshop, Byrd Polar Research Center, The Ohio State University.0896-2472, 1993.

Bromwich, D. H., and Fogt, R. L.: Strong trends in the skill of the ERA-40 and NCEP–NCAR reanalyses in the high and midlatitudes of the Southern Hemisphere, 1958–2001, Journal of Climate, 2004, 17; 23, p. 4603-4619.

Bromwich, D. H., Fogt, R. L., Hodges, K. I., and Walsh, J. E.: A tropospheric assessment of the ERA-40, NCEP, and JRA-25 global reanalyses in the polar regions, Journal of Geophysical Research: Atmospheres, 2007, 112; D10, p. 1-21.

Bromwich, D. H., Nicolas, J. P., and Monaghan, A. J.: An assessment of precipitation changes over Antarctica and the Southern Ocean since 1989 in contemporary global reanalyses, Journal of Climate, 2011, 24; 16, p. 4189-4209.

Bromwich, D. H., Steinhoff, D. F., Simmonds, I., Keay, K., and Fogt, R. L.: Climatological aspects of cyclogenesis near Adélie Land Antarctica, Tellus A, 2011, 63; 5, p. 921-938.

Bromwich, D. H., Nicolas, J. P., Monaghan, A. J., Lazzara, M. A., Keller, L. M., Weidner, G. A., and Wilson, A. B.: Central West Antarctica among the most rapidly warming regions on Earth, Nature Geoscience, 2013, 6; 2, p. 139-145.

Brutsaert, W.: A theory for local evaporation (or heat transfer) from rough and smooth surfaces at ground level, Water resources research, 1975, 11; 4, p. 543-550.

Butzin, M., Werner, M., Masson-Delmotte, V., Risi, C., Frankenberg, C., Gribanov, K., Jouzel, J., and Zakharov, V. I.: Variations of oxygen-18 in West Siberian precipitation during the last 50 years, Atmospheric Chemistry and Physics, 2014, 14; 11, p. 5853-5869.

Caiazzo, L., Becagli, S., Frosini, D., Giardi, F., Severi, M., Traversi, R., and Udisti, R.: Spatial and temporal variability of snow chemical composition and accumulation rate at Talos Dome site (East Antarctica), Science of the Total Environment, 2016, 550, p. 418-430.

Campbell, G., Pope, A., Lazzara, M., and Scambos, T.: The Coldest Place On Earth:-90° C and Below in East Antarctica from Landsat-8 and other Thermal Sensors, AGU Fall Meeting Abstracts, 2013.

Cappa, C. D., Hendricks, M. B., DePaolo, D. J., and Cohen, R. C.: Isotopic fractionation of water during evaporation, Journal of Geophysical Research: Atmospheres, 2003, 108; D16, p. 1-10.

Casado, M., Landais, A., Masson-Delmotte, V., Genthon, C., Kerstel, E., Kassi, S., Arnaud, L., Picard, G., Prie, F., and Cattani, O.: Continuous measurements of isotopic composition of water vapour on the East Antarctic Plateau, Atmospheric Chemistry and Physics, 2016, 16; 13, p. 8521-8538.

Casado, M., Landais, A., Masson-Delmotte, V., Genthon, C., Kerstel, E., Kassi, S., Arnaud, L., Picard, G., Prie, F., Cattani, O., Steen-Larsen, H. C., Vignon, E., and Cermak, P.: Continuous measurements of isotopic composition of water vapour on the East Antarctic Plateau, Atmos. Chem. Phys., 2016, 16; 13, p. 8521-8538.

Cassou, C., and Guilyardi, É.: Modes de variabilité et changement climatique: Synthèse du quatrième rapport d'évaluation du Giec, La Météorologie, 2007, 59, p. 22-30.

Cavalieri, D., Parkinson, C., Gloersen, P., and Zwally, H.: updated yearly: Sea Ice Concentrations from Nimbus-7 SMMR and DMSP SSM/I-SSMIS Passive Microwave Data, Version 1 [1979-2014]. Boulder, Colorado USA. NASA National Snow and Ice Data Center Distributed Active Archive Center, 1996.

Chapman, W. L., and Walsh, J. E.: A synthesis of Antarctic temperatures, Journal of Climate, 2007, 20; 16, p. 4096-4117.

Chen, X., Zhang, X., Church, J. A., Watson, C. S., King, M. A., Monselesan, D., Legresy, B., and Harig, C.: The increasing rate of global mean sea-level rise during 1993–2014, Nature Climate Change, 2017, 7; 7, p. 492-495.

Cherel, Y.: Isotopic niches of emperor and Adélie penguins in Adélie Land, Antarctica, Marine Biology, 2008, 154; 5, p. 813-821.

Cherel, Y., Koubbi, P., Giraldo, C., Penot, F., Tavernier, E., Moteki, M., Ozouf-Costaz, C., Causse, R., Chartier, A., and Hosie, G.: Isotopic niches of fishes in coastal, neritic and oceanic waters off Adélie Land, Antarctica, Polar Science, 2011, 5; 2, p. 286-297.

Church, J. A., Clark, P. U., Cazenave, A., Gregory, J. M., Jevrejeva, S., Levermann, A., Merrifield, M. A., Milne, G. A., Nerem, R. S., and Nunn, P. D.: Sea level change, PM Cambridge University Press, 2013.

Ciais, P., and Jouzel, J.: Deuterium and oxygen 18 in precipitation: Isotopic model, including mixed cloud processes, Journal of Geophysical Research: Atmospheres, 1994, 99; D8, p. 16793-16803.

Ciais, P., White, J., Jouzel, J., and Petit, J.: The origin of present-day Antarctic precipitation from surface snow deuterium excess data, Journal of Geophysical Research: Atmospheres, 1995, 100; D9, p. 18917-18927.

Collins, W. D., Bitz, C. M., Blackmon, M. L., Bonan, G. B., Bretherton, C. S., Carton, J. A., Chang, P., Doney, S. C., Hack, J. J., and Henderson, T. B.: The community climate system model version 3 (CCSM3), Journal of Climate, 2006, 19; 11, p. 2122-2143.

Comiso, J. C.: Variability and trends in Antarctic surface temperatures from in situ and satellite infrared measurements, Journal of Climate, 2000, 13; 10, p. 1674-1696.

Comiso, J. C., Gersten, R. A., Stock, L. V., Turner, J., Perez, G. J., and Cho, K.: Positive trend in the Antarctic sea ice cover and associated changes in surface temperature, Journal of Climate, 2017, 30; 6, p. 2251-2267.

Connolley, W.: The Antarctic temperature inversion, International Journal of Climatology: A Journal of the Royal Meteorological Society, 1996, 16; 12, p. 1333-1342.

Connolley, W. M., and Bracegirdle, T. J.: An Antarctic assessment of IPCC AR4 coupled models, Geophysical Research Letters, 2007, 34; 22, p. 1-6.

Cotte, C., and Guinet, C.: Historical whaling records reveal major regional retreat of Antarctic sea ice, Deep Sea Research Part I: Oceanographic Research Papers, 2007, 54; 2, p. 243-252.

Craig, H., and Gordon, L.: Stable Isotopes in Oceanographic Studies and Paleotemperatures, Tongiorgi, 1965, p. 9-130.

Cristofari, R., Bertorelle, G., Ancel, A., Benazzo, A., Le Maho, Y., Ponganis, P. J., Stenseth, N. C., Trathan, P. N., Whittington, J. D., and Zanetti, E.: Full circumpolar migration ensures evolutionary unity in the Emperor penguin, Nature communications, 2016, 7; 11842, p. 1-9.

Crosta, X., Denis, D., and Ther, O.: Sea ice seasonality during the Holocene, Adélie Land, East Antarctica, Marine Micropaleontology, 2008, 66; 3-4, p. 222-232.

Cuffey, K. M., and Steig, E. J.: Isotopic diffusion in polar firn: implications for interpretation of seasonal climate parameters in ice-core records, with emphasis on central Greenland, Journal of Glaciology, 1998, 44; 147, p. 273-284.

Cuffey, K. M., Clow, G. D., Steig, E. J., Buizert, C., Fudge, T., Koutnik, M., Waddington, E. D., Alley, R. B., and Severinghaus, J. P.: Deglacial temperature history of West Antarctica, Proceedings of the National Academy of Sciences, 2016, 113; 50, p. 14249-14254.

Cunde, X., Jiawen, R., Dahe, Q., Zhongqin, L., Weizhen, S., and Allison, I.: Complexity of the climatic regime over the Lambert Glacier basin of the East Antarctic ice sheet: firn-core evidences, Journal of Glaciology, 2001, 47; 156, p. 160-162.

Dahl-Jensen, D., Mosegaard, K., Gundestrup, N., Clow, G. D., Johnsen, S. J., Hansen, A. W., and Balling, N.: Past temperatures directly from the Greenland ice sheet, Science, 1998, 282; 5387, p. 268-271.

Dansgaard, W.: The Abundance of O18 in Atmospheric Water and Water Vapour, Tellus, 1953, 5; 4, p. 461-469.

Dansgaard, W.: Stable isotopes in precipitation, Tellus, 1964, 16; 4, p. 436-468.

Dee, D., Uppala, S., Simmons, A., Berrisford, P., Poli, P., Kobayashi, S., Andrae, U., Balmaseda, M., Balsamo, G., and Bauer, P.: The ERA-Interim reanalysis: Configuration and performance of the data assimilation system, Quarterly Journal of the Royal Meteorological Society, 2011, 137; 656, p. 553-597.

Dee, D. P., Uppala, S., Simmons, A., Berrisford, P., Poli, P., Kobayashi, S., Andrae, U., Balmaseda, M., Balsamo, G., and Bauer, P.: The ERA-Interim reanalysis: Configuration and performance of the data assimilation system, Quarterly Journal of the royal meteorological society, 2011, 137; 656, p. 553-597.

Delaygue, G., Jouzel, J., Masson, V., Koster, R. D., and Bard, E.: Validity of the isotopic thermometer in central Antarctica: limited impact of glacial precipitation seasonality and moisture origin, Geophysical Research Letters, 2000, 27; 17, p. 2677-2680.

Delmas, R., and Pourchet, M.: Utilisation de filtres échangeurs d'ions pour l'étude de l'activité globale d'un carottage glaciologique, International Association of Hydrological Sciences Publication, 1977, 118, p. 159-163.

Delmotte, M., Masson, V., Jouzel, J., and Morgan, V. I.: A seasonal deuterium excess signal at Law Dome, coastal eastern Antarctica: a southern ocean signature, Journal of Geophysical Research: Atmospheres, 2000, 105; D6, p. 7187-7197.

Denis, D., Crosta, X., Zaragosi, S., Romero, O., Martin, B., and Mas, V.: Seasonal and subseasonal climate changes recorded in laminated diatom ooze sediments, Adelie Land, East Antarctica, The Holocene, 2006, 16; 8, p. 1137-1147.

Ding, Q., Steig, E. J., Battisti, D. S., and Wallace, J. M.: Influence of the tropics on the Southern Annular Mode, Journal of Climate, 2012, 25; 18, p. 6330-6348.

Dittmann, A., Schlosser, E., Masson-Delmotte, V., Powers, J. G., Manning, K. W., Werner, M., and Fujita, K.: Precipitation regime and stable isotopes at Dome Fuji, East Antarctica, Atmospheric Chemistry and Physics, 2016, 16; 11, p. 6883-6900.

Dowsett, H., Barron, J., and Poore, R.: Middle Pliocene sea surface temperatures: a global reconstruction, Marine Micropaleontology, 1996, 27; 1-4, p. 13-25.

Draxler, R. R., and Hess, G.: An overview of the HYSPLIT_4 modelling system for trajectories, Australian meteorological magazine, 1998, 47; 4, p. 295-308.

Drumond, A., Muñiz, R. N., and Presa, L. G.: A Lagrangian approach for investigating anomalies in the moisture transport during drought episodes, Cuadernos de investigación geográfica, 2016; 42, p. 113-125.

Dufour, A.: Water vapour transport to the high latitudes : mechanisms and variability from reanalyses and radiosoundings, Th. : Terre Univers Environnement, Université Grenoble Alpes, 2016, 110 pp.

Durre, I., Vose, R. S., and Wuertz, D. B.: Overview of the integrated global radiosonde archive, Journal of Climate, 2006, 19; 1, p. 53-68.

Dütsch, M., Pfahl, S., and Sodemann, H.: The impact of nonequilibrium and equilibrium fractionation on two different deuterium excess definitions, Journal of Geophysical Research: Atmospheres, 2017, 122; 23, p. 732-746.

Eisen, O., Frezzotti, M., Genthon, C., Isaksson, E., Magand, O., van den Broeke, M. R., Dixon, D. A., Ekaykin, A., Holmlund, P., and Kameda, T.: Ground-based measurements of spatial and temporal variability of snow accumulation in East Antarctica, Reviews of Geophysics, 2008, 46; 2, p. 1-39.

Eisenman, I., Meier, W. N., and Norris, J. R.: A spurious jump in the satellite record: has Antarctic sea ice expansion been overestimated?, The Cryosphere, 2014, 8, p. 1289-1296.

Ekaykin, A., Kozachek, A., Lipenkov, V. Y., and Shibaev, Y. A.: Multiple climate shifts in the Southern Hemisphere over the past three centuries based on central Antarctic snow pits and core studies, Annals of Glaciology, 2014, 55; 66, p. 259-266.

Ekaykin, A. A., Lipenkov, V. Y., Kuzmina, I. N., Petit, J. R., Masson-Delmotte, V., and Johnsen, S. J.: The changes in isotope composition and accumulation of snow at Vostok station, East Antarctica, over the past 200 years, Annals of Glaciology, 2004, 39, p. 569-575.

Ekaykin, A. A., Vladimirova, D. O., Lipenkov, V. Y., and Masson-Delmotte, V.: Climatic variability in Princess Elizabeth Land (East Antarctica) over the last 350 years, Climate of the Past, 2017, 13; 1, p. 61-71.

Emanuelsson, B. D., Bertler, N. A., Neff, P. D., Renwick, J. A., Markle, B. R., Baisden, W. T., and Keller, E. D.: The role of Amundsen–Bellingshausen Sea anticyclonic circulation in forcing marine air intrusions into West Antarctica, Climate Dynamics, 2018, p. 1-18.

Essou, G. R. C.: Potentiel des données de précipitation et température des réanalyses atmosphériques en modélisation hydrologique, Th. : École de technologie supérieure, Université du Québec, 2016, 271 pp.

Etheridge, D. M., Steele, L. P., Francey, R., and Langenfelds, R.: Atmospheric methane between 1000 AD and present: Evidence of anthropogenic emissions and climatic variability, Journal of Geophysical Research: Atmospheres, 1998, 103; D13, p. 15979-15993.

Fan, T., Deser, C., and Schneider, D. P.: Recent Antarctic sea ice trends in the context of Southern Ocean surface climate variations since 1950, Geophysical Research Letters, 2014, 41; 7, p. 2419-2426.

Favier, V., Agosta, C., Genthon, C., Arnaud, L., Trouvillez, A., and Gallée, H.: Modeling the mass and surface heat budgets in a coastal blue ice area of Adelie Land, Antarctica, Journal of Geophysical Research: Earth Surface, 2011, 116; F3, p. 1-14.

Favier, V., Agosta, C., Parouty, S., Durand, G., Delaygue, G., Gallée, H., Drouet, A.-S., Trouvilliez, A., and Krinner, G.: An updated and quality controlled surface mass balance dataset for Antarctica, The Cryosphere, 2013, 7; 2, p. 583-597.

Favier, V., Agosta, C., Parouty, S., Durand, G., Delaygue, G., Gallée, H., Drouet, A.-S., Trouvilliez, A., and Krinner, G.: An updated and quality controlled surface mass balance dataset for Antarctica, Cryosphere, 2013, 7; 2, p. p. 583-p. 597.

Favier, V., Agosta, C., Parouty, S., Durand, G., Delaygue, G., Gallée, H., Drouet, A. S., Trouvilliez, A., and Krinner, G.: An updated and quality controlled surface mass balance dataset for Antarctica, The Cryosphere, 2013, 7; 2, p. 583-597.

Favier, V., Krinner, G., Amory, C., Gallée, H., Beaumet, J., and Agosta, C.: Antarctica-Regional Climate and Surface Mass Budget, Current Climate Change Reports, 2017, 3; 4, p. 303-315.

Fegyveresi, J. M., Alley, R., Spencer, M., Fitzpatrick, J., Steig, E., White, J., McConnell, J., and Taylor, K.: Late-Holocene climate evolution at the WAIS Divide site, West Antarctica: bubble number-density estimates, Journal of Glaciology, 2011, 57; 204, p. 629-638.

Fernandoy, F., Meyer, H., Oerter, H., Wilhelms, F., Graf, W., and Schwander, J.: Temporal and spatial variation of stable-isotope ratios and accumulation rates in the hinterland of Neumayer station, East Antarctica, Journal of glaciology, 2010, 56; 198, p. 673-687.

Fernandoy, F., Meyer, H., and Tonelli, M.: Stable water isotopes of precipitation and firn cores from the northern Antarctic Peninsula region as a proxy for climate reconstruction, The Cryosphere, 2012, 6; 2, p. 313-330.

Fernandoy, F., Tetzner, D., Meyer, H., Gacitúa, G., Hoffmann, K., Falk, U., Lambert, F., and MacDonell, S.: New insights into the use of stable water isotopes at the northern Antarctic Peninsula as a tool for regional climate studies, The Cryosphere, 2018, 12; 3, p. 1069-1090.

Fischer, E. M., Luterbacher, J., Zorita, E., Tett, S., Casty, C., and Wanner, H.: European climate response to tropical volcanic eruptions over the last half millennium, Geophysical research letters, 2007, 34; 5, p. 1-6.

Fischer, H., Severinghaus, J., Brook, E., Wolff, E., Albert, M., Alemany, O., Arthern, R., Bentley, C., Blankenship, D., and Chappellaz, J.: Where to find 1.5 million yr old ice for the IPICS" Oldest-Ice" ice core, Climate of the Past, 2013, 9; 6, p. 2489-2505.

Flato, G., Marotzke, J., Abiodun, B., Braconnot, P., Chou, S. C., Collins, W. J., Cox, P., Driouech, F., Emori, S., and Eyring, V.: Evaluation of climate models. In: climate change 2013: the physical science basis. Contribution of working group I to the fifth assessment report of the intergovernmental panel on climate change, Climate Change 2013, 2013, 5, p. 741-866.

Fogg, G. E., and Fogg, G. E.: A history of Antarctic science, Cambridge University Press, 1992.

Fogt, R. L., Perlwitz, J., Monaghan, A. J., Bromwich, D. H., Jones, J. M., and Marshall, G. J.: Historical SAM variability. Part II: Twentieth-century variability and trends from reconstructions, observations, and the IPCC AR4 models, Journal of Climate, 2009, 22; 20, p. 5346-5365.

Fogt, R. L., Goergens, C. A., Jones, J. M., Schneider, D. P., Nicolas, J. P., Bromwich, D. H., and Dusselier, H. E.: A twentieth century perspective on summer Antarctic pressure change and variability and contributions from tropical SSTs and ozone depletion, Geophysical Research Letters, 2017, 44; 19, p. 9918-9927.

Fogt, R. L., Clark, L. N., and Nicolas, J. P.: A New Monthly Pressure Dataset Poleward of 60° S since 1957, Journal of Climate, 2018, 31; 10, p. 3865-3874.

Frezzotti, M., Urbini, S., Proposito, M., Scarchilli, C., and Gandolfi, S.: Spatial and temporal variability of surface mass balance near Talos Dome, East Antarctica, Journal of Geophysical Research: Earth Surface, 2007, 112; F2, p. 1-15.

Fudge, T., Markle, B. R., Cuffey, K. M., Buizert, C., Taylor, K. C., Steig, E. J., Waddington, E. D., Conway, H., and Koutnik, M.: Variable relationship between accumulation and temperature in West Antarctica for the past 31,000 years, Geophysical Research Letters, 2016, 43; 8, p. 3795-3803.

Fujita, K., and Abe, O.: Stable isotopes in daily precipitation at Dome Fuji, East Antarctica, Geophysical Research Letters, 2006, 33; 18, p. 1-4.

Gallée, H., and Schayes, G.: Development of a three-dimensional meso-γ primitive equation model: katabatic winds simulation in the area of Terra Nova Bay, Antarctica, Monthly Weather Review, 1994, 122; 4, p. 671-685.

Gallée, H.: Simulation of the mesocyclonic activity in the Ross Sea, Antarctica, Monthly Weather Review, 1995, 123; 7, p. 2051-2069.

Gallée, H., and Pettré, P.: Dynamical constraints on katabatic wind cessation in Adélie Land, Antarctica, Journal of the atmospheric sciences, 1998, 55; 10, p. 1755-1770.

Gallée, H., Guyomarc'h, G., and Brun, E.: Impact of snow drift on the Antarctic ice sheet surface mass balance: possible sensitivity to snow-surface properties, Boundary-Layer Meteorology, 2001, 99; 1, p. 1-19.

Gallée, H., Trouvilliez, A., Agosta, C., Genthon, C., Favier, V., and Naaim-Bouvet, F.: Transport of snow by the wind: A comparison between observations in Adélie Land, Antarctica, and simulations made with the regional climate model MAR, Boundary-layer meteorology, 2013, 146; 1, p. 133-147.

Genthon, C., Lardeux, P., and Krinner, G.: The surface accumulation and ablation of a coastal blue-ice area near Cap Prudhomme, Terre Adélie, Antarctica, Journal of Glaciology, 2007, 53; 183, p. 635-645.

Genthon, C., Six, D., Favier, V., Lazzara, M., and Keller, L.: Atmospheric temperature measurement biases on the Antarctic plateau, Journal of Atmospheric and Oceanic Technology, 2011, 28; 12, p. 1598-1605.

Gignac, C.: Utilisation de la télédétection radar haute-résolution pour l'étude du régime glaciel marin au voisinage des infrastructures maritimes du Nunavik, Th. , Université du Québec, Institut national de la recherche scientifique, 2012.

Ginot, P., Stampfli, F., Stampfli, D., Schwikowski, M., and Gaggeler, H.: FELICS, a new ice core drilling system for high-altitude glaciers, Memoirs of National Institute of Polar Research. Special issue, 2002, 56, p. 38-48.

Gloersen, P.: Global maps of sea ice cencentration age and surface temperature derived from NIMBUS-7 SSMR: A case study, Oceanography from Space, 1981, 777, p.

Gonfiantini, R.: Standards for stable isotope measurements in natural compounds, Nature, 1978, 271; 5645, p. 534-536.

Goosse, H., Braida, M., Crosta, X., Mairesse, A., Masson-Delmotte, V., Mathiot, P., Neukom, R., Oerter, H., Philippon, G., and Renssen, H.: Antarctic temperature changes during the last millennium: evaluation of simulations and reconstructions, Quaternary Science Reviews, 2012, 55, p. 75-90.

Goosse, H.: Reconstructed and simulated temperature asymmetry between continents in both hemispheres over the last centuries, Climate Dynamics, 2017, 48; 5-6, p. 1483-1501.

Gordon, C., Cooper, C., Senior, C. A., Banks, H., Gregory, J. M., Johns, T. C., Mitchell, J. F., and Wood, R. A.: The simulation of SST, sea ice extents and ocean heat transports in a version of the Hadley Centre coupled model without flux adjustments, Climate dynamics, 2000, 16; 2-3, p. 147-168.

Gorodetskaya, I., Kneifel, S., Maahn, M., Van Tricht, K., Thiery, W., Schween, J., Mangold, A., Crewell, S., and Van Lipzig, N.: Cloud and precipitation properties from ground-based remote-sensing instruments in East Antarctica, The Cryosphere, 2015, 9; 1, p. 285-304.

Goursaud, S., Masson-Delmotte, V., Favier, V., Preunkert, S., Fily, M., Gallée, H., Jourdain, B., Legrand, M., Magand, O., and Minster, B.: A 60-year ice-core record of regional climate from Adélie Land, coastal Antarctica, The Cryosphere, 2017, 11; 1, p. 343-362.

Goursaud, S., Masson-Delmotte, V., Favier, V., Orsi, A., and Werner, M.: Water stable isotope spatio-temporal variability in Antarctica in 1960–2013: observations and simulations from the ECHAM5-wiso atmospheric general circulation model, Clim. Past, 2018, 14; 6, p. 923-946.

Goursaud, S., Masson-Delmotte, V., Favier, V., Preunkert, S., Legrand, M., Minster, B., and Werner, M.: Challenges associated with the climatic interpretation of water stable isotope records from a highly resolved firn core from Adélie Land, coastal Antarctica, The Cryosphere Discuss., 2018, 2018, p. 1-55.

Graf, W., Reinwarth, O., Moser, H., Minikin, A., Wagenbach, D., Kipfstuhl, J., and Oerter, H.: Isotopic and chemical investigations of 10 m firn cores from the eastern part of the Ronne Ice Shelf, Antarctica, FRISP Rep, 1991, 5, p. 45-53.

Graf, W., Oerter, H., Reinwarth, O., Stichler, W., Wilhelms, F., Miller, H., and Mulvaney, R.: Stable-isotope records from Dronning Maud Land, Antarctica, Annals of Glaciology, 2002, 35; 1, p. 195-201.

Grazioli, J., Genthon, C., Boudevillain, B., Duran-Alarcon, C., Del Guasta, M., Jean-Baptiste, M., and Berne, A.: Measurements of precipitation in Dumont d'Urville, Adélie Land, East Antarctica, The Cryosphere, 2017, 11; 4, p. 1797-1811.

Grazioli, J., Madeleine, J.-B., Gallée, H., Forbes, R. M., Genthon, C., Krinner, G., and Berne, A.: Katabatic winds diminish precipitation contribution to the Antarctic ice mass balance, Proceedings of the National Academy of Sciences, 2017, 114; 41, p. 10858-10863.

Guillet, S., Corona, C., Stoffel, M., Khodri, M., Lavigne, F., Ortega, P., Eckert, N., Sielenou, P. D., Daux, V., and Churakova, O. v.: Climate response to the Samalas volcanic eruption in 1257 revealed by proxy records, Nature Geoscience, 2017, 10; 2, p. 123-127.

Hack, J. J., Caron, J. M., Yeager, S. G., Oleson, K. W., Holland, M. M., Truesdale, J. E., and Rasch, P. J.: Simulation of the global hydrological cycle in the CCSM Community Atmosphere Model version 3 (CAM3): Mean features, Journal of climate, 2006, 19; 11, p. 2199-2221.

Hakim, G. J., Emile-Geay, J., Steig, E. J., Noone, D., Anderson, D. M., Tardif, R., Steiger, N., and Perkins, W. A.: The last millennium climate reanalysis project: Framework and first results, Journal of Geophysical Research: Atmospheres, 2016, 121; 12, p. 6745-6764.

Helsen, M.: On the interpretation of stable isotopes in Antarctic precipitation, Th. : Institute for Marine and Atmospheric research Utrecht, Department of Physics and Astronomy, Utrecht University, 2006, 158 pp.

Helsen, M., Van de Wal, R., Van den Broeke, M., Masson-Delmotte, V., Meijer, H., Scheele, M., and Werner, M.: Modeling the isotopic composition of Antarctic snow using backward trajectories: Simulation of snow pit records, Journal of Geophysical Research: Atmospheres, 2006, 111; D15, p. 1-19.

Helsen, M., Van de Wal, R., and Van den Broeke, M.: The isotopic composition of present-day Antarctic snow in a Lagrangian atmospheric simulation, Journal of Climate, 2007, 20; 4, p. 739-756.

Hines, K. M., Bromwich, D. H., and Marshall, G. J.: Artificial surface pressure trends in the NCEP–NCAR reanalysis over the Southern Ocean and Antarctica, Journal of Climate, 2000, 13; 22, p. 3940-3952.

Hobbs, W. R., Massom, R., Stammerjohn, S., Reid, P., Williams, G., and Meier, W.: A review of recent changes in Southern Ocean sea ice, their drivers and forcings, Global and Planetary Change, 2016, 143, p. 228-250.

Hoffmann, G., Werner, M., and Heimann, M.: Water isotope module of the ECHAM atmospheric general circulation model: A study on timescales from days to several years, Journal of Geophysical Research: Atmospheres, 1998, 103; D14, p. 16871-16896.

Holland, P. R., and Kwok, R.: Wind-driven trends in Antarctic sea-ice drift, Nature Geoscience, 2012, 5; 12, p. 872-875.

Holloway, M. D., Sime, L. C., Singarayer, J. S., Tindall, J. C., Bunch, P., and Valdes, P. J.: Antarctic last interglacial isotope peak in response to sea ice retreat not ice-sheet collapse, Nature communications, 2016, 7; 12293, p. 1-9.

Hoshina, Y., Fujita, K., Nakazawa, F., Iizuka, Y., Miyake, T., Hirabayashi, M., Kuramoto, T., Fujita, S., and Motoyama, H.: Effect of accumulation rate on water stable isotopes of near-surface snow in inland Antarctica, Journal of Geophysical Research: Atmospheres, 2014, 119; 1, p. 274-283.

Hosking, J. S., Fogt, R., Thomas, E. R., Moosavi, V., Phillips, T., Coggins, J., and Reusch, D.: Accumulation in coastal West Antarctic ice core records and the role of cyclone activity, Geophysical Research Letters, 2017, 44; 17, p. 9084-9092.

Hourdin, F., Mauritsen, T., Gettelman, A., Golaz, J.-C., Balaji, V., Duan, Q., Folini, D., Ji, D., Klocke, D., and Qian, Y.: The art and science of climate model tuning, Bulletin of the American Meteorological Society, 2017, 98; 3, p. 589-602.

Inoue, M., Curran, M. A., Moy, A. D., van Ommen, T. D., Fraser, A. D., Phillips, H. E., and Goodwin, I. D.: A glaciochemical study of the 120 m ice core from Mill Island, East Antarctica, Climate of the Past, 2017, 13; 5, p. 437-453.

IPCC: Fifth Assessment Report (AR5): Climate Change 2013/2014: Climate Change 2014: Impacts, Adaptation, and Vulnerability; Part B. Regional Aspects/Edited by Vicente R. Barros (Working Group II Co-Chair, Centro de Investigaciones Del Mar Y la Atmósfera, Universidad de Buenos Aires), Christopher B. Field (Working Group II Co-Chair, Department of Global Ecology, Carnegie Institution for Science), David Jon Dokken (Executive Director), Michael D. Mastrandrea (Co-Director of Science), Katharine J. Mach (Co-Director of Science), T. Eren Bilir, Monalisa Chatterjee, Kristie L. Ebi, Yuka Otsuki Estrada, Robert C. Genova, Betelhem Girma, Eric S. Kissel, Andrew N. Levy, Sandy MacCracken, Patricia R. Mastrandrea, Leslie L. White, Cambridge University Press, 2014.

IPCC, W.: Contribution to the IPCC Fifth Assessment Report, Climate Change, 2013, p. 36.

Isaksson, E., and Karlén, W.: High resolution climatic information from short firn cores, western Dronning Maud Land, Antarctica, Climatic Change, 1994, 26; 4, p. 421-434.

Isaksson, E., and Karlén, W.: Spatial and temporal patterns in snow accumulation, western Dronning Maud Land, Antarctica, Journal of Glaciology, 1994, 40; 135, p. 399-409.

Isaksson, E., Karlén, W., Gundestrup, N., Mayewski, P., Whitlow, S., and Twickler, M.: A century of accumulation and temperature changes in Dronning Maud Land, Antarctica, Journal of Geophysical Research: Atmospheres, 1996, 101; D3, p. 7085-7094.

Jakob, C.: An improved strategy for the evaluation of cloud parameterizations in GCMs, Bulletin of the American Meteorological Society, 2003, 84; 10, p. 1387-1401.

Johnsen, S.: Stable isotope homogenization of polar firn and ice, Isotopes and impurities in snow and ice, 1977, 118, p. 210-219.

Johnsen, S. J., Clausen, H. B., Cuffey, K. M., Hoffmann, G., Schwander, J., and Creyts, T.: Diffusion of stable isotopes in polar firn and ice: the isotope effect in firn diffusion, Physics of ice core records, 2000, 121-140,

Johnsen, S. J., Clausen, H. B., Cuffey, K. M., Hoffmann, G., Schwander, J., and Creyts, T.: Diffusion of stable isotopes in polar firn and ice: the isotope effect in firn diffusion, Physics of ice core records, 2000, 159, p. 121-140.

Jones, D. A., and Simmonds, I.: Time and space spectral analyses of Southern Hemisphere sea level pressure variability, Monthly weather review, 1993, 121; 3, p. 661-672.

Jones, J. M., Gille, S. T., Goosse, H., Abram, N. J., Canziani, P. O., Charman, D. J., Clem, K. R., Crosta, X., De Lavergne, C., and Eisenman, I.: Assessing recent trends in high-latitude Southern Hemisphere surface climate, Nature Climate Change, 2016, 6, p. 917-926.

Jones, P.: Recent variations in mean temperature and the diurnal temperature range in the Antarctic, Geophysical Research Letters, 1995, 22; 11, p. 1345-1348.

Jones, P., and Lister, D.: Antarctic near-surface air temperatures compared with ERA-Interim values since 1979, International Journal of Climatology, 2015, 35; 7, p. 1354-1366.

Jones, P. D., Briffa, K., Osborn, T., Lough, J., Van Ommen, T., Vinther, B., Luterbacher, J., Wahl, E., Zwiers, F., and Mann, M.: High-resolution palaeoclimatology of the last millennium: a review of current status and future prospects, The Holocene, 2009, 19; 1, p. 3-49.

Jones, T., Cuffey, K., White, J., Steig, E., Buizert, C., Markle, B., McConnell, J., and Sigl, M.: Water isotope diffusion in the WAIS Divide ice core during the Holocene and last glacial, Journal of Geophysical Research: Earth Surface, 2017, 122; 1, p. 290-309.

Jourdain, B.: Etude du maillon atmosphérique du cycle biogéochimique du soufre aux hautes latitudes sud (station Dumont d'Urville), Th. : Océan, Atmosphère, Université Joseph-Fourier - Grenoble, I, 2001.

Jourdain, B., and Legrand, M.: Seasonal variations of atmospheric dimethylsulfide, dimethylsulfoxide, sulfur dioxide, methanesulfonate, and non-sea-salt sulfate aerosols at Dumont d'Urville (coastal Antarctica)(December 1998 to July 1999), Journal of Geophysical Research: Atmospheres, 2001, 106; D13, p. 14391-14408.

Jourdain, B., and Legrand, M.: Year-round records of bulk and size-segregated aerosol composition and HCl and HNO3 levels in the Dumont d'Urville (coastal Antarctica) atmosphere: Implications for sea-salt aerosol fractionation in the winter and summer, Journal of Geophysical Research: Atmospheres, 2002, 107; D22, p. 1-13.

Joussaume, S., Sadourny, R., and Jouzel, J.: A general circulation model of water isotope cycles in the atmosphere, Nature, 1984, 311; 5981, p. 24-29.

Jouzel, J., Merlivat, L., and Lorius, C.: Deuterium excess in an East Antarctic ice core suggests higher relative humidity at the oceanic surface during the last glacial maximum, Nature, 1982, 299; 5885, p. 688-691.

Jouzel, J., and Merlivat, L.: Deuterium and oxygen 18 in precipitation: Modeling of the isotopic effects during snow formation, Journal of Geophysical Research: Atmospheres, 1984, 89; D7, p. 11749-11757.

Jouzel, J., Lorius, C., Petit, J., Genthon, C., Barkov, N., Kotlyakov, V., and Petrov, V.: Vostok ice core: a continuous isotope temperature record over the last climatic cycle (160,000 years), Nature, 1987, 329; 6138, p. 403-408.

Jouzel, J., and Koster, R. D.: A reconsideration of the initial conditions used for stable water isotope models, Journal of Geophysical Research: Atmospheres, 1996, 101; D17, p. 22933-22938.

Jouzel, J., Alley, R. B., Cuffey, K., Dansgaard, W., Grootes, P., Hoffmann, G., Johnsen, S. J., Koster, R., Peel, D., and Shuman, C.: Validity of the temperature reconstruction from water isotopes in ice cores, Journal of Geophysical Research: Oceans, 1997, 102; C12, p. 26471-26487.

Jouzel, J., Hoffmann, G., Koster, R., and Masson, V.: Water isotopes in precipitation:: data/model comparison for present-day and past climates, Quaternary Science Reviews, 2000, 19; 1, p. 363-379.

Jouzel, J., Masson-Delmotte, V., Cattani, O., Dreyfus, G., Falourd, S., Hoffmann, G., Minster, B., Nouet, J., Barnola, J.-M., and Chappellaz, J.: Orbital and millennial Antarctic climate variability over the past 800,000 years, science, 2007, 317; 5839, p. 793-796.

Jouzel, J., Delaygue, G., Landais, A., Masson-Delmotte, V., Risi, C., and Vimeux, F.: Water isotopes as tools to document oceanic sources of precipitation, Water Resources Research, 2013, 49; 11, p. 7469-7486.

Jouzel, J.: Water stable isotopes: atmospheric composition and applications in polar ice core studies, in: Treatise on Geochemistry, 2nd Edn., edited by: Keeling, R. a. R., L., Elsevier, 213-256, 2014.

Junying, S., Jiawen, R., and Dahe, Q.: 60 years record of biogenic sulfur from Lambert Glacier basin firn core, East Antarctica, Annals of Glaciology, 2002, 35, p. 362-367.

Kalnay, E., Kanamitsu, M., Kistler, R., Collins, W., Deaven, D., Gandin, L., Iredell, M., Saha, S., White, G., and Woollen, J.: The NCEP/NCAR 40-year reanalysis project, Bulletin of the American meteorological Society, 1996, 77; 3, p. 437-471.

Kanamitsu, M., Ebisuzaki, W., Woollen, J., Yang, S.-K., Hnilo, J., Fiorino, M., and Potter, G.: Ncep–doe amip-ii reanalysis (r-2), Bulletin of the American Meteorological Society, 2002, 83; 11, p. 1631-1643.

Karlöf, L., Isaksson, E., Winther, J.-G., Gundestrup, N., Meijer, H. A., Mulvaney, R., Pourchet, M., Hofstede, C., Lappegard, G., and Pettersson, R.: Accumulation variability over a small area in east Dronning Maud Land, Antarctica, as determined from shallow firn cores and snow pits: some implications for ice-core records, Journal of Glaciology, 2005, 51; 174, p. 343-352.

Kaufman, D. S., Schneider, D. P., McKay, N. P., Ammann, C. M., Bradley, R. S., Briffa, K. R., Miller, G. H., Otto-Bliesner, B. L., Overpeck, J. T., and Vinther, B. M.: Recent warming reverses long-term Arctic cooling, Science, 2009, 325; 5945, p. 1236-1239.

Kawamura, K., Abe-Ouchi, A., Motoyama, H., Ageta, Y., Aoki, S., Azuma, N., Fujii, Y., Fujita, K., Fujita, S., and Fukui, K.: State dependence of climatic instability over the past 720,000 years from Antarctic ice cores and climate modeling, Science advances, 2017, 3; e1600446, p. 1-13.

Kay, J., Deser, C., Phillips, A., Mai, A., Hannay, C., Strand, G., Arblaster, J., Bates, S., Danabasoglu, G., and Edwards, J.: The Community Earth System Model (CESM) large ensemble project: A community resource for studying climate change in the presence of internal climate variability, Bulletin of the American Meteorological Society, 2015, 96; 8, p. 1333-1349.

Kessler, E.: On the distribution and continuity of water substance in atmospheric circulations, in: On the distribution and continuity of water substance in atmospheric circulations, Springer, 1-84, 1969.

Kidson, J. W.: Interannual variations in the Southern Hemisphere circulation, Journal of Climate, 1988, 1; 12, p. 1177-1198.

Kiehl, J. T., and Gent, P. R.: The community climate system model, version 2, Journal of Climate, 2004, 17; 19, p. 3666-3682.

Kodama, Y., Wendler, G., and Ishikawa, N.: The diurnal variation of the boundary layer in summer in Adélie Land, eastern Antarctica, Journal of Applied Meteorology, 1989, 28; 1, p. 16-24.

König-Langlo, G., King, J., and Pettré, P.: Climatology of the three coastal Antarctic stations Dumont d'Urville, Neumayer, and Halley, Journal of Geophysical Research: Atmospheres, 1998, 103; D9, p. 10935-10946.

Korona, J., Berthier, E., Bernard, M., Rémy, F., and Thouvenot, E.: SPIRIT. SPOT 5 stereoscopic survey of polar ice: reference images and topographies during the fourth International Polar Year (2007–2009), ISPRS Journal of Photogrammetry and Remote Sensing, 2009, 64; 2, p. 204-212.

Koster, R. D., Jouzel, J., Suozzo, R. J., and Russell, G. L.: Origin of July Antarctic precipitation and its influence on deuterium content: a GCM analysis, Climate Dynamics, 1992, 7; 4, p. 195-203.

Kreutz, K., Mayewski, P. A., Twickler, M., Whitlow, S., White, J., Shuman, C., Raymond, C., Conway, H., and McConnell, J.: Seasonal variations of glaciochemical, isotopic and stratigraphic properties in Siple Dome (Antarctica) surface snow, Annals of Glaciology, 1999, 29, p. 38-44.

Krinner, G., and Werner, M.: Impact of precipitation seasonality changes on isotopic signals in polar ice cores: a multi-model analysis, Earth and Planetary Science Letters, 2003, 216; 4, p. 525-538.

Krinner, G., Magand, O., Simmonds, I., Genthon, C., and Dufresne, J.-L.: Simulated Antarctic precipitation and surface mass balance at the end of the twentieth and twenty-first centuries, Climate Dynamics, 2007, 28; 2-3, p. 215-230.

Krinner, G., Guicherd, B., Ox, K., Genthon, C., and Magand, O.: Influence of oceanic boundary conditions in simulations of Antarctic climate and surface mass balance change during the coming century, Journal of Climate, 2008, 21; 5, p. 938-962.

Kurita, N., Noone, D., Risi, C., Schmidt, G. A., Yamada, H., and Yoneyama, K.: Intraseasonal isotopic variation associated with the Madden-Julian Oscillation, Journal of Geophysical Research: Atmospheres, 2011, 116; D24, p. 1-20.

Kurita, N., Hirasawa, N., Koga, S., Matsushita, J., Steen-Larsen, H. C., Masson-Delmotte, V., and Fujiyoshi, Y.: Influence of large-scale atmospheric circulation on marine air intrusion toward the East Antarctic coast, Geophysical Research Letters, 2016, 43; 17, p. 9298-9305.

Küttel, M., Steig, E. J., Ding, Q., Monaghan, A. J., and Battisti, D. S.: Seasonal climate information preserved in West Antarctic ice core water isotopes: relationships to temperature, large-scale circulation, and sea ice, Climate Dynamics, 2012, 39; 7-8, p. 1841-1857.

Laepple, T., Münch, T., Casado, M., Hoerhold, M., Landais, A., and Kipfstuhl, S.: On the similarity and apparent cycles of isotopic variations in East Antarctic snow pits, The Cryosphere, 2018, 12; 1, p. 169-187.

Landais, A., Ekaykin, A., Barkan, E., Winkler, R., and Luz, B.: Seasonal variations of 17O-excess and d-excess in snow precipitation at Vostok station, East Antarctica, Journal of Glaciology, 2012, 58; 210, p. 725-733.

Landais, A., Casado, M., Prié, F., Magand, O., Arnaud, L., Ekaykin, A., Petit, J.-R., Picard, G., Fily, M., and Minster, B.: Surface studies of water isotopes in Antarctica for quantitative interpretation of deep ice core data, Comptes Rendus Geoscience, 2017, 349; 4, p. 139-150.

Lazzara, M. A., Weidner, G. A., Keller, L. M., Thom, J. E., and Cassano, J. J.: Antarctic automatic weather station program: 30 years of polar observation, Bulletin of the American Meteorological Society, 2012, 93; 10, p. 1519-1537.

Lee, J. E., Fung, I., DePaolo, D. J., and Henning, C. C.: Analysis of the global distribution of water isotopes using the NCAR atmospheric general circulation model, Journal of Geophysical Research: Atmospheres, 2007, 112; D16, p. 1-14.

Lee, J. E., Fung, I., DePaolo, D. J., and Otto-Bliesner, B.: Water isotopes during the Last Glacial Maximum: New general circulation model calculations, Journal of Geophysical Research: Atmospheres, 2008, 113; D19109, p. 1-15.

Legrand, M., Ducroz, F., Wagenbach, D., Mulvaney, R., and Hall, J.: Ammonium in coastal Antarctic aerosol and snow: Role of polar ocean and penguin emissions, Journal of Geophysical Research: Atmospheres, 1998, 103; D9, p. 11043-11056.

Legrand, M., and Wagenbach, D.: Impact of the Cerro Hudson and Pinatubo volcanic eruptions on the Antarctic air and snow chemistry, Journal of Geophysical Research: Atmospheres, 1999, 104; D1, p. 1581-1596.

Legrand, M., Preunkert, S., Jourdain, B., Gallée, H., Goutail, F., Weller, R., and Savarino, J.: Year-round record of surface ozone at coastal (Dumont d'Urville) and inland (Concordia) sites in East Antarctica, Journal of Geophysical Research: Atmospheres, 2009, 114; D20, p. 1-12.

Legrand, M., Yang, X., Preunkert, S., and Theys, N.: Year-round records of sea salt, gaseous, and particulate inorganic bromine in the atmospheric boundary layer at coastal (Dumont d'Urville) and central (Concordia) East Antarctic sites, Journal of geophysical research: atmospheres, 2016, 121; 2, p. 997-1023.

Legrand, M., Preunkert, S., Weller, R., Zipf, L., Elsässer, C., Merchel, S., Rugel, G., and Wagenbach, D.: Year-round record of bulk and size-segregated aerosol composition in central Antarctica (Concordia site)–Part 2:

Biogenic sulfur (sulfate and methanesulfonate) aerosol, Atmospheric Chemistry and Physics, 2017, 17; 22, p. 14055-14073.

Legrand, M., Preunkert, S., Wolff, E., Weller, R., Jourdain, B., and Wagenbach, D.: Year-round records of bulk and size-segregated aerosol composition in central Antarctica (Concordia site)–Part 1: Fractionation of sea-salt particles, Atmospheric Chemistry and Physics, 2017, 17; 22, p. 14039.

Lejiang, Y., Zhanhai, Z., Mingyu, Z., Zhong, S., Lenschow, D., Hsu, H., Huiding, W., and Bo, S.: Validation of ECMWF and NCEP--NCAR Reanalysis Data in Antarctica, 大气科学进展, 2010, 27; 5, p. 1151-1168.

Lemeur: The Cryosphere, submitted.

Lenaerts, J., Den Broeke, M., Berg, W., Meijgaard, E. v., and Kuipers Munneke, P.: A new, high-resolution surface mass balance map of Antarctica (1979–2010) based on regional atmospheric climate modeling, Geophysical Research Letters, 2012, 39; 4, p. 1-5.

Lenaerts, J., den Broeke, M., Déry, S., Meijgaard, E., Berg, W., Palm, S. P., and Sanz Rodrigo, J.: Modeling drifting snow in Antarctica with a regional climate model: 1. Methods and model evaluation, Journal of Geophysical Research: Atmospheres, 2012, 117; D5, p. 1-17.

Levkov, L., Rockel, B., Kapitza, H., and Raschke, E.: 3D mesoscale numerical studies of cirrus and stratus clouds by their time and space evolution, Contributions to atmospheric physics, 1992, 65; 1, p. 35-58.

Lewis, S. C., LeGrande, A. N., Kelley, M., and Schmidt, G. A.: Modeling insights into deuterium excess as an indicator of water vapor source conditions, Journal of Geophysical Research: Atmospheres, 2013, 118; 2, p. 243-262.

Libois, Q., Picard, G., Arnaud, L., Morin, S., and Brun, E.: Modeling the impact of snow drift on the decameter-scale variability of snow properties on the Antarctic Plateau, Journal of Geophysical Research: Atmospheres, 2014, 119; 20, p. 11-662.

Lin, Y.-L., Farley, R. D., and Orville, H. D.: Bulk parameterization of the snow field in a cloud model, Journal of Climate and Applied Meteorology, 1983, 22; 6, p. 1065-1092.

Lisiecki, L. E., and Raymo, M. E.: A Pliocene-Pleistocene stack of 57 globally distributed benthic δ18O records, Paleoceanography, 2005, 20; 1, p. 1-17.

Liu, H., Jezek, K., Li, B., and Zhao, Z.: Radarsat Antarctic Mapping Project digital elevation model version 2, Radarsat Antarctic Mapping Project digital elevation model version 2, Boulder, Colorado USA: National Snow and Ice Data Center. Digital media., 2001.

Loewe, F.: The land of storms, Weather, 1972, 27; 3, p. 110-121.

Lorius, C.: A physical and chemical study of the coastal ice sampled from a core drilling in Antarctica, Expéditions polaires françaises. Missions Paul-Emile Victor, 1967.

Lorius, C., Hagemann, R., Nief, G., and Roth, E.: Teneurs en deuterium le long d'un profil de 106 m dans le neve antarctique. Application a l'etude des variations climatiques, Earth and Planetary Science Letters, 1968, 4; 3, p. 237-244.

Lorius, C., Merlivat, L., and Hagemann, R.: Variation in the mean deuterium content of precipitations in Antarctica, Journal of Geophysical Research, 1969, 74; 28, p. 7027-7031.

Lorius, C., and Merlivat, L.: Distribution of mean surface stable isotopes values in East Antarctica; observed changes with depth in coastal area, CEA Centre d'Etudes Nucleaires de Saclay, 1975.

Lorius, C., Raynaud, D., Petit, J.-R., Jouzel, J., and Merlivat, L.: Late-glacial maximum-Holocene atmospheric and ice-thickness changes from Antarctic ice-core studies, Annals of glaciology, 1984, 5, p. 88-94.

Lüthi, D., Le Floch, M., Bereiter, B., Blunier, T., Barnola, J.-M., Siegenthaler, U., Raynaud, D., Jouzel, J., Fischer, H., and Kawamura, K.: High-resolution carbon dioxide concentration record 650,000–800,000 years before present, Nature, 2008, 453; 7193, p. 379-382.

Maahn, M., Burgard, C., Crewell, S., Gorodetskaya, I. V., Kneifel, S., Lhermitte, S., Van Tricht, K., and Lipzig, N. P.: How does the spaceborne radar blind zone affect derived surface snowfall statistics in polar regions?, Journal of Geophysical Research: Atmospheres, 2014, 119; 24, p. 13,604-613,620.

Magand, O.: Bilan de masse de surface Antarctique: techniques de mesure et analyse critique, Citeseer, 2009.

Majoube, M.: Fractionnement en oxygene 18 et en deuterium entre l'eau et sa vapeur, Journal de Chimie Physique, 1971, 68, p. 1423-1436.

Manguin, É.: Premier inventaire des diatomées de la Terre Adélie Antarctique: espèces nouvelles.(First inventory of diatoms from Adélie Land, Antarctica: new species.), Revue Algologique Nouvelle Série, 1957, 3, p. 111-134.

Markle, B., Bertler, N., Sinclair, K., and Sneed, S.: Synoptic variability in the Ross Sea region, Antarctica, as seen from back-trajectory modeling and ice core analysis, Journal of Geophysical Research: Atmospheres, 2012, 117; D2, p. 1-17.

Markle, B. R., Steig, E. J., Buizert, C., Schoenemann, S. W., Bitz, C. M., Fudge, T., Pedro, J. B., Ding, Q., Jones, T. R., and White, J. W.: Global atmospheric teleconnections during Dansgaard–Oeschger events, Nature Geoscience, 2017, 10; 1, p. 36-40.

Marshall, G. J., and Harangozo, S. A.: An appraisal of NCEP/NCAR reanalysis MSLP data viability for climate studies in the South Pacific, Geophysical Research Letters, 2000, 27; 19, p. 3057-3060.

Marshall, G. J.: Analysis of recent circulation and thermal advection change in the northern Antarctic Peninsula, International journal of climatology, 2002, 22; 12, p. 1557-1567.

Marshall, G. J.: Trends in the Southern Annular Mode from observations and reanalyses, Journal of Climate, 2003, 16; 24, p. 4134-4143.

Marshall, G. J., and Thompson, D. W.: The signatures of large-scale patterns of atmospheric variability in Antarctic surface temperatures, Journal of Geophysical Research: Atmospheres, 2016, 121; 7, p. 3276-3289.

Marshall, G. J., Thompson, D. W., and Broeke, M. R.: The signature of Southern Hemisphere atmospheric circulation patterns in Antarctic precipitation, Geophysical Research Letters, 2017, 44; 22, p. 11,580-511,589.

Martin, A.: Circulation et transport des masses d'eau sur le plateau Est-Antarctique au large de la Terre Adélie, Th. : Sciences de la Terre, Université Pierre et Marie Curie - Paris VI, 2016, 261 pp.

Massom, R., Reid, P., Stammerjohn, S., Raymond, B., Fraser, A., and Ushio, S.: Change and variability in East Antarctic sea ice seasonality, 1979/80–2009/10, PLoS One, 2013, 8; 5, p. 1-14.

Massom, R. A., Hill, K., Barbraud, C., Adams, N., Ancel, A., Emmerson, L., and Pook, M. J.: Fast ice distribution in Adélie Land, East Antarctica: interannual variability and implications for emperor penguins Aptenodytes forsteri, Marine Ecology Progress Series, 2009, 374, p. 243-257.

Massom, R. A., and Stammerjohn, S. E.: Antarctic sea ice change and variability–physical and ecological implications, Polar Science, 2010, 4; 2, p. 149-186.

Masson-Delmotte, V., Delmotte, M., Morgan, V., Etheridge, D., Van Ommen, T., Tartarin, S., and Hoffmann, G.: Recent southern Indian Ocean climate variability inferred from a Law Dome ice core: New insights for the interpretation of coastal Antarctic isotopic records, Climate Dynamics, 2003, 21; 2, p. 153-166.

Masson-Delmotte, V., Hou, S., Ekaykin, A., Jouzel, J., Aristarain, A., Bernardo, R., Bromwich, D., Cattani, O., Delmotte, M., Falourd, S., Frezzotti, M., Gallée, H., Genoni, L., Isaksson, E., Landais, A., Helsen, M., Hoffmann, G., Lopez, J., Morgan, V., Motoyama, H., Noone, D., Oerter, H., Petit, J., Royer, A., Uemera, R., Schmidt, G., Schlosser, E., Simões, J., Steig, E., Stenni, B., Stievenard, M., van den Broeke, M., van de Wal, R., van de Berg, W., Vimeux, F., and White, J.: A review of Antarctic surface snow isotopic composition: Observations, atmospheric circulation, and isotopic modeling, Journal of Climate, 2008, 21; 13, p. 3359-3387.

Masson-Delmotte, V., Buiron, D., Ekaykin, A., Frezzotti, M., Gallée, H., Jouzel, J., Krinner, G., Landais, A., Motoyama, H., and Oerter, H.: A comparison of the present and last interglacial periods in six Antarctic ice cores, Climate of the Past, 2011, 7; 2, p. 397-423.

Masson-Delmotte, V., Steen-Larsen, H., Ortega, P., Swingedouw, D., Popp, T., Vinther, B., Oerter, H., Sveinbjornsdottir, A., Gudlaugsdottir, H., and Box, J.: Recent changes in north-west Greenland climate documented by NEEM shallow ice core data and simulations, and implications for past-temperature reconstructions, Cryosphere (The), 2015, 9, p. 1481-1504.

Mayewski, P. A., and Goodwin, D.: International Trans-Antarctic Scientific Expedition (ITASE): 200 years of past Antarctic climate and environmental change: science and implementation plan, 1996: report from the ITASE Workshop, Cambridge, United Kingdom, 2-3 August, 1996, 1, PAGES, 1997.

Mayewski, P. A., Frezzotti, M., Bertler, N., Ommen, T. V., Hamilton, G., Jacka, T. H., Welch, B., Frey, M., Dahe, Q., and Jiawen, R.: The international trans-antarctic scientific expedition (ITASE): an overview, Annals of Glaciology, 2005, 41, p. 180-185.

McGregor, H. V., Evans, M. N., Goosse, H., Leduc, G., Martrat, B., Addison, J. A., Mortyn, P. G., Oppo, D. W., Seidenkrantz, M.-S., and Sicre, M.-A.: Robust global ocean cooling trend for the pre-industrial Common Era, Nature Geoscience, 2015, 8; 9, p. 671-677.

McKinney, W.: pandas: a foundational Python library for data analysis and statistics, Python for High Performance and Scientific Computing, 2011, p. 1-9.

Merlivat, L.: Molecular diffusivities of H 2 16 O, HD 16 O, and H 2 18 O in gases, The Journal of Chemical Physics, 1978, 69; 6, p. 2864-2871.

Merlivat, L., and Jouzel, J.: Global climatic interpretation of the deuterium-oxygen 18 relationship for precipitation, Journal of Geophysical Research: Oceans, 1979, 84; C8, p. 5029-5033.

Meyers, M. P., DeMott, P. J., and Cotton, W. R.: New primary ice-nucleation parameterizations in an explicit cloud model, Journal of Applied Meteorology, 1992, 31; 7, p. 708-721.

Mezgec, K., Stenni, B., Crosta, X., Masson-Delmotte, V., Baroni, C., Braida, M., Ciardini, V., Colizza, E., Melis, R., and Salvatore, M.: Holocene sea ice variability driven by wind and polynya efficiency in the Ross Sea, Nature Communications, 2017, 8; 1334, p. 1-12.

Minikin, A., Legrand, M., Hall, J., Wagenbach, D., Kleefeld, C., Wolff, E., Pasteur, E. C., and Ducroz, F.: Sulfur-containing species (sulfate and methanesulfonate) in coastal Antarctic aerosol and precipitation, Journal of Geophysical Research: Atmospheres, 1998, 103; D9, p. 10975-10990.

Mo, K. C., and Higgins, R. W.: The Pacific–South American modes and tropical convection during the Southern Hemisphere winter, Monthly Weather Review, 1998, 126; 6, p. 1581-1596.

Mo, K. C.: Relationships between low-frequency variability in the Southern Hemisphere and sea surface temperature anomalies, Journal of Climate, 2000, 13; 20, p. 3599-3610.

Monaghan, A. J., Bromwich, D. H., and Wang, S.-H.: Recent trends in Antarctic snow accumulation from Polar MM5 simulations, Philosophical Transactions of the Royal Society of London A: Mathematical, Physical and Engineering Sciences, 2006, 364; 1844, p. 1683-1708.

Morcrette, J.-J.: Assessment of the ECMWF model cloudiness and surface radiation fields at the ARM SGP site, Monthly weather review, 2002, 130; 2, p. 257-277.

Morgan, V., and van Ommen, T. D.: Seasonality in late-Holocene climate from ice-core records, The Holocene, 1997, 7; 3, p. 351-354.

Morgan, V. I., Wookey, C., Li, J., Van Ommen, T., Skinner, W., and Fitzpatrick, M.: Site information and initial results from deep ice drilling on Law Dome, Antarctica, Journal of Glaciology, 1997, 43; 143, p. 3-10.

Müller, K., Sinisalo, A., Anschütz, H., Hamran, S.-E., Hagen, J.-O., McCONNELL, J. R., and Pasteris, D. R.: An 860 km surface mass-balance profile on the East Antarctic plateau derived by GPR, Annals of Glaciology, 2010, 51; 55, p. 1-8.

Mulvaney, R., Wagenbach, D., and Wolff, E.: Postdepositional change in snowpack nitrate from observation of year-round near-surface snow in coastal Antarctica, Journal of geophysical research, 1998, 103; D9, p. 11,021-011,031.

Mulvaney, R., Oerter, H., Peel, D. A., Graf, W., Arrowsmith, C., Pasteur, E. C., Knight, B., Littot, G. C., and Miners, W. D.: 1000 year ice-core records from Berkner Island, Antarctica, Annals of Glaciology, 2002, 35; 1, p. 45-51.

Mulvaney, R., Abram, N. J., Hindmarsh, R. C., Arrowsmith, C., Fleet, L., Triest, J., Sime, L. C., Alemany, O., and Foord, S.: Recent Antarctic Peninsula warming relative to Holocene climate and ice-shelf history, Nature, 2012, 489; 7414, p. 141-144.

Münch, T., Kipfstuhl, S., Freitag, J., Meyer, H., and Laepple, T.: Constraints on post-depositional isotope modifications in East Antarctic firn from analysing temporal changes of isotope profiles, The Cryosphere, 2017, 11; 5, p. 2175-2188.

Naud, C. M., Booth, J. F., and Del Genio, A. D.: Evaluation of ERA-Interim and MERRA cloudiness in the Southern Ocean, Journal of Climate, 2014, 27; 5, p. 2109-2124.

Neff, P. D., and Bertler, N. A.: Trajectory modeling of modern dust transport to the Southern Ocean and Antarctica, Journal of Geophysical Research: Atmospheres, 2015, 120; 18, p. 9303-9322.

Nerem, R. S., Beckley, B. D., Fasullo, J. T., Hamlington, B. D., Masters, D., and Mitchum, G. T.: Climate-change–driven accelerated sea-level rise detected in the altimeter era, Proceedings of the National Academy of Sciences, 2018, 201717312, p. 1-4.

Neukom, R., Gergis, J., Karoly, D. J., Wanner, H., Curran, M., Elbert, J., González-Rouco, F., Linsley, B. K., Moy, A. D., and Mundo, I.: Inter-hemispheric temperature variability over the past millennium, Nature Climate Change, 2014, 4; 5, p. 362-368.

Neumann, T. A., and Waddington, E. D.: Effects of firn ventilation on isotopic exchange, Journal of Glaciology, 2004, 50; 169, p. 183-194.

Nicolas, J. P., and Bromwich, D. H.: Precipitation changes in high southern latitudes from global reanalyses: A cautionary tale, Surveys in geophysics, 2011, 32; 4-5, p. 475-494.

Nicolas, J. P., and Bromwich, D. H.: New Reconstruction of Antarctic Near-Surface Temperatures: Multidecadal Trends and Reliability of Global Reanalyses, Journal of Climate, 2014, 27; 21, p. 8070-8093.

Noone, D., and Simmonds, I.: Associations between δ 18O of water and climate parameters in a simulation of atmospheric circulation for 1979–95, Journal of Climate, 2002, 15; 22, p. 3150-3169.

Noone, D., and Simmonds, I.: Annular variations in moisture transport mechanisms and the abundance of δ18O in Antarctic snow, Journal of Geophysical Research: Atmospheres, 2002, 107; D24, p. 1-11.

Noone, D., and Simmonds, I.: Sea ice control of water isotope transport to Antarctica and implications for ice core interpretation, Journal of Geophysical Research: Atmospheres, 2004, 109; D7, p. 1-13.

Noone, D.: Evaluation of hydrological cycles and processes with water isotopes: Report to GEWEX-GHP from the Stable Water-isotope Intercomparison Group (SWING), Pan-GEWEX Meeting, Frascati, Italy, 2006,

Noone, D.: Assessing global model hydrology with simulations from the Stable Water-isotope INtercomparison Group, Research Activities in Atmospheric and Oceanic Modeling, Report, 2007; 36, p. 4-21.

Noone, D.: The influence of midlatitude and tropical overturning circulation on the isotopic composition of atmospheric water vapor and Antarctic precipitation, Journal of Geophysical Research: Atmospheres, 2008, 113; D4, p. 1-13.

Nusbaumer, J.: An examination of atmospheric river moisture transport and hydrology using isotope-enabled CAM5, Th. : Department of Atmospheric and Oceanic Sciences, University of Colorado, 2016, 149 pp.

Oerter, H., Wilhelms, F., Jung-Rothenhäusler, F., Göktas, F., Miller, H., Graf, W., and Sommer, S.: Accumulation rates in Dronning Maud Land, Antarctica, as revealed by dielectric-profiling measurements of shallow firn cores, Annals of Glaciology, 2000, 30, p. 27-34.

Orsi, A. J., Cornuelle, B. D., and Severinghaus, J. P.: Little Ice Age cold interval in West Antarctica: evidence from borehole temperature at the West Antarctic Ice Sheet (WAIS) divide, Geophysical Research Letters, 2012, 39; 9, p. 1-7.

Ortega, P., Lehner, F., Swingedouw, D., Masson-Delmotte, V., Raible, C. C., Casado, M., and Yiou, P.: A model-tested North Atlantic Oscillation reconstruction for the past millennium, Nature, 2015, 523; 7558, p. 71-74.

Otterå, O. H., Bentsen, M., Drange, H., and Suo, L.: External forcing as a metronome for Atlantic multidecadal variability, Nature Geoscience, 2010, 3; 10, p. 688-694.

Paillard, D., Labeyrie, L., and Yiou, P.: Macintosh program performs time-series analysis, Eos, Transactions American Geophysical Union, 1996, 77; 39, p. 379-379.

Palerme, C., Genthon, C., Claud, C., Kay, J. E., Wood, N. B., and L'Ecuyer, T.: Evaluation of current and projected Antarctic precipitation in CMIP5 models, Climate Dynamics, 2016, p. 1-15.

Palerme, C., Genthon, C., Claud, C., Kay, J. E., Wood, N. B., and L'Ecuyer, T.: Evaluation of current and projected Antarctic precipitation in CMIP5 models, Climate Dynamics, 2017, 48; 1-2, p. 225-239.

Palm, S. P., Kayetha, V., Yang, Y., and Pauly, R.: Blowing snow sublimation and transport over Antarctica from 11 years of CALIPSO observations, The Cryosphere, 2017, 11; 6, p. 2555-2569.

Paolo, F., Padman, L., Fricker, H., Adusumilli, S., Howard, S., and Siegfried, M.: Response of Pacific-sector Antarctic ice shelves to the El Niño/Southern Oscillation, Nature geoscience, 2018, 11, p. 121-126.

Parish, T. R., and Waight III, K. T.: The forcing of Antarctic katabatic winds, Monthly Weather Review, 1987, 115; 10, p. 2214-2226.

Parkinson, C. L., Comiso, J. C., Zwally, H. J., Cavalieri, D. J., Gloersen, P., and Campbell, W. J.: Arctic sea ice, 1973-1976: Satellite passive-microwave observations, 1987.

Parrenin, F., Dreyfus, G., Durand, G., Fujita, S., Gagliardini, O., Gillet, F., Jouzel, J., Kawamura, K., Lhomme, N., and Masson-Delmotte, V.: 1-D-ice flow modelling at EPICA Dome C and Dome Fuji, East Antarctica, Climate of the Past, 2007, 3; 2, p. 243-259.

Parrenin, F., Cavitte, M. G., Blankenship, D. D., Chappellaz, J., Fischer, H., Gagliardini, O., Masson-Delmotte, V., Passalacqua, O., Ritz, C., and Roberts, J.: Is there 1.5-million-year-old ice near Dome C, Antarctica?, The Cryosphere, 2017, 11; 6, p. 2427-2437.

Pépy, G.: Etude du formaldéhyde (HCHO) en zone côtière Antarctique, Th. , Université Grenoble Alpes, 2011.

Périard, C., and Pettré, P.: Some aspects of the climatology of dumont D'Irville, adélie land, Antarctica, International Journal of Climatology, 1993, 13; 3, p. 313-328.

Petit, J.-R., Jouzel, J., Raynaud, D., Barkov, N. I., Barnola, J.-M., Basile, I., Bender, M., Chappellaz, J., Davis, M., and Delaygue, G.: Climate and atmospheric history of the past 420,000 years from the Vostok ice core, Antarctica, Nature, 1999, 399; 6735, p. 429-436.

Petit, J., White, J., Young, N., Jouzel, J., and Korotkevich, Y. S.: Deuterium excess in recent Antarctic snow, Journal of Geophysical Research: Atmospheres, 1991, 96; D3, p. 5113-5122.

Pettré, P., Pinglot, J., Pourchet, M., and Reynaud, L.: Accumulation distribution in Terre Adélie, Antarctica: effect of meteorological parameters, Journal of Glaciology, 1986, 32; 112, p. 486-500.

Pettré, P., and André, J.-C.: Surface-pressure change through Loewe's phenomena and katabatic flow jumps: Study of two cases in Adélie Land, Antarctica, Journal of the atmospheric sciences, 1991, 48; 4, p. 557-571.

Pettré, P., and Périard, C.: Aspects du climat de Dumont-d'Urviller et de l'Antarctique, Rubrique: Climatologie, 1996, 13, p. 55-62.

Pfahl, S., and Sodemann, H.: What controls deuterium excess in global precipitation?, Climate of the Past, 2014, 10; 2, p. 771-781.

Phillpot, H., and Zillman, J.: The surface temperature inversion over the Antarctic continent, Journal of Geophysical Research, 1970, 75; 21, p. 4161-4169.

Picciotto, E. a., and Wilgain, S.: Fission products in Antarctic snow, a reference level for measuring accumulation, Journal of Geophysical Research, 1963, 68; 21, p. 5965-5972.

Plummer, C., Curran, M., van Ommen, T. D., Rasmussen, S. O., Moy, A., Vance, T., Clausen, H. B., Vinther, B. M., and Mayewski, P.: An independently dated 2000-yr volcanic record from Law Dome, East Antarctica, including a new perspective on the dating of the 1450s CE eruption of Kuwae, Vanuatu, Climate of the Past, 2012, 8; 6, p. 1929-1940.

Pope, J. O., Holland, P. R., Orr, A., Marshall, G. J., and Phillips, T.: The impacts of El Niño on the observed sea ice budget of West Antarctica, Geophysical Research Letters, 2017, 44, p. 6200-6208.

Preunkert, S., Legrand, M., Jourdain, B., Moulin, C., Belviso, S., Kasamatsu, N., Fukuchi, M., and Hirawake, T.: Interannual variability of dimethylsulfide in air and seawater and its atmospheric oxidation by-products (methanesulfonate and sulfate) at Dumont d'Urville, coastal Antarctica (1999–2003), Journal of Geophysical Research: Atmospheres, 2007, 112; D6, p. 1-13.

Preunkert, S., Jourdain, B., Legrand, M., Udisti, R., Becagli, S., and Cerri, O.: Seasonality of sulfur species (dimethyl sulfide, sulfate, and methanesulfonate) in Antarctica: Inland versus coastal regions, Journal of Geophysical Research: Atmospheres, 2008, 113; D15, p. 1-10.

Preunkert, S., and Legrand, M.: Towards a quasi-complete reconstruction of past atmospheric aerosol load and composition (organic and inorganic) over Europe since 1920 inferred from Alpine ice cores, Climate of the Past, 2013, 9; 4, p. 1403-1416.

Rahaman, W., Thamban, M., and Laluraj, C.: Twentieth-century sea ice variability in the Weddell Sea and its effect on moisture transport: Evidence from a coastal East Antarctic ice core record, The Holocene, 2016, 26; 3, p. 338-349.

Randall, D. A., Xu, K.-M., Somerville, R. J., and Iacobellis, S.: Single-column models and cloud ensemble models as links between observations and climate models, Journal of Climate, 1996, 9; 8, p. 1683-1697.

Raymond, B., Lea, M. A., Patterson, T., Andrews-Goff, V., Sharples, R., Charrassin, J. B., Cottin, M., Emmerson, L., Gales, N., and Gales, R.: Important marine habitat off east Antarctica revealed by two decades of multi-species predator tracking, Ecography, 2015, 38; 2, p. 121-129.

Raynaud, D., Lorius, C., Budd, W., and Young, N.: Ice flow along an IAGP flow line and interpretation of data from an ice core in Terre Adelie, Antarctica, Journal of Glaciology, 1979, 24; 90, p. 103-115.

Reid, P., Stammerjohn, S., Massom, R., Scambos, T., and Lieser, J.: The record 2013 Southern Hemisphere sea-ice extent maximum, Annals of Glaciology, 2015, 56; 69, p. 99-106.

Rémy, F.: L'Antarctique: la mémoire de la terre vue de l'espace, CNRS, 2003.

Richardson, C., Aarholt, E., Hamran, S. E., Holmlund, P., and Isaksson, E.: Spatial distribution of snow in western Dronning Maud Land, East Antarctica, mapped by a ground-based snow radar, Journal of Geophysical Research: Solid Earth, 1997, 102; B9, p. 20343-20353.

Rintoul, S.: On the origin and influence of Adelie Land bottom water, Antarctic Research Series, 1998, 75, p. 151-171.

Risi, C., Bony, S., Vimeux, F., and Jouzel, J.: Water-stable isotopes in the LMDZ4 general circulation model: Model evaluation for present-day and past climates and applications to climatic interpretations of tropical isotopic records, Journal of Geophysical Research: Atmospheres, 2010, 115; D12, p. 1-27.

Risi, C., Noone, D., Worden, J., Frankenberg, C., Stiller, G., Kiefer, M., Funke, B., Walker, K., Bernath, P., and Schneider, M.: Process-evaluation of tropospheric humidity simulated by general circulation models using water vapor isotopic observations: 2. Using isotopic diagnostics to understand the mid and upper tropospheric moist bias in the tropics and subtropics, Journal of Geophysical Research: Atmospheres, 2012, 117; D5, p. 1-26.

Risi, C., Landais, A., Winkler, R., and Vimeux, F.: Can we determine what controls the spatio-temporal distribution of d-excess and 17 O-excess in precipitation using the LMDZ general circulation model?, Climate of the Past, 2013, 9; 5, p. 2173-2193.

Ritter, F., Steen-Larsen, H. C., Werner, M., Masson-Delmotte, V., Orsi, A., Behrens, M., Birnbaum, G., Freitag, J., Risi, C., and Kipfstuhl, S.: Isotopic exchange on the diurnal scale between near-surface snow and lower atmospheric water vapor at Kohnen station, East Antarctica, The Cryosphere, 2016, 10; 4, p. 1647-1663.

Ritter, F., Steen-Larsen, H. C., Werner, M., Masson-Delmotte, V., Orsi, A., Behrens, M., Birnbaum, G., Freitag, J., Risi, C., and Kipfstuhl, S.: Isotopic exchange on the diurnal scale between near-surface snow and lower atmospheric water vapor at Kohnen station, East Antarctica, The Cryosphere, 2016, 10, p. 1647-1663.

Rodrigo, J. S., Buchlin, J.-M., van Beeck, J., Lenaerts, J. T., and van den Broeke, M. R.: Evaluation of the antarctic surface wind climate from ERA reanalyses and RACMO2/ANT simulations based on automatic weather stations, Climate dynamics, 2013, 40; 1-2, p. 353-376.

Roeckner, E., Bäuml, G., Bonaventura, L., Brokopf, R., Esch, M., Giorgetta, M., Hagemann, S., Kirchner, I., Kornblueh, L., and Manzini, E.: The atmospheric general circulation model ECHAM 5. PART I: Model description, Report / MPI für Meteorologie, 2003, 349, p. 1-140.

Rozanski, K., Araguás-Araguás, L., and Gonfiantini, R.: Isotopic patterns in modern global precipitation, Climate change in continental isotopic records, 1993, 78, p. 1-36.

Saha, S., Moorthi, S., Wu, X., Wang, J., Nadiga, S., Tripp, P., Behringer, D., Hou, Y.-T., Chuang, H.-y., and Iredell, M.: The NCEP climate forecast system version 2, Journal of Climate, 2014, 27; 6, p. 2185-2208.

Scarchilli, C., Frezzotti, M., Grigioni, P., De Silvestri, L., Agnoletto, L., and Dolci, S.: Extraordinary blowing snow transport events in East Antarctica, Climate Dynamics, 2010, 34; 7-8, p. 1195-1206.

Schleussner, C.-F., Divine, D., Donges, J. F., Miettinen, A., and Donner, R.: Indications for a North Atlantic ocean circulation regime shift at the onset of the Little Ice Age, Climate dynamics, 2015, 45; 11-12, p. 3623-3633.

Schlosser, E., Reijmer, C., Oerter, H., and Graf, W.: The influence of precipitation origin on the δ18O–T relationship at Neumayer station, Ekstrmisen, Antarctica, Annals of Glaciology, 2004, 39, p. 41-48.

Schlosser, E., Duda, M., Powers, J., and Manning, K. W.: Precipitation regime of Dronning Maud Land, Antarctica, derived from Antarctic Mesoscale Prediction System (AMPS) archive data, Journal of Geophysical Research: Atmospheres, 2008, 113; D24, p. 1-9.

Schlosser, E., Oerter, H., Masson-Delmotte, V., and Reijmer, C.: Atmospheric influence on the deuterium excess signal in polar firn: implications for ice-core interpretation, Journal of glaciology, 2008, 54; 184, p. 117-124.

Schlosser, E., Anschütz, H., Divine, D., Martma, T., Sinisalo, A., Altnau, S., and Isaksson, E.: Recent climate tendencies on an East Antarctic ice shelf inferred from a shallow firn core network, Journal of Geophysical Research: Atmospheres, 2014, 119; 11, p. 6549-6562.

Schlosser, E., Stenni, B., Valt, M., Cagnati, A., Powers, J. G., Manning, K. W., Raphael, M., and Duda, M. G.: Precipitation and synoptic regime in two extreme years 2009 and 2010 at Dome C, Antarctica–implications for ice core interpretation, Atmospheric Chemistry and Physics, 2016, 16; 8, p. 4757-4770.

Schlosser, E., Dittmann, A., Stenni, B., Powers, J. G., Manning, K. W., Masson-Delmotte, V., Valt, M., Cagnati, A., Grigioni, P., and Scarchilli, C.: The influence of the synoptic regime on stable water isotopes in precipitation at Dome C, East Antarctica, The Cryosphere, 2017, 11; 5, p. 2345-2361.

Schlosser, E., Haumann, F. A., and Raphael, M. N.: Atmospheric influences on the anomalous 2016 Antarctic sea ice decay, The Cryosphere, 2018, 12; 3, p. 1103-1119.

Schmidt, G. A., LeGrande, A. N., and Hoffmann, G.: Water isotope expressions of intrinsic and forced variability in a coupled ocean-atmosphere model, Journal of Geophysical Research: Atmospheres, 2007, 112; D10, p. 1-18.

Schneider, D. P., Steig, E. J., and Van Ommen, T.: High-resolution ice-core stable-isotopic records from Antarctica: towards interannual climate reconstruction, Annals of Glaciology, 2005, 41, p. 63-70.

Schneider, D. P., Steig, E. J., van Ommen, T. D., Dixon, D. A., Mayewski, P. A., Jones, J. M., and Bitz, C. M.: Antarctic temperatures over the past two centuries from ice cores, Geophysical Research Letters, 2006, 33; 16, p. 1-5.

Schoenemann, S. W., Steig, E. J., Ding, Q., Markle, B. R., and Schauer, A. J.: Triple water-isotopologue record from WAIS Divide, Antarctica: Controls on glacial-interglacial changes in 17Oexcess of precipitation, Journal of Geophysical Research: Atmospheres, 2014, 119; 14, p. 8741-8763.

Schoenemann, S. W., and Steig, E. J.: Seasonal and spatial variations of 17Oexcess and dexcess in Antarctic precipitation: Insights from an intermediate complexity isotope model, Journal of Geophysical Research: Atmospheres, 2016, 121; 19, p. 11,215-211,247.

Schroeter, S., Hobbs, W., and Bindoff, N. L.: Interactions between Antarctic sea ice and large-scale atmospheric modes in CMIP5 models, The Cryosphere, 2017, 11; 2, p. 789-803.

Schwanck, F., Simões, J. C., Handley, M., Mayewski, P. A., Auger, J. D., Bernardo, R. T., and Aquino, F. E.: A 125-year record of climate and chemistry variability at the Pine Island Glacier ice divide, Antarctica, The Cryosphere, 2017, 11; 4, p. 1537-1552.

Shindell, D. T., and Schmidt, G. A.: Southern Hemisphere climate response to ozone changes and greenhouse gas increases, Geophysical Research Letters, 2004, 31; 18, p. 1-4.

Shu, Q., Qiao, F., Song, Z., and Wang, C.: Sea ice trends in the Antarctic and their relationship to surface air temperature during 1979–2009, Climate dynamics, 2012, 38; 11-12, p. 2355-2363.

Sigl, M., McConnell, J. R., Toohey, M., Curran, M., Das, S. B., Edwards, R., Isaksson, E., Kawamura, K., Kipfstuhl, S., and Krüger, K.: Insights from Antarctica on volcanic forcing during the Common Era, Nature Climate Change, 2014, 4; 8, p. 693-697.

Sigl, M., Fudge, T., Winstrup, M., Cole-Dai, J., Ferris, D., McConnell, J., Taylor, K., Welten, K., Woodruff, T., and Adolphi, F.: The WAIS Divide deep ice core WD2014 chronology-Part 2: Annual-layer counting (0-31 ka BP), Climate of the Past Discussions, 2015, 11, p. 3425-3474.

Sigl, M., Winstrup, M., McConnell, J., Welten, K., Plunkett, G., Ludlow, F., Büntgen, U., Caffee, M., Chellman, N., and Dahl-Jensen, D.: Timing and climate forcing of volcanic eruptions for the past 2,500 years, Nature, 2015, 523; 7562, p. 543-549.

Sigmond, M., and Fyfe, J. C.: The Antarctic sea ice response to the ozone hole in climate models, Journal of Climate, 2014, 27; 3, p. 1336-1342.

Sime, L., Wolff, E., Oliver, K., and Tindall, J.: Evidence for warmer interglacials in East Antarctic ice cores, Nature, 2009, 462; 7271, p. 342-345.

Sime, L. C., Tindall, J. C., Wolff, E. W., Connolley, W. M., and Valdes, P. J.: Antarctic isotopic thermometer during a CO2 forced warming event, Journal of Geophysical Research: Atmospheres, 2008, 113; D24119, p. 1-16.

Simmonds, I., and Jacka, T.: Relationships between the interannual variability of Antarctic sea ice and the Southern Oscillation, Journal of Climate, 1995, 8; 3, p. 637-647.

Simmonds, I., Keay, K., and Lim, E.-P.: Synoptic activity in the seas around Antarctica, Monthly Weather Review, 2003, 131; 2, p. 272-288.

Simmons, A., Jones, P., da Costa Bechtold, V., Beljaars, A., Kållberg, P., Saarinen, S., Uppala, S., Viterbo, P., and Wedi, N.: Comparison of trends and low-frequency variability in CRU, ERA-40, and NCEP/NCAR analyses of surface air temperature, Journal of Geophysical Research: Atmospheres, 2004, 109; D24115, p. 1-18.

Sinclair, K., Bertler, N., and Trompetter, W.: Synoptic controls on precipitation pathways and snow delivery to high-accumulation ice core sites in the Ross Sea region, Antarctica, Journal of Geophysical Research: Atmospheres, 2010, 115; D22112, p. 1-11.

Sinclair, K. E., Bertler, N. A., Bowen, M. M., and Arrigo, K. R.: Twentieth century sea-ice trends in the Ross Sea from a high-resolution, coastal ice-core record, Geophysical Research Letters, 2014, 41; 10, p. 3510-3516.

Smith, S. R., and Stearns, C. R.: Antarctic pressure and temperature anomalies surrounding the minimum in the Southern Oscillation index, Journal of Geophysical Research: Atmospheres, 1993, 98; D7, p. 13071-13083.

Sodemann, H., and Stohl, A.: Asymmetries in the moisture origin of Antarctic precipitation, Geophysical research letters, 2009, 36; L22803, p. 1-5.

Sokratov, S. A., and Golubev, V. N.: Snow isotopic content change by sublimation, Journal of Glaciology, 2009, 55; 193, p. 823-828.

Southwell, C., Emmerson, L., McKinlay, J., Newbery, K., Takahashi, A., Kato, A., Barbraud, C., DeLord, K., and Weimerskirch, H.: Spatially extensive standardized surveys reveal widespread, multi-decadal increase in East Antarctic Adélie penguin populations, PloS one, 2015, 10; e0139877, p. 1-18.

Spikes, V. B., Hamilton, G. S., Arcone, S. A., Kaspari, S., and Mayewski, P. A.: Variability in accumulation rates from GPR profiling on the West Antarctic plateau, Annals of Glaciology, 2004, 39, p. 238-244.

Stammerjohn, S., Martinson, D., Smith, R., Yuan, X., and Rind, D.: Trends in Antarctic annual sea ice retreat and advance and their relation to El Niño–Southern Oscillation and Southern Annular Mode variability, Journal of Geophysical Research: Oceans, 2008, 113; C03S90, p. 1-20.

Steen-Larsen, H. C., Masson-Delmotte, V., Hirabayashi, M., Winkler, R., Satow, K., Prié, F., Bayou, N., Brun, E., Cuffey, K. M., Dahl-Jensen, D., Dumont, M., Guillevic, M., Kipfstuhl, S., Landais, A., Popp, T., Risi, C., Steffen, K., Stenni, B., and Sveinbjörnsdottír, A. E.: What controls the isotopic composition of Greenland surface snow?, Climate of the Past, 2014, 10; 1, p. 377-392.

Steen-Larsen, H., Risi, C., Werner, M., Yoshimura, K., and Masson-Delmotte, V.: Evaluating the skills of isotope-enabled general circulation models against in situ atmospheric water vapor isotope observations, Journal of Geophysical Research: Atmospheres, 2017, 122; 1, p. 246-263.

Steig, E. J., Schneider, D. P., Rutherford, S. D., Mann, M. E., Comiso, J. C., and Shindell, D. T.: Warming of the Antarctic ice-sheet surface since the 1957 International Geophysical Year, Nature, 2009, 457; 7228, p. 459-462.

Steig, E. J., Ding, Q., Battisti, D., and Jenkins, A.: Tropical forcing of Circumpolar Deep Water inflow and outlet glacier thinning in the Amundsen Sea Embayment, West Antarctica, Annals of Glaciology, 2012, 53; 60, p. 19-28.

Steig, E. J., Ding, Q., White, J. W., Küttel, M., Rupper, S. B., Neumann, T. A., Neff, P. D., Gallant, A. J., Mayewski, P. A., and Taylor, K. C.: Recent climate and ice-sheet changes in West Antarctica compared with the past 2,000 years, Nature Geoscience, 2013, 6; 5, p. 372-375.

Steiger, N. J., Steig, E. J., Dee, S. G., Roe, G. H., and Hakim, G. J.: Climate reconstruction using data assimilation of water isotope ratios from ice cores, Journal of Geophysical Research: Atmospheres, 2017, 122; 3, p. 1545-1568.

Stein, A., Draxler, R. R., Rolph, G. D., Stunder, B. J., Cohen, M., and Ngan, F.: NOAA's HYSPLIT atmospheric transport and dispersion modeling system, Bulletin of the American Meteorological Society, 2015, 96; 12, p. 2059-2077.

Stenni, B., Caprioli, R., Cimino, L., Cremisini, C., Flora, O., Gragnani, R., Longinelli, A., Maggi, V., and Torcini, S.: 200 years of isotope and chemical records in a firn core from Hercules Neve, northern Victoria Land, Antarctica, Annals of Glaciology, 1999, 29, p. 106-112.

Stenni, B., Serra, F., Frezzotti, M., Maggi, V., Traversi, R., Becagli, S., and Udisti, R.: Snow accumulation rates in northern Victoria Land, Antarctica, by firn-core analysis, Journal of Glaciology, 2000, 46; 155, p. 541-552.

Stenni, B., Masson-Delmotte, V., Johnsen, S., Jouzel, J., Longinelli, A., Monnin, E., Röthlisberger, R., and Selmo, E.: An oceanic cold reversal during the last deglaciation, Science, 2001, 293; 5537, p. 2074-2077.

Stenni, B., Scarchilli, C., Masson-Delmotte, V., Schlosser, E., Ciardini, V., Dreossi, G., Grigioni, P., Bonazza, M., Cagnati, A., Karlicek, D., Risi, C., Udisti, R., and Valt, M.: Three-year monitoring of stable isotopes of precipitation at Concordia Station, East Antarctica, The Cryosphere, 2016, 10; 5, p. 2415-2428.

Stenni, B., Curran, M. A., Abram, N. J., Orsi, A., Goursaud, S., Masson-Delmotte, V., Neukom, R., Goosse, H., Divine, D., and Van Ommen, T.: Antarctic climate variability on regional and continental scales over the last 2000 years, Climate of the Past, 2017, 13; 11, p. 1609-1634.

Stenni, B., Curran, M. A. J., Abram, N. J., Orsi, A., Goursaud, S., Masson-Delmotte, V., Neukom, R., Goosse, H., Divine, D., van Ommen, T., Steig, E. J., Dixon, D. A., Thomas, E. R., Bertler, N. A. N., Isaksson, E., Ekaykin, A., Frezzotti, M., and Werner, M.: Antarctic climate variability at regional and continental scales over the last 2,000 years, Clim. Past Discuss., 2017, 2017, p. 1-35.

Stoffel, M., Khodri, M., Corona, C., Guillet, S., Poulain, V., Bekki, S., Guiot, J., Luckman, B. H., Oppenheimer, C., and Lebas, N.: Estimates of volcanic-induced cooling in the Northern Hemisphere over the past 1,500 years, Nature Geoscience, 2015, 8; 10, p. 784-788.

Stohl, A., Wotawa, G., Seibert, P., and Kromp-Kolb, H.: Interpolation errors in wind fields as a function of spatial and temporal resolution and their impact on different types of kinematic trajectories, Journal of Applied Meteorology, 1995, 34; 10, p. 2149-2165.

Stohl, A., Forster, C., Frank, A., Seibert, P., and Wotawa, G.: The Lagrangian particle dispersion model FLEXPART version 6.2, Atmospheric Chemistry and Physics, 2005, 5; 9, p. 2461-2474.

Sturm, C., Zhang, Q., and Noone, D.: An introduction to stable water isotopes in climate models: benefits of forward proxy modelling for paleoclimatology, Climate of the Past, 2010, 6; 1, p. 115-129.

Swingedouw, D., Ortega, P., Mignot, J., Guilyardi, E., Masson-Delmotte, V., Butler, P. G., Khodri, M., and Séférian, R.: Bidecadal North Atlantic ocean circulation variability controlled by timing of volcanic eruptions, Nature communications, 2015, 6; 6545, p. 1-12.

Tamura, T., Ohshima, K. I., and Nihashi, S.: Mapping of sea ice production for Antarctic coastal polynyas, Geophysical Research Letters, 2008, 35; L07606, p. 1-5.

Telford, P., Braesicke, P., Morgenstern, O., and Pyle, J.: Description and assessment of a nudged version of the new dynamics Unified Model, Atmospheric Chemistry and Physics, 2008, 8; 6, p. 1701-1712.

Thomas, E., Dennis, P., Bracegirdle, T. J., and Franzke, C.: Ice core evidence for significant 100-year regional warming on the Antarctic Peninsula, Geophysical Research Letters, 2009, 36; L20704, p. 1-5.

Thomas, E. R., Bracegirdle, T. J., Turner, J., and Wolff, E. W.: A 308 year record of climate variability in West Antarctica, Geophysical Research Letters, 2013, 40; 20, p. 5492-5496.

Thomas, E. R., and Bracegirdle, T. J.: Precipitation pathways for five new ice core sites in Ellsworth Land, West Antarctica, Climate dynamics, 2015, 44; 7-8, p. 2067-2078.

Thomas, E. R., van Wessem, J. M., Roberts, J., Isaksson, E., Schlosser, E., Fudge, T., Vallelonga, P., Medley10, B., Lenaerts, J., and Bertler11, N.: Review of regional Antarctic snow accumulation over the past 1000 years, Climate of the Past Discussion, 2017, p.

Thomas, E. R., van Wessem, J. M., Roberts, J., Isaksson, E., Schlosser, E., Fudge, T. J., Vallelonga, P., Medley, B., Lenaerts, J., and Bertler, N.: Regional Antarctic snow accumulation over the past 1000 years, Climate of the Past, 2017, 13; 11, p. 1491-1513.

Thompson, D. W., and Wallace, J. M.: Annular modes in the extratropical circulation. Part I: Month-to-month variability, Journal of climate, 2000, 13; 5, p. 1000-1016.

Thompson, D. W., Solomon, S., Kushner, P. J., England, M. H., Grise, K. M., and Karoly, D. J.: Signatures of the Antarctic ozone hole in Southern Hemisphere surface climate change, Nature Geoscience, 2011, 4; 11, p. 741-749.

Tindall, J., Valdes, P., and Sime, L. C.: Stable water isotopes in HadCM3: Isotopic signature of El Niño–Southern Oscillation and the tropical amount effect, Journal of Geophysical Research: Atmospheres, 2009, 114; D04111, p. 1-12.

Toggweiler, J. R., and Russell, J.: Ocean circulation in a warming climate, Nature, 2008, 451; 7176, p. 286-288.

Touzeau, A., Landais, A., Stenni, B., Uemura, R., Fukui, K., Fujita, S., Guilbaud, S., Ekaykin, A., Casado, M., and Barkan, E.: Acquisition of isotopic composition for surface snow in East Antarctica and the links to climatic parameters, The Cryosphere, 2016, 10; 2, p. 837-852.

Touzeau, A., Landais, A., Morin, S., Arnaud, L., and Picard, G.: Numerical experiments on isotopic diffusion in polar snow and firn using a multi-layer energy balance model, Geosci. Model Dev. Discuss., 2017, 2017, p. 1-58.

Turner, J., Bromwich, D., Colwell, S., Dixon, S., Gibson, T., Hart, T., Heinemann, G., Hutchinson, H., Jacka, K., and Leonard, S.: The Antarctic first regional observing study of the troposphere (FROST) project, Bulletin of the American Meteorological Society, 1996, 77; 9, p. 2007-2032.

Turner, J., Leonard, S., Marshall, G. J., Pook, M., Cowled, L., Jardine, R., Pendlebury, S., and Adams, N.: An assessment of operational Antarctic analyses based on data from the FROST project, Weather and forecasting, 1999, 14; 6, p. 817-834.

Turner, J.: The El Niño–Southern Oscillation and Antarctica, International Journal of climatology, 2004, 24; 1, p. 1-31.

Turner, J., Colwell, S. R., Marshall, G. J., Lachlan-Cope, T. A., Carleton, A. M., Jones, P. D., Lagun, V., Reid, P. A., and Iagovkina, S.: The SCAR READER project: toward a high-quality database of mean Antarctic meteorological observations, Journal of Climate, 2004, 17; 14, p. 2890-2898.

Turner, J., Phillips, T., Marshall, G. J., Hosking, J. S., Pope, J. O., Bracegirdle, T. J., and Deb, P.: Unprecedented springtime retreat of Antarctic sea ice in 2016, Geophysical Research Letters, 2017, 44; 13, p. 6868-6875.

Uemura, R., Matsui, Y., Yoshimura, K., Motoyama, H., and Yoshida, N.: Evidence of deuterium excess in water vapor as an indicator of ocean surface conditions, Journal of Geophysical Research: Atmospheres, 2008, 113; D19114, p. 1-10.

Uemura, R., Masson-Delmotte, V., Jouzel, J., Landais, A., Motoyama, H., and Stenni, B.: Ranges of moisture-source temperature estimated from Antarctic ice cores stable isotope records over glacial-interglacial cycles, Climate of the Past, 2012, 8; 3, p. 1109-1125.

Uemura, R., Masson-Delmotte, V., Jouzel, J., Landais, A., Motoyama, H., and Stenni, B.: Ranges of moisture-source temperature estimated from Antarctic ice cores stable isotope records over glacial–interglacial cycles, Climate of the Past, 2012, 8; 3, p. 1109-1125.

Uppala, S. M., Kållberg, P., Simmons, A., Andrae, U., Bechtold, V. d., Fiorino, M., Gibson, J., Haseler, J., Hernandez, A., and Kelly, G.: The ERA-40 re-analysis, Quarterly Journal of the royal meteorological society, 2005, 131; 612, p. 2961-3012.

Van de Berg, W., Van den Broeke, M., Reijmer, C., and Van Meijgaard, E.: Reassessment of the Antarctic surface mass balance using calibrated output of a regional atmospheric climate model, Journal of Geophysical Research: Atmospheres, 2006, 111; D11104, p. 1-15.

van der Wel, G., Fischer, H., Oerter, H., Meyer, H., and Meijer, H.: Estimation and calibration of the water isotope differential diffusion length in ice core records, The Cryosphere, 2015, 9; 4, p. 1601-1616.

Van Liefferinge, B., Pattyn, F., Cavitte, M. G., Karlsson, N. B., Young, D. A., Sutter, J., and Eisen, O.: Promising Oldest Ice sites in East Antarctica based on thermodynamical modelling, The Cryosphere Discuss., 2018, p. 1-22.

van Lipzig, N. P. M.: The surface mass balance of the Antarctic ice sheet: a study with a regional atmospheric model, 1999.

Van Loon, H.: The half-yearly oscillations in middle and high southern latitudes and the coreless winter, Journal of the Atmospheric Sciences, 1967, 24; 5, p. 472-486.

van Ommen, T. D., and Morgan, V.: Calibrating the ice core paleothermometer using seasonality, Journal of Geophysical Research: Atmospheres, 1997, 102; D8, p. 9351-9357.

Van Wessem, J., Reijmer, C., Morlighem, M., Mouginot, J., Rignot, E., Medley, B., Joughin, I., Wouters, B., Depoorter, M., and Bamber, J.: Improved representation of East Antarctic surface mass balance in a regional atmospheric climate model, Journal of Glaciology, 2014, 60; 222, p. 761-770.

Vaughan, D. G., Comiso, J. C., Allison, I., Carrasco, J., Kaser, G., Kwok, R., Mote, P., Murray, T., Paul, F., and Ren, J.: Observations: cryosphere, Climate change, 2013, 2103, p. 317-382.

Vega, C. P., Schlosser, E., Divine, D. V., Kohler, J., Martma, T., Eichler, A., Schwikowski, M., and Isaksson, E.: Surface mass balance and water stable isotopes derived from firn cores on three ice rises, Fimbul Ice Shelf, Antarctica, The Cryosphere, 2016, 10; 6, p. 2763-2777.

Verfaillie, D., Fily, M., Le Meur, E., Magand, O., Jourdain, B., Arnaud, L., and Favier, V.: Snow accumulation variability derived from radar and firn core data along a 600 km transect in Adelie Land, East Antarctic plateau, The Cryosphere, 2012, 6, p. 1345-1358.

Vimeux, F., Masson, V., Jouzel, J., Stievenard, M., and Petit, J.: Glacial-interglacial changes in ocean surface conditions in the Southern Hemisphere, Nature, 1999, 398; 6726, p. 410-413.

Vimeux, F., Masson, V., Delaygue, G., Jouzel, J., Petit, J., and Stievenard, M.: A 420,000 year deuterium excess record from East Antarctica: Information on past changes in the origin of precipitation at Vostok, Journal of Geophysical Research: Atmospheres, 2001, 106; D23, p. 31863-31873.

Waddington, E. D., Steig, E. J., and Neumann, T. A.: Using characteristic times to assess whether stable isotopes in polar snow can be reversibly deposited, Annals of Glaciology, 2002, 35, p. 118-124.

Wagenbach, D., Ducroz, F., Mulvaney, R., Keck, L., Minikin, A., Legrand, M., Hall, J., and Wolff, E.: Sea-salt aerosol in coastal Antarctic regions, Journal of Geophysical Research: Atmospheres, 1998, 103; D9, p. 10961-10974.

Wagenbach, D., Ducroz, F., Mulvaney, R., Keck, L., Minikin, A., Legrand, M., Hall, J. S., and Wolff, E. W.: Sea-salt aerosol in coastal Antarctic regions, J. Geophys. Res.-Atmos., 1998, 103; D9, p. 10961-10974.

Wagenbach, D., Legrand, M., Fischer, H., Pichlmayer, F., and Wolff, E.: Atmospheric near-surface nitrate at coastal Antarctic sites, Journal of Geophysical Research: Atmospheres, 1998, 103; D9, p. 11007-11020.

Walt, S. v. d., Colbert, S. C., and Varoquaux, G.: The NumPy array: a structure for efficient numerical computation, Computing in Science & Engineering, 2011, 13; 2, p. 22-30.

Wang, C., and Fiedler, P. C.: ENSO variability and the eastern tropical Pacific: A review, Progress in Oceanography, 2006, 69; 2-4, p. 239-266.

Wang, Y., Ding, M., Van Wessem, J., Schlosser, E., Altnau, S., van den Broeke, M. R., Lenaerts, J. T., Thomas, E. R., Isaksson, E., and Wang, J.: A comparison of Antarctic Ice Sheet surface mass balance from atmospheric climate models and in situ observations, Journal of Climate, 2016, 29; 14, p. 5317-5337.

Wang, Y., Zhou, D., Bunde, A., and Havlin, S.: Testing reanalysis data sets in Antarctica: Trends, persistence properties, and trend significance, Journal of Geophysical Research: Atmospheres, 2016, 121; 21, p. 12,839-812,855.

Welch, B. C., Jacobel, R. W., and Arcone, S. A.: First results from radar profiles collected along the US-ITASE traverse from Taylor Dome to South Pole (2006–2008), Annals of Glaciology, 2009, 50; 51, p. 35-41.

Welhouse, L. J., Lazzara, M. A., Keller, L. M., Tripoli, G. J., and Hitchman, M. H.: Composite analysis of the effects of ENSO events on Antarctica, Journal of Climate, 2016, 29; 5, p. 1797-1808.

Wendler, G., Stearns, C., Weidner, G., Dargaud, G., and Parish, T.: On the extraordinary katabatic winds of Adélie Land, Journal of Geophysical Research: Atmospheres, 1997, 102; D4, p. 4463-4474.

Werner, M., Heimann, M., and Hoffmann, G.: Isotopic composition and origin of polar precipitation in present and glacial climate simulations, Tellus B: Chemical and Physical Meteorology, 2001, 53; 1, p. 53-71.

Werner, M., and Heimann, M.: Modeling interannual variability of water isotopes in Greenland and Antarctica, Journal of Geophysical Research: Atmospheres, 2002, 107; D1, p. ACL 1-1 - ACL 1-13.

Werner, M., Barras, V., Brown, J., Gourcy, L., Henderson-Sellers, A., Hoffmann, G., Ichiyanagi, K., Kelley, M., Noone, D., and Roads, J.: SWING-The Stable Water Isotope Intercomparison Group, AGU Fall Meeting Abstracts, 2004,

Werner, M., Langebroek, P. M., Carlsen, T., Herold, M., and Lohmann, G.: Stable water isotopes in the ECHAM5 general circulation model: Toward high-resolution isotope modeling on a global scale, Journal of Geophysical Research: Atmospheres, 2011, 116; D15109, p. 1-14.

Werner, M., Jouzel, J., Masson-Delmotte, V., and Lohmann, G.: Reconciling glacial Antarctic water stable isotopes with ice sheet topography and the isotopic paleothermometer, Nature communications, in press.

Whillans, I., and Grootes, P.: Isotopic diffusion in cold snow and firn, Journal of Geophysical Research: Atmospheres, 1985, 90; D2, p. 3910-3918.

Wienecke, B., Lawless, R., Rodary, D., Bost, C.-A., Thomson, R., Pauly, T., Robertson, G., Kerry, K., and LeMaho, Y.: Adélie penguin foraging behaviour and krill abundance along the Wilkes and Adélie land coasts, Antarctica, Deep Sea Research Part II: Topical Studies in Oceanography, 2000, 47; 12-13, p. 2573-2587.

William, K.: Abrupt mid-twentieth-century decline in Antarctic sea-ice extent from whaling records, Nature, 1997, 389; 6646, p. 57-60.

Wit, J., Straaten, C., and Mook, W.: Determination of the Absolute Hydrogen Isotopic Ratio of V-SMOW and SLAP, Geostandards and Geoanalytical Research, 1980, 4; 1, p. 33-36.

Wolff, E., Hall, J., Mulvaney, R., Pasteur, E., Wagenbach, D., and Legrand, M.: Relationship between chemistry of air, fresh snow and firn cores for aerosol species in coastal Antarctica, Journal of Geophysical Research, 1998, 103; D9, p. 11057-11070.

Xiao, C., Ding, M., Masson-Delmotte, V., Zhang, R., Jin, B., Ren, J., Li, C., Werner, M., Wang, Y., and Cui, X.: Stable isotopes in surface snow along a traverse route from Zhongshan station to Dome A, East Antarctica, Climate dynamics, 2013, 41; 9-10, p. 2427-2438.

Xie, P., and Arkin, P. A.: Global precipitation: A 17-year monthly analysis based on gauge observations, satellite estimates, and numerical model outputs, Bulletin of the American Meteorological Society, 1997, 78; 11, p. 2539-2558.

Xin, Y., Bian, L., Rinke, A., and Dethloff, K.: Simulation and evaluation of 2-m temperature over Antarctica in polar regional climate model, Science China Earth Sciences, 2014, 57; 4, p. 703-709.

Yao, T., Petit, J., Jouzel, J., Lorius, C., and Duval, P.: Climatic record from an ice margin area in East Antarctica, Annals of Glaciology, 1990, 14; 1, p. 323-327.

York, D., Evensen, N. M., Martınez, M. L., and De Basabe Delgado, J.: Unified equations for the slope, intercept, and standard errors of the best straight line, American Journal of Physics, 2004, 72; 3, p. 367-375.

Yoshimura, K., Kanamitsu, M., Noone, D., and Oki, T.: Historical isotope simulation using reanalysis atmospheric data, Journal of Geophysical Research: Atmospheres, 2008, 113; D19108, p. 1-15.

Yoshimura, K., Frankenberg, C., Lee, J., Kanamitsu, M., Worden, J., and Röckmann, T.: Comparison of an isotopic atmospheric general circulation model with new quasi-global satellite measurements of water vapor isotopologues, Journal of Geophysical Research: Atmospheres, 2011, 116; D19118, p. 1-15.

Young, N., Raynaud, D., De Angelis, M., Petit, J.-R., and Lorius, C.: Past changes of the Antarctic Ice Sheet in Terre Adélie as deduced from ice-core data and ice modelling, Annals of Glaciology, 1984, 5, p. 239-239.

Yuan, X., and Yonekura, E.: Decadal variability in the Southern Hemisphere, Journal of Geophysical Research: Atmospheres, 2011, 116; D19, p.

Annexe A.

Coastal water vapor isotopic composition driven by katabatic wind variability in summer at Dumont d'Urville, coastal East Antarctica (Bréant et al., soumis)

Résumé. La station de Dumont d'Urville, située sur la côte est de l'Antarctique en Terre Adélie, est une des plus venteuse régions côtières du monde, à cause des vents catabatiques dévalant le long des pentes descendantes de la calotte de l'Antarctique de l'est. En été, saison d'intérêt dans cette étude, le climat côtier est caractérisé par des cycles dials très marqués de la température et des vents, associé à l'influence contrastée des vents catabatiques pendant la nuit comparé au jour. Des études récentes de mesures d'observation ont mis en évidence l'importance des rafales de vents ainsi que des processus de sublimation pour le bilan de masse de surface régional de la calotte antarctique. Notre étude a pour objectif d'explorer la valeur ajoutée des isotopes de l'eau dans la région côtière de la Terre Adélie pour fournir de nouvelles informations du cycle de l'eau atmosphérique local. Nous présentons les premières mesures continues de $\delta^{18}O$ et d-excess dans la vapeur d'eau de la Terre Adélie. Pendant notre période de mesure (26/12/2016 au 03/02/2017), nous avons observé des cycles dials en termes de température, humidité et composition isotopique. Les cycles de la composition isotopique sont particulièrement larges comparés aux variabilités faibles de la température contrairement à d'autres site d'Antarctique où des mesures similaires ont été effectuées. Nous suggérons c'est la force du vent catabatique qui contrôle la variabilité dial du $\delta^{18}O$ et du d-excess en été à Dumont d'Urville : les forts vents catabatiques apportent un air relativement sec avec de la vapeur d'eau composée de faibles $\delta^{18}O$ et de forts d-excess depuis le plateau de l'Antarctique jusqu'au basses couches atmosphériques de DDU. Finalement, notre étude a des conséquences pour l'interprétation de la neige des profils isotopiques enregistrés dans les carottes de glace des régions côtières aussi bien pour l'évaluation des modèles atmosphériques équipés des isotopes de l'eau que pour l'interprétation des carottes de glace.

Coastal water vapor isotopic composition driven by katabatic wind variability in summer at Dumont d'Urville, coastal East Antarctica

Camille Bréant[1], Christophe Leroy Dos Santos[1], Mathieu Casado[1], Elise Fourré[1], Sentia Goursaud[1], Valérie Masson-Delmotte[1], Vincent Favier[2], Cécile Agosta[1,2], Olivier Cattani[1], Frédéric Prié[1], Benjamin Golly[2], Anaïs Orsi[1], Patricia Martinerie[2], Amaëlle Landais[1,]*

[1] Laboratoire des Sciences du Climat et de l'Environnement (LSCE) - IPSL, UMR 8212, CEA-CNRS-UVSQ, Université Paris-Saclay, F-91190 Gif sur Yvette, France

[2] Univ. Grenoble Alpes, CNRS, IRD, Grenoble INP, Institut de Géophysique de l'Environnement (IGE), F-38000 Grenoble, France

[*] corresponding author : amaelle.landais@lsce.ipsl.fr

Abstract

Dumont d'Urville station, located on the East coast of Antarctica in Adélie Land, is in one of the windiest coastal region on Earth, due to katabatic winds downslope from the East Antarctic ice sheet. In summer, the season of interest in this study, coastal weather is characterized by well-marked diel cycles in temperature and wind patterns, associated with the contrasted influence of katabatic winds during night time and during day time. Recent monitoring studies have evidenced the importance of blowing snow as well as snow sublimation processes for the regional surface mass balance of the Antarctic ice sheet. Our study aims at exploring the added value of water stable isotopes in coastal Adélie Land to provide new information on the local atmospheric water cycle. We present the first continuous measurements of $\delta^{18}O$ and d-excess in water vapor over Adélie Land. During our measurements period (26/12/2016 to 03/02/2017), we observed clear diel cycles in term of temperature, humidity and isotopic composition. The cycles in isotopic composition are particularly large given the muted variations in temperature when compared to other Antarctic sites where similar monitoring have been performed. We suggest that the driver for $\delta^{18}O$ and d-excess diel variability in summer at Dumont d'Urville is the katabatic wind force: strong katabatic winds bring relative dry air with water vapor associated with low $\delta^{18}O$ and high d-excess from the Antarctic plateau to the low level atmospheric layer of DDU. Finally, our study has implications for the interpretation of snow and ice core isotopic profiles in these coastal regions as well as for the evaluation of atmospheric models equipped with water isotopes and ice core interpretation.

1. Introduction

Adélie Land, located on the coast of Antarctica, in the Indian Ocean sector (Figure 1) is one of the windiest coastal regions on Earth, due to katabatic winds blowing downslope from the East Antarctic Plateau (Pettré et al., 1993; Wendler et al., 1997; König-Langlo et al., 1998). This region is also associated with a coastal winter polynya playing a key role on sea ice formation, deep water formation, and associated food webs (Kusahara et al., 2017). Large variations of regional sea ice extent have been monitored since 1979 (Massom et al., 2013), with maximum expansion of pack ice up to 300 km from the coast (Massom & Stammerjohn, 2010; Tamura et al., 2016). Sea ice may persist during summer months (Smith et al., 2011). Located at (66°39'N, 140°00 E) in Adélie Land, the Dumont d'Urville station (hereafter DDU) has provided continuous weather monitoring since 1957 (Périard & Pettré, 1993). In summer, the season of interest in this study, coastal weather is in general characterized by well-marked diel cycles in temperature and wind patterns, associated with the contrasted influence of katabatic winds during night time and upslope sea breezes during day time (Gallée & Pettré, 1998). Recent monitoring studies have evidenced the importance of blowing snow as well as snow sublimation processes for the regional surface mass balance of the Antarctic ice sheet (Grazioli et al., 2017; Barral et al., 2014; Amory et al., 2015). Along traverses from DDU to Dome C, repeated accumulation measurements on stake areas provide key information on the spatio-temporal patterns of ice sheet surface mass balance in coastal East Antarctica (Agosta et al., 2012; Favier et al., 2013). Still, the contribution of the different surface and atmospheric processes related to water cycle on the surface mass balance remains unknown and may bias the final estimate. As an example, the recent study of (Grazioli et al., 2017) suggests that low-level sublimation linked to katabatic winds can lead to a 35% reduction of snowfall on the East Antarctic coast and to a 17% reduction when considering whole Antarctica. Our study is thus motivated by the need to better document and understand the processes affecting atmospheric moisture transport and snow-air exchanges in coastal polar areas with climatic conditions comparable to Adélie Land.

Here, we explore the added value of water isotopes to document the local and regional atmospheric water cycle through presentation of new stable isotopic measurements on water vapor performed in the summer season during 40 days at DDU near the surface. Water stable isotopes are integrated tracers of the atmospheric water cycle, as equilibrium and kinetic fractionation leave an imprint of each process occurring along the moisture path: evaporation, atmospheric moisture transport, and condensation (Jouzel, 2013). In ice cores, water stable isotopes are amongst the core classical measurements. In high accumulation regions, they are combined with ice core chemistry measurements to identify seasonal cycles and develop ice core layer counted chronologies (e.g. Thomas et al., 2017; Roberts et al., 2015). In central Antarctic regions, the variability of water stable

isotopes ($\delta^{18}O$ or δD) in precipitation is dominated by a fingerprint of local temperature variability at daily, seasonal and inter-annual scales (Stenni et al., 2016). In contrast to sites located on the East Antarctic plateau where the temperature-driven distillation effect is more important than oceanic source effects on precipitation water isotopic variations (e.g. Touzeau et al., 2016), the climatic interpretation of water isotopic composition in coastal regions is more ambiguous (e.g. Altnau et al., 2014; Goursaud et al., 2016). Indeed, the influence of the origin of precipitation on water isotopes composition is probably more important in coastal regions than in the Antarctic plateau (Jouzel et al., 2013). In addition, in coastal areas characterized by intense winds, deposition effects linked to sublimation of falling snow and post-deposition effects linked with remobilization of surface snow (e.g. blowing snow) are expected to alter the snow isotopic composition, hence complicating the climatic interpretation of the water stable isotope variability (e.g. Landais et al., 2017). Recently, one 22.4 m ice core spanning the period 1946-2006 was retrieved 10.24 km far from DDU. Decadal variations in $\delta^{18}O$ are parallel to decadal variations in DDU surface air temperature (Goursaud et al., 2017), but sub-decadal variations remain unexplained and could arise from variations in moisture origin as well as deposition or post-deposition "noise", calling for water isotope measurements in the vapor to decipher the processes at play at the scale of weather events.

Recent studies have used continuous monitoring of water stable isotopes in surface water vapour and surface snow in Antarctica to explore the influences of both atmospheric dynamic and post-deposition effects on surface snow isotopic composition (Ritter et al., 2016; Casado et al., 2016). These studies have evidenced patterns of diel variations, and demonstrated that the surface snow isotopic composition can change in-between precipitation events in parallel with changes in vapour isotopic composition, itself driven by changes in atmospheric advection patterns, as initially observed above the Greenland ice sheet (Steen-Larsen et al., 2014). Diel variations in surface vapour isotopic composition were also reported in summer in polar regions with no snow cover, for instance in Kangerlussuaq, West Greenland (Kopec et al., 2014). In this site, the diel variations were attributed to local boundary layer characteristics involving sea breeze processes. Day to day surface vapour isotopic variations monitored from a ship were also related to shifts in very local atmospheric circulation patterns near Syowa, on the East Antarctic coast (e.g. Kurita et al., 2016a; Kurita et al., 2016b).

Our study is motivated by the need to better understand the drivers of water vapour isotope variations in Adélie Land for (i) ice core interpretation, (ii) exploring the added value of water stable isotopes to provide new information on the local atmospheric moisture budget and thus (iii) improving our knowledge of the present and recent coastal climate and water cycle variations. This is relevant for the regional surface mass balance of the ice sheet as well as for the evaluation of atmospheric models equipped with water isotopes. We have thus implemented a laser spectroscopy instrument to measure

continuously the isotopic composition of water vapor at DDU during summer 2016-2017, taking advantage of the excellent facilities of the station.

This paper is organized as follows. We first report (Section 2 and SOM) the experimental set up, as well as the calibration of the isotopic measurements to provide continuous $\delta^{18}O$ and d-excess measurements in the water vapor at DDU during 40 days. The analysis of the calibrated dataset (Section 3) depicts different periods of measurements based on weather conditions, especially wind regimes, sky conditions and one snowfall event. The unequivocal isotopic diel cycles in DDU surface water isotopes are characterized in terms of amplitude and timing (Section 4) and compared with local meteorological data as well as diel cycles observed in continuous water vapor $\delta^{18}O$ time series in other polar regions. We then summarize our key findings and suggest ways forward (Section 5).

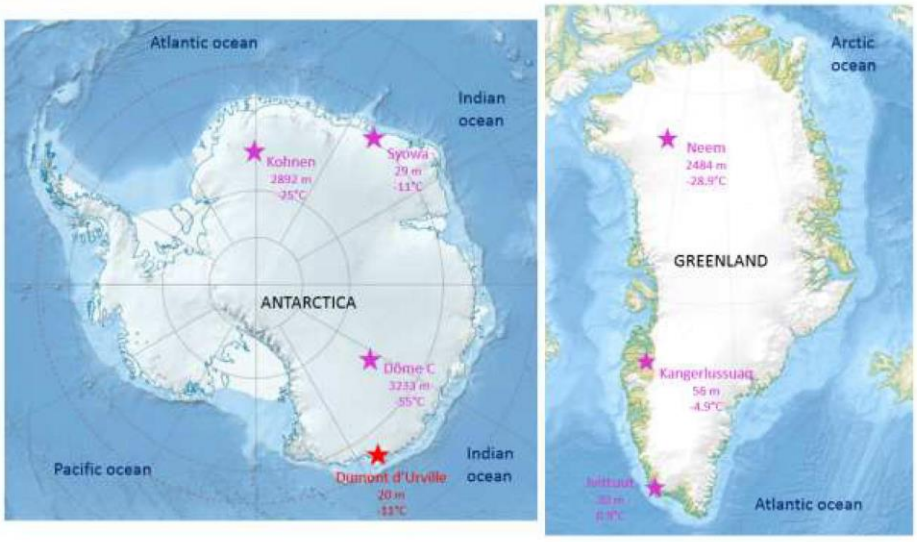

Figure 1: Maps of Antarctica (left) and Greenland (right) showing the location of our study site (red) and the location of other sites where continuous water stable isotope records have provided insights on diel variations (pink). For each site, height and near-surface mean annual temperature are given.

2. Analytical method

We installed a PICARRO Li-2130 laser spectroscopy in the "Laboratoire 3" shelter, located on the inland side of DDU station (Figure 2). A 6 m length heated copper tube has been deployed to continuously sample water vapor at 2 m above the snow surface. The extremity of the tube was covered by a Gelman Zefluor 0.5 µm filter to prevent the inflow of precipitation or blowing snow. Continuous measurements of water vapor isotopic composition took place during 40 days from

December 26th 2016 to February 3rd 2017. Except for one electrical shutdown on January 4th 2017, the only interruptions of our monitoring occurred during bi-daily calibrations.

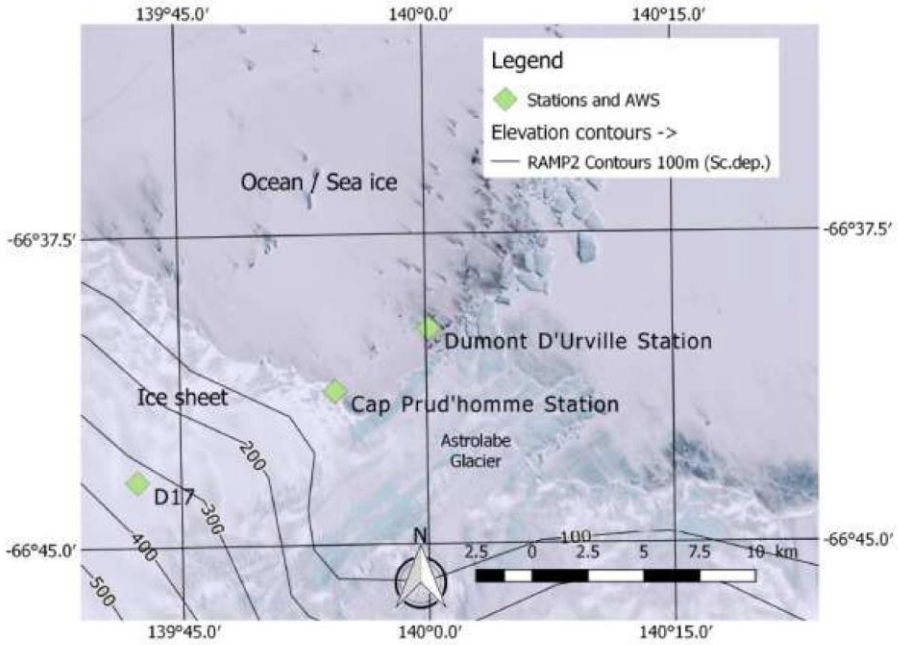

Figure 2: Map of DDU station showing the location of the two AWS installed at Cap Prud'homme and D17. Background image is a 15-m resolution Landsat Image Mosaic of Antarctica from the area taken between 1999-2002 (Bindschadler et al., 2008). Elevation lines are extracted from the digital elevation model from Radarsat Antarctic Mapping Project Digital Elevation Model Version 2 (RAMP2, Liu et al., 2001). The map was designed with Quantarctica3 (https://www.qgis.org/fr/site/about/case_studies/antarctica.html).

During our monitoring period, the humidity varied between 2000 and 6000 ppmv. The raw $\delta^{18}O$ values varied typically between -23 and -35‰ (Figure 3). The procedure for calibration of the raw data is detailed in supplementary material. Despite problems with the calibration module, we followed as much as possible the correction proposed in previous studies. We thus corrected the raw laser spectroscopy $\delta^{18}O$ measurements for (1) shifts between measured $\delta^{18}O$ and δD and true $\delta^{18}O$ and δD values , (2) the temporal drift of the instrument for $\delta^{18}O$ and δD and (3) the influence of humidity on $\delta^{18}O$ and δD values (Tremoy et al., 2012; Hans Christian Steen-Larsen et al., 2013). The uncertainties on the isotopic measurements then mainly result from scattering of the calibration points as well as missing calibration points during several weeks. The upper limits of uncertainties on the absolute values of $\delta^{18}O$ and d-excess (δD-8*$\delta^{18}O$) vary respectively between 1‰ and 3.5‰ and between 5‰ and 25‰.

This uncertainty, mainly linked to unknown drift, should be applied on the absolute values of $\delta^{18}O$ and d-excess but not on their short-term variations, at the timescale of a few days. In the following sections of this manuscript, we thus do not discuss much the absolute values of $\delta^{18}O$ and d-excess but rather focus on the short-term (diel) variability.

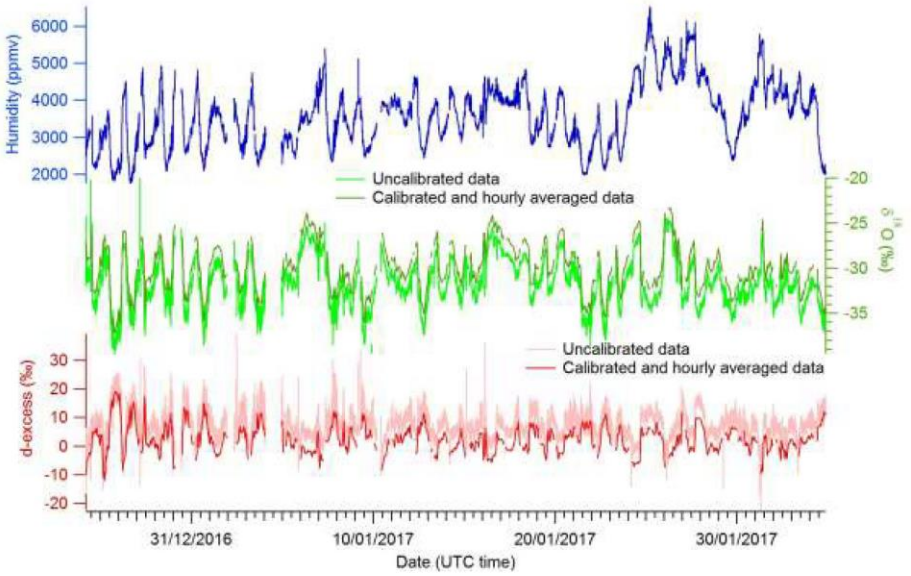

Figure 3: Humidity (blue), $\delta^{18}O$ (green) and d-excess (δD-8$\delta^{18}O$, red) measured by the laser spectroscopy instrument at DDU. Raw data (resolution of one minute) are shown in light green and light red for $\delta^{18}O$ and d-excess respectively. Calibrated $\delta^{18}O$ and d-excess data (hourly resolution) are shown in dark green and brown, respectively.*

The DDU weather station provides continuous measurements at hourly resolution. Temperature and humidity are measured from a Vaisala HMP 110 probe in a standard meteorological shelter, 1.5 m above the ground surface. Wind speed and direction are measured on a 10 m tower located a few meters from the meteorological shelter. Surface wind directions can be used to separate between winds with continental origin and winds with oceanic origins. Jourdain (2001) and Angot et al. (2016) identified oceanic winds at DDU in the range from 270 to 110°, the other winds having a continental origin.

January 2017 is a relatively warm month with a mean monthly air temperature of -0.4°C, compared to a mean January temperature of -0.9 °C (±0.9°C) over the whole 1957 -2017 record, though not extreme

(a mean air temperature of 1°C was recorded in January 1972 and 2010). In January 2017, the sea ice extent around DDU is among the three largest summer sea ice extents observed around DDU (with January 2012 and January 2013) over the last 44 years, as estimated from the Hadley Center Sea Ice and Sea Surface Temperature data set HadISST.2 (Titchner & Rayner, 2014), comparable to the sea ice extent observed in January 2012 and 2013. Even though a direct causal link has not been proven with sea ice extent, we note that the January 2017 Southern Annular Mode index is unusually low, showing the lowest value since 1993, and the 5th lowest value since 1984 (Marshall, 2003).

In addition, for this study we used the meteorological data recorded by the automated weather station (AWS) set up at Cap Prud'homme (66.688°S, 139.907°E, 5 km from Dumont d'Urville on the continent, 27 m above sea level, Figure 2). The sensor characteristics are listed in Favier et al. (2011). Quantities were recorded as half-hourly means of measurements performed at 10 s time intervals.

The data obtained at DDU and at Cap Prud'homme are well correlated at the hourly scale over the whole period of measurements. In the following, we present the temperature and wind speed data from Cap Prud'homme because (1) they were obtained on the continent, in an area more directly influenced by the katabatic winds and (2) the data are less affected by buildings on the station as in DDU.

3. Results

Figure 4 displays our 40-day record of DDU water vapor isotopic composition in parallel with temperature, humidity, wind speed, wind direction and incoming longwave indicating the cloud coverage. The isotopic composition time series are overall well correlated with humidity and temperature. While we do not comment on the long term trends of the water isotopic ratios because of calibration issues reported above, we note that humidity measured with the same instrument and validated by other sensors reaches high levels (above 5000 ppmv) during the period between January 25th and 28th, corresponding to the longest snowfall event of the monitoring period. This period is also associated with high incoming longwave showing radiation as expected under wet and cloudy conditions. Wind speed does not exhibit much long term variability (i.e. at the timescale of a few days/weeks) except for a period with almost no wind between the 16th and the 18th of January and periods of strong winds at the end of January / beginning of February when cloudy conditions prevail.

At shorter timescales, we observe strong diel cycles in δD, $\delta^{18}O$, temperature, humidity, and wind characteristics. The diel variations in wind direction are however beyond detectability in the case of

very low wind speeds (i.e. below 3 $m.s^{-1}$ such as between the 16th and the 18th of January). The most reliable wind direction is the one measured when wind speed is larger than 5 $m.s^{-1}$: in this case, wind mainly originates from katabatic forcing and has a continental origin. Diel cycles of $\delta^{18}O$, temperature, humidity, wind speed and d-excess are visible almost over the whole period. We nevertheless observe a strong variability on the amplitude of the different cycles. As examples, maximal (minimal) amplitudes of diel cycles in $\delta^{18}O$, temperature and humidity are respectively 11.5‰ (0.9‰), 8°C (1°C), 2640 ppmv (280 ppmv).

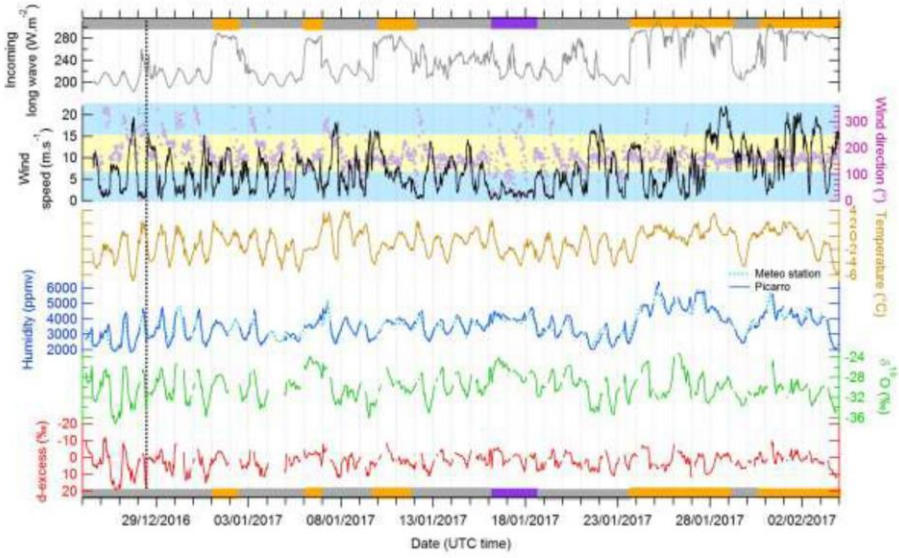

Figure 4: Evolution of incoming long wave (used here to differentiate cloudy from clear sky conditions), wind strength, wind direction and temperature from the Cap Prud'homme automatic weather station and humidity from DDU meteorological station together with the evolution of humidity, $\delta^{18}O$ and d-excess recorded by our laser instrument. In the second upper panel, the horizontal blue and yellow bands stand for the range of direction winds originating from the ocean or from the continent respectively. The grey, orange and violet rectangles indicate the periods which are the focus of Figure 5 (clear sky, cloudy, no wind). The snowy period (25th to 28th of January 2017) is included in the cloudy periods. The dashed vertical line corresponds to a specific event discussed in section 4.

4. Discussion

4-1- Characteristics of diel cycles

We have clustered our measurements based on the weather conditions in periods with clear sky (grey on Figure 4), cloudy conditions (orange on Figure 4) and no wind conditions (violet on Figure 4, corresponding to days without katabatic wind occurrence even during the night). During the period without wind, only a small diel cycle is observed in the temperature record but no clear diel cycles are observed in the humidity and $\delta^{18}O$ records. On the contrary, during the clear sky periods, clear diel cycles are observed in temperature (mean amplitude of 4.5°C), humidity (mean amplitude of 1300 ppmv), $\delta^{18}O$ (mean amplitude of 5.4 ‰), d-excess (mean amplitude of 10 ‰) and wind speed (mean amplitude of 7 $m.s^{-1}$) (Figure 5a). In most cases, there are significant correlations (Table 1) between temperature, humidity and $\delta^{18}O$ while both d-excess and wind speed are significantly anti-correlated with these 3 parameters. However, the correlation between $\delta^{18}O$ and near surface temperature diel cycles is surprisingly low (R^2=0.24), given the relationship between temperature, atmospheric distillation and isotopic depletion leading to a strong correlation (R^2=0.9) on the Antarctic plateau between near surface temperature and $\delta^{18}O$ of precipitation or surface snow along transects (Touzeau, et al., 2016; Stenni et al., 2016; Masson-Delmotte et al., 2008). When extracted the typical average diel cycles for the 5 parameters mentioned above (Figure 5a), we do not observe significant temporal shift between the maxima / minima in each record: temperature maximum is synchronous with minimum in wind speed, maximum in $\delta^{18}O$, maximum in humidity and minimum in d-excess. During the cloudy periods, diel cycles are less marked and the (anti-)correlations between the different parameters are much less clear (Figure 5b). In this case, we note a correlation between temperature and humidity as well as an anti-correlation between $\delta^{18}O$ and d-excess.

The relatively low correlation between temperature and $\delta^{18}O$ even during the clear sky conditions rules out local air temperature as the main driver of vapor $\delta^{18}O$ diel variations. In order to progress in our understanding of the mechanisms leading to vapor $\delta^{18}O$ variations in January 2017, back-trajectories were calculated over the whole period using the HYSPLIT trajectory model, with the global data assimilation system from the US national weather service (NCEP, National Centers for Environmental Prediction). Calculations were performed over 5 days prior to arrival at an elevation of 20 m at the location of DDU, with a time step of 3 hours. Except for the heavy snowfall event (from the 25th to the 28th of January), all other back-trajectories show an origin of air masses from the Antarctic continent (Figure 6). This is not in agreement with the measured local wind direction showing very weak winds from an oceanic origin during the warmest periods. Still, as mentioned, these periods are associated with very weak wind speed so that the wind direction measured locally at 20 m height is not very reliable.

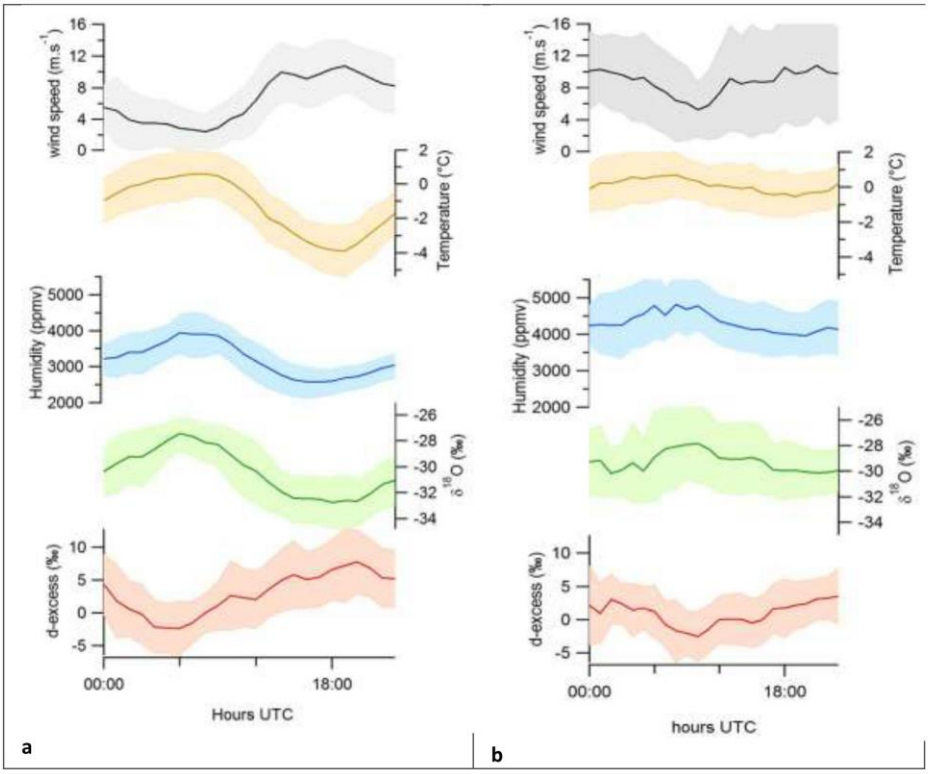

Figure 5: Average diel cycles of wind speed, temperature, humidity, $\delta^{18}O$ and d-excess during periods with clear sky conditions (a) and cloudy conditions (b) (see Figure 4 for identification of these time periods). The hourly data for the two different periods were averaged to produce the respective mean diel cycles. The envelopes in light colors were obtained from the standard deviation of the data obtained over the different days within each period. The time zone at DDU is UTC+ 10.

Variables \ Periods	Clear Sky	Cloudy
d-excess vs temperature	0.18 (-6 ‰.K^{-1})	0.01
humidity vs temperature	0.49 (221 ppmv.K^{-1})	0.32
$\delta^{18}O$ vs temperature	0.24 (0.39 ‰.K^{-1})	0.11
d-excess vs $\delta^{18}O$	0.73 (-0.42)	0.56
$\delta^{18}O$ vs humidity	0.73 (0.003 ‰.$ppmv^{-1}$)	< 0.01
d-excess vs humidity	0.51 (-0.42 ‰.$ppmv^{-1}$)	< 0.01
Wind speed vs temperature	0.27 (1.1 $m.s^{-1}.K^{-1}$)	0.05
Humidity vs wind speed	0.36 (-244 ppmv.$s.m^{-1}$)	0.09
$\delta^{18}O$ vs wind speed	0.36 (-0.34 ‰.$s.m^{-1}$)	0.11
d-excess vs wind speed	0.11 (-0.42 ‰.$s.m^{-1}$)	< 0.01

Table 1: Correlation coefficients (R^2) between different climatic and/or isotopic parameters during the clear sky and cloudy periods at DDU based on hourly data (N=505 for clear sky periods; N=289 for cloudy periods). The slope between the two parameters is also reported within brackets for clear sky conditions when correlation and anti-correlation coefficients are at the highest. Note that although wind speed and d-excess appear correlated on figure 5b on an average diel cycle, this is not the case when taking all the individual data from the cloudy period.

261

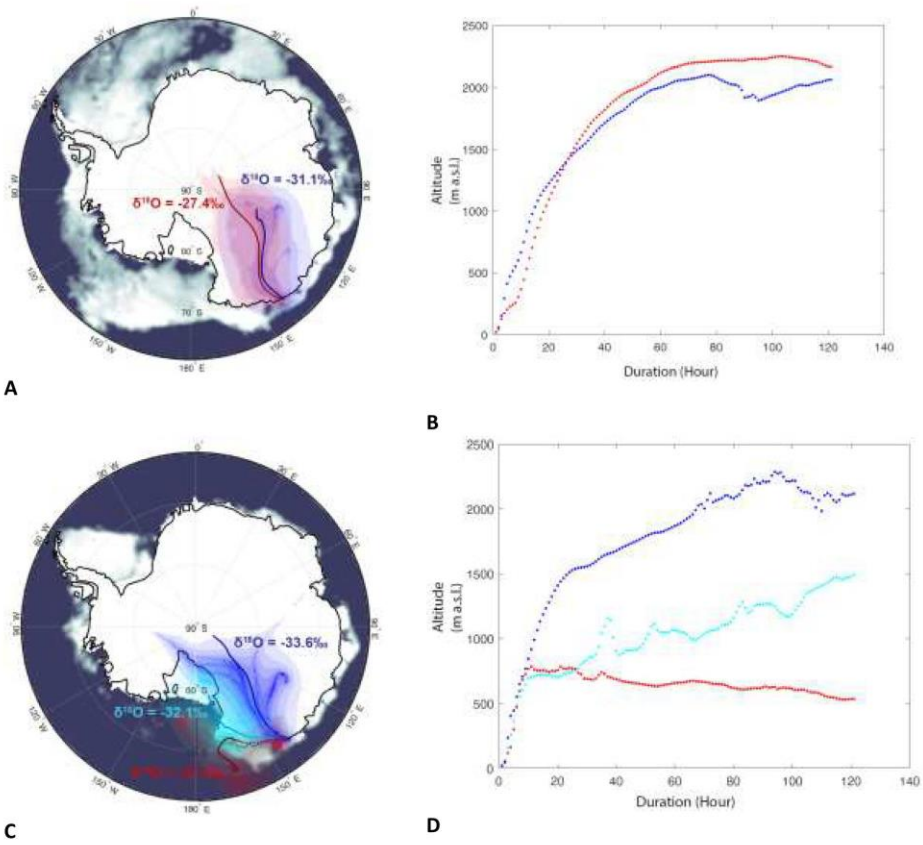

262 *Figure 6: Back trajectories leading to different isotopic composition at DDU during clear sky conditions*
263 *(a and b, 2nd to 5th of January) and during snow conditions (c and d, 25th to 28th of January 2018). Maps*
264 *a and c present (i) the clusters of back-trajectories (shades) separated according to the $\delta^{18}O$ values (a:*
265 *red for $\delta^{18}O$ higher than -29 ‰; blue for $\delta^{18}O$ lower than -29 ‰; c: red for $\delta^{18}O$ higher than -30 ‰; blue*
266 *for $\delta^{18}O$ lower than -30 ‰) and (ii) the barycentres of the ensemble of trajectories (lines) of the water*
267 *vapor. Plots b and d present the mean altitudes along each cluster identified by same colors as in maps*
268 *a and c. Note that 2 clusters and barycentres of back trajectories (deep blue and light blue) are observed*
269 *for $\delta^{18}O$ values lower than -30 ‰ in map c (snow conditions).*

270

271 We propose that the coastal atmospheric dynamics around DDU are the driver of the diel cycles during
272 clear sky summer conditions. While the surface ocean temperature remains mostly stable during the
273 day, the continental temperature above DDU region exhibits a diel cycle linked to incoming shortwave
274 with a minimum at 18:00 UTC (Figure 5a). A temperature gradient between the continent and the coast
275 occurs between ~12:00 and 24:00 UTC (cold phase at DDU) enhancing the dry katabatic winds flowing
276 downslope from the relatively cold continent to the coastal region. These strong continental winds

277 bring cold air mass with low humidity, water vapor being characterized by low $\delta^{18}O$ and high d-excess
278 since surface snow $\delta^{18}O$ has been shown to decrease and d-excess to increase from the coast to inland
279 Antarctica (e.g. Masson-Delmotte et al., 2008; Touzeau et al., 2016).
280 During cloudy period, diel temperature variations are muted (Figure 5b). The wind speed cycles are
281 also less systematic over this period with days associated with relatively strong wind (e.g. beginning of
282 February). As already pointed out, only the anti-correlation between $\delta^{18}O$ and d-excess is preserved.
283 During the arrival of a low pressure system at DDU (as observed between the 25th and the 28th of
284 January), higher winds are associated with trajectories originating from the ocean with distinctive
285 higher $\delta^{18}O$ and lower d-excess signatures as compared to the continental water vapor. In this case,
286 wind speed is correlated with relative humidity (and with $\delta^{18}O$ to a lesser extent). The anti-correlation
287 between $\delta^{18}O$ and d-excess is preserved, as also observed during cloudy and clear sky conditions. Only
288 with very weak surface winds (lower than 3 m.s^{-1}) does the anti-correlation between $\delta^{18}O$ and d-excess
289 at the diel scale disappear.
290 Diel isotopic cycles in this region may also arise from other processes, such as the influence of
291 sublimation of blowing snow. Indeed, Barral et al. (2014) and Grazioli et al. (2017) showed that
292 sublimation of blowing snow affects vertical humidity profiles in Adélie land. Barral et al. (2014)
293 evidenced a correlation between relative humidity of the low level of the atmosphere and katabatic
294 wind speed at the windy plateau station D17. This is interpreted as an increase in sublimation of
295 blowing snow during strong wind conditions. At DDU, the situation is however different. First, using
296 our temperature and humidity records to calculate relative humidity, we show that the atmosphere is
297 always undersaturated at DDU, except during snowfall events. Second, under clear sky conditions, diel
298 cycles of relative humidity are anti-correlated with wind speed at DDU (similarly to the anti-correlation
299 between specific humidity and wind speed observed in Figure 5a) in contrast with the positive
300 correlation observed by Barral et al. (2014) at D17. Third, if sublimation of local blowing or precipitating
301 snow was a large source of surface vapor in response to strong katabatic winds as proposed by Grazioli
302 et al. (2017), then one would expect to observe a parallel increase of surface vapor $\delta^{18}O$ as snow is
303 enriched in heavier isotopes compared to water vapor. In contrast, we observe an anti-correlation
304 between $\delta^{18}O$ and wind speed (Figure 5a). Based on these lines of evidence, we conclude that diel
305 variations in atmospheric dynamics and associated variations in transport of air masses from the
306 plateau to the coast are better candidates to explain the $\delta^{18}O$ and d-excess diel cycles than diel
307 variations in the sublimation of blowing snow at DDU. This contrasts with the situation on a coastal
308 plateau station such as D17.
309
310 **4-2- Comparison between DDU diel cycles and diel cycles at other polar locations**

We now compare the occurrence, amplitude and characteristics of diel cycles in DDU isotopic records with other available records from polar regions. We explore whether there are systematic links between the characteristics of diel cycles in surface water vapor $\delta^{18}O$ and those in meteorological variables, as well as the relationships between diel isotopic cycles and geographic characteristics such as the distance to the open sea. Table 2 summarizes the characteristics of diel cycles observed in all available water vapor isotopic datasets from Greenland and Antarctica. These records encompass summer seasons, most of them with documented snowfall events. At each site, diel cycles of temperature and humidity are identified most of the time. We thus calculated a characteristic diel cycle at each site through an average over a period of 5-7 consecutive days with unequivocal diel cycles of average amplitude. The smallest amplitudes of temperature diel cycles are observed in coastal regions of Antarctica (DDU and Syowa) as expected from the oceanic influence. The smallest amplitudes of the water vapor $\delta^{18}O$ and d-excess diel cycles are also observed at some coastal stations (Syowa, Ivittuut). Inland Antarctica, $\delta^{18}O$ diel cycles display amplitudes larger than 4.5‰; diel temperature variations are also large (larger than 8°C). There is however no systematic correspondence between the amplitude of the temperature diel cycle and the amplitude of the $\delta^{18}O$ diel cycle. This is particularly remarkable at DDU, where we observe a relatively small amplitude of temperature diel cycles (comparable to the other coastal station in Antarctica), but an unusually large amplitude of the $\delta^{18}O$ diel variations (5.4 ‰ against 1 ‰ at the coastal locations of Syowa and Ivittuut). The relatively strong $\delta^{18}O$ diel variations observed at the coastal DDU station is in fact rather comparable to the one observed in the coastal station of Kangerlussuaq in summer 2011 (amplitude of $\delta^{18}O$ diel cycle of 3.5 ‰ to be compared to 1.4 ‰ at the Greenland coastal station of Ivittut). This pattern was attributed to the alternation between sea breeze and katabatic winds (Kopec et al., 2014).

		Dôme C[a]	Kohnen Station[b]	NEEM[c]	Ivittuut[d]	Syowa[e]	Kangerlussuaq[f]	DDU[g]
Temperature (°C)	Average value	-30.8	-23.4	-10.3	9.5	-1.9	10.0	**-0.5**
	Diel cycle amplitude	11.1	8.7	9.7	7.6	3.2	10.3	**4.5**
Humidity (ppmv)	Average value	600	1200	3100	11100	3900	7400	**3200**
	Diel cycle amplitude	500	1000	2100	1900	600	2200	**1300**
$\delta^{18}O$ (‰)	Average value	-68.94	-54.74	-43.83	-18.88	-28.12	-30.50	**-30.37**
	Diel cycle amplitude	6.48	4.87	3.01	1.36	2.23	3.51	**5.40**
d-excess (‰)	Average value	58	30	37	9	15	14	**3**
	Diel cycle amplitude	22	11	4	7	8	11	**10**
Period used for cycles characterization (days)		04/01/15 to 11/01/15	20/12/13 to 27/12/13	01/07/10 to 08/07/10	13/07/12 to 20/07/12	28/01/14 to 04/02/14	08/08/11 to 15/08/11	**Clear sky periods of this study**
Period of measurements (days)		25/12/14 to 17/01/15	17/12/13 to 01/01/14	24/05/10 to 29/07/10	01/07/12 to 31/07/12	20/01/14 to 09/02/14	21/07/11 to 15/08/11	**25/12/16 to 03/02/17**
Height of measurements (m)		2	0.2 – 3	0.1 – 1.5	5	1	1	**2**
Strong snowy period (days)		Not documented	19/12/12, 03/01/13, 07/01/13 and 17/01/13	28/06/10	Not documented	17/01/15 to 19/01/15	Not documented	**25/01/17 to 28/01/17**

333

334 *Table 2: Comparison of the diurnal evolutions of the climatic (temperature, humidity) and isotopic ($\delta^{18}O$, d-excess) parameters for different polar sites where*
335 *isotopic composition of water vapor is available.* [a]Casado et al., 2016 ; [b]Ritter et al., 2016 ; [c]Steen-Larsen et al., 2011 ; Steen-Larsen et al., 2013 ; [d]Bonne et
336 al., 2014 ; [e]Kurita et al., 2016b, Kurita et al., 2016a ; [f]Kopec et al., 2014; [g] *This study*

337

At all sites exhibiting a diel cycle, the warmest hours are also associated with the highest humidity level and the highest $\delta^{18}O$ values. The link with wind speed is less systematic: higher wind speeds are observed during the warmest hours at Dome C, but during the coldest hours at DDU. A significant correlation is identified between $\delta^{18}O$ and temperature diel variations at most polar sites (DDU, Kohnen, Dome C, Ivittuut, Kangerlussuaq, NEEM), and for intra-seasonal variations in the absence of strong snow events at NEEM and Ivittuut, Greenland. At the diurnal scale, the $\delta^{18}O$ vs temperature slope is lower for continental sites (~ 0.6 ‰.°C^{-1} on average) than for coastal sites where isotopic diurnal cycles are clearly visible (i.e. Kangerlussuaq and DDU, 1.2 ‰.°C^{-1} on average). This confirms the similarities of the diel cycles identified in the short records available at Kangerlussuaq (25 days) and DDU (40 days), and motivates a detailed analysis of the water vapor isotopic variations on the two sites. We note that both records are hampered by calibration issues. No calibration of the isotopic data is presented for the Kangerlussuaq record, and we have reported the problems encountered with the standard delivery module at DDU and the resulting uncertainties.

The meteorological characteristics encountered during boreal summer 2011 in Kangerlussuaq and austral summer 2016-2017 in DDU reveals some similarities. Both exhibit a rather large amplitude of diel cycle for water vapor $\delta^{18}O$ in link with wind speed cycles. These two locations are affected by katabatic winds, stronger at DDU than at Kangerlussuaq (between 2 and 7 m.s^{-1} at Kangerlussuaq and between 0 and 20 m.s^{-1} at DDU). Despite these similarities, local summer humidity levels are much lower at DDU than at Kangerlussuaq. Kangerlussuaq is located in an alluvial flatland, near the confluence of two major regional rivers originating from the Russell Glacier, and its peak precipitation usually occurs in July-August. In summer 2016-2017, the presence of sea ice up to a distance of 70 km from DDU probably also explains our low humidity levels.

At Kangerlussuaq, the $\delta^{18}O$ and d-excess diel variations are explained by shifts in moisture origin, linked to local wind directions (Kopec et al., 2011). At night, continental winds bring relatively dry air with low $\delta^{18}O$ (high d-excess) of water vapor from the continent to the coastal station in the atmospheric boundary layer. During the day, due to increasing coastal land surface temperature, a sea breeze phenomenon occurs, bringing air masses with higher humidity levels of oceanic origin associated with high $\delta^{18}O$ (low d-excess). At DDU, we could not identify such a sea breeze phenomenon during summer 2016-2017 since, based on back-trajectory analyses, the origin of low level air mass remains always the same (i.e. from the continent). The diel cycles may thus rather be triggered by variations in the intensity of continental winds, themselves related to diel temperature variations over the continent. The occurrence of a summer sea breeze phenomenon was clearly observed at DDU in earlier years (Angot et al., 2016; Pettré et al., 1993; Jourdain, 2001). It may have been prevented by the particularly large sea ice extent during January 2017.

372

373 **4-3- Sharp intra-daily isotopic variations and added value of water isotopes measurements**

374 Finally, the fact that the impact of katabatic winds is also obvious in diel cycles of humidity and
375 temperature questions the added value of measuring the isotopic composition of water vapor. Still,
376 our record permits to identify at least one case in which continuous measurements of $\delta^{18}O$ and d-
377 excess in the water vapor reveal an event not captured in the temperature and humidity series. We
378 focus on a particular rapid event which occurred on December 28th, with a 3h sharp negative peak of
379 $\delta^{18}O$ of 8.5 ‰ (with $\delta^{18}O$ values reaching -34 ‰), close to the amplitude of the average diel cycle
380 (Figure 7). The associated d-excess increase is very strong and reaches 26 ‰, i.e. more than twice
381 larger than the amplitude of the diel cycle during clear sky conditions. These remarkable isotopic
382 excursions correspond to an abrupt change in the wind strength and direction, the 3-hour isotopic
383 peak itself corresponding to winds originating from the continent, hence probably bringing air masses
384 reflecting the isotopic composition of the East Antarctic plateau surface vapor, with low $\delta^{18}O$ and high
385 d-excess. This particular event confirms the influence of the atmospheric dynamic on the isotopic
386 composition of low level water vapor. It shows that the atmospheric dynamic and associated wind
387 characteristics should be considered when interpreting water isotopic records in coastal Adélie Land.

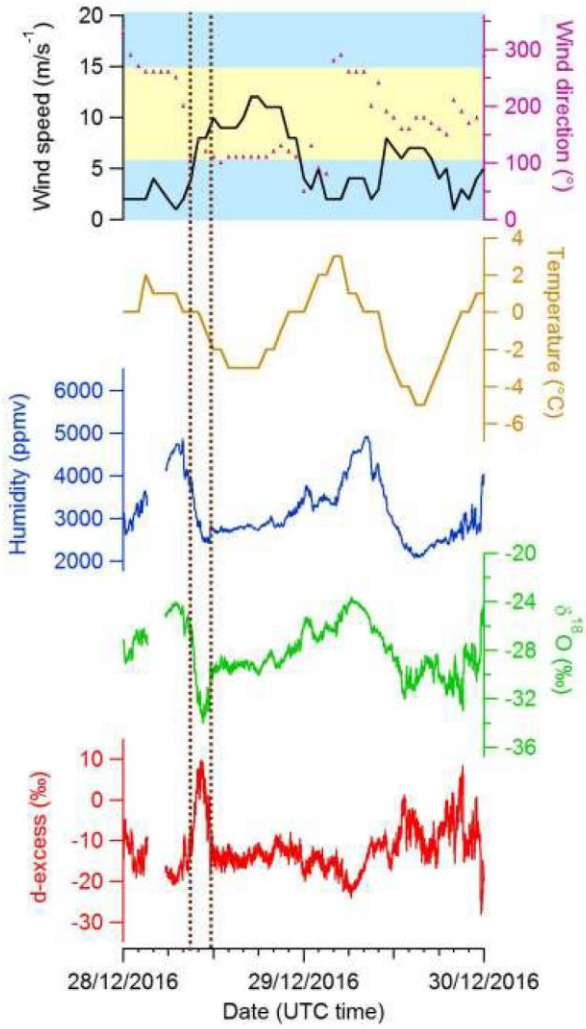

388

389 *Figure 7: Focus on a peak of $\delta^{18}O$ and d-excess (vertical dashed brown lines) on the 28th of December*
390 *2016 (zoom from Figure 4).*
391

392 **5. Conclusion and perspectives**

393 We presented the first water vapor isotopic record at the coastal station DDU in Adélie Land, a region
394 strongly influenced by katabatic winds. During a 40 days measurement period, we evidenced clear and
395 strong diel cycles especially during clear sky conditions. They can be explained by the occurrence of
396 strong katabatic winds when continental temperature is low. During the coldest hours of the day,
397 continental gravity winds increase downslope leading to enhanced arrival of low $\delta^{18}O$ and high d-

398 excess in the water vapor at DDU. The comparison with available water vapor records in other polar
399 sites supports close links between katabatic wind regimes and isotopic diel variations. Indeed, while
400 diel cycles are not clearly seen in the water vapor isotopic composition of polar coastal sites of Ivittuut
401 and Syowa, strong isotopic diurnal cycles are observed in the water vapor of the windiest coastal sites
402 affected by diel variations of katabatic wind speed (Kangerlussuaq and DDU).

403 Since our water vapor isotopic record is longer at DDU than the one recorded at Kangerlussuaq, we
404 are also able to highlight the added value of water isotopes with respect to humidity record. In
405 particular, short (~3 hours) peaks in $\delta^{18}O$ and d-excess as captured in our record that may correspond
406 to abrupt changes in wind origin. This confirms that $\delta^{18}O$ of water vapor in coastal regions affected by
407 katabatic winds is much more sensitive to air mass origins than e.g. to temperature or humidity. This
408 finding has the potential to influence the interpretation of coastal ice core records in these regions
409 (Goursaud et al., 2017).

410 The insights from our field campaign may not be fully representative of average conditions at DDU.
411 One of the limits of our study is that sea ice did not break down at DDU during the 2016-2017 summer
412 season, a rare but not unusual situation which very probably affected DDU weather conditions,
413 including surface water vapor and its isotopic composition. Obtaining longer records is important to
414 encompass a larger range of weather and climate conditions to further inform the interpretation of
415 the isotopic records in Adélie Land.

416

417 **Acknowledgments**

418 The research leading to these results has received funding from the European Research Council under
419 the European Union's Seventh Framework Programme (FP7/2007-2013) / ERC grant agreement n°
420 [306045]. We acknowledge the programs ASUMA and NIVO2 and the support of IPEV. Many thanks to
421 Bruno Jourdain, Doris Thuillier and the technical staff at the Dumont d'Urville station in summer 2016-
422 2017 for strong support. Support for this study was also obtained from the LEFE programs ADELISE and
423 NEVE-CLIMAT as well as ANR ASUMA. Finally, we thank deeply Hans Christian Steen Larsen, Jean-Louis
424 Bonne, Naoyuki Kurita, Ben Kopec and François Ritter for sharing the raw files of climate and isotopic
425 data used for building Table 2.

References

Agosta, C., Favier, V., Genthon, C., Gallée, H., Krinner, G., Lenaerts, J. T. M., & van den Broeke, M. R. (2012). A 40-year accumulation dataset for Adelie Land, Antarctica and its application for model validation. *Climate Dynamics*, *38*(1–2), 75–86.

Altnau, S., Schlosser, E., Isaksson, E., & Divine, D. (2014). Climatic signals from 76 shallow firn cores in Dronning Maud Land, East Antarctica. *The Cryosphere Discussions*, *8*, 5961–6005. http://doi.org/10.5194/tcd-8-5961-2014

Amory, C., Trouvilliez, A., Gallée, H., Favier, V., Naaim-Bouvet, F., Genthon, C., … Bellot, H. (2015). Comparison between observed and simulated aeolian snow mass fluxes in Adélie Land, East Antarctica. *The Cryosphere*, *9*(4), 1373–1383. http://doi.org/10.5194/tc-9-1373-2015

Angot, H., Dion, I., Vogel, N., Legrand, M., Magand, O., & Dommergue, A. (2016). Multi-year record of atmospheric mercury at Dumont d'Urville, East Antarctic coast: continental outflow and oceanic influences. *Atmospheric Chemistry and Physics*, *16*(13), 8265–8279.

Barral, H., Genthon, C., Trouvilliez, A., Brun, C., & Amory, C. (2014). Blowing snow in coastal Adélie Land, Antarctica: three atmospheric-moisture issues. *The Cryosphere*, *8*(5), 1905–1919.

Bindschadler, R., Vornberger, P., Fleming, A., Fox, A., Mullins, J., Binnie, D., … Gorodetzky, D. (2008). The Landsat image mosaic of Antarctica. *Remote Sensing of Environment*, *112*(12), 4214–4226.

Bonne, J.-L., Masson-Delmotte, V., Cattani, O., Delmotte, M., Risi, C., Sodemann, H., & Steen-Larsen, H. (2014). The isotopic composition of water vapour and precipitation in Ivittuut, southern Greenland. *Atmospheric Chemistry and Physics*, *14*(9), 4419–4439.

Casado, M., Landais, A., Masson-Delmotte, V., Genthon, C., Kerstel, E., Kassi, S., … Cermak, P. (2016). Continuous measurements of isotopic composition of water vapour on the East Antarctic Plateau. *Atmospheric Chemistry and Physics Discussions*, 1–26. http://doi.org/10.5194/acp-2016-8

Favier, V., Agosta, C., Genthon, C., Arnaud, L., Trouvillez, A., & Gallée, H. (2011). Modeling the mass and surface heat budgets in a coastal blue ice area of Adelie Land , Antarctica, *116*, 1–14. http://doi.org/10.1029/2010JF001939

Favier, V., Agosta, C., Parouty, S., Durand, G., Delaygue, G., Gallée, H., … Krinner, G. (2013). An updated and quality controlled surface mass balance dataset for Antarctica. *The Cryosphere*, *7*(2), 583.

Gallée, H., & Pettré, P. (1998). Dynamical constraints on katabatic wind cessation in Adélie Land, Antarctica. *Journal of the Atmospheric Sciences*, *55*(10), 1755–1770.

Goursaud, S., Masson-Delmotte, V., Favier, V., Preunkert, S., Fily, M., Gallée, H., … Minster, B. (2017). A 60-year ice-core record of regional climate from Adélie Land, coastal Antarctica. *The Cryosphere*, *11*(1), 343–362.

Goursaud, S., Masson-Delmotte, V., Favier, V., Preunkert, S., Fily, M., Gallée, H., … Werner, M. (2016). A sixty year ice-core record of regional climate from Adélie Land, coastal Antarctica. *The Cryosphere Discuss.*, *2016*, 1–36. http://doi.org/10.5194/tc-2016-179

Grazioli, J., Genthon, C., Boudevillain, B., Duran-Alarcon, C., Del Guasta, M., Jean-Baptiste, M., &

Berne, A. (2017). Measurements of precipitation in Dumont d'Urville, Adélie Land, East Antarctica. *The Cryosphere*, *11*(4), 1797.

Jourdain, B. (2001). Etude du maillon atmosphérique du cycle biogéochimique du soufre aux hautes latitudes sud (station Dumont d'Urville), phD thesis, 350 p.

Jouzel, J. (2013). *Water Stable Isotopes: Atmospheric Composition and Applications in Polar Ice Core Studies*. *Treatise on Geochemistry: Second Edition* (2nd ed., Vol. 5). Elsevier Ltd. http://doi.org/10.1016/B978-0-08-095975-7.00408-3

Jouzel, J., Delaygue, G., Landais, A., Masson-Delmotte, V., Risi, C., & Vimeux, F. (2013). Water isotopes as tools to document oceanic sources of precipitation. *Water Resources Research*, *49*(11). http://doi.org/10.1002/2013WR013508

König-Langlo, G., King, J., & Pettré, P. (1998). Climatology of the three coastal Antarctic stations Dumont d'Urville, Neumayer, and Halley. *Journal of Geophysical Research: Atmospheres*, *103*(D9), 10935–10946.

Kopec, B., Lauder, A., Posmentier, E., & Feng, X. (2014). The diel cycle of water vapor in west Greenland. *Journal of Geophysical Research: Atmospheres*, *119*(15), 9386–9399.

Kurita, N., Hirasawa, N., Koga, S., Matsushita, J., Steen-Larsen, H. C., Masson-Delmotte, V., & Fujiyoshi, Y. (2016a). Identification of Air Masses Responsible for Warm Events on the East Antarctic Coast. *SOLA*, *12*, 307–313.

Kurita, N., Hirasawa, N., Koga, S., Matsushita, J., Steen-Larsen, H. C., Masson-Delmotte, V., & Fujiyoshi, Y. (2016b). Influence of large-scale atmospheric circulation on marine air intrusion toward the East Antarctic coast. *Geophysical Research Letters*, *43*(17), 9298–9305. http://doi.org/10.1002/2016GL070246

Kusahara, K., Hasumi, H., Fraser, A. D., Aoki, S., Shimada, K., Williams, G. D., … Tamura, T. (2017). Modeling Ocean–Cryosphere Interactions off Adélie and George V Land, East Antarctica. *Journal of Climate*, *30*(1), 163–188.

Landais, A., Casado, M., Prié, F., Magand, O., Arnaud, L., Ekaykin, A., … Orsi, A. (2017). Surface studies of water isotopes in Antarctica for quantitative interpretation of deep ice core data. *Comptes Rendus - Geoscience*. http://doi.org/10.1016/j.crte.2017.05.003

Liu, H., Jezek, K., Li, B., & Zhao, Z. (2001). Radarsat Antarctic Mapping Project digital elevation model version 2. *Radarsat Antarctic Mapping Project Digital Elevation Model Version 2, Boulder, Colorado USA: National Snow and Ice Data Center. Digital Media.*

Marshall, G. J. (2003). Trends in the Southern Annular Mode from observations and reanalyses. *Journal of Climate*, *16*(24), 4134–4143.

Massom, R. A., & Stammerjohn, S. E. (2010). Antarctic sea ice change and variability–physical and ecological implications. *Polar Science*, *4*(2), 149–186.

Massom, R., Reid, P., Stammerjohn, S., Raymond, B., Fraser, A., & Ushio, S. (2013). Change and variability in East Antarctic sea ice seasonality, 1979/80–2009/10. *PloS One*, *8*(5), e64756.

Masson-Delmotte, V., Hou, S., Ekaykin, A., Jouzel, J., Aristarain, A., Bernardo, R. T., … White, J. W. C. (2008). A review of antarctic surface snow isotopic composition: Observations, atmospheric

circulation, and isotopic modeling. *Journal of Climate*, *21*(13), 3359–3387. http://doi.org/10.1175/2007JCLI2139.1

Périard, C., & Pettré, P. (1993). Some aspects of the climatology of dumont D'Irville, adélie land, Antarctica. *International Journal of Climatology*, *13*(3), 313–328.

Pettré, P., Payan, C., & Parish, T. R. (1993). Interaction of katabatic flow with local thermal effects in a coastal region of Adelie Land, East Antarctica. *Journal of Geophysical Research: Atmospheres*, *98*(D6), 10429–10440.

Ritter, F., Steen-larsen, H. C., Werner, M., Masson-delmotte, V., Orsi, A., Behrens, M., … Kipfstuhl, S. (2016). Isotopic exchange on the diurnal scale between near-surface snow and lower atmospheric water vapor at Kohnen station , East Antarctica, (February), 1–35. http://doi.org/10.5194/tc-2016-4

Smith, J. A., Hillenbrand, C.-D., Kuhn, G., Larter, R. D., Graham, A. G., Ehrmann, W., … Forwick, M. (2011). Deglacial history of the West Antarctic Ice Sheet in the western Amundsen Sea embayment. *Quaternary Science Reviews*, *30*(5), 488–505.

Steen-Larsen, H. C., Johnsen, S. J., Masson-Delmotte, V., Stenni, B., Risi, C., Sodemann, H., … Ellehøj, M. (2013). Continuous monitoring of summer surface water vapor isotopic composition above the Greenland Ice Sheet. *Atmospheric Chemistry and Physics*, *13*(9), 4815–4828.

Steen-Larsen, H. C., Masson-Delmotte, V., Hirabayashi, M., Winkler, R., Satow, K., Prié, F., … Sveinbjörnsdottír, A. E. (2014). What controls the isotopic composition of Greenland surface snow? *Climate of the Past*, *10*(1), 377–392. http://doi.org/10.5194/cp-10-377-2014

Steen-Larsen, H. C., Masson-Delmotte, V., Sjolte, J., Johnsen, S. J., Vinther, B. M., Bréon, F.-M., … White, J. (2011). Understanding the climatic signal in the water stable isotope records from the NEEM shallow firn/ice cores in northwest Greenland. *Journal of Geophysical Research: Atmospheres*, *116*(D6), n/a--n/a. http://doi.org/10.1029/2010JD014311

Stenni, B., Scarchilli, C., Masson-Delmotte, V., Schlosser, E., Ciardini, V., Dreossi, G., … others. (2016). Three-year monitoring of stable isotopes of precipitation at Concordia Station, East Antarctica. *The Cryosphere*, *10*(5), 2415.

Tamura, T., Ohshima, K. I., Fraser, A. D., & Williams, G. D. (2016). Sea ice production variability in Antarctic coastal polynyas. *Journal of Geophysical Research: Oceans*, *121*(5), 2967–2979.

Thomas, E. R., van Wessem, J. M., Roberts, J., Isaksson, E., Schlosser, E., Fudge, T. J., … others. (2017). Review of regional Antarctic snow accumulation over the past 1000 years. *Climate of the Past Discussion*.

Titchner, H. A., & Rayner, N. A. (2014). The Met Office Hadley Centre sea ice and sea surface temperature data set, version 2: 1. Sea ice concentrations. *Journal of Geophysical Research: Atmospheres*, *119*(6), 2864–2889.

Touzeau, A., Landais, A., Stenni, B., Uemura, R., Fukui, K., Fujita, S., … Barkan, E. (2016). Acquisition of isotopic composition for surface snow in East Antarctica and the links to climatic parameters. *The Cryosphere*, *10*(2), 837–852.

Tremoy, G., Vimeux, F., Mayaki, S., Souley, I., Cattani, O., Risi, C., … Oi, M. (2012). A 1-year long$\delta^{18}O$ record of water vapor in Niamey (Niger) reveals insightful atmospheric processes at different

544 timescales. *Geophysical Research Letters*, *39*(8).

545 Wendler, G., Stearns, C., Weidner, G., Dargaud, G., & Parish, T. (1997). On the extraordinary katabatic
546 winds of Adélie Land. *Journal of Geophysical Research: Atmospheres*, *102*(D4), 4463–4474.

547

Supplementary material (analytical methods) for the manuscript:

Coastal water vapor isotopic composition driven by katabatic wind variability in summer at Dumont d'Urville, coastal East Antarctica

Camille Bréant[1], Christophe Leroy Dos Santos[1], Mathieu Casado[1], Elise Fourré[1], Sentia Goursaud[1], Valérie Masson-Delmotte[1], Vincent Favier[2], Cécile Agosta[1,2], Olivier Cattani[1], Frédéric Prié[1], Benjamin Golly[2], Anaïs Orsi[1], Patricia Martinerie[2], Amaëlle Landais[1,]*

[1] Laboratoire des Sciences du Climat et de l'Environnement (LSCE) - IPSL, UMR 8212, CEA-CNRS-UVSQ, Université Paris-Saclay, F-91190 Gif sur Yvette, France

[2] Univ. Grenoble Alpes, CNRS, IRD, Grenoble INP, Institut de Géophysique de l'Environnement (IGE), F-38000 Grenoble, France

1- Isotopic calibrations

During our monitoring period, the PICARRO humidity measurements varied between 2000 and 6000 ppmv. The raw $\delta^{18}O$ values varied typically between -23 and -35‰ and we used two LSCE internal water standards for calibration. They have $\delta^{18}O$ values (themselves calibrated with respect to VSMOW) of -27.23 +/- 0.05‰ (D47-CB) and -52.6 +/- 0.05‰ (DomeC-CB).

It is now well established that raw laser spectroscopy $\delta^{18}O$ measurements must be corrected for (1) shifts between measured $\delta^{18}O$ and δD and true $\delta^{18}O$ and δD values , (2) the drift of the instrument for $\delta^{18}O$ and δD and (3) the influence of humidity on $\delta^{18}O$ and δD values,(Tremoy et al., 2012); (Steen-Larsen et al., 2013). Our calibration procedure was the following. Every day, our two standards of known $\delta^{18}O$ and δD were introduced using the PICARRO standard delivery module (SDM) and measured during 30 to 40 minutes each, at an average humidity of 5600 ppmv, in the cavity of the laser spectroscopy instrument. Only the results obtained during the last 10 minutes of the measurement period were retained for calibration purpose, to avoid potential memory effects. In addition, each week, one of the two standard waters was introduced 5 times during 30 minutes at 5 different humidity levels (1000, 2000, 3000, 4000 and 5000 ppmv). Unfortunately, due to issues with injections in the vaporizer within the standard delivery calibration module, numerous calibration points could not be used because of scattering in the data: the standard deviations of the humidity and $\delta^{18}O$ over 10 minutes exceed respectively 100 ppmv and 1‰.

Robust calibration points (i.e. with stable humidity level - standard deviations of the humidity over 10 minutes lower than 100 ppmv) were identified between January 13th and February 2nd after most issues with the injection in the calibration module have been fixed. To establish the isotopes vs humidity calibration curve, we selected the 11 data points obtained from measurements spanning more than 10 minutes from one water isotope standard (D47-CB). The resulting isotope vs humidity calibration curves (Figure S1) were drawn through linear interpolation over the calibration points obtained on the 0 to 2000 ppmv section making the assumption that drift over this short measurement period was of second order. The uncertainties associated with this assumption are discussed in next section. These calibration curves are similar to previous calibration results obtained with the same instrument (Casado et al., 2016). In the rest of the section (2000 ppmv to 8000 ppmv) we consider the humidity dependence as null based on the few calibration points at DDU and laboratory calibration. Still, because no calibration point was obtained between 1500 and 4400 ppmv, an alternative calibration curve over this period is proposed and used for the uncertainty estimate (cf next section).

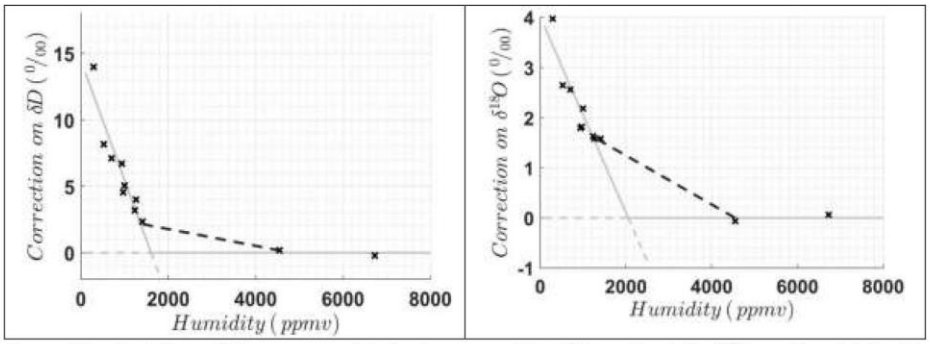

Figure S1: Evolution of the measured isotopic composition (δD on the left, $\delta^{18}O$ on the right) with respect to humidity during the calibrations performed in the field. The grey solid lines show the calibration curves (we choose the simplest fit, i.e. through a linear function). The black dashed line show an alternative calibration line for humidity between 1500 and 4400 ppmv that has been included in our uncertainty calculation (next section).

The two other steps of the corrections (drift and VSMOW-SLAP scale) were performed simultaneously using measurements of the two standards DomeC-CB and D47-CB chosen to cover the span of isotopic values measured at DDU. The drift over the whole period of measurements is difficult to estimate because of the short period of robust calibration data and scattering of the calibration points (Figure S2). In addition, the correction for humidity is not independent from the drift as explained above. This is the reason why we could not deduce a robust drift effect from the points displayed on Figure 4. We thus did not impose any temporal drift for measurements over the whole

period. We used the average measured values of the high and low standards in order to do the VSMOW-SLAP scale correction. The uncertainty associated with this approach is reported in section 2.3.

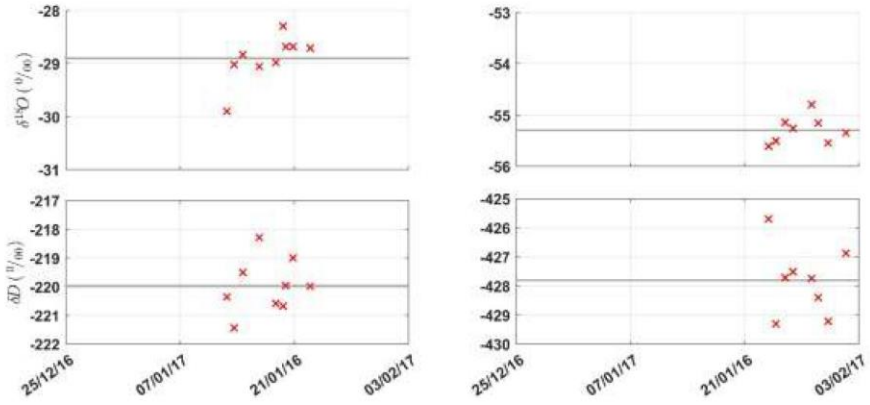

Figure S2: Temporal e*volution of the measured* $\delta^{18}O$ *(upper panel) and* δD *(lower panel) after correction for the influence of humidity (left: for standard D47-CB; right: for standard DomeC-CB). The calibration points are indicated as red crosses. The solid grey lines show the mean values used for the SMOW-SLAP calibration.*

2- Uncertainties associated with calibrated isotopic data

The final uncertainties on $\delta^{18}O$, δD and d-excess of the water vapor results from: (1) uncertainty on the humidity vs isotopes correction, (2) scattering of the $\delta^{18}O$ and δD of measuring standards within the calibration period (Figure S2) and (3) uncertainty on the drift outside of calibration period.

(1) The uncertainty for the humidity – isotopes correction deduced from figure S1 is of up to 1‰, and up to 3.2‰ for $\delta^{18}O$ and d-excess respectively when humidity of our measurements is at its minimum (2000 ppmv).

(2) The scattering of the calibration points leads to uncertainty and is estimated as the 2σ width of the distribution of the measured isotopic composition of our known standards. This is the minimal uncertainty to be associated with measurements in the calibration period: respectively 1‰ and 5‰ for $\delta^{18}O$ and d-excess.

(3) We are aware of the limitation of the extrapolation for the drift correction of our data. The calibration points display a rather large scattering and the extrapolated drift cannot be well defined. It is therefore crucial to carefully assess the time-dependent uncertainty associated

with our calibrated measurements. In order to estimate the uncertainty linked to our assumption of a no drift outside the calibration period, we used different alternative scenarios for the drift to correct the data. Despite scattering of the calibration point, linear regressions were obtained on the calibration points for the different standards and applied as correction for our data within and outside the calibration range. Combined with uncertainty linked to the humidity – isotopes correction, the maximum difference between the different scenarios is used to define the maximum uncertainty of our dataset: it reaches up to 3.5‰ and 25‰ (respectively for $\delta^{18}O$ and d-excess) at the beginning of the measurement period when no faithful calibration points could be obtained. Finally, it should be noted that this largest source of uncertainty due to drift should be applied on the absolute values of $\delta^{18}O$ and d-excess but not on their short-term variations.

References

Casado, M., Landais, A., Masson-Delmotte, V., Genthon, C., Kerstel, E., Kassi, S., … Cermak, P. (2016). Continuous measurements of isotopic composition of water vapour on the East Antarctic Plateau. *Atmospheric Chemistry and Physics Discussions*, 1–26. http://doi.org/10.5194/acp-2016-8

Steen-Larsen, H. C., Johnsen, S. J., Masson-Delmotte, V., Stenni, B., Risi, C., Sodemann, H., … Ellehøj, M. (2013). Continuous monitoring of summer surface water vapor isotopic composition above the Greenland Ice Sheet. *Atmospheric Chemistry and Physics*, *13*(9), 4815–4828.

Tremoy, G., Vimeux, F., Mayaki, S., Souley, I., Cattani, O., Risi, C., … Oi, M. (2012). A 1-year longδ18O record of water vapor in Niamey (Niger) reveals insightful atmospheric processes at different timescales. *Geophysical Research Letters*, *39*(8).

Annexe B.

Surface studies of water isotopes in Antarctica for quantitative interpretation of ice core data (Landais, et al., *Comptes Rendus Geoscience*, 2017)

Résumé. Les carottes de glace polaires sont des archives climatiques uniques. En effet, la plupart d'entre elles présentent une stratigraphie continue et une haute résolution temporelle de plusieurs variables climatiques dans une seule archive. Alors que les enregistrements des isotopes de l'eau (δD ou $\delta^{18}O$) dans les carottes de glace servent de références pour les variations de températures atmosphériques passées, leur relation à la température est associée à une large incertitude ; en particulier, des effets de post-dépôt sont très importants en Antarctique de l'Est à cause de bas taux d'accumulation. La forte influence des processus de post-dépôt souligne la nécessité de programmes de recherche sur la surface polaire, en plus des programmes de forages profonds. Nous présentons ici de nouveaux résultats sur les isotopes de l'eau issus de différents programmes récents de surface, la plupart pour l'Antarctique de l'Est. Avec des données publiés précédemment, les nouvelles données présentent dans cette étude ont des implications pour les reconstructions de climat à partir des données isotopes enregistrées dans les carottes de glace : (1) la relation spatiale entre la température de surface moyenne et la composition isotopique de la neige moyennée sur les premiers mètres de profondeur peut s'expliquer directement en utilisant un modèle isotopique simple ajusté à l'évolution du d-excess par rapport au $\delta^{18}O$ issue des transects du secteur de l'Antarctique de l'Est. Les pentes spatiales observées sont significativement plus hautes (~ 0,7 à 0,8 ‰ $°C^{-1}$ pour la relation $\delta^{18}O$ vs température) que les pentes saisonnières obtenues à partir des données de précipitation de Vostok et Dome C (0,35 à 0,46 ‰ $°C^{-1}$). Nous expliquons ces différences par des changements de la relation température de condensation vs température de surface entre l'été et l'hiver sur le plateau central de l'Antarctique de l'Est, où la couche d'inversion disparait en été. (2) Les effets de post-dépôt liés aux changements entre la surface neigeuse et la vapeur d'eau atmosphérique modifient le $\delta^{18}O$ dans la neige de surface, même en l'absence d'évènements de précipitation. Cette évolution préserve la corrélation positive entre le $\delta^{18}O$ de la neige et la température de surface, mais est associée à une bien plus petite pente du $\delta^{18}O$ vs température comparée à la

pente observée dans la relation saisonnière issue des précipitations. (3) Les effets de post-dépôt limitent clairement l'archivage de la variabilité de haute résolution (saisonnière) dans la neige polaire, mais non suggérons que les sites avec un taux d'accumulation de l'ordre de 40 $kg.m^{-2}.yr^{-1}$ devraient enregistrer un cycle saisonnier à des profondeurs peu profondes.

C. R. Geoscience 349 (2017) 139–150

Contents lists available at ScienceDirect

Comptes Rendus Geoscience

www.sciencedirect.com

External Geophysics, Climate (Glaciology)

Surface studies of water isotopes in Antarctica for quantitative interpretation of deep ice core data

Amaelle Landais [a,d,*], Mathieu Casado [a,d], Frédéric Prié [a,d], Olivier Magand [b,d], Laurent Arnaud [b,d], Alexey Ekaykin [c,d], Jean-Robert Petit [b,d], Ghislain Picard [b,d], Michel Fily [b,d], Bénédicte Minster [a,d], Alexandra Touzeau [a,d], Sentia Goursaud [a,d], Valérie Masson-Delmotte [a,d], Jean Jouzel [a,d], Anaïs Orsi [a,d]

[a] *UMR8212, CEA–CNRS–UVSQ–UPS, Laboratoire des sciences du climat et de l'environnement (IPSL), 91190 Gif-sur-Yvette, France*
[b] *IRD, IGE, Université Grenoble Alpes, CNRS, 38000 Grenoble, France*
[c] *Arctic and Antarctic Research Institute, 199397 St Petersburg, Russia*
[d] *Institute of Earth Sciences, Saint Petersburg State University, 199397 Saint Petersburg, Russia*

ARTICLE INFO

Article history:
Received 2 May 2017
Accepted after revision 11 May 2017
Available online 1 August 2017

Handled by François Chabaux

Keywords:
Ice core
Water isotopes
Antarctica

ABSTRACT

Polar ice cores are unique climate archives. Indeed, most of them have a continuous stratigraphy and present high temporal resolution of many climate variables in a single archive. While water isotopic records (δD or δ^{18}O) in ice cores are often taken as references for past atmospheric temperature variations, their relationship to temperature is associated with a large uncertainty. Several reasons are invoked to explain the limitation of such an approach; in particular, post-deposition effects are important in East Antarctica because of the low accumulation rates. The strong influence of post-deposition processes highlights the need for surface polar research programs in addition to deep drilling programs. We present here new results on water isotopes from several recent surface programs, mostly over East Antarctica. Together with previously published data, the new data presented in this study have several implications for the climatic reconstructions based on ice core isotopic data: (1) The spatial relationship between surface mean temperature and mean snow isotopic composition over the first meters in depth can be explained quite straightforwardly using simple isotopic models tuned to d-excess vs. δ^{18}O evolution in transects on the East Antarctic sector. The observed spatial slopes are significantly higher ($\sim$ 0.7–0.8‰·°C^{-1} for δ^{18}O vs. temperature) than seasonal slopes inferred from precipitation data at Vostok and Dome C (0.35 to 0.46‰·°C^{-1}). We explain these differences by changes in condensation versus surface temperature between summer and winter in the central East Antarctic plateau, where the inversion layer vanishes in summer. (2) Post-deposition effects linked to exchanges between the snow surface and the atmospheric water vapor lead to an evolution of δ^{18}O in the surface snow, even in the absence of any precipitation event. This evolution preserves the positive correlation between the δ^{18}O of snow and surface temperature, but is associated with a much slower δ^{18}O-vs-temperature slope than the slope observed in the seasonal precipitation. (3) Post-deposition effects clearly limit the archiving of high-resolution (seasonal) climatic variability in the polar snow, but we suggest that sites with an accumulation rate of the order of 40 kg.m^{-2}.yr^{-1} may record a seasonal cycle at shallow depths.

* Corresponding author. UMR8212, CEA–CNRS–UVSQ–UPS, Laboratoire des sciences du climat et de l'environnement (IPSL), 91190 Gif-sur-Yvette, France.
E-mail address: AmaelleLandais[ad].amaelle.landais@lsce.ipsl.fr">AmaelleLandais[ad].amaelle.landais@lsce.ipsl.fr ().

http://dx.doi.org/10.1016/j.crte.2017.05.003
1631-0713/

1. Introduction

Polar ice cores are unique archives of multiple sources of information on past changes in climate and environment. Indeed, most polar ice cores have a continuous stratigraphy, and allow extracting highly resolved records, reaching seasonal resolution in Greenland and coastal Antarctica. Today, the ice core spanning continuously the longest period is the EPICA Dome C ice core, drilled on the East Antarctic plateau and covering the last 800 ka, hence eight climatic cycles (EPICA Community Members, 2004). Earlier discontinuous records have been extracted from blue ice fields (Higgins et al., 2015). The International Partnership for Ice Core Science is searching drilling sites where records spanning the last 1.5 million years could be extracted (Fischer et al., 2013). In central Greenland, where accumulation rates are at least 10 times larger than in the East Antarctic plateau, the longest continuous climatic record from NorthGRIP is limited to the last 120 ka (NorthGRIP-community-members, 2004), but information back to 130 ka has been extracted from an undisturbed section of the NEEM ice core (NEEM community members, 2013).

Various proxies are measured in ice cores enabling the reconstruction of climatic and environmental variables. While concentration of greenhouse gases (CO_2, CH_4, NO_2) is directly measured by the extraction of the air trapped in the ice, other proxies are more indirect, such as chemical proxies to infer changes in distal climatic conditions, atmospheric circulation, atmospheric chemistry, sea ice extent or fire records (e.g., Legrand et al., 2016; Wolff et al., 2010). Similarly, while high-resolution water isotopic records (δD or δ^{18}O) in ice cores are often taken as references for past atmospheric temperature variations, their quantitative interpretation is not straightforward and may be associated with large uncertainties. The initial method of temperature reconstruction from water isotopes is based on the present-day spatial relationship between δD or δ^{18}O and surface temperature on polar transects. This spatial slope is then used as a surrogate for the relationship between changes in water isotopic composition and temperature from past to present ("temporal slope"). In East Antarctica, the amplitude of temperature change over glacial–interglacial transitions was mainly estimated based on water isotopes with an associated error of −10 to +30%. In West Antarctica, the amplitude of the last deglaciation has been estimated to +11.3 °C based on measurements of isotopic composition of air isotopes, i.e. 2 to 4 °C larger than the water isotopes estimated amplitude of the last deglaciation in East Antarctica (Cuffey et al., 2016). At the glacial-interglacial scale, most atmospheric General Circulation Models equipped with water isotopes suggest that temporal slopes are close to spatial slopes (Jouzel et al., 2007; Risi et al., 2010; Stenni et al., 2010) with one exception (Lee et al., 2008) producing smaller slopes attributed to evaporative recharge over the Southern Ocean. For interannual variations under present-day climate or for simulated climates warmer than today due to increased greenhouse gas concentration, several studies produce temporal slopes up to twice smaller than the spatial ones, mostly because of precipitation-temperature covariance effects through precipitation intermittency (Schmidt et al., 2007; Sime et al., 2009). Temporal slopes lower than spatial slopes for climates warmer than pre-industrial ones (early Holocene, earlier interglacial periods) are also supported independently by investigations of isotope–temperature–accumulation relationships (Cauquoin et al., 2015).

Sources of uncertainties in the use of the spatial slope as a surrogate for temporal slopes emerge from (1) past changes in moisture source regions and the corresponding climatic variations, affecting the isotopic composition of the water vapor that will finally precipitate in polar regions (e.g., Lee et al., 2008), (2) past changes in the trajectories of water masses toward the polar regions affecting water isotopes in precipitation independently of changes in local condensation temperature (Helsen et al., 2006), (3) past changes in precipitation intermittency including seasonal effects (Krinner and Werner, 2003; Laepple et al., 2011; Masson-Delmotte et al., 2006; Sime et al., 2009) causing a distortion between the ice core signal (precipitation-weighted) and annual mean temperature; and finally (4) post-deposition effects leading to a modification of the isotopic composition of the surface snow after its deposition and before it is buried (Johnsen et al., 2000; Neumann and Waddington, 2004; Town et al., 2008).

In Greenland, the diffusion of the δ^{18}O seasonal signal can be corrected (e.g., Steen-Larsen et al., 2011) and other post-deposition effects have long been estimated to be of second order because of the high accumulation rate. However, recent studies claim that post-deposition processes could represent a significant contribution to the isotopic signal (Steen-Larsen et al., 2014). Still, alternative temperature measurements have been developed such as borehole temperature measurements (Dahl-Jensen, 1998) or direct quantification of the amplitude of temperature changes through air isotopic measurements (Landais et al., 2004a, b; Orsi et al., 2014; Severinghaus and Brook, 1999). These methods allow estimating temperature changes with an accuracy estimated at ±3 °C for Dansgaard–Oeschger abrupt events (Buizert et al., 2014; Kindler et al., 2014). These analyses reveal that, in Greenland, temporal isotope–temperature slopes are systematically lower than spatial slopes, with marked regional characteristics (e.g., Guillevic et al., 2013).

In the central East-Antarctic plateau, low accumulation rate and slow past temperature make borehole temperature reconstructions more difficult to interpret (Salamatin et al., 1998) and preclude the use of air isotopic measurements for quantitative temperature reconstructions (Landais, 2011). In this region, there is thus a strong need to better understand and quantify the processes potentially affecting the relationship between water isotopes and temperature, and specifically post-deposition processes that may have a strong influence when surface snow is exposed to exchanges with air during long time periods.

These facts have motivated the development of two types of surface polar programs in addition to deep drilling programs. The first type of surface program is focused on investigating the surface characteristics of a deep drilling

site through the deployment of numerous instruments to monitor the variability of weathering conditions and/or surface snow characteristics, as implemented at Concordia Station for the EPICA Dome C (Champollion et al., 2013; Genthon et al., 2013; Libois et al., 2015). Other programs explore the variability of surface characteristics (accumulation rate, layer structure, isotopic and chemistry composition...) through traverse expeditions, and information retrieved from the network of pits and shallow ice cores (Goursaud et al., 2016; Mayewski and Al, 2006).

Here, we review the importance of surface programs for the climatic interpretation of ice core water isotopic records. For this purpose, we report new results on water isotopes from several recent surface programs, mostly over East Antarctica. These new results are confronted to previous data and used to update guidelines for interpretation of water isotopic records in ice core.

2. Methods

Various datasets from several campaigns are used in this manuscript. We first describe the sample collection, then the measurements techniques and the calibration protocol.

2.1. Sample collection

2.1.1. Transects

Several transects have been performed in the recent years with sampling of surface snow down to a depth sufficient to characterize the average isotopic composition at the site. On each sampling site, a metallic tube (titanium) is used to penetrate into the first 30–100 cm of the snow and extract a snow sample, which is then mixed for homogenization. In low accumulation sites, this simple method enables the collection of a sample of the average snow isotopic composition over several years.

We present here water isotopic datasets from two new transects in Antarctica (Fig. 1): the French–Russian Taste-Idea Explore campaign performed in 2011–2012 in the central East Antarctic Plateau (hereafter referred to as TI11) and the Spanish expedition Expedicion Acciona Windpowered Antarctica, performed in 2011–2012 in the inland Atlantic sector of East Antarctica. The TI11 campaign provided samples in very cold and low-accumulation regions of East Antarctica, between Dome C and Vostok, hence completing a previous transect between the coastal site of Terra Nova Bay and Dome C where δD, δ^{18}O and δ^{17}O were already documented (Landais et al., 2008). The Spanish expedition provided samples from the edge of the East Antarctic plateau south of the coastal Novolazareskaja station to South Pole Station. These transects are compared to previously published datasets: one Swedish-Japanese transect from Syowa to Dome F and one Chinese transect from Zongshan to Dome A (Fig. 1).

2.1.2. Precipitation and surface snow

Surface studies have been developed thanks to the establishment of the permanent overwintering stations in East Antarctica, for instance at Dome C and Vostok (Fig. 1). Sampling of precipitation is being performed routinely since 2008 at Dome C (Stenni et al., 2016). Precipitation is sampled on a wood table covered by a polystyrene/Teflon plate and standing 1 m above the snow surface. The precipitated snow layer is removed ideally every day at 1 am UTC (Coordinated Universal Time). Few snow samples were collected annually as precipitation events are rare at Dome C. Moreover, even if the wood table is

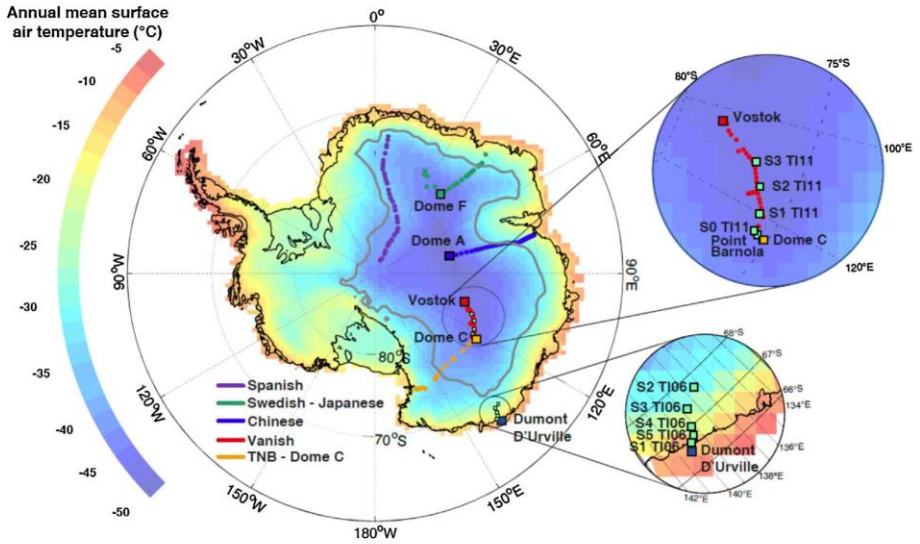

Fig. 1. Recent surface transects performed in East Antarctica and location of the different snow-pit sampling sites mentioned in this study, with indication of the mean surface air temperature (Nicolas and Bromwich, 2014).

Table 1
Summary of the different snow pits used in this study.

Sites	Latitude S	Longitude E	Resolution (cm)	Accumulation ($kg \cdot m^{-2} \cdot yr^{-1}$)	10 m depth Temperature (°C)	Altitude (m)	Year of sampling
S1 TI06	66°42′25	139°49′53	5	219	−13.1	279	2007[3]
S2 TI06	67°39′35	137°31′26	5	360	−29.5	1808	2007[3]
S3 TI06	67°24′39	138°37′53	5	260	−25.8	1578	2007[3]
S4 TI06	67°02′29	139°08′12	5	280	−22.4	1170	2007[3]
S5 TI06	66°46′30	139°33′25	5	310	NA	653	2007[3]
S0 TI11	75°42′44	123°16′49	3	25.7	−55.1	3197	2012[3]
S1 TI11	75°42′97	120°13′54	10	22.4	−56.0	3206	2012[3]
S2 TI11	76°17′37	117° 16′56.3	3	21	−55.1	3229	2012[2]
S3 TI11	76°50′	113° 01′46	10	22.2	−54.5	3324	2012[3]
Point Barnola	75°42′55	123°15.50′	5	26	NA	3236	2012[3]
Vostok	78°27′52	106°50′14	3	21	−57	3488	2008[2] and 2014[2]
Dome C	75°06′	123°19′48	1.5 to 3	27–35	−54.3	3233	1978[1] and 2007[2] and 2012[1]

Superscript numbers indicate the reference for the subset of records recently published by: (1) Casado et al. (2016b) and (2) Touzeau et al. (2016); (3) indicate new unpublished datasets (this study).

placed 1 m above the surface, it is not always simple to distinguish between blowing snow and precipitation events. Finally, the distance between the main building and the wood table (800 m) makes manual sampling sometimes impossible under very cold weather conditions.

In parallel, other polar programs have implemented routine sampling of surface snow (Casado et al., 2016a; Touzeau et al., 2016). For the data presented here, surface snow was sampled on random spots of a clean area about 1 km from the Concordia station on a weekly basis. Samples from the surface were gathered from the surface skin layer (the few upper millimeters).

2.1.3. Snowpits collection

We present depth profiles of isotopic composition from snow pits realized over different locations of the Antarctic Plateau (Table 1 and Fig. 1). The samples were taken in plastic flasks and shipped frozen to France where they were analyzed. First, in the Austral summer 2006–2007, five 1–2-meter-deep snow pits have been sampled during the Taste Idea campaign (hereafter TI06) with a vertical resolution of 5 cm. These snow pits were taken on the slope of the Antarctic plateau with an accumulation rate varying between 200 and 400 $kg \cdot m^{-2} \cdot yr^{-1}$, i.e. approximately 90 cm of snow each year. In 2011/12, another series of snow pits was realized in the framework of the TI11 campaign between Dome C and Vostok. Four 1–3-meter-deep snow pits were realized with a resolution from 3 to 10 cm in an area with accumulation rates around 20 to 30 mm $kg \cdot m^{-2} \cdot yr^{-1}$. A 110 m core has also been sampled at Point Barnola during this campaign.

In addition to the pits and cores realized during transect, three snow pits from Dome C and two from Vostok are included in this study. They were sampled from 2008 to 2015.

2.2. Snow isotopes analysis

After collection, the snow samples were placed in closed corning tubes or sealed bags and kept frozen all the way back from Antarctica to France. They were melted only prior to measurement to ensure correct conservation of the water isotopic composition.

Two methods for $\delta^{18}O$ measurements were used in this study. The samples from the TI06 campaign were measured at the "Laboratoire des sciences du climat et de l'environnement" (LSCE) by water–CO_2 equilibration using a calibration performed vs V-SMOW and V-SLAP. The most recent measurements of $\delta^{18}O$ (after 2011) and δD measurements presented here were also performed at LSCE, but using a laser cavity ring-down spectroscopy (CRDS) analyzer PICARRO. A special care has been dedicated to the calibration of this instrument since many data displayed here have a $\delta^{18}O$ lower than −55.5‰. This means that the usual V-SMOW vs V-SLAP calibration on the range −55.5‰ to 0‰ cannot be applied directly. To address this issue, a calibration study has been performed during the measurement period through the realization of water samples with $\delta^{18}O$ as low as −80‰ (Casado et al., 2016a). Finally, the accuracy for $\delta^{18}O$ and δD measurements displayed here is about 0.1 and 1‰, respectively.

3. Results

3.1. Isotopic composition of surface snow along transects

3.1.1. Motivation

Transects are key to document the spatial distribution of the multi-annual average isotopic composition, and, together with average temperature measurements, estimate the spatial relationships between $\delta^{18}O$ and temperature (Lorius and Merlivat, 1977; Lorius et al., 1969; Masson-Delmotte et al., 2008; Touzeau et al., 2016). They are of primary importance to benchmark atmospheric general circulation models equipped with water isotopes (e.g., Risi et al., 2010; Werner et al., 2015), especially in central East Antarctica, where modeling uncertainties also arise from poorly characterized fractionation coefficients at low temperature.

Over the last decades, numerous analytical and theoretical studies have been devoted to constrain the fractionation coefficients associated with water isotopes (e.g., Cappa et al., 2003; Ellehoj et al., 2013; Horita et al., 2008; Luz et al., 2009; Majoube, 1971a, b; Merlivat and Nief, 1967; Pinilla et al., 2014; Van Hook, 1968).

Nevertheless, uncertainties remain associated with the quantification of isotopic fractionation between water vapor and snow during condensation in polar regions, where several specific effects should be taken into account. First, unlike for condensation of rainwater in clouds, snowflakes formation does not occur at equilibrium between the vapor and the condensed phase. The air is generally oversaturated with water vapor and strong kinetic fractionation (i.e. linked with diffusivity) occurs in addition to equilibrium fractionation between water vapor and snow. This kinetic effect is enhanced when supersaturation increases, which is the case when air temperature decreases. The parameterization of the vapor–snow fractionation proposed by Jouzel and Merlivat (1984) expresses the fractionation coefficient (α_{v-s}) during snow formation by the formula:

$$\alpha_{V-S} = \frac{S}{(S-1)D/D^{*} + 1/\alpha_{eq}} \quad (1)$$

where α_{eq} is the fractionation coefficient at equilibrium between vapor and solid, D and D^{*} are the diffusion coefficients of the light and heavy water isotopes in air. In the classical approach, supersaturation S is related to inversion temperature, T in °C, at which precipitation is assumed to form, so that $S = 1-aT$, with a varying between 0.002 and 0.007 (Ciais and Jouzel, 1994; Jouzel and Merlivat, 1984). This relationship is constrained by atmospheric measurements and the "a" coefficient is adjusted to reduce model-data mismatches for polar precipitation. The second-order parameter d-excess, defined as d-excess = $\delta D - 8 \times \delta^{18}O$ (Dansgaard, 1964), is indeed very sensitive to kinetic effects at condensation in cold polar regions. As a consequence, the tuning of the supersaturation relationship to temperature is performed so that the observed relationship between $\delta^{18}O$ and d-excess in Antarctica can be reproduced by GCMs (Risi et al., 2010; Schmidt et al., 2007). Adequate tuning of supersaturation in mixed-cloud distillation models is essential for quantitative reconstructions of climate variables (site temperature, evaporation conditions at moisture sources) based on $\delta^{18}O$ and d-excess from deep ice core records (Ciais and Jouzel, 1994; Masson-Delmotte et al., 2005; Stenni et al., 2010; Winkler et al., 2012).

3.1.2. Results

The new data from the TI11 and Spanish expeditions provide water isotopic data in very cold regions. Snow in these regions is particularly depleted in both $H_2{}^{18}O$ and $HD^{18}O$, and we focus here on snow with $\delta^{18}O$ lower than –40‰. This snow is also associated with an increase in the second-order parameter d-excess, which is a result of the strong distillation of the moist air mass when it arrives at the end point of its trajectory; the amplitude of this d-excess increase is attenuated by kinetic effects at condensation that decrease d-excess in precipitation. The increase in snow d-excess when $\delta^{18}O$ is decreasing is evidenced by TI11 data, showing much smaller isotopic scattering than in the Chinese transect near Dome A (Pang et al., 2015). This new set of data will therefore help better tuning of models implemented with water isotopes for Antarctica.

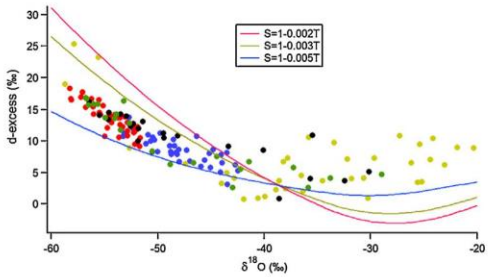

Fig. 2. Evolution of the d-excess vs $\delta^{18}O$ for the samples obtained on transects from Fig. 1, using the same color code (red, blue, yellow, green and black circles correspond respectively to the French–Russian TI11, Spanish, Chinese, Swedish–Japanese and Italian–French transects) together with MCIM simulations of d-excess calculated along a cooling trajectory for different parameterizations of the supersaturation function (thin lines). Note that it is not expected that one single distillation trajectory should encompass all traverse data, given the fact that different locations receive moisture from different sources and through different cooling trajectories.

Fig. 2 displays a comparison between the new transect data and outputs of the Mixed Cloud Isotopic Model (MCIM) (Ciais and Jouzel, 1994), which computes the evolution of the isotopic composition of water vapor and condensed liquid and snow along a moist air trajectory, allowing for a proportion of the condensed water to remain in the cloud and the coexistence of liquid water and ice in intermediate temperature ranges. This model is commonly used for a first-order quantitative interpretation of water stable isotope records from Antarctic deep ice cores (e.g., Landais et al., 2008; Stenni et al., 2003; Vimeux et al., 2001; Winkler et al., 2012). Fig. 2 shows the sensitivity of d-excess simulated by MCIM to the supersaturation parameterization, especially for low $\delta^{18}O$ (for $\delta^{18}O > -40$‰, temperature is not low enough for the supersaturation influence to be significant). The best fit between the model outputs and all datasets (Fig. 2) is obtained for a parameterization of S in the range from $S = 1-0.003\ T$ to $S = 1-0.005\ T$, which is also the range commonly used in general circulation models equipped with water stable isotopes (e.g., Risi et al., 2010; Schmidt et al., 2005; Werner et al., 2011). The new data presented here lead to a tuning of the supersaturation as $S = 1-0.004\ T$ over the two transects (Fig. 2). Note that the isotopic data with $\delta^{18}O > -40$‰ are of no use to tune supersaturation, and the scattering of the data reflects the different moisture source and trajectories of the water mass toward Antarctica (influences of temperature, humidity of the evaporative region as well as presence of sea ice).

3.2. Precipitation vs surface snow at Dome C

Fig. 3 displays daily variations in surface air temperature, precipitation, $\delta^{18}O$ of precipitation events and $\delta^{18}O$ of weekly sampled surface snow during year 2011. Stenni et al. (2016) already stressed the close day-to-day correlation between temperature and the $\delta^{18}O$ of the precipitation. First, seasonal variations are marked by higher precipitation $\delta^{18}O$ in austral summer (with a

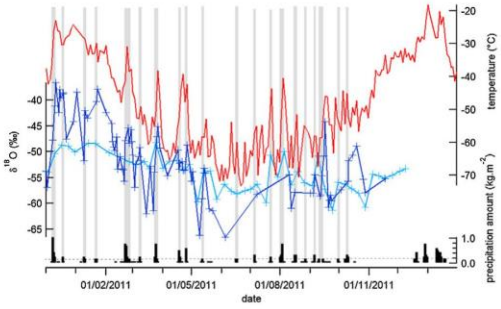

Fig. 3. Variations of 2 m surface air temperature measured by an automatic weather station (red, Genthon et al., 2013), $\delta^{18}O$ of precipitation (dark blue crosses) and $\delta^{18}O$ of surface snow (light blue crosses) for the year 2011 at Dome C. The amount of precipitation is a product of ERA-interim reanalyses (Dee et al., 2011). The grey bars indicate precipitation amounts larger than 0.2 kg·m^{-2}.

maximum value of −37‰) and lower values in austral winter (with a minimum value of −67‰). Second, short-lived warm events associated with significant precipitation events are also associated with $\delta^{18}O$ peaks (e.g., 21–22 February 2011, 25 March 2011). Such a correlation between temperature and the $\delta^{18}O$ of precipitation is not unexpected; it results from the distillation of the water mass from the low to high latitudes associated with the gradual decrease of $\delta^{18}O$ in water vapor and precipitation. The relationship obtained between $\delta^{18}O$ and temperature for the annual distribution of precipitation at Dome C is on average 0.49 ± 0.01‰·°C^{-1} (Stenni et al., 2016); for the year 2011 displayed in Figs. 3 and 4, the slope is of 0.48 ± 0.035‰·°C^{-1} ($R^2 = 0.29$, $N = 80$). This slope is significantly lower than the spatial $\delta^{18}O$-vs-temperature relationship of 0.8 ± 0.01‰·°C^{-1} given by Masson-Delmotte et al. (2008).

More surprisingly, despite the very small cumulative snow accumulation over one year at Dome C and strong blowing snow events that regularly remove the recently deposited snow, the surface snow $\delta^{18}O$ also follows the temperature evolution at the annual scale, even in the absence of abundant precipitation (e.g., from January to March). Still, the amplitude is much smaller (0.14 ± 0.01‰ °C^{-1}, Fig. 4) than the amplitude of the

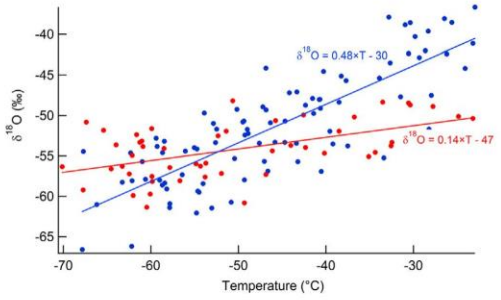

Fig. 4. Relationship between $\delta^{18}O$ and temperature for surface snow (red) and precipitation (blue) at Dome C for the year 2011.

precipitation $\delta^{18}O$-vs-temperature evolution. The correlation between $\delta^{18}O$ and temperature in the absence of precipitation events necessarily reflects post-deposition processes of exchange between water vapor and surface snow, as observed in Greenland (Steen-Larsen et al., 2014). In addition, some warming events often associated with precipitation during the austral winter are also clearly imprinted in the surface snow $\delta^{18}O$ (e.g., 22 July and 3 August). These results suggest that even if important deposition and post-deposition processes affect surface snow isotopic composition, the co-variations of $\delta^{18}O$ with temperature are preserved in the surface snow. Still, quantifying the link between temperature and the $\delta^{18}O$ of precipitation as currently performed with models equipped with isotopes is not sufficient; surface exchanges should be implemented, which strengthens the need for surface studies as the one presented here.

3.3. Snow pits

Deposition and post-deposition processes may not only affect the surface layer as documented in the previous section, but also deeper snow layers. At shallow depth, snow porosity is large and wind ventilation favors water vapor circulation and hence exchange with snow crystals (Neumann and Waddington, 2004). Surface snow also undergoes sublimation and wind blowing effects, leading to complex accumulation patterns affecting the whole snow stratigraphy (Groot Zwaaftink et al., 2013, Libois et al., 2014). Wind speeds are remarkably high on the margin of the Antarctic plateau due to katabatic winds (gravity-driven downslope descent of cold surface air towards the coastal areas), leading to large blowing snow events (Scarchilli et al., 2010). In order to assess how the initial seasonal or inter-annual variability of precipitation isotopic signal is preserved down into the firn, numerous shallow snow pits have been sampled and analyzed for water stable isotopes.

Earlier studies have demonstrated that annual layer counting is possible using water isotopes records, but often more equivocal than through seasonally resolved records of major ions on the Antarctic plateau (probably continental erosion and sea ice for Ca^{2+} and Na^{+}), or seasonal signals evidenced through electrical conductivity or dielectric continuous measurements (e.g., Rasmussen et al., 2006). This mismatch is particularly true for sites with relatively low accumulation rate where diffusion of water vapor will affect more strongly the isotopic composition of snow than the concentration of chemical species (Hoshina et al., 2016).

Despite limitations by diffusion, water isotopes in snow pits and shallow ice cores are still largely used for the reconstruction of recent climate variations (Altnau et al., 2014; Goursaud et al., 2016; Jouzel et al., 1983; Küttel et al., 2012; Schneider et al., 2006). For sites characterized by low accumulation rate, stacking several pits enables one to increase the ratio between signal and noise, hence improving the climatic reconstruction (Ekaykin et al., 2014; Münch et al., 2015).

We present here a compilation of new water isotopic records obtained over the recent years from Taste-Idea transects (Fig. 1, Table 1). These data are also complemented by snow pits from Dome C sampled at a resolution

down to 1.5 cm in depth. Our analysis of these records is devoted to the cause of the observed variability through depth: under which conditions and until which depth can an annual cycle be recorded? What is the significance of centimetric variations in surface snow water stable isotope records?

3.3.1. Taste Idea snow pits

At the coastal site S1 TI06, where the highest temperature was recorded at a depth of 10 m (−13 °C), we can compare isotopic profiles from one snow pit with one 22.4 m shallow core drilled at a distance of about 5 m (Goursaud et al., 2016). The parallel $\delta^{18}O$ variations (Fig. 5) suggest limited noise associated with spatial variability at a site where the accumulation rate is high and corresponds to an annual mean deposition of $190 \pm 60\ kg{\cdot}m^{-2}{\cdot}yr^{-1}$ (Goursaud et al., 2016). The maximum of $\delta^{18}O$ observed at about 1 m depth in the pit most likely corresponds to the snow layer of the previous summer, as expected from the range of snow accumulation. For the S2 TI06 pit, the depth difference of about 130 cm between the two $\delta^{18}O$ minima also corresponds to the average accumulation rate obtained from nearby stakes ($\sim 320\ kg{\cdot}m^{-2}{\cdot}yr^{-1}$).

The detection of an annual cycle is more complicated at other sites, because the snow pits are too shallow. The top layer does not systematically correspond to high $\delta^{18}O$ values (especially at S306) despite the fact that sampling was performed during the warmest summer months. This suggests that, even at sites with relatively high accumulation rates, deposition and post-deposition effects (including snow blowing and intermittency of precipitation) complicate the identification of summer layers in shallow ice cores and hence limit the resolution of the associated climate reconstructions. Duplicate and longer records from deeper pits or shallow cores are needed to deconvolve post-deposition from climatic signals.

3.3.2. Snow pits on the East Antarctic plateau

Fig. 5 displays $\delta^{18}O$ variations over the top 1 m of snow on several snow pits sampled in 2011–2012 during the TI11 campaign. Altogether, $\delta^{18}O$ values range between −58 and −46‰; this 8‰ amplitude is twice smaller than that observed in precipitation samples from Dome C and Vostok (Ekaykin et al., 2004; Stenni et al., 2016), and similar to the seasonal amplitude observed in surface snow samples at Dome C (Fig. 3). Comprehensive statistical analyses cannot be applied on such short records, but we may identify 2–3 cycles of $\delta^{18}O$ variations within 1 m (Fig. 6), corresponding to a depth periodicity of 20 to 50 cm in the $\delta^{18}O$ signal. Because the annual accumulation rate is in general

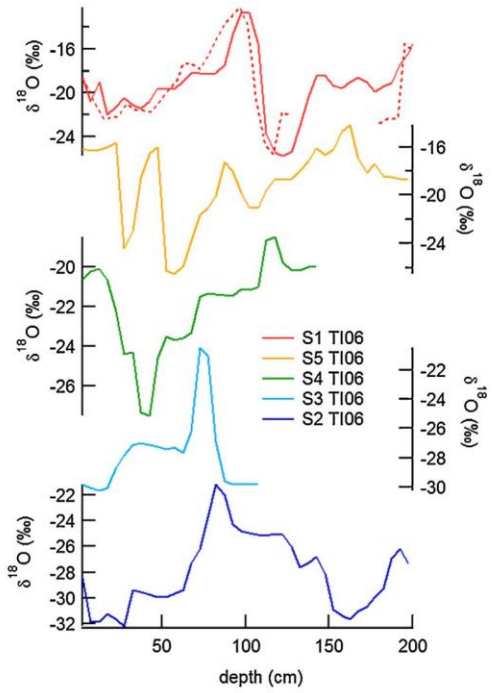

Fig. 5. Depth evolution of $\delta^{18}O$ in the five snow pits from the Taste Idea campaign 2006–07 (TI06) (see Fig. 1 for locations). For S1 TI06, we represent the records from the snow pit (red solid line) and 22 m shallow core (red dotted line, Goursaud et al., 2016).

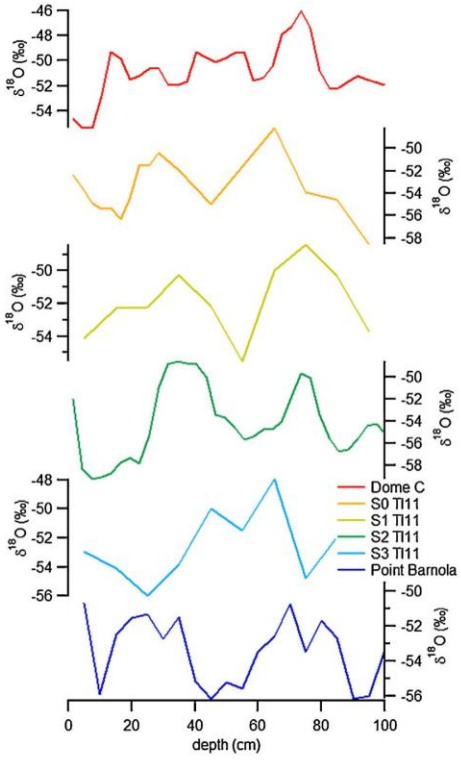

Fig. 6. $\delta^{18}O$ evolution on the first meter of East Antarctic snow pits at low-accumulation sites from the Vanish-Explore campaign (2011–2012). The data from Dome C and S2 TI11 were published in Touzeau et al. (2016).

lower than 100 kg·m^{-2}·yr^{-1} on the Antarctic plateau, these δ^{18}O "cycles" cannot be understood as reflecting seasonal variations, as discussed previously for the coastal site S1 TI06.

The periodicity of the signal can be investigated in more details using the δ^{18}O records obtained from 3 m-deep snow pits in the same region (Fig. 7). The records confirm the previous observation of much longer periodicity than the annual accumulation rate for the different sites as also detailed in Casado et al. (2016a, b). There is only one exception for this behavior from the Dome C δ^{18}O record, obtained on the snow pit dug in 2007. On this snow pit, the scattering of δ^{18}O data obtained on a 3-cm resolution observed over the first meter can be related to a high-frequency variability of δ^{18}O (~6–9 cm). Deeper in the firn, the record is smoother, possibly due to diffusion. Diffusion is indeed expected to increase strongly on the first meters of snow as shown by calculations of diffusion given in Johnsen et al. (2000). The diffusion length increases rapidly from the surface, reaching 2 cm at 1 m depth and more than 6 cm at 4 m at Dome C. This means that a signal associated with a 10 cm periodicity will be attenuated by a factor of 2 at 1 m and by a factor of 10 at 4 m. An annual cycle should hence be visible at 1 m at Dome C, but vanishes deeper as observed for the snow pit drilled in 2007.

We finally stress here the large dispersion between δ^{18}O records from the same site (e.g., for Vostok and Dome C). This confirms the strong spatial variability already observed on records of impurities, densities and isotopes from different snow pits drilled the same year, but at distances of several tenths of meters (Ekaykin et al., 2014; Gautier et al., 2016; Hoshina et al., 2016; Laepple et al., 2016; Libois et al., 2014; Münch et al., 2015).

Intermittency of precipitation, sublimation of snow, deposition and post-deposition effects (e.g., firn ventilation, diffusion and blowing snow) are good candidates for explaining the lack of seasonal record archived in snow pits. Several studies have also highlighted the discontinuous accumulation process at sites like Dome C linked to wind events (Groot Zwaaftink et al., 2013, Libois et al., 2014). Still, the fact that the 2007 Dome C δ^{18}O record displays high-frequency variability over the first meter raises the question of a possible missing seasonal signal in the other records. Indeed, Dome C is the site with the highest accumulation rate beyond the different sites presented in Fig. 7 and the sampling resolution of 3 cm may not be enough to capture the high-frequency (seasonal) variability present in the other records.

3.3.3. Focus on Dome C

The previous results suggest that seasonal cycles might be identified at Dome C with a higher-resolution sampling. We thus performed high-resolution (1.5 cm) δ^{18}O measurements on two snow pits drilled during the summer season 2014–2015 at Dome C (Fig. 8). It is possible to identify three maxima (indicated by arrows) and two minima over the top 20 cm, as expected from the average accumulation rate of ~ 8–10 cm of snow per year (27–35 kg·m^{-2}·yr^{-1}) at Dome C. These results confirm that seasonal cycles may be recorded in the upper 20 cm of the snow layers at Dome C. At deeper depths, a longer periodicity (at least 20 cm) appears more prominent, similar to that evidenced from the 3 m snow pits described in the previous section.

Finally, we investigate δ^{18}O profiles over the upper 50 cm of snow performed every 4 hours at Dome C between 21 and 23 December 2015 (Fig. 9). All eight profiles exhibit relatively low δ^{18}O values near the surface and a strong δ^{18}O increase up to −42‰ at depths between 6 and 10 cm. Such coherency between the δ^{18}O profiles is

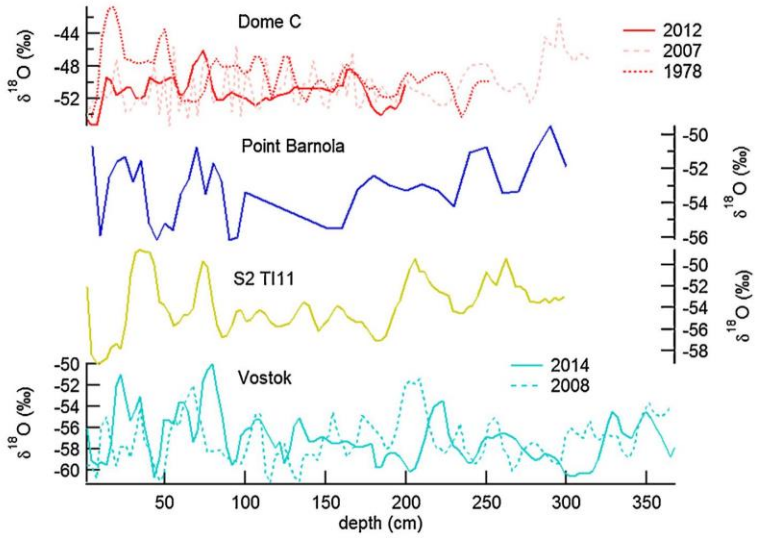

Fig. 7. A compilation of δ^{18}O records from 3-4 m deep snow pits in low accumulation sites from East Antarctica (see Fig. 1 for the location of these sites).

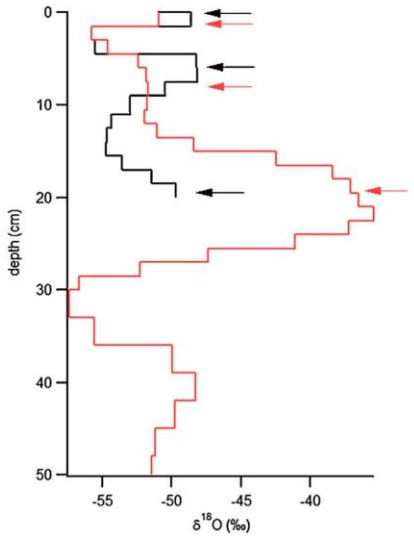

Fig. 8. $\delta^{18}O$ records from two snow pits (black and red) drilled at Dome C in summer 2014–2015 and sampled at a depth of 1.5 cm. The arrows show the location of the three first $\delta^{18}O$ maxima (or inflexion point for the second red arrow).

supported by a principal components (PC) analysis, with PC1 capturing 67% of the variance, showing the strong $\delta^{18}O$ peak depths of 6–10 cm as well as two oscillations of smaller amplitude at higher depths. This suggests that a common signal can be extracted from high-resolution $\delta^{18}O$ snow pit profiles. This common signal may either be produced by deposition (snowfall $\delta^{18}O$ signal linked to atmospheric processes along transport and at condensation) or produced by post-deposition processes and snow–air isotopic exchanges with a spatial coherence at the scale of a few meters at least.

The eight $\delta^{18}O$ profiles exhibit significant differences, such as the amplitude of the peak observed at depths between 6 and 10 cm. There is no link between the variations of amplitude of this sub-surface $\delta^{18}O$ peak and the surface temperature, hence with the temperature gradient at the very surface of the snow. Even if the pits are rather close (1 m distance between successive pits), variations in $\delta^{18}O$ from one snow pit to the next one may be affected by wind blowing or wind scouring effects (Libois et al., 2014). Some small surface inhomogeneity or snow dunes at Dome C are indeed observed at the meter scale (Picard et al., 2014), reflecting erosion and enhanced deposition on different sites of the snow dunes. Such snow redistribution processes probably explains stratigraphic noise and/or hiatus observed in the different snow pits at very low accumulation rates (e.g., Kameda et al., 2008).

4. Conclusions and perspectives

Together with previously published data, the new data presented in this study have several implications for the climatic reconstruction based on ice core isotopic data.

The spatial relationship between surface temperature and isotopic composition of precipitation can be explained quite straightforwardly using simple isotopic models tuned on d-excess vs $\delta^{18}O$ evolution in transects on the East Antarctic sector. The spatial slopes deduced from the transects are however systematically higher ($\sim$ 0.7–0.8‰·°C^{-1} for $\delta^{18}O$ vs temperature, Masson-Delmotte et al., 2008; Touzeau et al., 2016) than temporal slopes calculated from seasonal variations in precipitation $\delta^{18}O$ at sites from East Antarctica like Vostok and Dome C (0.35 to 0.46‰·°C^{-1} (Landais et al., 2012; Stenni et al., 2016). These

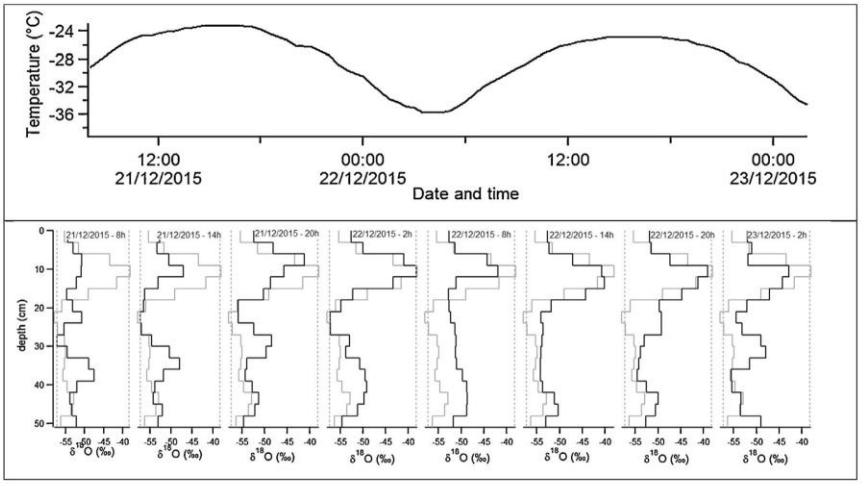

Fig. 9. Top: 2 m surface air temperature measurements at Dome C. Bottom: 8 $\delta^{18}O$ records (black) from eight snow pits located at 1 m distance drilled every 6 h between 21 and 23 December 2015 at Dome C. The grey curve displays the first component (PC1) of a principal component analysis and captures 67% of the common variance of the eight $\delta^{18}O$ records.

differences may be explained by the vanishing inversion layer in summer (Casado et al., 2016a, b; Landais et al., 2012), and therefore different relationships between condensation and surface temperature.

Post-deposition effects linked to exchanges between the snow surface and the atmospheric water vapor lead to an evolution of $\delta^{18}O$ in the surface snow in the absence of any precipitation event in Antarctica, as previously evidenced for Greenland. This process preserves the positive correlation between the $\delta^{18}O$ of snow and surface temperature at the seasonal scale, but with a much slower $\delta^{18}O$-vs-temperature slope than observed with seasonal precipitation data (Casado et al., 2016b; Touzeau et al., 2016). Such relationship likely involves equilibrium and kinetic fractionation at the interface between snow and atmosphere at sublimation and hoar condensation (Casado et al., 2016b; Ritter et al., 2016; Steen-Larsen et al., 2014). It is now a priority to quantify the importance of these processes for different deep-drilling sites, as it is highly important both for the comparison of ice core data with atmospheric model outputs and for assessing uncertainties attached to past temperature reconstructions from ice cores. Implementing isotopes in snow models is a crucial step forward.

Post-deposition effects clearly limit the possible archiving of high-resolution (seasonal) climatic variability in the polar snow. Earlier studies suggested that seasonal cycles could not be recorded in snow water isotopes from low accumulation rate sites of East Antarctica (Ekaykin et al., 2014). Using new isotopic records from snow pits drilled in high-accumulation and low-accumulation sites of East Antarctica, we are able to adjust/refine this statement. Sites with an accumulation rate larger than 70–80 $kg \cdot m^{-2} \cdot yr^{-1}$ such as Kohnen (Münch et al., 2015) record a seasonal cycle in the absence of large wind effects. It is challenging to identify seasonal cycles on sites from the East Antarctic plateau: in the different snow pits recovered associated with the TI11 campaign and at Vostok, no variations are identified at depths corresponding to the average annual accumulation rate. The only exception is for one snow pit drilled at Dome C in 2007, where the water isotopic record depicts high-frequency variations over the first meter, which may correspond to seasonal signals. This finding is further supported by water isotopic records from two snow pits from Dome C, analyzed at 1.5 cm resolution. Our results also depict a smoothing of these signals below one meter in depth, probably due to diffusion.

An important result of our study is that seasonal climate variability may affect the surface snow isotopic composition at the surface and possibly over the top 50 cm, at least at Dome C. We are still lacking high-resolution (1 cm) deep snow pits and associated snow modeling to study how the seasonal cycle is preserved or not in the snow when diffusion and wind ventilation induce important water vapor transport in the zone where porosity is still important.

Acknowledgments

The research leading to these results has received funding from the European Research Council under the European Union's Seventh Framework Program (FP7/2007–2013)/RC grant agreement number 306045. Ice cores, snow samples (pits and surface) were drilled within the International TASTE-IDEA (Trans-Antarctic Scientific Traverse Expeditions–Ice Divide of East Antarctica)/VANISH (Vulnerability of ANtarctic Ice SHeet and its atmosphere) programs supported by the "Agence nationale de la recherche" (Project No. ANR-07-VULN-0013), during the 2006/2007 and 2011/2012 summer campaigns, with logistical support from "Institut polaire français Paul-Émile-Victor" (IPEV). We thank all the field team members who contributed to the success of the 2006–2007 TASTE-IDEA/VANISH summer campaigns.

Appendix A. Supplementary data

Supplementary data associated with this article can be found, in the online version, at http://dx.doi.org/10.1016/j.crte.2017.05.003.

References

Altnau, S., Schlosser, E., Isaksson, E., Divine, D., 2014. Climatic signals from 76 shallow firn cores in Dronning Maud Land, East Antarctica. Cryosph. Discuss. 8, 5961–6005, http://dx.doi.org/10.5194/tcd-8-5961-2014.

Buizert, C., Gkinis, V., Severinghaus, J.P., He, F., Lecavalier, B.S., Kindler, P., Leuenberger, M., Carlson, A.E., Vinther, B., Masson-Delmotte, V., White, J.W.C., Liu, Z., Otto-Bliesner, B., Brook, E.J., 2014. Greenland temperature response to climate forcing during the last deglaciation. Science 345 (6201), 1177–1180, http://dx.doi.org/10.1126/science.1254961.

Cappa, C.D., Hendricks, M.B., DePaolo, D.J., Cohen, R.C., 2003. Isotopic fractionation of water during evaporation. J. Geophys. Res. 108 (D16), 4525, http://dx.doi.org/10.1029/2003JD003597.

Casado, M., Landais, A., Masson-Delmotte, V., Genthon, C., Kerstel, E., Kassi, S., Arnaud, L., Picard, G., Prie, F., Cattani, O., Steen-Larsen, H.-C., Vignon, E., Cermak, P., 2016a. Continuous measurements of isotopic composition of water vapour on the East Antarctic Plateau. Atmos. Chem. Phys. 16, 8521–8538, http://dx.doi.org/10.5194/acp-16-8521-2016.

Casado, M., Landais, A., Picard, G., Münch, T., Laepple, T., Stenni, B., Dreossi, G., Ekaykin, A., Arnaud, L., Genthon, C., Touzeau, A., Masson-Delmotte, V., Jouzel, J., 2016b. Archival of the water stable isotope signal in East Antarctic ice cores. Cryosph. Discuss. 2016, 1–33, http://dx.doi.org/10.5194/tc-2016-263.

Cauquoin, A., Landais, A., Raisbeck, G.M., Jouzel, J., Bazin, L., Kageyama, M., Peterschmitt, J.-Y., Werner, M., Bard, E., Team, A., 2015. Comparing past accumulation rate in East Antarctic ice cores using ^{10}Be, water isotopes and CMIPS-PMIP3 models. Clim. Past 11, 355–367, http://dx.doi.org/10.5194/cp-11-355-2015.

Champollion, N., Picard, G., Arnaud, L., Lefebvre, E., Fily, M., 2013. Hoar crystal development and disappearance at Dome C, Antarctica: observation by near-infrared photography and passive microwave satellite. Cryosphere 7 (4), 1247–1262, http://dx.doi.org/10.5194/tc-7-1247-2013.

Ciais, P., Jouzel, J., 1994. Deuterium and oxygen 18 in precipitation: isotopic model, including mixed cloud processes. J. Geophys. Res. Atm. 99 (D8), 16793–16803.

Cuffey, K.M., Clow, G.D., Steig, E.J., Buizert, C., Fudge, T.J., Koutnik, M., Waddington, E.D., 2016. Deglacial temperature history of West Antarctica. PNAS 113 (50), 14249–14254, http://dx.doi.org/10.1073/pnas.1609132113.

Dahl-Jensen, D., 1998. Past Temperatures Directly from the Greenland Ice Sheet. Science 282 (5387), 268–271, http://dx.doi.org/10.1126/science.282.5387.268.

Dansgaard, W., 1964. Stable isotopes in precipitation. Tellus 16, 436–468.

Dee, D.P., Uppala, S·m., Simmons, A.J., Berrisford, P., Poli, P., Kobayashi, S., Andrae, U., Balmaseda, M.A., Balsamo, G., Bauer, P., Bechtold, P., Beljaars, A.C.M., van de Berg, L., Bidlot, J., Bormann, N., Delsol, C., Dragani, R., Fuentes, M., Geer, A.J., Malmberger, L., Healy, S.B., Hersbach, H., Hólm, E.V., Isaksen, L., Kållberg, P., Köhler, M., Matricardi, M., McNally, A.P., Monge-Sanz, B.M., Morcrette, J.-J., Park, B.-K., Peubey, C., de Rosnay, P., Tavolato, C., Thépaut, J.N., Vitart, F., 2011. The ERA-Interim: configuration and performance of the data assimilation system. Q. J. R. Meteorol. Soc. 137, 553–597, http://dx.doi.org/10.1002/qj.828.

Ekaykin, A.A., Kozachek, A.V., Lipenkov, V.Y., Shibaev, Y.A., 2014. Multiple climate shifts in the Southern Hemisphere over the past three centuries based on central Antarctic snow pits and core studies. Ann. Glaciol. 55 (66), 259–266, http://dx.doi.org/10.3189/2014AoG66A189.

Ekaykin, A.A., Lipenkov, V.Y., Kuzmina, I.N., Petit, J.R., Masson-Delmotte, V., Johnsen, S.J., 2004. The changes in isotope composition and accumulation of snow at Vostok station, East Antarctica, over the past 200 years. Ann. Glaciol. 39 (1), 569–575.

Ellehoj, M.D., Steen-Larsen, H.C., Johnsen, S.J., Madsen, M.B., 2013. Ice-vapor equilibrium fractionation factor of hydrogen and oxygen isotopes: experimental investigations and implications for stable water isotope studies. Rapid Commun. Mass Spectrom. 27 (19), 2149–2158, http://dx.doi.org/10.1002/rcm.6668.

Epica Community Members, 2004. Eight glacial cycles from an Antarctic ice core. Nature 429 (6992), 623–628., http://www.nature.com/nature/journal/v429/n6992/suppinfo/nature02599_S1.html.

Fischer, H., Severinghaus, J., Brook, E., Wolff, E., Albert, M., Alemany, O., Arthern, R., Bentley, C., Blankenship, D., Chappellaz, J., Creyts, T., Dahl-Jensen, D., Dinn, M., Frezzotti, M., Fujita, S., Gallee, H., Hindmarsh, R., Hudspeth, D., Jugie, G., Kawamura, K., Lipenkov, V., Miller, H., Mulvaney, R., Parrenin, F., Pattyn, F., Ritz, C., Schwander, J., Steinhage, D., Van Ommen, T., Wilhelms, F., 2013. Where to find 1.5 million yr old ice for the IPICS "Oldest-Ice" ice core. Clim. Past 9 (6), 2489–2505, http://dx.doi.org/10.5194/cp-9-2489-2013.

Gautier, E., Savarino, J., Erbland, J., Lanciki, A., Possenti, P., 2016. Variability of sulfate signal in ice core records based on five replicate cores. Clim. Past 12 (1), 103–113, http://dx.doi.org/10.5194/cp-12-103-2016.

Genthon, C., Six, D., Gallée, H., Grigioni, P., Pellegrini, A., 2013. Two years of atmospheric boundary layer observations on a 45-m tower at Dome C on the Antarctic plateau. J. Geophys. Res. Atmos. 118 (8), 3218–3232, http://dx.doi.org/10.1002/jgrd.50128.

Goursaud, S., Masson-Delmotte, V., Favier, V., Preunkert, S., Fily, M., Gallée, H., Jourdain, B., Legrand, M., Magand, O., Minster, B., Werner, M., 2016. A sixty year ice-core record of regional climate from Adélie Land, coastal Antarctica. Cryosph. Discuss. 2016, 1–36, http://dx.doi.org/10.5194/tc-2016-179.

Groot Zwaaftink, C.D., Cagnati, A., Crepaz, A., Fierz, C., MacElloni, G., Valt, M., Lehning, M., 2013. Event-driven deposition of snow on the Antarctic Plateau: analyzing field measurements with SNOWPACK. Cryosphere 7 (1), 333–347, http://dx.doi.org/10.5194/tc-7-333-2013.

Guillevic, M., Bazin, L., Landais, A., Kindler, P., Orsi, A., Masson-Delmotte, V., Blunier, T., Buchardt, S.L., Capron, E., Leuenberger, M., Martinerie, P., Prié, F., Vinther, B.M., 2013. Spatial gradients of temperature, accumulation and ∂^{18}O-ice in Greenland over a series of Dansgaard-Oeschger events. Clim. Past 9 (3), 1029–1051, http://dx.doi.org/10.5194/cp-9-1029-2013.

Helsen, M.M., van de Wal, R.S.W., van den Broeke, M.R., Masson-Delmotte, V., Meijer, H.A.J., Scheele, M.P., Werner, M., 2006. Modeling the isotopic composition of Antarctic snow using backward trajectories: simulation of snow pit records. J. Geophys. Res. Atmos. 111 (15), 1–19, http://dx.doi.org/10.1029/2005JD006524.

Higgins, J.A., Kurbatov, A.V., Spaulding, N.E., Brook, E., Introne, D.S., Chimiak, L.M., Yan, Y., Mayewski, P., Bender, M.L., 2015. Atmospheric composition 1 million years ago from blue ice in the Allan Hills, Antarctica. Proc. Natl. Acad. Sci. USA 112 (22), 6887–6891, http://dx.doi.org/10.1073/pnas.1420232112.

Horita, J., Rozanski, K., Cohen, S., 2008. Isotope effects in the evaporation of water: a status report of the Craig-Gordon model. Isotop. Environ. Health Stud. 44 (1), 23–49, http://dx.doi.org/10.1080/10256010801887174.

Hoshina, Y., Fujita, K., Iizuka, Y., Motoyama, H., 2016. Inconsistent relationships between major ions and water stable isotopes in Antarctic snow under different accumulation environments. Polar Sci. 10 (1), 1–10, http://dx.doi.org/10.1016/j.polar.2015.12.003.

Johnsen, S.J., Clausen, H.B., Cuffey, K.M., Hoffmann, G., Schwander, J., Creyts, T., 2000. Diffusion of stable isotopes in polar firn and ice: the isotope effect in firn diffusion. Phys. Ice Core Rec. 159, 121–140.

Jouzel, J., Merlivat, L., 1984. Deuterium and oxygen 18 in precipitation: modeling of the isotopic effects during snow formation. J. Geophys. Res. Atmos. 89 (D7), 11749–11757.

Jouzel, J., Merlivat, L., Petit, J.-R., Lorius, C., 1983. Isotopic Record in the South Pole Snow. J. Geophys. Res. 88 (2), 2693–2703.

Jouzel, J., Masson-Delmotte, V., Cattani, O., Dreyfus, G., Falourd, S., Hoffmann, G., Minster, B., Nouet, J., Barnola, J.-M., Chappellaz, J., Fischer, H., Gallet, J.C., Johnsen, S., Leuenberger, M., Loulergue, L., Luethi, D., Oerter, H., Parrenin, F., Raisbeck, G., Raynaud, D., Schilt, A., Schwander, J., Selmo, E., Souchez, R., Spahni, R., Sauffer, B., Steffensen, J.P., Stenni, B., Stocker, T.F., Tison, J.L., Werner, M., Wolff, E.W., 2007. Orbital and millennial Antarctic climate variability over the past 800,000 years. Science 317 (5839), 793–796.

Kindler, P., Guillevic, M., Baumgartner, M., Schwander, J., Landais, A., Leuenberger, M., 2014. Temperature reconstruction from 10 to 120 kyr b2k from the NGRIP ice core. Clim. Past 10 (2), 887–902, http://dx.doi.org/10.5194/cp-10-887-2014.

Krinner, G., Werner, M., 2003. Impact of precipitation seasonality changes on isotopic signals in polar ice cores: A multi-model analysis. Earth Planet Sci. Lett. 216 (4), 525–538, http://dx.doi.org/10.1016/S0012-821X(03)00550-8.

Küttel, M., Steig, E.J., Ding, Q., Monaghan, A.J., Battisti, D.S., 2012. Seasonal climate information preserved in West Antarctic ice core water isotopes: relationships to temperature, large-scale circulation, and sea ice. Clim. Dynam. 39 (7), 1841–1857, http://dx.doi.org/10.1007/s00382-012-1460-7.

Laepple, T., Hörhold, M., Münch, T., Freitag, J., Wegner, A., Kipfstuhl, S., 2016. Layering of surface snow and firn at Kohnen Station, Antarctica - noise or seasonal signal? J. Geophys. Res. Earth Surf., http://dx.doi.org/10.1002/2016JF003919.

Laepple, T., Werner, M., Lohmann, G., 2011. Synchronicity of Antarctic temperatures and local solar insolation on orbital timescales. Nature 471 (7336), 91–94.

Landais, A., 2011. Utility of stable isotopes of N and Ar as tracers to retrieve past air temperature from air trapped in ice cores. In: Handbook of Environmental Isotope Geochemistry. 865–886.

Landais, A., Barkan, E., Luz, B., 2008. Record of δ^{18}O and ^{17}O-excess in ice from Vostok Antarctica during the last 150,000 years. Geophys. Res. Lett. 35 (2), L02709.

Landais, A., Caillon, N., Severinghaus, J., Barnola, J.M., Goujon, C., Jouzel, J., Masson-Delmotte, V., 2004a. Analyse isotopique de l'air piégé dans la glace pour quantifier les variations de température. C. R. Geoscience 336 (11), 963–970.

Landais, A., Jouzel, J., Masson-Delmotte, V., Caillon, N., 2004b. Large temperature variations over rapid climatic events in Greenland: a method based on air isotopic measurements. C. R. Geoscience 337 (10–11), 947–956.

Landais, A., Ekaykin, A., Barkan, E., Winkler, R., Luz, B., 2012. Seasonal variations of ^{17}O-excess and d-excess in snow precipitation at Vostok station. East Antarctica. J. Glaciol. 58 (210), 725–733, http://dx.doi.org/10.3189/2012JoG11J237.

Lee, J., Fung, I., Depaolo, D.J., Otto-bliesner, B., 2008. Water isotopes during the last glacial maximum: new general circulation model calculations. J. Geophys. Res. 113 , http://dx.doi.org/10.1029/2008JD009859.

Legrand, M., McConnell, J., Fischer, H., Wolff, E.W., Preunkert, S., Chellman, N., Leuenberger, D., Maselli, O., Sigl, M., Schüpbach, S., Flannigan, M., 2016. Boreal fire records in Northern Hemisphere ice cores: a review. Clim. Past Disc. 1–43, http://dx.doi.org/10.5194/cp-2016-70.

Libois, Q., Picard, G., Arnaud, L., Dumont, M., Lafaysse, M., Morin, S., Lefebvre, E., 2015. Summertime evolution of snow specific surface area close to the surface on the Antarctic Plateau. Cryosphere 9 (6), 2383–2398, http://dx.doi.org/10.5194/tc-9-2383-2015.

Libois, Q., Picard, G., Arnaud, L., Morin, S., Brun, E., 2014. Modeling the impact of snow drift on the decameter-scale variability of snow properties on the Antarctic Plateau. J. Geophys. Res. Atmos. 119 (20), 11662–11681, http://dx.doi.org/10.1002/2014JD022361.

Lorius, C., Merlivat, L., 1977. Distribution of mean surface stable isotope values in East Antarctica: observed changes with depth in coastal area. In: Isotopes and impurities in snow and ice. IAHS Grenoble, France127–137.

Lorius, C., Merlivat, L., Hagemann, R., 1969. Variation in the mean deuterium content of precipitations in Antarctica. J. Geophys Res. 74 (28), 7027–7031.

Luz, B., Barkan, E., Yam, R., Shemesh, A., 2009. Fractionation of oxygen and hydrogen isotopes in evaporating water. Geochim. Cosmochim. Acta 73 (22), 6697–6703, http://dx.doi.org/10.1016/j.gca.2009.08.008.

Majoube, M., 1971a. Fractionnement en oxygène 18 entre la glace et la vapeur d'eau. J. Chim. Phys. 68 (4), 625–636.

Majoube, M., 1971b. Fractionnement en oxygène 18 et en deutérium entre l'eau et sa vapeur. J. Chim. Phys. 68 (7–8), 1423–1436.

Masson-Delmotte, V., Jouzel, J., Landais, A., Stievenard, M., Johnsen, S.J., White, J.W.C., Werner, M., Sveinbjornsdottir, A., Fuhrer, K., 2005. GRIP deuterium excess reveals rapid and orbital-scale changes in Greenland moisture origin. Science 309 (5731), 118–121.

Masson-Delmotte, V., Dreyfus, G., Braconnot, P., Johnsen, S., Jouzel, J., Kageyama, M., Landais, A., Loutre, M.F., Nouet, J., Parrenin, F., Raynaud, D., Stenni, B., Tuenter, E., 2006. Past temperatures reconstructions from deep ice cores: relevance for future climate changes. Clim. Past 2, 145–165.

Masson-Delmotte, V., Hou, S., Ekaykin, A., Jouzel, J., Aristarain, A., Bernardo, R.T., Bromwich, D., Cattani, O., Delmotte, M.M., Falourd, S.,

Frezzotti, M., Gallée, H., Genoni, L., Isaksson, E., Landais, A., Helsen, M.M., Hoffmann, G., Lopez, J., Morgan, V., Motoyama, H., Noone, D., Oerter, H., Petit, J.R., Royer, A., Uemura, R., Schmidt, G.A., Schlosser, E., Simoes, J.C., Steig, E.J., Stenni, B., Stievenard, M., Van Den Broeke, M.R., Van De Wal, R.S.W., Van De Berg, W.J., Vimeux, F., White, J.W.C., 2008. A review of Antarctic surface snow isotopic composition: observations, atmospheric circulation, and isotopic modeling. J. Climate 21 (13), 3359–3387, http://dx.doi.org/10.1175/2007JCLI2139.1.

Mayewski, P., Al, E., 2006. The International Trans-Antarctic Scientific Expedition (ITASE): An overview. Ann. Glaciol. 41, 180–185.

Merlivat, L., Nief, G., 1967. Fractionnement isotopique lors des changements d'état solide-vapeur et liquide-vapeur de l'eau à des températures inférieures à 0 °C. Tellus 19 (1), 122–127.

Münch, T., Kipfstuhl, S., Freitag, J., Meyer, H., Laepple, T., 2015. Regional climate signal vs. local noise: a two-dimensional view of water isotopes in Antarctic firn at Kohnen station. Clim. Past Discuss. 5605–5649, http://dx.doi.org/10.5194/cpd-11-5605-2015.

NEEM Community members, 2013, 2013. Eemian interglacial reconstructed from a Greenland folded ice core. Nature 493 (7433), 489–494, http://dx.doi.org/10.1038/nature11789.

Neumann, T., Waddington, E.D., 2004. Effects of firn ventilation on isotopic exchange. J. Glaciol. 50 (169), 183–194.

Nicolas, J.P., Bromwich, D.H., 2014. New reconstruction of Antarctic near-surface temperatures: multidecadal trends and reliability of global reanalyses. J. Climate 27, 8070–8093, http://dx.doi.org/10.1175/JCLI-D-13-00733.1.

NorthGRIP-community-members, 2004. High resolution climate record of the northern hemisphere reaching into last interglacial period. Nature 431, 147–151.

Orsi, A.J., Cornuelle, B.D., Severinghaus, J.P., 2014. Magnitude and temporal evolution of Dansgaard–Oeschger event 8 abrupt temperature change inferred from nitrogen and argon isotopes in GISP2 ice using a new least-squares inversion. Earth Planet Sci. Lett. 395 , http://dx.doi.org/10.1016/j.epsl.2014.03.030.

Pang, H., Hou, S., Landais, A., Masson-Delmotte, V., Prie, F., Steen-Larsen, H.C., Risi, C., Li, Y., Jouzel, J., Wang, Y., He, J., Minster, B., Falourd, S., 2015. Spatial distribution of ^{17}O-excess in surface snow along a traverse from Zhongshan station to Do, me A, East Antarctica. Earth Planet. Sci. Lett. Lett. 414, 126–133, http://dx.doi.org/10.1016/j.epsl.2015.01.014.

Picard, G., Royer, A., Arnaud, L., Fily, M., 2014. Influence of meter-scale wind-formed features on the variability of the microwave brightness temperature around Dome C in Antarctica. Cryosphere 8 (3), 1105–1119, http://dx.doi.org/10.5194/tc-8-1105-2014.

Pinilla, C., Blanchard, M., Balan, E., Ferlat, G., Vuilleumier, R., Mauri, F., 2014. Equilibrium fractionation of H and O isotopes in water from path integral molecular dynamics. Geochim. Cosmochim. Acta 135, 203–216, http://dx.doi.org/10.1016/j.gca.2014.03.027.

Rasmussen, S.O., Andersen, K.K., Svensson, A.M., Steffensen, J.P., Vinther, B.M., Clausen, H.B., Siggaard-Andersen, M.L., Johnsen, S.J., Larsen, L.B., Dahl-Jensen, D., Bigler, M., Rothlisberger, R., Fischer, H., Goto-Azuma, K., Hansson, M.E., Ruth, U., 2006. A new Greenland ice core chronology for the last glacial termination. J. Geophys. Res. Atmos. 111 (6), 1–16, http://dx.doi.org/10.1029/2005JD006079.

Risi, C., Bony, S., Vimeux, F., Jouzel, J., 2010. Water-stable isotopes in the LMDZ4 general circulation model: Model evaluation for present-day and past climates and applications to climatic interpretations of tropical isotopic records. J. Geophys. Res. Atmos. 115 (12) , http://dx.doi.org/10.1029/2009JD013255.

Ritter, F., Steen-Larsen, H.C., Werner, M., Masson-Delmotte, V., Orsi, A., Behrens, M., Birnbaum, G., Freitag, J., Risi, C., Kipfstuhl, S., 2016. Isotopic exchange on the diurnal scale between near-surface snow and lower atmospheric water vapor at Kohnen station, East Antarctica. Cryosphere 10, 1647–1663, http://dx.doi.org/10.5194/tc-10-1647-2016.

Salamatin, A.N., Lipenkov, V.Y., Barkov, N.I., Jouzel, J., Petit, J.R., Raynaud, D., 1998. Ice core age dating and paleothermometer calibration based on isotope and temperature profiles from deep boreholes at Vostok Station (East Antarctica). J. Geophys. Res. 103 (8), 8963, http://dx.doi.org/10.1029/97JD02253.

Scarchilli, C., Frezzotti, M., Grigioni, P., De Silvestri, L., Agnoletto, L., Dolci, S., 2010. Extraordinary blowing snow transport events in East Antarctica. Clim. Dynam. 34 (7), 1195–1206, http://dx.doi.org/10.1007/s00382-009-0601-0.

Schmidt, G.A., Hoffmann, G., Shindell, D.T., Hu, Y., 2005. Modeling atmospheric stable water isotopes and the potential for constraining cloud processes and stratosphere-troposphere water exchange. J. Geophys. Res. Atmos. 110 (21), 1–15, http://dx.doi.org/10.1029/2005JD005790.

Schmidt, G.A., LeGrande, A.N., Hoffmann, G., 2007. Water isotope expressions of intrinsic and forced variability in a coupled ocean-atmosphere model. J. Geophys. Res. Atmos. 112 (D10), D10103, http://dx.doi.org/10.1029/2006JD007781.

Schneider, D.P., Steig, E.J., Van Ommen, T.D., Dixon, D.A., Mayewski, P.A., Jones, J.M., Bitz, C.M., 2006. Antarctic temperatures over the past two centuries from ice cores. Geophys. Res. Lett. 33 (16), 1–5, http://dx.doi.org/10.1029/2006GL027057.

Severinghaus, J.P., Brook, E.J., 1999. Abrupt climate change at the end of the last glacial period inferred from trapped air in polar ice. Science 286, 930–933, http://dx.doi.org/10.1126/science.286.5441.930.

Sime, L.C., Wolff, E.W., Oliver, K.I.C., Tindall, J.C., 2009. Evidence for warmer interglacials in East Antarctic ice cores. Nature 462 (7271), 342–345.

Steen-Larsen, H.C., Masson-Delmotte, V., Hirabayashi, M., Winkler, R., Satow, K., Prié, F., Bayou, N., Brun, E., Cuffey, K.M., Dahl-Jensen, D., Dumont, M., Guillevic, M., Kipfstuhl, S., Landais, A., Popp, T., Risi, C., Steffen, K., Stenni, B., Sveinbjörnsdottír, A.E., 2014. What controls the isotopic composition of Greenland surface snow? Clim. Past 10 (1), 377–392, http://dx.doi.org/10.5194/cp-10-377-2014.

Steen-Larsen, H.C., Masson-Delmotte, V., Sjolte, J., Johnsen, S.J., Vinther, B.M., Bréon, F.-M., Clausen, H.B., Dahl-Jensen, D., Falourd, S., Fettweis, X., Gallée, H., Jouzel, J., Kageyama, M., Lerche, H., Minster, B., Picard, G., Punge, H.J., Risi, C., Salas, D., Schwander, J., Steffen, K., Sveinbjörnsdóttir, A.E., Svensson, A., White, J., 2011. Understanding the climatic signal in the water stable isotope records from the NEEM shallow firn/ice cores in northwest Greenland. J. Geophys. Res. Atmos. 116 (D6) , http://dx.doi.org/10.1029/2010JD014311.

Stenni, B., Jouzel, J., Masson-Delmotte, V., Rothlisberger, R., Castellano, E., Cattani, O., Falourd, S., Johnsen, S.J., Longinelli, A., Sachs, J.P., Selmo, E., Souchez, R., Steffensen, J.P., Udisti, R., 2003. A late-glacial high-resolution site and source temperature record derived from the EPICA Dome C isotope records (East Antarctica). Earth Planet. Sci. Lett. 217, 183–195.

Stenni, B., Masson-Delmotte, V., Selmo, E., Oerter, H., Meyer, H., Röthlisberger, R., Jouzel, J., Cattani, O., Falourd, S., Fischer, H., Hoffmann, G., Iacuminc, P., Johnsen, S.J., Minster, B., Udisti, R., 2010. The deuterium excess records of EPICA Dome C and Dronning Maud Land ice cores (East Antarctica). Quatern. Sci. Rev. 29 (1), 146–159.

Stenni, B., Scarchilli, C., Masson-Delmotte, V., Schlosser, E., Ciardini, V., Dreossi, G., Grigioni, P., Bonazza, M., Cagnati, A., Karlicek, D., 2016. Three-year monitoring of stable isotopes of precipitation at Concordia Station. East Antarctica. Cryosphere 10 (5), 2415.

Touzeau, A., Landais, A., Stenni, B., Uemura, R., Fukui, K., Fujita, S., Guilbaud, S., Ekaykin, A., Casado, M., Barkan, E., Luz, B., Magand, O., Teste, G., Le Meur, E., Baroni, M., Savarino, J., Bourgeois, I., Risi, C., 2016. Acquisition of isotopic composition for surface snow in East Antarctica and the links to climatic parameters. Cryosphere 10, 837–852, http://dx.doi.org/10.5194/tc-10-837-2016.

Town, M.S., Warren, S.G., Walden, V.P., Waddington, E.D., 2008. Effect of atmospheric water vapor on modification of stable isotopes in near-surface snow on ice sheets. J. Geophys. Res. Atmos. 113 (24), 1–16, http://dx.doi.org/10.1029/2008JD009852.

Van Hook, W.A., 1968. Vapor pressures of the isotopic waters and ices. J. Phys. Chem. 72 (4), 1234–1244.

Vimeux, F., Masson, V., Delaygue, G., Jouzel, J., Petit, J.R., Stievenard, M., 2001. A 420,000 year deuterium excess record from East Antarctica: Information on past changes in the origin of precipitation at Vostok. J. Geophys. Res. Atmos. 106 (D23), 31863–31873.

Werner, M., Haese, B., Xu, X., Zhang, X., Butzin, M., Lohmann, G., 2015. Glacial–interglacial changes of $H_2{}^{18}O$, HDO and deuterium excess–results from the fully coupled Earth System Model ECHAM5/MPI-OM. Geosci. Model Dev. Discuss. 8 (10), 8835–8894, http://dx.doi.org/10.5194/gmdd-8-8835-2015.

Werner, M., Langebroek, P.M., Carlsen, T., Herold, M., Lohmann, G., 2011. Stable water isotopes in the ECHAM5 general circulation model: toward high-resolution isotope modeling on a global scale. J. Geophys. Res. Atmos. 116 (D15) .

Winkler, R., Landais, A., Sodemann, H., Dumbgen, L., Prie, F., Masson-Delmotte, V., Stenni, B., Jouzel, J., 2012. Deglaciation records of ^{17}O-excess in East Antarctica: Reliable reconstruction of oceanic normalized relative humidity from coastal sites. Clim. Past 8 (1), 1–16, http://dx.doi.org/10.5194/cp-8-1-2012.

Wolff, E.W., Barbante, C., Becagli, S., Bigler, M., Boutron, C.F., Castellano, E., de Angelis, M., Federer, U., Fischer, H., Fundel, F., Hansson, M., Hutterli, M., Jonsell, U., Karlin, T., Kaufmann, P., Lambert, F., Littot, G.C., Mulvaney, R., Röthlisberger, R., Ruth, U., Severi, M., Siggaard-Andersen, M.L., Sime, L.C., Steffensen, J.P., Stocker, T.F., Traversi, R., Twarloh, B., Udisti, R., Wagenbach, D., Wegner, A., 2010. Changes in environment over the last 800,000 years from chemical analysis of the EPICA Dome C ice core. Quat. Sci. Rev. 29 (1–2), 285–295, http://dx.doi.org/10.1016/j.quascirev.2009.06.013.

Annexe C.

*P*ublications et communications liées à cette thèse

Publications.

Bréant, C., Leroy Dos Santos, C., Casado, M., Fourré, E., **Goursaud, S.**, Masson-Delmotte, V., Favier, V., Agosta, C., Cattani, O., Prié, F., Golly, B., Orsi, A., and Martinerie, P.: Coastal water vapor isotopic composition driven by katabatic wind variability in summer at Dumont d'Urville, coastal East Antarctica, Earth and Planetary Science Letters, *submitted.*

Klein, F., Abram, N.J., Curran, M.a., Goosse, H., **Goursaud, S.**, Masson-Delmotte, V., Moy, A., Neukom, R., Orsi, A., Sjolte, J., Steiger, N., Stenni, B., and Werner, M., Assessing the robustness of Antarctic temperature reconstructions over the past two millennia using pseudoproxy and data assimilation experiments, Clim. Past Discuss., 2018, in review.
https://doi.org/10.5194/cp-2018-90

Goursaud, S., Masson-Delmotte, V., Favier, V., Preunkert, S., Legrand, M., Minster, B., and Werner, M.: Challenges associated with the climatic interpretation of water stable isotope records from a highly resolved firn core from Adélie Land, coastal Antarctica, The Cryosphere Discuss., 2018, 1-55, 10.5194/tc-2018-121, 2018.
https://doi.org/10.5194/tc-2018-121

Goursaud, S., Masson-Delmotte, V., Favier, V., Orsi, A., and Werner, M.: Water stable isotope spatio-temporal variability in Antarctica in 1960–2013: observations and simulations from the ECHAM5-wiso atmospheric general circulation model, Clim. Past, 14, 923-946, 10.5194/cp-14-923-2018, 2018.
https://doi.org/10.5194/cp-14-923-2018

Landais, A., Casado, M., Prié, F., Magand, O., Arnaud, L., Ekaykin, A., Petit, J.-R., Picard, G., Fily, M., Minster, B., Touzeau, A., **Goursaud, S.**, Masson-Delmotte, V., Jouzel, J., and Orsi, A.: Surface studies of water isotopes in Antarctica for quantitative interpretation of deep ice core data, Comptes Rendus Geoscience, 2017.
https://doi.org/10.1016/j.crte.2017.05.003

Stenni, B., Curran, M. A., Abram, N. J., Orsi, A., **Goursaud, S.**, Masson-Delmotte, V., Neukom, R., Goosse, H., Divine, D., and Van Ommen, T.: Antarctic climate variability on regional and continental scales over the last 2000 years, Climate of the Past, 13, 1609, 2017.
https://doi.org/10.5194/cp-13-1609-2017

Goursaud, S., Masson-Delmotte, V., Favier, V., Preunkert, S., Fily, M., Gallée, H., Jourdain, B., Legrand, M., Magand, O., Minster, B., and Werner, M. (2017). A 60-year ice-core record of regional climate from Adélie Land, coastal Antarctica. *The Cryosphere*, *11*(1), 343-362.
https://doi.org/10.5194/tc-11-343-2017

Goursaud, S., Agu**,** A., Wojkiewicz, J.L., Redon, N., Lahcen Khouchaf, .-Enhanced metrological performances of organic electronic ammonia sensors using electro spinning techniques, *Procedia Engineering*, 87, 204-207, 2014
https://doi.org/10.1016/j.proeng.2014.11.619

Communications.

19-23 June 2018 What Controls Deuterium Excess in Coastal Antarctica?, *POLAR2018 Open Science Conference OSC*, Davos (Switzerland), Poster

08-12 May 2017 Goursaud et al., Assessing nudged atmospheric model performance using Antarctic ice core water stable isotope data for the period 1960-2013, *Open Scientific Meeting*, Saragoza (Spain), Poster

24-28 April 2017 Goursaud et al., Assessment of local and regional climate signals in water stable isotopes and chemistry records from new high resolution shallow ice cores in Adelie Land, Antarctica, *European Geosciences Union*, Vienna (Austria) (oral)

07-11 March 2016 Goursaud et al., What control the triple isotopic composition of oxygen in the precipitations of Bolivia?, *International Partnerships in Ice Core Sciences 2016*, Hobart (Tasmania, Australia), Poster

07-10 Sept. 2014 Goursaud et al., Enhanced Metrological Performances of Organic Electronic Ammonia Sensors Using Electro Spinning Techniques, *EUROSENSORS 2014*, Brescia (Italia), Poster